UNIVERSITÉ D'ORLÉANS

ÉCOLE DOCTORALE SCIENCES BIOLOGIQUES ET CHIMIE DU VIVANT

Centre de Biophysique Moléculaire, Orléans

THÈSE présentée par :

Ons KHARRAT

soutenue le : 14 Janvier 2025

pour obtenir le grade de : **Docteur de l'Université d'Orléans**

Discipline/ Spécialité : Biologie

Deciphering the mechanisms of action of promising defensins to design a new generation of antimicrobials

THÈSE dirigée par :

Dr. LANDON Céline	Directrice de recherche CNRS, CBM, Orléans

RAPPORTEURS :

Dr. WEINGARTH Markus	Associate Professor, Université de Utrecht, Pays-Bas
Dr. ALVES Isabel	Directrice de recherche CNRS, CBMN, Pessac

JURY :

Dr. BENEDETTI Hélène	Directrice de recherche CNRS, CBM, Orléans, président du jury
Dr. WEINGARTH Markus	Associate Professor, Université de Utrecht, Pays-Bas
Dr. ALVES Isabel	Directrice de recherche CNRS, CBMN, Pessac
Dr. DESTOUMIEUX-GARZON Delphine	Directrice de recherche CNRS, IHPE, Montpellier
Dr. BULET Philippe	Directeur de recherche CNRS, IAB, Grenoble
Dr. LANDON Céline	Directrice de recherche CNRS, CBM, Orléans

Acknowledgements

The thesis work presented in this manuscript was carried out at the Centre de Biophysique Moléculaire (CBM), a unit of the Centre National de la Recherche Scientifiques (CNRS).

I would like to thank the SSBCV doctoral school for the granting of a thesis scholarship, and the Agence Nationale de la Recherche (ANR) for funding the associated costs. I would also like to thank the laboratory director, Dr. Matthieu Réfrégiers, for allowing me to carry out this thesis at CBM. More importantly, for his real support, his positive vibes and for the excellent exchanges, scientific and otherwise, that I've had with him. “Thank you, Mathieu”. I would also like to thank Dr. Hélène Bénédetti, Deputy Director of the CBM, who agreed to be a member of the jury for my thesis defense. “Thanks Hélène for your support and for listening to the students’ concerns”.

I would like to thank Dr. Markus Weingarth and Dr. Isabel Alves for agreeing to act as rapporteurs for this manuscript, despite their busy schedules. I would also like to thank Dr. Delphine Destoumieux-Garzon and Dr. Philippe Bulet for agreeing to serve on my thesis defense jury. "Thank you to all of you, members of the jury, and believe me, I've done my best to write this manuscript in a short space of time. I hope you enjoy reading it. See you soon on D-day".

My warmest thanks go to Dr. Céline Landon, my thesis supervisor, for trusting me to carry out this project. I would also like to thank her for the extensive training she has given me, for her daily availability, her constant support, her efficient supervision and for all the sound advice she has given me. I have learned a lot from you, especially how to observe an antimicrobial peptide from a structural perspective and how we should have a critical eye on what we do. To Céline: "Thank you for all these things; supporting my ideas, encouraging me, discussing scientific topics or others, making me feel comfortable, and not putting up barriers."

For the two people I spent the most time with during these three years, Françoise Paquet and Hervé Meudal. All my thanks will not be enough to express my gratitude towards you. Our deep discussions, our scientific exchanges on NMR, politics, daily life, sports, our meals together in the cantine. You are friends to me and you will remain so. I will never forget your support, your listening...I learnt a lot from you both humanly and professionally. Thank you so much with all my heart.

I would like to thank also Dr. Karine Loth for the conversations we've had together and the meals we've shared. “Thank you Karine for your scientific advice and your support, I really like the person you are”. I also thank Dr. Marylène Bertrand for helping me during these three years, for examining the products, the equipment, the orders, as well as for our exchanges together, especially in the morning. “Marylène, I truly respect your values and the principles you stand for, including equality.” I thank also Dr. Laurence Jouvensal for sharing some conversations with me and I appreciate her perfectionism for preparing the

classes. I would also like to express my gratitude to Dr. Agnès Delmas for allowing me to benefit from her extensive scientific experience.

A big think to David Gosset for all microscopy and flow cytometry experiments, who were an excellent work partner and without him a whole part of the thesis never saw the light of day. Thank you, David, for your support and the good vibes of work.

I thank also all the incredible collaborators with whom I had the chance to work and to learn a lot: Dr. Vincent Aucagne and Jean-Baptiste Madinier for peptide labeling (CBM, Orléans), Dr. Philippe Bulet and Dr. Sébastien Voisin for all experiments on fungal cells (BioPark, Archamps), Dr. Rouba Nassreddine and Dr. Reine Nehmé for MST experiments (ICOA, Orléans), Dr. Cyrille Botté and Dr. Yoshiki Botté for MS experiments (IAB, Grenoble), Dr. Caroline Mas (ISBG, Grenoble) and Dr. Frank Coste (CBM, Orléans) for ITC experiments, and Dr. Dror Warschawski for solid-state NMR experiments (LBM, Paris).

I express my warmest thanks to Eric Kaya, my friend and colleague, for everything he has done for me: for listening and supporting me. Thank you, Eric. I was very spoiled to meet you. Also, I would like to thank Dr. El-Hadji Cisse for teaching me a lot about peptide synthesis and purification and helping me to analyze data and for sharing interesting scientific or other discussion. I think also all PhD students in the CBM (Ayoub, Sara, Océane, Albert, Clémence….) and I wish them all the best for their projects.

I am deeply grateful to my family for their unconditional support, encouragement, and understanding throughout my journey. Thank you for your patience with me, and I hope you are proud of me.

Lastly, but certainly not least, I would like to express my deep gratitude to my Loulou, my friend, my companion, my soulmate, for these three "incredible years" with him. Your presence has undoubtedly changed many things. I am honored to share moments of my life with such an exceptional person. Thank you for everything.

Abbreviations

2D: Two-dimensional

3D: Three-dimensional

3-keto DhSph: 3-keto dihydrosphingosine

AFPs: Antifungal peptides

AIDS: acquired immunodeficiency syndrome

AMPs: Antimicrobial peptides

AMR: Antimicrobial resistance

AvBDs: Avian β-defensins

CFU: Colony-forming unit

CGT: ceramide galactosyltransferase

CPMG: Carr-Purcell-Meiboom-Gill

CSA: Chemical shift anisotropy

CSαβ: Cysteine-stabilized αβ motif

CSP: Chemical shift perturbation

CW: cell wall

CWI: Cell Wall Integrity

d_{31}-POPC: deuterated 1-palmitoyl-d_{31}-2-oleoyl-sn-glycero-3-phosphocholine

DAPI: 4',6-diamidino-2-phenylindole

D_2O: deuterated water

DhSph: dihydrosphingosine

DLS: Dynamic light scattering

DNA: Deoxyribonucleic acid

DRPs: disulfide-rich peptides

DP: Differential power

ELISA: Enzyme-linked immunosorbent assay

ESI: electrospray ionization

ESI-MS: Electrospray ionization mass spectrometry

EZRDM: EZ Rich Defined Medium

FDA: Food and Drug Administration

fGlcCer: fungal glucosylceramides

FITC: Fluorescein isothiocyanate

GalCer: galactosylceramides

GC-MS: gas-chromatography coupled with mass spectrometry

GCS: glucosylceramide synthase

GlcCer: Glucosylceramides

GFP: Green fluorescent protein

GSL: Glycosphingolipids

HDPs: Host defense peptides

HEPES: 4-(2-Hydroxyethyl) piperazine-1-ethanesulfonic acid

HIV: Human immunodeficiency virus

HMQC: Heteronuclear multiple quantum coherence

HPLC: High-pressure liquid chromatography

HPTLC: high-performance thin layer chromatography

HSQC: Heteronuclear single quantum coherence

IC_{50}: Half maximal inhibitory concentration

IM: Inner membrane

IPC: inositol phosphorylceramides

ITC: Isothermal titration calorimetry

L: loop

LB: Luria-Bertani

LCB: Long chain base

LED: Light Emitting Diode

LPS: Lipopolysaccharides

LSDs: Lysosomal storage disorders

LUVs: Large unilamellar vesicles

M9 supp. media: M9 minimal medium supplemented by 0.4% glucose

M: Molecular mass

MAPK: classical mitogen-activated protein kinase

MDR: multi-drug resistant

MeCN: Acetonitrile

MIC: minimum inhibitory concentration

MIPC: Mannosylated IPC

MLVs: Multilamellar vesicles

MOAs: Mechanisms of action

MS: Mass spectrometry

MS/MS: Tandem mass spectrometry

MST: Microscale thermophoresis (MST)

m/z: Mass-to-charge ratio

NMR: Nuclear magnetic resonance

NO: Nitric Oxide

NOE: Nuclear Overhauser Effect

NRPs: Non-ribosomal peptides

OD_{600nm}: Optical density at 600 nm

OM: Outer membrane

PAMPs: pathogen-associated molecular patterns

PBS: Phosphate buffer saline

PC: Egg L-α-phosphatidylcholine

PDB: Potato Dextrose Broth

PDMS: polydimethylsiloxane

PDMP: 1-phenyl-2-decanoylamino-3-morpholino- 1-propanol

PG: Peptidoglycan

PI: propidium iodide

PRRs: Pattern recognition receptors

Q-TOF: Quadrupole Time-of-Flight

RiPPs: Ribosomally synthesized and post-translationally modified peptides

RNA: Ribonucleic acid

ROI: Region of interest

ROS: Reactive Oxygen Species (ROS)

RT: room temperature

SD: Standard deviation

SDS: sodium dodecyl sulfate

SDS-PAGE: Sodium Dodecyl Sulfate - PolyAcrylamide Gel Electrophoresis

SEM: standard error of the mean

SL: Sphingolipids

SMT: Sphingolipid C9-methyltransferase

SOFAST: band-Selective Optimized-Flip-Angle Short-Transient

sp/mL: spores/mL

SPR: Surface plasmon resonance

SPT: Sphingolipid palmitoyltransferase

SPPS: Solid phase peptide synthesis

TFA: Trifluoroacetic acid

TLRs: Toll-like receptors

UDP: Uridine diphosphate

UV: Ultraviolet

v/v: Volume per volume percentage concentration

WHO: World Health Organization

wt: wild-type

Symbols

K_d: Dissociation constant

ΔH: Enthalpy

-T ΔS: Entropy

g: gravitational force

^{1}H Hydrogen

^{31}P: Phosphorus 31

^{15}N: Nitrogen 15

Units

%: percent

°C: Celsius degree

Å: angström (10-10 m)

Cal: calorie

Da (ou g.mol-1): Dalton

g: gram

h: hour

Hz: hertz

K: Kelvin degree

L: liter

µL: microliter

µM: micromolar

Min: minute

nm: nanometer

ppm: Parts per million

Rpm: rotation per minute

s: second

General table of contents

Résumé de thèse

Les **antimicrobiens**- antibactériens, antiviraux, antifongiques et antiparasitaires - sont des substances largement utilisées pour prévenir et traiter les infections chez les humains, les animaux et les plantes. Malheureusement, leur efficacité est aujourd'hui menacée, car de nombreux traitements antimicrobiens qui fonctionnaient auparavant ne fonctionnent plus, les micro-organismes y étant devenus résistants. On parle de **résistance aux antimicrobiens (AMR)** lorsque les bactéries, les virus, les parasites ou les champignons ne réagissent plus aux agents antimicrobiens auxquels ils étaient auparavant sensibles. Pire encore, certaines souches bactériennes, connues sous le nom de "superbactéries", ont développé une résistance multiple, c'est–à–dire à plusieurs types d'antibiotiques, provoquant des infections extrêmement difficiles à traiter. L'utilisation accrue et le mauvais usage des antimicrobiens, combinés au nombre limité de médicaments nouvellement développés, sont les principales causes de l'émergence d'agents pathogènes résistants.

Aujourd'hui, la résistance aux antimicrobiens figure dans le **top 10 de la liste des menaces pour la santé mondiale établie par l'Organisation Mondiale de la Santé** (OMS). Elle menace la santé et le bien-être des humains et des animaux, en augmentant le risque de propagation des maladies et en entraînant des conséquences néfastes, des handicaps et des décès. De plus, les maladies infectieuses des plantes deviennent difficiles, voire impossibles, à traiter, ce qui réduit la productivité des exploitations agricoles et menace la sécurité alimentaire et nutritionnelle. On estime que l'AMR a été directement responsable de 1,27 million de décès dans le monde en 2019. Aujourd'hui, le taux de mortalité mondial dû à l'AMR dépasse celui du paludisme ou du cancer du sein et est comparable à celui de la tuberculose et du VIH.

Pour éviter de perdre notre capacité à contrôler les pathogènes résistants aux médicaments actuels et pour éviter des échecs critiques en médecine et en sécurité alimentaire, nous devons absolument améliorer rapidement notre gestion de l'utilisation des médicaments, promouvoir la découverte de nouveaux médicaments et **trouver des solutions alternatives** aux composés antimicrobiens actuellement utilisés. Parmi les alternatives prometteuses, il y a les **peptides antimicrobiens (PAMs)** connus aussi sous le nom de peptides de défense de l'hôte (HDP pour Host defense Peptides). Les PAMs font partie du système immunitaire inné des vertébrés, des invertébrés et des plantes. Ils possèdent un large spectre antimicrobien ainsi que des activités de régulation immunitaire. Les familles de PAMs sont nombreuses et présentent des structures extrêmement diverses. Parmi elles se trouve la superfamille de peptides riches en ponts disulfure connue sous le nom de "défensines".

Les défensines sont des peptides antimicrobiens (PAMs) très structurés, avec un repliement caractéristique riche en feuillets β et un réseau bien définis de ponts disulfure. Elles contiennent au moins six résidus de cystéine conservés impliqués dans trois ponts disulfures. Les défensines sont généralement cationiques, avec pourcentage élevé de résidus hydrophobes, leur taille est généralement inférieure à 10 kDa. Elles sont exprimées par de très nombreux animaux, plantes et champignons en tant

que composants essentiels de leur système de défense de l'hôte. Il convient de noter que le terme "défensine" recouvre au moins deux superfamilles de peptides riches en ponts disulfure (DRP Disulfide-Rich Peptides), phylogénétiquement indépendantes : les cis-défensines et les trans-défensines (figure 1). La superfamille cis est largement répandue dans les champignons, les plantes et la majorité des invertébrés, y compris les insectes. La superfamille trans est apparue et a évolué exclusivement chez les animaux.

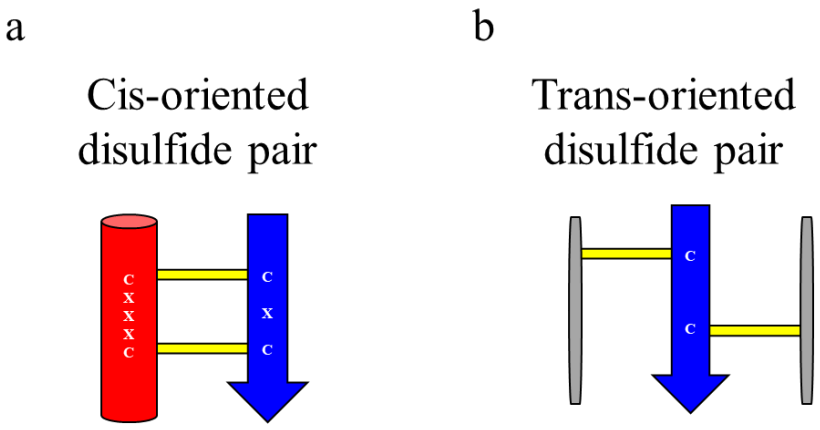

Figure 1 : Les deux superfamilles de défensines. (a) Cis-défensines où le motif CXC conservé dans le feuillet β oriente naturellement les ponts disulfure correspondants dans la même direction. (b) Défensines trans où les cystéines vicinales conservées (motif CC) dans le feuillet β orientent automatiquement les ponts disulfure correspondants dans des directions opposées. La flèche bleue indique un brin β, le cylindre rouge indique une hélice α, les lignes jaunes indiquent les ponts disulfure, les barres grises indiquent une partie de la molécule que peut être structurée ou non structurée. C pour cystéine et X pour n'importe quel acide aminé.

Les activités antimicrobiennes des défensines, ainsi que leurs caractéristiques structurales sont bien décrites dans la litérature. Par contre, leurs mécanismes d'action (MOA) sont beaucoup moins connus, d'autant plus qu'il est désormais reconnu qu'ils disposent d'une grande variété de MOA, optimisés au cours de millions d'années d'évolution dans leur environnement naturel. En effet, pendant longtemps, on a considéré que les modes d'action de tous les PAMs cationiques étaient principalement basés sur la perméabilisation des membranes (attraction électrostatique sur les membranes microbiennes chargées négativement), car les PAMs lytiques linéaires et non structurés ont été les premiers (et les plus largement) étudiés. Mais au cours des dix dernières années, de nombreuses études sur d'autres familles de PAMs non lytiques ont montré que leurs modes d'actions, étaient souvent beaucoup plus complexes que la seule perméabilisation des membranes, qui ne représente en fait qu'une toute petite partie du panel de mécanismes développés pas les PAM. C'est le cas en particulier avec des structures complexes telles que celles des défensines, dont le MOA mérite d'être exploré. En effet, pour générer rationnellement des molécules efficaces à partir des PAMs, la première étape cruciale consiste à

comprendre à l'échelle moléculaire/atomique comment ils agissent dans la nature. Cela fournira des informations importantes sur leurs applications thérapeutiques potentielles.

Mon projet de doctorat porte sur le décryptage des modes d'action de deux défensines prometteuses, une défensine Cis, à savoir ETD151, un peptide antifongique de 44 résidus optimisé à partir de défensines d'insectes (partie I, figure 2a), et une défensine Trans, AvBD103b, un peptide antimicrobien de 38 résidus provenant du manchot royal, pour son activité antibactérienne (partie II, figure 2b).

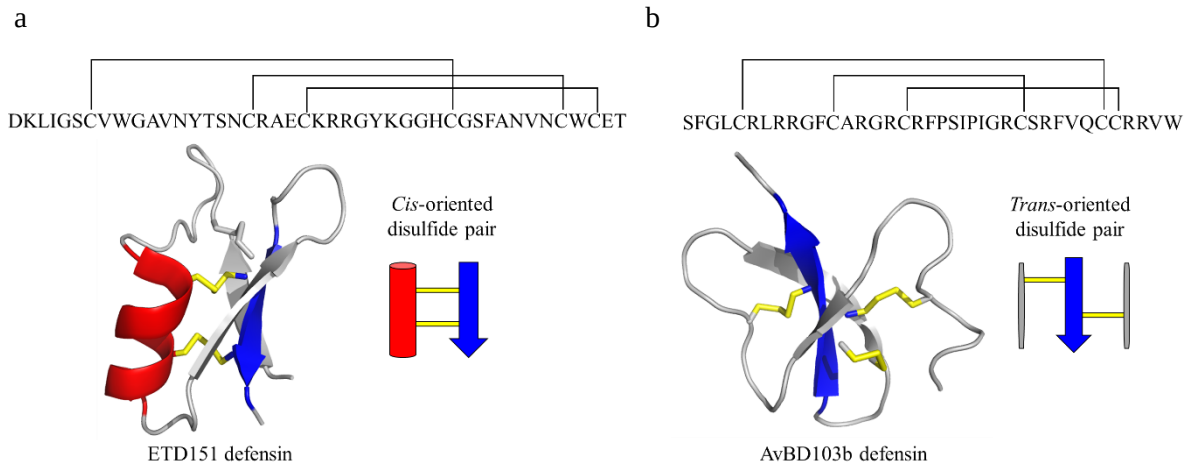

Figure 2 : Séquences et structures 3D des défensines étudiées dans le cadre de cette thèse. (a) La défensine ETD151 dérivée des insectes (code PDB : 1P00). (b) La défensine aviaire AvBD103b (code PDB : 1UT3). Les ponts disulfure sont indiqués en jaune.

Partie I : ETD151, une cis-défensine antifongique prometteuse

La défensine ETD151 est très active contre les champignons pathogènes pour l'homme et les plantes, et ne présente pas de toxicité. ETD151 a été optimisé au début des années 2000 par la société biotechnologique EntoMed SA (d'où son nom ETD), lors de l'optimisation de la défensine Heliomicin du papillon *Heliothis virescens*. Le mode d'action de ETD151 a de multiples facettes, et nécessite la présence de glucosylcéramides (GlcCer), lipides membranaires fongiques déterminants de la croissance cellulaire et de la virulence chez les champignons. Les GlcCer fongiques sont donc considérés comme des cibles prometteuses, avec un faible risque d'induire une résistance. ETD151 apparait donc comme candidat prometteur pour la lutte contre les souches fongiques résistantes. Cependant, son mode d'action antifongique - en particulier sa cible membranaire et les mécanismes moléculaires par lesquels il interagit avec cette cible - reste à élucider.

La première partie comprend :

Le chapitre 1 : Introduction

La chapitre 1 présente une introduction bibliographique sur le problème de la résistance antifongique et les nouveaux agents antifongiques permettant de traiter les champignons pathogènes. Un accent particulier a été mis sur la présentation de certaines défensines de plantes et d'insectes ciblant les GlcCers, qui pourraient inspirer de nouvelles alternatives thérapeutiques aux options de traitement existantes.

Le chapitre 2 : Identification de la cible membranaire de l'ETD151

Ce chapitre est consacré à l'étude de la première étape du MOA de ETD151 contre un champignon phytopathogène, *Botrytis cinerea*, en identifiant sa cible au niveau de la membrane du champignon, et en examinant dans quelle mesure la présence de cette cible est liée à l'activité antifongique de ETD151. **Ce chapitre comprend essentiellement un article publié dans "Proceedings of the National Academy of Sciences" (PNAS): Ons Kharrat *et al*. 2025 intitulé "The antimicrobial activity of ETD151 defensin is dictated by the presence of glycosphingolipids in the targeted organisms".**

Avant le début de ma thèse, il avait été montré que la présence de GlcCer dans les membranes était indispensable à la sensibilité de *Pichia pastoris* et de *Candida albicans* à la défensine ETD151. Notre principal objectif dans cette section était de démontrer si le glycolipide, GlcCer, présent dans les membranes fongiques était la cible membranaire directe du peptide ETD151. Pour cela, (i) nous avons caractérisé structurellement le(s) GlcCer(s) isolé(s) de *B. cinerea* par spectrométrie de masse (MS), (ii) nous avons évalué par thermophorèse microscopique (MST) l'affinité de ETD151 pour les GlcCer(s) isolés de *B. cinerea* et étudié dans un contexte membranaire, et enfin (iii) nous avons évalué l'effet de ETD151 sur *Novosphingobium capsulatum*, une des rares bactéries Gram-négatives qui expriment des glycosphingolipides (GSL) au lieu de lipopolysaccharides (LPS).

Dans un premier temps, les GlcCer ont été extraits des mycéliums de *B. cinerea* par chromatographie sur couche mince à haute performance et deux espèces de ce sphingolipide ont été identifiées par spectrométrie de masse avec les structures d19:2/h16:1 et d19:2/h16:0 (Figure 3). **Ce travail est le premier dans lequel les glycosphingolipides de *B. cinerea* ont été caractérisés structurellement, augmentant ainsi notre connaissance de la composition de la membrane de ce champignon pathogène.**

L'interaction directe de la défensine ETD151 avec le GlcCer a été démontrée par thermophorèse microscopique (MST) en utilisant le peptide ETD151 fluorescent mono-marqué (Atto647-ETD151) et des liposomes de phosphatidylcholine (PC) contenant du GlcCer isolé du champignon *B. cinerea*. **Cette analyse a pour la première fois permis d'évaluer l'affinité de liaison, avec une valeur de K_d de 0,5 ± 0,3 µM** (Figure 4).

La majorité des cellules procaryotes ne contiennent pas de GSL, ce qui explique leur résistance à l'action de ETD151. Nous avons étudié la sensibilité de *Novosphingobium capsulatum*, une des rares bactéries contenant des GSL, au peptide ETD151. Le peptide provoque des changements morphologiques transitoires de la bactérie. L'activité de croissance inhibitrice (IC_{50}) est de l'ordre de ~75 µM, avec une affinité pour la surface cellulaire, soulignant **l'importance critique de la GSL en tant que cible membranaire** (Figure 5).

Cette étude a permis de mieux comprendre le MOA de l'ETD151, un candidat prometteur pour développer un nouveau médicament antifongique, et pourrait ouvrir la voie à de nouvelles perspectives en matière de santé humaine et de protection des cultures. De plus, cette identification de la cible membranaire et l'établissement du lien direct entre cette étape de liaison à la cible et l'activité de l'ETD151 pourraient permettre d'étendre le potentiel du peptide ETD151 à d'autres pathologies humaines dans lesquelles les GlcCers sont surexprimés, notamment certaines maladies cancéreuses.

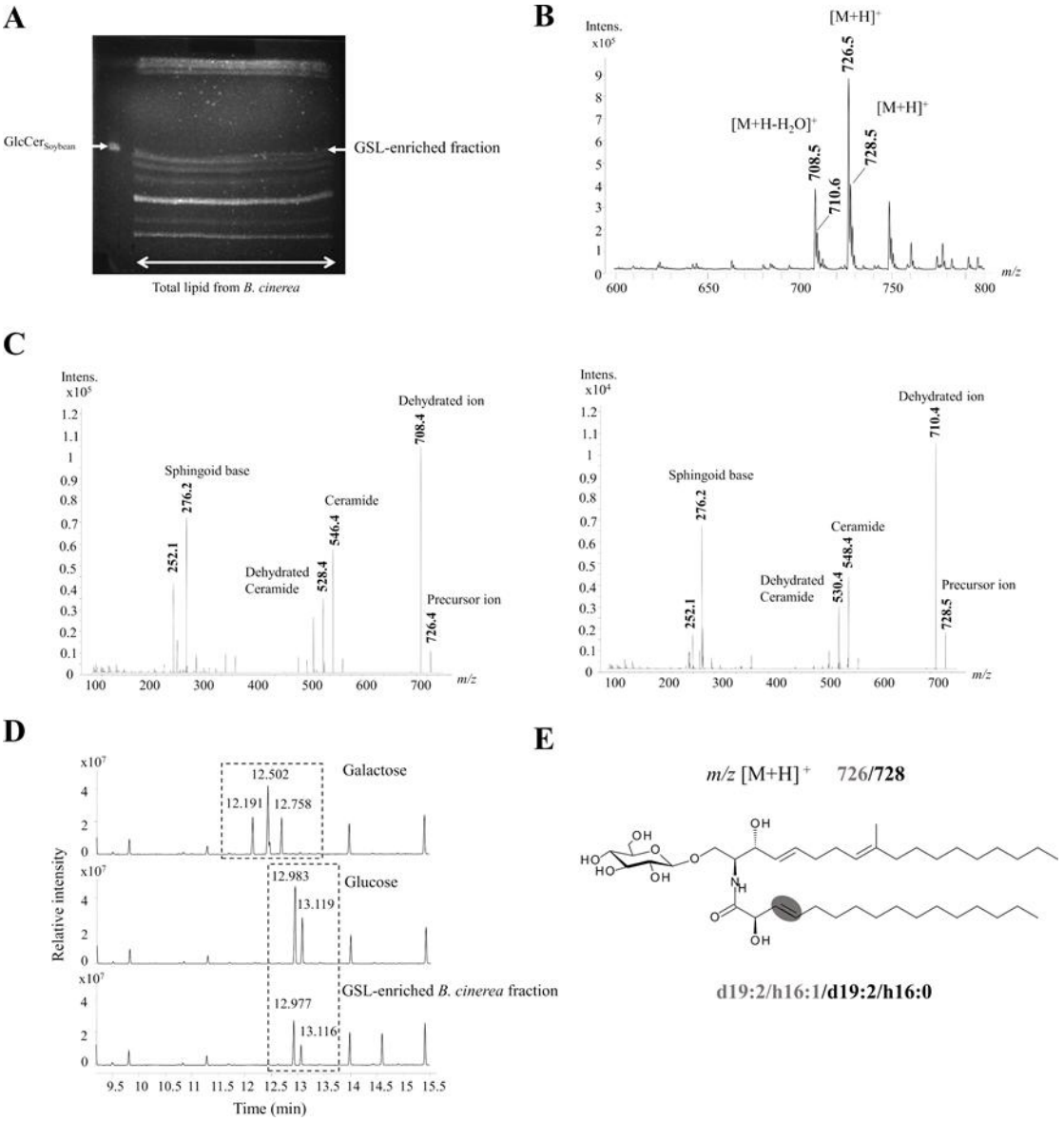

Figure 3 : Analyse structurale des glucosylcéramides (GlcCer) obtenus à partir des mycéliums de *B. cinerea* B05.10. (A) Isolement de la fraction enrichie en glycosphingolipides des lipides totaux bruts extraits de *B. cinerea* par chromatographie sur couche mince à haute performance (HPTLC). La migration HPTLC a été réalisée avec du dichlorométhane/méthanol/ammoniaque 2M (65:25:4, vol/vol/vol) et les bandes de lipides ont été visualisées sous lumière UV après coloration à la primuline. Le GlcCer de soja (GlcCer$_{Soybean}$) a été utilisé comme étalon. (B) Spectres ESI-MS de la fraction purifiée enrichie en glycosphingolipides. (C) ESI-MS/MS des ions précurseurs moléculaires à *m/z* 726,4 et 728,5 observés dans ESI-MS. (D) Analyse GC-MS de la fraction enrichie en glycosphingolipides après extraction, méthanolyse et dérivatisation au triméthylsilyle (TMS). Chromatogrammes des ions totaux pour le glucose et le galactose en tant qu'étalons et la fraction enrichie en glycosphingolipides de *B. cinerea*. (E) Structure proposée pour les principales espèces de GlcCer trouvées chez *B. cinerea*. Par analogie avec le GlcCer des plantes, la double liaison de l'acide gras a été proposée en position C3-C4.

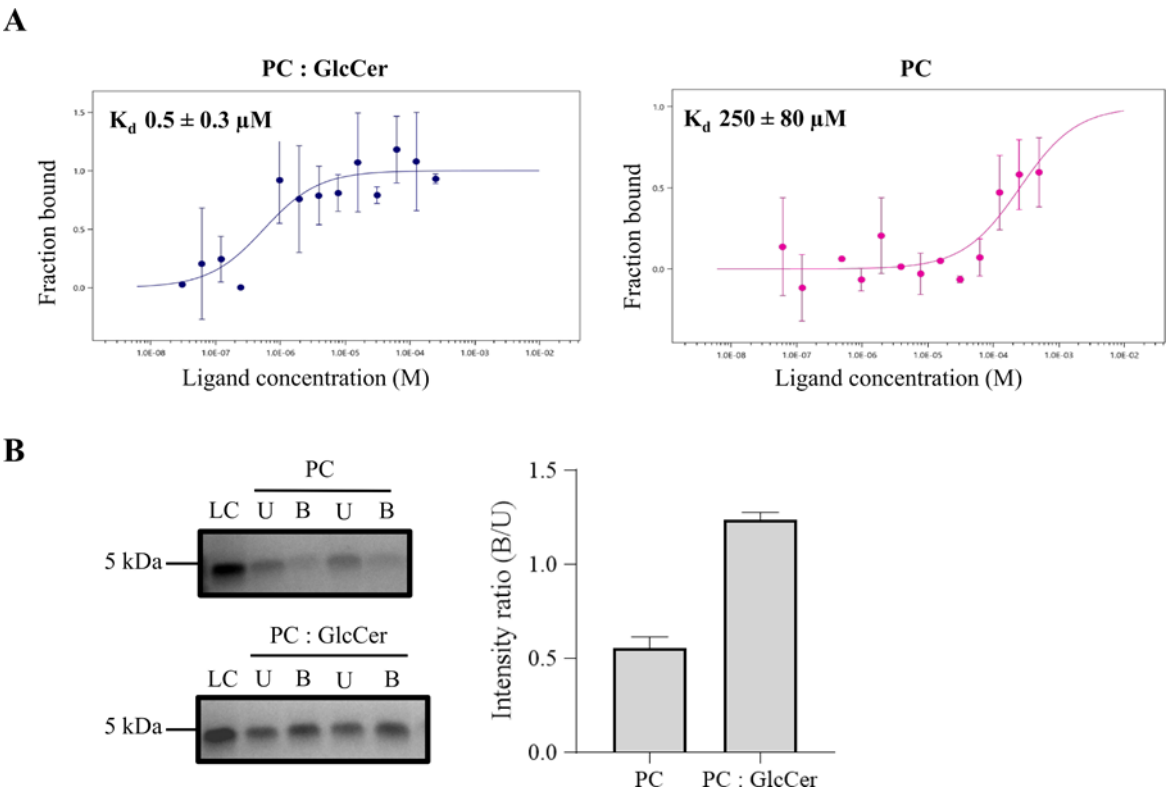

Figure 4 : ETD151 se lie préférentiellement aux liposomes contenant des glucosylcéramides fongiques. (A) Courbes de liaison MST de l'Atto647-ETD151. A gauche : des liposomes de phosphatidylcholine (PC) contenant des des GlcCer extraits de *B. cinerea* ($GlcCer_{B.\ cinerea}$) avec un rapport molaire de 10/90 (GlcCer/PC) ; à droite des liposomes sans GlcCer, fabriqués uniquement avec du PC, ont été utilisés comme contrôle. K_d est la constante de dissociation donnée comme moyenne de trois expériences indépendantes ± SD. Toutes les expériences ont été réalisées avec une concentration constante d'Atto647-ETD151 (50 nM) à 22°C. Une puissance d'excitation à détection automatique et une puissance de MST de 40 % ont été utilisées. Le tampon utilisé est un tampon phosphate (10 mM, pH 5,8). (B) Expérience de centrifugation de liposomes comparant la liaison du peptide ETD151 aux liposomes 100% PC et aux liposomes PC : GlcCer fongique (rapport molaire 90 :10). Les fractions liées (B) et non liées (U) ont été soumises à une analyse SDS-PAGE et à une coloration colloïdale de Coomassie. Le peptide ETD151 seul a été utilisé comme contrôle de charge (LC). Les intensités des bandes ont été calculées à l'aide du logiciel ImageJ. Les moyennes du rapport des intensités (lié/non lié) ont ensuite été calculées pour n = 2 expériences (indiquées dans le gel). Les données représentent la moyenne ± SEM, n = 2.

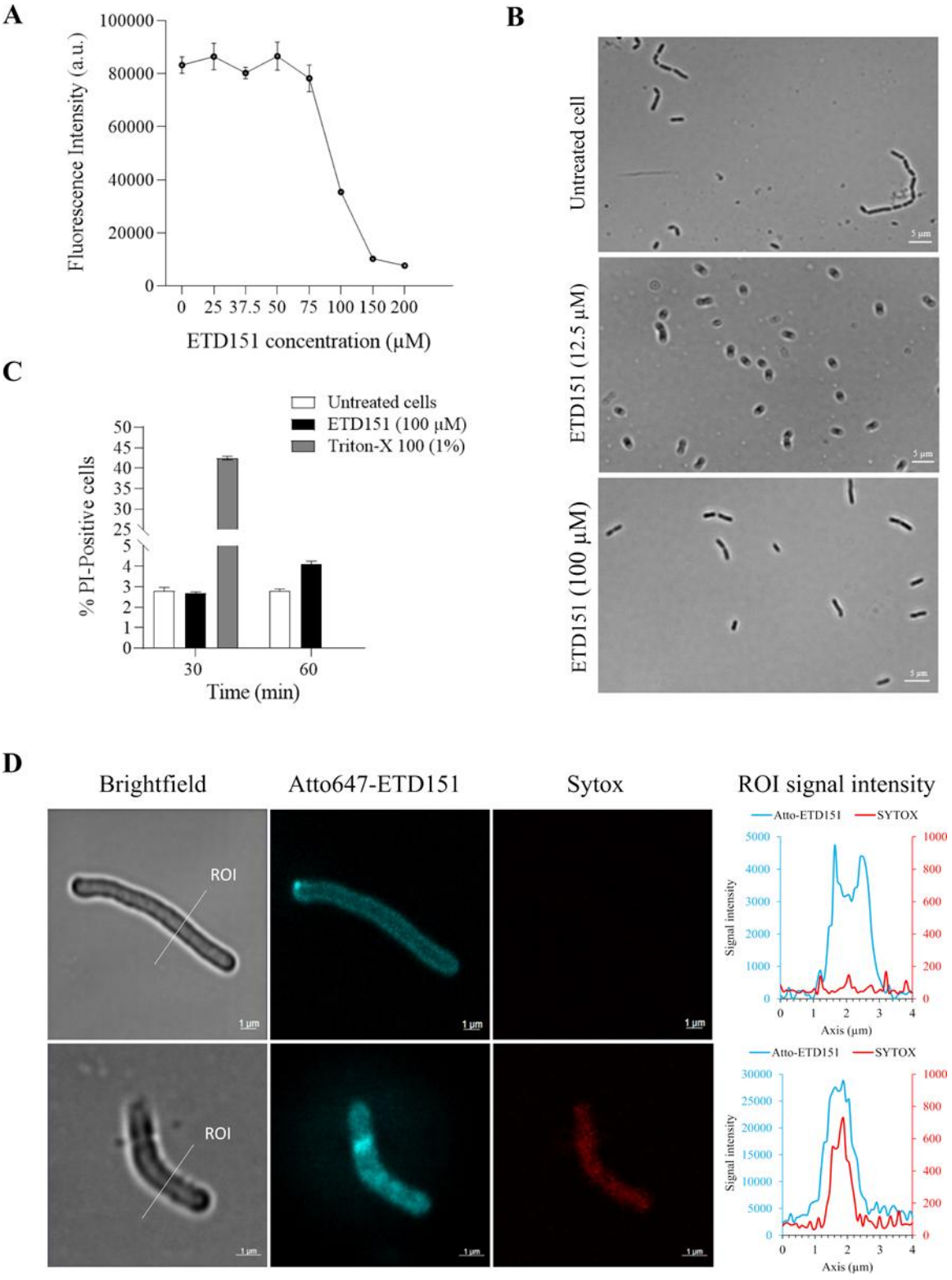

Figure 5 : Effet de l'ETD151 sur la bactérie *Novosphingobium capsulatum* contenant des glycosphingolipides. (A) L'activité antibactérienne de l'ETD151 contre *N. capsulatum* a été déterminée à l'aide du test de viabilité cellulaire à la résazurine. Différentes concentrations du peptide ETD151 (25-200 µM) ont été utilisées pour l'incubation avec *N. capsulatum*, pendant 24 heures. L'intensité de la fluorescence a été mesurée après 2 heures d'ajout de résazurine (10 %, v/v). Les cellules

métaboliquement actives peuvent réduire la résazurine non fluorescente en forme fluorescente. Les données sont représentées comme des moyennes ± SEM pour des mesures triplicats. (B) Images microscopiques représentatives de *N. capsulatum* traité après 24 heures avec deux concentrations d'ETD151 (12,5 et 100 µM). Les cellules non traitées montrent des cellules normales en forme de bâtonnets. À 12,5 µM, l'ETD151 induit des changements de forme des cellules bactériennes, montrant des cellules sphériques de *N. capsulatum*. A 100 µM, l'ETD151 semble n'avoir aucun effet sur la morphologie cellulaire. Barre d'échelle = 2µm. (C) Perméabilisation de la membrane cytoplasmique de *N. capsulatum* traité avec 100 µM d'ETD151 déterminée par cytométrie en flux avec 30 µM d'iodure de propidium (PI imperméable à la membrane). La proportion de cellules perméabilisées a été détectée par la fluorescence due à la liaison de la sonde fluorescente iodure de propidium (PI) avec l'ADN après 30 et 60 minutes d'incubation avec l'ETD151. Les cellules non traitées et les cellules traitées avec du Triton-X 100 (1%, v/v) ont été utilisées comme contrôles négatifs et positifs, respectivement. Les données sont des moyennes ± SEM pour des mesures en trois exemplaires. (D) Localisation subcellulaire de l'Atto647-ETD151 dans *N. capsulatum*. A gauche : Images de microscopie confocale de cellules de *N. capsulatum* exposées simultanément à 2 µM d'Atto647-ETD151 (bleu) et à 10 nM de Sytox orange (rouge) pendant 30 minutes. Barre d'échelle = 1 µM. A droite : Intensité du signal (unités arbitraires) dans la région d'intérêt (ROI) de chaque cellule.

Chapitre 3 : Étude de l'interaction moléculaire de l'ETD151 avec sa cible

Le chapitre 3 se concentre sur l'étude de l'interaction directe *in vitro*, au niveau moléculaire et atomique, entre ETD151 et sa cible membranaire fongique, GlcCer, identifiée dans le chapitre 2. Des essais biochimiques et biophysiques ont été utilisés pour comprendre certains éléments clés de cette interaction défensine-GlcCer, qui est nécessaire à l'activité antifongique de plusieurs défensines. L'implication de caractéristiques spécifiques de la structure de la cible dans cette interaction a également été étudiée. **Ce chapitre est essentiellement basé sur un article en cours de révision dans « Journal of Biological Chemistry » (JBC) : Ons Kharrat *et al*. 2025 et intitulé "ETD151 defensin targets fungal methylated glucosylceramides".**

Notre objectif dans ce travail est de caractériser, à l'aide de tests biophysiques, l'interaction directe entre la défensine ETD151 et les membranes contenant du GlcCer aux échelles moléculaire et atomique. A cette fin, nous avons réalisé une étude à l'échelle moléculaire combinant plusieurs techniques biophysiques : (i) les techniques de thermophorèse à micro-échelle (MST) et de calorimétrie par titrage isotherme (ITC) pour estimer l'affinité de liaison entre ETD151 et le GlcCer fongique (méthylé), (ii) la résonance magnétique nucléaire (RMN) en solution pour déterminer quelle partie du peptide ETD151 est affectée par l'interaction avec le GlcCer fongique, (iii) la RMN solide (ss-NMR) pour évaluer l'effet de la présence de ETD151 sur la dynamique des lipides membranaires, et enfin (iv) l'ensemble de ces techniques pour étudier l'implication du C9-méthyle de la base sphingoïde du GlcCer dans l'interaction

moléculaire entre ETD151-GlcCer, en comparant le GlcCer fongique méthylé et un GlcCer non méthylé de plante.

L'affinité de liaison ETD151-GlcCer méthylé, mesurée expérimentalement par calorimétrie de titrage isotherme (ITC) et thermophorèse à micro-échelle (MST), est de l'ordre du micromolaire (Figure 6). La RMN en solution a ensuite permis d'identifier la zone du peptide ETD151 impliquée dans la liaison avec GlcCer méthylé et qui comprend les deux boucles hydrophobes adjacentes (Figure 7). Nous avons également révélé que ETD151 s'insérait spécifiquement dans les vésicules lipidiques de phosphatidylcholine (PC) contenant du GlcCer méthylé et les fluidifiait (Figure 8). Enfin, nous avons montré que le C9-méthyl de la base sphingoïde jouait un rôle majeur dans l'interaction ETD151-GlcCer. Sa présence augmente en effet l'affinité de liaison entre les deux partenaires, ce qui entraîne des changements structurels plus importants chez ETD151 et une insertion plus profonde dans le cœur hydrophobe des membranes modèles (Figure 6-8).

Cette étude, qui révèle des éléments biochimiques et structurels clés de l'interaction ETD151-GlcCer, fournit une base pour élucider la structure et la dynamique d'autres défensines en relation avec leur fonction, et peut aussi servir de base pour le développement d'antifongiques mimétiques de la défensine.

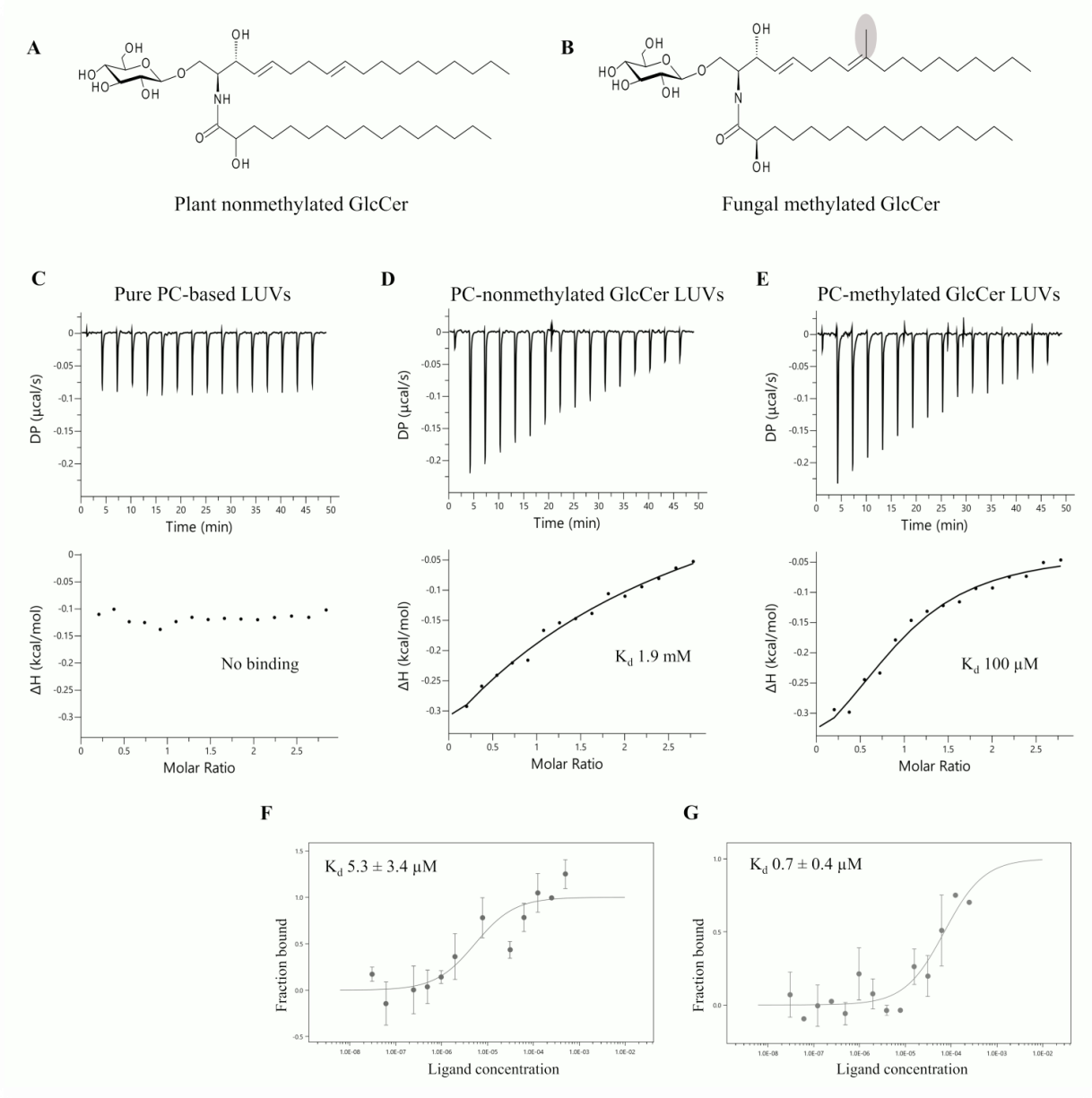

Figure 6 : Structures des glucosylcéramides, analyse thermodynamique (ITC) et thermophorétique (MST) de l'affinité de liaison de l'ETD151 avec différentes compositions de larges vésicules uni lamellaires (LUVs) dans un tampon phosphate (10 mM, pH 5,8). K_d est la constante de dissociation du complexe ETD151-LUVs. (A-B) Structures chimiques du GlcCer végétal (A) et du GlcCer fongique (B). (C-E) Titrages ITC d'une suspension de LUVs de 3,5 mM dans une solution de 250 µM d'ETD151. (En haut) Les thermogrammes ITC présentent la puissance différentielle (DP) en fonction du temps. (En bas) Les isothermes de liaison présentent l'enthalpie (ΔH) pour différents rapports molaires. Les résultats ITC présentés sont représentatifs des titrages en triple pour chaque condition. Courbes de liaison MST de l'ETD151 marqué par fluorescence (Atto647-ETD151) à (F) des LUVs PC contenant du GlcCer non méthylées et (G) des LUVs PC contenant du GlcCer méthylées. Les valeurs K_d estimées par les expériences de MST sont données comme moyenne de trois expériences indépendantes ± SD.

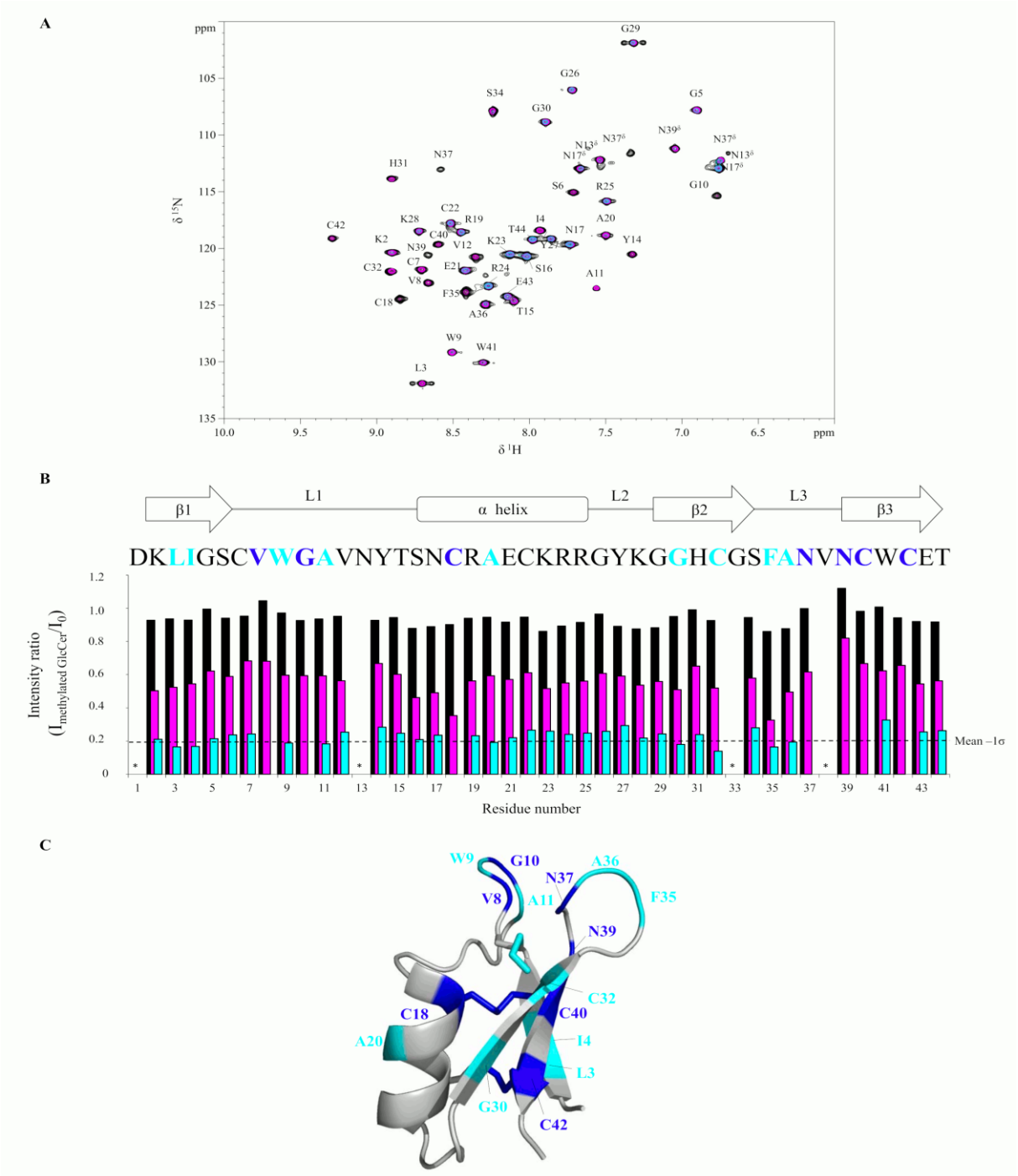

Figure 7 : Analyse RMN en solution de la structure du peptideETD151 en présence de LUVs PC contenant du GlcCer méthylé. (A) Spectres 2D SOFAST-HMQC superposés de ^{15}N -ETD151 (50 µM) en présence de LUVs PC contenant le GlcCer méthylés, à différents rapports molaires ETD151 : GlcCer méthylé : 10 :1 (noir), 1 :1 (rose) et 1 :10 (blue). (B) Rapports d'intensité des pics de ^{15}N-ETD151 (50 µM) en présence de LUVs PC contenant le GlcCer méthylés à différents rapports molaires ETD151 : GlcCer méthylées ; 10 :1 (noir), 1 :1 (rose) et 1 :10 (blue) par rapport à l'intensité I_0 du pic correspondant dans le spectre de référence (^{15}N-ETD151 à l'état libre à 50 µM). La numérotation des résidus du peptide ETD151 sont représentés sur l'axe des x. La ligne horizontale marque la moyenne du rapport d'intensité

en présence d'ETD151 : GlcCer méthylé au rapport molaire de 1 :10, moins un écart-type (-1σ). Les * indiquent les résidus pour lesquels les pics sont absents dans les états libre et lié du peptide ETD151. La séquence et les structures secondaire de ETD151 sont représentées, les flèches noires représentant les positions des β-brins et le rectangle noir représentant la position de l'hélice α. Les 3 boucles reliant ces éléments de structure secondaire sont numérotées L1, L2 et L3. (C) Structure 3D de ETD151 indiquant les acides aminés les plus perturbés, révélés dans la figure 7B (>-1σ), par l'ajout de PC : LUVs GlcCer méthylés. Les résidus dont l'intensité de pic diminue fortement sont indiqués en blue clair, et les résidus dont les pics ne sont pas visibles en raison d'un très fort élargissement et significatif de l'échange sont indiqués en blue foncé.

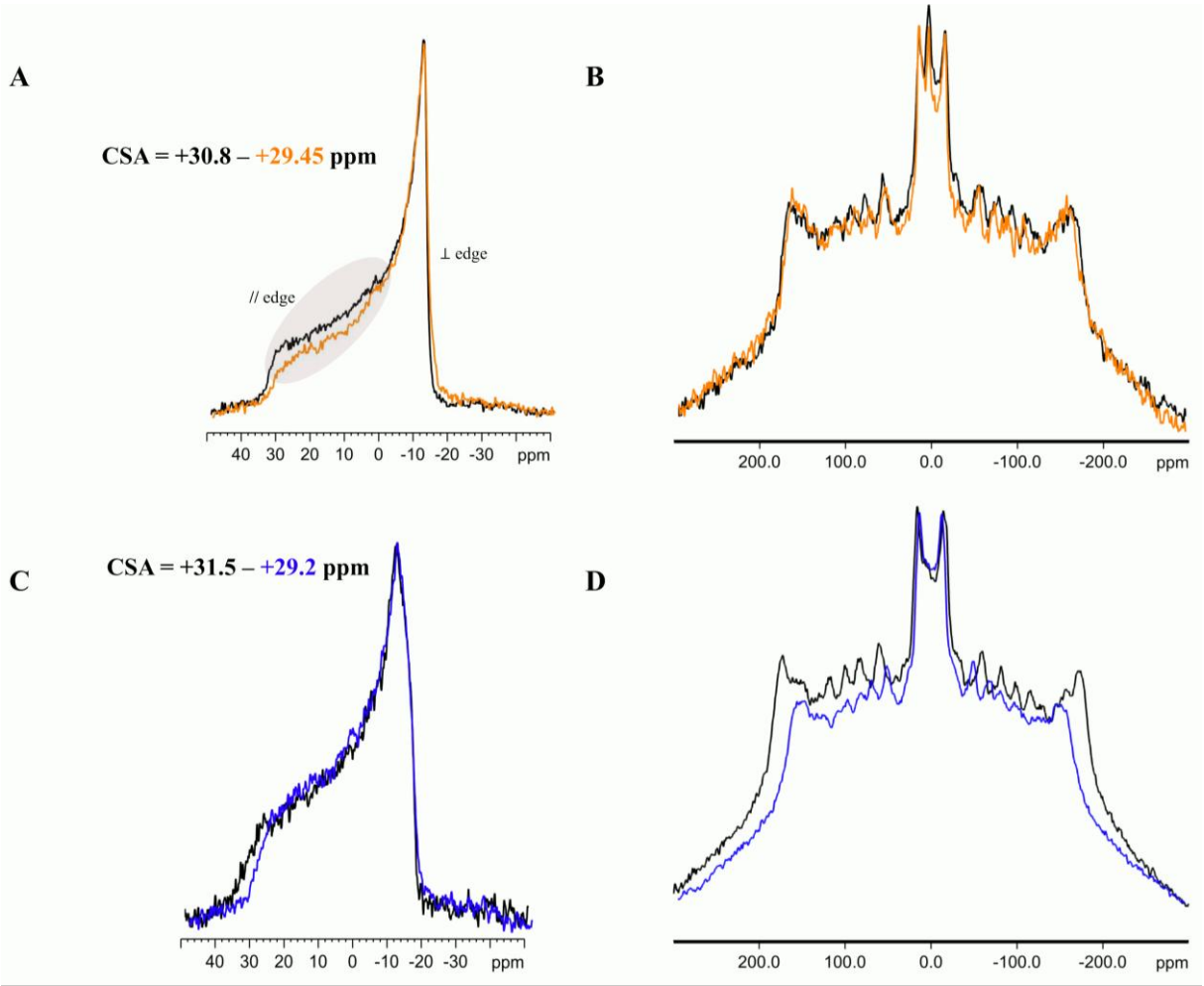

Figure 8 : Etude en RMN solide (ss-RMN) de l'impact du peptide ETD151 sur la dynamique des vésicules de PC contenant des GlcCer à un ratio peptide/lipide de 1 :20. (A) Spectres ^{31}P statiques et (B) spectres ^{2}H statiques des vésicules contenant des GlcCer non méthylés en l'absence (en noir) ou en présence (en orange) de l'ETD151. (C) Spectres ^{31}P statiques et (D) spectres ^{2}H statiques de vésicules contenant du GlcCer méthylé en l'absence (en noir) ou en présence (en bleu) d'ETD151. Les valeurs d'anisotropie du déplacement chimique (CSA) sont indiquées en ppm dans les figures 8A et 8C.

Partie II : AvBD103b, une trans-défensine antibactérienne prometteuse

La β-défensine aviaire AvBD103b a été isolée de l'estomac du manchot royal mâle. Elle y est fortement exprimée pendant la dernière partie de l'incubation de l'œuf. AvBD103b est active contre un large panel de bactéries Gram-positives et Gram-négatives, avec l'avantage de maintenir son activité en présence de sels (ce qui présente un intérêt notable par exemple pour traiter des infections chez des patients atteints de mucoviscidose) et sans présenter de toxicité. L'hypothèse actuelle est que son mécanisme est non-spécifique (pas d'existence d'une cible de forte affinité reconnue stéréo-spécifiquement) et multifonctionnel (cumul de plusieurs effets délétères pour la bactérie) ce qui le rendrait serait peu enclin au développement de résistance de la part des bactéries, mais ce mécanisme est loin d'être compris.

Cette deuxième partie comprend :

Le chapitre 4 : Introduction

Ce chapitre propose une revue bibliographique de la littérature sur les défensines aviaires, présentant leurs caractéristiques structurales, leurs activités biologiques antibactériennes, et les données disponibles concernant les MOAs antibactériens. Ce travail bibliographique sera complété et finalisé pour une valorisation sous la forme d'une revue.

Le chapitre 5 : Premiers éléments sur le mécanisme antibactérien de la défensine AvBD103b

Ce chapitre est consacré à l'étude en temps réel du mode d'action de la défensine AvBD103b sur les bactéries vivantes *Escherichia coli* par microscopie à fluorescence, en utilisant un dispositif microfluidique. Pour ce faire, nous avons d'abord transposé au laboratoire une technique innovante d'imagerie de fluorescence sur cellule unique qui permet de disséquer le mécanisme antibactérien de peptides antimicrobiens en temps réel, sur des bacteries *E. coli* vivantes, et dans des conditions physiologiques.

Mon objectif global dans cette partie de la thèse est de suivre la trajectoire en temps réel d'une version fluorescente du peptideAvBD103b sur des bactéries vivantes en utilisant l'imagerie de fluorescence sur cellule unique, méthode décrite ci-dessus (Figure 9). Pour y parvenir, les étapes suivantes ont été nécessaires : (i) transposer la méthode développée par J.C. Weisshaar (Madison, WI, USA) et l'adapter au microscope du CBM. Des peptides de contrôle, tels que la cathélicidine LL-37 et le peptide AvBD103b non marqués, sont utilisés pour fixer les premiers paramètres ; (ii) marquer chimiquement la défensine AvBD103b avec un groupe fluorescent et vérifier que ce marquage n'a pas d'impact sur l'activité ni sur le MOA du peptide AvBD103b; et (iii) réaliser des expériences préliminaires de microscopie de fluorescence avec le peptide AvBD103b fluorescent pour définir sa (ses) localisation(s) précise(s) et sa distribution spatiale tout au long du mécanisme. L'objectif est d'émettre des hypothèses

sur des partenaires moléculaires privilégiés qui pourraient entrer en interaction avec AvBD103b au cours du processus.

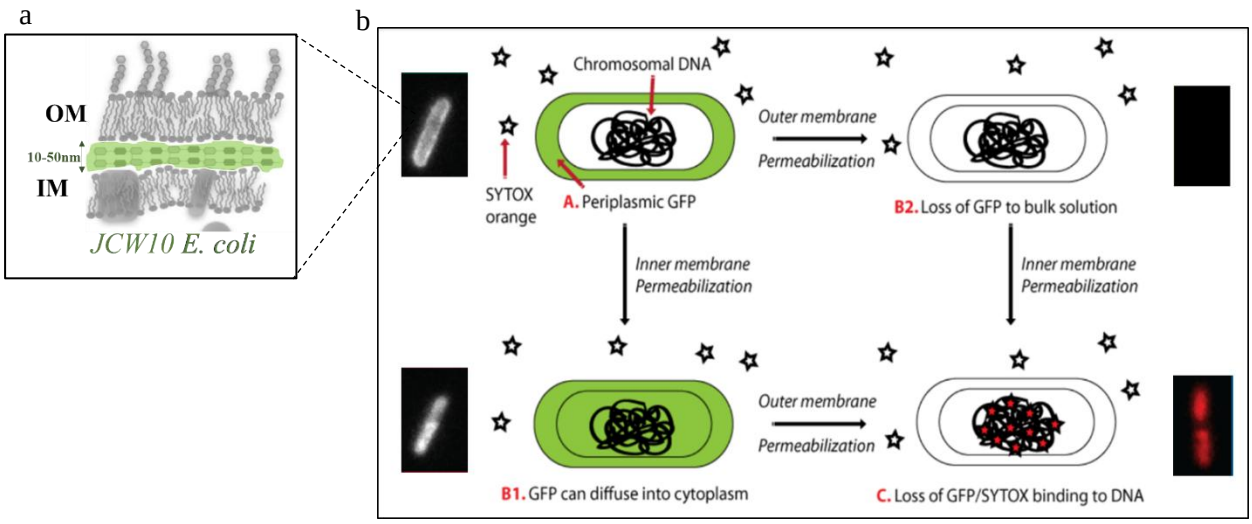

Figure 9 : Vue schématique de la perméabilisation de la membrane bactérienne suite à l'attaque des bactéries par le peptide antimicrobien (PAM), en utilisant la microscopie à fluorescence. (a) Souche *E. coli* JCW10 exprimant la protéine fluorescente verte (GFP) dans le périplasme, espace d'environ 10-50 nm d'épaisseur entre la membrane externe (MO) et la membrane cytoplasmique (CM) des bactéries. (b) *E. coli* JCW10 avec GFP périplasmique exposée à un milieu de croissance bactérien contenant le PAM et du Sytox, une sonde fluorescente liant l'ADN (A). Le PAM peut théoriquement affecter la perméabilisation de la membrane de deux manières : soit il perméabilise d'abord la MO, permettant à la GFP de se disperser dans la solution (B2), puis il perméabilise la CM, ce qui est rendu visible par la fluorescence du Sytox, qui devient fortement fluorescent lors de sa liaison à l'ADN (C) ; soit le PAM rompt d'abord la CM, permettant à la GFP périplasmique de diffuser dans le cytoplasme (B1), puis il perméabilise la MO, ce qui permet l'entrée du Sytox, sa liaison à l'ADN et sa fluorescence (C).

Le peptide a été marqué avec le groupement fluorescent Cyanine5 (Cy5-AvBD103b) pour permettre de suivre précisément sa distribution spatiale pendant son attaque bactérienne. Une stratégie sélective directe a été mise en œuvre pour marquer la Serine N-terminale (Figure 10). Malgré les deux étapes de la réaction de conjugaison, le rendement global était bon, autour de 50%. **Nous avons obtenu 7,5 mg de Cy5-AvBD103b avec une grande pureté, ce qui nous permet de réaliser toutes nos expériences facilement.** Comme la localisation cellulaire du peptide sera basée sur le signal de fluorescence du groupement greffé sur le peptide, un essai de concentration minimale inhibitrice (CMI) (Tableau 1) et une localisation cellulaire ont été réalisés pour vérifier que le groupement Cyanine5 ne modifiait pas l'activité du peptide, ni son mécanisme d'action.

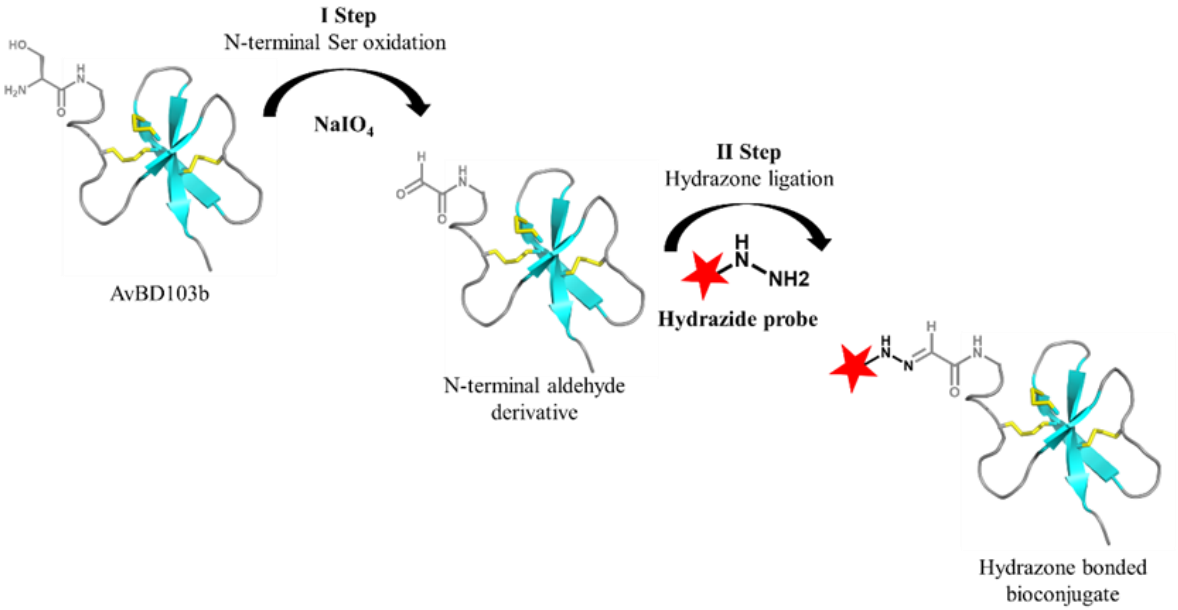

Figure 10 : Stratégie chimique suivie pour le marquage du peptide AvBD103b. La stratégie de bioconjugaison basée sur la réaction de ligation chimique de l'hydrazone conjuguant un dérivé aldéhyde N-terminal du peptide AvBD103b à une sonde moléculaire portant un groupe fonctionnel hydrazide, a permis d'obtenir le conjugué hydrazone-peptide de manière covalente.

Tableau 1 : Valeurs de MIC du peptide AvBD103b natif, de sa version fluorescente Cy5-AvBD103b, de la cathelicidine LL-37 utilisée comme contrôle positif et du peptide SERINENTER utilisé comme contrôle négatif, contre la souche *E. coli* JCW10 dans le milieu indiqué. MIC = concentration minimale inhibitrice qui inhibe la croissance de ≥ 90 % des cellules. Données présentées sous forme de moyennes d'expériences répétées trois fois.

		Bactérie : *E. coli* JCW10		
Milieu de culture		**Minimal M9 supp. 0.4% glucose** 303 mOsmoL, pH 7.2		
Peptides	**AvBD103b**	**LL-37**	**Cy5-AvBD103b**	**SERINENTER**
MIC µM	**4 µM**	**8 µM**	**4 µM**	**>64 µM**

Nous avons suivi en temps réel la localisation cellulaire de Cy5-AvBD103b et ses effets sur la perméabilisation des membranes externe (OM) et cytoplasmique (CM) des bactéries *E. coli* vivantes. Pour cela, nous avons réalisé une vidéo de 75 minutes en enregistrant toutes les 20 secondes des images de contraste de phase (suivi de la croissance bactérienne), de fluorescence GFP (suivi de la perméabilisation membranaire), de fluorescence Sytox Orange (suivi de la perméabilisation membranaire) et de la fluorescence de Cy5-AvBD103b (localisation du peptide). Toutes les expériences utilisant Cy5-AvBD103b ont été réalisées à 24 µM en présence de 50 nM Sytox Orange et ont été répétées plusieurs fois. La localisation de Cy5-AvBD103b en temps réel pendant l'attaque bactérienne,

simultanément avec l'effet de perméabilisation de la membrane, a montré 4 cas de figure possibles (Figure 11). **Nos résultats préliminaires ont montré que le peptide AvBD103b se localisait préférentiellement dans l'anneau Z, où se trouvent les protéines de division cellulaire, et dans la région septale, où la synthèse du peptidoglycane est active** (Figure 12). Tout au long de son attaque, le peptide AvBD103b reste principalement à la surface de la cellule. Cependant, une partie du peptide peut éventuellement atteindre le cytoplasme et ainsi de multiples partenaires moléculaires intracellulaires potentiels.

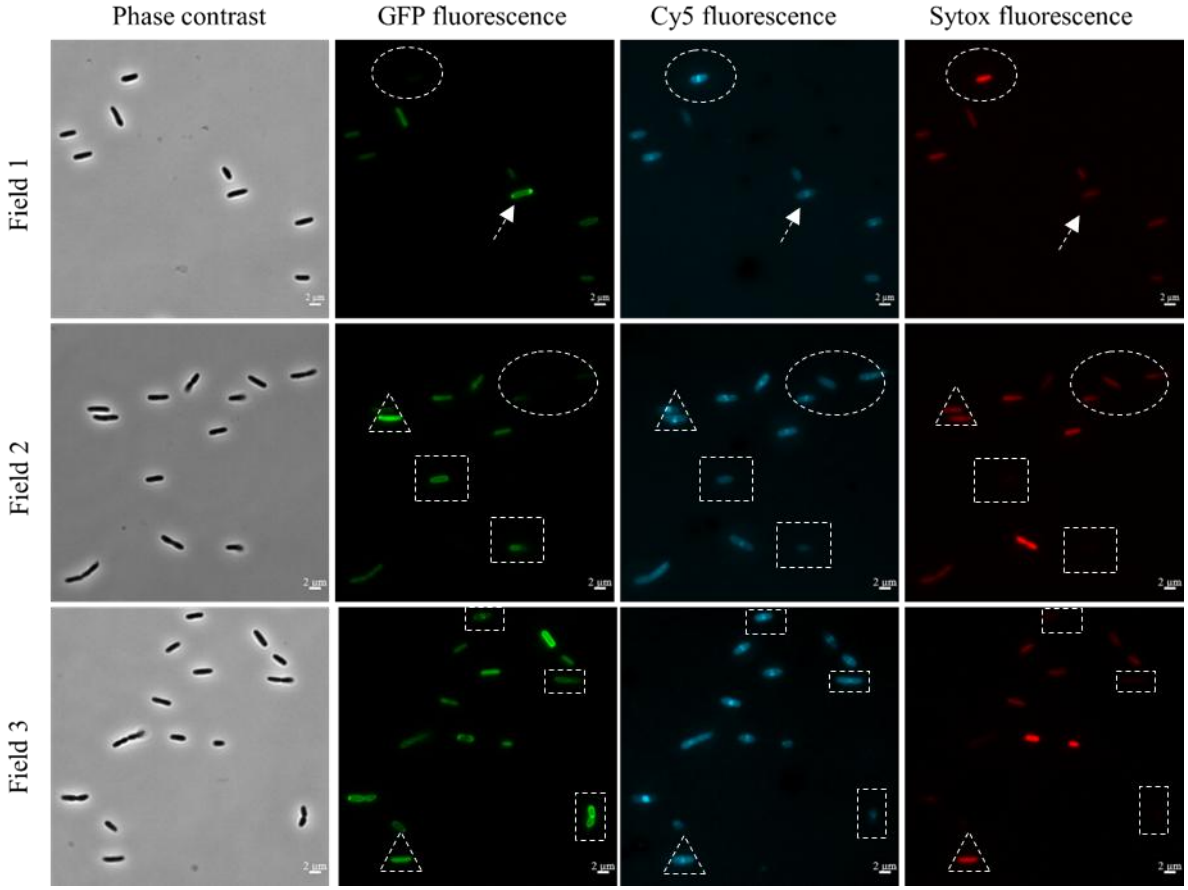

Figure 11 : Trois champs représentatifs des observations faites au microscope à champ large sur des bactéries exposées pendant ~ 120 min à un flux constant (0,2 mL/h) de 24 µM de Cy5-AvBD103b sous flux dans la chambre microfluidique. De gauche à droite, les images montrent le contraste de phase, la fluorescence verte GFP (488 nm), la fluorescence de Cy5-AvBD103b (650 nm) et la fluorescence du Sytox Orange (548 nm). Les rectangles blancs indiquent les bactéries dont la fluorescence GFP est localisée dans le périplasme, faiblement marquées par le peptide Cy5-AvBD103b et non marquées par le Sytox. Les flèches blanches indiquent des bactéries avec un marquage Cy5-AvBD103b important, une faible fluorescence Sytox et une fluorescence GFP périplasmique. Les triangles blancs montrent des bactéries marquées avec Cy5-AvBD103b, avec une forte intensité de fluorescence Sytox et une partie de la GFP entrée dans le cytoplasme de la bactérie. Les cercles blancs

montrent des bactéries marquées avec le peptide Cy5-AvBD103b, avec une fluorescence Sytox et une disparition totale de la fluorescence du signal GFP.

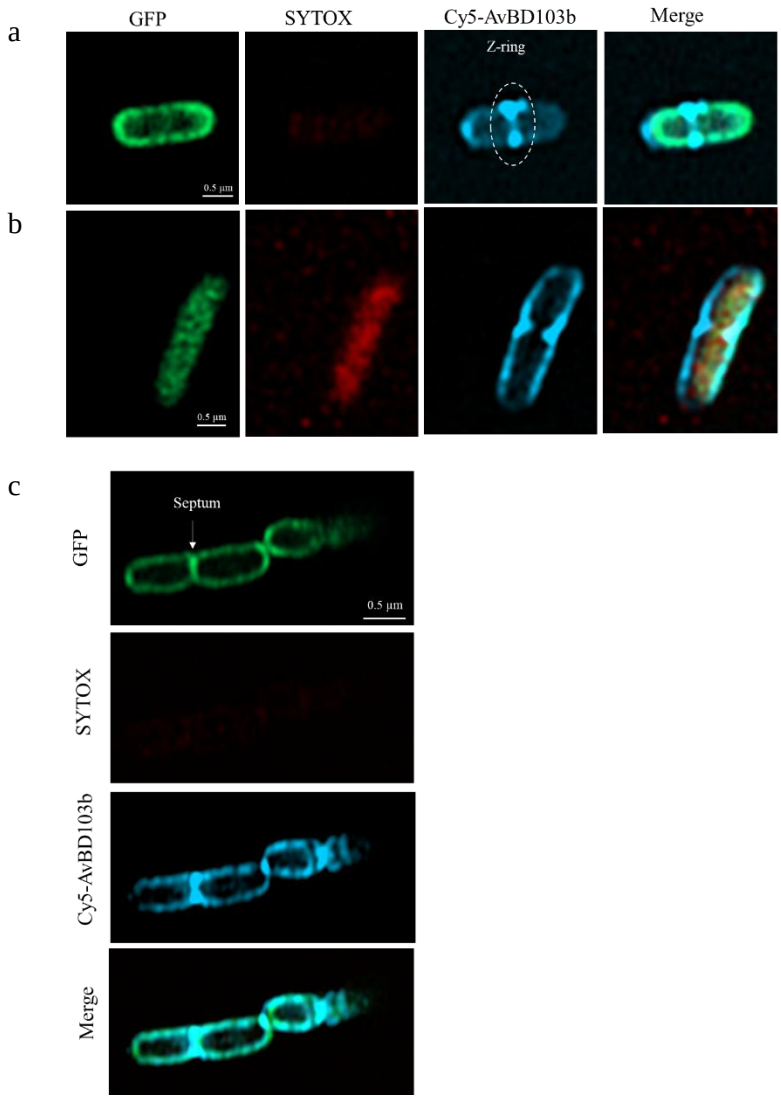

Figure 12 : Images de microscopie confocale illustrant les différentes possibilités de localisation du peptide, avec des effets de perméabilisation des membranes. (a) Cellule non-septante avec GFP périplasmique, fluorescence Sytox très faible et fluorescence Cy5 localisée au niveau des membranes, avec une intensité élevée dans l'anneau Z. (b) Cellule non septante avec GFP cytoplasmique, Sytox se liant à l'ADN et Cy5-AvBD103b se liant aux membranes des bactéries. (c) Cellule septante avec GFP périplasmique, sans fluorescence Sytox et avec la fluorescence Cy5 localisée au niveau des membranes, avec une intensité élevée dans la région septale.

Ce travail de thèse utilisant la technique innovante de microscopie de fluorescence sur cellule unique, en temps réel et en conditions physiologiques, nous a permis de fournir de nouveaux éléments sur le

mécanisme d'action, en particulier la distribution spatiale directe du peptide lors de son attaque de la bactérie. Cela ouvrira la voie à l'exploration des partenaires moléculaires potentiels et/ou des processus cellulaires impliqués dans le mécanisme antibactérien du peptideAvBD103b. **Cette compréhension est essentielle pour explorer le potentiel de la défensineAvBD103b en tant que candidat pour la conception d'une nouvelle génération de molécules antibactériennes.**

General Introduction

Antimicrobials—antibiotics, antivirals, antifungals, and antiparasitics—are substances widely used to prevent and treat infections in humans, animals, and plants. Unfortunately, their effectiveness is now in jeopardy because a number of antimicrobial treatments that used to work no longer do, as microorganisms have become resistant to them. **Antimicrobial resistance (AMR)** is when bacteria, viruses, parasites, or fungi no longer respond to antimicrobial medicines to which they were previously susceptible. More seriously, some bacterial strains develop resistance to several types of antibiotics, causing hard-to-treat infections and are referred to as "superbugs." Increased use and misuse of antimicrobials, coupled with the limited number of the newly developed drugs, are the main drives behind the emergence of drug-resistant pathogens.

Today, AMR appears in the top 10 of the threats list for global health established by the World Health Organization (WHO). It threatens the health and well-being of humans and animals, increasing the risk of disease spread and leading to adverse consequences, disabilities, and deaths. Moreover, infectious plant diseases are becoming difficult, if not impossible, to treat, thereby reducing the productivity of farms and threatening food and nutritional security. It is estimated that AMR was directly responsible for 1.27 million global deaths in 2019 and contributed to 4.95 million deaths. Today, the global mortality rate from AMR exceeds that of malaria or breast cancer and is comparable to that of tuberculosis and HIV. In addition, AMR has significant economic costs in public health and in agriculture, resulting in US$ 1 trillion to US$ 3.4 trillion in gross domestic product (GDP) losses per year by 2030 (WHO, 2023).

To avoid a global collapse in our ability to control drug-resistant pathogens and to avoid critical failures in medicine and food safety, we need to improve our management of drug use, promote the discovery of new drugs, and find alternative solutions to the antimicrobial drugs commonly used. Among the promising alternatives to AMR, there are **antimicrobial peptides (AMPs)** known as host defense peptides (HDPs). AMPs are part of the innate immune system of vertebrates, invertebrates, and plants, known for their broad antimicrobial spectrum as well as immune regulatory activities. Structurally, AMPs are diverse, including disulfide-rich peptide superfamily known as "**defensins**".

Defensins are highly structured antimicrobial peptides (AMP), with characteristic β-sheet rich folds and well-defined frameworks of disulfide-linked cysteines. They are generally cationic, with a high level of hydrophobic residues, <10 kDa, and are expressed by a wide array of animals, plants, and fungi as essential components of their host defense system. Note that the term "defensin" covers at least two phylogenetically independent disulfide-rich peptide (DRP) superfamilies of AMPs: **cis-defensins and trans-defensins** (Figure 1) [1]. Defensins contain at least six conserved cysteine residues involved in 3 disulfide bridges.

The **cis super-family** is widely distributed across fungi, plants and the majority of invertebrates, including insects. The **trans super-family** has arisen and evolved exclusively in animals.

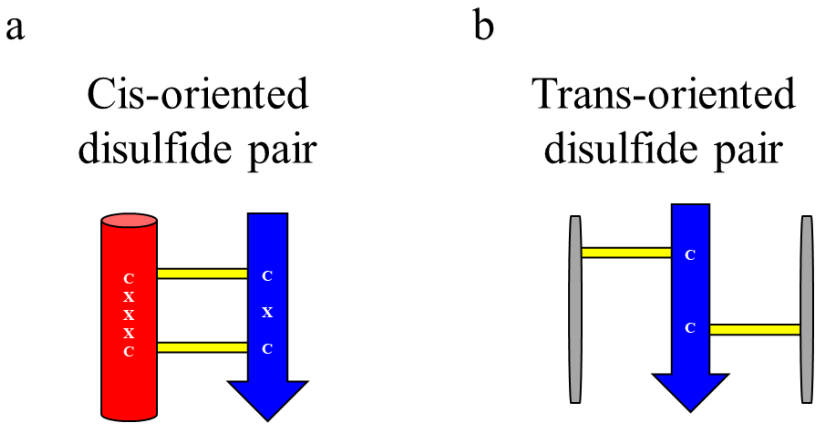

Figure 1: The two super-families of defensins. (a) **Cis-defensins** where the conserved CXC motif in the β-sheet naturally orients the corresponding disulfide bridges in the same direction. (b) **Trans-defensins** where the conserved vicinal cysteines (CC motif) in the β-sheet automatically orients the corresponding disulfides bridges in opposite directions. The blue arrow indicates a β-sheet, the red cylinder indicates an α-helix, the yellow lines indicate disulfide bridges, the gray lines indicate a structured or unstructured part, C for cysteine and X for any amino acid.

Although their antimicrobial activities and their structural characteristics have been extensively reported, their mechanisms of action (MOAs) are less well-understood, especially with evidence now that they have a wide variety of MOAs optimized over millions of years in nature. Indeed, for a long time, it was believed that the MOAs of all cationic AMPs were primarily based on membrane permeabilization due to their electrostatic attraction to negatively charged microbial membranes. This is because linear, unstructured lytic AMPs have been the most studied. Over the last ten years, real evidence has shown that the mode of action of AMPs, particularly with complex structures such as defensins, is more complicated than membrane permeabilization, and therefore needs to be explored.

To rationally generate highly effective molecules from AMPs for therapeutic application, the first crucial step is to understand at the molecular/atomic scale how they act in nature. This will provide important information on their potential therapeutic applications.

My PhD project is focused on deciphering the MOAs of two promising defensins, a Cis-defensin namely ETD151, a 44-residue antifungal peptide optimized from insect defensins (Part I, Figure 2a), and a Trans-defensin AvBD103b a 38-residue antimicrobial peptide from the king penguin for its antibacterial activity (Part II, Figure 2b).

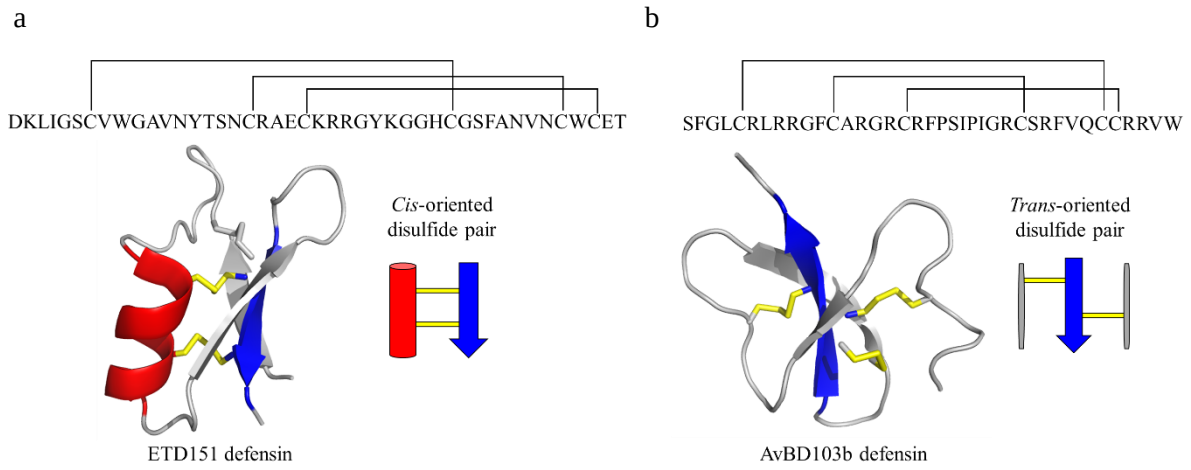

Figure 2: Sequences and 3D structures of defensins of interest in this thesis. (a) The **insect-derived defensin ETD151** (PDB code: 1P00). (b) The **avian defensin AvBD103b** (PDB code: 1UT3). Disulfide bridges are shown in black brackets for sequences and in yellow for structures.

Part I: ETD151 a promising antifungal cis-defensin

The defensin ETD151 is highly active against human and plant pathogenic fungi without toxicity. The name ETD151 stands for EntoMed peptide number 151. Indeed, the ETD151 peptide has been optimized by the former French biotechnology company EntoMed SA during its lead optimisation of the defensin Heliomicin, isolated from *Heliothis virescens*. Its multifaceted MOA requires the presence of glucosylceramides (GlcCers), fungal membrane lipids that are determinants of cell growth and virulence in fungi, and are therefore considered promising targets. Targeting fungal GlcCer is unlikely to quickly induce resistance, which makes ETD151 one of promising candidates to be a solution against resistant-fungal strains. However, its antifungal MOA - particularly its membrane target and the molecular by which it interacts with this target - remain to be elucidated. **The first part** includes:

Chapter 1 presents a **bibliographic introduction** about the **antifungal resistance** problem and the novel investigational agents to treat pathogenic fungi. A particular emphasis was put on presenting some **defensins from plants and insects** targeting a promising cellular target, which may provide therapeutic alternatives to existing treatment options.

Chapter 2 is devoted to study the first step of the MOA of ETD151 against a phytopathogenic fungus *Botrytis cinerea* by **identifying its cellular membrane target** and **investigating to which extent the presence of this putative target in microbial membrane may dictate the antimicrobial activity of ETD151**. This chapter essentially includes an article that is under revision in *Proceedings of the National Academy of Sciences* (PNAS): Ons Kharrat *et al*. 2024 intitled "**The antimicrobial activity of ETD151 defensin is dictated by the presence of glycosphingolipids in the targeted organisms**".

Chapter 3 focuses on the study of the **direct *in vitro* interaction**, at **molecular and atomic level**, between **ETD151** and its fungal **membrane target**, identified in chapter 2. **Biochemical and**

biophysical assays were used to the comprehension of some key elements of this defensin-target interaction, which is required for the antifungal activity of several defensins. Also, the implication of specific features of target structure in this interaction has been investigated. This chapter is essentially based on a manuscript that will be submitted in *Journal of Biological Chemistry* (JBC): Ons Kharrat *et al.* 2024 and intitled "**ETD151 defensin targets fungal methylated glucosylceramides**".

This **first part** ends with a **conclusion and perspectives** summarizing the main findings, conclusions and outlook.

Part II: AvBD103b a promising antibacterial trans-defensins

The **avian β-defensin** AvBD103b has been isolated from the stomach of the king penguin male and is highly expressed during the last part of egg incubation. AvBD103b is active against a wide panel of Gram-positive and Gram-negative bacteria, with the advantage of being salt-insensitive, and without toxicity. Its antibacterial MOA, supposed to be non-specific and multifaceted, preventing bacteria from developing a resistance mechanism is not fully understood. This **second part** includes:

Chapter 4 provides a **bibliographic review** of the literature on **avian defensins**, presenting their structural characteristics, **antibacterial** biological activities, and what we know up to date about their **antibacterial** MOA. This bibliographical work will be the subject of a review to be completed and submitted.

Chapter 5 is dedicated to study the **MOA in real time** of **AvBD103b** on *Escherichia coli* **living bacteria** in **microfluidic device** using **fluorescence microscopy**. To achieve this, we first implemented an innovative single-cell fluorescence imaging technique that allows to dissect the antibacterial mechanism of AMPs in real time, on living *E. coli*, and in physiological conditions. The aim here is to label the peptide and monitor precisely its spatial distribution during its bacterial attack.

This second part will end with a conclusion and perspectives summarizing the main findings, conclusions and the envisaged perspectives.

Note: For ease of reading, the numbering of figures, tables and bibliographical references is independent of each chapter.

References

[1] T. M. A. Shafee, F. T. Lay, M. D. Hulett, et M. A. Anderson, « The Defensins Consist of Two Independent, Convergent Protein Superfamilies », *Mol Biol Evol*, vol. 33, nº 9, p. 2345-2356, sept. 2016, doi: 10.1093/molbev/msw106.

Part I.

ETD151 a promising antifungal cis-defensin

Chapter 1: Introduction

Table of contents

I. Fungal infections and current antifungal agents

1. Fungal infections

Annually, fungal pathogens infect billions of people and cause at least 1.5 million deaths [1, 2]. This high global mortality rate caused by fungal infections exceeds that of malaria and breast cancer and is comparable to that of tuberculosis, one of the top global killers in 2016 according to the World Health Organization (WHO). The elderly, immunocompromised patients (Human immunodeficiency virus (HIV)/ acquired immunodeficiency syndrome (AIDS) sufferers) or patients receiving cancer therapy are the most susceptible to systemic fungal infections.

Fungal diseases have historically been underestimated and neglected in disease research. In view of this alarming situation, in 2022 the World Health Organization (WHO) drew up -for the first time - a priority list of 19 pathogenic fungi, classified into three groups: critical group, high group and medium group (Figure 1), on the basis of several criteria such as resistance to antifungal agents, annual incidence, access to diagnosis, complications and sequelae [3].

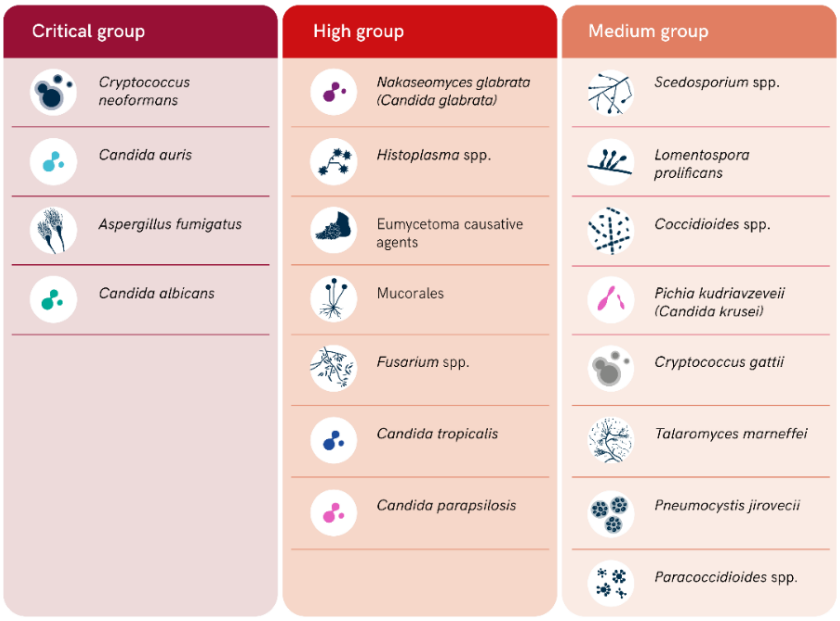

Figure 1: First fungal priority pathogens list established by the WHO in 2022 (adapted from ref [3])

Fungal pathogens are transmitted to human predominantly by direct contact (e.g. dermatophytic fungi can cause superficial skin infections) and/or inhalation of spores/conidia causing pulmonary and systemic infections (e.g. Aspergillosis is caused by inhaling *Aspergillus fumigatus* and *A. flavus* spores, Cryptococcosis is caused by inhaling *C. neoformans* and *C. gattii* spores). Besides, organisms such as

Candida spp. are commensals of the mammalian microbiome and are normally harmless but can become opportunistic pathogens for some immunocompromised individuals. Table 1 lists a number of human diseases caused by fungi, and the burden they represent [4].

The main causative agents of systemic fungal infections are *Cryptococcus, Candida* and *Aspergillus* species. Cryptococcal infections take the lives of approximately 112,000 people every year. Invasive candidiasis can cause life-threatening infections for immunocompromised patients with mortality rates exceeding 40% even with treatment. Invasive aspergillosis causes severe diseases in people with weakened immune systems, with a mortality rate of 50% despite appropriate care. In France, invasive aspergillosis is the third leading cause of invasive fungal infection according to Institut Pasteur, Paris [5].

Table 1: Main human pathogenic fungi associated diseases and symptoms. Data obtained from ref [4]

Fungal pathogens	Diseases	symptoms	Burden
Aspergillus fumigatus, Aspergillus flavus	Aspergillosis	-Lung infection or invasive aspergillosis: fever, cough, thoracic pain, hemoptysis and breathing difficulties.	-Allergic bronchopulmonary, ~4.8 million global burden -Chronic pulmonary, ~3 million global burden; -Invasive, >300,000 annually;
Crytococcus neoformans, Cryptococcus gattii	Cryptococcosis	-Infection can be localized to the lungs or skin lesions or disseminated, with the most common clinical form of cryptococcosis is meningoencephalitis.	-Infection touch ~223,000 annually, -Meningoencephalitis represents more than 60% of cases, and in more than 80% of cases in patients with HIV.
Candida albicans, Candida glabrata, Candida auris	Candidiasis	-Localized candidiasis (Oral cavity, vaginal mucosa or esophagus). -Systemic candidiasis may result from nosocomial infections.	-Invasive, ~750,000 annually; -Oral, ~2 million annually; -Esophageal, ~1.3 million annually; -Vulvovaginal, ~134 million global burden -Mortality is still approximately 40% and has not fallen despite therapeutic and diagnostic breakthroughs.
Fusarium solani, Fusarium oxysporum	Fusariosis	-Localized skin infection, mycetoma, or pneumonia.	~Hundreds
Histoplasma capsulatum	Histoplasmosis	-Shortness of breath, possible signs of respiratory failure.	-Infections, ~500,000 annually; -Disseminated, ~100,000 annually;

As well as threatening human health, fungi are among the dominant causal agents of plant diseases affecting agricultural crops, leading to a drop-in quality and yield, thus jeopardizing food security. In fact, crop-destroying fungi are responsible for perennial yield losses of around 20% worldwide, plus a further 10% in post-harvest losses. Losses due to fungal diseases affecting wheat, rice, corn, potatoes and soybeans have been estimated at the equivalent of the food needed to feed 600 million people for a year [6]. Table 2 summarizes some of the most economically threat phytopathogenic fungi [7],the

associated diseases and their impact on agricultural crop losses [8]. Fungi use two main strategies to infect plants and are classified as necrotrophs or biotrophs. The first class, necrotrophs (e.g. *Botrytis cinerea*), kill their hosts by secreting toxins and feed on dead tissues. The second class, biotrophs (e.g. *Puccinia* spp), colonize the living tissues of their hosts using effector molecules that suppress plant cell death and manipulate plant metabolism in favor of the pathogen [9, 10].

Table 2: Main phytopathogenic fungi, associated plant diseases and impacts on crop losses. Data obtained from ref [7].

Fungal pathogens	Main affected crops	Diseases	Crop loss (%)
Magnaporthe oryzae	Rice	Rice blast	Up to 35% harvest losses
Botrytis cinerea	Fruits and ornamental flowers	Gray mold	Up to 30% to 40% loss of strawberries
Puccinia spp.	Soybean	Rust	Up to 70% loss
Fusarium graminearum	Cereals	Fusarium head blight, Fusarium ear blight	In China, 5-10% loss. In Europe and South America, up to 50-60% and 70% of loss
Fusarium spp.	potato	Dry rot tubers	Crop losses of up to 25%. During storage, >60% of tubers can be infected

2. Conventional antifungal drugs

In the clinic

Despite the profound impact of pathogenic fungi on human health, the antifungal drugs currently available used in clinical practices for superficial and systemic infections are limited to only five frontline classes of drugs, namely azoles, polyenes, allylamines, echinocandins, and pyrimidines analogs. These antifungal agents usually targeted ergosterol biosynthesis pathway, fungal cell wall or fungal DNA/RNA (Figure 2). Based on their cellular targets, they can be classified into three categories: ergosterol inhibitors (azoles, polyenes and allylamines), glucan synthase inhibitors (echinocandins) and antimetabolites (pyrimidine analogs). Representative structures of one molecule in each class are shown in Figure 3.

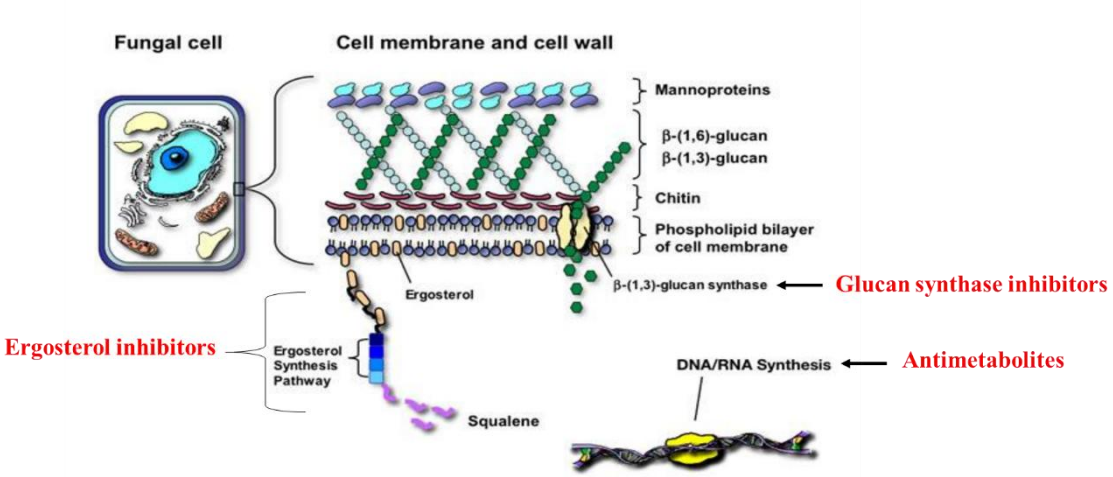

Figure 2: Schematic representation of the composition of the cell wall and plasma membrane in fungal cells (adapted from reference [11]) and the main three classes of antifungal agents (in red). The cell wall is composed of glucans (50-60% dry weight), chitin (1-20% dry weight) and glycoproteins (20-50% dry weight). The plasma membrane is mainly composed of three classes of lipids: phospholipids, sphingolipids and ergosterol.

(i) The azoles (e.g. fluconazole, Figure 3-1), are the most widely used class of fungicides in the clinic for systemic fungal infections because of their higher solubility in mammalian body fluids. The azoles inhibit 14α-demethylase, which converts lanesterol to ergosterol, and thus causes the accumulation of toxic intermediates. Unfortunately, the azoles inhibit mammalian cytochrome P450, leading to the disruption of the metabolism of other drugs.

(ii) The polyenes (e.g. amphotericin B, Figure 3-2), are the oldest antifungals drugs used to treat invasive fungal infections with a broad-spectrum activity. The polyenes target the cell membrane by binding to ergosterol, the most abundant sterol in fungal membranes, resulting in permeabilization and destabilization of the cell membrane. Although the polyenes bind preferentially to ergosterol rather than cholesterol, unfortunately, their low affinity to cholesterol on the host membranes cause high toxicity [12], disfavoring their clinical use.

(iii) Allylamines (e.g. terbinafine, Figure 3-3) inhibit ergosterol biosynthesis by targeting squalene epoxidase, a key enzyme in fungal sterol biosynthesis, which converts squalene to lanosterol. This results in a deficiency in ergosterol, regulator of membrane fluidity, and therefore an increasing of membrane permeability and leakage of cellular components, ultimately leading to fungal cell death. The clinical application of this class is mainly limited to the control of superficial dermatophytoses.

(iv) The echinocandins (e.g. caspofungin, Figure 3-4) are the newest class of antifungals with a unique mechanism of action, targeting the cell wall by inhibiting β-1,3-glucan synthase, a key enzyme for cell wall integrity. β-1,3-glucan, a branched matrix of polysaccharides,

present in fungi but not in higher eukaryotes such as mammals. While they have milder side effects compared to azoles, echinocandins have a narrow spectrum of activity and lack of oral formulations. They are recommended as primary therapy for invasive candidiasis.

(v) Finally, pyrimidines analogs (e.g. 5-fluorocytosine (5-FC), Figure 3-5) are synthetic analogues of the nucleotide cytosine (5-FU). Cytidine deaminase transforms the pyrimidine analogue 5-FC into 5-FU, which is then incorporated into DNA and RNA during their synthesis and suppresses cellular activity by either preventing protein synthesis or preventing DNA replication. Pyrimidines analogs are mainly used for the infections caused by fungal strains such as *candida albicans* and *cryptococcus neoformans*. However, they are not active against filamentous fungi lacking thymidylate synthase, which limits their therapeutic use.

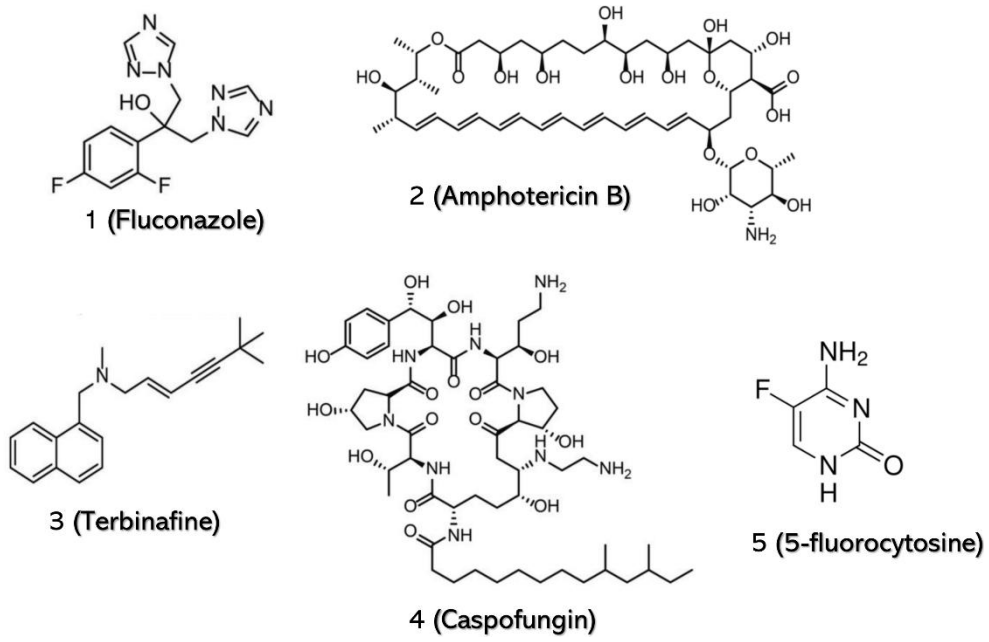

Figure 3: Structures of presentative molecules of each class of current antifungal agents. (1) Azoles are a class of heterocyclic compounds containing a nitrogen atom and at least one other non-carbon atom as part of the ring. (2) Polyenes are actinomycetes-derived unsaturated macrolactones. (3) Allylamines (4). Echinocandins are semi-synthetic amphiphilic lipopeptides composed of a cyclic hexapeptide core with different lipid side chains. (5) Pyrimidine analogs are the synthetic structural analogs of nucleotide cytosine.

Unfortunately, these antifungals had numerous drawbacks or limitations in their therapeutic use, including host toxicity, unfavorable pharmacokinetics, lack of oral formulations and limited spectrum of activity [13]. For example, azoles disrupt the metabolism of other drugs by inhibiting mammalian cytochrome P450; polyenes are highly toxic, causing nephrotoxicity and hepatotoxicity in particular;

pyrimidine analogues have a limited spectrum; and, finally, echinocandins have no oral formulations and must be administered intravenously daily, which is problematic in the event of prolonged treatment.

It is therefore necessary to develop a new antifungal agent to overcome these limitations and treat invasive fungal infections. However, due to the close evolutionary relationship between fungi and humans, drug development in the clinic is slow and limited.

In the field

In agriculture, historically, **multi-site fungicides** targeting a range of cellular processes in fungi were developed between the 1940s and 1970s. But the vast majority (90%) of fungicides developed since the 1960s have a supposed **single-site action**, i.e. they only act on a single site and disrupt a particular cellular process. Today, there are around nine times as many antifungal compounds available to combat fungal diseases of plants as there are to treat systemic fungal infections in humans. The six main classes of fungicides for crop diseases target mitochondrial function (succinate dehydrogenase inhibitors (SDHIs), anilinopyrimidines (AP) and strobilurins (QoIs)), the cytoskeleton (benzimidazoles (MBCs)) or ergosterol biosynthesis (azoles and morpholines) (Figure 4) [8]. SDHIs inhibit the electron transfer chain of mitochondrial respiration, by binding to the ubiquinone-binding site in the complex II of mitochondria. AP target mitochondrial signaling pathways through inhibition of methionine synthesis and secretion of hydrolytic enzymes. AP could be toxic by inhalation. QoIs target mitochondrial respiration by binding to the Qo site of complex III, blocking therefore fungal energy production. This class causes environmental contamination and non-target toxicity [14]. MBCs inhibit the assembly of microtubules by interfering with the cytoskeleton by binding to β-tubulin. Unfortunately, MBCs have high risk to induce resistance. Azoles inhibit 14α-demethylase, which converts lanesterol to ergosterol, and thus cause the accumulation of toxic intermediates. Morpholines inhibit two target sites within the ergosterol biosynthetic pathway, Δ14-reductase and Δ8-Δ7-isomerase. Their narrow spectrum of activity limited their use in fields.

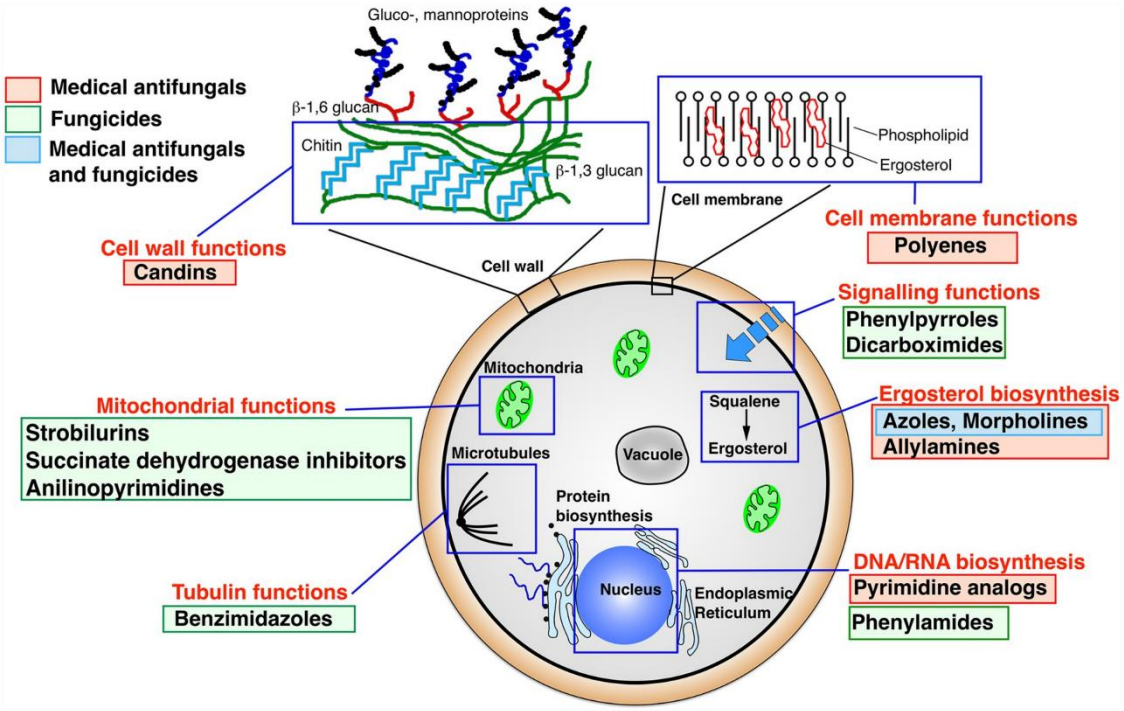

Figure 4: Cellular targets of principal antifungals used in medicine and in agriculture (adapted from ref [15]).

Modern agricultural practices rely on chemical-derived fungicides to control plant fungal diseases; however, they present potential risks to the environment and human health. They are a source of air, water and soil contamination, and their effects on human after oral consumption promote allergies, asthma and bronchopulmonary diseases. In addition, these pesticides can have adverse effects on crop physiology, such as altering photosynthesis, leading to reduced growth and yield of cultivated plants (for example, benzimidazoles and anilinopyrimidines are phytotoxic) [23]. Unfortunately, SDHIs binding is not specific to fungal SDH as they can also inhibit SDH activity in mitochondria of non-target organisms. Succinate dehydrogenase (SDH) is a universal mitochondrial enzymatic complex, its deficiency in human leads to neurological pathologies and cancer. The carcinogenic potential of mitotoxic fungicides (e.g. SDH inhibitors) has been shown in animals [24].

These synthetic fungicides are widely used by farmers, improving crop yields and quality, but leading to environmental contamination and risks to human health. In a One Health context, it is therefore necessary to develop alternatives to synthetic fungicides for agricultural applications.

II. Fungal resistance and alternatives to current antifungal agents

1. Fungal pathogenicity and resistance to host immune system

The pathogen recognition starts with complex interactions between the invading pathogen and the host's immune system, which plays a crucial role in detecting and eliminating fungal pathogens. Once fungal cells breach the host's physical barriers, they are recognized by pattern recognition receptors (PRRs) (e.g. Toll-like receptors (TLRs) and dectins) of the immune system through pathogen-associated molecular patterns (PAMPs) found in the fungal cell wall, include components like chitin and β-1,3-glucans. The pathogen recognition by PRRs triggers signal transduction pathways and initiates a host immune response including phagocytosis, the production of reactive oxygen and nitrogen species (ROS/RNS), the release of cytokines and chemokines, which stimulate a potent inflammatory reaction to neutralize the fungal pathogen. Fungi that survive this initial innate immune response, led by monocytes, macrophages, dendritic cells and neutrophils, encounter the adaptive immune system which helps in clearing and eliminating fungal infections.

Fungi have evolved numerous mechanisms to evade innate and adaptive immune responses. They can modulate their surface structures to conceal conserved PAMPs, preventing detection by PRRs. For example, a major surface glycoprotein that masks surface β-1,3-glucan and the cell wall is devoid of chitin [16], polysaccharides β-1,3-glucan exposed on the surface were cut by endo β-1,3-glucanase, resulting in reduced pathogen recognition and stimulation of pro-inflammatory reaction. Additionally, fungi undergo morphological adaptations and transitions during their life cycle, such as spore formation, filamentous growth, mycelial aggregation, formation of titan cells, asteroid bodies, that allow them to evade immune surveillance and adapt to varying environmental conditions, including changes in nutrient availability and interactions with the host. In addition to immune evasion, biofilm formation in fungi such as *Candida albicans*, *Aspergillus fumigatus*, and *Cryptococcus neoformans* enhances their ability to survive hostile environments and resist antifungal treatments. To further undermine host defenses, some fungi produce mycotoxins that damage host cells and disrupt critical cellular functions, resulting in tissue injury, inflammation, and immunosuppression. Fungal pathogens can also secrete immunomodulatory molecules to interfere with the host's immune processes [17].

2. Fungal resistance to drugs

Besides human and environmental toxicity of currently available antifungal agents, which is the main drawback of their application, these drugs are now faced with the emergence of (multi)-resistant fungal strains [18]. Indeed, the long-term use of a limited repertoire of antifungals in the clinic and the excessive and widespread use of fungicides in the field have led to the emergence of drug-resistant fungal pathogens to most of antifungal classes. Fungi develop several physiological adaptations, mutations in target genes followed by selection, sexual reproduction and horizontal gene transfer to escape the toxic

effect of antifungal agents. Fungal biofilm formation, in addition to its role in resistance to the host immune response as mentioned above, exhibits greater drug tolerance due to several factors (e.g. extracellular polymeric matrix of substances, slow growth rates, synergistic interactions in biofilm cells). The major resistance mechanisms are (i) increasing the drug efflux by upregulating multidrug transporters and (ii) target modification or overexpression which limits the efficacy of the drug [19]. Table 3 summarizes the main mechanisms of resistance developed against antifungal agents currently used in the clinic and in the field.

Table 3: The main classes of drugs used against plant fungal infections, their principal mechanism of action, their drawbacks and known mechanisms of resistance to them.

Antifungal class (representative molecule)	Mechanisms of resistance
Used for both plant and human fungal infections	
Azoles (fluconazole)	-Target site conformational changes (mutation in *cyp51or ERG11* gene) with low/no affinity to azoles -Target overexpression (*cyp51)* -Efflux pump (ABC transporters, MFS) overexpression
Used for human fungal infections	
Polyenes (amphotericin B)	-Regulation of stress response pathways -Mutations in *Erg1* gene encoding squalene epoxidase impair binding of drug -Mutations leading to loss of ERG3 function result in low ergosterol content
Pyrimidine analogs (flucytosine)	-Target overexpression -Efflux pump overexpression -Mutations in enzymes involved in the pyrimidine salvage pathways
Echinocandins (caspofungin)	- Regulation of stress response pathways -Target site conformational changes alter binding affinity to drug (FKS glucan synthase)
Used for plant fungal infections	
Succinate dehydrogenase inhibitors (SDHIs)	-Target site conformational changes (mutations in succinate dehydrogenase gene (*sdh)*) - Efflux pump overexpression
Anilinopyrimidines (AP)	- Efflux pump overexpression or modification of the target sites
Benzimidazoles (MBCs)	- Target site conformational changes (point mutation in β-tubulin gene)
Strobilurins (QoIs)	-Target site conformational changes (point mutations in the mitochondrial cytochrome b gene (*cyt b*))
Morpholines	-Unknown

The azoles are the most widely used due to their broad spectrum of activity and low cost. Unfortunately, the extensive use of the azoles in the field has promoted the emergence of azole-resistant phytopathogenic fungi, such as *B. cinerea, Penicillium digitatum,* and so on. Azole fungicide-resistance involves an amino acid substitution in codon 136 (Y136F) of *CYP51*, encoding gene of 14 α-demethylase enzyme (*CYP51*) and/or an increase in *CYP51* expression (e.g. *Uncinula necator* [20]). Moreover, it has been described the transmission of azole-resistant *A. fumigatus* from the field to the

clinic [21]. *Aspergillus* spp. strains develop resistance to azoles treatment in the field, they survive in the environment, soil and in food, producing airborne spores that can be inhaled by human [17, 21].

The resistance of *Candida* spp. and *Aspergillus* spp. to polyenes is due to reduced ergosterol content and the incorporation of modified sterols with low affinity for amphotericin B [23] . The majority of 5-FC resistance mechanisms occur due to mutations in crucial enzymes involved in the pyrimidine salvage pathways. The absence and/or alteration of any of the enzymes responsible for the activity of cytosine permease (*FCY2*), cytosine deaminase (*FCA1, FCY1*), or uracil phosphoribosyl transferase (*FUR1*) have been shown to cause resistance in *S. cerevisiae* and *C. albicans* to pyrimidine analogs [24, 25]. Resistance to echinocandin drugs remains relatively low, but some echinocandin-resistant *C. glabrata* isolates show cross-resistance to azole drugs [26], making the situation more dangerous. The target of echinocandins, β (1,3)-glucan synthase, is encoded by the *FKS1* and *FKS2* genes in *Candida* spp. Resistance to echinocandins in *Candida* spp. has been reported due to mutations in highly conserved "hot spot" regions of the *FKS*-encoded subunits of glucan synthase, resulting in decreased sensitivity of the enzyme to the drug. *FKS* mutations mainly occur in *FKS1* region encompassing residues F641-P649 and at position A1361 (*C. albicans* equivalent) [27].

The frequent application of single-site fungicides in agricultural production leads to selective pressure and the development of resistance in plant pathogens mainly by single-point mutation. Reduced susceptibility or field resistance to SDHI has been reported in over 20 fungal species, including economically important plant pathogens such as *B. cinerea*. Target site mutations in the Sdh subunits (mainly SdhB and SdhC) have been shown to confer reduced sensitivity to SDHIs in a fungal species. Specific mutations of amino acids P225, N230 and H272 in the SdhB of *B. cinerea* have been shown to be the cause of SDHI resistance [28]. Resistance to AP due to P319A or L412F mutations in *Pos5* gene were identified in *B. cinerea* isolates [29]. Fungi resistant to MBCs have been reported to carry point mutations in the β-tubulin gene at the codon 200 (F200Y) or 198 (E198A/K/V) (e.g. *B. cinerea* [30]). QoIs resistance is conferred by mainly G143A mutation in mitochondrial cytochrome b gene (*cytb*) of many plant pathogenic fungi (e.g. *Cercospora beticola* [31], *Botrytis cinerea* [32]).

The growing prevalence of antifungal-resistant infections along with the therapeutic limitations of the current limited antifungal agents emphasize the imminent need for researching new cellular fungal-specific targets allowing the development of drugs exerting effective antifungal activity and overcoming drug resistance.

3. Alternative treatment strategies

Several strategies have been proposed to combat the dramatical emergence of resistance, coupled with the limited number of newly developed antifungals. The relatively easiest strategy is to start from

existing drugs i) by optimizing traditional antifungal agents' properties and minimizing their side effects; ii) by repositioning the use of commercially drug; or iii) by combining different drugs for a synergistic effect. The second strategy is to develop new antifungal agents (small molecules similar to clinically available antifungal drugs) with new targets. Several new antifungal agents are currently in development, offering advantages over current drugs in terms of antifungal resistance and absence of adverse effects. Unfortunately, this strategy involves several years of research and is associated with extended timelines. The third strategy is to develop new biopharmaceuticals via immunotherapy to enhance patients' immune systems [33] or exploring antimicrobial peptides (AMPs).

a. Development of new agents from existing drugs

Optimization of current antifungal agents

We discuss new agents within existing antifungal classes with improved safety and tolerability profiles due to enhanced pharmacokinetic and pharmacodynamic properties (Figure 5)**.** One simple way to find a solution to treat invasive fungal infections is to optimize the available antifungal classes to overcome their limitations. Oteseconazole (VT-1161) is a tetrazole designed to increase the selectivity to fungal CYP51 rather than human cytochrome enzyme and thus fewer side effects compared to currently available azoles. It has over 2000-fold selectivity for fungal CYP51 over the human enzyme, potentially reducing drug interactions and toxicity. Oral oteseconazole is FDA-approved for treatment of acute vaginal candidiasis. Opelconazole (PC945) is the first inhaled triazole antifungal agent for the treatment of respiratory fungal infections. PC945 is a potent CYP51 inhibitor, designed to be administered by inhalation to achieve high local pulmonary concentrations and limited systemic exposure. It has a broad spectrum of activity even against azole-resistant *A. fumigatus* strains. Opelconazole is currently under clinical trials (phase 2: NCT05037851). Encochleated Amphotericin B (C-AmB) is a polyene with orally administration as lipid nanocrystal amphotericin B has been developed to overcome the significant toxicities (e.g. renal toxicity) of amphotericin B deoxycholate only intravenously administrated. This developed formulation, lipid nanocrystal amphotericin B, allows a target delivery of the drug, improving the efficacy and minimizing the toxicity compared with lipid formulation of AmB. Oral C-AmB is FDA-approved for treatment of vulvovaginal candidiasis (VVC). Rezafungin (CD 101) is an optimized echinocandin with improvement of pharmacokinetic properties (long half-life) allowing for weekly, rather than daily, dosing, which is the case of already this FDA-approved agent [34]. This IV dose spacing of the drug minimizes its hepatotoxicity. Actually, rezafungin is prescribed for acute moderate to severe VVC treatment. Certainly, these optimized drugs are less toxic than their parental drugs, however, they are not a solution for the drug resistance problem as they have the same cellular target and MOA.

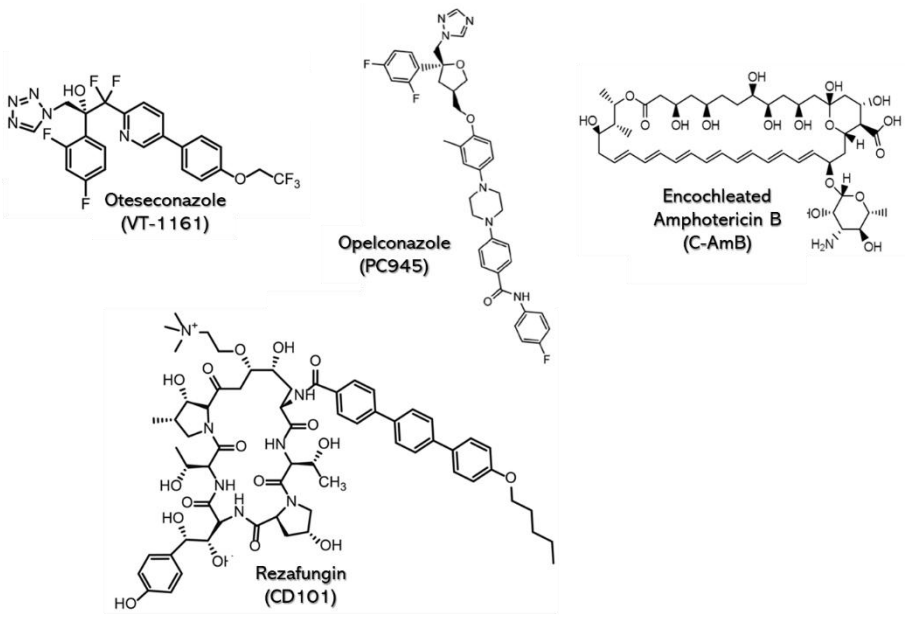

Figure 5: Structures of optimized antifungal agents newly approved by the FDA and/or under clinical trials.

Drug repositioning

Repurposed drug is an interesting alternative to achieve new strategies to treat fungal infections. This approach has allowed to identify potential antifungal activity of non-antifungal drugs [35]. For example, Atorvastatin, a drug for hyphercholesterolaemia treatment, used as an adjuvant with fluconazole, has shown anti-cryptococcal effect in mice infected by *C. gatti* [36]. Tamoxifen, anti-cancer drug, has shown an antifungal activity against pathogenic yeasts (e.g. *Candida* spp. and *C. neoformans*) [37].

Combination approach

Monotherapy is the most recommended to treat fungal infections; however, in some cases, it presents therapeutic failure due to drug bioavailability and resistance problems. Combination therapy could be an alternative to monotherapy for patients with invasive infections that are difficult to treat, such as those due to multi-resistant species and those who fail to respond to standard treatment. The synergistic activity of a combination therapy enhances the efficacy of drugs with different cellular targets or improves drug bioavailability [38]. The combination can be between two antifungal drugs, or between an antifungal drug and a non-antifungal agent. The combination of Amphotericin B and flucytosine has been the most frequently tested (as a combination between antifungals), and has previously been considered the standard treatment for cryptococcal meningitis [39]. The *in vitro* effect of azole drug combined with tobramycin analogues, displaying antifungal activities in addition to their antibacterial activities, has demonstrated to synergistically inhibit *C. albicans* strains growth [40].

b. Development of new small antifungal drugs

Apart from improving antifungals inhibiting the traditional cell targets, efforts have been made to seek new targets. We discuss three first-in-class members of three novel antifungal classes, GPI inhibitors, triterpenoids and orotomides [37, 38], which are under advanced clinical trials and that target, glycosyl-phosphatidylinositol (GPI), chitin synthase and pyrimidine synthesis, respectively (Figure 6) [43]. Table 4 summarizes antifungal agents currently in clinical trials and/or recently approved by the FDA, which optimize existing drugs or constitute a new class of antifungal agents.

Fosmanogepix is a first-in-class antifungal that targets the cell wall by blocking GPI production through inhibition of the fungal enzyme Gwt1. GPIs are important compounds for cell wall construction and maintenance of homeostasis. This new agent has a broad antifungal spectrum (*Candida* spp., *Cryptococcus* spp., *Aspergillus* spp., *Fusarium* spp.) and is active against highly resistant fungi. Phase 2 clinical trials (NCT04240886) have been completed for this drug.

Irexafungerp is the first of the triterpenoid antifungals, targeting the cell wall via inhibition of β-1,3-glucan synthase. Importantly, it has an activity against resistant *Candida* species. Its structure and mechanism of action are similar to those of the echinocandins, with slightly different binding sites. Of the three echinocandins currently available, none is available orally. Ibrexafungerp is therefore the first in a new class of oral glucan synthase inhibitors. Ibrexafungerp is FDA-approved for the treatment of vulvovaginal candidiasis.

Olorofim is the first in a new class of antifungal agents known as orotomides, which target nucleic acid metabolism. Olorofim shows activity against highly resistant molds. This compound inhibits pyrimidine biosynthesis by inhibiting the enzyme dihydroorotate dehydrogenase. Olorofim is currently in phase 2 clinical trials (NCT03583164).

Recently, a compound called **T-2307**, belonging to a new class of arylamidines, has already started clinical trials. However, no data is available on the progress of trials. It has a broad spectrum of activity, with the advantage of being active against echinocandin-resistant *C. glabrata*. T-2307 targets mitochondria, collapsing its membrane potential. In vitro studies showed that T-2307 was more selective in inhibiting fungal mitochondrial function than that observed against rat and bovine mitochondria [39, 40].

a

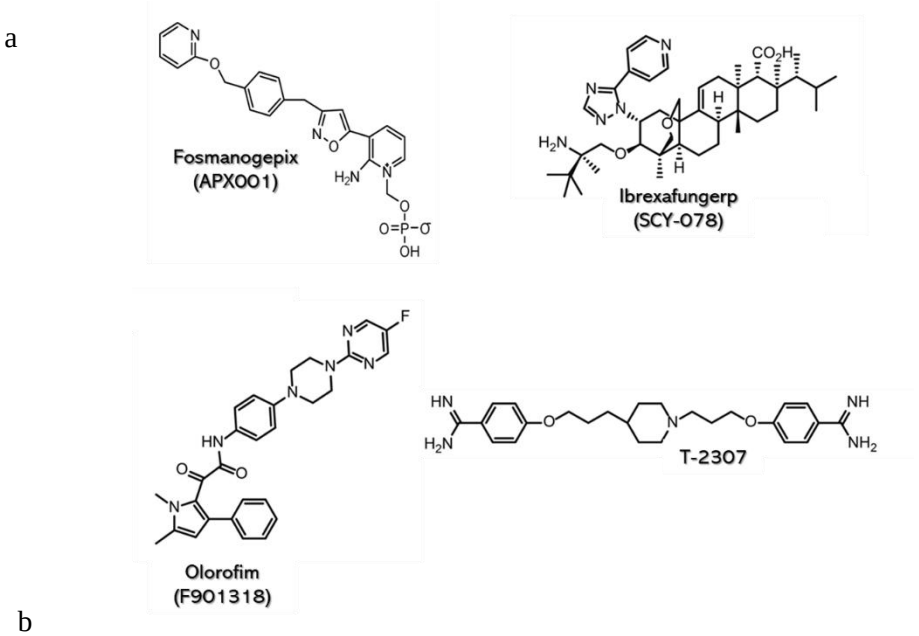

b

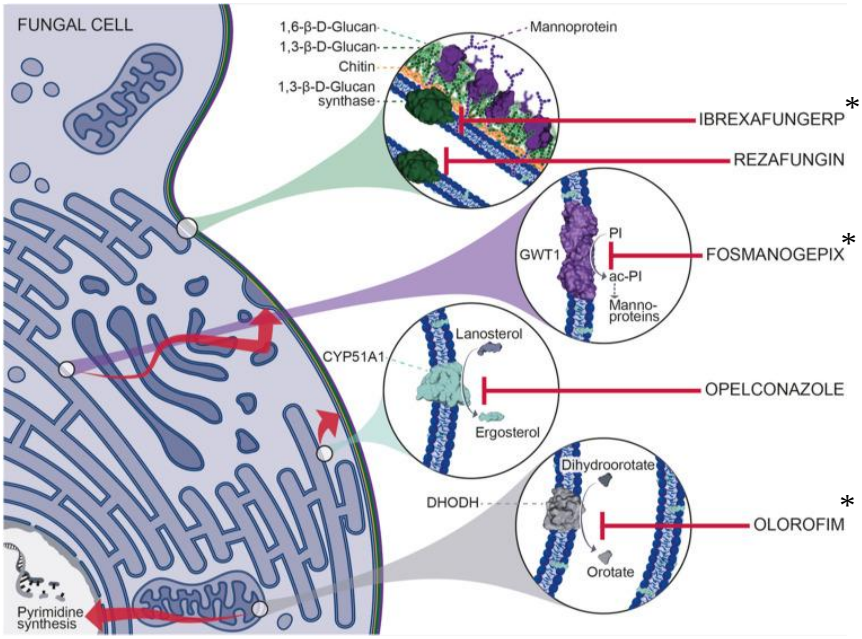

Figure 6: Structures and MOAs of new developed small antifungal drugs. (a) Structures of new class of antifungal agents newly approved by the FDA or in clinical trials. (b) Mechanism of action of new antifungal drugs, whether optimized from an existing antifungal class or first-in-class (adapted from ref [46]). Asterisks indicate the three new classes of antifungal agents.

Table 4: Summary of new antifungal agents in clinical trials and/or newly approved by the FDA

Antifungal agent	Class	Route of administration	Current stage of development
Opelconazole (PC945)	Triazoles	Inhalation	-Phase 2 (NCT05037851): Prophylaxis or pre-emptive therapy against *pulmonary Aspergillosis* in lung transplant recipients
Oteseconazole (VT-1161)	Tetrazoles	Oral	-FDA-approved for treatment of acute vaginal candidiasis -Phase 3 (NCT03561701): Recurrent vulvovaginal candidiasis treatment
Rezafungin (CD101)	Echinocandins	IV	-FDA-approved for acute moderate to severe VVC treatment -Ongoing: Treatment of candidemia and/or invasive candidiasis (NCT03667690) Prevention of invasive fungal disease in patients undergoing allogeneic HCT (NCT04368559)
Encochleated Amphotericin B (C-AmB or MAT2203)	Polyenes	Oral	-FDA-approved for VVC treatment (NCT05541107) -Ongoing: Treatment of cryptococcal meningitis in HIV infected patients (NCT04031833)
Fosmanogepix (APX001)	Glycosylphos-phatidylinositol (GPI) inhibitors	Oral & IV	-Phase 2 (NCT04240886): Treatment of invasive fungal infections caused by *Aspergillus* spp. or rare molds -Treatment of candidemia or invasive candidiasis due to *C. auris* (NCT04148287) -Treatment of candidemia in non-neutropenic patients (NCT03604705)
Ibrexafungerp (SCY-078)	Triterpenoids	Oral	-FDA-approved: Vulvovaginal Candidiasis treatment -Phase 3 (NCT03059992): Treatment in patients with refractory or intolerant fungal diseases - Phase 2 (NCT03672292): Ibrexafungerp and voriconazole combination for treatment of invasive pulmonary aspergillosis
Olorofim (F901318)	Orotomides	Oral & IV	-Phase 2 (NCT03583164): Treatment of invasive fungal infections lacking suitable alternative treatment options.
T-2307	Arylamidines	IV	No available data on progress of trials

c. Development of non-traditional antifungal therapies

In addition to chemical antifungal agents, new biopharmaceuticals have emerged to prevent or treat fungal infections, including immunotherapy using cytokine, monoclonal antibodies, therapeutic vaccines and antimicrobial peptides [47].

Immunomotherapy

The evidence of fungal infections occurs usually in immune-compromised people, whereas immune-competent people are rarely intact with these infections, which highlights the resistance of immunity mediates to fungal attacks. Recently, targeting the host immune system to enhance patient's immune system responses efficacy to eradicate fungal pathogens becomes a reasonable approach to overcome the toxicity to conventional antifungal therapy [48]. In general, immunomodulating therapeutic agents

have a broad activity spectrum, are safe and with low risk to induce resistance [49]. Various immunotherapies show their effectiveness in the context of fungal infections including cytokine therapy (e.g. Recombinant macrophage colony-stimulating factor (M-CSF), granulocyte-macrophage colony-stimulating factor (GM-CSF) and interferon gamma), cellular therapy (e.g. granulocyte transfusion, adoptive T-cell and monoclonal antibodies). Mab 2G8 [50] and efungumab (mycograb) [51] are among the few antifungal drugs based on monoclonal antibodies to have reached an advanced stage of clinical development. However, despite all these promising potential benefits, immunomodulating agents are cost-intensive and may induce some toxicities and inflammation.

Antifungal peptides

There is an increasing interest in peptides as promising novel antimicrobial agents as they are generally effective and well-tolerated. Natural antifungal peptides (AFPs) are AMPs with antifungal activity, produced by several organisms (e.g. mammalian, fungi, plants, insects) as natural molecules belonging to the defense system of each organism against fungal pathogens [52]. Among the many families of AFPs in mammalian, Histatins are one of the most extensively studied, and most of the peptides currently in clinical trials are derived from them [47]. They are cationic histidine-rich linear peptides isolated from human saliva. They have strong and specific antifungal activity against many human pathogenic fungi, e.g., *Candida* spp., *C. neoformans, Aspergillus fumigates*). Among the many families of AFP found in plants and insects are defensins, small cysteine-rich peptides, exhibiting direct antifungal activity against pathogenic fungi, as well as immunomodulatory activities. In addition to their potent *in vitro* antifungal activity, most defensins are non-cytotoxic, making them suitable candidate molecules for optimizing antifungal leads [53].

A very few of AFPs are reached clinical trials [54]. Among them, P-113, known also as PAC-113, is a peptide (AKRHHGYKRKFH) derived from the human salivary protein histatin 5. P-113 particularly has a potent activity against *C. albicans* [55]. It was effective in phase II human trials as mouth rinse to treat oral candidiasis in human immunodeficiency virus (HIV) seropositive patients, which compared favorably to the efficacy of nystatin, a standard treatment for oral candidiasis [56]. NP213, known as Novexatin, is a cyclic cationic novel antifungal peptide specifically designed for the topical treatment of infections caused by dermatophytes and non-dermatophytes fungi. NP213 was designed using human defensins as a template. It was effective in two phase IIa human trials, as a promise peptide-based candidate for the topical treatment of fungal nail infections [57].

Despite the large number of AFP identified with potent antifungal activity in vitro and in animal models, only a few have been tested in clinical trials. The therapeutic use of AFP requires a better understanding of these substances, particularly those with complex structures such as defensins, and their various mechanisms of action.

III. Antifungal CSαβ defensins

Plants and insects produce a variety of antifungal compounds, including AMPs such as defensins, to protect themselves from invasive fungal diseases. Interestingly, these plant and insect defensins also exhibit antimicrobial activity against human fungal pathogens such as *Candida* and *Aspergillus*, in addition to plant and insect pathogens [47, 46]. Structurally, plant antifungal defensins share with insect defensins a folding pattern known as CSαβ motif (Cystein-stabilized α-helix β-sheet motif) [59]. Numerous reviews have reported on the therapeutic potential of plant and insect defensins, for use alone or in combination, as alternative antimycotics and/or their application in the field as alternatives to synthetic fungicides to combat phytopathogenic fungi and their mycotoxins [46, 43, 47, 48]. The next section of this chapter focuses on these antifungal CSαβ defensins, presenting their activity, 3D structures, and mechanisms of action.

1. Plant defensins

As part of the innate immune system, plants produce a variety of proteins and peptides, including α/β-thionins, cyclotides, snakins, heveins, glycine-rich peptides, and defensins, to defend against potential invaders [63]. Defensins are widely distributed in plants and are found in various parts, for example, seeds, roots, stems, flowers, and leaves [64]. The expression of these small cationic proteins can be induced by pathogen attack, injury and certain abiotic stresses [65]. Although the spectrum of activity of plant defensins is quite broad, they are primarily recognized for their antifungal activity. Indeed, most plant defensins isolated to date display antifungal activity against a wide range of fungi, including various plant pathogens, but also human pathogens [54, 55]. However, some plant defensins do not inhibit fungal growth but rather α-amylase, an insect intestinal enzyme, thus protecting themselves from feeding insects [68]. With a few exceptions [56, 57, 58, 59], plant defensins show no antibacterial activity. Conversely, defensins isolated from insects and mussels are mainly active against Gram-positive bacteria and only occasionally against Gram-negative strains or fungi [73]. This may reflect the relative importance of infection pressure exerted by fungal versus bacterial pathogens on plants. It should be noted that other biological activities of plant defensins, including ion channel blocking activity [74], antiviral activity and anticancer properties [61, 62], have been reported.

Antifungal activity

Among the plant defensins most studied for their potent antifungal activity are RsAFP2 from *Raphanus sativus*, NaD1 from *Nicotiana alata*, MsDef1 from *Medicago sativa*, MtDef4 from *Medicago truncatula*, Psd1 from *Pisum sativum* and HsAFP1 from *Heuchera sanguinea*. RsAFP2 inhibits the growth of various pathogenic fungal species, including *Aspergillus flavus*, *B. cinerea*, *C. albicans*, *Fusarium solani*, at a low micromolar concentrations [77, 78]. This defensin is nontoxic to mammalian cells [79]. In addition, RsAFP2 was shown to have anti-biofilm activity, acting synergistically with caspofungin to prevent biofilm formation by *C. albicans* [78]. It has been demonstrated the

prophylactically effectiveness of RsAFP2 against murine candidiasis upon intravenous administration [79]. NaD1 exhibits a large spectrum of activity by inhibiting, *A. nidulans*, *B. cinerea*, *C. albicans*, *C. neoformans*, *F. graminearum*, *S. cerevisiae* [80]. Both MsDef1 and MtDef4 show an activity against *Fusarium graminearum* and *N. crassa* [74, 81]. Psd1 is active against *A. niger*, *F. oxysporum*, *F. solani*, *N. crassa* and *S. cerevisae* [82]. HsAFP1 exhibits activity against *A. flavus*, *B. cinerea*, *C. albicans*, *F. solani*, *N. crassa* and *Penicilium digitatum* [83].

Plant defensins have been widely exploited to protect crops against phytopathogenic fungi and mycotoxin contamination, and to replace the use of synthetic fungicides [62]. Transgenic plants that overexpress an antifungal defensin have been developed, showing an enhanced resistance to pathogenic fungi [84, 85]. Tomato plant transformed by MsDef1 or RsAFP2 defensins has been shown to have higher protection against *F. oxysporum*. Similarly, tomato plants, tobacco and wheat, overexpressing RsAFP2 defensin, showed resistance to *Alternaria longipes* and *Rhizoctonia solani* [85].

Sequence and 3D structure

Structurally, plant defensins consist of an α-helix and three antiparallel β-strands (in the order β1-α-β2-β3) organized into the so-called CSαβ-motif (Cysteine-stabilized α-helix β-sheet motif) [59]. Most plant defensins have eight conserved cysteine residues, linked by a conserved array of four disulfide bonds, with the following connectivities: C1-C8, C2-C5, C3-C6 and C4-C7. The number of amino acid residues between certain cysteines is conserved, in particular three residues between C3 and C4 in the α-helix (C3-x-x-x-C4, where x denotes any amino acid, Figure 6) and one residue between C6 and C7 in the β-strand that is connected to the helix by the two disulfide bridges (C3-C6 and C4-C7). Apart from the conserved cysteines, the primary sequences of plant defensins show a very low percentage of homology with each other (Figure 6). Only rare residues are well-conserved, such as two glycines with a structural role.

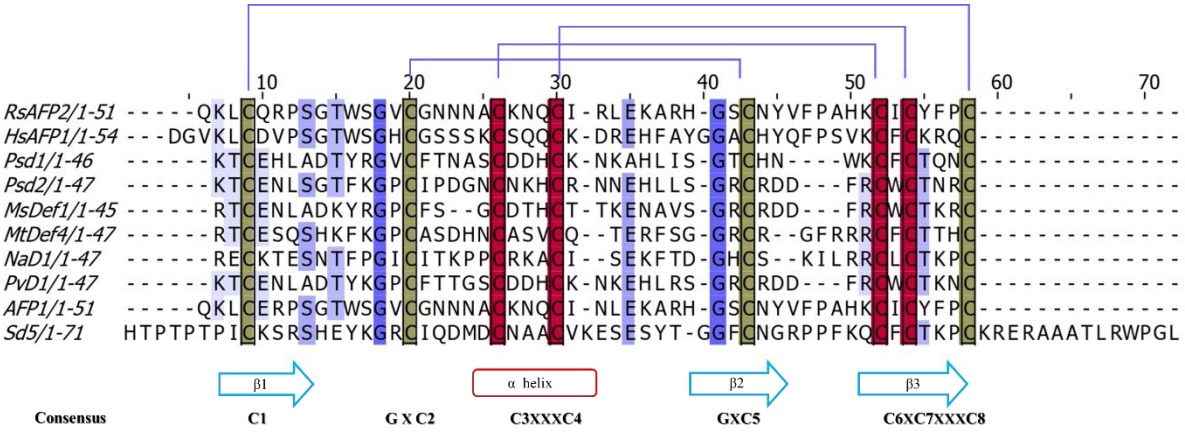

Figure 6: Sequence alignment of some of the plant defensins mentioned in this chapter of the thesis, using the Clustal alignment tool. (-) indicates gaps in the alignment. Highly conserved residues are highlighted in dark blue and slightly conserved residues in light blue. Cysteines involved in CSαβ

folding are highlighted in orange. (Top) Black brackets represent disulfide bridges between the corresponding cysteine residues. (Bottom) 2D structures, the blue arrows representing the positions of the β-strands and the red rectangle representing the position of the α-helix. Schematic representation of the consensus sequence with G for Gly, C for Cys, and x for any amino acid.

To date, 24 tridimensional structures of plant defensins have been experimentally resolved by NMR or X-ray crystallography, showing great similarity. Only monomeric forms have been reported by NMR (selected examples represented Figure 7a, b and c), whereas dimeric forms have been reported by X-Ray (example Figure 7d). This large number of resolved three-dimensional structures has allowed to study structure-activity relationships of this family of proteins, and to identify some amino acid residues and/or region of the proteins that are important for their antifungal activity. Although it differs from one plant defensin to another, the region consisting of the β2 and β3 strands and their connecting loop, called the γ-core, has been proposed to be important for antifungal activity.

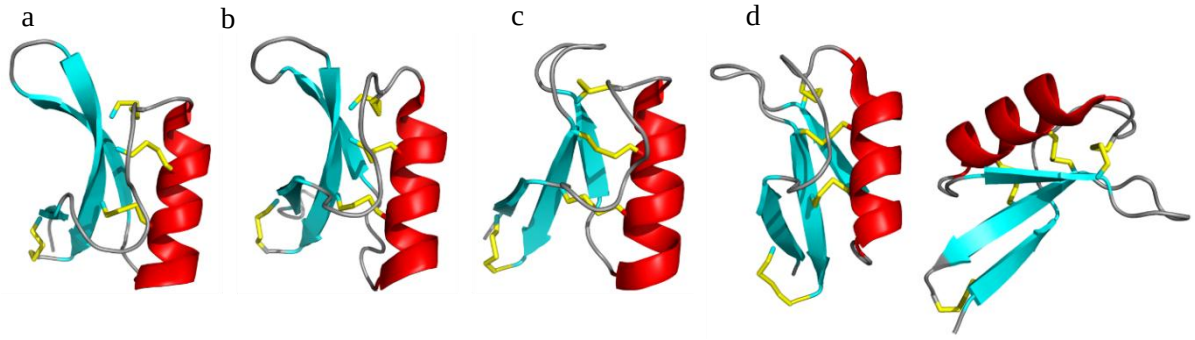

Figure 7: Examples of 3D structures of antifungal plant defensins. (a) Radish RsAFP2 (PDB code: 2N2R) [78] ; (b) Coral Bells HsAFP1 (PDB code: 2N2Q) [83] ; (C) Truncated alfalfa MtDef4 (PDB code: 2LR3) [86] ; (D) Winged tobacco NaD1 (PDB code: 4AAZ) [87]. The α-helix is shown in red, β-strands in blue and disulfide bridges in yellow.

Antifungal mechanisms of action

Despite their similarities in biological activities and global fold structures, plant defensins appear to act via different and complex mechanisms. In general, it has been reported that they interact with one or more cell wall and/or plasma membrane compound(s) as the first step in their mechanism, inducing various downstream effects responsible for fungistatic/fungicidal activity [73, 74]. RsAFP2 specifically interacts with fungal glucosylceramides present in the Cell Wall (CW)/ plasma membrane, activates the cell-wall integrity (CWI) pathway, induces the formation of Reactive Oxygen Species (ROS), the influx of Ca^{2+} and the efflux of K^{+}, leading to apoptosis (Figure 8 (A)) [75, 76, 77]. NaD1 interacts with CW, internalizes into fungal cell by energy-dependent mechanism, induces ROS and NO production, binds with several plasma membrane lipids (e.g. PA, PS, PIP, cardiolipin) and causes membrane permeabilization (Figure 8 (B)) [78, 79, 80]. MtDef4 dysregulates Ca^{2+} levels and binds to PA in plasma

membrane (Figure 8 (C)). MsDef1 interacts with $Ca_V1.2$ channels in the membrane, blocking Ca^{2+} influx, and activates the CWI pathway (Figure 8 (D)) [81, 82]. This multi-effect mechanism of plant defensins is highly valuable for reducing the emerging threat of multi-resistant fungal strains.

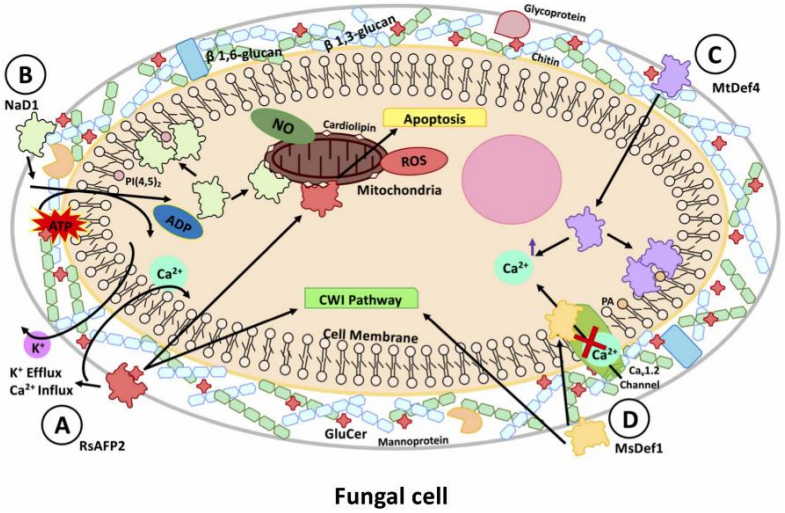

Figure 8: Mechanisms of action of four plant defensins, namely RsAFP2, NaD1, MsDef1 and MsDef1, downstream of lipid binding (adapted from ref [98]).

Each defensin seems to have its own MOA, which is highly valuable for countering the emerging threat of multi-resistant fungal strains, and their complex multi-effect mechanism.

2. Insect defensins

Insects produce defensins as part of an inducible systemic response and secrete them into the hemolymph (equivalent to blood) in response to microbial attack. Conversely to plant defensins, insect defensins are mainly recognized for their antibacterial properties rather than antifungal ones. Particularly, insect defensins are efficient against Gram-positive bacteria, including plant and human pathogens, at micromolar range [73]. However, some insect defensins show potent activity against Gram-negative bacteria, or are mainly active against fungi [74, 75].

Antifungal activity

The insect defensins with antifungal activity known to date are Drosomycin from *Drosophila melanogaster* [101], Heliomicin from *Heliothis virescens* [100], ARD1 from *Archaeoprepona demophon* [102], Termicin from *Pseudocanthotermes spiniger* [103], in addition to three other defensins identified from *Galleria mellonella;* Gallerimycin [104], Gm defensin [51, 52], and Gm defensin-like peptide from (Table 5). Drosomycin is the first isolated insect defensin from Drosophila melanogaster with exclusively antifungal properties. It is active against a broad spectrum of filamentous fungi pathogenic to human and plants [76, 82]. Heliomicin is a peptide extracted from *Heliothis virescens* with a potent activity against numerous filamentous fungi in addition to some yeasts, e.g., *C. albicans*,

C. neoformans [108]. Although ARD1 peptide from *Archaeoprepona demophon* differs from Heliomicin by only two amino acids (D17N and G20A in the α-helix), ARD1 is more efficient against fungi, particularly against *C. albicans* and *A. fumigatus* [102]. Termicin is a termite-specific peptide displaying antifungal activity against filamentous fungi and yeasts at low concentration (minimal inhibitory concentrations (MIC) < 10µM). Also, it shows an activity against Gram-positive bacteria at relatively high concentration (MIC > 50 µM) [103]. Coprisin peptide, isolated from the dung beetle, *Copris tripartitus*, exhibiting antifungal activity with MIC values range between 5 and 20 µM without exerting hemolytic activity against human erythrocytes [109]. Gallerimycin has antifungal activity against the entomopathogenic fungus *M. anisopliae*, but does not display any antifungal activity against *S. cerevisiae* nor any antimicrobial activity against *M. luteus, B. subtilis,* and *E. coli* [104]. GmDefensin (also known as Galleria defensin) was active against some filamentous fungi and yeast strains (MIC < 50 µM) however does not shown any activity against the series of bacteria tested (at the highest concentration tested, CMI > 50 µM) [51, 52]. Gm-defensin like peptide has no antibacterial activity except against *S. lutea* (MIC = 1.9 µM), exhibits similar antifungal activity to GmDefensin, but lacks antifungal activity against *C. albidus*, *F. oxysporum*, and *S. cerevisiae* [106].

None of the antibacterial assays realized with these defensins could highlight any antibacterial activity (no assays with ARD1) with the exception of the termicin and defensin-like Gm peptide, which showed activity against Gram-positive bacteria [106].

Table 5: State of the art of antifungal activities reported for insect defensins

Organism	Insect defensin	Length (AA), net charge,	Antifungal activity	References
Drosophila melanogaster	Drosomycin	44, +1	*Alternaria brassicicola, Botrytis cinerea, Fusarium culmorum, Geotrichum candidum, Neurospora crassa, Septoria tritici*	[101]
Heliothis virescens	Heliomicin	44, +1	*Aspergillus fumigatus, B. cinerea, Candida albicans, Cryptococcus neoformans, F. culmorum, N. crassa, S. tritici*	[100]
Archaeoprepona demophon	ARD1	44, +2	*A. fumigatus, C. albicans, C. neoformans*	[102]
Pseudocanthotermes spiniger	Termicin	36, +4	*C. albicans, C. neoformans, F. culmorum, N. crassa, Nectria haematococca, Saccharomyces cerevisiae, Trichoderma viride*	[103]
Copris tripartitus	Coprisin	43, +3	*A. flavus, A. fumigatus, Aspergillus parasiticus, C. albicans, Malassezia furfur, Trichosporon beigelii, Trichophyton rubrum*	[109]
Galleria mellonella	Gallerimycin	42, +4	*M.nisopliae*	[104]
	GmDefensin (Galleria)	43, 0	*T. viride, P. grisea, F. oxysporum, C. albicans, G. candidium, C. neoformans* *P. pastoris, A. niger, T. harzianum, C. fructus, P. tannophilus*	[105] [106]

	GmDef-like	44, 0	*P. pastoris, P. stipites, C. albicans, A. niger, T. harzianum, C. fructus, P. tannophilus*	[106]

Sequence and 3D structure

Structurally, insect defensins contain at least six conserved cysteines that form a typical arrangement of three disulfide bonds with the following connectivities: C1-C4, C2-C5 and C3-C6. As with plant defensins, the primary sequences of insect defensins vary considerably (see alignment Figure 9).

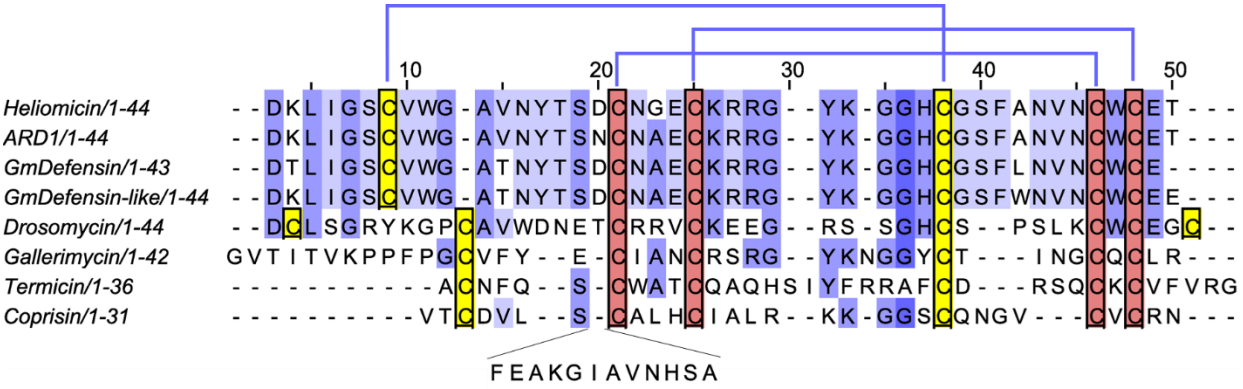

Figure 9: Sequence alignment of insect defensins with described antifungal activity using the Clustal alignment tool. For a more appropriate alignment, we preferred to show the additional coprisin loop below. Cysteines involved in CSαβ folding are highlighted in orange.

One of the main limitations of studying structure-activity relationships of insect defensins is the lack of experimentally resolved 3D structures. Currently only nine insect defensins have been characterized, using solution NMR spectroscopy, including five antifungal peptides (Figure 10): Termicin, Coprisin, Heliomicin, ARD1, and Drosomycin. Their 3D folds consist of one α-helix connected to a two-stranded antiparallel β-sheet (αββ, e.g termicin and coprisin, Figure 10 (a) and (b), respectively) [110], or a three-stranded antiparallel β-sheet (βαββ, e.g. Heliomicin [111] and Drosomycin, Figure 10 (d) and (f), respectively). They contain at least a third disulfide bond connecting the N-terminal part with the central β-strand. Drosomycin contains eight cysteines forming an additional 4th disulfide bridge, connecting the N-terminal strand to the C-terminus, consolidating an already compact structure, and making its fold very similar to that of plant defensins [112]. Structural prediction of gallerimycin using Alphafold v2.0 shows a structure composed of an α-helix and a two-stranded antiparallel β-sheet (αββ), with a long unstructured N-terminal region. Note that the model confidence score per residue (pLDDT) for the N-terminal part is between 50 and 70, indicating a low prediction score.

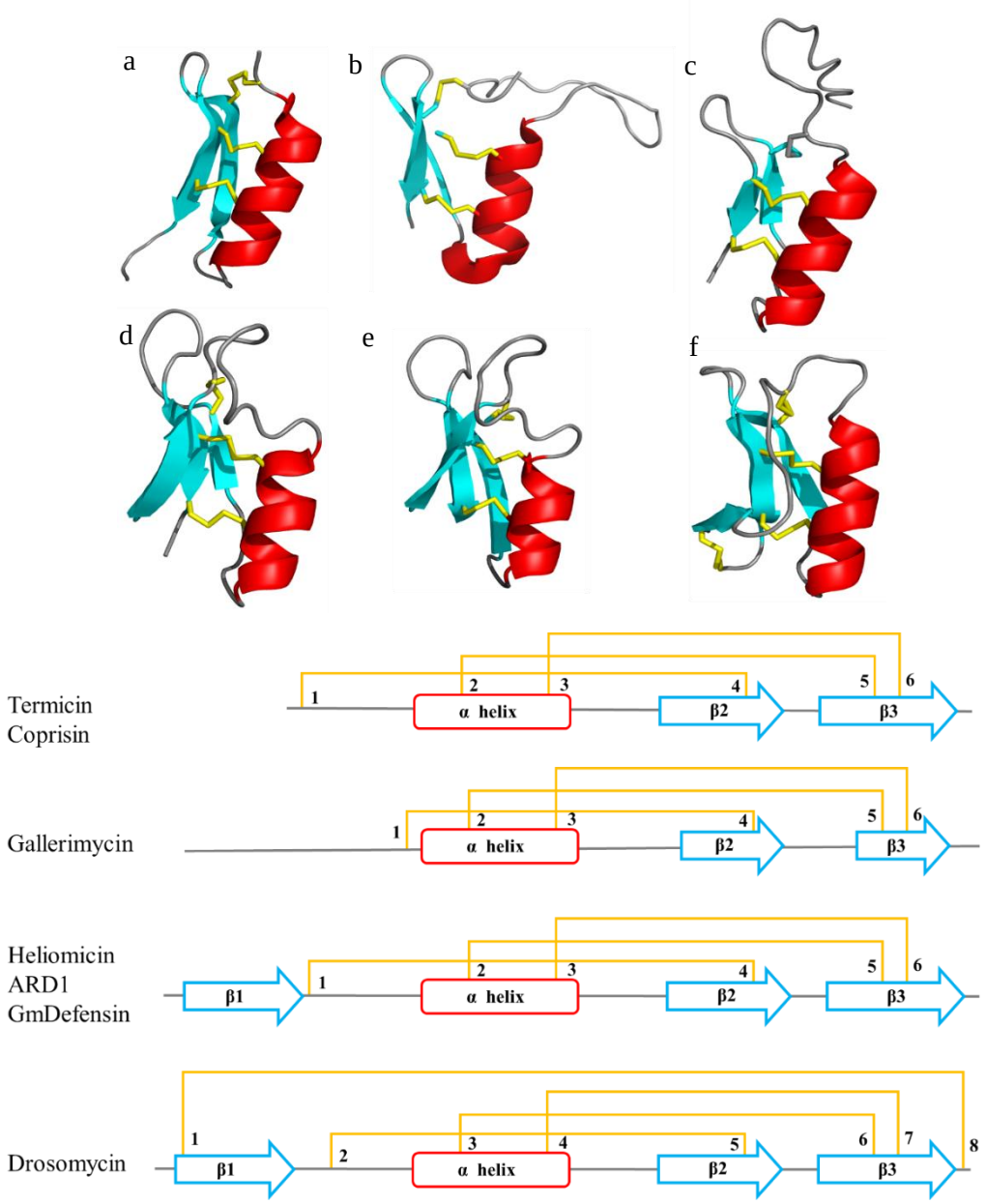

Figure 10: 3D structures of antifungal insect defensins. (a) Termicin (PDB: 1MM0) [113]; (b) Coprisin (PDB: 2LN4) [114]; (c) Gallerimycin (structure predicted by Alphafold v2.0); (d) Heliomicin (PDB: 1I2U) [115]; (e) GmDefensin (structure predicted by Alphafold v2.0); (f) Drosomycin (PDB: 1MYN) [107]. (Below) Secondary structure organization and disulfide bridge connectivity. The α-helix is shown in red, β-sheet in blue and disulfide bridges in yellow.

For insect defensins, attempting to link the activity to structural features is difficult, as a very restricted set of 3D structures is available. Antifungal insect peptides exhibit an amphiphilic character, however with different positions of hydrophilic and hydrophobic residues exposed on the surface. It has been suggested that the N-terminal region and the distribution of hydrophobic and charged residues play a role in the specificity of certain insect defensins towards fungi. In an attempt to impart antibacterial

activity to the antifungal Heliomicin, changes in the N-terminal sequence resulted in a loss of antifungal activity, underscoring its functional importance [111]. It has been suggested that a hydrophobic patch in which a lysine residue is embedded may play a role in Drosomycin antifungal activity [61, 62]. For both Heliomicin and ARD1, it has been shown via site-directed mutagenesis study that increasing the cationicity and hydrophobicity enhance the antifungal spectrum and the potency of activity [102].

Morphological effects and mechanisms of action

Unlike plant defensins, the antifungal modes of action of insect defensins have been poorly studied. As all antimicrobial cationic peptides, the toxic effect of these defensins is thought to involve, wholly or at least partially, interaction with negatively charged microbial membranes, leading to membrane permeabilization and rupture. However as the mechanism of action of AMPs become better understood, and with the few examples of anionic or neutral peptides (e.g., GmDefensin and GmDefensin-like) exhibiting antimicrobial activity [118], it is increasingly recognized that electrostatic interactions with microbial membranes cannot fully explain the mode of action of certain molecules, including the antifungal defensins.

The limited information available on the antifungal actions of insect defensins is reported below. The antifungal effect of Termicin against *A. fumigatus* has been reported. Although at 400 mg/mL Termicin is unable to inhibit spores, it induces morphogenic changes in hyphae and can cause cell wall perforation, occasionally leading to cytoplasmic leakage [119]. In the case of Drosomycin, it has been shown that at high concentrations, 800 mg/mL, it can inhibit the germination of fungal spores. At lower concentrations, it causes stunted growth and abnormal hyphal morphology. After treatment at 10 mg/mL, Drosomycin induces partial lysis of over 50% of *B. cinerea* hyphae, resulting in leakage of cytoplasmic material [101]. The structural and functional similarity between Heliomicin and the plant defensin RsAFP2 led Thevissen et al. [90] to suggest a similar antifungal mechanism for both defensins. Indeed, it has been shown that Heliomicin interacts directly with RsAFP2's membrane partner, glucosylceramides, as the first step in its MOA. However, no further information on its molecular antifungal MOA is currently available.

The similarity of their antifungal activity and 3D structures suggests a close relationship between plant and insect defensins, supporting the hypothesis of a common origin. Furthermore, it is possible that insect defensins have a similar mode of antifungal action to plant defensins. Interestingly, both plant and insect defensins, RsAFP2 and Heliomicin, target the same fungal membrane partner, glucosylceramides, which is one of the promising targets for the development of new antifungals, making them of great interest. The following section will present this membrane partner of antifungal defensins, highlighting the therapeutic potential of targeting it.

IV. Fungal glucosylceramides

1. Biosynthesis and structures

Sphingolipids (SL) constitute a group of membrane lipids characterized by a sphingoid base or long chain base (LCB) linked with a fatty acid through an amide bond, forming the ceramide backbone. To this ceramide structure, a polar group is attached via C_1-OH [120]. Depending on the nature of this polar group, there are two major classes of sphingolipids, the glycosphingolipids (GSL) (that can be acids or neutrals) and phosphosphingolipids. The major fungal sphingolipids are glucosylceramides (GlcCer) an a neutral GSL (Figure, A) and inositol phosphorylceramides (IPCs), an acidic GSL (Figure 11, B).

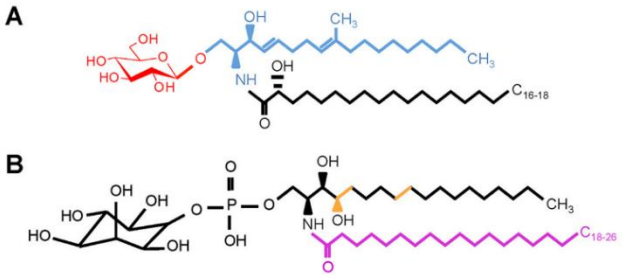

Figure 11: Main glycosphingolipids (GSL) structures in fungi: (A) glucosylceramides (GlcCer) and (B) inositol phosphorylceramides (IPC) (adapted from reference [121]). (A) The basic structure of fungal GlcCer contains a long chain base (LCB) composed of 9-methyl-4,8-sphingadienine (blue), which is amide linked to α-hydroxylated C_{16}-C_{18} fatty acid (black) at C2 and ester linked to a sugar head group (red) at C_1 position. (B) The basic structure of IPC consists of a 4-hydroxysphinganine (phytosphingosine) as the LCB linked to a very long fatty acid chain C_{18}-C_{26} (pink).

The GSL biosynthetic pathway has been described and well-reviewed [64, 65]. The first step begins in the endoplasmic reticulum and involves the condensation of serine and palmitoyl-CoA, catalyzed by serine palmitoyltransferase (SPT). This condensation leads to the formation of 3-keto dihydrosphingosine (3-keto DhSph), which is then reduced by 3-keto DhSph reductase. The precursor formed, dihydrosphingosine (DhSph), will be acylated by ceramide synthase enzymes and can generate two distinct pools of ceramides, dihydroceramide and phytoceramide, which are the building blocks for the formation of neutral or acidic GSLs, respectively (Figure 10, C).

For neutral GSL biosynthesis, the dihydroceramide formed is then desaturated in C_4 and C_8 of the LCB by sphingolipid Δ4-desaturase and Δ8-desaturase, respectively. The resulted ceramide is methylated by sphingolipid C_9-methyl transferase (SMT) to form the mature ceramide, OH-Δ8-C_9-methyl ceramide. Once produced, ceramides are then transported to the Glogi, where the final step of the neutral GSL synthesis occurs, involving the transfer of a sugar residue from UDP-glucose or UDP-galactose to the ceramide backbone to form glucosylceramides (GlcCer) or galactosylceramides (GalCer), respectively, by GlcCer synthase (GCS) or ceramide galactosyltransferase (CGT) (Figure 12). In fungi, GlcCer and

GalCer are considered the final step of the neutral GSL pathway, whereas in mammalian cells they are then used for the formation of hundreds of complex glycosphingolipids (e.g. cerebrosides, gangliosides).

Acidic GSL are formed by the transfer of a phosphoinositol from phosphatidylinositol to the C_1-OH of phytoceramides leading to IPC formation, catalyzed by IPC synthase (Figure 12). Conversely to neutral GSL, acidic GSL include inositol phosphorylceramides (IPC) are used as building blocks for more complex molecules (e.g. mannosylated IPC (MIPC) and $M(IP)_2C$) in fungi as well as in plants.

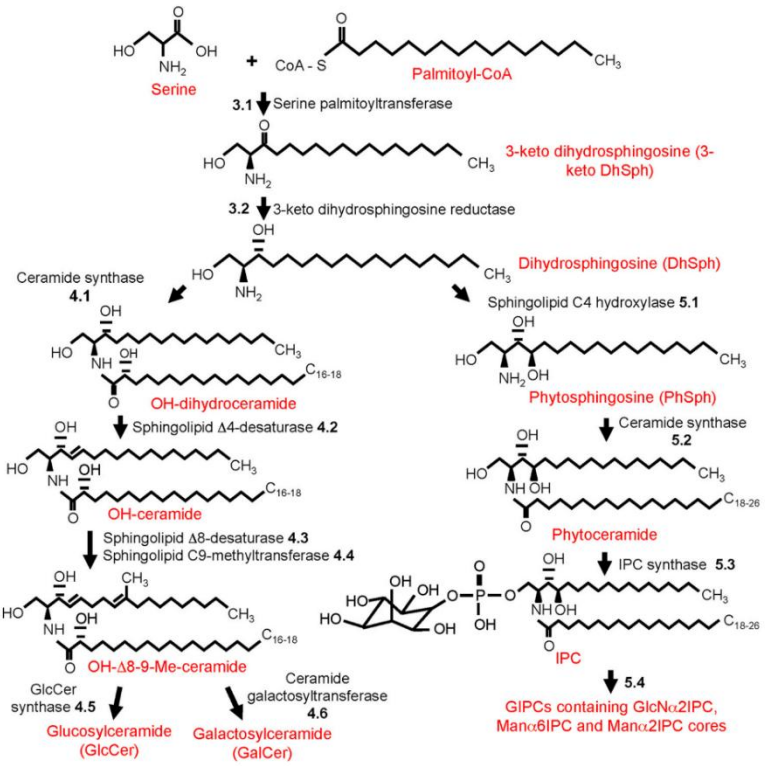

Figure 12: GSL biosynthesis pathway in fungi (adapted from reference [121])

Fungal GlcCer are present in the plasma membrane of almost all fungi, except *C. glabrata, S. cerevisiae* and *Schizosaccharomyces pombe*, but they are also found in the cell wall or in the extracellular environment secreted in vesicles. GlcCer structures isolated from several fungi pathogenic to human (e.g. *Candida albicans*, *Cryptococcus neoformans*, *Aspergillus fumigatus*, *Scedosporium*) as well to plant (e.g. *Fusarium oxysporum*, *Fusarium graminearum*, *Penicillium digitatum*, *Cladosporium*) have been characterized by mainly mass spectrometry approaches [123] (Table 6). Although their structures are globally well conserved, fungal cells can produce GlcCer structures differing by the number of hydroxylation, the degree of unsaturation and/or the length of fatty acids chains [124]. Barreto-Bergter and colleagues have shown that even fungi belonging to the same species can have different structure of GlcCer [125].

Table 6: GlcCer structures of some fungal species pathogenic to human and/or plant.

fungi	GlcCer structure described*		References
	Sugar	Major fatty acid	
Aspergillus fumigatus	Glucose/Galactose	C18:1, Δ3	[126]
Candida albicans	Glucose	C18:0	[127]
Cryptococcus neoformans	Glucose	C18:0	[128]
Lomentospora prolificans	Glucose	C18:0	[129]
Fusarium solani	Glucose	C18:1, Δ3	[130]
Pichia pastoris	Glucose	C18:0	[131]

*9-methyl-4,8-sphingadienine (d19:2) is the long chain base composing the ceramide unit of all the molecules described in this table. Except for *L. prolificans*, the sphingoid base is 4-hydroxy-9-methyl-4,8-sphingadienine (d19:2OH). All fatty acids are hydroxylated.

2. Biological roles

Several studies have reported the involvement of GlcCer in crucial fungal biological functions, such as growth, morphogenesis and pathogenicity/virulence. In addition to the complete GlcCer molecule, certain structural features specific to fungal GlcCer, notably the C8-C9 double bond and the C9 methyl of LCB, have been shown to be important for normal growth, fungal morphogenesis and virulence in certain fungal species. Interestingly, this double bond between C8-C9 and methylation are structural features unique to fungi, distinguishing them from their mammalian and plant counterparts.

The biological roles of GlcCer and/or a specific feature were demonstrated using mutant deletion of the gene encoding the enzyme responsible for the biosynthesis step in yeasts and filamentous fungi, as shown in figure 13.

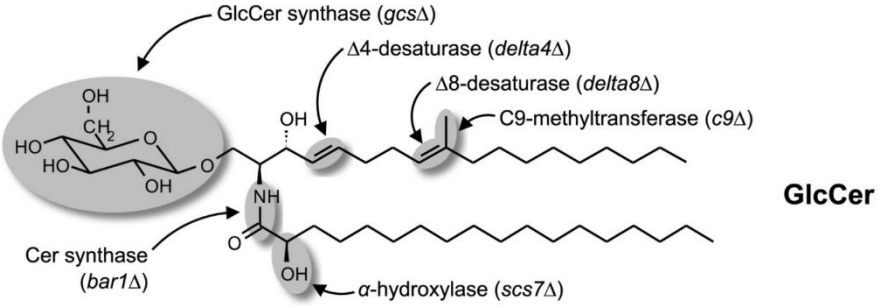

Figure 13: Fungal GlcCer structure with highlighted structural features, responsible enzymes for introducing these structural features as well as the corresponding gene names and the knock-out strains names used (adapted from ref [132]**).**

Role in fungal growth, morphogenesis and virulence

Human pathogenic fungi, *Cryptococcus neoformans* and *Candida albicans*, have been shown to require GlcCer as a key regulator of pathogenicity [73, 74]. Indeed, *C. neoformans* Δ*gcs* strains were not able to growth in neutral/alkaline pH, characteristic of extracellular host environments, which is essential to infect cells [134]. It is also worth noting that many plant pathogenic fungi mutants lacking GlcCer show impaired growth and loss or reduction of virulence compared with wild-type strains. For instance, (i) Δ*FocGCS* null mutant of *Fusarium oxysporum* showed reduced mycelial growth and lost the ability to

cause fusarium wilt in banana [135], (ii) Δ*CgGCS* mutants of *Colletotrichum gloeosporioides* showed a reduced mycelial growth and were almost disable to invade tomato and mango hosts [136], (iii) Δ*PdGcs1* mutants of *Penicillium digitatum* showed a decrease in vegetation growth and sporulation as well as an impairment in the virulence on citrus fruits by delaying the occurrence of water soaking lesion and the formation of smaller size of lesion [137], and (iv) Δ*Fggcs1* mutant of *F. graminearum* showed a significant reduction to spread in wheat heads and corn silk tissues after colonization [81].

Also, fungal GlcCer have been reported to contribute in lipid raft organization involving in the membrane integrity and the lipid order. Thus, its absence or even changes in its structure led to the fragility of the membrane (increase the membrane permeability), making fungal cells more vulnerable and less resistant to antifungal molecules. In *Scedosporium aurantiacum*, monoclonal anti-GlcCer altered lipid rafts organization, as shown by using the fluorescent stain filipin, and reduced total biomass and viability in biofilms formed on polystyrene plates [138]. In addition, it has been demonstrated that this glycolipid is important for biofilm formation in *A. fumigatus* and for biofilm adhesion in *Scedosporium aurantiacum* [138].

Role of the C8-C9 double bond and the methylation of the long chain base

Moreover, yeast and filamentous fungi mutants' strains have been developed lacking key enzymes such as sphingolipid C_9-methyl transferase (SMT), fungus-specific enzyme, and Δ8-desaturase. Importantly, these knockout strains have defects in fungal growth, hyphal elongation, lipid raft organization [139] and a decreased virulence *in vitro* model [140]. SMT encoding gene has been reported to be not necessary for the vegetative growth of yeast but is necessary for the growth of filamentous fungi. Indeed, the *P. pastoris* and *C. albicans* knock-out strains, lacking completely the production of C9-methylated GlcCer, were viable and not impaired in growth compared with the wild-type strain [82, 83]. However, *F. graminearum* ΔFgmt2, *N. crassa* ΔSMT and *A. nidulans* ΔSMT mutants' strains, still produced methylated and unmethylated GlcCer, exhibited severe growth defects [84, 85]. The disruption of SMT1 encoding gene in *C. neoformans* was studied by Singh et al. The Δsmt1 mutant strain exhibited decreased virulence in a murine model of cryptococcosis and an increased susceptibility to sodium dodecyl sulfate (SDS), suggesting a defect in cell membrane structures confirmed by fluorescence spectroscopy and atomic force microscopy studies [74, 86]. In addition, the presence of the methyl group in the ceramide backbone influences the physical properties of the fungal cell membrane, affecting membrane fluidity, stability (contribute to the hydrophobic interactions within the lipid bilayers) and permeability (disruption of the fungal membrane integrity, leading to fungal growth inhibition or cell death). Indeed, it has been supposed that the C9-methylation, with the additional Δ-8 double bond, increase the physical distance between the hydrophobic core of GlcCer and other lipids [124]. The lack of these features, C9 methyl group, may disrupt the proper lipid organization of the plasma membrane.

This role of membrane order regulator has been demonstrated to be required for fungal pathogenicity in the mouse model [139].

V. Targeting fungal glucosylceramides

Due to the importance of GlcCer for fungal growth and pathogenesis and their conserved structure, targeting fungal GlcCer is a promising strategy for developing the next-generation antifungals [66, 87, 88], needed to overcome some of the limitations of currently available antifungals (azoles, polyenes and echinocandins). There are two ways to target GlcCer: (i) by inhibiting the activity of enzymes implicated in the biosynthesis pathways, or (ii) by directly targeting GlcCer, thereby inhibiting their function.

1. Targeting glucosylceramides biosynthesis pathway

SPT inhibitors are drugs that target the first enzyme (SPT) involved in the biosynthesis pathway of SGL. They are highly active with a broad spectrum of activity; however, they also inhibit human SPT1. Myriocin, a metabolite from the entomopathogenic fungus *Isaria sinclairii,* is one of the best-known irreversible inhibitors of SPT. It can prevent germination and induce abnormal branching in hyphae in *Aspergillus*. Unfortunately, the application of myriocin is limited due to its lack of specificity for fungal SPTs, resulting in toxicity to the cellular host. However, improve its selectivity against the fungal counterpart appears to be possible [148].

Ceramide glucosyl synthase (**CGS) inhibitors** lead to depletion of sphingolipids content and increase levels of toxic sphingoid bases (dihydrosphingosine DHS and phytosphingosine). They have shown moderate *in vitro* and *in vivo* antifungal activities. Fumonisin B1 and australifungin, mycotoxins from *Fusarium* and *Sporormiella australis*, respectively, have been reported as two inhibitors of fungal ceramide synthase. The lack of specificity towards fungal ceramide synthase and their toxicity to mammalian cells limit the use of these compounds as antifungal drugs. Similarly, treatment with PDMP (1-phenyl-2-decanoylamino-3-morpholino- 1-propanol), a GCS inhibitor, affected hyphal growth and spore germination of *Aspergillus nidulans* and *A. fumigatus,* but had the drawback of being toxic to the host [149]. Interestingly, acylhydrazones, PDMP derivatives, inhibit specifically fungal GCS with lower toxicity toward mammalian cells.

Generally, SGL enzyme inhibitors appear to be a good alternative to inhibit pathogenic fungal growth however their main drawback is the lack of selectivity toward fungal enzymes resulting in toxicity to mammalian cells.

2. Targeting directly glucosylceramides

a. Antibodies

As GlcCer are immunologically active components, they induce the production of monoclonal antibodies directed against fungal GlcCer. These antibodies have been shown to possess antifungal

activity [90, 91]. They can constitute therefore an antifungal immunotherapy tool, which could be used as alternatives to chemical fungicides in order to control plant diseases, or in medical application as a vaccination therapy. Here are a few non-exhaustive examples: (i) Single-domain antibodies (VHH) generated after immunization of camelids with fungal GlcCer were able to bind specifically to fungal GlcCer, and not to mammalian or plant GlcCer. Interestingly, these VHHs demonstrated their ability to inhibit *B. cinerea* growth *in vitro* and on tomato leaves when sprayed, thus reducing *B. cinerea*-induced disease symptoms [152]; (ii) Monoclonal antibodies to *Fonsecaea pedrosoi* have resulted in a marked reduction of fungal growth after treatment of murine cells infected with *F. pedrosoi*, the most causative agent of chromoblastomycosis [153]; (iii) Immunization with a monoclonal antibody to fungal GlcCer showed a significant reduction in host inflammation and prolongation of survival in the *C. neoformans*-infected mouse model [154]; and (iv) The therapeutic potential of cryptococcosis after fungal GlcCer administration in a mouse model, eliciting an anti-fungal GlcCer antibody response, demonstrated that it prevented the dissemination of *C. neoformans* from the lungs to the brain [155].
Together, antibodies against fungal GlcCer are potentially active against pathogenic fungi and have shown a synergistic effect when combined with antifungal compounds without being toxic to mammalian or plant cells.

b. GlcCer-targeting CSαβ defensins

It has been reported that fungal GlcCer are recognized by some antifungal defensins belonging to the subfamily of defensins found in plants and insects, and referred to as "CSαβ defensins" because of their characterized cysteine-stabilized α-helix β-sheet structural motif (CSαβ). Antifungal defensins targeting GlcCer are considered promising molecules for combating pathogenic fungi [96, 97, 98] for the following reasons: (i) they are effective in *vitro* at micromolar concentrations against fungi; (ii) they are non/lowly-toxic to human cells and the environment compared to synthetic fungicides; (iii) they exhibit relatively high structural stability after heat treatment and exposure to extreme pH levels due to their compact structure; (iv) they target GlcCer, which are virulence determinants and essential for infection *in vivo*. The last point is crucial in the context of development of new antifungals, as it makes the frequency of resistance development *in vivo* relatively low, and even if mutations have occurred, mutants with defective sphingolipid biosynthesis are not effective and therefore do not survive *in vivo* [124].

Fungal GlcCer-dependent activity

For some CSαβ defensins, the presence of GlcCer in fungal membranes has been shown to be required for their optimal activity against yeast strains and/or filamentous fungi. Indeed, these defensins show a decrease or complete abolition of the activity against Δ*gcs* mutants (lacking GlcCer) compared to their wild-type (wt) strains (Table 7). These defensins include six plant defensins: RsAFP2 from *Raphanus sativus*, Psd1 and Psd2 from *Pisum sativum*, MsDef1 from *Medicago sativa*, PvD1 from *Phaseolus vulgaris*, and AFP1 from *Brassica juncea* [159], and only one insect defensin, Heliomicin from *Heliothis*

virescens. Furthermore, since *S. cerevisiae* and *C. glabrata* (yeasts that do not contain GlcCer) and bacteria do not possess membrane-bound GlcCer, these defensins are generally inactive or active at high concentrations against *S. cerevisiae* and *C. glabrata* and bacteria cells [160].

Table 7: Plant/insect defensins for which GlcCer has been reported to be a determining factor in their antifungal activity. The data are reported as median inhibitory concentration (IC_{50})[b] or minimum inhibitory concentration (MIC) [a], expressed in micromolar (µM).

Defensins (organism)	*P. pastoris*		*C. albicans*		*F. graminearum*		*A. nidulans*		Ref
	WT	Δ*gcs*	*WT*	Δ*gcs*	*WT*	Δ*gcs*	*WT*	Δ*gcs*	
RsAFP2 (*Raphanus sativus)*	2[a]	> 40[a]	2.5[a]	> 40[a]	0.25-0.4[b]	0.6-07[b]	-	-	[160], [81]
Psd1 (*Pisum sativum*)	-	-	9 µM[b]	15 µM[b]	-	-	-	-	[161]
Psd2 (*Pisum sativum*)	-	-	Δ*gcs* mutants are more resistant than wt strains at 20 µM Psd2		-	-	Δ*gcs* mutants are more resistant than wt strains at 20 µM Psd2		[162]
MsDef1 (*Medicago sativa*)	-	-	-	-	1.5-3[b]	6-9[b]	-	-	[81]
PvD1 (*Phaseolus vulgaris*)	-	-	Δ*gcs* mutants are more resistant than wt strains		-	-	-	-	[163]
AFP1 (*Brassica juncea*)	-	-	0.6[b]	> 5[b]	-	-	-	-	[164]
Heliomicin (*Heliothis virescens*)	2.5[a]	> 40[a]	2.5[a]	> 20[a]	-	-	-	-	[160]

Although these results clearly show the relevance of the presence of GlcCer in fungal membranes for the activity of certain defensins, they do not demonstrate a direct interaction between defensin and GlcCer. Given that GlcCer contributes to the regulation of membrane fluidity and order [142, 143], their absence in the membranes of yeast/filamentous fungi mutants can alter the biophysical properties of the cell membrane (as mentioned in the previous section of this chapter), thereby affecting susceptibility to peptides. Therefore, to confirm that GlcCer is the molecular membrane target of defensin, additional biochemical or biophysical assays are necessary.

Defensins for which molecular interaction with fungal GlcCer has been confirmed by *in vitro* assays, we refer to them as "GlcCer-targeting defensins". This group includes RsAFP2, Psd1, Psd2, and Heliomicin. It includes also sd5, a plant defensin from *Saccharum officinarum*, that shows *in vitro* recognition of fungal GlcCer (no biological data available for Δ*gcs* mutants). For the second group, gathering MsDef1, PvD1, and AFP1, i.e. defensins where this molecular interaction has not (yet) been reported, we refer to them as "GlcCer-associated defensins".

Fungal GlcCer-defensin molecular interaction studies

Only a few studies have examined the binding between defensins and fungal GlcCer under non-membrane conditions, for example, through the reverse enzyme-linked immunosorbent assay (rELISA) or under membrane conditions using lipid vesicles containing GlcCer as a simplified model to mimic fungal membranes.

Reverse ELISA

Using rELISA assay (Table 8), in which glycolipids are immobilized in the wells of microtiter plates and bound defensin is detected immunologically, it was shown that RsAFP2 interacts specifically with fungal GlcCer (C9-methylated with a C18 fatty acid chain) in a dose-dependent manner, but not with plant GlcCer (unmethylated with a C16 fatty acid chain) (Figure 14 (A)). This indicates that the binding of RsAFP2 to GlcCer is structurally dependent as the C9-methyl in the sphingoid base is important for the recognition of GlcCer by RsAFP2 [167]. Under the same conditions, Heliomicin was found able to bind both fungal GlcCer and plant GlcCer (Figure 14 (B)), unlike RsAFP2 [167]. Although, RsAFP2 and Heliomicin target the same membrane partner in fungi, the presence of one of these two defensins does not inhibit the interaction of the other one with fungal GlcCer [167]. These results demonstrate that each defensin has a different GlcCer recognition site, including the C9-methyl for RsAFP2, but not for Heliomicin. Interestingly, both defensins show reduced interaction with human GlcCer (Figure 14) which demonstrate their low toxicity to human cells.

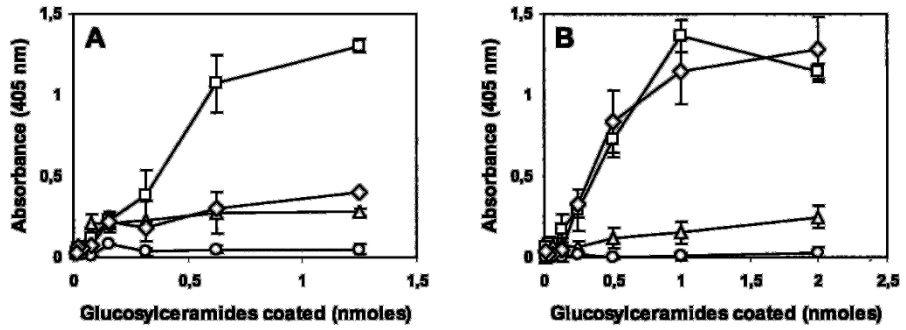

Figure 14: Interaction of RsAFP2 and Heliomicin with GlcCer using rELISA (adapted from ref [167]). Dose-response curves are presented for the interaction of RsAFP2 (A) and heliomicin (B) with GlcCer from *P. pastoris* (squares), human spleen (triangles), soybean (diamonds), and monogalactosyldiacylglycerols from soybean (circles). RsAFP2 and heliomicin were used at a concentration of 50 nM.

Table 8: *In vitro* molecular recognition of plant/insect defensins to fungal GlcCer

Techniques	Defensins	Experimental conditions	Results and conclusion	References
rELISA	**RsAFP2**	rELISA-based binding assay in which glycolipids (GlcCer from *P. pastoris* or unmethylated GlcCer from soybean) are coated to the wells of microtiter plates and peptide was detected immunologically.	**RsAFP2** interacts in a dose-dependent manner with purified GlcCer from *P. pastoris*, however, no significant interaction of RsAFP2 with different concentrations of soybean (unmethylated GlcCer).	[167]
	Heliomicin		**Heliomicin** interacts with fungal GlcCer and plant GlcCer in a dose-dependent manner.	
SPR	**Psd1**	Small unilamellar vesicles (SUVs) (1 mM) with Egg phosphatidylcholine (PC) or PC: $GlcCer_{soybean}$ (7:3, molar: molar), or PC: $GlcCer_{F.\ solani}$ (7:3, molar: molar) or pure $GlcCer_{F.\ solani}$ in buffer (10 mM HEPES, pH 7.4 and 150 mM NaCl) or PBS, pH 7.4. SUVs were immobilized on the chip surface and the amount of lipids was normalized using a fixed value for the base lie (3500 RU) before peptide addition. The protein-lipid interaction was measured by injection of 100 µL of Psd1 (3.5-28 µM) or Psd2 (5-100 µM) at a constant flow 30 µL/min for 200 s (Psd1) or 10 µL/min for 600 s (Psd2). The dissociation was measured for 300 s or 600 s after the injection endpoint.	The incorporation of 30% mol $GlcCer_{F.\ solani}$ to PC-SUV increased the Psd1 binding response (α values 8 x higher) and the response was 60-fold greater with SUV containing only $GlcCer_{F.\ solani}$. The presence of 30 % mol of $GlcCer_{Soybean}$ induced a slightly higher response to that observed with pure PC vesicles (α values 2 x higher) but lower than PC: $GlcCerF._{solani}$ (α values 2.5 x lower).	[168]
	Psd2		The binding response intensity was greater with pure PC vesicles than PC: $GlcCerF._{solani}$ (70:30) although the association rate was similar.	[162]
Liquid-state NMR	**Sd5**	^{15}N-labeled Sd5 (200 µM) in 5 mM sodium phosphate buffer (pH 4.0), in the presence or absence of 5 mM PC or PC: fungal GlcCer (9:1, molar ratio) vesicles.	NMR and relaxation studies demonstrated that Sd5 showed conformational changes with the presence of PC: fungal GlcCer vesicles.	[169]
	Psd1	NMR spectra were recorded on 0.5 mL samples of ^{15}N-labeled Psd1 (50–200 µM) in 20 mM sodium phosphate buffer pH 5-, and 20-mM sodium chloride in the presence or absence of 5 mM PC or PC: fungal GlcCer (9:1, molar ratio) vesicles.	NMR and relaxation studies showed that Psd1 interacts with vesicles of PC and PC: fungal GlcCer (9:1 molar ratio) in slightly different manner and the major binding epitope showed conformational changes supporting the conformation selection as the binding mechanism.	[170]
Liposome leakage assay	**Sd5**	Large unilamellar vesicles (LUVs) containing the dye/quencher pair (ANTS/DPX) were incubated in the presence of Sd5 and the fluorescence was measured after the addition of the defensin at different concentration.	Sd5 was able to promote vesicle leakage when they include membrane total lipids of *F. solani* or PC: $GlcCer_{F.\ solani}$ compared to no effect was observed	[169]

		An increase in fluorescence is observed in the event of dye leakage.	with PC: Phosphatidylethanolamine (PE) or PC: Phosphatidylglycerol (PG) up to 100 µM Sd5.	

Surface plasmon resonance (SPR)

For both pea defensins Psd1 and Psd2, the interaction with GlcCer isolated from *F. solani* ($GlcCer_{F. solani}$) incorborated in small unilamellar vesicles (SUVs) have been investigated using SPR experiments (Table 8). SUVs were composed mainly with phophatidylcholine (PC) containing 30% mol of $GlcCer_{F. solani}$. In SPR experiments, SUVs are immobilized on the chip surface prior to peptide injection at a given concentration under constant flow. Usually, SPR assay provides binding affinity and kinetic parameters, association and dissociation rates (K_a and K_d), of the interaction in real time, which can be used to determine an equilibrium dissociation constant K_D. However, with pea defensins and GlcCer-containing SUVs interaction, kinetic data (K_a and K_d values) could not be obtained since the dissociation phase was insignificant (K_a >>> K_d). Thus, the difference and quantification of membrane-binding affinities of defensins were based on the equilibrium response before dissociation (Req values) and how fast the initial association occurred indicated by the initial association rate (α values). The higher the Req and α values, the greater the peptide's binding affinity to membranes.

SPR results showed that Psd1 has greater binding affinity to PC-based SUVs when they contained $GlcCer_{F.solani}$ rather than SUVs containing only PC and/or 30% mol of plant GlcCer (unmethylated GlcCer) [168]. Compared to fungal membrane model Psd1 shows reduced interaction with cholesterol-rich mammalian membranes (Figure 15). In accordance with SPR results, partition studies have shown that Psd1 has a high affinity for model membranes enriched in ergosterol, the main sterol present in fungal membranes, and GlcCer [145]. For Psd2, the binding affinity is higher to pure PC-based SUVs than those containing $GlcCer_{F. solani}$ [162]. Using PIP strips, Psd2 has been shown to bind to several lipid targets in addition to GlcCer, such as ergosterol, phosphatidylcholine and other phospholipids [140]. These findings suggest the difference of defensin selectivity to fungal GlcCer.

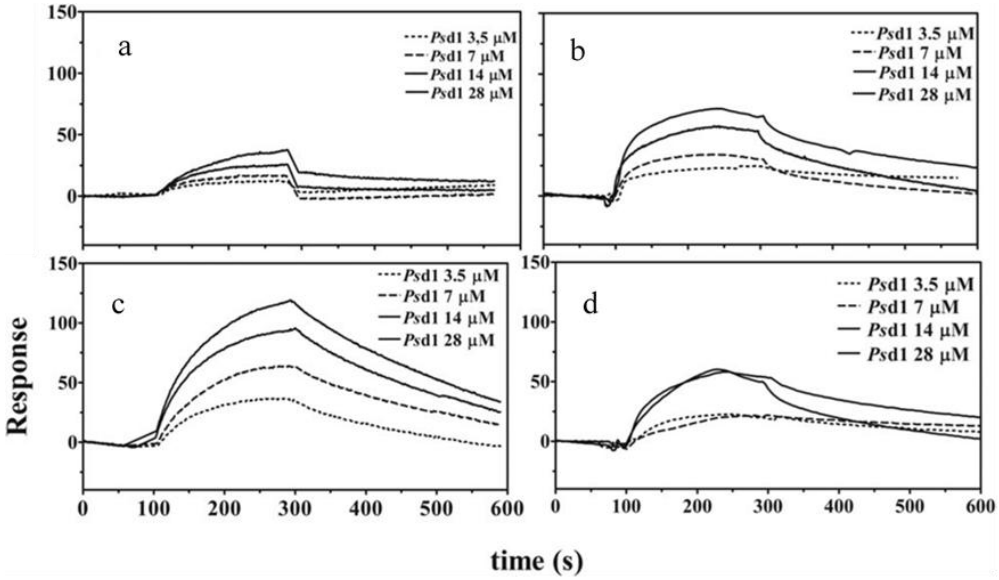

Figure 15: Real-time interaction of Psd1 at different concentrations with SUVs using SPR (adapted from ref [168]). The different SUVs compositions: (a) only PC, (b) PC: Cholesterol (PC: Chol, 7:3), (c) PC: GlcCer$_{F.\ solani}$ (7:3) and (d) PC: GlcCer$_{Soybean}$ (7:3).

NMR in solution

Structural and dynamic properties are thought to play a role in the activities of plant defensins, particularly in the membrane interaction and recognition of their molecular target. However, to our knowledge, only two studies have examined the effect of fungal GlcCer presence in a membrane context on the structure of defensin.

The monitoring of the chemical shift perturbation (CSP) of ^{15}N-labeled Psd1 showed that mainly loops L1 and L3 were perturbated by the presence of PC-based vesicles containing GlcCer$_{F.\ solani}$ (9:1 molar ratio). Additionally, several cysteines were disrupted, suggesting conformational adaptation of Psd1 in the membrane recognition. This interaction Psd1-fungal GlcCer suggested to involve other types of interactions than electrostatic ones such as hydrogen bonds (T16 and N17) and hydrophobic interactions (V13, F15, A18 and W38) (Figure 16a) [170].

The second study has been performed with the plant defensin Sd5. Liposome leakage assay showed that this defensin disturbs selectively and in a concentration-dependent manner PC-based vesicle containing fungal GlcCer (GlcCer$_{F.\ solani}$), or vesicles made with fungal whole lipid extract, unlike other negatively charged lipids-based vesicles [169]. Therefore, the recognition of membranes by sd5 seems not to depend only on the lipid surface charge. Upon addition of fungal GlcCer-enriched PC vesicles, a series of residues of sd5, mainly clustered in part of the α-helix and in the loop between the α-helix and the β2 (loop L2) are disrupted. Namely, residues V31, K32, S34, E35, S36 and Y37 were reported as likely to respond to specific interaction with fungal GlcCer (Figure 16b) [169].

Although Psd1 and Sd5, are two defensins with completely different dynamic properties, NMR dynamic studies, both in the free state and in the presence of target membranes (GlcCer), showed a molecular recognition of fungal GlcCer by conformational selection. Indeed, the region of Psd1 probably involved in the interaction (L1 and L3) displayed reduced conformational exchange, probably due to the stabilization of a specific membrane-bound conformation of Psd1 [170], while the presence of vesicles containing fungal GlcCer led to an increase in Sd5 conformational exchange processes [169].

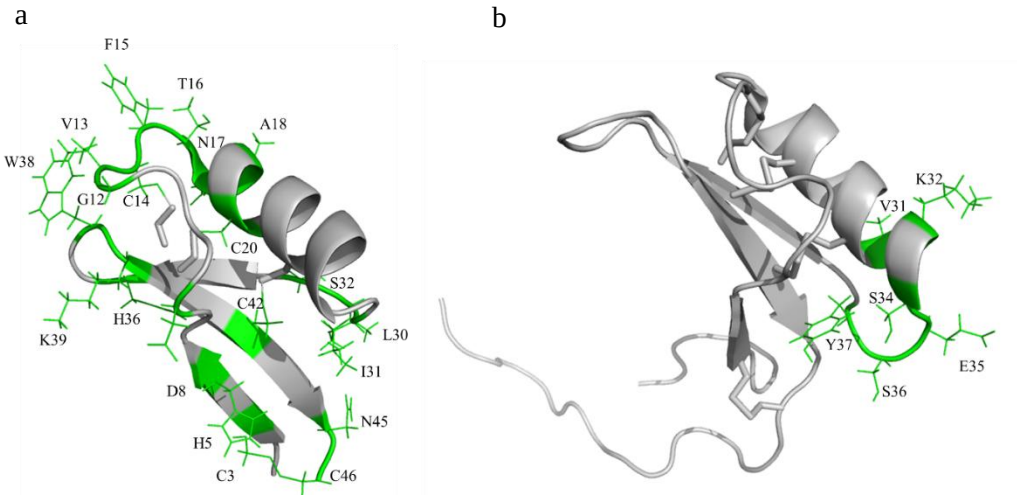

Figure 16: Cartoon representations of (a) Psd1 (PDB code: 1JKZ) and (b) Sd5 (PDB code: 2KSK) defensins. Residues highlighted in green were the most affected by the presence of vesicles of phosphatidylcholine (PC): fungal GlcCer (9:1, molar ratio) vesicles (adapted from ref [169, 170]).

Reported fungal GlcCer structural features for fungal sensitivity to defensins

For some antifungal CSαβ defensins, it was investigated whether the presence of certain structural features in GlcCer, in particular the C8-C9 double bond and the C9-methyl in the GlcCer LCB, was required for full antifungal activity. *C. albicans* (Δ*smt*) mutants lacking a methyl group in the sphingoid base were found to be more resistant to the AFP1 peptide than wt strains [159]. *A. nidulans* Δ*smtA* and Δ*smtB* mutants, lacking methylation in GlcCer, were more resistant to 20 µM Psd2 than wt strains and strains lacking C8-C9 unsaturation (Δ*sde8*) [162]. The Δ*sde8* mutant of *Aspergillus nidulans*, lacking the C8-C9 unsaturation in GlcCer, showed resistance to Psd1 compared with wt strains [140]. On the contrary, the defensins RsAFP2 and MsDef1 showed similar activity on *F. gramineurum* Δsmt mutants (produce 65-75% unmethylated GlcCer and 25-35% methylated GlcCer) and wt strains [143]. *P. pastoris* mutants lacking the C9-methyl in the LCB showed similar sensitivity to RsAFP2 as wt strains [143].

Overall, although binding to GlcCer is a crucial step common to some antifungal defensins sharing the same CSαβ folding, each of these defensins appears to interact differently with GlcCer, which may or may not involve the C9 methyl group. Consequently, there seems to be no consensus on how antifungal defensins interact with fungal GlcCer.

Available data about defensin internalization (or not) and downstream effects

Upon target interaction, defensins are either internalized into fungal cells which suggest possible intracellular target(s) or remained outside the cell. The interaction with CW/membrane target and/or cell internalization induces different downstream effects, all of which contribute to the killing process [88]. RsAFP2 has been shown to remain mainly in the CW, colocalized with Uvitex fluorescent dye which bind to the chitin in fungal walls (Figure 17a). This prudentially localization in the CW has been attributed to the presence of 42% of GlcCer [171]. The PvD_1r, with only an additional methionine in the N-terminus compared to PvD_1, conjugated to FITC, has been shown to colocalize with DAPI, nucleus staining dye, in *C. albicans* cells (Figure 17b, E-H) [163]. This localization may suggest possible intracellular target(s) of PvD_1r, which is a GlcCer-associated defensin. The FITC-conjugated Psd1 has been shown to internalize and disperse in *C. albicans* DAPI-staining cells (Figure 17c, Top) [168]. Lobo and colleagues also reported the internalization of Psd1 in *F. solani* hyphae by colocalization with DAPI. They showed that Psd1 induces the cell cycle arrest by interacting with cyclin F, a cell cycle regulator nucleus protein [172]. For these defensins, e.g., RsAFP2, PvD1, and Psd1 the subcellular localization has been demonstrated to be dependent of the presence of GlcCer in fungal membrane (Figure 17). Indeed, RsAFP2 did not show any localization on Δgcs *C. albicans* mutants [171]. PvD1 and Psd1 were not able to internalize Δgcs *C. albicans* mutants compared to wild-type strains [163, 168].

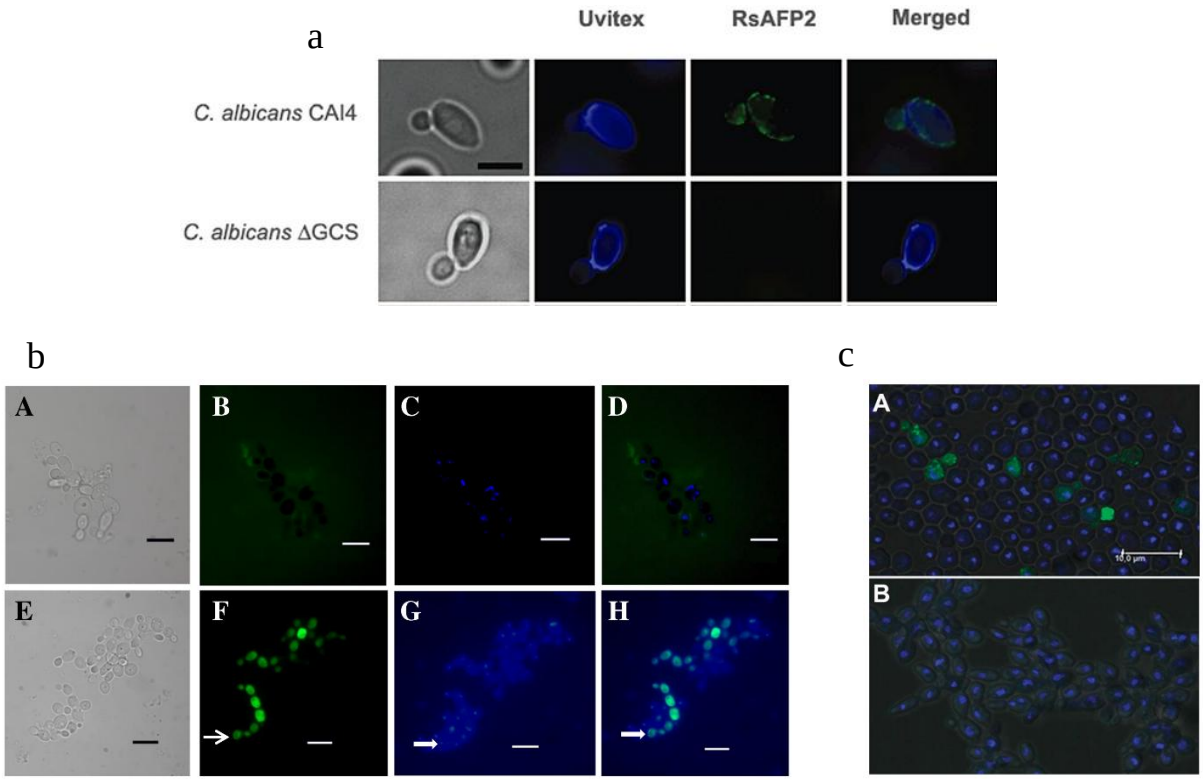

Figure 17: Localization of RsAFP2, PvD1 and Psd1 defensins in *C. albicans* wt and mutant strains lacking GlcCer in their membranes (Δ*gcs*).

(a) Localization of RsAFP2 (50 µg/mL) after 3h at the fungal cell *C. albicans* (CAI4 and Δ*gcs* strains) surface by epifluorescence microscopy and further incubated with Uvitex B2 (blue) and anti-RsAFP2 antibodies in combination with a FITC-labelled goat anti-rabbit IgG (green) [171].
(b) Fluorescence microscopy of *C. albicans* cells treated by FITC-conjugated PvD1r (50 µg/mL). (A-D) Mutant cells; (E-H) Wild-type cells. Cells were incubated for 24 h with FITC-conjugated PvD1r (50 µg/mL) (green fluorescence) (B and F). After the incubation period, the nuclei were stained with DAPI (blue fluorescence) (C and G). Light microscopy (A and E). Overlap of the DAPI and FITC images (D and H). The open arrow shows the FITC labeling (F); the filled arrows show the DAPI nuclei labeling (G) and the colocalization of FITC and DAPI (H) [163].
(c) Confocal fluorescence microscopic images of (A) SC5314 CAI4 *C. albicans* strain treated with 20 µM Psd1 and (B) Δgcs1 *C. albicans* treated with 20 µM Psd1. Green - FITC-conjugated Psd1, Blue - DAPI [168].

Multiple downstream signals leading to cell death may be induced by GlcCer-associated defensins, which include membrane permeabilization, reactive oxygen species (ROS) and /or nitric oxide (NO) induction (oxidative stress), dysregulation of ionic homeostasis and CW integrity pathway activation [88]. RsAFP2 has been shown to induce ROS production in *C. albicans*, which is essential for the initial phase of apoptosis. This ROS induction is a downstream effect of the GlcCer binding event [91]. The defensins PvD1 and AFP1 have also been reported to induce ROS production as part of their antifungal MoAs [159]. Defensins RsAFP2 and MsDef1 have both been demonstrated to activate the CWI pathway and increase classical mitogen-activated protein kinase (MAPK) signaling [104, 108]. RsAFP2 and both *Medicago defensins* MsDef1 and MtDef4 have been reported to disrupt cellular ionic homeostasis. In cells, RsAFP2 induce the influx of Ca^{2+} and efflux of K^{+} [174]. MsDef1 has a potent inhibitor activity specifically of the Cav1.2 (L-type) channel in mammalian cells and can block up to 90% of Ca^{2+} channel activity. Interestingly, MtDef4 defensin showed an activity against fungal cells GlcCer- independent, however its Ca^{2+} modulation activity requires the presence of GlcCer [175].

VI. GlcCer-targeting defensins: ETD151 as a promising example

Targeting an essential component for growth and virulence combining to the multifaceted mechanisms of action, antifungal defensins are highly valuable for reducing the emerging threat of multi-resistant strains. GlcCer-targeting defensins provide therefore an avenue for antifungal therapeutic design and their efficiency have proved beneficial in treating fungal diseases models in animals and plants. Despite this evidence, the development of defensin-based drugs for therapeutic and/or agricultural applications requires solutions to several obstacles, *in vivo* lack of toxicity data, optimized process of their production on a large scale, *in vivo* stability data and last but not least, acceptance of their use as fungicides by farmers.

1. The ETD151 story

Optimization of ETD151 from butterflies defensins

Nosocomial infections (which may include bacteria, fungi and viruses), also called hospital-acquired infections because they occur in patients during their hospital stay, are widespread throughout the world affecting around 15% of all hospitalized patients. In the 2000s, to combat nosocomial infections, French biotech company EntoMed SA drew on the immune system of insects, which are exceptionally resistant to microbes, to develop new antimicrobial molecules.

The ETD151 peptide (EnToMed peptide number 151) was developed in the context of antifungal agents to combat *Candida* spp., *Aspergillus* spp., *Fusarium* spp., and other molds, including *Scedosporium* spp. These fungi are opportunistic pathogens causing nosocomial infections in immunocompromised patients through environmental contamination or from endogenous microflora. These nosocomial fungal infections are difficult to diagnose and lead to high morbidity and mortality despite antifungal treatment. The 44 amino acid peptide called "ETD151" was optimized on the basis of fine mutagenesis, from the two lepidopteran insect antifungal peptides; Heliomicin from *Heliothis virescens*, and ARD1 from *Archeoprepona demophoon*. ETD151 differs from ARD1 by a single N19R mutation and from Heliomicin by two further mutations, D17N and G20A (Figure 16). The 3D structure of ETD151 in solution resolved by NMR is similar to those of Heliomicin and ARD1. It showed a compact fold consisting of a three-stranded antiparallel β-sheet and an α-helix linked by the three conserved disulfide bridges, typical of CSαβ defensins (Figure 18).

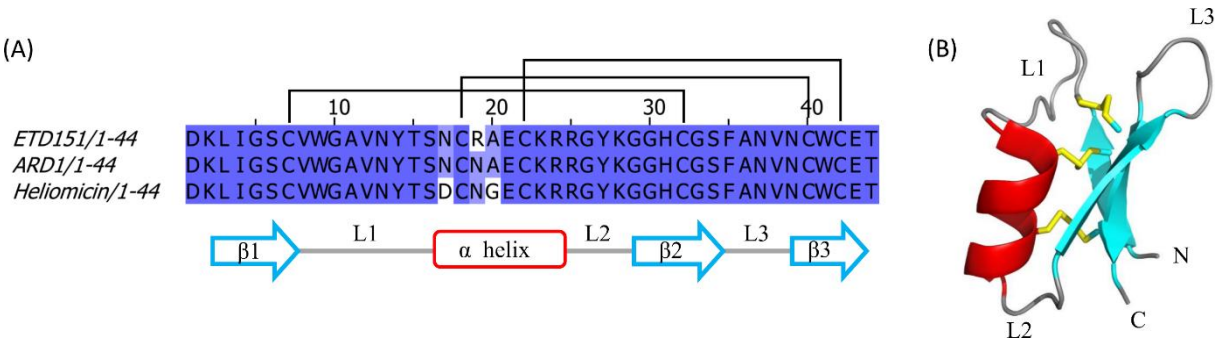

Figure 18: ETD151 Primary sequence, secondary and tertiary structure. (A) Sequence alignment of ETD151, ARD1 and Heliomicin defensins. Conserved residues are highlighted in purple. The secondary structures are shown below. The blue arrows indicate the β-sheet and the red rectangle for the α-helix and L1, L2 and L3 for loop 1, loop 2 and loop 3, respectively. (B) 3D NMR structure of ETD151 (PDB code 1P00 [102]). The α-helix is shown in red, the β-sheet in blue and the disulfide bridges in yellow. C and N indicate the C-terminus and N-terminus, respectively.

The increased of cationicity and hydrophobicity enhanced ETD151's activity against fungal species compared with its analogues. ETD151 is active *in vitro* at micromolar concentrations against a broad range of fungi responsible for systemic fungal infections (Table 9), particularly *Fusarium* and *Scedosporium* [102]. Thanks to the successful large-scale production of ETD151 in *S. cerevisiae*, its *in*

vivo efficacy and toxicity were evaluated. ETD151 administered intravenously proved more effective than amphotericin B, one of the standard treatments for invasive infections, against a murine model infected with *C. albicans* and *A. fumigatus* [176]. In addition, ETD151 proved to be non-toxic, even after systemic administration in mice at doses up to 600 mg/kg.

Table 9: Antifungal activity of ETD151. Data obtained from ref [87, 168]

	ETD151	
Fungal pathogen	IC_{50}(µg/mL)	IC_{50}(µM)
Aspergillus fumigatus	6.25	1,09
Candida albicans	3.12	0,54
Cryptococcus neoformans	1.56	0,27
Lomentospora prolificans	0.1	0,02
Fusarium solani	0.4	0,07
Botrytis cinerea	3.4	0.59

Efficacy of ETD151 against the phytopathogenic fungus Botrytis cinerea

In addition to its efficacy against human fungal pathogens, ETD151 has shown strong growth-inhibiting activity against the phytopathogenic fungus *B. cinerea*. This filamentous fungus is an example of a broad host range necrotrophic pathogen that primarily infects dicotyledonous plants. The best-known disease caused by *B. cinerea* is gray mold. This disease is widespread and causes severe economic damage worldwide. In general, the fungus enters these tissues at an early stage in the crop's development and remains dormant until the environment is favorable and the host's physiology changes. As a result, severe damage is caused during post-harvest storage of apparently healthy crops. *B. cinerea* also causes massive losses in field and greenhouse horticultural crops prior to harvest, mainly in fruits, vegetables, and ornamental flowers [118, 119, 120]. Over the past decade, the situation has worsened with the discovery of multi-resistant strains of *B. cinerea* in the field [121, 122, 123].

To fight this phytopathogenic fungus, new fungicides with innovative mechanisms of action or other approaches using nonchemical items are thus required. Interestingly, ETD151 is a potent inhibitor of the growth of both spore and mycelium forms of *B. cinerea* at µM level [177], which is not the case of neither Heliomicin nor drosomycin, which have a weak activity against the mycelium form of *B. cinerea* [184]. Aumer *et al.* reported that ETD151 induces morphological changes in *B. cinerea* mycelia and lysis of hyphae even after 1h of incubation (Figure 19) [177]. Indeed, the peptide inhibits spore germination and hyphal elongation while at the same time altering the morphology of the fungus.

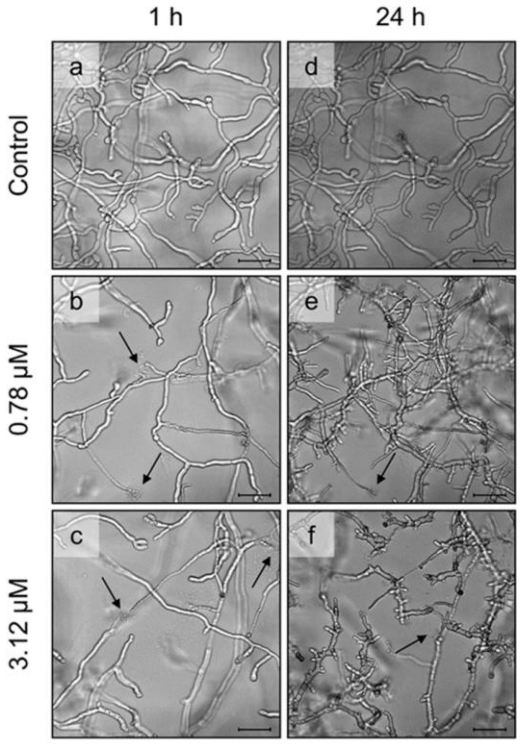

Figure 19: Morphogenic alterations induced by ETD151 in *B. cinerea* mycelia after 1 h and 24 h of incubation (adapted from ref [177]). Untreated mycelia were used as a control experiment (a and d). Mycelia treated with 0.78 µM (b, e) and (c, f) 3.12 µM of ETD151. Arrows indicate the lysis of hyphae. Scale bars, 50 µm.

Dissecting the mechanism of ETD151 action

Understanding the MOA is an important aspect of FDA drug approval, particularly in the documents used to request authorization to conduct phase 2 and 3 clinical trials. Indeed, knowledge of a drug's MOA determines both its therapeutic applications and its potential adverse effects.

ETD151's MOA started to be studied against *B. cinerea* a few years ago (Figure 20), and it has been shown that ETD151 treatment of *B. cinerea* mycelium disrupts 300 proteins belonging to 6 different pathways namely spliceosome, ribosome, protein processing in endoplasmic reticulum, endocytosis, MAPK signaling pathway, and oxidative phosphorylation. However, ETD151 does not have a direct effect on the mitochondrial respiration chain [177]. Furthermore, ETD151 causes membrane disruption in *B. cinerea* mycelia with increasing the impermanent cell dye uptake, Sytox, leading to the release of intracellular content [177]. ETD151 also induces morphogenic alterations in *B. cinerea* by reducing hyphal elongation with a concomitant disorder in hyphal branching. These morphological changes defined ETD151 as a morphogenic defensin of *B. cinerea* [177], likely to a few insect and plant antifungal defensins.

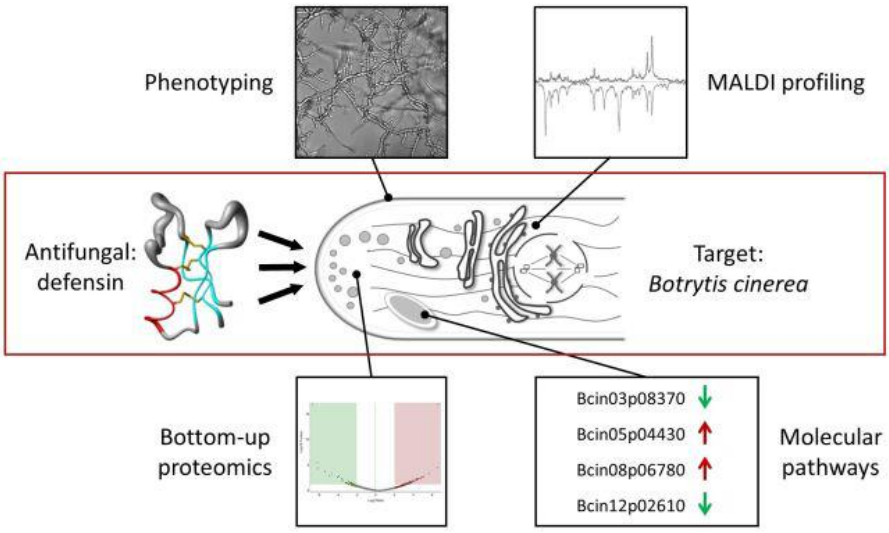

Figure 20: Insights into the MOA of ETD151 on the phytopathogenic fungus *Botrytis cinerea* (adapted from ref [177]).

These mechanistic data highlight that certain actions of ETD151 on *B. cinerea* (e.g. activation of the CWI pathway, morphological changes, membrane disruption) are similar to those reported for plant defensins such as the radish defensin RsAFP2, which may suggest a close mechanism of action. This means that the first step in ETD151's MOA is probably an interaction with a component of the CW/plasma membrane, followed or not by cell internalization.

ETD151 as a promising candidate

All these findings suggest that this cationic, cysteine-rich and non-cytotoxic ETD151 peptide could be a promising antifungal alternative to current conventional drugs for the systemic fungal infection treatment and/or to control phytopathogenic fungi as an environmentally friendly molecule. Moreover, its multifaceted MOA is supposed to have a lower likelihood of causing antifungal resistance. Moreover, its multifaceted mechanism of action is supposed to have a lower probability of causing antifungal resistance. However, further information about its mechanism of action is needed to harness the full potential of ETD151 for diseases control.

2. Aim of my work

The overall aim of this part of my thesis is to decipher the first step in ETD151's mechanism of action at the molecular level by identifying its membrane target and the extent to which the presence of this target is important for ETD151's activity (Chapter 2) and then provide the key elements of the direct *in vitro* interaction between the ETD151 peptide and its molecular target (Chapter 3).

VII. References

[1] G. D. Brown, D. W. Denning, N. A. R. Gow, S. M. Levitz, M. G. Netea, et T. C. White, « Hidden killers: human fungal infections », *Sci Transl Med*, vol. 4, n° 165, p. 165rv13, déc. 2012, doi: 10.1126/scitranslmed.3004404.

[2] F. Bongomin, S. Gago, R. O. Oladele, et D. W. Denning, « Global and Multi-National Prevalence of Fungal Diseases—Estimate Precision », *J Fungi (Basel)*, vol. 3, n° 4, p. 57, oct. 2017, doi: 10.3390/jof3040057.

[3] « WHO fungal priority pathogens list to guide research, development and public health action ». Consulté le: 24 juin 2024. [En ligne]. Disponible sur: https://iris.who.int/bitstream/handle/10665/363682/9789240060241-eng.pdf?sequence=1

[4] A. Rokas, « Evolution of the human pathogenic lifestyle in fungi », *Nat Microbiol*, vol. 7, n° 5, p. 607-619, mai 2022, doi: 10.1038/s41564-022-01112-0.

[5] « Aspergillose », Institut Pasteur. Consulté le: 16 septembre 2024. [En ligne]. Disponible sur: https://www.pasteur.fr/fr/centre-medical/fiches-maladies/aspergillose

[6] M. C. Fisher *et al.*, « Emerging fungal threats to animal, plant and ecosystem health », *Nature*, vol. 484, n° 7393, Art. n° 7393, avr. 2012, doi: 10.1038/nature10947.

[7] R. Dean *et al.*, « The Top 10 fungal pathogens in molecular plant pathology », *Molecular Plant Pathology*, vol. 13, n° 4, Art. n° 4, mai 2012, doi: 10.1111/j.1364-3703.2011.00783.x.

[8] V. S. Brauer *et al.*, « Antifungal Agents in Agriculture: Friends and Foes of Public Health », *Biomolecules*, vol. 9, n° 10, p. 521, sept. 2019, doi: 10.3390/biom9100521.

[9] G. Doehlemann, B. Ökmen, W. Zhu, et A. Sharon, « Plant Pathogenic Fungi », *Microbiology Spectrum*, vol. 5, n° 1, p. 10.1128/microbiolspec.funk-0023-2016, janv. 2017, doi: 10.1128/microbiolspec.funk-0023-2016.

[10] J. Mapuranga, N. Zhang, L. Zhang, J. Chang, et W. Yang, « Infection Strategies and Pathogenicity of Biotrophic Plant Fungal Pathogens », *Front Microbiol*, vol. 13, p. 799396, juin 2022, doi: 10.3389/fmicb.2022.799396.

[11] A. Alzohairy, A. bra, G. Elsharbina, et M. Abohashem, « Characterization of new isolates of some Geophilic yeast from Egypt », 2014.

[12] T. Roemer et D. J. Krysan, « Antifungal Drug Development: Challenges, Unmet Clinical Needs, and New Approaches », *Cold Spring Harb Perspect Med*, vol. 4, n° 5, p. a019703, janv. 2014, doi: 10.1101/cshperspect.a019703.

[13] S. Campoy et J. L. Adrio, « Antifungals », *Biochemical Pharmacology*, vol. 133, p. 86-96, juin 2017, doi: 10.1016/j.bcp.2016.11.019.

[14] Y. Feng, Y. Huang, H. Zhan, P. Bhatt, et S. Chen, « An Overview of Strobilurin Fungicide Degradation:Current Status and Future Perspective », *Front Microbiol*, vol. 11, p. 389, mars 2020, doi: 10.3389/fmicb.2020.00389.

[15] D. Sanglard, « Finding the needle in a haystack: Mapping antifungal drug resistance in fungal pathogen by genomic approaches », *PLoS Pathog*, vol. 15, n° 1, p. e1007478, janv. 2019, doi: 10.1371/journal.ppat.1007478.

[16] L. Ma *et al.*, « Genome analysis of three Pneumocystis species reveals adaptation mechanisms to life exclusively in mammalian hosts », *Nat Commun*, vol. 7, n° 1, p. 10740, févr. 2016, doi: 10.1038/ncomms10740.

[17] G. K. K. Reddy, A. R. Padmavathi, et Y. V. Nancharaiah, « Fungal infections: Pathogenesis, antifungals and alternate treatment approaches », *Curr Res Microb Sci*, vol. 3, p. 100137, avr. 2022, doi: 10.1016/j.crmicr.2022.100137.

[18] M. C. Fisher *et al.*, « Tackling the emerging threat of antifungal resistance to human health », *Nat Rev Microbiol*, vol. 20, n° 9, p. 557-571, sept. 2022, doi: 10.1038/s41579-022-00720-1.

[19] Y. Lee, N. Robbins, et L. E. Cowen, « Molecular mechanisms governing antifungal drug resistance », *NPJ Antimicrob Resist*, vol. 1, n° 1, p. 5, 2023, doi: 10.1038/s44259-023-00007-2.

[20] O. Frenkel, L. Cadle-Davidson, W. F. Wilcox, et M. G. Milgroom, « Mechanisms of Resistance to an Azole Fungicide in the Grapevine Powdery Mildew Fungus, Erysiphe necator », *Phytopathology*, vol. 105, nº 3, p. 370-377, mars 2015, doi: 10.1094/PHYTO-07-14-0202-R.

[21] M. Woods, J. A. McAlister, et J. Geddes-McAlister, « A One Health approach to overcoming fungal disease and antifungal resistance », *WIREs Mechanisms of Disease*, vol. 15, nº 4, p. e1610, 2023, doi: 10.1002/wsbm.1610.

[22] S. R. Lockhart, A. Chowdhary, et J. A. W. Gold, « The rapid emergence of antifungal-resistant human-pathogenic fungi », *Nat Rev Microbiol*, vol. 21, nº 12, p. 818-832, déc. 2023, doi: 10.1038/s41579-023-00960-9.

[23] H. Carolus, S. Pierson, K. Lagrou, et P. Van Dijck, « Amphotericin B and Other Polyenes—Discovery, Clinical Use, Mode of Action and Drug Resistance », *Journal of Fungi*, vol. 6, nº 4, Art. nº 4, déc. 2020, doi: 10.3390/jof6040321.

[24] M. R. Chevallier, R. Jund, et F. Lacroute, « Characterization of cytosine permeation in Saccharomyces cerevisiae », *Journal of Bacteriology*, vol. 122, nº 2, p. 629-641, mai 1975, doi: 10.1128/jb.122.2.629-641.1975.

[25] A. R. Dodgson, K. J. Dodgson, C. Pujol, M. A. Pfaller, et D. R. Soll, « Clade-Specific Flucytosine Resistance Is Due to a Single Nucleotide Change in the FUR1 Gene of Candida albicans », *Antimicrobial Agents and Chemotherapy*, vol. 48, nº 6, p. 2223-2227, juin 2004, doi: 10.1128/aac.48.6.2223-2227.2004.

[26] C. D. Pham *et al.*, « Role of FKS Mutations in Candida glabrata: MIC Values, Echinocandin Resistance, and Multidrug Resistance », *Antimicrobial Agents and Chemotherapy*, vol. 58, nº 8, p. 4690-4696, juill. 2014, doi: 10.1128/aac.03255-14.

[27] S. Park *et al.*, « Specific substitutions in the echinocandin target Fks1p account for reduced susceptibility of rare laboratory and clinical Candida sp. isolates », *Antimicrob Agents Chemother*, vol. 49, nº 8, p. 3264-3273, août 2005, doi: 10.1128/AAC.49.8.3264-3273.2005.

[28] A. Lalève, S. Gamet, A.-S. Walker, D. Debieu, V. Toquin, et S. Fillinger, « Site-directed mutagenesis of the P225, N230 and H272 residues of succinate dehydrogenase subunit B from otrytis cinerea highlights different roles in enzyme activity and inhibitor binding », *Environmental Microbiology*, vol. 16, nº 7, p. 2253-2266, 2014, doi: 10.1111/1462-2920.12282.

[29] S. Saito et C.-L. Xiao, « Understanding resistance to Anilinopyrimidine fungicides », 2023, p. 341-366. doi: 10.19103/AS.2022.0116.13.

[30] C. Q. Zhang, Y. H. Liu, et G. N. Zhu, « Detection and characterization of benzimidazole resistance of Botrytis cinerea in greenhouse vegetables », *Eur J Plant Pathol*, vol. 126, nº 4, p. 509-515, avr. 2010, doi: 10.1007/s10658-009-9557-5.

[31] J. Piszczek, K. Pieczul, et A. Kiniec, « First report of G143A strobilurin resistance in Cercospora beticola in sugar beet (Beta vulgaris) in Poland », *J Plant Dis Prot*, vol. 125, nº 1, p. 99-101, févr. 2018, doi: 10.1007/s41348-017-0119-3.

[32] J. Jiang, L. Ding, T. J. Michailides, H. Li, et Z. Ma, « Molecular characterization of field azoxystrobin-resistant isolates of Botrytis cinerea », *Pesticide Biochemistry and Physiology*, vol. 93, nº 2, p. 72-76, févr. 2009, doi: 10.1016/j.pestbp.2008.11.004.

[33] X. Cui, L. Wang, Y. Lü, et C. Yue, « Development and research progress of anti-drug resistant fungal drugs », *J Infect Public Health*, vol. 15, nº 9, p. 986-1000, sept. 2022, doi: 10.1016/j.jiph.2022.08.004.

[34] G. R. Thompson *et al.*, « Efficacy and safety of rezafungin and caspofungin in candidaemia and invasive candidiasis: pooled data from two prospective randomised controlled trials », *The Lancet Infectious Diseases*, vol. 24, nº 3, p. 319-328, mars 2024, doi: 10.1016/S1473-3099(23)00551-0.

[35] R. Das, K. Kotra, P. Singh, B. Loh, S. Leptihn, et U. Bajpai, « Alternative Treatment Strategies for Secondary Bacterial and Fungal Infections Associated with COVID-19 », *Infect Dis Ther*, vol. 11, nº 1, p. 53-78, févr. 2022, doi: 10.1007/s40121-021-00559-8.

[36] N. de Q. Ribeiro *et al.*, « Atorvastatin as a promising anticryptococcal agent », *Int J Antimicrob Agents*, vol. 49, nº 6, p. 695-702, juin 2017, doi: 10.1016/j.ijantimicag.2017.04.005.

[37] K. Dolan, S. Montgomery, B. Buchheit, L. Didone, M. Wellington, et D. J. Krysan, « Antifungal activity of tamoxifen: in vitro and in vivo activities and mechanistic characterization », *Antimicrob Agents Chemother*, vol. 53, nº 8, p. 3337-3346, août 2009, doi: 10.1128/AAC.01564-08.

[38] R. G. Vitale, « Role of Antifungal Combinations in Difficult to Treat Candida Infections », *Journal of Fungi*, vol. 7, nº 9, Art. nº 9, sept. 2021, doi: 10.3390/jof7090731.

[39] M. Cuenca-Estrella, « Combinations of antifungal agents in therapy–what value are they? », *Journal of Antimicrobial Chemotherapy*, vol. 54, nº 5, p. 854-869, nov. 2004, doi: 10.1093/jac/dkh434.

[40] S. K. Shrestha, M. Y. Fosso, et S. Garneau-Tsodikova, « A combination approach to treating fungal infections », *Sci Rep*, vol. 5, nº 1, p. 17070, nov. 2015, doi: 10.1038/srep17070.

[41] S. E. Jacobs, P. Zagaliotis, et T. J. Walsh, « Novel antifungal agents in clinical trials », *F1000Res*, vol. 10, p. 507, janv. 2022, doi: 10.12688/f1000research.28327.2.

[42] T. J. Gintjee, M. A. Donnelley, et G. R. Thompson, « Aspiring Antifungals: Review of Current Antifungal Pipeline Developments », *Journal of Fungi*, vol. 6, nº 1, Art. nº 1, mars 2020, doi: 10.3390/jof6010028.

[43] T. P. McCarty et P. G. Pappas, « Antifungal Pipeline », *Front. Cell. Infect. Microbiol.*, vol. 11, sept. 2021, doi: 10.3389/fcimb.2021.732223.

[44] J. Mitsuyama *et al.*, « In Vitro and In Vivo Antifungal Activities of T-2307, a Novel Arylamidine », *Antimicrobial Agents and Chemotherapy*, vol. 52, nº 4, p. 1318-1324, avr. 2008, doi: 10.1128/aac.01159-07.

[45] K. Yamashita *et al.*, « The Novel Arylamidine T-2307 Selectively Disrupts Yeast Mitochondrial Function by Inhibiting Respiratory Chain Complexes », *Antimicrobial Agents and Chemotherapy*, vol. 63, nº 8, p. 10.1128/aac.00374-19, juill. 2019, doi: 10.1128/aac.00374-19.

[46] H. M *et al.*, « The Antifungal Pipeline: Fosmanogepix, Ibrexafungerp, Olorofim, Opelconazole, and Rezafungin », *Drugs*, vol. 81, nº 15, oct. 2021, doi: 10.1007/s40265-021-01611-0.

[47] A. Nicola *et al.*, « Antifungal drugs: New insights in research & development », *Pharmacology & Therapeutics*, vol. 195, oct. 2018, doi: 10.1016/j.pharmthera.2018.10.008.

[48] M. Ademe, « Immunomodulation for the Treatment of Fungal Infections: Opportunities and Challenges », *Front Cell Infect Microbiol*, vol. 10, p. 469, 2020, doi: 10.3389/fcimb.2020.00469.

[49] Q. H. Sam, W. S. Yew, C. J. Seneviratne, M. W. Chang, et L. Y. A. Chai, « Immunomodulation as Therapy for Fungal Infection: Are We Closer? », *Front Microbiol*, vol. 9, p. 1612, 2018, doi: 10.3389/fmicb.2018.01612.

[50] A. Rachini *et al.*, « An Anti- -Glucan Monoclonal Antibody Inhibits Growth and Capsule Formation of Cryptococcus neoformans In Vitro and Exerts Therapeutic, Anticryptococcal Activity In Vivo », *Infection and immunity*, vol. 75, p. 5085-94, janv. 2007, doi: 10.1128/IAI.00278-07.

[51] R. C. Matthews *et al.*, « Preclinical Assessment of the Efficacy of Mycograb, a Human Recombinant Antibody against Fungal HSP90 », *Antimicrobial Agents and Chemotherapy*, vol. 47, nº 7, p. 2208-2216, juill. 2003, doi: 10.1128/aac.47.7.2208-2216.2003.

[52] M. Fernández de Ullivarri, S. Arbulu, E. Garcia-Gutierrez, et P. D. Cotter, « Antifungal Peptides as Therapeutic Agents », *Front. Cell. Infect. Microbiol.*, vol. 10, mars 2020, doi: 10.3389/fcimb.2020.00105.

[53] B. P. H. J. Thomma, B. P. A. Cammue, et K. Thevissen, « Mode of Action of Plant Defensins Suggests Therapeutic Potential », *Current Drug Targets - Infectious Disorders*, vol. 3, nº 1, p. 1-8, mars 2003, doi: 10.2174/1568005033342000.

[54] G. S. Dijksteel, M. M. W. Ulrich, E. Middelkoop, et B. K. H. L. Boekema, « Review: Lessons Learned From Clinical Trials Using Antimicrobial Peptides (AMPs) », *Front. Microbiol.*, vol. 12, févr. 2021, doi: 10.3389/fmicb.2021.616979.

[55] D. Rothstein *et al.*, « Anticandida Activity Is Retained in P-113, a 12-Amino-Acid Fragment of Histatin 5 », *Antimicrobial agents and chemotherapy*, vol. 45, p. 1367-73, mai 2001, doi: 10.1128/AAC.45.5.1367-1373.2001.

[56] W. S. Jang, X. S. Li, J. N. Sun, et M. Edgerton, « The P-113 Fragment of Histatin 5 Requires a Specific Peptide Sequence for Intracellular Translocation in Candida albicans, Which Is Independent of Cell Wall Binding », *Antimicrobial Agents and Chemotherapy*, vol. 52, nº 2, p. 497-504, févr. 2008, doi: 10.1128/aac.01199-07.

[57] D. Mercer, J. Robertson, L. Miller, C. Stewart, et D. O'Neil, « NP213 (Novexatin®): A unique therapy candidate for onychomycosis with a differentiated safety and efficacy profile », *Medical mycology*, vol. 58, mars 2020, doi: 10.1093/mmy/myaa015.

[58] B. P. H. J. Thomma, B. P. A. Cammue, et K. Thevissen, « Plant defensins », *Planta*, vol. 216, nº 2, p. 193-202, déc. 2002, doi: 10.1007/s00425-002-0902-6.

[59] B. Cornet, J. M. Bonmatin, C. Hetru, J. A. Hoffmann, M. Ptak, et F. Vovelle, « Refined three-dimensional solution structure of insect defensin A », *Structure*, vol. 3, nº 5, p. 435-448, mai 1995, doi: 10.1016/s0969-2126(01)00177-0.

[60] K. Thevissen, H.-H. Kristensen, B. P. H. J. Thomma, B. P. A. Cammue, et I. E. J. A. François, « Therapeutic potential of antifungal plant and insect defensins », *Drug Discovery Today*, vol. 12, nº 21-22, p. 966-971, nov. 2007, doi: 10.1016/j.drudis.2007.07.016.

[61] N. Robbins, G. D. Wright, et L. E. Cowen, « Antifungal Drugs: The Current Armamentarium and Development of New Agents », *Microbiology Spectrum*, vol. 4, nº 5, p. 10.1128/microbiolspec.funk-0002-2016, oct. 2016, doi: 10.1128/microbiolspec.funk-0002-2016.

[62] V. Leannec-Rialland, V. Atanasova, S. Chereau, M. Tonk-Rügen, A. Cabezas-Cruz, et F. Richard-Forget, « Use of Defensins to Develop Eco-Friendly Alternatives to Synthetic Fungicides to Control Phytopathogenic Fungi and Their Mycotoxins », *Journal of Fungi*, vol. 8, nº 3, Art. nº 3, mars 2022, doi: 10.3390/jof8030229.

[63] W. F. Broekaert *et al.*, « Antimicrobial Peptides from Plants », *Critical Reviews in Plant Sciences*, vol. 16, nº 3, p. 297-323, janv. 1997, doi: 10.1080/07352689709701952.

[64] W. F. Broekaert, FRG. Terras, BPA. Cammue, et R. W. Osborn, « Plant Defensins: Novel Antimicrobial Peptides as Components of the Host Defense System », *Plant Physiology*, vol. 108, nº 4, p. 1353-1358, août 1995, doi: 10.1104/pp.108.4.1353.

[65] F. Lay et M. Anderson, « Defensins - Components of the Innate Immune System in Plants », *CPPS*, vol. 6, nº 1, p. 85-101, févr. 2005, doi: 10.2174/1389203053027575.

[66] P. Silva, S. Goncalves, et N. Santos, « Defensins: Antifungal lessons from eukaryotes », *Frontiers in microbiology*, vol. 5, p. 97, mars 2014, doi: 10.3389/fmicb.2014.00097.

[67] K. Vriens, B. P. A. Cammue, et K. Thevissen, « Antifungal Plant Defensins: Mechanisms of Action and Production », *Molecules*, vol. 19, nº 8, Art. nº 8, août 2014, doi: 10.3390/molecules190812280.

[68] P. B. Pelegrini, F. T. Lay, A. M. Murad, M. A. Anderson, et O. L. Franco, « Novel insights on the mechanism of action of α-amylase inhibitors from the plant defensin family », *Proteins: Structure, Function, and Bioinformatics*, vol. 73, nº 3, p. 719-729, 2008, doi: 10.1002/prot.22086.

[69] A. E. Sathoff et D. A. Samac, « Antibacterial Activity of Plant Defensins », 2019.

[70] M. A. Anderson et M. R. Bleackley, « Salt-Tolerant Antifungal and Antibacterial Activities of the Corn Defensin ZmD32 », *Frontiers in Microbiology*, vol. 10, 2019.

[71] A. E. Sathoff, S. Velivelli, D. M. Shah, et D. A. Samac, « Plant Defensin Peptides have Antifungal and Antibacterial Activity Against Human and Plant Pathogens », *Phytopathology®*, vol. 109, nº 3, p. 402-408, mars 2019, doi: 10.1094/PHYTO-09-18-0331-R.

[72] A. E. Sathoff, « Plant defensin antibacterial mode of action against Pseudomonas species », 2020.

[73] P. Bulet et R. Stöcklin, « Insect antimicrobial peptides: structures, properties and gene regulation », *Protein Pept Lett*, vol. 12, nº 1, p. 3-11, janv. 2005, doi: 10.2174/0929866053406011.

[74] R. G. Spelbrink, N. Dilmac, A. Allen, T. J. Smith, D. M. Shah, et G. H. Hockerman, « Differential Antifungal and Calcium Channel-Blocking Activity among Structurally Related Plant

Defensins », *Plant Physiology*, vol. 135, nº 4, p. 2055-2067, août 2004, doi: 10.1104/pp.104.040873.

[75] J. Skalska *et al.*, « Plant defensin PvD1 modulates the membrane composition of breast tumour-derived exosomes », *Nanoscale*, vol. 11, nº 48, p. 23366-23381, déc. 2019, doi: 10.1039/C9NR07843F.

[76] V. S. G. do Amaral *et al.*, « Pisum sativum Defensin 1 Eradicates Mouse Metastatic Lung Nodules from B16F10 Melanoma Cells », *Int J Mol Sci*, vol. 21, nº 8, p. 2662, avr. 2020, doi: 10.3390/ijms21082662.

[77] F. R. Terras *et al.*, « Analysis of two novel classes of plant antifungal proteins from radish (Raphanus sativus L.) seeds. », *J. Biol. Chem.*, vol. 267, nº 22, Art. nº 22, mai 1992.

[78] K. Vriens *et al.*, « The radish defensins RsAFP1 and RsAFP2 act synergistically with caspofungin against Candida albicans biofilms », *Peptides*, vol. 75, p. 71-79, janv. 2016, doi: 10.1016/j.peptides.2015.11.001.

[79] P. M. Tavares *et al.*, « In Vitro Activity of the Antifungal Plant Defensin RsAFP2 against Candida Isolates and Its In Vivo Efficacy in Prophylactic Murine Models of Candidiasis », *Antimicrobial Agents and Chemotherapy*, vol. 52, p. 4522-4525, 2008, doi: 10.1128/AAC.00448-08.

[80] F. T. Lay, H. J. Schirra, M. J. Scanlon, M. A. Anderson, et D. J. Craik, « The Three-dimensional Solution Structure of NaD1, a New Floral Defensin from Nicotiana alata and its Application to a Homology Model of the Crop Defense Protein alfAFP », *Journal of Molecular Biology*, vol. 325, nº 1, Art. nº 1, janv. 2003, doi: 10.1016/S0022-2836(02)01103-8.

[81] V. Ramamoorthy, E. B. Cahoon, J. Li, M. Thokala, R. E. Minto, et D. M. Shah, « Glucosylceramide synthase is essential for alfalfa defensin-mediated growth inhibition but not for pathogenicity of Fusarium graminearum », *Molecular Microbiology*, vol. 66, nº 3, p. 771-786, 2007, doi: 10.1111/j.1365-2958.2007.05955.x.

[82] M. S. Almeida, K. M. S. Cabral, E. Kurtenbach, F. C. L. Almeida, et A. P. Valente, « Solution structure of Pisum sativum defensin 1 by high resolution NMR: plant defensins, identical backbone with different mechanisms of action », *Journal of Molecular Biology*, vol. 315, nº 4, Art. nº 4, janv. 2002, doi: 10.1006/jmbi.2001.5252.

[83] K. Vriens *et al.*, « Synergistic Activity of the Plant Defensin HsAFP1 and Caspofungin against Candida albicans Biofilms and Planktonic Cultures », *PLOS ONE*, vol. 10, nº 8, Art. nº 8, août 2015, doi: 10.1371/journal.pone.0132701.

[84] H. U. Stotz, J. Thomson, et Y. Wang, « Plant defensins: Defense, development and application », *Plant Signaling & Behavior*, vol. 4, nº 11, p. 1010-1012, nov. 2009, doi: 10.4161/psb.4.11.9755.

[85] A. F. Lacerda, É. A. R. Vasconcelos, et P. B. Pelegrini, « Antifungal defensins and their role in plant defense. », *Frontiers in Microbiology*, 2014.

[86] U. S. Sagaram *et al.*, « Structural and Functional Studies of a Phosphatidic Acid-Binding Antifungal Plant Defensin MtDef4: Identification of an RGFRRR Motif Governing Fungal Cell Entry », *PLOS ONE*, vol. 8, nº 12, p. e82485, déc. 2013, doi: 10.1371/journal.pone.0082485.

[87] F. T. Lay *et al.*, « Dimerization of plant defensin NaD1 enhances its antifungal activity », *J Biol Chem*, vol. 287, nº 24, p. 19961-19972, juin 2012, doi: 10.1074/jbc.M111.331009.

[88] T. L. Cools, C. Struyfs, B. P. Cammue, et K. Thevissen, « Antifungal plant defensins: increased insight in their mode of action as a basis for their use to combat fungal infections », *Future Microbiology*, vol. 12, nº 5, Art. nº 5, mars 2017, doi: 10.2217/fmb-2016-0181.

[89] K. Parisi, T. M. A. Shafee, P. Quimbar, N. L. van der Weerden, M. R. Bleackley, et M. A. Anderson, « The evolution, function and mechanisms of action for plant defensins », *Seminars in Cell & Developmental Biology*, févr. 2018, doi: 10.1016/j.semcdb.2018.02.004.

[90] K. Thevissen *et al.*, « Defensins from Insects and Plants Interact with Fungal Glucosylceramides », *J. Biol. Chem.*, vol. 279, nº 6, Art. nº 6, juin 2004, doi: 10.1074/jbc.M311165200.

[91] A. M. Aerts, I. E. J. A. François, E. M. K. Meert, Q.-T. Li, B. P. A. Cammue, et K. Thevissen, « The Antifungal Activity of RsAFP2, a Plant Defensin from Raphanus sativus, Involves the Induction

of Reactive Oxygen Species in Candida albicans », *MMB*, vol. 13, nº 4, Art. nº 4, 2007, doi: 10.1159/000104753.

[92] K. Thevissen *et al.*, « The plant defensin RsAFP2 induces cell wall stress, septin mislocalization and accumulation of ceramides in Candida albicans », *Molecular Microbiology*, vol. 84, nº 1, Art. nº 1, 2012, doi: 10.1111/j.1365-2958.2012.08017.x.

[93] N. L. van der Weerden, R. E. W. Hancock, et M. A. Anderson, « Permeabilization of Fungal Hyphae by the Plant Defensin NaD1 Occurs through a Cell Wall-dependent Process », *J. Biol. Chem.*, vol. 285, nº 48, Art. nº 48, nov. 2010, doi: 10.1074/jbc.M110.134882.

[94] B. M. E. Hayes, M. R. Bleackley, J. L. Wiltshire, M. A. Anderson, A. Traven, et N. L. van der Weerden, « Identification and Mechanism of Action of the Plant Defensin NaD1 as a New Member of the Antifungal Drug Arsenal against Candida albicans », *Antimicrobial Agents and Chemotherapy*, vol. 57, nº 8, Art. nº 8, août 2013, doi: 10.1128/AAC.00365-13.

[95] J. A. E. Payne *et al.*, « The plant defensin NaD1 introduces membrane disorder through a specific interaction with the lipid, phosphatidylinositol 4,5 bisphosphate », *Biochimica et Biophysica Acta (BBA) - Biomembranes*, vol. 1858, nº 6, Art. nº 6, juin 2016, doi: 10.1016/j.bbamem.2016.02.016.

[96] R. G. Spelbrink, N. Dilmac, A. Allen, T. J. Smith, D. M. Shah, et G. H. Hockerman, « Differential Antifungal and Calcium Channel-Blocking Activity among Structurally Related Plant Defensins », *Plant Physiology*, vol. 135, nº 4, Art. nº 4, août 2004, doi: 10.1104/pp.104.040873.

[97] V. Ramamoorthy, E. B. Cahoon, J. Li, M. Thokala, R. E. Minto, et D. M. Shah, « Glucosylceramide synthase is essential for alfalfa defensin-mediated growth inhibition but not for pathogenicity of Fusarium graminearum », *Molecular Microbiology*, vol. 66, nº 3, Art. nº 3, nov. 2007, doi: 10.1111/j.1365-2958.2007.05955.x.

[98] M. J. A. Hein, M. Kvansakul, F. T. Lay, T. K. Phan, et M. D. Hulett, « Defensin–lipid interactions in membrane targeting: mechanisms of action and opportunities for the development of antimicrobial and anticancer therapeutics », *Biochemical Society Transactions*, vol. 50, nº 1, p. 423-437, janv. 2022, doi: 10.1042/BST20200884.

[99] P. Bulet, « Les peptides antimicrobiens de la drosophile. », *Med Sci (Paris)*, vol. 15, nº 1, p. 23, 1999, doi: 10.4267/10608/1192.

[100] M. Lamberty *et al.*, « Insect immunity. Isolation from the lepidopteran Heliothis virescens of a novel insect defensin with potent antifungal activity », *J Biol Chem*, vol. 274, nº 14, p. 9320-9326, avr. 1999, doi: 10.1074/jbc.274.14.9320.

[101] P. Fehlbaum *et al.*, « Insect immunity: Septic injury of Drosophila induces the synthesis of a potent antifungal peptide with sequence homology to plant antifungal peptides. », *J. Biol. Chem.*, vol. 269, nº 52, Art. nº 52, déc. 1994.

[102] C. Landon *et al.*, « Lead optimization of antifungal peptides with 3D NMR structures analysis », *Protein Science*, vol. 13, nº 3, Art. nº 3, mars 2004, doi: 10.1110/ps.03404404.

[103] M. Lamberty *et al.*, « Insect immunity. Constitutive expression of a cysteine-rich antifungal and a linear antibacterial peptide in a termite insect », *J. Biol. Chem.*, vol. 276, nº 6, Art. nº 6, sept. 2001, doi: 10.1074/jbc.M002998200.

[104] B. Schuhmann, V. Seitz, A. Vilcinskas, et L. Podsiadlowski, « Cloning and expression of gallerimycin, an antifungal peptide expressed in immune response of greater wax moth larvae, Galleria mellonella », *Archives of Insect Biochemistry and Physiology*, vol. 53, nº 3, Art. nº 3, juill. 2003, doi: 10.1002/arch.10091.

[105] Y. S. Lee *et al.*, « Purification, cDNA cloning and expression of an insect defensin from the great wax moth, Galleria mellonella », *Insect Molecular Biology*, vol. 13, nº 1, Art. nº 1, févr. 2004, doi: 10.1111/j.1365-2583.2004.00462.x.

[106] M. Cytryńska, P. Mak, A. Zdybicka-Barabas, P. Suder, et T. Jakubowicz, « Purification and characterization of eight peptides from Galleria mellonella immune hemolymph », *Peptides*, vol. 28, nº 3, Art. nº 3, mars 2007, doi: 10.1016/j.peptides.2006.11.010.

[107] C. Landon, P. Sodano, C. Hetru, J. Hoffmann, et M. Ptak, « Solution structure of drosomycin, the first inducible antifungal protein from insects », *Protein Science*, vol. 6, n° 9, Art. n° 9, sept. 1997, doi: 10.1002/pro.5560060908.

[108] N. Banzet, M.-P. Latorse, P. Bulet, E. François, C. Derpierre, et M. Dubald, « Expression of insect cystein-rich antifungal peptides in transgenic tobacco enhances resistance to a fungal disease », *Plant Science*, vol. 162, n° 6, Art. n° 6, juin 2002, doi: 10.1016/S0168-9452(02)00053-5.

[109] J. Lee *et al.*, « Coprisin-induced antifungal effects in Candida albicans correlate with apoptotic mechanisms », *Free radical biology & medicine*, vol. 52, p. 2302-11, avr. 2012, doi: 10.1016/j.freeradbiomed.2012.03.012.

[110] P. Da Silva, L. Jouvensal, M. Lamberty, P. Bulet, A. Caille, et F. Vovelle, « Solution structure of termicin, an antimicrobial peptide from the termite Pseudacanthotermes spiniger », *Protein Science*, vol. 12, n° 3, p. 438-446, 2003, doi: 10.1110/ps.0228303.

[111] M. Lamberty *et al.*, « Solution structures of the antifungal heliomicin and a selected variant with both antibacterial and antifungal activities », *Biochemistry*, vol. 40, n° 40, Art. n° 40, oct. 2001, doi: 10.1021/bi0103563.

[112] C. Landon, P. Sodano, C. Hetru, J. Hoffmann, et M. Ptak, « Solution structure of drosomycin, the first inducible antifungal protein from insects », *Protein Science*, vol. 6, n° 9, p. 1878-1884, 1997, doi: 10.1002/pro.5560060908.

[113] P. Da Silva, L. Jouvensal, M. Lamberty, P. Bulet, A. Caille, et F. Vovelle, « Solution structure of termicin, an antimicrobial peptide from the termite Pseudacanthotermes spiniger », *Protein Science*, vol. 12, n° 3, Art. n° 3, mars 2003, doi: 10.1110/ps.0228303.

[114] E. Lee *et al.*, « Insight into the antimicrobial activities of coprisin isolated from the dung beetle, Copris tripartitus, revealed by structure-activity relationships », *Biochimica et biophysica acta*, vol. 1828, nov. 2012, doi: 10.1016/j.bbamem.2012.10.028.

[115] M. Lamberty *et al.*, « Solution structures of the antifungal heliomicin and a selected variant with both antibacterial and antifungal activities », *Biochemistry*, vol. 40, n° 40, p. 11995-12003, oct. 2001, doi: 10.1021/bi0103563.

[116] C. Landon, F. Vovelle, P. Sodano, et A. Pajon, « The active site of drosomycin, a small insect antifungal protein, delineated by comparison with the modeled structure of Rs-AFP2, a plant antifungal protein », *The Journal of Peptide Research*, vol. 56, n° 4, p. 231-238, 2000, doi: 10.1034/j.1399-3011.2000.00757.x.

[117] Z. Zhang et S. Zhu, « Functional role of charged residues in drosomycin, a Drosophila antifungal peptide », *Dev Comp Immunol*, vol. 34, n° 9, p. 953-958, sept. 2010, doi: 10.1016/j.dci.2010.04.003.

[118] X.-X. Xu *et al.*, « An anionic defensin from Plutella xylostella with potential activity against Bacillus thuringiensis », *Bull. Entomol. Res.*, vol. 106, n° 6, p. 790-800, déc. 2016, doi: 10.1017/S0007485316000596.

[119] M. Lamberty *et al.*, « Insect Immunity: constitutive expression of a cysteine-rich antifungal and a linear antibacterial peptide in a termite insect. », *Journal of Biological Chemistry*, vol. 276, n° 6, p. 4085-4092, févr. 2001, doi: 10.1074/jbc.M002998200.

[120] D. G. Sant, S. G. Tupe, C. V. Ramana, et M. V. Deshpande, « Fungal cell membrane-promising drug target for antifungal therapy », *J Appl Microbiol*, vol. 121, n° 6, p. 1498-1510, déc. 2016, doi: 10.1111/jam.13301.

[121] C. M. Fernandes, G. H. Goldman, et M. Del Poeta, « Biological Roles Played by Sphingolipids in Dimorphic and Filamentous Fungi », *mBio*, vol. 9, n° 3, p. e00642-18, mai 2018, doi: 10.1128/mBio.00642-18.

[122] C. Jiang, J. Ge, B. He, et B. Zeng, « Glycosphingolipids in Filamentous Fungi: Biological Roles and Potential Applications in Cosmetics and Health Foods », *Frontiers in Microbiology*, vol. 12, 2021, Consulté le: 2 février 2022. [En ligne]. Disponible sur: https://www.frontiersin.org/article/10.3389/fmicb.2021.690211

[123] A. Singh et M. Del Poeta, « Sphingolipidomics: An Important Mechanistic Tool for Studying Fungal Pathogens », *Front Microbiol*, vol. 7, p. 501, avr. 2016, doi: 10.3389/fmicb.2016.00501.
[124] M. Del Poeta, L. Nimrichter, M. L. Rodrigues, et C. Luberto, « Synthesis and Biological Properties of Fungal Glucosylceramide », *PLoS Pathog*, vol. 10, nº 1, p. e1003832, janv. 2014, doi: 10.1371/journal.ppat.1003832.
[125] E. Barreto-Bergter, G. L. Sassaki, et L. M. de Souza, « Structural Analysis of Fungal Cerebrosides », *Front Microbiol*, vol. 2, p. 239, déc. 2011, doi: 10.3389/fmicb.2011.00239.
[126] M. H. S. Villas Boas, H. Egge, G. Pohlentz, R. Hartmann, et E. Barreto Bergter, « Structural determination of N-2'-hydroxyoctadecenoyl-1-O-β-d-glucopyranosyl-9-methyl-4, 8-sphingadienine from species of Aspergillus », *Chemistry and Physics of Lipids*, vol. 70, nº 1, p. 11-19, mars 1994, doi: 10.1016/0009-3084(94)90043-4.
[127] T. Matsubara, A. Hayashi, Y. Banno, T. Morita, et Y. Nozawa, « Cerebroside of the dimorphic human pathogen, *Candida albicans* », *Chemistry and Physics of Lipids*, vol. 43, nº 1, p. 1-12, janv. 1987, doi: 10.1016/0009-3084(87)90012-0.
[128] M. Rodrigues *et al.*, « Human Antibodies against a Purified Glucosylceramide from Cryptococcus neoformans Inhibit Cell Budding and Fungal Growth », *Infection and Immunity*, vol. 68, p. 7049-7060, 2000, doi: 10.1128/IAI.68.12.7049-7060.2000.
[129] M. I. D. da S. Xisto *et al.*, « Glucosylceramides From Lomentospora prolificans Induce a Differential Production of Cytokines and Increases the Microbicidal Activity of Macrophages », *Front. Microbiol.*, vol. 10, mars 2019, doi: 10.3389/fmicb.2019.00554.
[130] R. S. Duarte, C. R. Polycarpo, R. Wait, R. Hartmann, et E. Barreto Bergter, « Structural characterization of neutral glycosphingolipids from *Fusarium* species », *Biochimica et Biophysica Acta (BBA) - Lipids and Lipid Metabolism*, vol. 1390, nº 2, p. 186-196, févr. 1998, doi: 10.1016/S0005-2760(97)00179-3.
[131] P. Ternes *et al.*, « Two pathways of sphingolipid biosynthesis are separated in the yeast Pichia pastoris », *J Biol Chem*, vol. 286, nº 13, p. 11401-11414, avr. 2011, doi: 10.1074/jbc.M110.193094.
[132] P. Ternes *et al.*, « Two Pathways of Sphingolipid Biosynthesis Are Separated in the Yeast Pichia pastoris », *J. Biol. Chem.*, vol. 286, nº 13, Art. nº 13, janv. 2011, doi: 10.1074/jbc.M110.193094.
[133] S. M. Noble, S. French, L. A. Kohn, V. Chen, et A. D. Johnson, « Systematic screens of a Candida albicans homozygous deletion library decouple morphogenetic switching and pathogenicity », *Nat Genet*, vol. 42, nº 7, p. 590-598, juill. 2010, doi: 10.1038/ng.605.
[134] P. C. Rittershaus *et al.*, « Glucosylceramide synthase is an essential regulator of pathogenicity of *Cryptococcus neoformans* », *J Clin Invest*, vol. 116, nº 6, Art. nº 6, juin 2006, doi: 10.1172/JCI27890.
[135] J. Wang *et al.*, « Loss of glucosylceramide synthase impairs the growth and virulence of Fusarium oxysporum f. sp. cubense », *Phytopathology Research*, vol. 4, nº 1, p. 31, août 2022, doi: 10.1186/s42483-022-00136-y.
[136] Y. Huang *et al.*, « CgGCS, Encoding a Glucosylceramide Synthase, Is Required for Growth, Conidiation and Pathogenicity in Colletotrichum gloeosporioides », *Front Microbiol*, vol. 10, p. 1016, mai 2019, doi: 10.3389/fmicb.2019.01016.
[137] C. Zhu *et al.*, « Glucosylceramides are required for mycelial growth and full virulence in *Penicillium digitatum* », *Biochemical and Biophysical Research Communications*, vol. 455, nº 3, p. 165-171, déc. 2014, doi: 10.1016/j.bbrc.2014.10.142.
[138] V. Rochetti, R. Rollin Pinheiro, E. Oliveira, M. Xisto, et E. Barreto-Bergter, « Glucosylceramide Plays a Role in Fungal Germination, Lipid Raft Organization and Biofilm Adhesion of the Pathogenic Fungus Scedosporium aurantiacum », *Journal of Fungi*, vol. 6, p. 345, déc. 2020, doi: 10.3390/jof6040345.
[139] S. Raj *et al.*, « Changes in glucosylceramide structure affect virulence and membrane biophysical properties of Cryptococcus neoformans », *Biochimica et Biophysica Acta (BBA) - Biomembranes*, vol. 1859, nº 11, p. 2224-2233, nov. 2017, doi: 10.1016/j.bbamem.2017.08.017.

[140] C. Fernandes *et al.*, « Functional characterization of the Aspergillus nidulans glucosylceramide pathway reveals that LCB Δ8-desaturation and C9-methylation are relevant to filamentous growth, lipid raft localization and Psd1 defensin activity », *Mol Microbiol*, vol. 102, nº 3, p. 488-505, nov. 2016, doi: 10.1111/mmi.13474.
[141] P. Ternes *et al.*, « Identification of Fungal Sphingolipid C9-methyltransferases by Phylogenetic Profiling », *J. Biol. Chem.*, vol. 281, nº 9, Art. nº 9, mars 2006, doi: 10.1074/jbc.M512864200.
[142] T. Oura et S. Kajiwara, « Candida albicans sphingolipid C9-methyltransferase is involved in hyphal elongation. », *Microbiology*, vol. 156 Pt 4, p. 1234-43, 2010, doi: 10.1099/mic.0.033985-0.
[143] V. Ramamoorthy, E. B. Cahoon, M. Thokala, J. Kaur, J. Li, et D. M. Shah, « Sphingolipid C-9 Methyltransferases Are Important for Growth and Virulence but Not for Sensitivity to Antifungal Plant Defensins in Fusarium graminearum », *Eukaryotic Cell*, vol. 8, nº 2, p. 217-229, févr. 2009, doi: 10.1128/EC.00255-08.
[144] A. Huber *et al.*, « Membrane Sphingolipids Regulate the Fitness and Antifungal Protein Susceptibility of Neurospora crassa », *Front Microbiol*, vol. 10, p. 605, 2019, doi: 10.3389/fmicb.2019.00605.
[145] A. Singh *et al.*, « Methylation of glycosylated sphingolipid modulates membrane lipid topography and pathogenicity of Cryptococcus neoformans », *Cellular Microbiology*, vol. 14, nº 4, p. 500-516, 2012, doi: 10.1111/j.1462-5822.2011.01735.x.
[146] R. Rollin-Pinheiro, A. Singh, E. Barreto-Bergter, et M. Del Poeta, « Sphingolipids as targets for treatment of fungal infections », *Future Medicinal Chemistry*, vol. 8, nº 12, p. 1469-1484, août 2016, doi: 10.4155/fmc-2016-0053.
[147] K. McEvoy, T. G. Normile, et M. Del Poeta, « Antifungal Drug Development: Targeting the Fungal Sphingolipid Pathway », *J Fungi (Basel)*, vol. 6, nº 3, p. 142, août 2020, doi: 10.3390/jof6030142.
[148] K. McEvoy, T. G. Normile, et M. Poeta, « Antifungal Drug Development: Targeting the Fungal Sphingolipid Pathway », *Journal of Fungi*, vol. 6, p. null, 2020, doi: 10.3390/jof6030142.
[149] S. B. Levery *et al.*, « Disruption of the glucosylceramide biosynthetic pathway in *Aspergillus nidulans* and *Aspergillus fumigatus* by inhibitors of UDP-Glc:ceramide glucosyltransferase strongly affects spore germination, cell cycle, and hyphal growth », *FEBS Letters*, vol. 525, nº 1, p. 59-64, août 2002, doi: 10.1016/S0014-5793(02)03067-3.
[150] M. L. Rodrigues *et al.*, « Human antibodies against a purified glucosylceramide from Cryptococcus neoformans inhibit cell budding and fungal growth », *Infect Immun*, vol. 68, nº 12, p. 7049-7060, déc. 2000, doi: 10.1128/IAI.68.12.7049-7060.2000.
[151] L. Nimrichter *et al.*, « A monoclonal antibody to glucosylceramide inhibits the growth of *Fonsecaea pedrosoi* and enhances the antifungal action of mouse macrophages », *Microbes and Infection*, vol. 6, nº 7, p. 657-665, juin 2004, doi: 10.1016/j.micinf.2004.03.004.
[152] B. De Coninck *et al.*, « Fungal Glucosylceramide-Specific Camelid Single Domain Antibodies Are Characterized by Broad Spectrum Antifungal Activity », *Frontiers in Microbiology*, vol. 8, 2017, Consulté le: 14 septembre 2022. [En ligne]. Disponible sur: https://www.frontiersin.org/articles/10.3389/fmicb.2017.01059
[153] L. Nimrichter *et al.*, « A monoclonal antibody to glucosylceramide inhibits the growth of Fonsecaea pedrosoi and enhances the antifungal action of mouse macrophages », *Microbes Infect*, vol. 6, nº 7, p. 657-665, juin 2004, doi: 10.1016/j.micinf.2004.03.004.
[154] M. L. Rodrigues *et al.*, « Monoclonal Antibody to Fungal Glucosylceramide Protects Mice against Lethal Cryptococcus neoformans Infection », *Clinical and Vaccine Immunology*, vol. 14, nº 10, p. 1372-1376, oct. 2007, doi: 10.1128/CVI.00202-07.
[155] V. Mor *et al.*, « Glucosylceramide Administration as a Vaccination Strategy in Mouse Models of Cryptococcosis », *PLOS ONE*, vol. 11, nº 4, p. e0153853, avr. 2016, doi: 10.1371/journal.pone.0153853.

[156] L. Nimrichter et M. L. Rodrigues, « Fungal Glucosylceramides: From Structural Components to Biologically Active Targets of New Antimicrobials », *Front Microbiol*, vol. 2, p. 212, oct. 2011, doi: 10.3389/fmicb.2011.00212.
[157] A. Kumar, P. Bansal, D. Katiyar, S. Prakash, et N. G. Raghavendra Rao, « Molecular Targeting and Novel Therapeutic Approaches against Fungal Infections », *Curr Mol Med*, vol. 23, nº 8, p. 726-736, 2023, doi: 10.2174/1566524023666230302123310.
[158] P. Manzanares, M. Giner-Llorca, J. F. Marcos, et S. Garrigues, « Fighting pathogenic yeasts with plant defensins and anti-fungal proteins from fungi », *Appl Microbiol Biotechnol*, vol. 108, nº 1, p. 277, mars 2024, doi: 10.1007/s00253-024-13118-1.
[159] Y. Oguro, H. Yamazaki, M. Takagi, et H. Takaku, « Antifungal activity of plant defensin AFP1 in Brassica juncea involves the recognition of the methyl residue in glucosylceramide of target pathogen Candida albicans », *Curr Genet*, vol. 60, nº 2, p. 89-97, mai 2014, doi: 10.1007/s00294-013-0416-8.
[160] K. Thevissen *et al.*, « Defensins from Insects and Plants Interact with Fungal Glucosylceramides* », *Journal of Biological Chemistry*, vol. 279, nº 6, p. 3900-3905, févr. 2004, doi: 10.1074/jbc.M311165200.
[161] L. Neves de Medeiros *et al.*, « Psd1 binding affinity toward fungal membrane components as assessed by SPR: The role of glucosylceramide in fungal recognition and entry », *Peptide Science*, vol. 102, nº 6, p. 456-464, 2014, doi: 10.1002/bip.22570.
[162] V. S. G. Amaral *et al.*, « Psd2 pea defensin shows a preference for mimetic membrane rafts enriched with glucosylceramide and ergosterol », *Biochim Biophys Acta Biomembr*, vol. 1861, nº 4, p. 713-728, avr. 2019, doi: 10.1016/j.bbamem.2018.12.020.
[163] E. de O. Mello *et al.*, « Functional expression and activity of the recombinant antifungal defensin PvD1r from Phaseolus vulgaris L. (common bean) seeds », *BMC Biochem*, vol. 15, p. 7, avr. 2014, doi: 10.1186/1471-2091-15-7.
[164] Y. Oguro, H. Yamazaki, M. Takagi, et H. Takaku, « Antifungal activity of plant defensin AFP1 in Brassica juncea involves the recognition of the methyl residue in glucosylceramide of target pathogen Candida albicans », *Curr Genet*, vol. 60, nº 2, p. 89-97, mai 2014, doi: 10.1007/s00294-013-0416-8.
[165] S. Raj *et al.*, « Changes in glucosylceramide structure affect virulence and membrane biophysical properties of Cryptococcus neoformans », *Biochimica et Biophysica Acta (BBA) - Biomembranes*, vol. 1859, nº 11, p. 2224-2233, nov. 2017, doi: 10.1016/j.bbamem.2017.08.017.
[166] A. Huber *et al.*, « Membrane Sphingolipids Regulate the Fitness and Antifungal Protein Susceptibility of Neurospora crassa », *Front Microbiol*, vol. 10, p. 605, 2019, doi: 10.3389/fmicb.2019.00605.
[167] K. Thevissen *et al.*, « Defensins from Insects and Plants Interact with Fungal Glucosylceramides », *The Journal of biological chemistry*, vol. 279, p. 3900-5, mars 2004, doi: 10.1074/jbc.M311165200.
[168] L. N. de Medeiros *et al.*, « Psd1 binding affinity toward fungal membrane components as assessed by SPR: The role of glucosylceramide in fungal recognition and entry », *Peptide Science*, vol. 102, nº 6, Art. nº 6, nov. 2014, doi: 10.1002/bip.22570.
[169] V. Silva de Paula, G. Razzera, E. Barreto-Bergter, F. C. L. Almeida, et A. P. Valente, « Portrayal of complex dynamic properties of sugarcane defensin 5 by NMR: multiple motions associated with membrane interaction », *Structure*, vol. 19, nº 1, p. 26-36, janv. 2011, doi: 10.1016/j.str.2010.11.011.
[170] L. Neves de Medeiros *et al.*, « Backbone dynamics of the antifungal Psd1 pea defensin and its correlation with membrane interaction by NMR spectroscopy », *Biochimica et Biophysica Acta (BBA) - Biomembranes*, vol. 1798, nº 2, p. 105-113, févr. 2010, doi: 10.1016/j.bbamem.2009.07.013.

[171] K. Thevissen *et al.*, « The plant defensin RsAFP2 induces cell wall stress, septin mislocalization and accumulation of ceramides in Candida albicans », *Molecular Microbiology*, vol. 84, n° 1, p. 166-180, 2012, doi: 10.1111/j.1365-2958.2012.08017.x.

[172] D. S. Lobo *et al.*, « Antifungal Pisum sativum Defensin 1 Interacts with Neurospora crassa Cyclin F Related to the Cell Cycle », *Biochemistry*, vol. 46, n° 4, p. 987-996, janv. 2007, doi: 10.1021/bi061441j.

[173] V. Ramamoorthy, X. Zhao, A. K. Snyder, J.-R. Xu, et D. M. Shah, « Two mitogen-activated protein kinase signalling cascades mediate basal resistance to antifungal plant defensins in Fusarium graminearum », *Cellular Microbiology*, vol. 9, n° 6, p. 1491-1506, 2007, doi: 10.1111/j.1462-5822.2006.00887.x.

[174] K. Thevissen, A. Ghazi, G. W. D. Samblanx, C. Brownlee, R. W. Osborn, et W. F. Broekaert, « Fungal Membrane Responses Induced by Plant Defensins and Thionins * », *Journal of Biological Chemistry*, vol. 271, n° 25, p. 15018-15025, juin 1996, doi: 10.1074/jbc.271.25.15018.

[175] A. Muñoz *et al.*, « Specific domains of plant defensins differentially disrupt colony initiation, cell fusion and calcium homeostasis in eurospora crassa », *Molecular Microbiology*, vol. 92, n° 6, p. 1357-1374, 2014, doi: 10.1111/mmi.12634.

[176] E. Andrès, « Cationic antimicrobial peptides in clinical development, with special focus on thanatin and heliomicin », *Eur J Clin Microbiol Infect Dis*, vol. 31, n° 6, Art. n° 6, juin 2012, doi: 10.1007/s10096-011-1430-8.

[177] T. Aumer, S. N. Voisin, T. Knobloch, C. Landon, et P. Bulet, « Impact of an Antifungal Insect Defensin on the Proteome of the Phytopathogenic Fungus Botrytis cinerea », *J Proteome Res*, vol. 19, n° 3, p. 1131-1146, mars 2020, doi: 10.1021/acs.jproteome.9b00638.

[178] L. Castillo, V. Plaza, L. F. Larrondo, et P. Canessa, « Recent Advances in the Study of the Plant Pathogenic Fungus Botrytis cinerea and its Interaction with the Environment », *Curr Protein Pept Sci*, vol. 18, n° 10, p. 976-989, 2017, doi: 10.2174/1389203717666160809160915.

[179] R. Dean *et al.*, « The Top 10 fungal pathogens in molecular plant pathology », *Molecular Plant Pathology*, vol. 13, n° 4, p. 414-430, 2012, doi: 10.1111/j.1364-3703.2011.00783.x.

[180] P. Canessa, J. Schumacher, M. A. Hevia, P. Tudzynski, et L. F. Larrondo, « Assessing the Effects of Light on Differentiation and Virulence of the Plant Pathogen Botrytis cinerea: Characterization of the White Collar Complex », *PLOS ONE*, vol. 8, n° 12, p. e84223, déc. 2013, doi: 10.1371/journal.pone.0084223.

[181] M. Hahn, « The rising threat of fungicide resistance in plant pathogenic fungi: Botrytis as a case study », *J Chem Biol*, vol. 7, n° 4, p. 133-141, oct. 2014, doi: 10.1007/s12154-014-0113-1.

[182] W. Shao, Y. Zhao, et Z. Ma, « Advances in Understanding Fungicide Resistance in Botrytis cinerea in China », *Phytopathology*, vol. 111, n° 3, p. 455-463, mars 2021, doi: 10.1094/PHYTO-07-20-0313-IA.

[183] S. Rupp *et al.*, « Botrytis fragariae, a New Species Causing Gray Mold on Strawberries, Shows High Frequencies of Specific and Efflux-Based Fungicide Resistance », *Appl Environ Microbiol*, vol. 83, n° 9, p. e00269-17, mai 2017, doi: 10.1128/AEM.00269-17.

[184] N. Banzet, M.-P. Latorse, P. Bulet, E. François, C. Derpierre, et M. Dubald, « Expression of insect cystein-rich antifungal peptides in transgenic tobacco enhances resistance to a fungal disease », *Plant Science*, vol. 162, n° 6, p. 995-1006, juin 2002, doi: 10.1016/S0168-9452(02)00053-5.

Chapter 2: Identification of the membrane target of ETD151

I. Aim of this work

The ETD151 peptide has been deemed worthy of selection as an antifungal candidate, and the identification of its molecular target(s) in the fungal membrane is paramount to the study of its mechanism of action (MOA). As antifungal defensins can have several membrane targets, identification of the target(s) relevant to its activity is crucial. Because the two structurally similar defensins Heliomicin and RsAFP2 are capable of binding fungal glucosylceramides (GlcCer), it was therefore hypothesized that GlcCer might be a potential target for ETD151 peptide. **Deciphering the mechanism of ETD151 actions against the model phytopathogenic fungus *Botrytis cinerea*** was carried out as part of a Thomas Aumer thesis' (2016-2019) supervised by Dr. P. Bulet (Biopark, Archamps) and Dr. C. Landon (CBM, Orléans).

During T. Aumer's thesis, the importance of the presence of GlcCer in fungal membranes for the full activity of ETD151 was confirmed by a deletion mutant assay. The growth inhibition activity of ETD151 against yeast mutants Δ*gcs Pichia pastoris* and *Candida albicans* lacking GlcCer and their wildtype (wt) strains was evaluated. The results confirmed the necessity of fungal GlcCer for ETD151 activity. In addition, the localization of ETD151 on *B. cinerea* by fluorescence microscopy showed that ETD151 remains mainly in CW, plasma membranes, the GlcCer-enriched compartment and intracellular vesicles involved in GlcCer transport. **These results were the starting point for my thesis and are included in the article of this chapter.**

Our main objective in this part was to demonstrate whether the glycolipid, GlcCer, in fungal membranes is the direct membrane target of the ETD151 peptide. To do this, (i) we structurally characterized the GlcCer(s) isolated from *B. cinerea* using mass spectrometry (MS) approach, (ii) we assessed the binding affinity of ETD151 to isolated GlcCer in a membrane context using microscale thermophoresis (MST), and (iii) we finally evaluated the effect of ETD151 on *Novosphingobium capsulatum*, a rare Gram-negative bacterium expressing glycosphingolipids (GSL) instead of lipopolysaccharides (LPS).

(i) To our knowledge, GlcCer(s) structures isolated from the fungus *B. cinerea* B05.10 have never been reported in the literature, so a sphingolipidomic study was carried out using MS approach. From the total lipid extracted from *B. cinerea* mycelium, GSL-enriched fraction was isolated and subjected to GC-MS analysis to identify the headgroup and MS fragmentation to characterize the ceramide moiety.

I performed the total lipid extraction from B. cinerea mycelia with Dr. S. Voisin under the supervision of Dr. P. Bulet (BioPark, Archamps). I carried out the GSL isolation and MS structure characterization with Dr. Yamaryo-Botte under the supervision of Dr. C. Botte (IAB, Grenoble). A commercially available soybean GlcCer was used to optimize the isolation and MS characterization procedure.

(ii) The binding affinity between a defensin and fungal GlcCer has rarely been studied. To estimate the binding affinity between ETD151 and simplified membrane models containing GlcCer extracted from

B. cinerea ($GlcCer_{B.\ cinerea}$), thermophoresis assays were performed. The interaction strength of the complex was evaluated by the determination of a dissociation constant (K_d). To get only the effect of $GlcCer_{B.\ cinerea}$ in the interaction with ETD151 peptide, GlcCer-free liposome (Phosphatidylcholine-based LUVs) control was used.

As MST is a fluorescence-based technique, I fluorescently labeled ETD151 by a dye NHS-ester, which reacts with the amino group of the peptide to build a covalent bond. I purified the mono-labeled ETD151 fraction by high performance liquid chromatography (HPLC) to be used for the interaction study. The conjugation reaction and purification were carried out with JB. Madinier under the supervision of Dr. V. Aucagne (CBM, Orléans). As MST has been described in few peptide-liposome interaction studies, an optimization step was necessary to find the optimal conditions. I performed the MST optimization, and assays were performed with Dr. R. Nassredine under the supervision of Dr. R. Nehme (ICOA, Orléans).

(iii) Defensins targeting GlcCer are generally devoid of antibacterial activity, which may be explained by the natural absence of glycosphingolipids (GSL) in bacterial membranes. ETD151 is also known to be exclusively antifungal and has not shown any activity against tested bacteria (e.g., *E. coli*). Exceptionally, few bacteria, including the genera *Sphingobacterium*, *Sphingomonas*, and *Bacteroides*, are able to synthesize sphingolipids. It is the case of, *N. capsulatum*, an infrequent Gram-negative bacterium expressing GSL instead of LPS. The susceptibility of *N. capsulatum* to ETD151 was investigated, as well as the localization of ETD151 on this bacterium using fluorescence microscopy.

I performed all assays to evaluate ETD151 activity, morphological effects, and subcellular localization on N. capsulatum using fluorescence-based assays. Fluorescence microscopy experiments were carried out with D. Gosset (MO2VING/P@cyfic platform, CBM, Orléans).

The identification of fungal GlcCer as a membrane target of the ETD151 peptide, and proof of the direct molecular interaction, which is an essential first step by which ETD151 exerts its antifungal activity, will pave the way for exploring the full therapeutic potential of this peptide.

II. Article

The results of this work have been submitted (01 August 2024) and accepted (8 January 2025) for publication in Proceedings of the National Academy of Sciences (PNAS) journal. In this thesis manuscript, we have chosen to reproduce the original paper.

PNAS RESEARCH ARTICLE | BIOCHEMISTRY

The antimicrobial activity of ETD151 defensin is dictated by the presence of glycosphingolipids in the targeted organisms

Ons Kharrat[a], Yoshiki Yamaryo-Botté[b], Rouba Nasreddine[c], Sébastien Voisin[d], Thomas Aumer[d,e,1], Bruno P. A. Cammue[f], Jean-Baptiste Madinier[a], Thomas Knobloch[e], Karin Thevissen[f], Reine Nehmé[c], Vincent Aucagne[a], Cyrille Botté[b], Philippe Bulet[b,d], and Céline Landon[a,2]

Affiliations are included on p. 11.

Edited by Hailing Jin, University of California, Riverside, CA; received August 1, 2024; accepted January 8, 2025 by Editorial Board Member Natasha V. Raikhel

Fungal infections represent a significant global health concern, with a growing prevalence of antifungal drug resistance. Targeting glucosylceramides (GlcCer), which are functionally important glycosphingolipids (GSL) present in fungal membranes, represents a promising strategy for the development of antifungal drugs. GlcCer are associated with the antifungal activity of certain plant and insect defensins. The 44-residue ETD151 peptide, optimized from butterfly defensins, is active against several fungal pathogens. ETD151 has been shown to induce a multifaceted mechanism of action (MOA) in *Botrytis cinerea*, a multiresistant phytopathogenic fungus. However, the target has yet to be identified. Our findings demonstrate that the presence of GlcCer in membranes determines the susceptibility of *Pichia pastoris* and *Candida albicans* toward ETD151. To ascertain whether this is due to direct molecular recognition, we demonstrate that ETD151 selectively recognizes liposomes containing GlcCer from *B. cinerea*, which reveals a methylated-sphingoid base structure. The dissociation constant was estimated by microscale thermophoresis to be in the μM range. Finally, fluorescence microscopy revealed that ETD151 localizes preferentially at the surface of *B. cinerea*. Furthermore, the majority of prokaryotic cells do not contain GSL, which explains their resistance to ETD151. We investigated the susceptibility of *Novosphingobium capsulatum*, one of the rare GSL-containing bacteria, to ETD151. ETD151 demonstrated transient morphological changes and inhibitory growth activity (IC_{50} ~75 μM) with an affinity for the cell surface, emphasizing the critical importance of GSL as target. Understanding the MOA of ETD151 could pave the way for new perspectives in human health and crop protection.

antifungal defensin | *Botrytis cinerea* | glucosylceramide | *Novosphingobium capsulatum* | molecular affinity

Significance

The multifaceted mechanisms of action of antifungal defensins make them promising candidates for combating fungal resistance. Identifying their relevant targets remains challenging. Glucosylceramides (GlcCer), glycosphingolipid (GSL) of fungal membranes, are promising targets for new antifungals. ETD151, optimized from butterfly defensins, inhibits the fungus responsible for the gray mold disease, *Botrytis cinerea*, which has become multidrug resistant. Our findings show that ETD151 binds directly to GlcCer, a crucial membrane component for its activity, and localizes preferentially at the membrane, from where it would induce various toxic effects. Having identified the molecular target of ETD151, we investigated the susceptibility of infrequent GSL-containing bacteria to ETD151. This highlights the necessity to identify molecular targets to unlock its full potential in medicine and agriculture.

Fungal infections represent a significant global threat to human health and food safety, largely due to the emergence of fungal resistance to currently available drugs (1). There is a clear need for new, effective, and safe antifungal drugs with different mechanisms of action to those currently used. Targeting compounds in the fungal cell wall (CW) and/or plasma membrane, which structurally differ from those in mammalian and plant cells and play important biological roles, may provide a solution to combat pathogenic fungi (2, 3). Glucosylceramides (GlcCer) are glycosphingolipids (GSL) found in the plasma membrane of almost all fungi. Fungal GlcCer (fGlcCer) have specific structural features distinct from those of plants and humans. They have been identified as playing crucial roles in fungal growth and pathogenicity/virulence (4, 5). It is also worth noting that many plant and human pathogenic fungi mutants lacking GlcCer show impaired growth and loss or reduction of virulence compared with wild-type (wt) strains (6–8). Therefore, targeting fGlcCer, directly or through inhibition of biosynthetic pathways, may prove an effective strategy for developing the next generation of antifungals (9, 10). Inhibitors of fungal synthesis enzymes, such as glucosylceramide synthase (GCS) inhibitors, have demonstrated potent in vitro and in vivo antifungal activities (11). Moreover, fGlcCer directly targeted by monoclonal antibodies to glucosylceramide (12, 13) showed remarkable efficacy in reducing symptoms of human and plant fungal infections (14, 15). Additionally, numerous reports identified fGlcCer as a possible binding target for certain antifungal peptides.

These peptides, found in plants and insects, are characterized by a cysteine-stabilized α-helix β-sheet structural motif (CSαβ). They are typically referred to as "antifungal defensins" (16). The susceptibility of yeasts and/or filamentous fungi to some of these plants [RsAFP2 from *Raphanus sativus* (17), MsDef1 from *Medicago sativa* (18), AFP1

The authors declare no competing interest.

This article is a PNAS Direct Submission. H.J. is a guest editor invited by the Editorial Board.

[1]Present address: EurofinsBTP Biologics, Lentilly, France.

[2]To whom correspondence may be addressed. Email: celine.landon@cnrs-orleans.fr.

This article contains supporting information online at https://www.pnas.org/lookup/suppl/doi:10.1073/pnas.2415524122/-/DCSupplemental.

Published February 12, 2025.

from *Brassica juncea* (19) and Psd2 from *Pisum sativum* (20)] or insect [Heliomicin from *Heliothis virescens* (17)] defensins is determined by the presence of GlcCer. These defensins are referred to as "GlcCer-associated defensins". There have only been a few instances where direct molecular interaction with fGlcCer has been demonstrated (*SI Appendix*, Table S1). The fGlcCer binding step may have a direct effect on the fungal membrane, leading to its permeabilization, and/or other downstream effects (e.g. activation of cell wall integrity (CWI), production of reactive oxygen species), all of which contribute to the killing process (21). This complex multitarget mechanism of action (MOA) of antifungal defensins is highly valuable for reducing the emerging threat of multiresistant strains.

Defensin-based protection represents a promising environmentally friendly alternative to synthetic fungicides for the protection of crops from phytopathogenic fungi (22). The filamentous fungus *Botrytis cinerea* is the causal agent of gray mold, responsible for a multitude of issues in crop fields. Over the past decade, the situation has worsened with the discovery of multiresistant strains of *B. cinerea* in the field (23). The ETD151 peptide is a cationic 44-amino acid disulfide-rich peptide (Isoelectric point 8.2, 32 % of hydrophobic residues, disulfide pairing C7-C32, C18-C40, C22-C42), which has been optimized from Heliomicin after three mutations (D17N/ N19R/G20A) by the former French Biotech company EntoMed S.A. (ETD standing for EnToMed) (24). It is a potent inhibitor of the growth of both the spore and mycelial forms of *B. cinerea* at the µM level (25), in contrast to Heliomicin or Drosomycin, which show weak activity against the mycelial form (26). A proteomic study was performed to elucidate the MOA of ETD151 on *B. cinerea*. The results demonstrated that this defensin modulated over 300 proteins corresponding to at least six molecular pathways in *B. cinerea.* Furthermore, ETD151 has been shown to induce membrane disruption in *B. cinerea* mycelia (25). Based on these results, defensin ETD151 was selected as a promising antifungal candidate. However, it remains unclear whether ETD151 is internalized or acts extracellularly on *B. cinerea*, and what is its molecular target in the fungal membrane.

We hypothesized that GlcCer in fungal membranes are a key component for the activity of ETD151, similar to its analog Heliomicin (17). In this study, antifungal activity assays were performed against yeast mutants lacking fGlcCer, our proposed membrane target, and showed that its presence is crucial for ETD151 to inhibit fungal growth. A multitechnique study was then conducted to elucidate the remaining aspects of the ETD151 MOA on *B. cinerea*: Fluorescence microscopy was employed to investigate the cellular localization of ETD151. By mass spectrometry (MS), we characterized the structure of its putative target (GlcCer) extracted from *B. cinerea*. We then used thermophoresis on a microscopic scale to evaluate the binding affinity between ETD151 and fGlcCer from *B. cinerea* incorporated into liposomes.

Finally, with the identification of ETD151's molecular target, we further investigated the susceptibility of GSL-containing bacteria to ETD151. Indeed, most prokaryotic cells do not contain sphingolipids, and only some bacteria, including the genera *Sphingobacterium*, *Sphingomonas,* and *Bacteroides,* can synthesize sphingolipids (27). Our study highlights the importance of analyzing the MOA of ETD151 at the molecular level, with a particular focus on identifying the relevant cellular targets. This is a crucial step in advancing the therapeutic and agricultural applications of ETD151.

Results and Discussion

fGlcCer Are Essential for the Antifungal Activity of ETD151 Defensin. GCS is an enzyme responsible for the final step in the biosynthesis of GlcCer, before its export to the plasma membrane or the CW or its secretion into the extracellular space in vesicles. Deletion of the *gcs* gene in yeasts therefore produces mutants devoid of GlcCer in their membranes. *C. albicans* and *Pichia pastoris* mutants lacking GlcCer (Δ*gcs* strains) exhibited resistance (minimum inhibitory concentration (MIC) > 40 µM) to ETD151, compared to their wt strains (MIC = 0.65 µM). This suggests that the presence of GlcCer is necessary for ETD151 to inhibit fungal cell growth (Fig. 1). These findings are consistent with previous observations made with the highly similar RsAFP2 and Heliomicin defensins against the same strains (17). Likewise, lower susceptibility or even resistance to other plant defensins was observed in various Δ*gcs* fungal strains (*SI Appendix*, Table S1), indicating that the presence of GlcCer in the membranes is relevant for their antifungal activity. In the membrane, GlcCer are associated with sterols and proteins to form lipid rafts. These microdomains impact membrane fluidity and regulate the organization and integrity of the membrane. Therefore, the correlation between the antifungal activity of ETD151 and the presence of GlcCer in the fungal membrane may involve either a direct molecular interaction between the two partners, or a modification of cell envelope organization due to the absence of fGlcCer in the membrane, which affects defensin activity. The literature and this study indicate that ETD151 is active only against GlcCer-containing pathogenic fungi, suggesting that fGlcCer may be a potential membrane target. However, the molecular interaction remains to be demonstrated (Table 1). Given our interest in the potency of ETD151 to control phytopathogenic fungi, we selected *B. cinerea* as the fungal model for our study.

***B. cinerea* GlcCer Has a Conserved Methylated sphingoid Base Linked to (un)Saturated Palmitic Acid.** fGlcCer contain a sphingoid base, which is connected *via* an amide bond to an

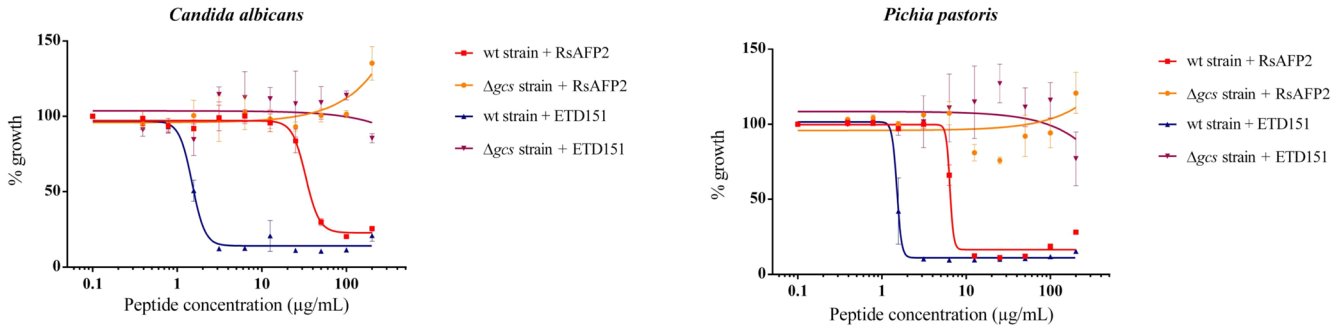

Fig. 1. Antifungal activity of ETD151 defensin on wt yeasts *C. albicans*, *P. pastoris,* and their mutants lacking GlcCer (Δ*gcs*). Dose–response curves illustrating the growth of yeasts in the presence of ETD151 and the radish defensin, RsAFP2, used as a positive control. Peptide activity is expressed as % growth relative to their concentrations in µg/mL (log scale from 0.1 to 200). The study was performed in triplicate, and results are represented as mean ± SD.

Table 1. Antifungal activity of ETD151 on several fungal species and yeast mutants lacking GlcCer (Δ*gcs*)

Fungal species	Presence of GlcCer	IC_{50} μM (μg/mL)	MIC μM (μg/mL)	References
Aspergillus fumigatus	Yes	1.3 (6.25)	–	(24)
C. albicans CAI4		–	0.13 (0.65)	
Cryptococcus neoformans		0.32 (1.56)	–	
Lomentospora prolificans		0.02 (0.1)	–	
Fusarium solani		0.08 (0.4)	–	
Pichia pastoris GS115			0.13 (0.65)	This work
Saccharomyces cerevisiae	No	No active		(24)
Pichia pastoris (Δgcs)		–	> 8.33 (> 40)	This work
C. albicans (Δgcs)		–	> 8.33 (> 40)	
B. cinerea	unknown	0.59 (2.8)	–	(25)

Summary of results available in the literature and from this work. Data are reported as medians (IC50, expressed in micromolar μM and in μg/mL and defined as the concentration that inhibits 50% of fungal growth) or minimum inhibitory concentration (MIC, expressed in micromolar μM and in μg/mL).

α-hydroxylated fatty acyl at C2. The latter structure comprises the ceramide moiety, bonded *via* an ester to a sugar head group at the C_1 position (28). However, fungal cells can produce a wide range of sphingolipid structures, differing in fatty acid chain length, number of hydroxylation, and degree of unsaturation. The MS approach has been extensively used to characterize various sphingolipid species extracted from different fungi (29). This has resulted in a large body of literature containing precursor ions and fragmentation patterns of various fungal sphingolipids being made available. The use of precursor *m/z* ion pairs and product *m/z* ions of molecular species of interest enables precise detection and quantification.

B. cinerea GlcCer have not been examined at the structural level; however, our BLAST search results support the presence of the *gcs* gene, which is responsible for the final step of GlcCer' biosynthesis (*SI Appendix*, Table S2). The chemical structure of the main GlcCer isolated from *B. cinerea* mycelia was analyzed (Fig. 2 for the B05.10 strain, and *SI Appendix*, Fig. S1 for B047 strain). After removal of glycerolipids, extracted lipids enriched in sphingolipids were separated by high-performance thin-layer chromatography (HPTLC). As shown in Fig. 2*A*, a band migrated onto a HPTLC similar to the commercially available GlcCer from soybean, used as an external standard ($GlcCer_{Soybean}$). The reactivity of the band to orcinol indicates the presence of sugar-containing lipids. It is therefore assumed that this fraction potentially contains the *B. cinerea* GlcCer. Using positive ion mode electrospray ionization (ESI)–MS, two molecular ions were observed at m/z 726.5 and 728.5 (Fig. 2*B*). When subjected to ESI–MS/MS (Fig. 2*C*), fragmentation of these molecular ions yielded fragments at *m/z* 708.4 and 710.4 (loss of water) and a daughter ion at *m/z* 276.2, which is characteristic of a 9-methyl-4,8-sphingadienine (d19:2) backbone as having an 18-carbon sphingadienine base with an additional methyl group (total of 19 carbons) after the loss of two water molecules. Although several sphingoid bases have been described, d19:2 is the predominant sphingoid base in most fungal species (29). MS/MS spectra also revealed the presence of a daughter ion at *m/z* 252.1 and 254 from the molecular ions at *m/z* 726 and 728, respectively. This suggests the presence of hydroxylated palmitic acid with or without unsaturation (C16:0 or C16:1). We have proposed that fatty acid unsaturation is localized between C3 and C4, as this is the most commonly reported position (30). The structure of the sugar head group released by hydrolysis from the glycosphingolipid-enriched fraction was identified as glucose by gas-chromatography (GC)–MS (Fig. 2*D*). As the positions of the double bonds, hydroxyl groups, and methylation could not be assigned based on MS analysis alone, we proposed the following structures, d19:2/h16:1 and d19:2/h16:0, for the two major GlcCer extracted from *B. cinerea* (Fig. 2*E*). The molecular ion recorded in our experimental conditions at *m/z* 728 is among the three most abundant fGlcCer described so far in the literature (29), with two additional molecular ions at *m/z* 756 and 754. The d19:2 sphingoid base has been identified in several fungi, including the *Fusarium, Pseudallescheria boydii, L. prolificans,* and *Cryptococcus* species (31). Interestingly, ETD151 was found to be active against *C. albicans, C. neoformans, A. fumigatus, F. solani,* and *L. prolificans* (24). In contrast, the molecular ion at *m/z* 726 (d19:2/h16:1) with a C16:1 unsaturated fatty acid has rarely been reported in the literature, the α-hydroxylated fatty acyl groups described in fungal sphingolipids are mainly C18:0, C18:1, and C16:0 (31).

Synthesized by specific enzymes, fGlcCer have specific structural characteristics that differ from plant and mammalian GlcCer. One such characteristic is the presence of a methyl group branching from C9 of the sphingoid base. In addition, the unsaturation between C8 and C9 in the sphingoid base distinguishes fGlcCer from mammalian GlcCer. These differences in GlcCer structures between fungi, plants, and mammals make GlcCer a potential target for antifungal therapeutics. Interestingly, the activity and/or interaction of certain GlcCer-associated proteins are associated with specific structural features (methylation at C9, unsaturation between C8 and C9, fatty acid length, and level of unsaturation) in fGlcCer. For example, the defensin RsAFP2 showed no binding to unmethylated human or plant GlcCer compared to methylated fGlcCer (17). The susceptibility of fungi to the antifungal protein AFP has been shown to depend on the saturation level of the fGlcCer fatty acid present in each fungus (32). We hypothesize that the efficacy of ETD151 is correlated with the presence of GlcCer on the membranes of microorganisms. We conducted a literature review to analyze the various GlcCer structures present in fungi for which the activity of ETD151 has been evaluated (*SI Appendix*, Table S3). This analysis revealed that ETD151 has broad-spectrum activity against fungi, all with methylated GlcCer. In addition, these fungal species sensitive to ETD151 show GlcCer structures with or without the C3-C4 double bond in the fatty acid and with a C16 or C18 fatty acid length. This independence of ETD151 activity from specific types of GlcCer structures will allow ETD151 to have broad-spectrum activity against fungi irrespective of their GlcCer structures.

***B. cinerea* GlcCer Is the Membrane Target of ETD151.** The in vitro molecular recognition of antifungal defensin for GlcCer has been documented in biophysical [surface plasmon resonance (SPR) and (NMR)] and biochemical (ELISA) studies. The radish RsAFP2 and the butterfly Heliomicin defensins interact with purified

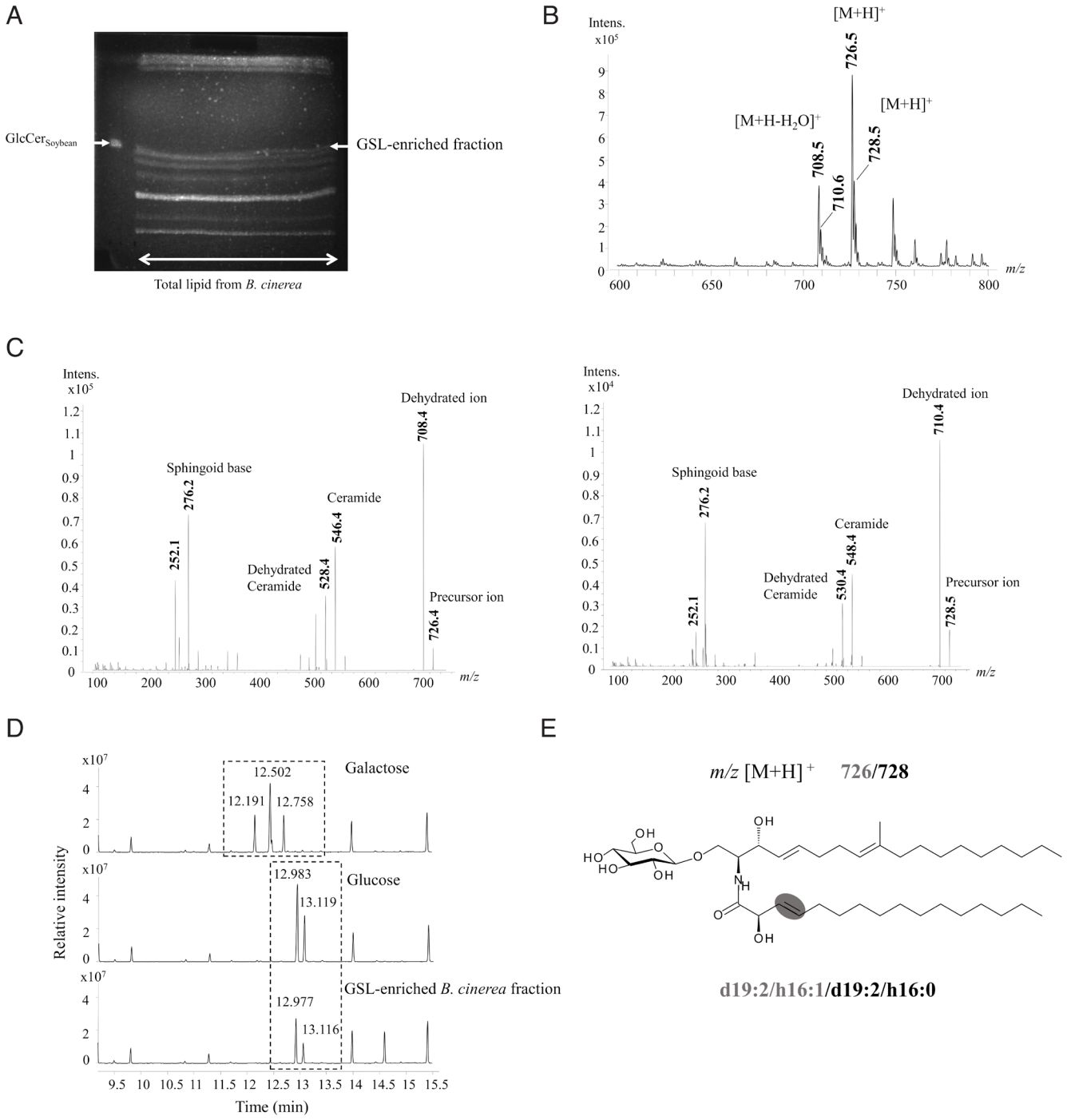

Fig. 2. Structural analysis of GlcCer obtained from *B. cinerea* B05.10 mycelia. (*A*) Isolation of glycosphingolipid-enriched fraction of crude total lipid extracted from *B. cinerea* using HPTLC. HPTLC migration was performed with dichloromethane/methanol/ammonia 2 M (65:25:4, vol/vol/vol), and lipid band was visualized under UV light after primulin staining. GlcCer from Soybean (GlcCer$_{Soybean}$) was used as a standard. (*B*) ESI–MS spectra of purified glycosphingolipid-enriched fraction. (*C*) ESI–MS/MS of molecular precursor ions at *m/z* 726.4 and 728.5 observed in ESI–MS. (*D*) GC–MS analysis of the glycosphingolipid-enriched fraction after extraction, methanolysis, and trimethylsilyl (TMS) derivatization. Total ion chromatograms (TIC) for glucose and galactose as standards and glycosphingolipid-enriched fraction from *B. cinerea*. (*E*) Proposed structure for the major GlcCer species found in *B. cinerea*. By analogy to plant GlcCer, the double bound of the fatty acid was proposed at C3-C4 position.

GlcCer from *P. pastoris* in a dose-dependent manner, as evidenced by immunological detection. SPR analysis revealed that the pea Psd1 defensin preferentially binds to vesicles containing GlcCer isolated from *F. solani*, as opposed to GlcCer-free liposomes (33). The structures of Psd1 and Sd5, defensins from *P. sativum* and *Saccharum officinarum,* respectively, exhibit conformational changes in the presence of *F. solani* GlcCer incorporated into vesicles. The binding affinity has been rarely studied between the two partners in any of the interaction studies conducted to date, apart from the SPR experiments. In these cases, Psd1-GlcCer affinities were estimated using the association rate constant (α-value) due to the insignificant dissociation rate constant.

To ascertain whether a direct molecular interaction exists between ETD151 and fGlcCer, we estimated the binding affinity of the fluorescently monolabeled-ETD151 (Atto647-ETD151) (*SI Appendix*, Figs. S2–S4 and Table S4) with GlcCer$_{B.\ cinerea}$-containing phosphatidylcholine (PC) liposomes (100 nm) using microscale thermophoresis (MST). Only a few micromolar of

target/ligand solutions are necessary to obtain a dissociation constant (K_d) value (34). MST does not require radioactivity or surface immobilization and is expected to perform well in complex matrices (35, 36). However, there are only a few examples of MST interaction studies of peptides with membrane models (37–40). By optimizing the experimental conditions and parameters, we prevented aggregation and adsorption of the labeled defensin during thermophoresis, ensuring good sensitivity and reproducibility (*SI Appendix*, Figs. S5–S7). In the MST-based binding experiments, the fluorescent ETD151 was maintained at a constant concentration (50 nM) and incubated with 16 different concentrations of $GlcCer_{B.\ cinerea}$-containing liposomes (from 1 mM to 30.5 nM). Upon binding to liposomes, the thermophoresis profile of ETD151 changed due to modifications in conformation, charge, and/or size of the molecule. The fluorescence of labeled ETD151 in the presence of the different concentrations of $GlcCer_{B.\ cinerea}$-containing liposomes was measured and converted into a binding curve from which the K_d was calculated and found to be 0.5 ± 0.3 µM (Fig. 3*A*). To ensure that the measured interaction truly represents specific binding to $GlcCer_{B.\ cinerea}$, control liposomes composed solely of PC ($GlcCer_{B.\ cinerea}$-free liposomes) were analyzed under the same conditions. Since buffer, ionic strength, and viscosity were unchanged in these experiments, the reduced apparent affinity is most likely the result of ETD151 binding to $GlcCer_{B.\ cinerea}$ -containing liposomes. The absence of $GlcCer_{B.\ cinerea}$ reduces the affinity to the membrane model since the K_d value was found to be 250 ± 80 µM (Fig. 3*A*).

This study provides an estimation of the K_d between an antifungal defensin and fungal liposomes containing GlcCer. As no binding affinity values are available in the literature for the interaction between defensin and fGlcCer, these data could serve as a reference point for future studies. It is worth noting that the values obtained are in the same order of magnitude as the rare K_d values obtained by MST for protein–lipid interactions. For example, the interaction of the phospholipid N-methyltransferase PmtA with cardiolipin has been estimated at around 5 µM (41), while the interaction of Drp1 cardiolipin-binding motif with cardiolipin has been estimated at 23 µM (42).

We further confirmed ETD151 binding to fGlcCer by performing liposome pulldown assays (Fig. 3*B*). Prepared PC-only and PC-GlcCer liposomes were incubated with ETD151 before being separated into bound and unbound fractions. We found that GlcCer incorporated in liposomes increased the membrane-bound ETD151 fraction. Taken together, MST and liposome pulldown assays demonstrate that ETD151 preferentially binds to liposomes containing fGlcCer.

ETD151 Localizes Particularly on *B. cinerea* Cell Surface. Upon interaction with GlcCer, antifungal plant defensins can either be internalized into the fungal cells, thereby affecting intracellular targets in the cytosol or nucleus, or remain on the outside of the fungal cells where they trigger cellular toxic effects for fungi. Plant defensins are classified according to their membrane partner, and MsDef1, RsAFP2, and Psd1 are classified as GlcCer-interacting

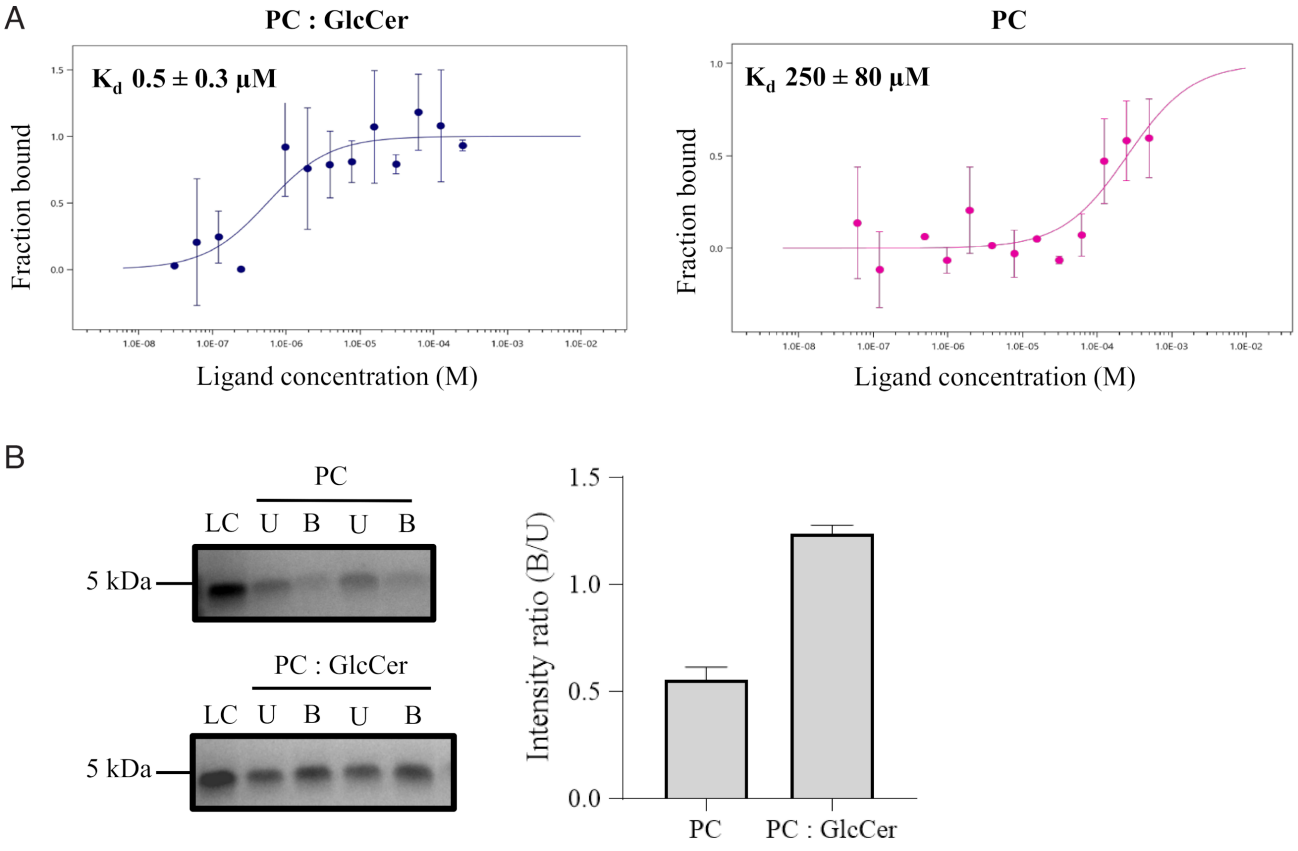

Fig. 3. ETD151 preferentially binds to liposomes containing fGlcCer. (*A*) Binding affinities by MST assay of Atto647-ETD151 to (*Right*) GlcCer-containing liposomes, GlcCer extracted from *B. cinerea* ($GlcCer_{B.\ cinerea}$) were incorporated into PC liposomes with a molar ratio at 10/90 (GlcCer/PC) and (*Left*) GlcCer-free liposomes, made with only PC, were used as a control. Kd is the dissociation constant given as mean of three independent experiments ± SD. All experiments were done with a constant concentration of Atto647-ETD151 (50 nM) at 22 °C. Autodetect excitation power and 40% MST power were used. MST buffer was phosphate buffer (10 mM, pH 5.8). (*B*) Liposome pulldown assay comparing the binding of ETD151 to PC only and PC: fGlcCer (90:10 molar ratio) liposomes. Bound (*B*) and unbound (*U*) fractions were subjected to SDS-PAGE analysis and colloidal Coomassie staining. ETD151 alone was used as loading control (LC). The intensities of the bands were calculated using ImageJ software. Averages of the ratio of intensities (Bound/Unbound) were then calculated for n = 2 experiments (shown in the gel). Data represent mean ± SEM, n = 2.

defensins. It is currently unclear whether MsDef1 is internalized by fungal cells (43). RsAFP2 is not internalized by fungi or yeasts (21), unlike Psd1, which interacts with cyclin F in the nucleus of the fungus *Neurospora crassa* (44).

To exploit the kinetics of the internalization and subcellular localization of ETD151 on fungal cells, live cell imaging was conducted on *B. cinerea* hyphae treated with green fluorescently labeled ETD151 (BODIPY-ETD151), a fluorescent labeling that did not affect the antifungal activity of ETD151 (*SI Appendix*, Table S5). Various concentrations (from 0.19 to 0.78 µM) were used, including the concentration that inhibits 50% of fungal growth (IC_{50}) (IC_{50} 0.59 µM, Table 1) and covering the entire inhibition profile of BODIPY-ETD151. After the addition of BODIPY-ETD151 at a concentration of 0.78 µM, confocal microscopy images showed a rapid and preferential localization of the peptide on the cell surface, characterized by a homogeneous distribution of the fluorescent signal along the hyphae (Fig. 4*A*, T0). This localization was independent of peptide concentration,

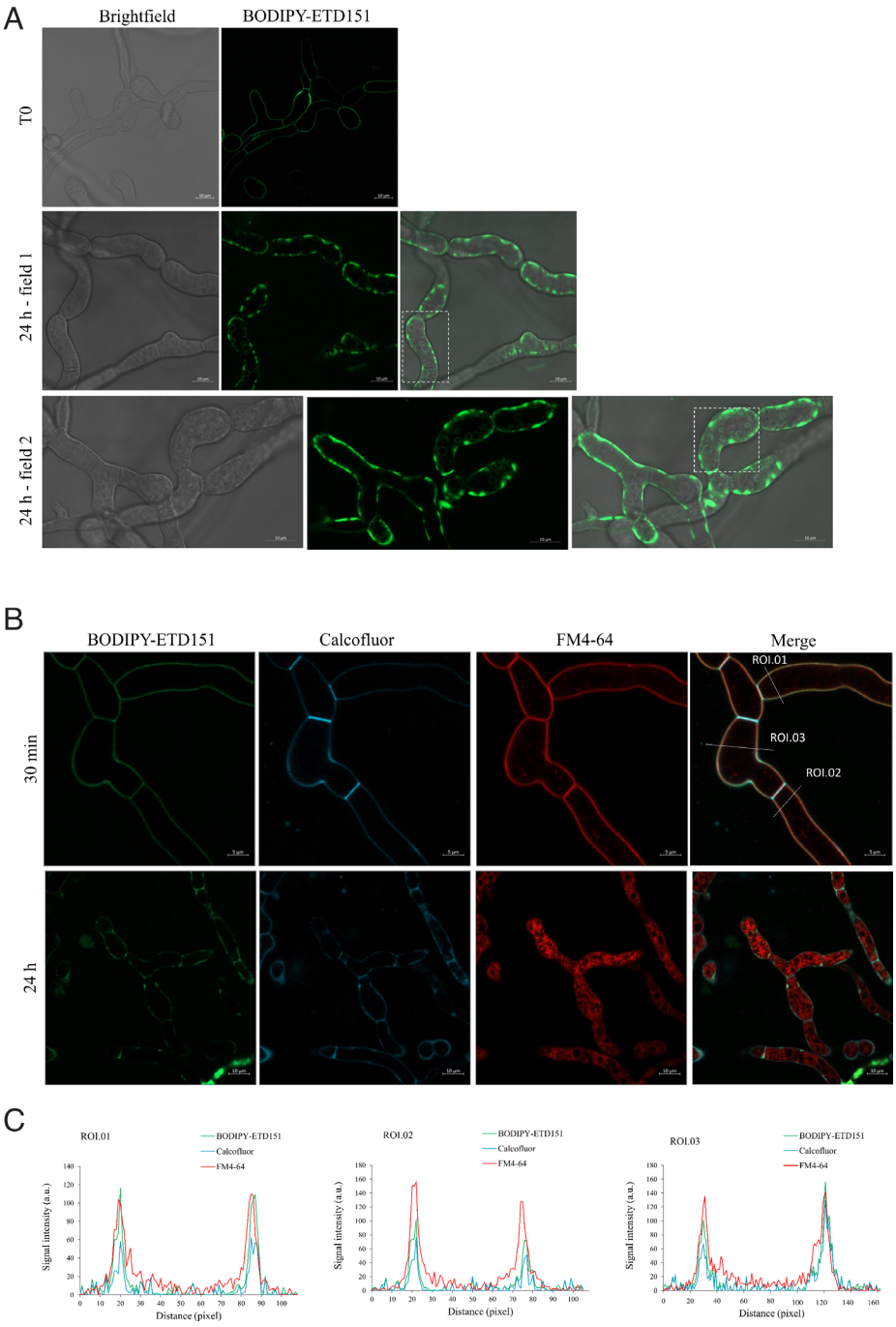

Fig. 4. BODIPY-ETD151 localization in B. *cinerea* cells. (*A*) Internalization of the BODIPY-ETD151 peptide (0.78 µM) on *B. cinerea*. Confocal microscopy images of *B. cinerea* (10^4 sp/mL in a 25% PDB medium) by 63x optical magnification. Hyphae examined in transmitted light and fluorescence at T0 and 24 h after addition of BODIPY-ETD151 (Scale bar, 10 µm). The white frames indicate the staining of the membranes around intracellular organelles by BODIPY-ETD151. (*B*) Subcellular localization of BODIPY-ETD151 (0.19 µM) on hyphae of the *B. cinerea*. Confocal observations made on *B. cinerea* (10^4 sp/mL in a 25% PDB medium) by 100x optical magnification. Hyphae examined by colabeling 30 min (Scale bar, 5 µm) and 24 h (Scale bar, 10 µm) in the presence of 0.19 µM BODIPY-ETD151 (green), Calcofluor (blue), and FM4-64 (red), respectively. (*C*) Signal intensities taken from regions of interest ROI.01, ROI.02, and ROI.03 from the merged image after 30-min treatment of mycelia *B. cinerea* (Fig. 4*B*).

as after 3 h incubation at 0.19, 0.39, and 0.78 μM, the labeled peptide showed the same distribution of fluorescence signal (*SI Appendix*, Fig. S8). This high affinity of ETD151 for CW and plasma membrane, known to be potentially rich in GlcCer, could be explained by the presence of its molecular target (45). Interestingly, after 24 h of incubation, the distribution of the labeled peptide has evolved. The fluorescence signal on the surface became stronger, showing accumulation at "patch" on the cell surface (Fig. 4*A*). Although BOPIPY-ETD151 did not spread into the cytoplasm, a fluorescent signal, weaker than at the cell surface, was detected, staining the membranes around intracellular organelles. These organelles vary in size, including vesicles, vacuoles, and nuclei, and are mainly attached to the plasma membrane (Fig. 4*A*, white frame). The affinity of the ETD151-BODIPY peptide for subcellular membranes could be explained by the presence of GlcCer in different cellular regions (46). The synthesis and degradation pathways of these sphingolipids involve the nuclei and Golgi apparatus, before being transported by vesicles to the plasma membrane.

To further explore the subcellular localization of ETD151 in *B. cinerea*, mycelia were incubated before being treated with BODIPY-ETD151, in the presence of FM4-64 as a membrane and endocytosis-specific dye, and Calcofluor as a CW dye that binds to cellulose and chitin. As shown in Fig. 4 *B* and 4 *C*, the fluorescence signals of BODIPY-ETD151 and Calcofluor overlap, indicating that the peptide remains on the cell surface after 30 min of treatment, particularly at the CW. After 24 h of treatment, we observed that the distribution of the calcofluor label showed significant similarities with that of the peptide, unlike the FM4-64 label, which diffused into the cytoplasm (Fig. 4*B*). This result suggests an effect of the ETD151 peptide on the CW, in line with the impact on the CWI pathway previously demonstrated in differential proteomic studies (25). This type of distribution has already been described for the plant defensin RsAFP2 in the yeast *C. albicans* and would correspond to an interaction of defensin with GlcCer present in the CW, where 43% of GlcCer are located (21).

Taken together, these observations demonstrate that ETD151 would preferentially remain in the fungal CW/plasma membrane, which is related to selective interactions with fungal membrane components, including GlcCer. However, we cannot rule out the possibility that a minor fraction of ETD151 may reach the cytoplasm, probably by a mode of entry other than endocytosis, to bind to membrane around intracellular organelles. It is also possible that ETD151 may exhibit selectivity for other fungal CW components (e.g. Chitin, β-Glucan, and Mannan), as antifungal defensins typically have multiple targets (16). To our knowledge, only NaD1 from *Nicotiana alata* has been reported to interact with the fungal CW components Chitin and Mannan (47).

Atypical Glycosphingolipid-Containing Bacteria Are Sensitive to ETD151.

ETD151 does not inhibit the growth of bacteria lacking sphingolipids. Plant and insect defensins are usually considered to possess antifungal activity but lack antibacterial activity. In the literature, this lack of antibacterial potency has only been reported for certain GlcCer-associated defensins. Among the eight bacterial strains tested, RsAFP2 only showed activity against *Bacillus megaterium* at a high concentration (IC_{50} ~ 200 μg/mL) (48). Heliomicin was also inactive against Gram-negative and -positive bacteria up to 100 μM (49). Sd5 has been reported to lack antibacterial properties (50). Up to 100 μM, ETD151 does not inhibit the growth of Gram-negative (*Escherichia coli* American Type Culture Collection (ATCC) 25944, *E. coli* D22) and -positive bacteria (*Bacillus subtilis* CV-1 and *Micrococcus luteus* ATCC 4698), which naturally lack GSL in their membranes, after overnight incubation (*SI Appendix*, Fig. S9). As we have demonstrated that the MOA of ETD151 requires interaction with a fungal membrane component, the lack of sensitivity of these bacteria to ETD151 could be attributed to the differences in microbial membranes.

ETD151 reduces the viability of Novosphingobium Capsulatum. *N. capsulatum* is one of the few Gram-negative bacteria that express GSL instead of lipopolysaccharides (LPS), assuming the same structural and functional role (27, 51). The structures of the sugar headgroups and ceramide backbones of the two main GSL in *Novosphingomonas* bacteria have been analyzed in detail (51). Therefore, we investigated the growth-inhibitory activity, morphological effects, membrane permeabilization, and localization of ETD151 on *N. capsulatum*.

The resazurin-based assay, which reflects cell metabolic activity, showed that ETD151 reduces the viability of *N. capsulatum* bacteria in a dose-dependent manner (IC_{50} ~ 75 μM) after 24 h of incubation (Fig. 5*A*). No morphological changes were observed at high concentrations of ETD151 (100 μM, above the IC_{50}). However, microscopy observations showed that *N. capsulatum* transitions from rod-shaped to spherical, viable cells upon treatment with low ETD151 concentration (12.5 μM, below the IC_{50}) (Fig. 5*B*). Similar morphological changes have been reported for *P. aeruginosa* after treatment with β-lactams, CW-targeting antibiotics (52). It is unclear whether these shape changes are a passive side effect of the antibiotic or whether they represent adaptive responses that promote bacterial fitness for surviving antibiotic exposure and thus counter the antibiotic's action (53). The spherical cells formed after ETD151 treatment remained viable and regained their natural rod shape after subculturing in peptide-free conditions. To ascertain whether the growth-inhibitory activity of ETD151 on *N. capsulatum* at high concentrations is a result of ETD151-induced membrane permeabilization, we performed a flow cytometry analysis to determine the percentage of propidium iodide (PI)-positive cells treated with ETD151. Our results showed that, even at 100 μM ETD151, the uptake of PI in bacterial cells was insignificant compared to untreated bacteria (Fig. 5*C*). In contrast, treatment with the positive control Triton-X 100 (1%, v/v) resulted in 42% of PI-positive cells over 30 min. This indicates that membrane permeabilization is not the primary mechanism through which ETD151 inhibits the growth of *N. capsulatum*. Overall, ETD151 selectively affects bacteria containing GSL in their membranes in a concentration-dependent manner. At low concentrations, it induces a shape transition in bacteria. At high concentrations, it triggers a growth-inhibitory effect without causing significant membrane damage".

ETD151 is mainly located on the N. capsulatum cell surface. Given ETD151's ability to bind fungal surfaces, we investigated the potential membrane-dependent localization of ETD151 on *N. capsulatum* cells using fluorescence-based techniques. Flow cytometry analysis of bacterial cultures treated with a low concentration of Atto647-ETD151 (2 μM) revealed the emergence of a bacterial subpopulation (78% of the treated culture) that tested positive for the labeled peptide after 10 min (*SI Appendix*, Fig. S10). This subpopulation may consist of cells that accumulate the peptide on the cell surface (membrane-bound fraction) and/or cells that accumulate the peptide intracellularly. Simultaneously, membrane perturbation was assessed using Sytox orange, a DNA-binding dye. As anticipated, cells treated with Atto647-ETD151 exhibited intact membranes even after 30 min. These results suggest that Atto647-ETD151 accumulates at the bacterial cell surface, indicating a strong affinity for membrane compounds without causing membrane damage. To gain further insight into the localization of Atto647-ETD151, *N. capsulatum* cells were exposed to Atto647-ETD151

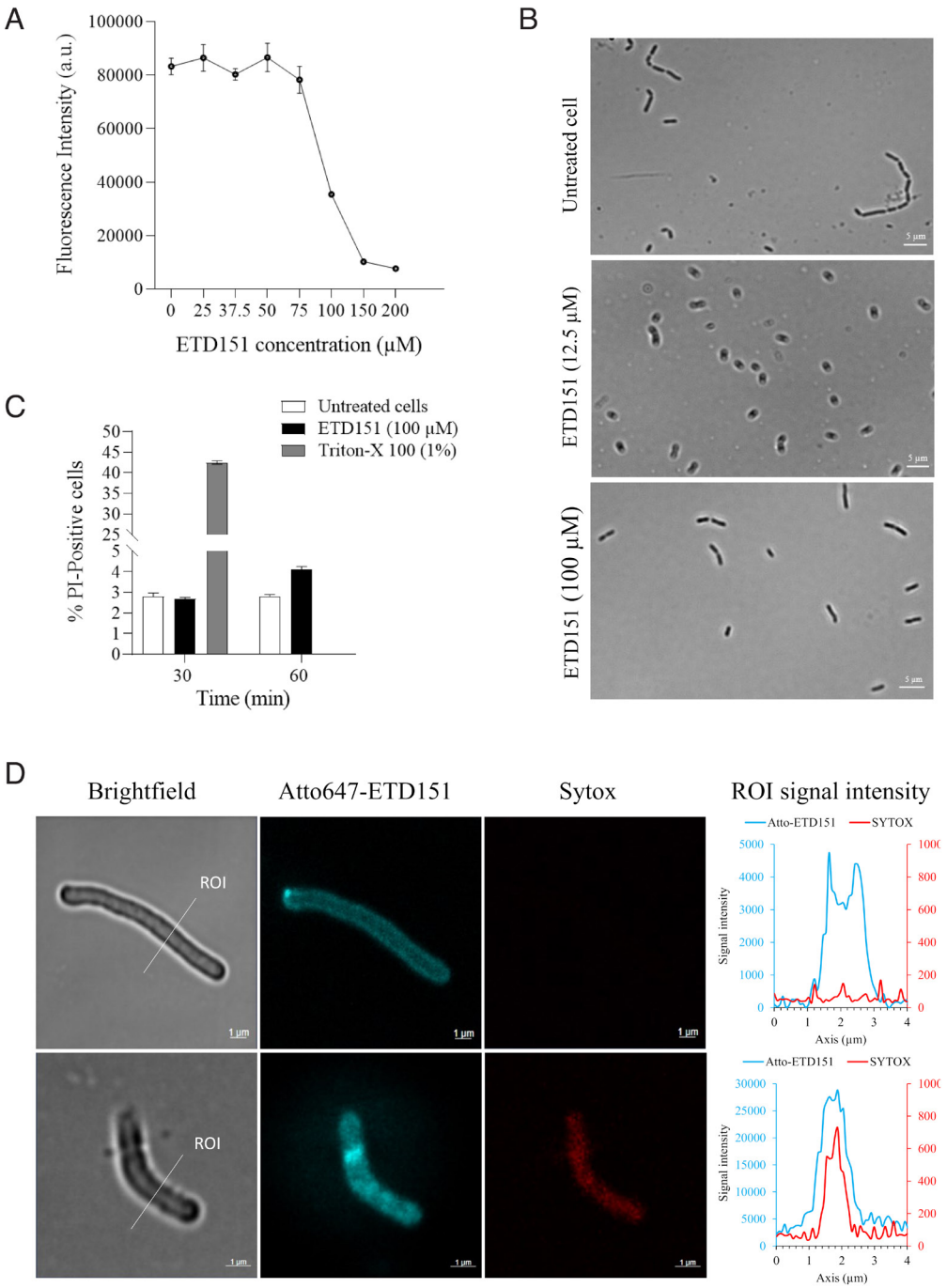

Fig. 5. Effect of ETD151 on glycosphingolipid-containing bacterium *N. capsulatum*. (*A*) Antibacterial activity of ETD151 against *N. capsulatum* was determined using the resazurin cell viability assay. Different concentrations of ETD151 (25 to 200 µM) were incubated with *N. capsulatum* for 24 h. Fluorescence intensity was measured after 2 h of adding resazurin (10%, v/v). The metabolically active cells can reduce nonfluorescent resazurin to fluorescent form. Data are represented as means ± SEM for triplicate measurements. (*B*) Representative microscopy images of *N. capsulatum* treated after 24 h with two concentrations of ETD151 (12.5 and 100 µM). Untreated cells, showing normal rod-shaped cells. At 12.5 µM, ETD151 induces bacterial cell shape changes, showing spherical cells of *N. capsulatum*. At 100 µM, ETD151 appears to have any effect on cellular morphology. (Scale bar, 2 µm.) (*C*) Cytoplasmic membrane permeabilization of *N. capsulatum* treated with 100 µM ETD151 determined via flow cytometry with 30 µM PI (PI membrane impermeable) stain. The proportion of permeabilized cells was detected by fluorescence due to binding of PI fluorescent probe with DNA after 30 and 60 min of incubation with ETD151. Untreated cells and cells treated with Triton-X 100 (1%, v/v) were used as negative and positive controls, respectively. Data are means ± SEM for triplicate measurements. (*D*) Subcellular localization of Atto647-ETD151 in *N. capsulatum*. *Left*: Confocal microscopy images of *N. capsulatum* cells simultaneously exposed to 2 µM Atto647-ETD151 (blue) and 10 nM Sytox orange (red) for 30 min. (Scale bar, 1 µm.) *Right*: Signal intensity (Arbitrary Units) taken from region of interest (ROI) of each cell.

(2 µM) in the presence of Sytox orange for 30 min and observed by confocal microscopy. The distinctive "camel profile" of Atto647-ETD151 fluorescence (Fig. 5*D*, *Top*) shows that the peptide tends to accumulate at the membrane level in areas enriched in GSL. This observation is consistent with our previous findings in the fungus *B. cinerea*. For a minor fraction of bacteria (around 1% of bacteria, according to flow cytometry analysis, see *SI Appendix*, Fig. S10), Atto647-ETD151 fluorescence can be seen within the bacterial cytoplasm, concomitantly with a weak fluorescent signal from the Sytox dye (~0.7 kDa) (Fig. 5*D*, *Bottom*). These observations may indicate a weak and/or transient disruption of the membrane allowing that part of the peptide to penetrate these cells and reach the bacterial cytoplasm. In these cases, the Atto-647 fluorescence profile switches from a camel to a dromedary profile (Fig. 5*D*, *Right*).

The data presented above confirm that the presence of GSL, the membrane target of ETD151, is crucial for its activity. Although the *N. capsulatum* glycosphingolipid is structurally different from fungal glucosylceramide, its presence in the bacterial outer membrane seems sufficient to observe the effect of ETD151, albeit at high concentrations.

The Potential of ETD151 May Apply to Other Human Pathologies. A strong connection was established between the target-binding step and the antifungal activity of ETD151, making it a promising candidate for targeting pathogenic fungi. This potential may apply to other human pathologies for which glucosylceramide metabolism is dysregulated, including lysosomal storage disorders (LSDs) and certain types of cancer. Indeed, Gaucher disease, one of the most prevalent LSDs, is caused by the deficiency of the lysosomal hydrolase β-glucocerebrosidase, which leads to pathological accumulation of GlcCer and glucosylsphingosine (54). In cancer cells, elevated levels of GlcCer can affect tumor progression and metastasis. Additionally, this accumulation of GlcCer has been observed in multidrug resistant (MDR) cancer cells (55, 56). Some GlcCer-associated plant defensins have been identified as potential anticancer agents with promising biological applications. Psd1 shows promise as a prototype for human lung antimetastatic melanoma therapy (57). MsDef1 has been demonstrated to sensitize MDR cancer cells to Doxorubicin chemotherapy, enhancing chemotherapy response (58). PvD1 modulates the membrane composition of breast cancer-derived exosomes (59). As with plant defensins, it would be beneficial to evaluate the potential of the insect-derived ETD151 (which combat pathogenic fungi through their essential GlcCer), as a possible anticancer agent.

Conclusions

GlcCer are pathogenicity determinants for numerous fungal pathogens. Antifungal compounds that target them directly represent a promising solution for combating fungal infections. The ETD151 defensin, optimized from butterfly defensins, exhibits potent antifungal activity against several human fungal pathogens, including *A. fumigatus*, *C. neoformans,* and *C. albicans*, which rank among the most critical fungal pathogens in the World Health Organization's fungal priority pathogens list (60). Its efficacy has also been observed against plant fungal pathogens such as *B. cinerea*. This activity is dependent on the GlcCer fungal membrane, making it one of the potential molecular targets of ETD151's MOA.

This multitechnique study provided essential insights into the MOA of ETD151 on *B. cinerea*. ETD151 was found to selectively bind to fGlcCer extracted from *B. cinerea*, revealing a well-conserved among fungi. GlcCer is also a determining factor in the cellular location of ETD151, as it is localized in the cell's enrichment regions (CW, plasma membrane, and intracellular vesicles). Following this interaction, ETD151 appears to modulate multiple cellular processes previously demonstrated by proteomic analysis (25), ultimately leading to fungal cell death. ETD151's antifungal activity is probably not ensured by a single mode of action, but involves a complex set of events, making the development of resistance rather unlikely.

Building on the understanding of ETD151's molecular target in fungi, we have studied rare bacteria containing GSL in their membranes. Although structurally distinct from fGlcCer, these bacteria have demonstrated some sensitivity to ETD151. We believe that ETD151 has the potential to be extended to other human GlcCer-related pathologies, such as cancer and GlcCer-related resistance to chemotherapeutic drugs, and thus pave the way for new perspectives in human health.

Materials and Methods

Reagents. The Potato Dextrose Broth (PDB) medium was purchased from Sigma-Aldrich (St. Louis, MO). SYTOX Orange Nucleic Acid Stain was purchased from Thermo Fisher Scientific (Waltham, MA). PC and Soybean GlcCer were purchased from Avanti Polar Lipids (Alabaster, AL, United States). The liquid minimum medium based on Tanaka's medium B was prepared according to (25). Ammonium hydroxide (NH_4OH), dichloromethane (DCM), and methanol (MeOH) were of reagent-grade or better quality and were purchased from Carlo-Erba (Val-de-Reuil, France).

Recombinant ETD151 and Labeled Peptide. The recombinant peptide ETD151 produced by high cell density fermentation of a modified *S. cerevisiae* strain developed by the former company EntoMed S.A. (Illkirch, France) was a gift from Philippe Bulet. Labeling of ETD151 peptide by BODIPY-FL-NHS ester (BDP, Lumiprobe) was performed by Genepep Society (Montpellier, France).

***B. cinerea* Strains and Growth Conditions.** Field-isolated *B. cinerea* spores B047 of agricultural interest were supplied by the Centre de Recherche de La Dargoire (Bayer CropScience, France). This strain was used for all experiments, as all previous data (25), proteomic analysis, and morphogenic alterations, as well as membrane permeabilization, concerning the MOA of ETD151, were obtained from this strain. For GlcCer extraction and identification, in addition to B047 strain, *B. cinerea* B05.10, a strain from Dr Paul Tudzynski's laboratory (Institut für Botanik, Münster, Germany) (61), was used.

B. cinerea strain B047 was grown and prepared as previously described (25). Strain B05.10 was available as "plugs" stored sterile in Milli-Q water at 4 °C. A culture was started by depositing a plug (approx. 0.5 cm^2) on potato dextrose agar medium (Oxoid, Basingstoke, U.K.) before incubation for 10 to 12 d at 21 ± 1 °C under ultraviolet light (UV, Vilber Lourmat 15 W 365 nm lamp). The B05.10 culture can be maintained by weekly subculturing (five maximum) from a plug taken from the previous week's dish.

To prepare a fresh spore solution, spores were harvested from a 7-d-old (for strain B047) or 10-d-old (for strain B05.10) culture dish using a Falcon cell scraper (Corning), filtered on a Falcon nylon 100 μm cell strainer (Corning), counted twice using a Malassez chamber, and adjusted to a final concentration of 10^4 sp/mL in minimal medium.

Activity Against Yeast Mutants Lacking GlcCer. *Pichia pastoris* strain GS115 (Invitrogen) and the corresponding *P. pastoris gcs*-deletion (Δ*gcs*) strain (62, 63), *C. albicans* strain SC5314 CAI4 and the corresponding *C. albicans gcs*-deletion strain (62) were used in this study. The antifungal activity of ETD151 against these yeast strains was assayed by microscopic analysis of liquid cultures grown in microtiter plates as described previously (17).

Extraction and Purification of GlcCer. For lipid extraction, *B. cinerea* mycelia were subjected to the Mandala extraction method, followed by a Bligh and Dyer extraction. Finally, a mild alkaline hydrolysis was performed to remove the glycerol backbone containing lipid contaminants (64). To isolate the glycosylceramides, the recovered lipids were purified by preparative thin layer chromatography (Silica Gel 60 Å, 10 × 10 cm plates, Merck, Germany) via elution with DCM: MeOH: 2 M NH_4OH (65:25:4; v/v/v). Commercial Soybean GlcCer ($GlcCer_{Soybean}$) was used as a standard. The spots were visualized under UV light (345 nm) after sprayed with primulin solution (0.05% primulin in 80% acetone). Glycosphingolipid-positive fractions were then extracted from the silica gel layer and used for either sphingolipid analysis by ESI–MS or sugar head group analysis by GC-MS.

Characterization of GlcCer. For sugar analysis, GSL-positive fractions were subjected to methanolysis followed by TMS-derivatization as previously described (65) before GC–MS analysis (*SI Appendix*, section 3). Sugar identification was performed by comparison with glucose and galactose as references.

For sphingolipids structure identification, MS analyses were performed using an HPLC coupled to a triple quadrupole mass spectrometry system (QqQ-MS, Agilent 1290 to 6495). Samples dissolved in methanol were subjected to full scanning MS (with scan range *m/z* 600 to 800) to detect characteristic *m/z* corresponding to fGlcCer and then MS/MS fragmentation (collision energy of 10, 20, 30, and 40 eV) to confirm the characteristic patterns (hexose, fatty acyl and sphingoid base) of the identified putative GlcCer. All the experimental parameters are detailed in *SI Appendix*, section 3. Data acquisition and processing were

performed using MassHunter software (Agilent) software. The Soybean GlcCer was used as a standard to validate the method.

Liposome Preparation and Characterization. Large unilamellar vesicles (LUV) were prepared with PC alone, referred to as "GlcCer-free liposomes" or with a PC/$GlcCer_{B.cinerea}$ molar ratio of 90/10 referred to as "GlcCer-containing liposomes". Lipids were dissolved in chloroform, dried under a nitrogen gas stream to create lipid films, and hydrated in 1 mL phosphate buffer (10 mM, pH 5.8). LUV were prepared by passing through a mini-extruder (Avanti Polar Lipids) using stacked 100 nm pore-size polycarbonate membrane filters. The particle size distribution and polydispersity index of vesicles generated were measured by dynamic light scattering analysis (Malvern Zetasizer Instruments ver. 7.11).

Labeling of ETD151 with Atto647 as Fluorophore for MST Affinity Assay. For MST experiments, ETD151 was labeled with the red fluorescent dye Atto647 NHS-ester (07376, Sigma-Aldrich) based on a classical N-hydroxy succinimidyl ester (NHS ester) chemistry. The protocol of labeling is detailed in *SI Appendix*, section 6).

To investigate the binding affinity between Atto647-ETD151 and $GlcCer_{B.cinerea}$-containing or -free liposomes, Atto647-ETD151 diluted in phosphate buffer (10 mM, pH 5.8) was centrifuged (10,000×*g*, 10 min) to remove potential peptide aggregates. The stock solution of each liposome (2 mM, 10 μL) was diluted 1:1 in phosphate buffer to make a 16-sample serial twofold dilution from 1 mM to 30.5 nM. Atto647-ETD151 was then added to obtain a final concentration of 50 nM in each ligand solution, well mixed and centrifuged (5,000×*g*, 2 min). Control liposomes containing only PC were incubated with Atto647-ETD151 under the same conditions.

MST experiments were performed on NanoTemper® Monolith NT.115 pico (NanoTemper Technologies GmbH, Munich, Germany). Standard silica capillaries from NanoTemper® (MO-K022) were filled with each sample and changes in Atto647-ETD151 fluorescence were detected by the MST device. Autodetect excitation power and 40% MST power with laser off/on times of 0 s and 20 s, respectively, were set up for all acquisitions. All measurements were performed at 22 °C and repeated three times.

Data analyses were performed using the MO.Affinity Analysis software (version 2.3, NanoTemper Technologies). The fluorescence change in the MST signal is normalized (F_{norm}), defined as F_{hot}/F_{cold} (F_{hot} as the hot region at 5 s after infrared (IR) laser heating and F_{cold} as the cold region at 0 s, before the laser is turned on). A dose–response curve is plotted as F_{norm} against the ligand concentration. The binding constants K_d between Atto647-ETD151 and liposomes were calculated using the saturation binding curve at equilibrium. The fitting function is derived from the law of mass action (66).

Liposome Pulldown Assay. Liposomes were prepared as previously described at final lipid concentrations equal to 2.5 mg/mL. 100 mL of liposomes were mixed with 50 μL of ETD151 peptide (0.1 mg/mL) and incubated at room temperature for 1 h. Liposome-peptide mixtures were centrifuged at 5,000×*g* rpm for 10 min at 20 °C. Pellets were washed twice with phosphate buffer (10 mM, pH 5.8), treated with Trion X-100 (1% final concentration), and centrifuged again (5,000×*g* rpm for 5 min). These experiments were repeated twice, and for each set, the bound and unbound peptide fractions were analyzed by SDS-PAGE. The protein bands were quantified by densitometry using ImageJ software. Averages of the ratio of intensities (bound: unbound) and SEM from all experiments were then calculated.

Fungal Growth Inhibition Assay. The antifungal activity of ETD151 and BODIPY-ETD151 against *B. cinerea* was determined as described in (25). Briefly, microplate wells (TPP Techno Plastic Products AG, Switzerland) were filled with 135 μL of the fresh suspension at 10^4 sp/mL before incubation. The addition of 15 μL of ETD151 solutions, resulting in final concentrations of 25 to 0.049 μM, occurred 3 d later. The plate was gently shaken and incubated for an additional 4 d. Evolution of the assay was monitored daily by absorbance measurement at 630 nm with an ELx808 microplate reader (BioTek, Winooski, USA). The dose–response curve was generated with Microsoft Excel software and XLfit plug-in (release 5.4). Data were fitted using the "Dose–response one site — 205" model to determine the concentration that inhibited at least 90% of growth (IC_{90}).

Confocal Microscopy of *B. cinerea* Treated with BODIPY-ETD151. A fresh spore solution at 1 × 10^4 sp/mL of *B. cinerea* was prepared in a 25% PDB medium and 200 μL of the solution was distributed in 96-well microplates (SensoPlate Glass Bottom, Greiner Bio-One). After 24 h of incubation and shaking, *B. cinerea* mycelia were treated by adding BODIPY-ETD151 at final concentrations of 0.19 and 0.78 μM. Imaging was performed immediately after addition of BODIPY-ETD151 using an inverted microscope (Axio Observer.Z1, Zeiss) combined with a confocal laser scanning unit (LSM 800, Zeiss). The latter was equipped with photomultiplier tubes, a transmitted light detector (ESID), three gallium phospho-arsenide detectors (GaAsP), and two oil-immersion objectives, Plan-Apochromat 63x/1.40 and 100x/1.40. Images were captured and processed using Zen software (v2.3). For microscopy experiments containing Calcofluor White M2R (F3543, Sigma-Aldrich) (final concentration of 9 μg/mL), a fluorophore that binds to the CW, and FM4-64 (T13320, Invitrogen) (final concentration of 5 μg/mL), a membrane-binding fluorophore, were added to the cell media immediately before imaging.

***N. capsulatum* Strains and Growth Conditions.** *N. capsulatum* DSMZ 30196 bacteria, were cultured on "nutrient" media recommended by the supplier (Peptone 5 g/L, meat extract 3 g/L, and ± agar 15 g/L in distilled water, pH adjusted to 7) at 30 °C under 180 rpm.

Resazurin-Based Assay and Microscopy Observation for *N. capsulatum* Treated with ETD151. A fresh inoculum of *N. capsulatum* was prepared in the nutrient media from the overnight bacterial suspensions of 1/100 and incubated until reaching 10^8 CFU/mL. The broth microdilution protocol, as previously described (67), was performed in a 96-well microtiter plate. Bacterial cells were incubated with different concentrations of ETD151 (25, 37.5, 50, 75, 100, 150, 200 μM) at 30 °C under 180 rpm. After overnight incubation at 30 °C, morphological changes caused by ETD151 were evaluated by microscopic observation of cells (untreated cells, cells treated with ETD151 at 12.5 and 100 μM). Then, 10 μL alamarBlue reagent (DAL1025, Invitrogen) was added to all wells and incubated at 37 °C for another 1 h. Color changes were observed and recorded by spectrophotometry. Bacterial cell viability was evaluated by fluorescence measurement (Ex 530–560 nm/ Em 590 nm) using a spectrophotometer plate reader (CLARIOstar Plus, BMG LABTECH). Only media without cells was included to determine the background signal and 100% reduced alamarBlue reagent without cells was included as a positive control. These experiments were performed in triplicate.

Membrane Permeabilization of *N. capsulatum* Treated with ETD151. All cell uptake assays were performed with a flow cytometer (LSRFortessa SORP) equipped with an argon laser. Detectors were set to logarithmic amplification. All experiments were performed in triplicate. Data were acquired and analyzed using BD FACSDiva software v8.0.1. A minimum of 20,000 events were recorded for each sample.

N. capsulatum cell membrane disruption was determined by measuring the percentage of PI incorporation (Invitrogen, Eugene, OR) into the cells. Bacterial cells suspended in a nutrient medium were incubated simultaneously with ETD151 and PI at concentrations of 100 and 30 μM, respectively, at room temperature. PI fluorescence intensity was recorded at different time points using the LSRFortessa SORP flow cytometer. The wavelength of red fluorescence was (610/20 nm) bandpass filter for PI. A positive control of 1% (v/v) Triton X-100 (Sigma Aldrich, St Louis, MO) in nutrient medium was used to disrupt the cytoplasmic membrane of bacteria, and bacteria incubated with PI without the peptide were considered a negative control.

Confocal Microscopy of *N. capsulatum* Cells Treated with Atto647-ETD151. Confocal laser scanning microscopy observation was used to localize Atto647-ETD151 at the cellular level. Live cell imaging was performed on an Axio Observer. Z1/7 confocal microscope using a 63X oil immersion objective. *N. capsulatum* cells suspended in nutrient media were treated for 30 min with Atto647-ETD151 (2 μM) in the presence of Sytox orange at 10 nM as a final concentration. Orange (excitation wavelength, 590 nm; emission wavelength, 618 nm) and red (excitation wavelength, 653 nm; emission wavelength, 668 nm) channels were used for Sytox and Atto647-ETD151 fluorescence, respectively. Image analysis and intensity profiles were performed using ZEN 2.3 lite software.

Data, Materials, and Software Availability. All study data are included in the article and/or *SI Appendix*.

ACKNOWLEDGMENTS. We would like to thank P. Soule (Nanotemper) for the initial discussion on the feasibility of MST experiments with liposomes. We thank also L. Trousseau and C. Struyfs for their technical support in the antibacterial and antifungal yeast trials, respectively. Finally, we are grateful to MO2VING facility (CBM, Orléans, France) and in particular to D. Gosset (P@CYFIC subplatform) for the confocal microscopy and flow cytometry experiments on bacteria.

Author affiliations: [a]Centre for Molecular Biophysics, CNRS, Orléans 45071, France; [b]Institute for Advanced Biosciences, University of Grenoble Alpes, Grenoble 38700, France; [c]Institute of Organic and Analytical Chemistry, University of Orléans, CNRS, Orléans 45069, France; [d]Plateform BioPark Archamps, Archamps 74160, France; [e]Bayer CropScience, Lyon 69263, France; and [f]Centre of Microbial and Plant Genetics, Katholieke Universiteit Leuven, Leuven 3001, Belgium

Author contributions: O.K., V.A., and C.L. designed research; O.K., Y.Y.-B., R. Nasreddine, S.V., T.A., B.P.A.C., J.-B.M., K.T., P.B., and C.L. performed research; O.K. contributed new reagents/analytic tools; O.K., Y.Y.-B., R. Nasreddine, T.A., B.P.A.C., T.K., K.T., R. Nehmé, V.A., C.B., P.B., and C.L. analyzed data; and O.K., P.B., and C.L. wrote the paper.

1. M. C. Fisher *et al.*, Tackling the emerging threat of antifungal resistance to human health. *Nat. Rev. Microbiol.* **20**, 557–571 (2022).
2. R. Garcia-Rubio, H. C. de Oliveira, J. Rivera, N. Trevijano-Contador, The fungal cell wall: *Candida*, *Cryptococcus*, and *Aspergillus* Species. *Front. Microbiol.* **10**, 2993 (2020).
3. D. G. Sant, S. G. Tupe, C. V. Ramana, M. V. Deshpande, Fungal cell membrane-promising drug target for antifungal therapy. *J. Appl. Microbiol.* **121**, 1498–1510 (2016).
4. P. C. Rittershaus *et al.*, Glucosylceramide synthase is an essential regulator of pathogenicity of *Cryptococcus neoformans*. *J. Clin. Invest.* **116**, 1651–1659 (2006).
5. S. M. Noble, S. French, L. A. Kohn, V. Chen, A. D. Johnson, Systematic screens of a *Candida albicans* homozygous deletion library decouple morphogenetic switching and pathogenicity. *Nat. Genet.* **42**, 590–598 (2010).
6. J. Wang *et al.*, Loss of glucosylceramide synthase impairs the growth and virulence of *Fusarium oxysporum* f. sp. cubense. *Phytopathol. Res.* **4**, 31 (2022).
7. Y. Huang *et al.*, CgGCS, Encoding a glucosylceramide synthase, is required for growth, conidiation and pathogenicity in *Colletotrichum gloeosporioides*. *Front Microbiol.* **10**, 1016 (2019).
8. C. Zhu *et al.*, Glucosylceramides are required for mycelial growth and full virulence in *Penicillium digitatum*. *Biochem. Biophy. Res. Commun.* **455**, 165–171 (2014).
9. R. Rollin-Pinheiro, A. Singh, E. Barreto-Bergter, M. Del Poeta, Sphingolipids as targets for treatment of fungal infections. *Future Med. Chem.* **8**, 1469–1484 (2016).
10. K. McEvoy, T. G. Normile, M. Del Poeta, Antifungal drug development: Targeting the fungal sphingolipid pathway. *J. Fungi (Basel)* **6**, 142 (2020).
11. S. B. Levery *et al.*, Disruption of the glucosylceramide biosynthetic pathway in *Aspergillus nidulans* and *Aspergillus fumigatus* by inhibitors of UDP-Glc:Ceramide glucosyltransferase strongly affects spore germination, cell cycle, and hyphal growth. *FEBS Lett.* **525**, 59–64 (2002).
12. L. Nimrichter *et al.*, A monoclonal antibody to glucosylceramide inhibits the growth of *Fonsecaea pedrosoi* and enhances the antifungal action of mouse macrophages. *Microbes infect.* **6**, 657–665 (2004).
13. M. L. Rodrigues *et al.*, Human antibodies against a purified glucosylceramide from *Cryptococcus neoformans* inhibit cell budding and fungal growth. *Infect. Immun.* **68**, 7049–7060 (2000).
14. M. L. Rodrigues *et al.*, Monoclonal antibody to fungal glucosylceramide protects mice against lethal C*ryptococcus neoformans* infection. *Clin. Vaccine Immunol.* **14**, 1372–1376 (2007).
15. B. De Coninck *et al.*, Fungal glucosylceramide-specific camelid single domain antibodies are characterized by broad spectrum antifungal activity. *Front. Microbiol.* **8**, 1059 (2017).
16. M. J. A. Hein, M. Kvansakul, F. T. Lay, T. K. Phan, M. D. Hulett, Defensin–lipid interactions in membrane targeting: Mechanisms of action and opportunities for the development of antimicrobial and anticancer therapeutics. *Biochem. Soc. Trans.* **50**, 423–437 (2022).
17. K. Thevissen *et al.*, Defensins from insects and plants interact with fungal glucosylceramides*. *J. Biol. Chem.* **279**, 3900–3905 (2004).
18. V. Ramamoorthy *et al.*, Glucosylceramide synthase is essential for alfalfa defensin-mediated growth inhibition but not for pathogenicity of *Fusarium graminearum*. *Mol. Microbiol.* **66**, 771–786 (2007).
19. Y. Oguro, H. Yamazaki, M. Takagi, H. Takaku, Antifungal activity of plant defensin AFP1 in *Brassica juncea* involves the recognition of the methyl residue in glucosylceramide of target pathogen *Candida albicans*. *Curr. Genet.* **60**, 89–97 (2014).
20. V. S. G. Amaral *et al.*, Psd2 pea defensin shows a preference for mimetic membrane rafts enriched with glucosylceramide and ergosterol. *Biochim. Biophys. Acta Biomembr.* **1861**, 713–728 (2019).
21. K. Thevissen *et al.*, The plant defensin RsAFP2 induces cell wall stress, septin mislocalization and accumulation of ceramides in *Candida albicans*. *Mol. Microbiol.* **84**, 166–180 (2012).
22. V. Leannec-Rialland *et al.*, Use of defensins to develop eco-friendly alternatives to synthetic fungicides to control phytopathogenic fungi and their mycotoxins. *J. Fungi* **8**, 229 (2022).
23. W. Shao, Y. Zhao, Z. Ma, Advances in understanding fungicide resistance in botrytis cinerea in China. *Phytopathology* **111**, 455–463 (2021).
24. C. Landon *et al.*, Lead optimization of antifungal peptides with 3D NMR structures analysis. *Protein Sci.* **13**, 703–713 (2004).
25. T. Aumer, S. N. Voisin, T. Knobloch, C. Landon, P. Bulet, Impact of an antifungal insect defensin on the proteome of the phytopathogenic fungus botrytis cinerea. *J. Proteome Res.* **19**, 1131–1146 (2020).
26. N. Banzet *et al.*, Expression of insect cystein-rich antifungal peptides in transgenic tobacco enhances resistance to a fungal disease. *Plant Sci.* **162**, 995–1006 (2002).
27. I. Olsen, E. Jantzen, Sphingolipids in bacteria and fungi. *Anaerobe* **7**, 103–112 (2001).
28. M. Del Poeta, L. Nimrichter, M. L. Rodrigues, C. Luberto, Synthesis and biological properties of fungal glucosylceramide. *PLoS Pathog.* **10**, e1003832 (2014).
29. A. Singh, M. Del Poeta, Sphingolipidomics: An important mechanistic tool for studying fungal pathogens. *Front Microbiol.* **7**, 501 (2016).
30. E. Barreto-Bergter, G. L. Sassaki, L. M. de Souza, Structural analysis of fungal cerebrosides. *Front Microbiol.* **2**, 239 (2011).
31. R. O. R. Calixto *et al.*, Structural analysis of glucosylceramides (GlcCer) from species of the *Pseudallescheria/Scedosporium* complex. *Fungal Biol.* **120**, 166–172 (2016).
32. N. Paege *et al.*, Species-specific differences in the susceptibility of fungi to the antifungal protein AFP depend on C-3 saturation of glycosylceramides. *mSphere* **4**, e00741 (2019).
33. L. Neves de Medeiros *et al.*, Psd1 binding affinity toward fungal membrane components as assessed by SPR: The role of glucosylceramide in fungal recognition and entry. *Peptide Sci.* **102**, 456–464 (2014).
34. S. Duhr, D. Braun, Why molecules move along a temperature gradient. *Proc. Natl. Acad. Sci. U.S.A.* **103**, 19678–19682 (2006).
35. G. Al Hamoui Dit Banni, *et al.*, Investigation of lipase-ligand interactions in porcine pancreatic extracts by microscale thermophoresis. *Anal. Bioanal. Chem.* **413**, 3667–3681 (2021).
36. E. Rascol, A. Dufourquet, R. Baccouch, P. Soule, I. D. Alves, An original approach to measure ligand/receptor binding affinity in non-purified samples. *Sci. Rep.* **12**, 5400 (2022).
37. G. van den Bogaart, K. Meyenberg, U. Diederichsen, R. Jahn, Phosphatidylinositol 4,5-bisphosphate increases Ca2+ affinity of synaptotagmin-1 by 40-fold *J. Biol. Chem.* **287**, 16447–16453 (2012).
38. L. Yu, Q. Fan, X. Yue, Y. Mao, L. Qu, Activity of a novel-designed antimicrobial peptide and its interaction with lipids. *J. Pept Sci.* **21**, 274–82 (2015).
39. M. Mahajan *et al.*, NMR identification of a conserved Drp1 cardiolipin-binding motif essential for stress-induced mitochondrial fission. *Proc. Natl. Acad. Sci. U.S.A.* **118**, e2023079118 (2021).
40. P. Rainsford *et al.*, Label-free measurement of antimicrobial peptide interactions with lipid vesicles and nanodiscs using microscale thermophoresis. *Sci. Rep.* **13**, 12619 (2023).
41. L. Danne *et al.*, Membrane-binding mechanism of a bacterial phospholipid N-methyltransferase. *Mol. Microbiol.* **95**, 313–331 (2015).
42. N. Bharambe, R. Ramachandran, Microscale thermophoresis (MST) as a tool for measuring dynamin superfamily protein (DSP)-lipid interactions. *Methods Mol. Biol.* **2159**, 85–92 (2020).
43. A. Muñoz *et al.*, Specific domains of plant defensins differentially disrupt colony initiation, cell fusion and calcium homeostasis in *Neurospora crassa*. *Mol. Microbiol.* **92**, 1357–1374 (2014).
44. D. S. Lobo *et al.*, Antifungal pisum sativum defensin 1 interacts with neurospora crassa cyclin F related to the cell cycle. *Biochemistry* **46**, 987–996 (2007).
45. L. Nimrichter, M. L. Rodrigues, E. Barreto-Bergter, L. R. Travassos, Sophisticated functions for a simple molecule: The role of glucosylceramides in fungal cells. *Lipid Insights* **2**, 61–73 (2008).
46. M. Lee, S. Y. Lee, Y.-S. Bae, Functional roles of sphingolipids in immunity and their implication in disease. *Exp. Mol. Med.* **55**, 1110–1130 (2023).
47. N. L. van der Weerden, R. E. W. Hancock, M. A. Anderson, Permeabilization of fungal hyphae by the plant defensin NaD1 Occurs through a cell wall-dependent process. *J. Biol. Chem.* **285**, 37513–37520 (2010).
48. F. R. Terras *et al.*, Analysis of two novel classes of plant antifungal proteins from radish (*Raphanus sativus L.*) seeds. *J. Biol. Chem.* **267**, 15301–15309 (1992).
49. M. Lamberty *et al.*, Insect immunity isolation from the lepidopteran heliothis virescens of a novel insect defensin with potent antifungal activity. *J. Biol. Chem.* **274**, 9320–9326 (1999).
50. V. Silva de Paula *et al.*, Evolutionary relationship between defensins in the Poaceae family strengthened by the characterization of new sugarcane defensins. *Plant Mol. Biol.* **68**, 321–335 (2008).
51. K. Kawahara, H. Moll, Y. A. Knirel, U. Seydel, Structural analysis of two glycosphingolipids from the lipopolysaccharidelacking bacterium *Sphingomonas capsulata*. *Eur. J. Biochem.* **267**, 1837–46 (2000).
52. L. G. Monahan *et al.*, Rapid conversion of *Pseudomonas aeruginosa* to a spherical cell morphotype facilitates tolerance to carbapenems and penicillins but increases susceptibility to antimicrobial peptides. *Antimicrob. Agents Chemother.* **58**, 1956–1962 (2014).
53. N. Ojkic, D. Serbanescu, S. Banerjee, Antibiotic Resistance via Bacterial Cell Shape-Shifting. *mBio* **13**, e00659–22 (2022).
54. J. Stirnemann *et al.*, A review of gaucher disease pathophysiology, clinical presentation and treatments. *Int. J. Mol. Sci.* **18**, 441 (2017).
55. Y. Y. Liu, T. Y. Han, A. E. Giuliano, M. C. Cabot, Expression of glucosylceramide synthase, converting ceramide to glucosylceramide, confers adriamycin resistance in human breast cancer cells. *J. Biol. Chem.* **274**, 1140–1146 (1999).
56. H. Huang *et al.*, LC-MS based sphingolipidomic study on A549 human lung adenocarcinoma cell line and its taxol-resistant strain. *BMC Cancer* **18**, 799 (2018).
57. V. S. G. do Amaral, *et al.*, Pisum sativum defensin 1 eradicates mouse metastatic lung nodules from B16F10 melanoma cells. *Int. J. Mol. Sci.* **21**, 2662 (2020).
58. R. Pandurangi, A. Karwa, U. S. Sagaram, K. Henzler-Wildman, D. Shah, Medicago Sativa Defensin1 as a tumor sensitizer for improving chemotherapy: Translation from anti-fungal agent to a potential anti-cancer agent. *Front Oncol.* **13**, 1141755 (2023).
59. J. Skalska *et al.*, Plant defensin PvD1 modulates the membrane composition of breast tumour-derived exosomes. *Nanoscale* **11**, 23366–23381 (2019).
60. WHO fungal priority pathogens list to guide research, development and public health action. https://www.who.int/publications/i/item/9789240060241. Accessed 27 July 2024.
61. P. Büttner *et al.*, Variations in ploidy among isolates of Botrytis cinerea: Implications for genetic and molecular analyses. *Curr. Genet* **25**, 445–450 (1994).
62. M. Leipelt *et al.*, Glucosylceramide synthases, a gene family responsible for the biosynthesis of glucosphingolipids in animals, plants, and fungi*. *J. Biol. Chem.* **276**, 33621–33629 (2001).
63. P. Ternes *et al.*, Two pathways of sphingolipid biosynthesis are separated in the yeast pichia pastoris. *J. Biol. Chem.* **286**, 11401–11414 (2011).
64. A. Singh, A. MacKenzie, G. Girnun, M. Del Poeta, Analysis of sphingolipids, sterols, and phospholipids in human pathogenic Cryptococcus strains. *J. Lipid Res.* **58**, 2017–2036 (2017).
65. M. J. McConville, S. W. Homans, J. E. Thomas-Oates, A. Dell, A. Bacic, Structures of the glycoinositolphospholipids from Leishmania major. A family of novel galactofuranose-containing glycolipids. *J. Biol. Chem.* **265**, 7385–7394 (1990).
66. C. J. Wienken, P. Baaske, U. Rothbauer, D. Braun, S. Duhr, Protein-binding assays in biological liquids using microscale thermophoresis. *Nat. Commun.* **1**, 100 (2010).
67. S. G. Franzblau *et al.*, Rapid, low-technology MIC determination with clinical mycobacterium tuberculosis isolates by using the microplate alamar blue assay. *J. Clin. Microbiol.* **36**, 362–366 (1998).

SUPPORTING INFORMATION (SI)

The antimicrobial activity of ETD151 defensin is dictated by the presence of glycosphingolipids in the targeted organisms

Ons Kharrat[a], Yoshiki Yamaryo-Botté[b], Rouba Nasreddine[c], Sébastien Voisin[d], Thomas Aumer[d,e,f], Bruno P.A. Cammue[g], Jean-Baptiste Madinier[a], Thomas Knobloch[e], Karin Thevissen[g], Reine Nehmé[c], Vincent Aucagne[a], Cyrille Botté[b], Philippe Bulet[b,d], Céline Landon[a]*

[a] Centre for Molecular Biophysics, CNRS, University of Orléans, Orléans, France; [b] Institute for Advanced Biosciences, University of Grenoble Alpes, Grenoble, France; [c] Institute of Organic and Analytical Chemistry, University of Orléans, CNRS, Orléans, France; [d] Plateform BioPark Archamps, Archamps, France; [e] Bayer SAS, Bayer CropScience, Lyon, France; [f] Present address: Eurofins BTP Biologics, Lentilly, France; [g] Centre of Microbial and Plant Genetics, KU Leuven, Leuven, Belgium;

Corresponding author: Céline Landon, celine.landon@cnrs-orleans.fr

Supporting Information Contents

1. Glucosylceramides (GlcCer)-associated defensins

Supplementary Table 1: Plant/insect defensins for which GlcCer has been reported to be a determining factor in their antifungal actions and/or which recognize GlcCer *in vitro*

Name (organism)	**The relevance of the presence of GlcCer in the activity and antifungal actions of defensins**	***In vitro* molecular recognition of a defensin to fungal GlcCer**
Heliomicin (*Heliothis virescens*)	-Mutant strains of *Pichia pastoris* (MIC = 2.5 µM for wild-type (wt) strains and MIC > 40 µM for mutant strains) and *Candida albicans* (MIC = 2.5 µM for wt strains and MIC > 20 µM for mutant strains) species lacking GlcCer or *S. cerevisiae* lacking GlcCer in their membranes are resistant to Heliomicin (1).	-Heliomicin was found to interact in a dose-dependent manner with GlcCer from *P. pastoris* using an ELISA-based binding assay (1).
RsAFP2 (*Raphanus sativus*)	-Mutant strains of *P. pastoris* (MIC = 2 µM for wt strains and MIC > 40 µM for mutant strains) and *C. albicans* (MIC = 2.5 µM for wt strains and MIC > 40 µM for mutant strains) species lacking GlcCer or *Saccharomyces cerevisiae* and *Candida glabrata* lacking GlcCer in their membranes are resistant to RsAFP2 (1). -In susceptible *C. albicans*, RsAFP2 induces endogenous reactive oxygen species (ROS), but not in the RsAFP2-resistant mutant lacking GlcCer (2). -*Fusarium graminearum* mutant lacking GlcCer (Δ*Fggcs*1) shows strong resistance to RsAFP2 (IC_{50} value between 0.6 - 0.7 µM) compared to wt PH-1 strain (IC_{50} value between 0.25 - 0.4 µM) (3).	-RsAFP2 was found to interact in a dose-dependent manner with GlcCer from *P. pastoris* using an ELISA-based binding assay (1).
Psd1 (*Pisum sativum*)	-The activity of Psd1 against *C. albicans* Δ*gcs* mutant (IC_{50} = 15 µM) was significantly reduced compared to *C. albicans* CAI4 (IC_{50} = 9 µM) (4). -PITC-conjugated Psd1 was internalized and dispersed in wt *C. albicans*, but not in *C. albicans* Δ*gcs* mutant (4).	-NMR and relaxation studies showed that Psd1 interacts with vesicles of phosphatidylcholine (PC) and PC: fungal GlcCer (9:1 molar ratio) in slightly different forms and the major binding epitope showed conformational changes supporting the conformation selection as the binding mechanism (5). -Surface plasmon resonance (SPR) analysis showed that Psd1 preferentially binds to vesicles containing GlcCer isolated from fungi (4).
Psd2 (*Pisum sativum*)	-*C. albicans* and *Aspergillus nidulans* mutants deficient in GCS (Δ*gcs*1 and Δ*gcs*A, respectively) showed increased resistance to 20 µM Psd2 compared to wt strains (6).	-SPR analysis showed that Psd2 has a higher affinity for pure 1-palmitoyl-2-oleoyl-glycero-3-phosphocholine (POPC) and POPC-based vesicles containing GlcCer and ergosterol in a 70:30 ratio (6).
MsDef1 (*Medicago sativa*)	-*Fusarium graminearum* mutant lacking GlcCer (Δ*Fggcs*1) shows increased resistance to MsDef1 (IC_{50} value between 6 - 9 µM) compared to wt PH-1 strain (IC_{50} value between 1.5 - 3 µM) (3).	No data available
PvD_1 (*Phaseolus vulgaris*)	-PvD_1 did not show growth inhibition on *C. albicans* mutant strains lacking GlcCer compared to wt strains (7). -FITC-conjugated PvD_1 was localized intracellularly in *C. albicans*, colocalized with DAPI staining, but no intracellular labeling was detected in *C. albicans* Δgcs1 mutant strains (7).	No data available
Sd5 (*Saccharum officinarium*)	No data available	-Sd5 was able to promote vesicle leakage when they contained total membrane lipids of *Fusarium solani* or PC: fungal GlcCer compared to no effect was observed with PC: phosphatidylethanolamine or PC: phosphatidylglycerol up to 100 µM Sd5 (8). -NMR and relaxation studies demonstrated that Sd5 undergoes conformational changes in the presence of PC: fungal GlcCer (9:1 molar ratio) vesicles (8).

2. Identification of the *gcs* gene in *B. cinerea*

General information

The BLAST results indicated that the Bcin02p00640.1 protein, transcribed from the *Bcin02g00640* gene, was the optimal match. The candidate protein is predicted to be localized in the endoplasmic reticulum, described as the production site of GlcCer. The candidate *gcs* gene (Bcin02g00640) of *B. cinerea* only shares 50 % identity (and around 65% similarity) with those of the filamentous fungi *Fusarium graminearum, Magnaporthe grisea, Aspergillus nidulans* and *Neurospora crassa.*

Supplementary Table 2: BLAST identification of the *gcs* gene in the fungus *Botrytis cinerea*

Sequence candidate		**Best match in *B. cinerea***		
Species	***gcs* gene**	**Gene**	**% identity**	**% similarity**
F. graminearum	FGSG_05955	*Bcin02g00640*	46 %	62 %
M. grisea	MGG_10668	*Bcin02g00640*	52 %	64 %
N. crassa	NCU01116	*Bcin02g00640*	53 %	66 %
A. nidulans	AN8806	*Bcin02g00640*	54 %	67 %

3. Experimental parameters of the characterization of glucosylceramides (GlcCer)

Analysis of the sugar moiety of GlcCer

GC-MS experiments were performed using a HP5-MS column (30 m x 250 um x 0.25 um (Agilent 19091S-433)) on an Agilent GC–MS (7890B-5977A) system in electron ionization mode coupled with an autosampler (Agilent 7393). The column temperature was programmed from 70°C (1 min hold) at 12.5°C per min then 25°C per min to 320°C (3 min hold). The front inlet temperature was kept at 270°C splitless and the MSD transfer line temperature was kept at 250°C. Inlet pressure was fixed at 8.573 psi. The helium gas flow rate was constant at 0.98.mL/min.

MS analysis of GlcCer

The flow injection conditions were as follows: mobile phase, eluent A (water: acetonitrile: isopropanol, 5:3:2, v/v/v) and eluent B (water: acetonitrile: isopropanol, 1:9:90, v/v/v), both containing 1 mM ammonium formate; flow rate: 0.05 mL/min and injection volume: 2 µL. The ionization conditions were as follows: ionization mode, positive; sheath gas flow rate, 10 L/min; nitrogen as a nebulizer and carrier gas, drying gas temperature, 150°C; drying gas flow 17 L/ min; nebulizer pressure 20 psi; sheath gas temperature 200°C; nozzle voltage, positive 1000 V-negative 1500 V and capillary voltage, positive 3500 V-negative 3000 V. In all cases, the mass accuracy was < 1 ppm.

4. Structural characterization of GlcCer extracted from *B. cinerea* B047

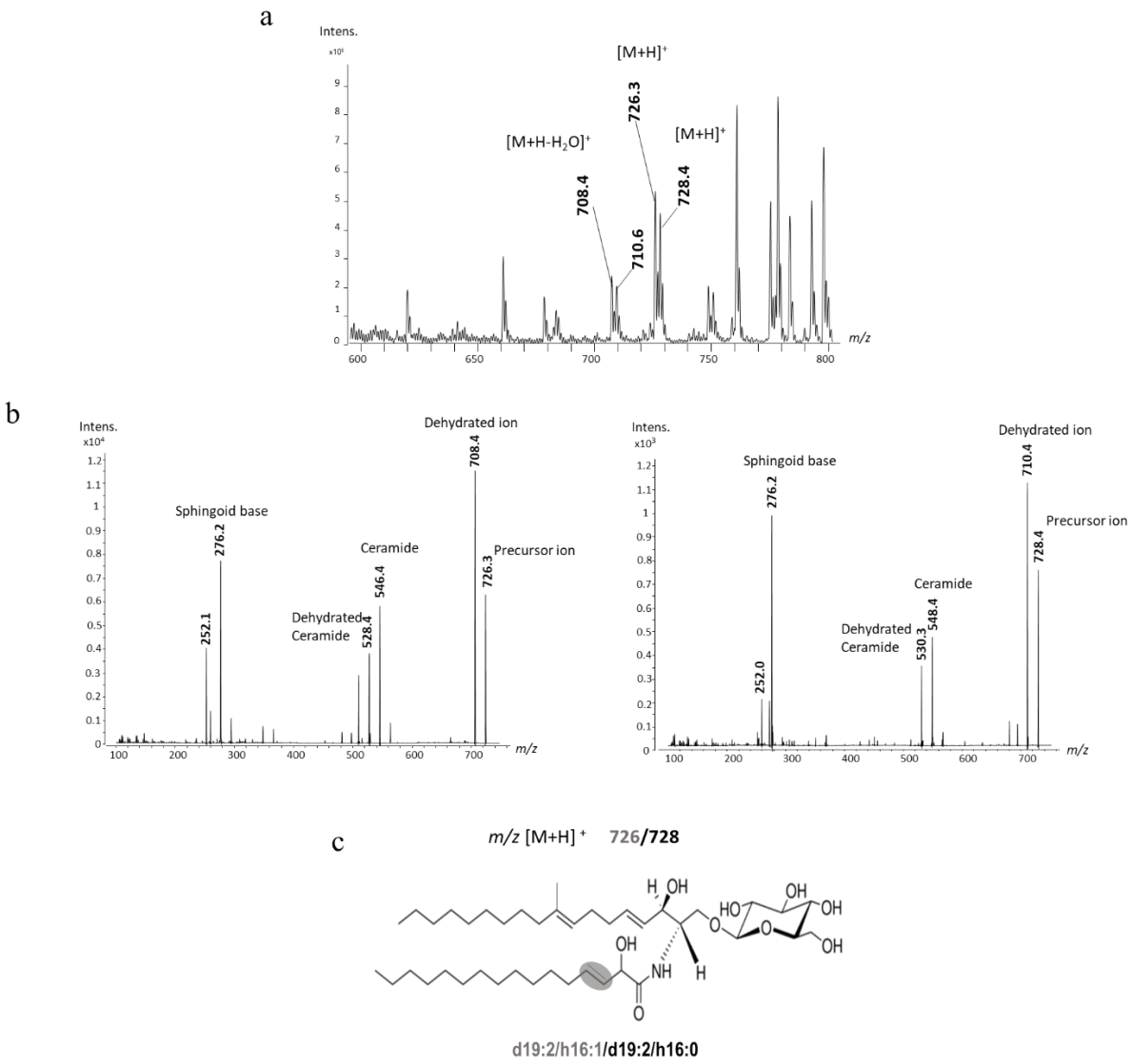

Supplementary Figure 1: Structural analysis of GlcCer extracted from *B. cinerea* B047 mycelia. (a) ESI-MS spectra of purified glycosphingolipid-enriched fraction. (b) ESI-MS/MS of molecular precursor ions at *m/z* 726.3 and 728.4 observed in ESI-MS. (c) Proposed structure for the major GlcCer species found in both strains *B. cinerea* B047 and B05.10. By analogy to plant GlcCer, the double bound of the fatty acid was proposed at C3-C4 position.

5. GlcCer structures of fungal species that are sensitive to ETD151

Supplementary Table 3: GlcCer structures of fungal species that are sensitive to ETD151

ETD151- sensitive fungi	GlcCer structure described*		References
	Sugar	Major fatty acid	
Aspergillus fumigatus	Glucose/Galactose	C18:1, Δ3	(9)
Candida albicans	Glucose	C18:0	(10)
Cryptococcus neoformans	Glucose	C18:0	(11)
Lomentospora prolificans	Glucose	C18:0	(12)
Fusarium solani	Glucose	C18:1, Δ3	(13)
Pichia pastoris	Glucose	C18:0	(14)
Botrytis cinerea	Glucose	C16:0 and C16:1	This work

*9-methyl-4,8-sphingadienine (d19:2) is the long-chain base forming the ceramide unit of all molecules described in this table. Except for *L. prolificans*, the sphingoid base is 4-hydroxy-9-methyl-4,8-sphingadienine (d19:2OH). All fatty acids are hydroxylated.

6. Labeling of ETD151 with Atto647 dye

General information

The peptide was labeled by grafting the Atto647 dye functionalized with an NHS ester, which is capable of forming a chemically stable amide bond with one of the four primary amine groups of ETD151 (N-terminus, Lys2, Lys23 and Lys28). Atto647 was chosen because it is a red-emitting dye, thus compatible with the MST apparatus used (NanoTemper ® Monolith NT.115 pico), with high fluorescence quantum yield, high photostability, and good water solubility. Moreover, Atto 647 has a neutral net charge and is photostable up to pH 8. Our goal was to preferentially label the N-terminus rather than lysine residues. Since decreasing the pH of the medium increases the N-terminal selectivity of the modification due to the different pKa of the primary amines on the lysine side chains (Nα-NH_2, ~10) and on the N-terminus (Nα-NH_2, ~8) (15). Conjugation was performed at pH 6.5, conditions that also reduce the unproductive reaction of hydrolysis of the NHS ester into its parent carboxylic acid. Briefly, lyophilized ETD151 (0.82 µmol) was resuspended in 205 µL of conjugation buffer (200 mM phosphate buffer, pH 6.5) followed by the addition of an equivalent molar amount of Atto647 NHS-ester previously dissolved in 102 µL acetonitrile (102µL). The reaction was incubated for 66 hours in the dark at 20 °C under stirring until total consumption of the dye (monitored by high-performance liquid chromatography (HPLC)). The crude labeling reaction mixture was analyzed, and the most-abundant mono-labeled fraction was purified by conventional reversed-phase HPLC (Chromaster system equipped with a 5160 pump, a 5430-diode array detector and a 5260-auto sampler, and fitted with a Chromolith High Resolution reverse phase-18e (150 Å, 10 × 4.6 mm, 3 mL/min flow rate) column. The molecular weights were

determined by ESI-MS (Agilent 1260 Infinity HPLC system coupled with an Agilent 6120 mass spectrometer (ESI + mode)).
HPLC and liquid chromatography (LC)-MS analysis of the crude reaction (**Supplementary Figure 2- Supplementary Table 4**) showed > 95% consumption of the starting Atto647-NHS ester. The most abundant mono-labeled peptide fraction (fraction D) was purified using reversed-phase HPLC (**Supplementary Figure 3**). ESI-MS analysis of this fraction confirmed a molecular ion at *m/z* 5417.79, corresponding to a mono-labeled ETD151. The overall yield of the labeling and purification steps for this fraction was approximately 10% (98% purity).
To determine the labeling site of fraction D, enzymatic digestion by pepsin (acidic medium at 37°C) was performed after reduction-alkylation (dithiothreitol was used for reduction and 4-vinyl pyridine for alkylation). The unlabeled ETD151 peptide was subjected to the same treatment. After enzymatic digestion treatment, MALDI-MS analysis showed no labeling on Lys23 and Lys28. Thus, the labeling site is either on the N-terminus or on Lys2. However, it was impossible to distinguish between selective labeling at either one of these two positions or a mixture at both (**Supplementary Figure 4**).

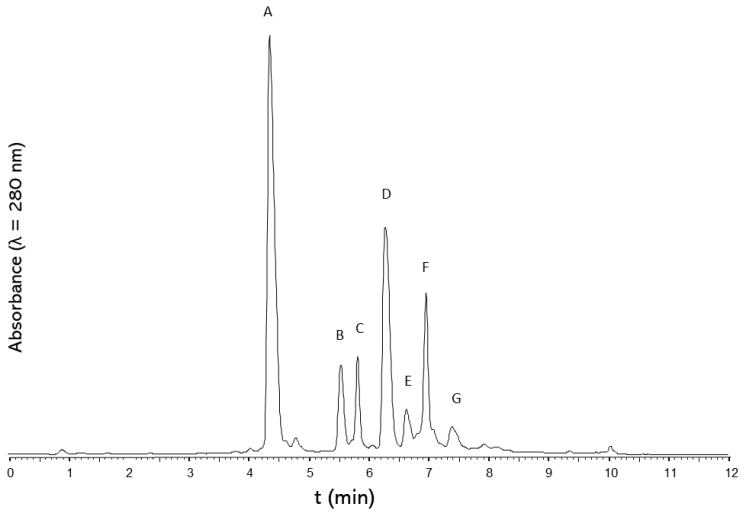

Supplementary Figure 2: Chromatogram of the crude mixture from the labeling reaction. HPLC analysis gradient: 25% - 45% solvent B (ACN + 0.1% TFA) for 5 minutes; Absorbance at 280 nm

Supplementary Table 4: Assignment of the main peaks observed during LC/MS analysis of the crude mixture from the labeling reaction.

Peak	[M] or $[M]^+$ calc.	[M] or $[M]^+$ found	Attributed to
A	4839.4	4838.9	Unlabeled ETD151
B	5414.4*	5413.4*	Mono-labeled ETD151
C	590.3	590.3*	Atto647-$CONH_2$**
D	**5414.4***	**5413.4***	**Mono-labeled ETD151**
E	5989.4*	5988.2*	Di-labeled ETD151
F	591.3*	591.3*	Atto647-COOH***
G	688.3*	688.3*	Atto647-CO-NHS

ESI-MS analyses were performed by injecting the collected HPLC peaks on the Agilent 6120 mass spectrometer (ESI + mode). The reported *m*/*z* values correspond to the monoisotopic ions for masses below 1000 Da, and to average masses for masses above 2000 Da (in the latter case, the multiply-charged envelope was deconvoluted using the charge deconvolution tool in Agilent OpenLab CDS ChemStation software). An asterisk (*) indicates that the $[M]^+$ value was used to calculate the theoretical mass, due to the permanent charge of Atto647 cationic fluorophore. The charge deconvolution tool in Agilent OpenLab CDS ChemStation software cannot take into consideration such a $[M]^+$ permanent positive charge, due to a small deviation from the calculated values for peaks B, D and E. **: Atto647-$CONH_2$ formation is likely due to the presence of ammonium in the conjugate mixture. ***: expected product resulting from the competing reaction of Atto647-NHS ester with water.

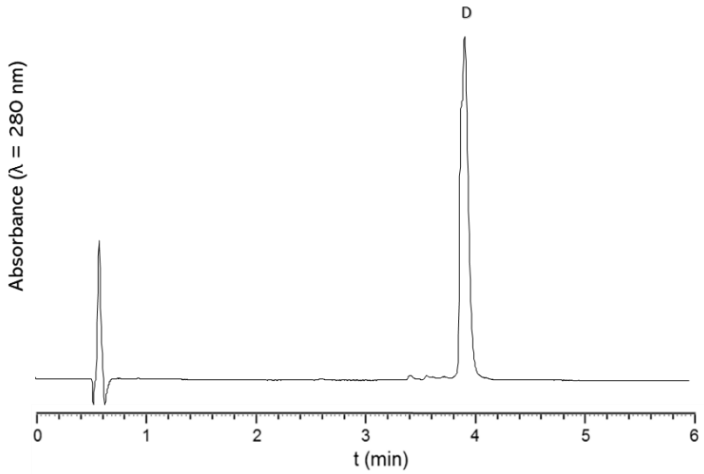

Supplementary Figure 3: Chromatogram of the purified Atto647-ETD151 fraction D used for MST experiments. HPLC purification and analysis of the purified fraction (retention time = 3.9 min, purity 98% purity): gradient 25% - 45% solvent B (ACN + 0.1% TFA) during 5 minutes; UV-detection at 280 nm.

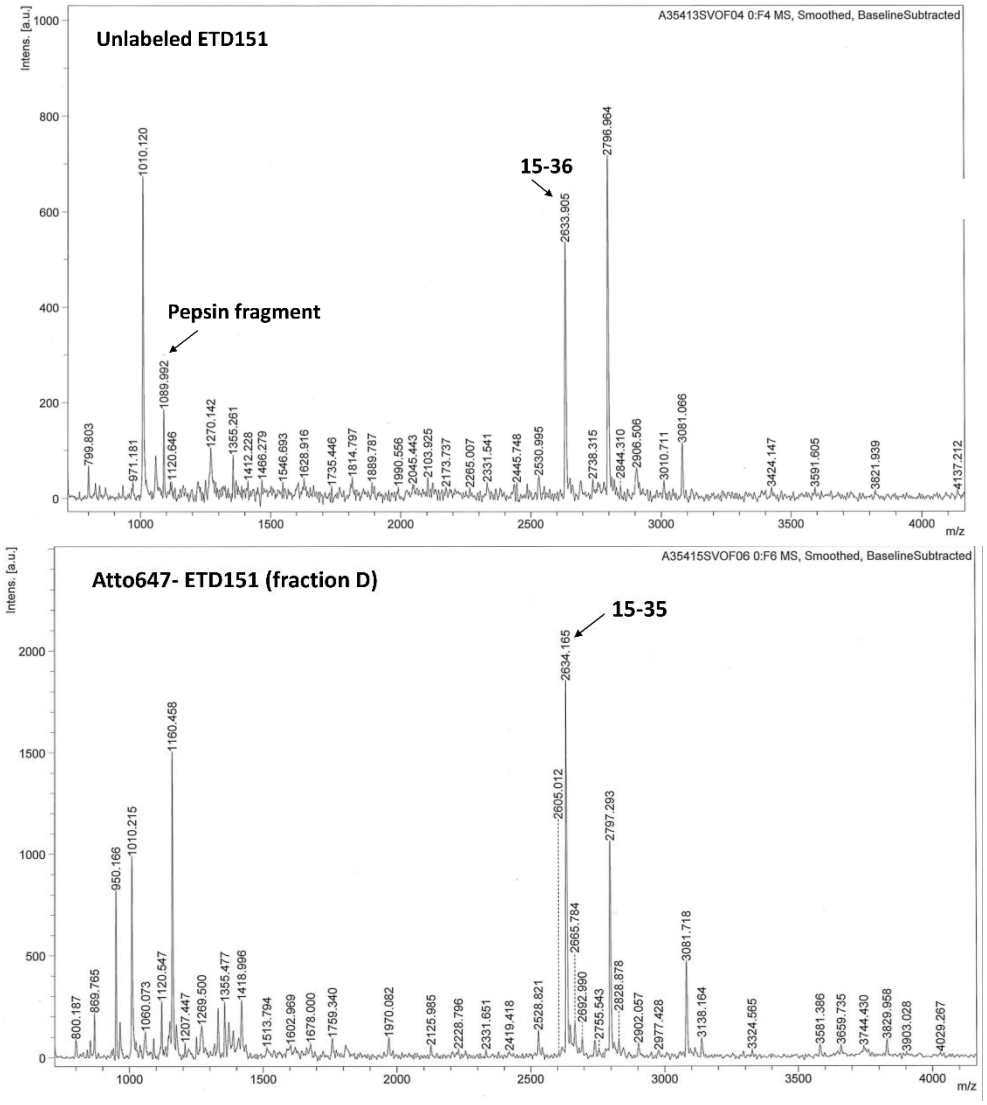

Supplementary Figure 4: MALDI-MS analysis of Atto647-ETD151 *vs* ETD151 after pepsin digestion.

7. MST optimization of experimental conditions

General information

To determine the optimal experimental conditions for analyzing the interaction between ETD151 and liposomes containing GlcCer$_{B.\ cinerea}$, we systematically tested various parameters and selected the optimal conditions based on fluorescence counts above the device threshold (>3000 counts). Optimized conditions also avoided asymmetric shapes indicating peptide adsorption, and bumpy thermographic curves suggesting aggregation during thermophoresis.

First, 3 solutions of Atto647-ETD151 at 25 nM were prepared in 3 different buffers to define the most suitable MST buffer composition. As shown in **Supplementary Figure 5 (a)**, phosphate buffer (10 mM and pH 5.8) containing non-ionic detergent Triton X-100 at concentrations ranging from 0.01 to 0.05% (v/v) all resulted in low fluorescence counts. The capillary shape graph showed a broad double peak, characteristic of the sample's adsorption into the inner capillary walls. Compared to phosphate buffer without any additive, we can assume that Triton X-100 promotes the adsorption of samples in this case. Moreover, phosphate buffer produces a bumpy thermograph curve in **Supplementary Figure 5 (b)** suggesting peptide aggregation. Since aggregation can also be caused by too low salt concentration and resulting charge-to-charge interaction of biomolecules, the addition of 100 mM NaCl (increase of ionic strength) to the phosphate buffer was tested. This resulted in double-peaks in the capillary shape graph again suggesting protein adsorption (**Supplementary Figure 5 (a)**, red curve). After centrifugation of the sample for 10 min at 10000 g in the phosphate buffer without additive, the thermographic profile showed a smooth curve (no aggregation) with no evidence of peptide aggregatio, which can interfere with the interpretation of the measurements (**Supplementary Figure 6)**. In addition, phosphate buffer provided the highest fluorescence counts, allowing further dilution of the target solution if necessary. Thus, 10 mM phosphate at pH 5.8 served as the most appropriate buffer composition for this study. The centrifugation step was mandatory to obtain a satisfactory signal. For the binding control test, the addition of ligand (liposomes made with phosphatidylcholine (PC)) induced a decrease in fluorescence intensity (< 2500 counts) which led us to test higher target concentrations, 50 and 100 nM. At 50 nM, the fluorescence intensity was acceptable and above the threshold value of 3000 counts (**Supplementary Figure 7**). The final target Atto647-ETD151 concentration was therefore kept constant at 50 nM. All measurements were performed at 22°C in standard uncoated capillaries with auto-detected excitation power and 40% of MST power.

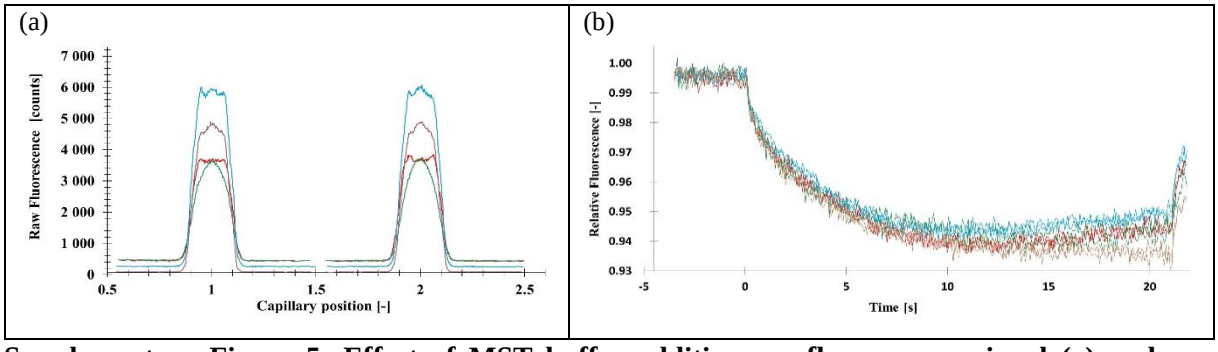

Supplementary Figure 5: Effect of MST buffer additives on fluorescence signal (a) and thermographs (b) inside the scanned capillaries: 10 mM phosphate buffer + 0% Triton X-100 (green), 10 mM phosphate buffer + 0.01% Triton X-100 (blue), 10 mM phosphate buffer + 0.05% Triton X-100 (brown) and 10 mM phosphate buffer + 100 mM NaCl (red).

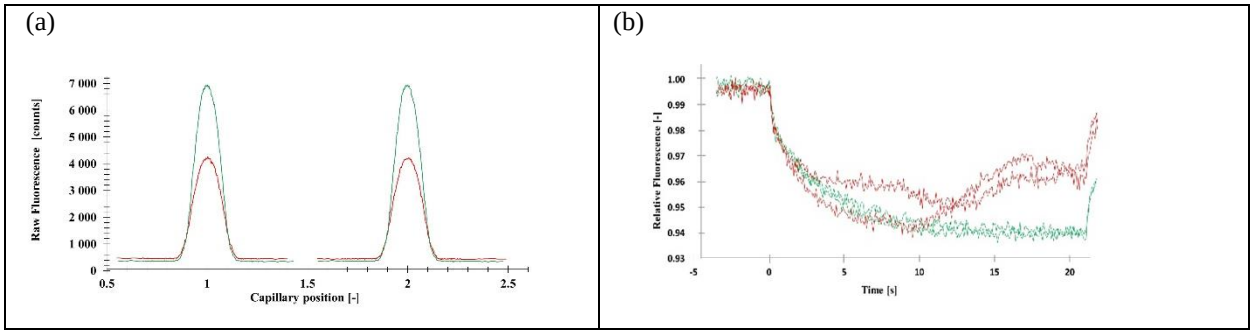

Supplementary Figure 6: Effect of centrifugation conditions on fluorescence signal (a) and on thermographs (b): without centrifugation (red) and with 10 min of centrifugation (green).

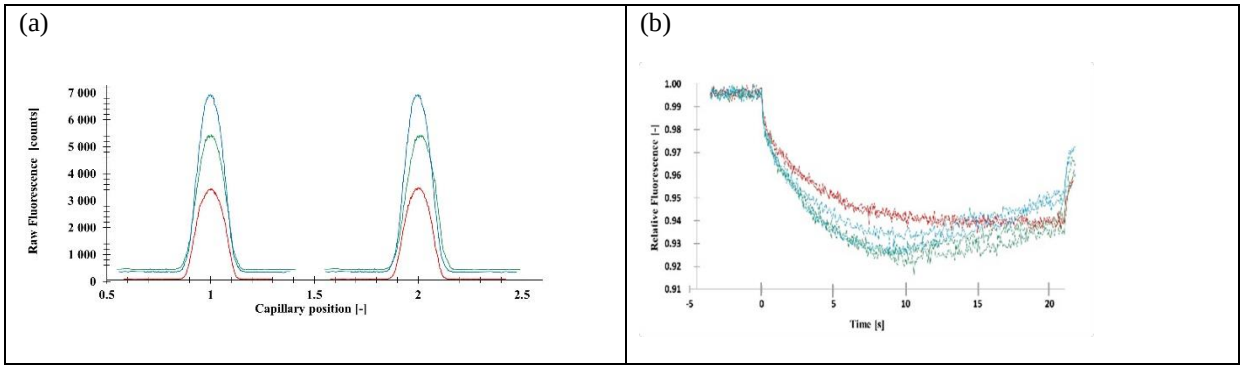

Supplementary Figure 7: Selection of target concentration on fluorescence signal (a) and on thermographs (b) 25nM (red), 50 nM (green) and 100 nM (blue).

8.Antifungal activity of BODIPY- ETD151 and ETD151

General information

The activity of BODIPY-ETD151 fractions was evaluated on B047 spores (10^4 sp/mL in a 25% PDB medium). Each labeled-peptide fraction was suspended in water/ dimethyl sulfoxide (0.1%, v/v). Sterile 96-well plates (TPP Techno Plastic Products AG, Trasadingen, Switzerland) were used to assess mycelial growth inhibition. A fresh spore preparation (10^4 sp/mL) suspended in a 25% PDB medium was deposited in each well (135 µL/well) before the addition of 15 µL of BODIPY-ETD151 solutions (final concentrations from 25 to 0.049 µM). After 7 days of incubation with gentle stirring, OD_{630nm} was measured using a plate reader (BioTek, Winooski, VT, USA) and the concentration that inhibited at least 90% of growth (IC_{90}) was determined. Untreated spores and spores treated with unlabeled-ETD151 were used as controls.

Supplementary Table 5: Antifungal activity of ETD151 and BODIPY-ETD151 obtained after conjugation of the fluorophore BODIPY-FL-NHS ester to the peptide ETD151

Fractions	Molecular mass (Da)	BODIPY	Purity	IC_{90} (µM)
ETD151	4 839.46	X	100 %	1.56
BODIPY-ETD151	5 113.56	1	92 %	1.56

9. BODIPY-ETD151 localization in *B. cinerea* cells at different concentration

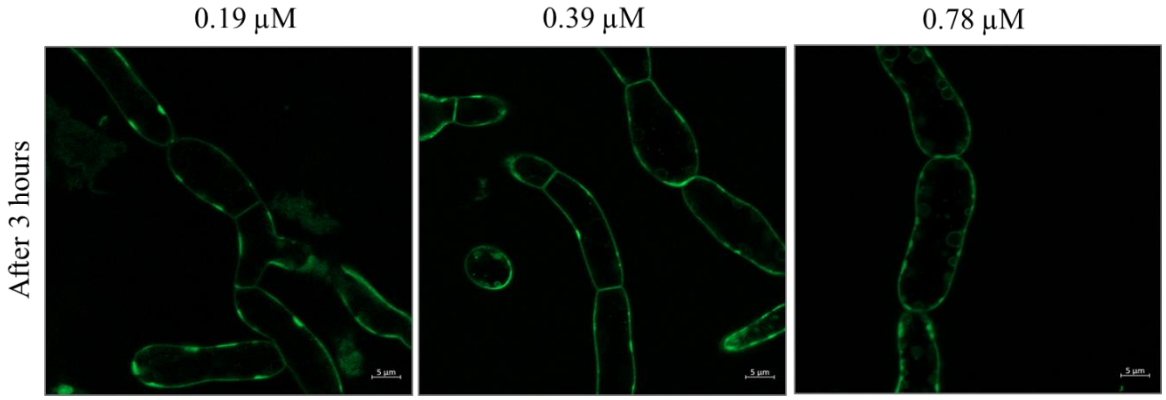

Supplementary Figure 8: Localization of BODIPY-ETD151 in *B. cinerea* cells. Confocal microscopy images of *B. cinerea* (10^4 sp/mL in a 25% PDB medium) using 63x optical magnification after incubation for 3 hours with different concentrations (0.19, 0.39 and 0.78 µM) of BODIPY-ETD151

10. Activity of ETD151 against a selected panel of bacteria

General information

The following strains were used to determine the minimum inhibitory concentrations (MICs): *Escherichia coli* ATCC 25922, *E. coli* D22, *Bacillus subtilis* CV-1 and *Micrococcus luteus* ATCC 4698. All strains were obtained from stock cultures maintained at -80 °C in culture media containing 25% glycerol.

The antibacterial activity of ETD151 was evaluated against bacteria using a modified version of the Clinical Laboratory and Standard Institute (CLSI) broth microdilution method as previously reported (16). Briefly, a fresh 1/100 dilution inoculum was prepared from an overnight bacterial culture. All bacteria were grown in MH II medium (Sigma-Aldrich), until reaching 10^8 colony-forming units (CFU)/mL. Bacterial cells diluted to 10^5 CFU/mL in the same media were deposited into a 96-well plate (Thermo Scientific) and incubated with ETD151 at various concentrations (from 100 µM to 0.2 µM, twofold serial dilutions). After incubation of the plates (30°C, 24h, shaking at 180 rpm), cell growth inhibition was evaluated by measuring the OD_{600nm} using a spectrophotometer microplate reader (BioTek, Winooski, VT, USA).

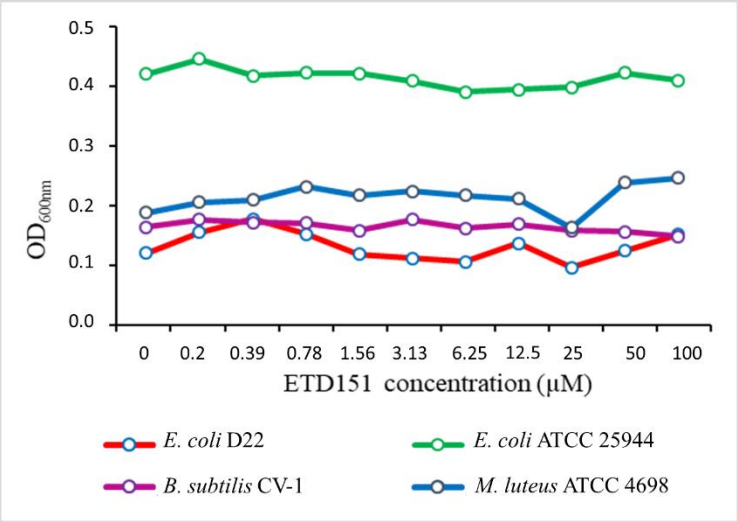

Supplementary Figure 9: Activity of ETD151 against a selected panel of bacteria. Bacterial growth assays for ETD151 at different concentrations against *Escherichia coli D22* (red), *E. coli* ATCC 25944 (green), *Bacillus subtilis* CV-1 (purple) and *Micrococcus. luteus* ATCC 4698 (bleu). Bacterial growth was measured by optical density at 600 nm (OD_{600nm}) after 24 hours of peptide treatment and plotted against ETD151 concentration.

11. Uptake of Atto647-ETD151 in *Novosphingobium capsulatum*

General information

The uptake of ETD151 labeled with Atto647-labeled ETD151 was assessed by flow cytometry as previously described (17). Mid-log phase bacteria were harvested, diluted to 10^6 CFU/mL and incubated with Atto647-ETD151 giving 2 µM as a final concentration at 30°C from 10 to 30 min in a "nutrient" medium. Treated cells were washed several times with buffered high-salt solution (10 mM Sodium-phosphate, 400 mM NaCl, 10 mM $MgCl_2$, pH 7.2), resuspended in phosphate-buffered saline (PBS) and immediately analyzed by the flow cytometer. The wavelength of red fluorescence was (610/20 nm) bandpass filter for Atto647. A solution of bacteria prepared in the same conditions, but not treated with ETD151, was used as a control.

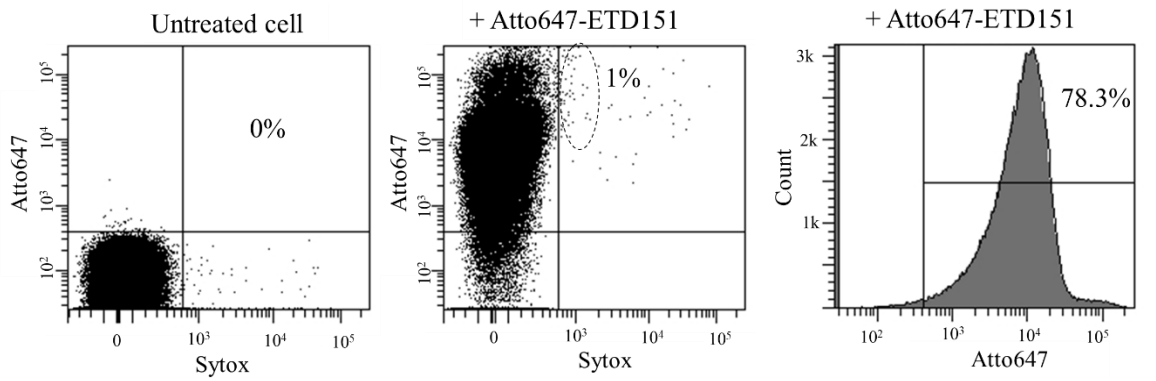

Supplementary Figure 10: Binding of Atto647-ETD151 in *N. capsulatum* by flow cytometry. Bacterial cells were treated with 2 µM Atto647-ETD151 for 10 min in the presence of 10 nM Sytox orange (DNA-binding strain). Untreated cells were used as a control incubated with 10 nM Sytox Orange. Analyses were performed after washing with a high-salt solution. Experiments were performed in triplicate.

References

1. K. Thevissen, *et al.*, Defensins from Insects and Plants Interact with Fungal Glucosylceramides*. *Journal of Biological Chemistry* **279**, 3900–3905 (2004).

2. A. M. Aerts, *et al.*, The antifungal activity of RsAFP2, a plant defensin from raphanus sativus, involves the induction of reactive oxygen species in Candida albicans. *J Mol Microbiol Biotechnol* **13**, 243–247 (2007).

3. V. Ramamoorthy, *et al.*, Glucosylceramide synthase is essential for alfalfa defensin-mediated growth inhibition but not for pathogenicity of Fusarium graminearum. *Molecular Microbiology* **66**, 771–786 (2007).

4. L. Neves de Medeiros, *et al.*, Psd1 binding affinity toward fungal membrane components as assessed by SPR: The role of glucosylceramide in fungal recognition and entry. *Peptide Science* **102**, 456–464 (2014).

5. L. Neves de Medeiros, *et al.*, Backbone dynamics of the antifungal Psd1 pea defensin and its correlation with membrane interaction by NMR spectroscopy. *Biochimica et Biophysica Acta (BBA) - Biomembranes* **1798**, 105–113 (2010).

6. V. S. G. Amaral, *et al.*, Psd2 pea defensin shows a preference for mimetic membrane rafts enriched with glucosylceramide and ergosterol. *Biochim Biophys Acta Biomembr* **1861**, 713–728 (2019).

7. E. de O. Mello, *et al.*, Functional expression and activity of the recombinant antifungal defensin PvD1r from Phaseolus vulgaris L. (common bean) seeds. *BMC Biochem* **15**, 7 (2014).

8. V. Silva de Paula, G. Razzera, E. Barreto-Bergter, F. C. L. Almeida, A. P. Valente, Portrayal of complex dynamic properties of sugarcane defensin 5 by NMR: multiple motions associated with membrane interaction. *Structure* **19**, 26–36 (2011).

9. M. H. S. Villas Boas, H. Egge, G. Pohlentz, R. Hartmann, E. Barreto Bergter, Structural determination of N-2′-hydroxyoctadecenoyl-1-O-β-d-glucopyranosyl-9-methyl-4, 8-sphingadienine from species of Aspergillus. *Chemistry and Physics of Lipids* **70**, 11–19 (1994).

10. T. Matsubara, A. Hayashi, Y. Banno, T. Morita, Y. Nozawa, Cerebroside of the dimorphic human pathogen, *Candida albicans*. *Chemistry and Physics of Lipids* **43**, 1–12 (1987).

11. M. Rodrigues, *et al.*, Human Antibodies against a Purified Glucosylceramide from Cryptococcus neoformans Inhibit Cell Budding and Fungal Growth. *Infection and Immunity* **68**, 7049–7060 (2000).

12. M. I. D. da S. Xisto, *et al.*, Glucosylceramides From Lomentospora prolificans Induce a Differential Production of Cytokines and Increases the Microbicidal Activity of Macrophages. *Front. Microbiol.* **10** (2019).

13. R. S. Duarte, C. R. Polycarpo, R. Wait, R. Hartmann, E. Barreto Bergter, Structural characterization of neutral glycosphingolipids from *Fusarium* species. *Biochimica et Biophysica Acta (BBA) - Lipids and Lipid Metabolism* **1390**, 186–196 (1998).

14. P. Ternes, *et al.*, Two pathways of sphingolipid biosynthesis are separated in the yeast Pichia pastoris. *J Biol Chem* **286**, 11401–11414 (2011).

15. A. Tantipanjaporn, M.-K. Wong, Development and Recent Advances in Lysine and N-Terminal Bioconjugation for Peptides and Proteins. *Molecules* **28**, 1083 (2023).

16. I. Wiegand, K. Hilpert, R. E. W. Hancock, Agar and broth dilution methods to determine the minimal inhibitory concentration (MIC) of antimicrobial substances. (2008).

17. M. Mattiuzzo, *et al.*, Role of the Escherichia coli SbmA in the antimicrobial activity of proline-rich peptides. *Mol Microbiol* **66**, 151–163 (2007).

Chapter 3: Molecular interaction study of ETD151 with its molecular target

I. **Aim of this work**

Our aim in this work is to characterize, using biophysical assays, the direct interaction between ETD151 defensin and its molecular target, fungal glucosylceramides (GlcCer), at the molecular and atomic scales. To this end, we carried out a molecular-scale study combining biophysical tools **(i)** to estimate the binding affinity between ETD151 and fungal (methylated) GlcCer using microscale thermophoresis (MST) and isothermal titration calorimetry (ITC) techniques, **(ii)** to determine which part of ETD151 is affected by the interaction with fungal GlcCer using solution nuclear magnetic resonance (NMR), **(iii)** to evaluate the effect of the presence of ETD151 on membrane lipid dynamics using solid-state NMR (ss-NMR), and finally **(iv)** to investigate the involvement of the C9-methyl sphingoid base of GlcCer in the molecular interaction between ETD151 and GlcCer.

This part of work was performed using commercially available GlcCer, fungal GlcCer (d19:2/h16:0) from *Pleurotus citrinopileatus*, and plant GlcCer (nonmethylated) (d18:2/h16:0) from soybean. *For all experiments, large unilamellar liposomes (LUVs) with 100 nm diameter, except for ss-NMR, were freshly prepared and controlled by dynamic light scattering (DLS). LUVs are composed of 90% mol phosphatidylcholine (PC) and 10% mol GlcCer. LUVs made only with PC were used as a control (PC-based LUVs) for all tests.*

(i) Evaluating the ligand's binding affinity to its target is an essential step for establishing the order strengths of biomolecular interactions. Utilizing both calorimetry (ITC) and thermophoresis (MST) approaches, we have estimated the dissociation constant (K_d) for the binding of ETD151 to fungal GlcCer contained in biomembranes. Gaining insight into the interaction's thermodynamic profile is the additional advantage of using ITC.

Because there's no data on defensin-GlcCer interaction studies by ITC in the literature, optimization part of protocoles has been performed. For ITC, I received financial assistance from Instruct-ERIC to have access to their platform (ISBG, Grenoble) as an ITC user, Dr. C. Mas trained and supervised me in the initial tests. After then, I carried out further ITC experiments in CBM after Dr. M. Suskiewicz's group obtained MicroCal PEAQ-ITC.

Under the supervision of Dr. R. Nasreddine and R. Nehme (ICOA, Orléans), I conducted MST assays using the previously fluorescently tagged ETD151 and the protocol optimized before.

(ii) For only two plant defensins namely Psd1 and Sd5, the identification of the peptide region that might be implicated in the recognition of GlcCer-containing liposomes has been investigated, demonstrating distinct regions disrupted of each defensin by fungal GlcCer. By NMR in solution, the disruption of ^{15}N-labeled ETD151 in presence of liposomes that contain fungal GlcCer has been monitored, and several residues of ETD151 that are affected by the presence of the fungal GlcCer have been identified.

^{1}H- ^{15}N HSQC NMR experiments, considered as the fingerprint of a peptide, were performed with Dr. F. Paquet (our team, CBM, Orléans). Structural changes in the peptide are reflected by changes in ^{1}H-^{15}N HSQC spectra in the absence (peptide free-state) and in the presence of GlcCer incorporated into liposomes. NMR Relaxation experiments of ETD151 in the free state were performed and analyzed by Dr. F. Paquet.

(iii) Glucosylceramides in plasma membranes contribute to maintaining lipid organization and membrane integrity. The recognition of fungal GlcCer by ETD151 therefore may result in lipid dynamic and order membrane perturbation. Using ss-NMR, the ETD151 peptide effect on the lipid order of multilamellar vesicles (MLV) containing fungal GlcCer was investigated. The lipid dynamics of the headgroup part (phosphate groups) as well as the hydrophobic core part (hydrocarbon chains) of PC were determined using static ^{31}P and static ^{2}H experiments, respectively.

Solid-state NMR static ^{31}P and ^{2}H experiments were performed and analyzed with Dr. D. Warschawski (Laboratory of Biomolecules, Paris).

(iv) The C9-methylation of GlcCer sphingoid base is a structural characteristic unique to fungi and has been shown to be involved in both fungal proliferation and pathogenicity. To investigate the impact of the C9-methyl of the GlcCer in ETD151-GlcCer interaction, all previous experiments (ITC, MTS, solution NMR, and ss-NMR) were performed with the nonmethylated GlcCer from Soybean in place of fungal (methylated) GlcCer under the same experimental settings.
In this study, **we provide an overview of the *in vitro* recognition of fungal GlcCer by ETD151 from the point of view of peptide structure and membrane lipid order using a simplified membrane model**. This **biochemical and structural characterization** of the interaction between ETD151 and its fungal molecular target may provide insights into the **development of new antifungal strategies specifically targeting pathogenic fungal cells via methylated GlcCer**.

II. Article

The results of this work were submitted on 25 February 2025 for publication in the Journal of Biological Chemistry (JBC) and are currently under revision. In this thesis manuscript, we have chosen to reproduce the submitted version.

How ETD151 defensin targets specifically methylated glucosylceramides to inhibit fungal growth

Ons Kharrat[a,b], Françoise Paquet[a], Rouba Nasreddine[c], Jean-Baptiste Madinier[a], Reine Nehmé[c], Vincent Aucagne[a], Philippe Bulet[d,e], Dror Warschawski[f], Céline Landon[a]*

[a] Centre for Molecular Biophysics, CNRS, Orléans, France; [b] University of Orléans, France; [c] Institute of Organic and Analytical Chemistry, University of Orléans, CNRS, Orléans, France; [d] Institute for Advanced Biosciences, University of Grenoble Alpes, Grenoble, France; [e] Plateform BioPark Archamps, Archamps, France; [f] Laboratory of Biomolecules, Paris, France;

*Corresponding author: celine.landon@cnrs-orleans.fr

Running title: ETD151 defensin targets fungal methylated glucosylceramides

Key Words:

Antimicrobial peptide, Defensin, Sphingolipid, Protein-lipid interaction, Membrane biophysics, Antifungal, Fungal glucosylceramides

Abstract

The growing resistance to antifungal drugs and the limited number of antifungals currently available highlight the need for new antifungal strategies. In this context, there is significant potential for plant and insect antifungal defensins, which target fungal glucosylceramides (GlcCer), a growth and virulence determinant. The ETD151 peptide, optimized from the insect defensin Heliomicin, binds to fungal GlcCer as a crucial step in its activity. Nevertheless, further investigation is necessary to elucidate the mechanisms by which ETD151 targets fungal GlcCer at the molecular and atomic scales. The binding affinity was experimentally measured with isothermal titration calorimetry (ITC) and microscale thermophoresis (MST). The results collectively revealed affinity with a membrane-bound methylated GlcCer in the micromolar range. Nuclear Magnetic Resonance (NMR) has been employed to identify the area of ETD151 that would monopolize methylated GlcCer binding, including the two adjacent hydrophobic loops. Furthermore, our findings indicate that ETD151 specifically inserts into and fluidifies phosphatidylcholine (PC) lipid vesicles containing methylated GlcCer. Finally, it is worth noting that the C9-methyl in the sphingoid base plays a pivotal role in the ETD151-GlcCer interaction. Its presence increases the binding affinity between the two partners, resulting in stronger structural changes in ETD151 and deeper insertion into the hydrophobic core of model membranes. This study reveals key biochemical and structural elements of the ETD151-GlcCer interaction, provides a basis for elucidating the structure and dynamics of other GlcCer-targeting defensins in relation to their function, and facilitates the development of defensin-mimetic antifungals.

INTRODUCTION

Fungal diseases have historically been underestimated and neglected. However, recent data indicates that fungal pathogens infect billions of people and cause at least 1.5 million deaths annually (1, 2). Despite the significant impact of fungal pathogens on global human health (3), only three frontline antifungal drug classes are currently employed in clinical practices to treat invasive infections: azoles, polyenes and echinocandins (4). These drugs target either the cell membrane or the cell wall to inhibit their fungistatic/fungicidal activities (5). Azoles bind to ergosterol, the primary sterol in fungal membranes. Polyenes inhibit the ergosterol biosynthesis pathway, while echinocandins inhibit β-1,3-glucan synthase, a crucial enzyme for maintaining cell wall integrity (6–8). Despite their efficacy in the treatment of systemic fungal infections, their toxicity to the host and unfavorable pharmacokinetics limit their clinical use (9). Furthermore, there is an increased risk of drug-resistant fungal pathogens emerging due to the overuse of these limited antifungal classes (10, 11). This highlights the urgent need to identify new antifungal agents with innovative mechanisms of action (MoAs) to treat systemic fungal infections. However, the development of new antifungals is challenging due to the close evolutionary relationship between fungi and humans (12).

Antifungal defensins, disulfide-rich peptides present in the immune systems of plants and insects (13), show great promise for drug development as a potential alternative to conventional antifungals (14, 15). This is attributed to three factors: (i) *in vivo* efficacy against a wide variety of fungi, (ii) minimal toxicity to human cells, and (iii) high stability against plasma proteases. Structurally, antifungal defensins share a common monomeric fold known as the cysteine-stabilized αβ motif (CSαβ). The latter comprises a three-stranded antiparallel β-sheet connected to an α-helix via two disulfide bridges. Despite their strong structural similarities, antifungal defensins act according to different MoAs, and are undoubtedly more complex than the membrane-lytic mechanism triggered by short linear antimicrobial peptides (AMPs). The MoAs of antifungal defensins involves interaction with one or more specific cell wall and/or plasma membrane compound(s), which can lead to membrane disruption and downstream events (16).

Among the promising cellular targets for antifungal defensins, glucosylceramides (GlcCer) have been identified as the most abundant neutral glycosphingolipid component in the fungal membranes. Their role as growth and virulence determinants has been established in various fungal species (17, 18). The presence of GlcCer in fungal membranes plays a pivotal role in the activity of certain plant and insect defensins, including RsAFP2 from the radish *Raphanus sativus* (19), Heliomicin from the tobacco budworm *Heliothis virescens* (19), Psd1 from the pea *Pisum sativum* (20), MsDef1 from the alfalfa/lucerne *Medicago sativa* (21) and PvD1 from the common bean *Phaseolus vulgaris* (22). On the one hand, direct *in vitro* molecular interaction with GlcCer has been demonstrated for RsAFP2, Heliomicin, Psd1, and Psd2 (19, 20, 23). Consequently, they are referred to as GlcCer-interacting defensins. On the other hand, the potential for GlcCer to serve as a target for some defensins (e.g.,

MsDef1 and PvD1) remains hypothetical, and further investigation is required to validate the direct molecular recognition with GlcCer.

We recently demonstrated that a recombinant form of ETD151 (produced in the yeast *Saccharomyces cerevisiae*), a 44-amino acid defensin derived from Heliomicin (24), requires the presence of GlcCer in fungal membranes to exert its full antifungal activity (25). The ETD151 peptide is active *in vitro* at micromolar concentrations against pathogenic fungi such as *Cryptococcus*, *Candida*, and *Aspergillus* (24), classified as a critical group in the World Health Organization (WHO) list of priority fungal pathogens (26). Furthermore, ETD151 was shown to be non-toxic after systemic administration and more effective than Amphotericin B, the current standard for the treatment of invasive infections, in a murine model infected with the yeast *Candida albicans* and the filamentous fungus *Aspergillus fumigatus* (27). Furthermore, ETD151 has demonstrated efficacy against the plant pathogenic fungus *Botrytis cinerea* (28). This filamentous fungus is a necrotrophic pathogen responsible for gray mold (29), which has developed resistance to current fungicides (30). The MoAs of ETD151 on *B. cinerea* have been partly elucidated, revealing a multifaceted mechanism (28) similar to that of certain plant defensins (31). To exert its anti-*Botrytis* activity, ETD151 binds directly to GlcCer located on the cell wall and/or plasma membrane, remaining mainly outside the cells (25) and causing membrane permeabilization (28). A proteomic study revealed that ETD151 disrupts proteins corresponding to six different pathways (spliceosome, ribosome, protein processing in endoplasmic reticulum endocytosis, Mitogen-Activated Protein Kinase signaling pathway and oxidative phosphorylation) in *B. cinerea* without directly affecting the respiratory chain (28). These findings collectively indicate that ETD151 represents a promising alternative to current therapies against fungal infections by targeting GlcCer. It is therefore crucial to elucidate the mechanisms by which ETD151 targets fungal GlcCer, at the molecular and atomic scale.

The typical structure of fungal GlcCer consists of a methylated sphingoid base (C9-methyl-4,8-sphingadienine; d19:2) linked to a 2-hydroxylated C16-C18 fatty acid and attached to glucose by an ester bond (32). Due to the addition of a methyl group by a specific fungal enzyme, sphingolipid C9-methyltransferase (SMT), to the sphingoid base at position C9, the fungal GlcCer structure differs from that of its mammalian and plant counterparts (33). Similarly to GlcCer synthesis, C9-methylation in the sphingoid base is essential for fungal growth, differentiation, and pathogenesis (34). Disruption of the gene encoding SMT in the encapsulated yeast *Cryptococcus neoformans* (Δ*smt*), which does not produce methylated GlcCer, resulted in a significant reduction in virulence in a murine model of cryptococcosis (35). The filamentous fungus *Neurospora crassa* Δ*smt* mutant cells were entirely devoid of methylated GlcCer production, exhibiting significant growth defects compared to their respective wildtype (WT) strains (36). In the case of the filamentous fungi *Fusarium gramineurum* and *Aspergillus nidulans*, the two SMTs encoded by respectively the *smt1* and *smt2* genes are suggested to exhibit redundant enzymatic functions (34, 37). *F. gramineurum* Δ*smt1* has been found to produce methylated GlcCer like the WT strains. However, *F. gramineurum* Δ*smt2* produces 75% of nonmethylated GlcCer, and exhibits

significant growth abnormalities and decreased pathogenicity in wheat (37). In addition to its critical role in fungal virulence, C9 methylation is a key factor influencing the activity of certain antifungal defensins. Indeed, the plant defensin AFP1 from the mustard plant *Brassica juncea* induces membrane permeabilization and reactive oxygen species (ROS) production in WT *C. albicans* strains. However, this effect is not observed in *C. albicans* Δ*mts1* mutants, which lack the methylated GlcCer (38). These observations demonstrate that targeting methylated GlcCer provides a selective approach to combat fungal infections while minimizing host toxicity. It is therefore crucial to investigate whether ETD151 is selective for methylated GlcCer.

This work presents evidence of the *in vitro* recognition of fungal methylated GlcCer by ETD151 from the perspective of peptide structure and membrane lipid order. In light of these considerations, we conducted a molecular-scale investigation employing biophysical approaches to (i) estimate the binding affinity between ETD151 and fungal methylated GlcCer using isothermal titration calorimetry (ITC) and microscale thermophoresis (MST) techniques; (ii) determine which part of ETD151 is impacted by the interaction with fungal methylated GlcCer using solution nuclear magnetic resonance (NMR); and (iii) assess the impact of ETD151 presence on membrane lipid dynamics using solid-state NMR (ss-NMR). We also examine the role of the methyl group in the molecular recognition between GlcCer and ETD151, by comparing methylated GlcCer and nonmethylated GlcCer. The biochemical and structural characterization of the interaction between ETD151 and its fungal molecular target could facilitate the development of novel antifungals strategies that target pathogenic fungal cells through methylated GlcCer.

RESULTS

To study the interaction between ETD151 and glucosylceramides (GlcCer) in a membrane context, 100 nm large unilamellar vesicles (LUVs) were created, primarily composed of phosphatidylcholine (PC), the main phospholipid present in the fungal plasma membrane (39). PC is a zwitterionic lipid, which prevents non-specific electrostatic attraction with the positively charged ETD151 (net charge +4 at physiological pH). Considering that sphingolipids account for approximately 7-16% of the fungal membrane lipid composition (40), GlcCer were incorporated into LUVs with 10% mol of total lipid. Two commercially available GlcCer were considered: a typical fungal GlcCer referred to as “methylated GlcCer”, and a plant GlcCer lacking the methyl group at C9 in the sphingoid base, referred to as “nonmethylated GlcCer”. The sole structural difference between these two GlcCer is the presence of the methyl group (Figures 1A and 1B).

1. The affinity of ETD151 for GlcCer is in the micromolar range, with a greater affinity observed when GlcCer is methylated

To investigate the binding affinity of ETD151 to GlcCer and to determine to what extent the C9-methyl structural feature in the sphingoid base may be involved in this binding affinity, ITC experiments were

carried out using PC-based LUVs as control vesicles, PC-nonmethylated GlcCer LUVs and PC-methylated GlcCer LUVs. As illustrated in Figure 1C, the titration of 3.5 mM pure PC-based vesicles into a ETD151 solution (250 µM, final concentration) did not generate any heat signal, confirming the absence of a strong interaction between PC and ETD151. The addition of 10% mol of nonmethylated- or methylated GlcCer incorporated into PC-based vesicles resulted in an exothermic binding isotherm (Figures 1D and 1E). This heat signal is associated with the specific interaction between ETD151 and GlcCer (methylated or not), as no such exothermic signal results were observed in the titration of these GlcCer-containing vesicles into 10 mM phosphate buffer at pH 5.8 (see supp info Figure S1). Using the "one-site binding model", the dissociation constant (K_d) values were determined of 1.9 mM and 100 µM were obtained with nonmethylated GlcCer (Figures 1D) and methylated GlcCer (Figure 1E,), respectively. The thermodynamic results demonstrated that the strength of the interaction between ETD151 and methylated GlcCer-containing vesicles (determined by a free energy of binding ΔG of -5.45 kcal/mol) appears to be primarily governed by an entropic contribution ($-T\Delta S$ = -5.03 kcal/mol) (see supp info Table S1), under our experimental conditions. The ITC results demonstrated that the incorporation of GlcCer enhances the binding affinity of ETD151 to the PC membrane, but also that the mere presence of the C9-methyl group significantly affects this binding (19-fold higher affinity).

As we have determined the binding affinity of ETD151 to GlcCer extracted from *B. cinerea* using the MST assays (25), the affinity of ETD151 was compared with nonmethylated GlcCer and methylated GlcCer, using the LUVs compositions defined in the ITC experiments. The reported values result from two distinct effects: a fast effect (e.g., the local responses of the fluorophore to the temperature jump, which depends on the environment), and a slow effect (e.g., the thermophoresis diffusion fluorescence changes). The MST results indicated that the K_d values of 50 µM fluorescently labeled ETD151 (Atto647-ETD151) for both GlcCer-containing PC vesicles are in the micromolar range: K_d 5.3 µM for nonmethylated GlcCer (Figure 1F) and K_d 0.7 µM for methylated GlcCer (Figure 1G). In line with the ITC results, the K_d estimated values using the single-site binding model from MST experiments showed that ETD151 binds to GlcCer-containing PC vesicles with a 7.5-fold higher affinity in the presence of C9-methyl.

2. The presence of GlcCer primarily affects the hydrophobic L1 and L3 loops of ETD151, with a greater alteration observed with methylated GlcCer

To determine which part of ETD151 governs its interaction with the lipid target, a series of NMR experiments were conducted with varying compositions and concentrations of LUVs. We selected the SOFAST-HMQC (selective optimized flip angle short transient-heteronuclear multiple quantum coherence) experiment, a variant of the conventional ^{1}H-^{15}N HSQC (heteronuclear single quantum coherence spectroscopy) experiment designed to shorten the measurement time by up to several folds with a significant gain in intensity. The reference ^{15}N-ETD151 spectrum displays a high degree of peak dispersion, typical of a well-structured peptide (see supp info Figure S2). Peaks corresponding to 40

residues were observed, i.e. 44 residues minus the N-terminal D1 residue, N13 which is masked under the intense C22 peak, G33 peak which is not in the range of the recorded chemical shift (6-10 ppm) and V38 located in the L3 loop. The latter residue is not visible, most likely due to intense peak broadening, a characteristic of an intermediate exchange regime.

Upon addition of 5 mM either PC-based LUVs or PC-nonmethylated GlcCer LUVs or PC-methylated GlcCer to a solution of ^{15}N-ETD151 (50 µM), no clear chemical shift perturbations (CSPs) were detected (see supp info Figure S3). An overall decrease in peak ratio intensity was observed for both LUVs-containing GlcCer (Figure 2, nonmethyalted GlcCer in orange and methylated GlcCer in cyan), in contrast to control PC-based LUVs (Figure 2, black). The loss of NMR peak intensity upon addition of PC-based LUVs containing nonmethylated or methylated GlcCer is likely due to an increase in the resonance line width of amides in the less mobile states of bound residues. Given their reduced mobility, the amide groups involved in GlcCer recognition will have a greater effective correlation time, resulting in greater broadening than those in unbound regions. As the peak ratio intensities for LUVs containing GlcCer were calculated relative to I_{PC} (intensity of peak in the ETD151-PC LUVs spectrum), the decrease in intensity is linked to the presence of GlcCer. Interestingly, the presence of methylated GlcCer results in a greater overall loss of mean intensity, decreasing by approximately 75%, compared to that of nonmethylated GlcCer, decreasing by around 60% (Figure 2). It is worth noting that three residues, namely G10, C18, and N37, are absent from the spectrum when GlcCer, methylated or not, is added. However, four residues, namely V8, N39, C40 and C42, are absent from the spectrum only when GlcCer is methylated, suggesting that they are specifically affected, directly or indirectly, by the presence of the C9 methyl (Figure 2).

To go further, NMR spectra of ETD151 (50 µM, final concentration) in the presence of PC-methylated GlcCer LUVs at different molar ratios (ETD151: methylated GlcCer; 10:1, 1:1, and 1:10) were performed to identify which residues were most affected in the binding, and thus define which part(s) of the peptide chain would play a key role in ETD151's affinity for the target, namely methylated GlcCer.

As seen in Figure 3A, the increased concentrations of methylated GlcCer-containing PC LUVs did not result in a discernible shift in the resonance positions of ETD151 residues. However, this resulted in a significant and progressive loss of the overall signal intensity of ^{15}N-ETD151 (Figure 3B). The progressive attenuation of ETD151 signal intensity is indicative of its binding to PC-methylated LUVs due to the slower tumbling of the large complex formed. Interestingly, differential perturbations in the intensity of the cross-peaks of certain residues were obtained, indicating a differential contribution to the interaction. To quantitatively discriminate the most perturbed residues in the presence of methylated GlcCer, we calculated the mean ratio intensity ($I_{methylated\ GlcCer}/I_0$, where I_0 is the intensity of ETD151 peak in free state), determined the standard deviation (σ), and set a threshold at minus one standard deviation from the mean (mean -1σ). Any residue with a ratio intensity below this threshold indicated a potential perturbation due to the presence of methylated GlcCer (Figure 3C). The absence of resonance

in some residues was attributed to line broadening, indicating complete partitioning of the peptide into the lipid bilayers or strong binding to the liposome surface. These residues, namely V8, G10, C18, N37, N39, C40, and C42 (Figure 3C, color blue), are likely to be the most affected by the presence of the methylated GlcCer. The intensity of several peaks decreased significantly (intensity below the threshold defined by mean -1σ), specifically the peaks of residues L3, I4, W9, A11, A20, G30, C32, F35, and A36 (Figure 3C, color cyan). The ETD151 residues highlighted in Figure 3C show that the area comprising the L1 and L3 loops is likely to be the most involved in lipid binding, involving mainly hydrophobic residues (W9, F35, V8, A11, F35, A36), and some polar residues (N37, N39).

3. ETD151 increases the lipid dynamics of GlcCer-containing membranes, with a more pronounced effect with methylated GlcCer

Methylation of GlcCer plays a pivotal role in regulating the physical properties of the plasma membrane in terms of lipid organization and membrane fluidity. Since GlcCer are the membrane target of ETD151, we suggest a biophysical link between GlcCer-containing vesicles and ETD151 interaction, raising the possibility of modification of lipid order and dynamics. Due to their high sensitivity to changes in lipid dynamics, ^{31}P and ^{2}H ss-NMR experiments have been widely used to investigate the impact of peptide presence on membrane models (41).

In this study, static ^{31}P ss-NMR experiments were conducted to gain insight into the molecular mobility of the polar head group of PC lipid and static ^{2}H ss-NMR provided additional information on the dynamics of the hydrophobic core using a deuterated POPC chain (d_{31}-POPC). Multilamellar vesicles (MLVs) containing GlcCer without ETD151 were used as a control and compared to MLVs with the presence of a ratio of 1 ETD151 to 20 lipids.

All ^{31}P spectra (Figure 4A and 4C), recorded with methylated or nonmethylated GlcCer-containing MLVs, in the absence or presence of ETD151, are characteristic of a lamellar phase with axial symmetry. Also characteristic of a lamellar fluid phase, all ^{2}H spectra (Figures 4B and 4D) exhibited a symmetric spectrum. For nonmethylated GlcCer-containing MLVs, ETD151 increased the dynamic of the phosphate group of PC lipids (chemical shift anisotropy (CSA) decreased from approx. 31 to 29.5 ppm), with a slight decrease in the downfield edge (// edge) intensity of the ^{31}P spectra (Figure 4A, circled gray area). This observation indicates the deformation of spherical liposomes into “prolate-like” liposomes in the magnetic field, following an increase in membrane elastic properties (42). However, no significant differences were observed in static ^{2}H spectra with or without ETD151 for these vesicles (Figure 4B), suggesting that ETD151 did not disrupt the dynamics of the d_{31}-POPC in this membrane model. This also suggests that the effect on nonmethylated GlcCer-containing MLVs order is very subtle, with a ^{31}P spectral shape modification indicating a change of orientation in the phosphate group.

Regarding methylated GlcCer-containing MLVs, a decrease in the CSA from 31.5 to approx. 29 ppm is also observed for lipid systems upon the addition of ETD151 (Figure 4C), indicating increased dynamics in the headgroup part of the membrane. The addition of ETD151 has a clear impact on static ^{2}H spectra

obtained with the methylated GlcCer model, leading to an overall decrease in spectral width (Figure 4D), corresponding to an increase in the dynamics of the hydrophobic core of the membrane, where the deuterons are located. While order parameters at each position could theoretically be measured, an overall quantification could be assessed easily by measuring the decrease of ^{2}H second spectral moment M_2, reflecting a more fluid membrane when containing ETD151 (see supp info Table S2).

Overall, the ss-NMR results obtained in our experimental conditions suggest that ETD151 was not deeply inserted into the hydrophobic part of the nonmethylated GlcCer-containing model membranes and is primarily located near the phosphate group of phospholipids, at the vesicle surface. However, ETD151 insertion in POPC containing methylated GlcCer is more profound, with a greater impact on overall membrane dynamics and a notable fluidification primarily observed of the hydrophobic part.

DISCUSSION

ETD151 was optimized from the defensin Heliomicin isolated from the tobacco budworm *Heliothis virescens* (24). It is highly effective against most fungal pathogens (e.g., *Aspergillus fumigatus*, *Candida albicans*, *Cryptococcus neoformans*) (24), which have developed multi-resistance to available antifungal drugs (26). Moreover, ETD151 showed low toxicity in mouse models (27). ETD151 therefore warrants further investigation as a promising antifungal peptide. While some steps of its MoAs (28) and the crucial role of fungal glucosylceramides (GlcCer) for ETD151 activity have been revealed (25), the mechanisms by which ETD151 targets fungal GlcCer, at the molecular and atomic scale require further investigation.

GlcCer are well-conserved glycosphingolipids in fungal membranes and play essential structural and signaling roles in cell survival and pathogenicity (17, 43). As their presence in the fungal membrane is important for the activity of certain CSαβ defensins (20–22, 38), there is a strong case for GlcCer to be a putative binding target for these defensins, such as Psd1, MtDef1, and AFP1. GlcCer interaction is a key step for antifungal defensin activity and the cascade of events leading to the attack on fungi. It is therefore essential to understand the structural and biochemical bases of this interaction to fully exploit the potential of GlcCer-interacting defensins as antifungal agents. In this study, we initially assessed the binding affinity using MST and ITC techniques. Then, we identified the disruptions at the atomic scale from the perspective of either the protein or the membrane, by NMR studies. Finally, given that methylated GlcCer are found only in fungi, we investigated the impact of the C9-methyl on the ETD151-GlcCer interaction. To characterize the molecular recognition between ETD151-fungal GlcCer and determine whether the methyl impacts this recognition, we used two commercially available GlcCer differing only by the presence of the C9-methyl: a fungal methylated GlcCer from the golden oyster mushroom *Pleurotus citrinopileatus* (d19:2/h16:0) and a plant nonmethylated GlcCer (d18:2/h16:0) from soybean. Each GlcCer was incorporated into PC-based LUVs at the same ratio to create simplified biomimetic membranes.

ETD151 demonstrates a greater affinity for methylated GlcCer

For the characterization of drug-target interactions, the determination of the binding (i.e. binding affinity) between the two partners is a key issue. This study combined ITC and MST assays, which indicated that ETD151 binds to PC-based vesicles when containing GlcCer. Unlike other GlcCer-interacting defensins, including Psd1, Psd2, and Sd5 defensins which have shown affinity for PC-based vesicles (20, 23, 44, 45), a non-significant interaction was observable between PC and ETD151 in PC-LUVs used as control. It is noteworthy that with both techniques, the measured affinity of ETD151 is higher when the incorporated GlcCer is methylated, clearly indicating the influence of the C9-methyl. Previous *in vitro* studies have demonstrated the following fungus-specific feature: C9 methylation plays a role in the binding of GlcCer by the pea defensin Psd1 (34) and AFP1 from the brown Eastern mustard *Brassica juncea* (38). Indeed, its absence in the sphingoid base prevents RsAFP2 from interacting with GlcCer (19) and reduces the binding affinity of Psd1 to GlcCer-containing lipid vesicles by 2.5-fold (20). It is worth noting that these previous studies (19, 20) used fungal and plant GlcCer, which, differ in fatty acid length and unsaturation state, in addition to the difference in C9-methyl in the sphingoid base. Therefore, the role of these structural variations in the binding affinity of antifungal CSαβ defensins to GlcCer cannot be ruled out. To our knowledge, this study demonstrates the *in vitro* impact of C9-methyl on ETD151-GlcCer binding.

There are limited data available in the literature regarding the estimation of defensin-GlcCer binding, data acquired with different biophysical techniques, such as reverse enzyme-linked immunosorbent assay (rELISA) (19), surface plasmon resonance (SPR) (20, 23), MST and ITC (this work). This makes affinity comparisons quite challenging (46). In an rELISA assay, glycolipids are immobilized on the hydrophobic surface of the wells of microtiter plates and the bound defensin is detected immunologically. This technique has been used to characterize the binding of RsAFP2 and Heliomicin to fungal methylated GlcCer and showed a dose-dependent interaction (20). SPR experiments were conducted to examine the interaction of mimetic fungal membranes with the pea defensins Psd1 and Psd2. In these experiments, liposomes were immobilized on the surface of the chip before peptide injection at a given concentration under constant flow. The SPR assay provides binding affinity and kinetic parameters, association and dissociation rates (K_a and K_d). However, in all studies of defensin-GlcCer interaction by SPR, the defensin-membrane dissociation phase was insignificant ($K_a >>> K_d$). Therefore kinetic data (K_a and K_d values) could not be obtained (20, 23). Binding affinity was therefore assessed by the equilibrium response before dissociation (Req) and/or by the speed of initial association indicated by the initial association rate (α-value). Higher Req and α values correlate with greater peptide binding affinity to membranes. The incorporation of 30% mol $GlcCer_{Fusarium\ solani}$ into a PC-based vesicles increased binding 5-fold for Psd1 compared to a PC-based vesicles, based on an α-value (20). However, Psd2, which shares approximately 45% sequence identity with Psd1, showed a 2-fold stronger binding

response intensity with pure POPC-based vesicles than with POPC: $GlcCer_{F.\ solani}$ vesicles (70:30), based on Req value (23).

To examine ETD151 interaction with methylated GlcCer, we employed both MST and ITC techniques to estimate the K_d values. The K_d value estimated by MST with the commercial fungal GlcCer (d19:2/h16:0, named methylated GlcCer in this work) is in the range of 0.7 µM. This value is consistent with that obtained in our previous work for ETD151 binding to liposomes containing GlcCer directly extracted from *B. cinerea* (mixture of d19:2/h16:0 and d19:2/h16:1, K_d is in the range of 0.5 µM) (25). With the commercial fungal GlcCer, we were able to evaluate the K_d value by ITC too. The K_d values are in the micromolar range, with values obtained with ITC higher than those obtained with MST. This discrepancy may be attributed to the experimental setup. Although ITC and MST report a signal proportional to the progression of the binding or saturation of the protein, the experimental procedure and the measured signal are different. With both techniques the binding affinity of ETD151 to GlcCer is greater when GlcCer is methylated.

The hydrophobic adjacent loops of ETD151 are impacted by the presence of GlcCer in model membranes

Identifying which parts of the ligand contribute to binding with the target is essential for understanding the ligand-target interaction at the atomic level. The positive charge of several antifungal defensins has been reported to determine membrane surface binding activity, particularly with the negatively charged phosphate head group of phospholipids (47). In solution NMR, signals of free-moving peptides in solution are typically sharp and intense. In contrast, peptides bound to liposomes are expected to show significant line broadening and intensity loss due to the slow tumbling motion of liposomes. Thus, if the addition of the liposomes does not induce a notable change in chemical shift or relative intensity to the peptide alone in the solution, it is considered a non-strong interaction. By contrast, when the addition of the liposomes results in a significant loss of intensity and/or clear chemical shift perturbation (CSP), the residues affected by the interaction can be identified. Moreover, at identical liposomes and peptide concentrations, greater attenuation of peptide signal intensity can be interpreted as higher peptide/liposomes affinity, allowing peptides to be classified according to their liposome affinity.

The NMR results suggest that the basic residues of ETD151 play a minor role in recognizing fungal GlcCer-containing vesicles. However, they demonstrate that the two L1 and L3 hydrophobic loops are seemingly those by which ETD151 interacts with or inserts into liposomes containing GlcCer (Figure 3B). This predominant hydrophobic role correlates with ITC results indicating an entropy-driven interaction. Except for the conservation of the disulfide bridges array (in yellow, Figure 5A), sequence conservation is generally low in the antifungal defensin family. In particular, the L1 loop of ETD151 is highly atypical and longer than usual (Figure 5A). The hydrophobic residues V8/W9/G10/A11/V12 of L1 are close to F35/A36/V38 of the L3 loop, forming a significant hydrophobic patch (Figure 5B-a). Note that V8, W9, G10, A11, F35 and A36 are among the most disturbed residues when ETD151 is in

interaction with GlcCer-containing membranes (Figure 3B). Such hydrophobic patches involving L1 and L3 loops are found in some antifungal plant defensins, with hydrophobic residues playing important biological roles, including activity, pathogen target recognition, and/or dimer formation (48, 49). For RsAFP2, mutagenesis of key hydrophobic residues in L3 loop, namely Y38, V39, F40, P41, and A42 (Figure 5B-b), resulted in a sharp decrease in antifungal activity compared to the WT (48). Note that V39, F40 and A42 correspond to F35, A36 and V38 in ETD151 (Figure 5A and 5B-a and 5B-b). In SPE10 from *Pachyrhizus erosus* jicama seeds, residues P13, F15 located in the L1 loop, and F39 located in the L3 loop forming the hydrophobic patch (Figure 5B-c) are required for antifungal activity and dimer formation (with F15 and F39 corresponding to V8 and V38 in ETD151, respectively). In particular, residue F39 has been identified as essential for antifungal activity (49). Solution NMR analysis of defensin Psd1, using CSP monitoring, showed that hydrophobic residues V13, F15, and A18 in the L1 loop and residue W38 in the L3 loop (Figure 5B-d) (with F15 and W38 corresponding to V8 and V38 in ETD151, respectively) are important for activity and are disrupted by $GlcCer_{F.\ solani}$ in PC lipid vesicles (50). Note that these four residues correspond to less hydrophobic residues in Psd2 (P13, I15, G18 and F39, respectively), for which no clear hydrophobic area is visible (Figure 5B-e) (51). In addition to the dominant hydrophobic interactions, the involvement of other types of interactions between ETD151 and methylated GlcCer, such as hydrogen bonds, remains a possibility. Furthermore, a conformational adaptation of the ETD151 structure to recognize GlcCer may be suggested, since two cysteines (C18, C40) forming one of the three disulfide-bridges were disrupted. The multiple effects induced by the interaction between defensin and GlcCer have already been postulated for Psd1 (50).

Structural changes in defensins recognizing GlcCer in the bound state have rarely been studied. However, there are indications that ETD151 shares structural changes in common with Psd1 when binding to fungal GlcCer. Indeed, for Psd1, the L1/L3 region exhibits reduced conformational exchange, likely due to the stabilization of a specific membrane-bound conformation of the peptide (50). In contrast, different structural regions of the sugar cane *Saccharum officinarum* defensin Sd5 were highlighted upon recognition of fungal GlcCer. The L1/L3 hydrophobic patch is small, involving I21 in the L1 loop and F48 in the L3 (corresponding to V8 and V38 in ETD151) (Figure 5B-f). The Sd5 region considered specific for Sd5-GlcCer interaction comprises part of the α-helix and the L2 loop (44).

Dynamic NMR studies for Psd1 and Sd5, two peptides with completely different dynamic properties, showed molecular recognition of fungal GlcCer by conformational selection. Upon binding to GlcCer, a modification of ETD151 dynamics could not be excluded. The internal dynamic of ETD151 in the free state, studied using NMR relaxation experiments, is in favor of a compact peptide (Longitudinal relaxation rate R1, sup data Figure S4a), without large amplitude internal motions on the ps~ns timescale (heteronuclear nuclear Overhauser effect, sup data Figure S4c). Interestingly, transverse relaxation rate values (R2) and dispersion experiments (CPMG) of ETD151 suggest that exchange processes occur on the µs~ms timescale (see supp info Figure S4b and S4d), particularly for residues I4, S34, F35, N37, N39 and C40 (see supp info Figure S4e). These residues are identified as potentially involved in the

target-binding event (solution NMR results). Importantly, the signal of V38 is undetectable due to an increase of its linewidth (via "exchange broadening") also reflecting the intermediate exchange regime. Dynamic processes in this time window include side chain reorientation, loop motion, secondary structure changes and hinged domain movements. Such motions may affect processes including ligand binding and release, folding and unfolding events, allostery and the rate of catalytic turnover. Therefore, despite sharing a common CSαβ structural fold, there seems to be no consensus among antifungal defensins regarding interaction with lipid targets, including fungal GlcCer. For ETD151, the two adjacent L1 and L3 loops constitute an essential region that would monopolize methylated GlcCer binding.

ETD151 specifically inserts into and fluidifies PC lipid vesicles containing methylated GlcCer

The lipid-binding activity of antimicrobial peptides (AMPs) is thought to modify several structural and dynamic properties of the membrane (52–54). While the effects of several linear AMPs with pore-forming activity (e.g., melittin, magainin, gramicidin, aurein, caerin) on lipids have been reported via ss-NMR (55, 56), the impact of disulfide-rich peptides has rarely been investigated (e.g., human β-defensin (HBD-3) analogs (57)). In this study, we employed ^{31}P and ^{2}H ss-NMR experiments to examine the disruption of lipid order caused by the interaction with ETD151. In the case of MLVs containing nonmethylated-GlcCer, ETD151 seems to remain on the lipid surface near the phosphate headgroup, deforming MLVs into non-spherical vesicles without disrupting the dynamics of lipid hydrophobic chains. In the case of MLVs containing methylated-GlcCer, ETD151-binding disrupts the order in the polar and hydrophobic parts of the lipid membranes, suggesting peptide insertion into the membrane. This suggests that the presence of the C9-methyl in GlcCer plays a role for ETD151-induced membrane fluidization and is a key factor for ETD151 to insert deeper into fungal membrane models. Moreover, our results show that ETD151 binding induces a slight increase in membrane disorder and therefore more fluid. Interestingly, analogous observations have been reported for rhamnolipids (RLs), potential biocontrol agents for crop protection with antifungal activities, using representative fungal membrane models (58). This differs from the HBD-3 analog, which rigidified negatively charged lipids mimicking bacterial membranes in addition to membrane morphological disruption (57). This indicates a possible different mechanism, at least in the membrane binding step of pore formation.

The C9-methyl in the sphingoid base plays a major role in the ETD151-GlcCer interaction

In a membrane context, the presence of C9-methyl in the GlcCer markedly enhances affinity with ETD151, influences the two adjacent loops of the ETD151 structure, and reinforces the destabilization of lipid dynamics caused by the peptide. Changes in the biophysical properties of membranes due to the presence of C9-methyl and/or the direct involvement of C9-methyl in the binding sites with ETD151 may explain the selectivity of ETD151 for membranes containing methylated GlcCer rather than nonmethylated GlcCer. Indeed, C9-methylation in GlcCer has been reported to influence membrane topography by affecting lipid organization, which directly impacts membrane permeabilization (36, 59,

60). Structural features of fungal GlcCer, e.g., C9-methylation and the Δ8 double bond, could increase the physical distance between the hydrophobic core of GlcCer and other membrane lipids (35). Such effects on the biophysical properties of membranes may facilitate ETD151 access to the hydrophobic core of fungal membranes. It is worth noting that a correlation between the structural role of methylated GlcCer in membranes and virulence in fungal cells has been documented. For example, Δ*smt C. neoformans* mutants, unable to infect a mouse model, showed a defect in cell membrane structures, as confirmed by fluorescence spectroscopy and atomic force microscopy studies (35). The second hypothesis is that C9-methyl is directly involved in the binding sites with ETD151. Our findings demonstrate that ETD151 binds primarily by hydrophobic effects to GlcCer-containing membranes and that increased hydrophobicity by C9 methyl correlates with enhanced affinity of ETD151 for GlcCer. The dependence of defensin activity on the presence of methylated GlcCer in fungal cells is controversial. Although RsAFP2, MsDef1 and Psd1 showed similar activity against Δ*smt* fungal mutants and their WT strains (23, 37), Psd2 showed reduced activity against Δ*smt* fungal mutants compared to WT strains (34). The C9-methyl in the sphingoid base plays a major role in the defensin-GlcCer interactions. However, the precise mechanism by which the C9-methyl is involved in GlcCer recognition by antifungal defensins has yet to be determined.

Finally, using biophysical and spectroscopic methods, this study provides molecular-level insights into how the antifungal insect defensin ETD151 interacts with its fungal membrane target, GlcCer. Furthermore, the presence of the methyl in GlcCer plays a role in ETD151-induced membrane fluidization and is a key factor in ETD151's deeper insertion into fungal membrane models, explaining why ETD151's binding affinity for GlcCer is greater when GlcCer is methylated. These new findings pave the way for the optimization and development of defensin mimetics to selectively combat pathogenic fungi by targeting methylated GlcCer while minimizing toxicity to the host.

EXPERIMENTAL PROCEDURES

Peptides and Lipids

The unlabeled recombinant ETD151 was provided by Dr. Philippe Bulet. Recombinant expression of the uniformly isotopically ^{15}N-labeled ETD151 peptide (^{15}N-ETD151) in *S. cerevisiae* was entrusted to the Promise company (Grenoble, France).

Glucosylceramide (GlcCer) from the golden oyster mushroom *Pleurotus citrinopileatus* was purchased from Funakoshi (Japan) and referred to here as “methylated GlcCer”. Soy GlcCer referred to here as “nonmethylated GlcCer” and egg L-α-phosphatidylcholine (PC) and deuterated 1-palmitoyl-d_{31}-2-oleoyl-sn-glycero-3-phosphocholine 16:0-d_{31}-18:1 POPC (d_{31}-POPC) were purchased from Avanti Polar Lipids (Alabaster, AL, USA).

Preparation of Large Unilamellar Vesicles (LUVs)

The lipid stock solutions (PC, nonmethylated GlcCer, and methylated GlcCer) were prepared in pure chloroform (purity higher than 99.8%, Sigma Aldrich) and mixed with appropriate volumes to obtain the desired concentrations. The organic solvent was dried under a stream of nitrogen and lyophilized overnight. The resulting dry lipid films were hydrated with phosphate buffer 10 mM, pH 5.8 (buffer A) and homogenized by five cycles of freezing (liquid nitrogen) and thawing (40°C) to produce vesicle suspensions. To calibrate and homogenize the size of the vesicles, the suspensions were passed 11 times using a mini-extruder through 0.1 µm pore-size polycarbonate membrane filters (Avanti Polar Lipids, Alabaster, AL, USA). The polydispersity index (PI) and the hydrodynamic diameter of the generated LUVs were assessed by dynamic light scattering (DLS) spectroscopy at 20°C. DLS experiments were conducted using a Zetasizer (Malvern Panalytical, Instruments version 7.11, UK) with low-volume cuvettes (VWR International, Leuven, Belgium). DLS data were acquired using the Zetasizer software version 7.11. All LUV suspensions were freshly prepared and presented a hydrodynamic diameter ~100 nm and a PI < 0.01, and used for all experiments, except for solid-state NMR.

Isothermal Titration Calorimetry (ITC)

Prior to the ITC experiment, all solutions (buffer A, peptide solution, liposome solutions) were degassed under vacuum to remove air bubbles. LUV suspensions of 3.5 mM PC or PC: nonmethylated GlcCer (9:1, molar ratio) or PC: methylated GlcCer (9:1, molar ratio) in buffer A were titrated into a 250 µM ETD151 solution in the same buffer. The freshly prepared LUVs suspensions were flushed with argon and kept at +4°C for a maximum of two days. Blank titrations were conducted by titrations of LUVs with varying compositions into the buffer.

All binding ITC experiments were performed using a MicroCal PEAQ-ITC microcalorimeter (Malvern Panalytical Ltd., Malvern, UK). Samples were equilibrated to 25°C before measurement. Titrations were performed at 25°C under constant stirring (750 rpm). Each experiment consisted of an initial injection of 0.3 µL followed by 16 separate injections of 2.5 µL into the sample calorimeter cell of 200 µL. The time between each injection was 180 s, and the measurements were performed with the reference power set to 5 µcal/s and the feedback mode set to “high”.

The acquired calorimetric data were analyzed using MicroCal PEAQ-ITC Analysis Software version 1.20 (Malvern Panalytical Ltd., Malvern, UK) and the graphs generated by the same software. To achieve the titrations with GlcCer-containing LUVs, the binding data were fit based on the “One set of sites” fitting model of the software, using the titrant concentration corresponding to that of GlcCer (10% mol of the total lipid concentration). Heat associated with the first injection was not included in the data analysis. Binding curves fitting generate a dissociation constant (K_d), stoichiometries (n), enthalpy of binding (ΔH) within 95% confidence intervals, from which the apparent binding free energy (ΔG) and entropy ($-T\Delta S$) are calculated. Thermodynamic parameters are reported as the average of triplicates with

standard deviation (SD). Blank titrations and dilution data were compared to and not subtracted from the binding data.

MicroScale Thermophoresis (MST)

MST experiments were performed using a Monolith NT.115 (red) instrument (NanoTemper Technologies). A serial dilution with liposome solution (½ dilution, 16 concentrations from 1 mM to 30.5 nM) were performed in buffer A. ETD151 was labeled with Atto647 (NHS ester reactive) from Sigma-Aldrich (07376) according to (25). The fluorescently labeled peptide (Atto647-ETD151) was diluted in buffer A and added to each liposome to a final concentration of 50 nM. All samples were measured after 5 min of incubation and centrifugation (2 min, 5000×g). The experiments were performed at 40% MST power and between 20-80% LED power at 22°C. MST traces were recorded using the following parameters: 5 s MST power off, 20 s MST power on, and 5 s MST power off. The dissociation constant (K_d) between peptide-liposome interaction was calculated based on the protocol provided by NanoTemper Technologies using the MO. Affinity Analysis 2.3 software.

Solution Nuclear Magnetic Resonance (NMR)

All NMR experiments were performed at 298 K on a 700 MHz Bruker Avance III HD spectrometer equipped with a triple resonance (^{1}H, ^{13}C, ^{15}N) cryoprobe. All data were processed using the Topspin ™ 3.2 Bruker software, cross peaks assignment and intensities (height extraction) were performed with CcpNmr (61). Sensitive fast-pulse experiments 2D ^{1}H-^{15}N SOFAST-HMQC (62) were recorded using Bruker pulse sequence "fhmqcf3gpph" with spectral widths of 1024 x 128 complex points in the ^{1}H and ^{15}N dimensions, respectively.

Lyophilized ^{15}N-ETD151 was dissolved in buffer A to 100 µM. ^{1}H-^{15}N SOFAST-HMQC spectra were recorded for free ETD151 in solution (50 µM as final concentration), and cross-peak assignment was based on PDB 1P00 deposited data. Peak intensities of free-state ^{15}N-ETD151 are referred to as I_0. Next, ^{1}H-^{15}N SOFAST-HMQC spectra were recorded for ^{15}N-ETD151 at 50 µM in the presence of 5 mM PC LUVs or PC-GlcCer LUVs (nonmethylated) or PC-methylated GlcCer LUVs, and the chemical shift and peak intensities were extracted. The peak intensities of ^{15}N-ETD151 in the presence of each LUVs composition are referred to as I_{PC}, $I_{\text{nonmethylated GlcCer}}$ and $I_{\text{methylated GlcCer}}$, respectively. The effects of adding PC-methylated GlcCer LUVs to ETD151 at different molar ratios (ETD151: methylated GlcCer; 10:1, 1:1, and 1:10) on the ^{1}H-^{15}N SOFAST-HMQC spectrum of ^{15}N-ETD151 at constant concentration (50 µM) were assessed. For each tube, 10% (v/v) of D_2O was added as a final concentration. The effect of the addition of PC LUVs, PC-GlcCer LUVs, and PC-methylated GlcCer LUVs on the ETD151 structure was evaluated by the intensity ratio, namely (I_{PC}/I_0), ($I_{\text{nonmethylated GlcCer}}/I_{PC}$), and ($I_{\text{methylated GlcCer}}/I_{PC}$), respectively. ETD151 residues showing a decrease in the intensity ratio of less than minus one standard deviation (-1σ) were considered to be significantly impacted by the presence of lipids contained in LUVs. Figures 3C and 5B were generated using PyMOL (63) and ChimeraX 1.4.

NMR Relaxation Experiments

The recombinant ^{15}N-ETD151 peptide was dissolved in tampon phosphate 40 mM pH 5.5 to obtain a final concentration of 0.4 mM. NMR relaxation experiments were performed at 298 K on an Avance III HD Bruker 700 MHz spectrometer equipped with a cryoprobe. ^{15}N R_1 relaxation delays of 10, 20, 30, 50, 75, 100, 150, 200, 300, 500, 1000, 2000 and 3000 ms and R_2 relaxation delays of 10, 20, 30, 40, 50, 60, 70, 80, 90, 100, 125, 150, 200, 250 and 300 ms were used for data collection. The above time series were fitted by a single exponential decay.

The ^{15}N-NOE spectra were collected with a 3 s relaxation delay. The ^{1}H–^{15}N heteronuclear NOE was calculated from the equation NOE = Isat/Ieq, where Isat and Ieq represent the volumes of a cross-peak in the spectra collected with and without proton saturation, respectively. All experiments were performed three times under identical conditions. Volumes for the amide ^{15}N-^{1}H cross peaks were measured using Topspin TM 3.2 Bruker software. Uncertainties in the volumes were determined from the duplicate spectra.

^{1}H-^{15}N CPMG experiments were recorded with ν_{CPMG} = 0, 50, 75, 100, 125, 150, 175, 200, 250, 300, 350, 400, 500, 600, 700, 800 and 900 Hz, and a CPMG constant time delay of 40 ms. Peak intensities were plotted as effective relaxation rates and relaxation dispersion curves were fitted using the ShereKhan web application (64). The data were fit using a global two-state exchange process with the Carver–Richards model for slow exchange (65).

Solid-State NMR (ss-NMR)

For ss-NMR experiments, multilamellar vesicles (MLVs) were prepared using the film method as previously described (66). Appropriate volumes of lipid stock solutions in chloroform were mixed to obtain the desired lipid compositions (i) PC: d_{31}-POPC: nonmethylated GlcCer and (ii) PC: d_{31}-POPC: methylated GlcCer, both with a molar ratio of 7:2:1. The organic solvent was dried under a nitrogen stream. The residual organic solvent in lipid film was removed by high vacuum for at least 4 h. The resulting dried lipid film was hydrated with 50 mM HEPES, 10 mM NaCl, pH 7.4 (buffer B) in deuterium-depleted water from Sigma Aldrich (7732-18-5). Lipid dispersion was vortexed and subjected to three cycles of freeze-thawing (10 min at -20°C followed by 10 min at 40°C) and transferred directly to an insert, which was then fitted into a 4 mm rotor. For samples containing ETD151, hydration of the lipid film was performed with buffer B containing ETD151 at a molar ratio equal to ½ that of GlcCer.

The ss-NMR experiments were performed at 298K on a Bruker Avance III 500 wide bore spectrometer (Wissembourg, France), with resonance frequencies of 500.5 MHz for ^{1}H, 202.6 MHz for ^{31}P spectra and 76.8 MHz for ^{2}H spectra, equipped with a 4-mm magic-angle spinning (MAS) triple-resonance probe. Static ^{31}P NMR spectra for the MLVs control sample and the ETD151-containing sample were acquired using a phase-cycled Hahn echo pulse sequence (67) with high-power (50 kHz) ^{1}H decoupling during acquisition. Using a 90° pulse length of 3 µs, an interpulse delay of 35 µs, data were collected

using 4 k data points with a recycle delay of 3 s and a total of 1 k scans per spectrum, amounting to 1 hour of acquisition. The static ^{2}H NMR experiments were carried out using a quadrupolar echo sequence (68) with 60 k data points, acquired with a 90° pulse length of 5 µs, an interpulse delay of 96 µs, and a recycle time set to 500 ms. A total of 100k scans per spectrum were acquired over 16 hours. Line broadening of 50 and 100 Hz was applied to the ^{31}P and ^{2}H spectra, respectively. The ^{31}P chemical shift anisotropy (CSA) was determined by line fitting using Bruker Topspin 3.2 and Sola (Solid Lineshape Analysis) softwares. MAS ^{2}H ss-NMR experiments were carried out using a 10 kHz spinning frequency and a phase-cycled quadrupolar echo sequence (69), with 100 k data points, acquired with a 90° pulse length of 4 µs, a rotor-synchronized interpulse delay of 96 µs and a recycle time of 500 ms. A total of 1 k scans per spectra were acquired for 10 min. ^{2}H spectral moment analysis was performed using MestRenova software V6.0 (Mestrelab Research, Santiago de Compostela, Spain). Second spectral moments (M_2) values, provide a quantitative description of the membrane lipid ordering, were calculated as previously described (69).

DATA AVAILABILITY

All the relevant data are contained within this manuscript and supporting information. Source data and additional data can be obtained from the corresponding author upon reasonable request.

SUPPORTING INFORMATION

This article contains supporting information.

AKNOWLEDGMENTS

We thank the MO2VING/NMR facility (CBM, Orléans, France), particularly Hervé Meudal for his technical advice in acquiring solution NMR experiments. For their technical assistance and helpful guidance in conducting and analyzing the ITC experiments, we also want to thank Caroline Mas (Grenoble Instruct-ERIC center, France), Franck Coste and Marcin Suskiewicz (Center for Molecular Biophysics, Orléans, France). This work used the platforms of the Grenoble Instruct-ERIC center (ISBG; UAR 3518 CNRS-CEA-UGA-EMBL) within the Grenoble Partnership for Structural Biology (PSB), supported by FRISBI (ANR-10-INBS-0005-02) and GRAL, financed within the University Grenoble Alpes graduate school (Ecoles Universitaires de Recherche) CBH-EUR-GS (ANR-17-EURE-0003).

CONFLICT OF INTEREST

Authors declare no competing interest in relation to the work described in this study.

REFERENCES

1. Bongomin, F., Gago, S., Oladele, R.O., *et al*. (2017) Global and Multi-National Prevalence of Fungal Diseases—Estimate Precision. J Fungi. **3**, 57
2. Denning, DW,. (2024) Global incidence and mortality of severe fungal disease. Lancet Infect Dis. **24**, 428–438

3. Brown, G. D., Ballou, E.R., Bates, S., *et al.* (2024) The pathobiology of human fungal infections. Nat Rev Microbiol. **22**, 687-704
4. Roemer, T., Krysan, D.J. (2014) Antifungal Drug Development: Challenges, Unmet Clinical Needs, and New Approaches. Cold Spring Harb Perspect Med. **4**, 019703
5. Odds, F. C., Brown, A. J. P., and Gow, N. A. R. (2003) Antifungal agents: mechanisms of action. Trends Microbiol. **11**, 272–279
6. Francois, I., Cammue, B., Borgers, M., et al. (2006) Azoles: Mode of Antifungal Action and Resistance Development. Effect of Miconazole on Endogenous Reactive Oxygen Species Production in Candida albicans. AIAMC. **5**, 3–13
7. Carolus, H., Pierson, S., Lagrou, K., *et al*. (2020) Amphotericin B and Other Polyenes—Discovery, Clinical Use, Mode of Action and Drug Resistance. J Fungi. **6**, 6(4)-321
8. Perlin, D. S. (2015) Mechanisms of echinocandin antifungal drug resistance. Ann N Y Acad of Sci. **1354**, 1–11
9. Houšť, J., Spížek, J., and Havlíček, V. (2020) Antifungal Drugs. Metabolites. **10**, 106
10. Lockhart, S. R., Chowdhary, A., and Gold, J. A. W. (2023) The rapid emergence of antifungal-resistant human-pathogenic fungi. Nat Rev Microbiol. **21**, 818–832
11. Lee, Y., Robbins, N., and Cowen, L. E. (2023) Molecular mechanisms governing antifungal drug resistance. NPJ Antimicrob Resist. **1**, 5
12. Robbins, N., Wright, GD., Cowen, L.E. (2016) Antifungal Drugs: The Current Armamentarium and Development of New Agents. Microbiol Spectr. **4**(5):10.1128.
13. Ganz, T. (2003) Defensins: antimicrobial peptides of innate immunity. Nat Rev Immunol. **3**, 710–720
14. Thevissen, K., Kristensen, H.-H., Thomma, B. P. H. J., *et al*. (2007) Therapeutic potential of antifungal plant and insect defensins. *Drug Discov Today*. **12**, 966–971
15. Silva, P. M., Gonçalves, S., and Santos, N. C. (2014) Defensins: antifungal lessons from eukaryotes. Front Microbiol. **5**, 97
16. Vriens, K., Cammue, B. P. A., and Thevissen, K. (2014) Antifungal Plant Defensins: Mechanisms of Action and Production. Molecules. **19**, 12280–12303
17. Fernandes, C.M., Goldman, G.H., Del Poeta, M. (2018) Biological Roles Played by Sphingolipids in Dimorphic and Filamentous Fungi. mBio. **9**, 00642-18
18. Rollin-Pinheiro, R., Singh, A., Barreto-Bergter, E., *et al*. (2016) Sphingolipids as targets for treatment of fungal infections. Future Med Chem. **8**, 1469–1484
19. Thevissen, K., Warnecke, D., François, I., *et al*. (2004) Defensins from Insects and Plants Interact with Fungal Glucosylceramides. J biol chem. **279**, 3900–5
20. Neves de Medeiros, L., Domitrovic, T., Cavalcante de Andrade, P., *et al*. (2014) Psd1 binding affinity toward fungal membrane components as assessed by SPR: The role of glucosylceramide in fungal recognition and entry. Biopolymers. **102**, 456–464
21. Ramamoorthy, V., Cahoon, E. B., Li, J., *et al*. (2007) Glucosylceramide synthase is essential for alfalfa defensin-mediated growth inhibition but not for pathogenicity of Fusarium graminearum. Mol Microbiol. **66**, 771–786
22. Mello, E. de O., dos Santos, I. S., Carvalho, A. de O., *et al*. (2014) Functional expression and activity of the recombinant antifungal defensin PvD1r from Phaseolus vulgaris L. (common bean) seeds. BMC Biochem. **15**, 7
23. Amaral, V. S. G., Fernandes, C. M., Felício, M. R., *et al*. (2019) Psd2 pea defensin shows a preference for mimetic membrane rafts enriched with glucosylceramide and ergosterol. Biochim Biophys Acta Biomembr. **1861**, 713–728
24. Landon, C., Barbault, F., Legrain, M., *et al*. (2004) Lead optimization of antifungal peptides with 3D NMR structures analysis. Protein Sci. **13**, 703–713
25. Kharrat, O., Yamaryo-Botté, Y., Nasreddine, R., *et al*. (2025) The antimicrobial activity of ETD151 defensin is dictated by the presence of glycosphingolipids in the targeted organisms. Proc Natl Acad Sci. **122**, e2415524122
26. Wold Health Organization. (2022) WHO fungal priority pathogens list to guide research, development and public health action
27. Andrès, E. (2012) Cationic antimicrobial peptides in clinical development, with special focus on thanatin and heliomicin. Eur J Clin Microbiol Infect Dis. **31**, 881–888

28. Aumer, T., Voisin, S. N., Knobloch, T., *et al*. (2020) Impact of an Antifungal Insect Defensin on the Proteome of the Phytopathogenic Fungus Botrytis cinerea. J Proteome Res. **19**, 1131–1146
29. Williamson, B., Tudzynski, B., Tudzynski, P., *et al*. (2007) Botrytis cinerea: the cause of grey mould disease. Mol Plant Pathol. **8**, 561–580
30. Hahn, M. (2014) The rising threat of fungicide resistance in plant pathogenic fungi: Botrytis as a case study. J Chem Biol. **7**, 133–141
31. Cools, T. L., Struyfs, C., Cammue, B. P., *et al*. (2017) Antifungal plant defensins: increased insight in their mode of action as a basis for their use to combat fungal infections. Future Microbiol. **12**, 441–454
32. Barreto-Bergter, E., Pinto, M. R., and Rodrigues, M. L. (2004) Structure and biological functions of fungal cerebrosides. An Acad Bras Cienc. **76**, 67–84
33. Ternes, P., Sperling, P., Albrecht, S., *et al*. (2006) Identification of Fungal Sphingolipid C9-methyltransferases by Phylogenetic Profiling. J. Biol. Chem. **281**, 5582–5592
34. Fernandes, C. M., de Castro, P. A., Singh, A., *et al*. (2016) Functional characterization of the Aspergillus nidulans glucosylceramide pathway reveals that LCB Δ8-desaturation and C9-methylation are relevant to filamentous growth, lipid raft localization and Psd1 defensin activity. Mol Microbiol. **102**, 488–505
35. Singh, A., Wang, H., Silva, L. C., *et al*. (2012) Methylation of glycosylated sphingolipid modulates membrane lipid topography and pathogenicity of Cryptococcus neoformans. Cell Microbiol. **14**, 500–516
36. Huber, A., Oemer, G., Malanovic, N., *et al*. (2019) Membrane Sphingolipids Regulate the Fitness and Antifungal Protein Susceptibility of Neurospora crassa. Front Microbiol. **10**, 605
37. Ramamoorthy, V., Cahoon, E. B., Thokala, M., *et al*. (2009) Sphingolipid C-9 Methyltransferases Are Important for Growth and Virulence but Not for Sensitivity to Antifungal Plant Defensins in Fusarium graminearum. Eukaryot Cell. **8**, 217–229
38. Oguro, Y., Yamazaki, H., Takagi, M., *et al*. (2014) Antifungal activity of plant defensin AFP1 in Brassica juncea involves the recognition of the methyl residue in glucosylceramide of target pathogen Candida albicans. Curr Genet. **60**, 89–97
39. Deleu, M., Crowet, J.-M., Nasir, M. N., *et al*. (2014) Complementary biophysical tools to investigate lipid specificity in the interaction between bioactive molecules and the plasma membrane: A review. Biochim Biophys Acta. **1838**, 3171–3190
40. Rautenbach, M., Troskie, A. M., and Vosloo, J. A. (2016) Antifungal peptides: To be or not to be membrane active. Biochimie. **130**, 132–145
41. Marcotte, I., Ouellet, M., and Auger, M. (2004) Insights on the interaction of met-enkephalin with negatively charged membranes--an infrared and solid-state NMR spectroscopic study. Chem Phys Lipids. **127**, 175–187
42. Picard, F., Paquet, M.-J., Levesque, J., *et al*. (1999) 31P NMR First Spectral Moment Study of the Partial Magnetic Orientation of Phospholipid Membranes. Biophys J. **77**, 888–902
43. Jiang, C., Ge, J., He, B., *et al*. (2021) Glycosphingolipids in Filamentous Fungi: Biological Roles and Potential Applications in Cosmetics and Health Foods. Front Microbiol. **12,** 690211
44. Silva de Paula, V., Razzera, G., Barreto-Bergter, E., *et al*. (2011) Portrayal of complex dynamic properties of sugarcane defensin 5 by NMR: multiple motions associated with membrane interaction. Structure. **19**, 26–36
45. Gonçalves, S., Teixeira, A., Abade, J., *et al*. (2012) Evaluation of the membrane lipid selectivity of the pea defensin Psd1. Biochim Biophys Acta. **1818**, 1420–1426
46. Luo, Y., and Chen, Y. (2024) Comparative Analysis of the Techniques for the Determination of Binding Affinity between a Small Molecule Inhibitor and a Protein Target. bioRxiv. 2024 Jan 1;594462.
47. Alvares, D. S., Viegas, T. G., and Ruggiero Neto, J. (2017) Lipid-packing perturbation of model membranes by pH-responsive antimicrobial peptides. Biophys Rev. **9**, 669–682
48. De Samblanx, G. W., Goderis, I. J., Thevissen, K., et al. (1997) Mutational Analysis of a Plant Defensin from Radish (Raphanus sativus L.) Reveals Two Adjacent Sites Important for Antifungal Activity. J Biol Chem. **272**, 1171–1179

49. Song, X., Zhang, M., Zhou, Z., *et al*. (2011) Ultra-high resolution crystal structure of a dimeric defensin SPE10. FEBS Letters. **585**, 300–306
51. Neves de Medeiros, L., Angeli, R., Sarzedas, C. G., *et al*. (2010) Backbone dynamics of the antifungal Psd1 pea defensin and its correlation with membrane interaction by NMR spectroscopy. Biochim Biophys Acta. **1798**, 105–113
50. Pinheiro-Aguiar, R., do Amaral, V. S. G., Pereira, I. B., *et al*. (2020) Nuclear magnetic resonance solution structure of Pisum sativum defensin 2 provides evidence for the presence of hydrophobic surface-clusters. Proteins. **88**, 242–246
52. Bechinger, B. (1999) The structure, dynamics and orientation of antimicrobial peptides in membranes by multidimensional solid-state NMR spectroscopy. Biochim Biophys Acta. **1462**, 157–183
53. Khandelia, H., Ipsen, J. H., and Mouritsen, O. G. (2008) The impact of peptides on lipid membranes. Biochim Biophys Acta. **1778**, 1528–1536
54. Iversen, A., Utterström, J., Khare, L. P., *et al*. (2024) Influence of lipid vesicle properties on the function of conjugation dependent membrane active peptides. J. Mater. Chem. B. **12**, 10320–10331
55. Ludtke, S. J., He, K., Heller, W. T., *et al*. (1996) Membrane Pores Induced by Magainin. Biochemistry. **35**, 13723–13728
56. Laadhari, M., Arnold, A. A., Gravel, A. E., *et al*. (2016) Interaction of the antimicrobial peptides caerin 1.1 and aurein 1.2 with intact bacteria by 2H solid-state NMR. Biochim Biophys Acta. **1858**, 2959–2964
57. Kang, X., Elson, C., Penfield, J., *et al*. (2019) Integrated solid-state NMR and molecular dynamics modeling determines membrane insertion of human β-defensin analog. Commun Biol. **2**, 402
58. Monnier, N., Furlan, A. L., Buchoux, S., *et al*. (2019) Exploring the Dual Interaction of Natural Rhamnolipids with Plant and Fungal Biomimetic Plasma Membranes through Biophysical Studies. Int J Mol Sci. **20**, 1009
59. Santos, F. C., Marquês, J. T., Bento-Oliveira, A., *et al*. (2020) Sphingolipid-enriched domains in fungi. FEBS Lett. **594**, 3698–3718
60. Raj, S., Nazemidashtarjandi, S., Kim, J., *et al*. (2017) Changes in glucosylceramide structure affect virulence and membrane biophysical properties of Cryptococcus neoformans. Biochim Biophys Acta. **1859**, 2224–2233
61. Vranken, W., Boucher, W., Stevens, T., *et al*. (2005) The CCPN Data Model for NMR Spectroscopy: development of a software pipeline. Proteins. **59**, 687–96
62. Schanda, P., Kupce, E., and Brutscher, B. (2006) SOFAST-HMQC Experiments for Recording Two-dimensional Deteronuclear Correlation Spectra of Proteins within a Few Seconds. J biomol NMR. **33**, 199–211
63. Delano W. (2002) The PyMOL Molecular Graphics System. 2002.
64. Mazur, A., Hammesfahr, B., Griesinger, C., *et al*. (2013) ShereKhan - Calculating exchange parameters in relaxation dispersion data from CPMG experiments. Bioinformatics. **29**, 1819-1820
65. Carver, J.P., and Richards, R.E. (1972) A general two-site solution for the chemical exchange produced dependence of T2 upon the carr-Purcell pulse separation. J Magn Reson. **6**, 89–105
66. Warschawski, D. E., Arnold, A., and Marcotte, I. (2018) A New Method of Assessing Lipid Mixtures by 31P Magic-Angle Spinning NMR. Biophys J. **114**, 1368–1376
67. Rance, M., and Byrd, R.A. (1983) Obtaining high-fidelity powder spectra in anisotropic media: Phase-cycled Hahn echo spectroscopy. J Magn Reson. **52**, 221–40
68. Davis, J. H., Jeffrey, K. R., Bloom, M., *et al*. (1976) Quadrupolar echo deuteron magnetic resonance spectroscopy in ordered hydrocarbon chains. Chem Phys Lett. **42**, 390–394
69. Warnet, X., Laadhari, M., Arnold, A., *et al*. (2015) A (2)H magic-angle spinning solid-state NMR characterisation of lipid membranes in intact bacteria. Biochim et biophys acta. **1858**, 146-152

ABBREVIATIONS

Antimicrobial peptides (**AMPs**), Band-Selective Optimized Flip Angle Short Transient Heteronuclear multiple quantum coherence (**SOFAST- HMQC**), Carr-Purcell-Meiboom-Gill (**CPMG**), Chemical shift anisotropy (**CSA**), Chemical shift perturbation (**CSP**), Cysteine-stabilized αβ motif (**CSαβ**), deuterated 1-palmitoyl-d_{31}-2-oleoyl-sn-glycero-3-phosphocholine 16:0-d_{31}-18:1 POPC (**d_{31}-POPC**), Differential power (**DP**), Dissociation constant (**K_d**), Dynamic light scattering (DLS), Egg L-α-phosphatidylcholine (**PC**), Enthalpy (**ΔH**), glucosylceramides (**GlcCer**), Heteronuclear single quantum correlation (**HSQC**), 4-(2-hydroxyethyl)-1-piperazineethanesulfonic acid (**HEPES**), Isothermal titration calorimetry (**ITC**), Large unilamellar vesicles (**LUVs**), mechanisms of action (**MoAs**), C9-methyltransferase (**SMT**), Microscale thermophoresis (**MST**), Multilamellar vesicles (**MLVs**), Nuclear Overhauser effect (**NOE**), Nuclear Magnetic Resonance (**NMR**), Phosphatidylcholine (**PC**), reactive oxygen species (**ROS**), Standard deviation (**SD**), wildtype (**WT**).

FIGURE AND LEGENDS

Figure 1.

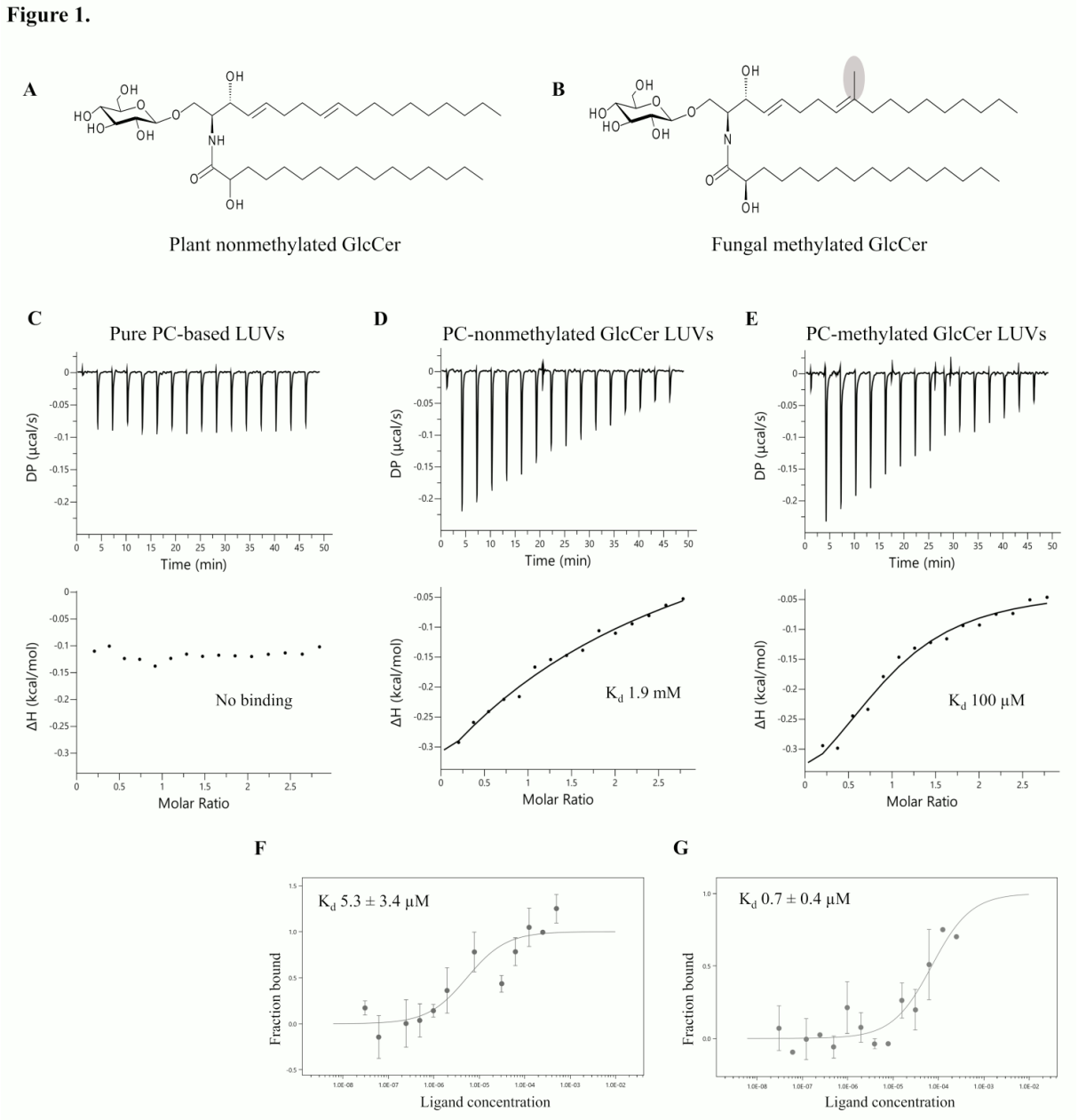

Figure 1. **Glucosylceramide (GlcCer) structures, thermodynamic (ITC) and thermophoretic (MST) analysis of the binding affinity of ETD151 with GlcCer-containing LUVs.**

(A-B) Chemical structures of plant nonmethylated GlcCer (A) and fungal methylated GlcCer (B). (C-E) ITC titrations of 3.5 mM LUVs suspension into a solution of 250 µM ETD151. (Top) ITC thermograms show the differential power (DP) over time. (Bottom) Binding isotherms present enthalpy (ΔH) in different molar ratios. Pure PC-based LUVs were used as a control (C). ITC results shown are representative of triplicate titrations for each condition. K_d is the dissociation constant of the ETD151-LUVs complex with PC-nonmethylated GlcCer LUVs (D) and PC-methylated GlcCer LUVs (E). (F-G) MST binding curves of fluorescently labeled ETD151 (Atto647-ETD151) to PC-nonmethylated GlcCer

LUVs (F) and PC-methylated GlcCer LUVs (G). K_d values estimated by MST assay are presented as the mean of three independent experiments ± SD. Peptide and liposome solutions were prepared in phosphate buffer 10mM, pH 5.8 for all ITC and MST experiments.

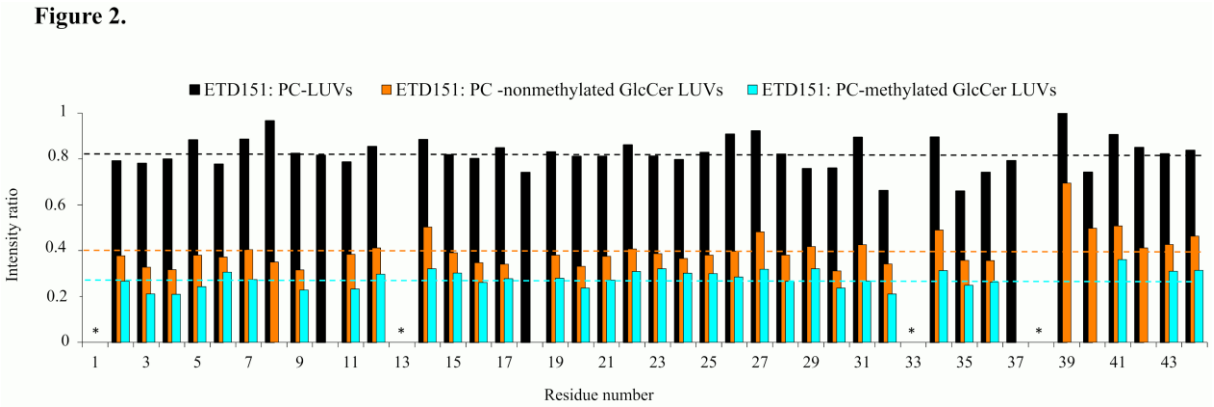

Figure 2. Relative ^{1}H-^{15}N SOFAST-HMQC signal intensities of ^{15}N-ETD151 in the presence of different compositions of LUVs.

All liposomes were used at the same concentration (5mM): PC-based LUVs (I_{PC}/I_0, in black), PC-nonmethylated GlcCer LUVs ($I_{nonmethylated\ GlcCer}/I_{PC}$, in orange), and PC-methylated GlcCer ($I_{methylated\ GlcCer}/I_{PC,}$ in cyan), with I_0 corresponding to the peak intensities of free-state ^{15}N-ETD151. The peptide ^{15}N-ETD151 was used at the same concentration (50 µM) for all samples. The horizontal lines indicate the mean ratio intensity for each sample. Residues of ETD151 are shown as consecutive numbers on the x-axis. Asterisks indicate residues where the resonance is absent in the free and bound states of ETD151.

Figure 3.

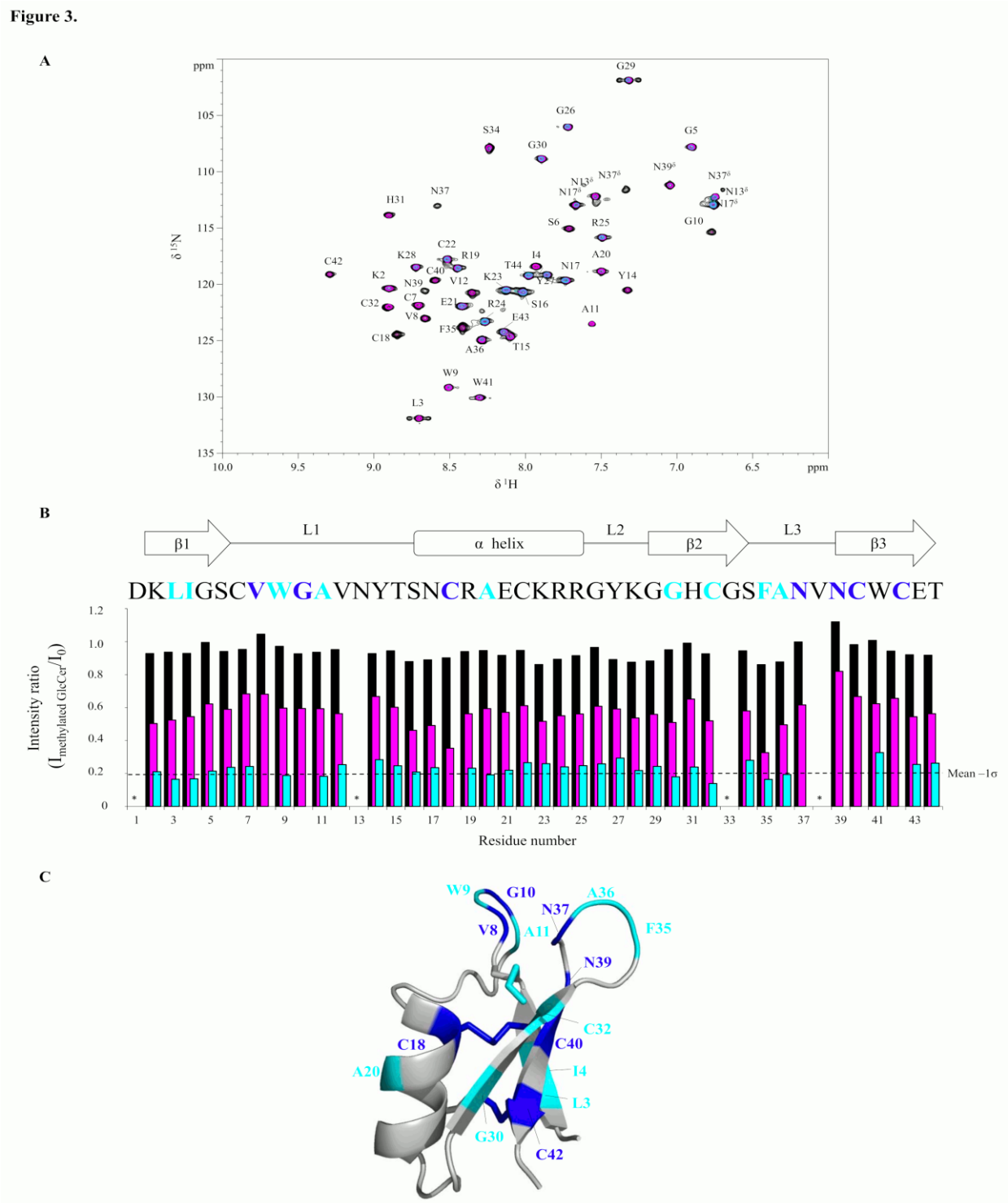

Figure 3. Solution NMR analysis for ETD151 structure in the presence of methylated GlcCer-containing PC-based LUVs.

(A) Superimposed ^{15}N -ETD151 (50 µM) 2D SOFAST-HMQC spectra in the presence of PC-methylated GlcCer LUVs at different ETD151: methylated GlcCer molar ratios; 10:1 (black), 1:1 (pink) and 1:10 (cyan). (B) Peak intensity ratios of ^{15}N-ETD151 (50 µM) in the presence of PC-methylated GlcCer LUVs at different ETD151: methylated GlcCer molar ratios; 10:1 (black), 1:1 (pink) and 1:10

(cyan) over the I_0 intensity of the corresponding peak in the reference spectrum (^{15}N-ETD151 free-state at 50 µM). Residues of ETD151 are shown as consecutive numbers on the x-axis. The horizontal line marks the mean of the intensity ratio in the presence of ETD151: methylated GlcCer at a molar ratio of 1:10, minus one standard deviation (-1σ). Asterisks indicate residues for which peaks are absent in the free and bound states of ETD151. In ETD151 sequence, residues with the most dramatic decrease in intensity due to significant exchange broadening are reported in cyan (below the threshold) or in blue (missing residues at ETD151: PC-methylated GlcCer LUV, 1:10 ratio). The secondary structure elements are displayed above the sequence, with black arrows indicating the three β-strands (β1, β2 and β3), and a black rectangle for the α-helix, connected by three loops (L1, L2, and L3). (C) 3D structure of ETD151 showing the most affected amino acids by the addition of PC: methylated GlcCer LUVs (intensity below the threshold defined in figure 3B). Residues with the most dramatic decrease in intensity due to significant exchange broadening are reported in cyan (below the threshold) or in blue (missing residues at ETD151: PC-methylated GlcCer LUV 1:10 ratio).

Figure 4.

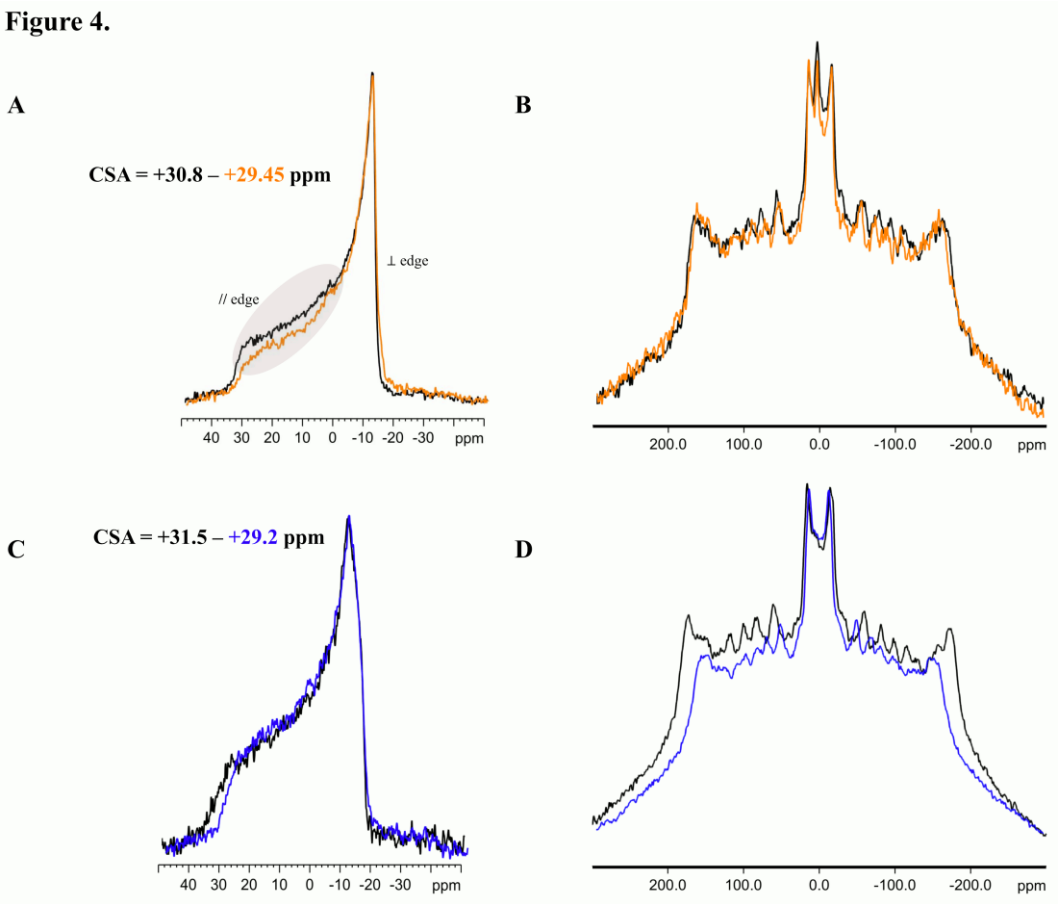

Figure 4. Solid state-NMR study of the effect of ETD151 presence on the dynamics of GlcCer-containing PC-based vesicles at a peptide/lipid ratio 1:20.

(A) Static ^{31}P spectra and (B) static ^{2}H spectra of nonmethylated GlcCer-containing vesicles in the absence (black) or presence (orange) of ETD151. // edge and ⊥ edge indicate the downfield edge and

perpendicular edge, respectively. (C) Static ^{31}P spectra and (D) static ^{2}H spectra of methylated GlcCer-containing vesicles in the absence (black) or presence (blue) of ETD151. Chemical shift anisotropy (CSA) values are indicated in ppm.

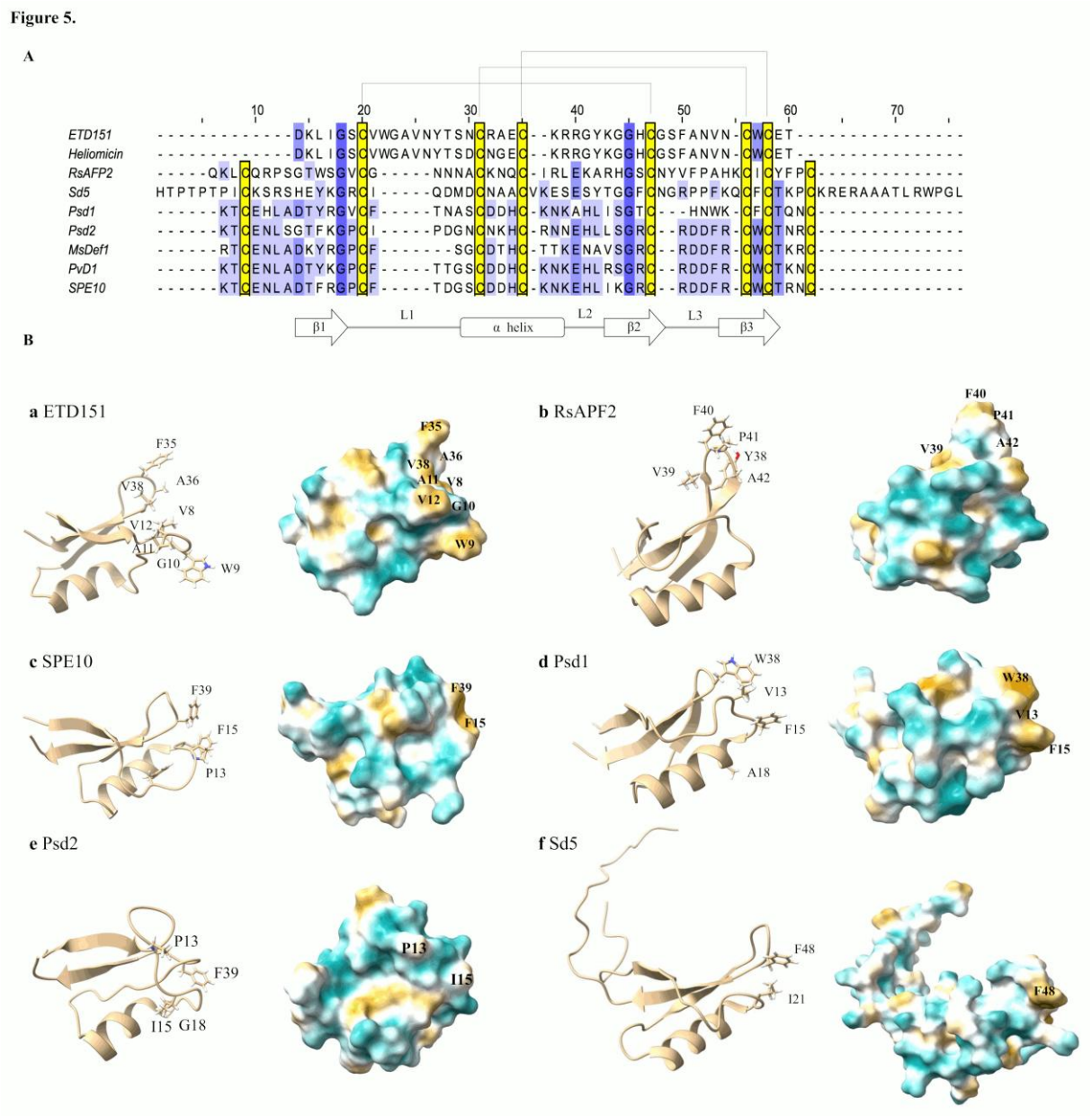

Figure 5. Sequences, 3D structures and hydrophobic surface properties of some antifungal defensins.

(A) Sequence alignment for a selected list of antifungal defensins. Cysteines are shown in yellow while conserved residues are highlighted in blue. (Top) Black brackets represent disulfide bridges between corresponding cysteine residues. (Bottom) The secondary structure elements are displayed above the sequence, with black arrows indicating the three β-strands (β1, β2 and β3), and a black rectangle for the α-helix, connected by three loops (L1, L2, and L3). (B) Structures of some of the discussed antifungal

defensins and their hydrophobic surface properties. Hydrophobic and hydrophilic potential areas are displayed in yellow and blue, respectively. Residues that are discussed are shown in 3D structures and surfaces. (B-a) ETD151 (PDB code: 1P00); (B-b) RsAFP2 (PDB code: 2n2r); (B-c) SPE10 (PDB code: 3psm); (B-d) Psd1 (PDB code: 1jkz); (B-e) Psd2 (PDB code: 6nom); and (B-f) Sd5 (PDB code: 2ksk).

Supporting information for:

How ETD151 defensin targets specifically methylated glucosylceramides to inhibit fungal growth

Ons Kharrat[a,b], Françoise Paquet[a], Rouba Nasreddine[c], Jean-Baptiste Madinier[a], Reine Nehmé[c], Vincent Aucagne[a], Philippe Bulet[d, e], Dror Warschawski[f], Céline Landon[a]*

[a] Centre for Molecular Biophysics, CNRS, Orléans, France; [b] University of Orléans, France; [c] Institute of Organic and Analytical Chemistry, University of Orléans, CNRS, Orléans, France; [d] Institute for Advanced Biosciences, University of Grenoble Alpes, Grenoble, France; [e] Plateform BioPark Archamps, Archamps, France; [f] Laboratory of Biomolecules, Paris, France;

Contact information:

*** Corresponding author:** Céline Landon, celine.landon@cnrs-orleans.fr

ITC control experiments

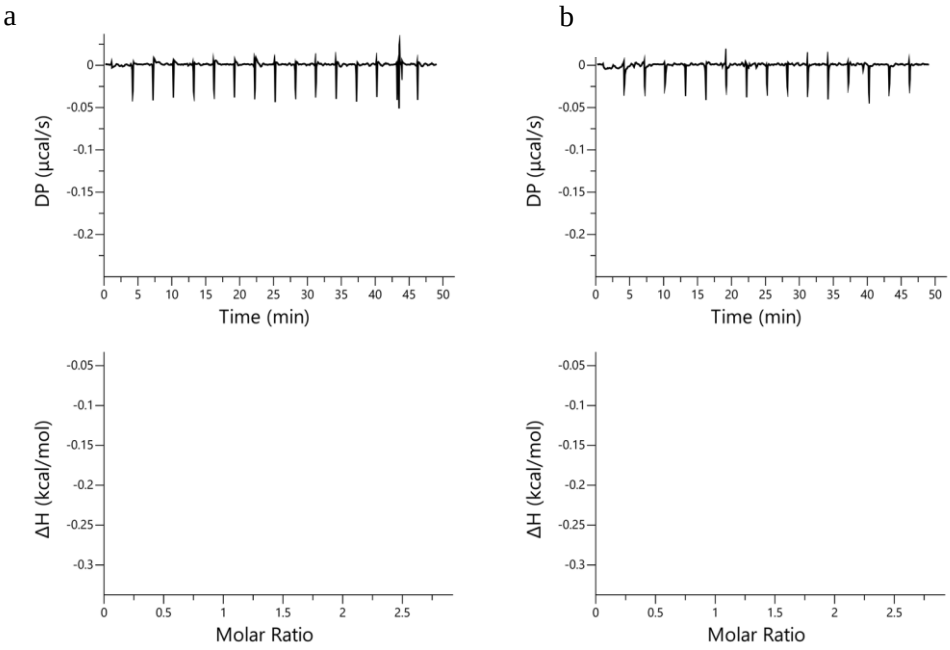

Figure S1: Blank titrations by injecting LUVs into buffer. (a) PC-nonmethylated GlcCer LUVs and (b) PC- methylated GlcCer LUVs into phosphate buffer 10 mM, pH 5.8 (buffer A). Experiments were carried out in the same conditions as other experiments presented in the article.

Table S1: Thermodynamic parameters for ETD151 binding methylated GlcCer-containing membranes by ITC.

	N (sites)	ΔG (kcal/mol)	ΔH (kcal/mol)	−TΔS (kcal/mol)
PC-methylated GlcCer LUVs	0.93 ± 0.1	-5.45	-0.42 ± 0.13	-5.03

Solution NMR experiments of ETD151 in the free state

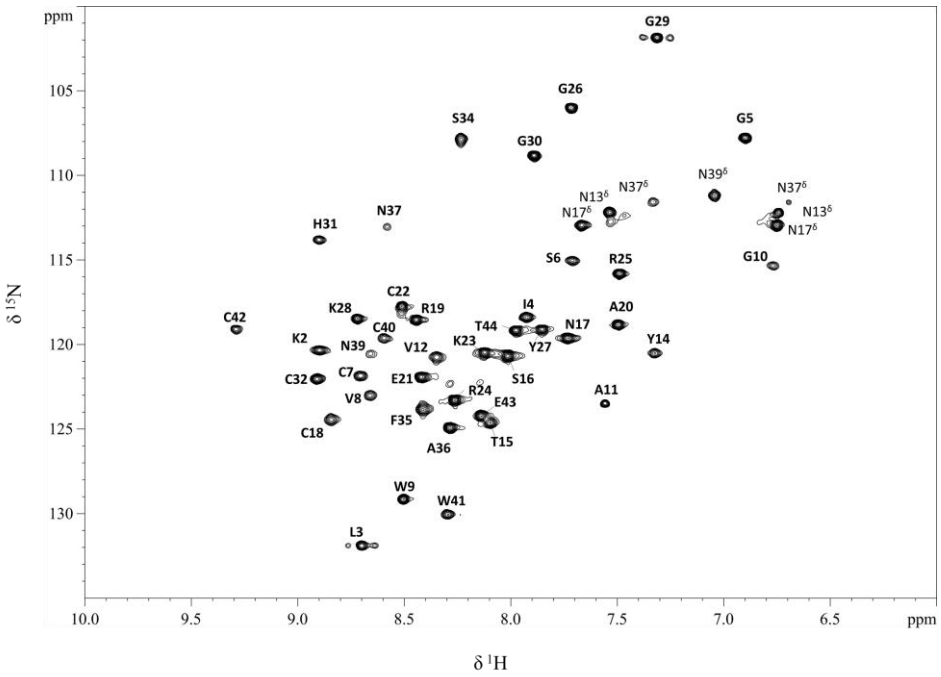

Figure S2: 2D ^{1}H-^{15}N SOFAST-HMQC of ^{15}N-ETD151 in free state at 50 µM as the final concentration in 10 mM phosphate buffer at pH 5.8 (buffer A).

Solution NMR experiments: ^{15}N-ETD151 with different compositions of LUVs

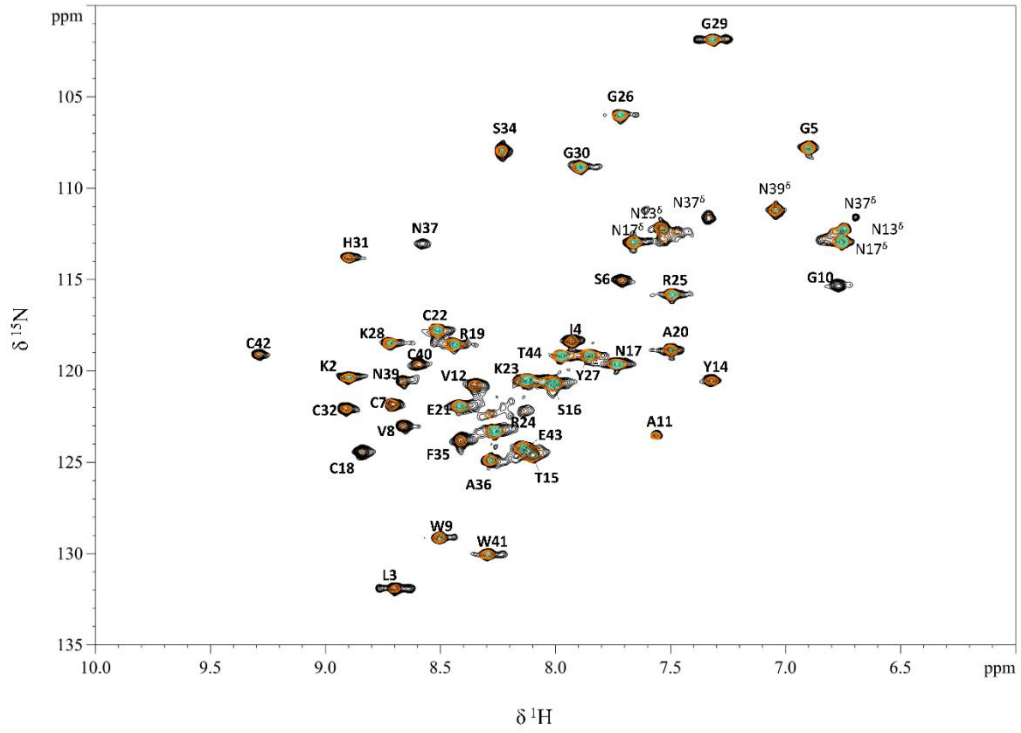

Figure S3: 2D ^{1}H-^{15}N SOFAST-HMQC of ^{15}N-ETD151 (50 µM) in the presence of 5 mM PC-based LUVs (black), 5 mM PC-nonmethylated GlcCer LUVs (orange) and 5 mM PC-methylated GlcCer LUVs (cyan) in buffer A at 298 K.

ss-NMR and spectral moment analysis

Table S2: ^{2}H second spectral moment (M_2) values obtained from Magic angle spinning (MAS) ^{2}H SS-NMR experiments were carried out using a 10 kHz spinning frequency. ^{2}H spectral moment analysis was performed using MestRenova software V6.0 (Mestrelab Research, Santiago de Compostela, Spain).

	^{2}H MAS (10 kHz)	
	M_2 (10^9 s^{-2})	
Samples	No ETD151	**With ETD151**
PC: nonmethylated GlcCer	3.15	**3.1**
PC: methylated GlcCer	3.5	**3.0**

Relaxation experiments of ^{15}N-ETD151 in the free state

Internal dynamics of ETD151 in the free state were studied using NMR relaxation experiments. Longitudinal relaxation rate (R1) values showed little perturbation along the sequence as expected for a compact peptide with three disulfide bridges (Figure S4a). Transverse relaxation rate (R2) values showed large deviations up to 5 times the mean value (6.5 s^{-1}) for I4, T15, C18, S34, F35, N37, N39 and C40 residues suggesting the presence of efficient exchange processes on the µs~ms timescale (Figure S4b). Such motions were only confirmed for I4, S34, F35, N37, N39 and C40 using NMR relaxation dispersion experiments (CPMG). These residues are mapped in Figure S4e. The CPMG curves were fitted with an intermediate-slow exchange between two states A and B, with k_{ex} = (3500 ± 500) s^{-1}, a minor population P_B of 5%, and a kinetic rate constant k_{AB} = (190 ± 75) s^{-1}. The CPMG fitting curves of S34, F35, N37, and N39 were presented in sup data Figure 5d. Small variations of heteronuclear nuclear Overhauser effect (^{1}H-^{15}N NOE) (0.65 - 0.82) observed along the sequence reflect the absence of internal motions on the ps~ns timescale with large amplitude (Figure S4c).

a

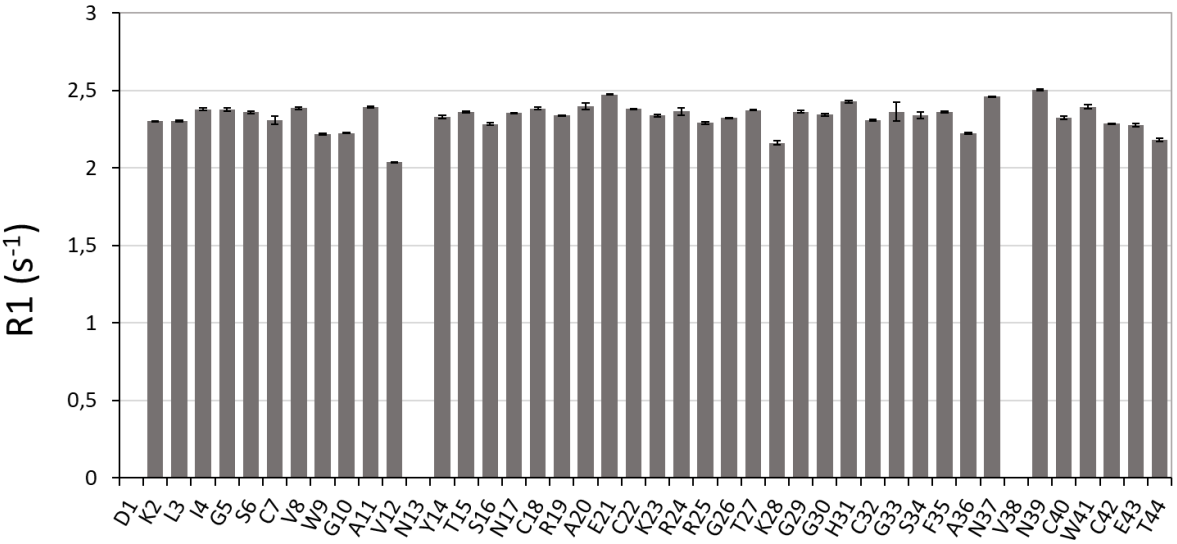
R1 (s-1)
3
2,5
2
1,5
1
0,5
0
D1 K2 L3 I4 G5 S6 C7 V8 W9 G10 A11 V12 N13 Y14 T15 S16 N17 C18 R19 A20 E21 C22 K23 R24 R25 G26 T27 K28 G29 G30 H31 C32 G33 S34 F35 A36 N37 V38 N39 C40 W41 C42 E43 T44

b

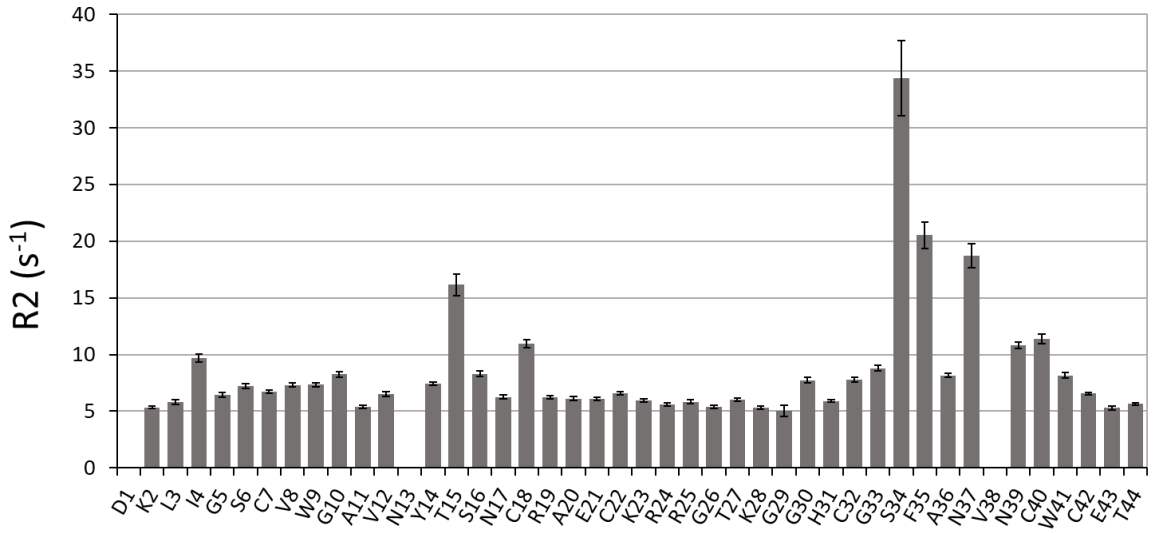
R2 (s-1)
40
35
30
25
20
15
10
5
0
D1 K2 L3 I4 G5 S6 C7 V8 W9 G10 A11 V12 N13 Y14 T15 S16 N17 C18 R19 A20 E21 C22 K23 R24 R25 G26 T27 K28 G29 G30 H31 C32 G33 S34 F35 A36 N37 V38 N39 C40 W41 C42 E43 T44

c

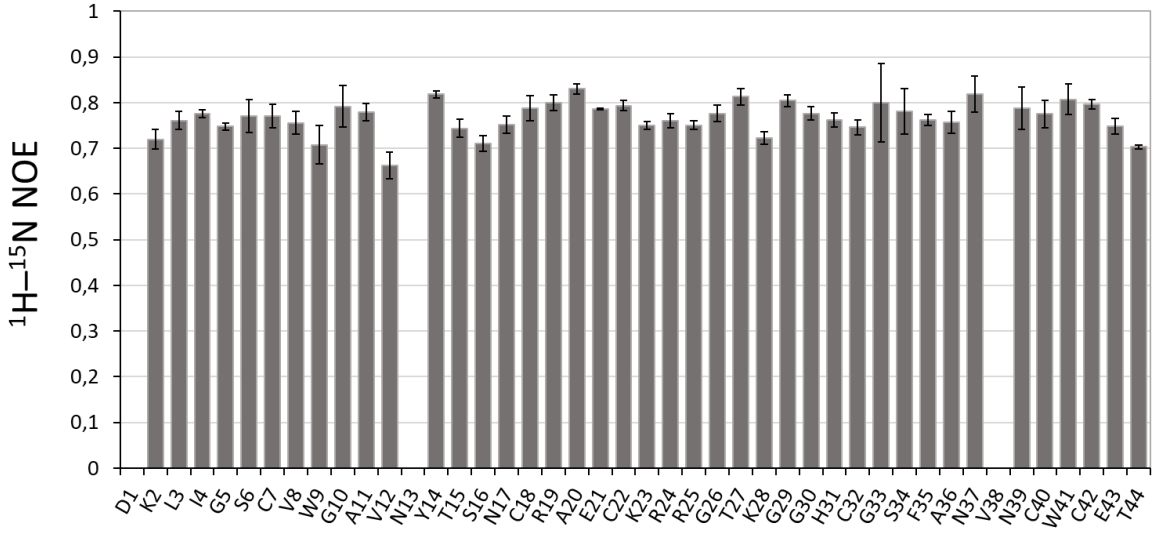
1H–15N NOE
1
0,9
0,8
0,7
0,6
0,5
0,4
0,3
0,2
0,1
0
D1 K2 L3 I4 G5 S6 C7 V8 W9 G10 A11 V12 N13 Y14 T15 S16 N17 C18 R19 A20 E21 C22 K23 R24 R25 G26 T27 K28 G29 G30 H31 C32 G33 S34 F35 A36 N37 V38 N39 C40 W41 C42 E43 T44

d

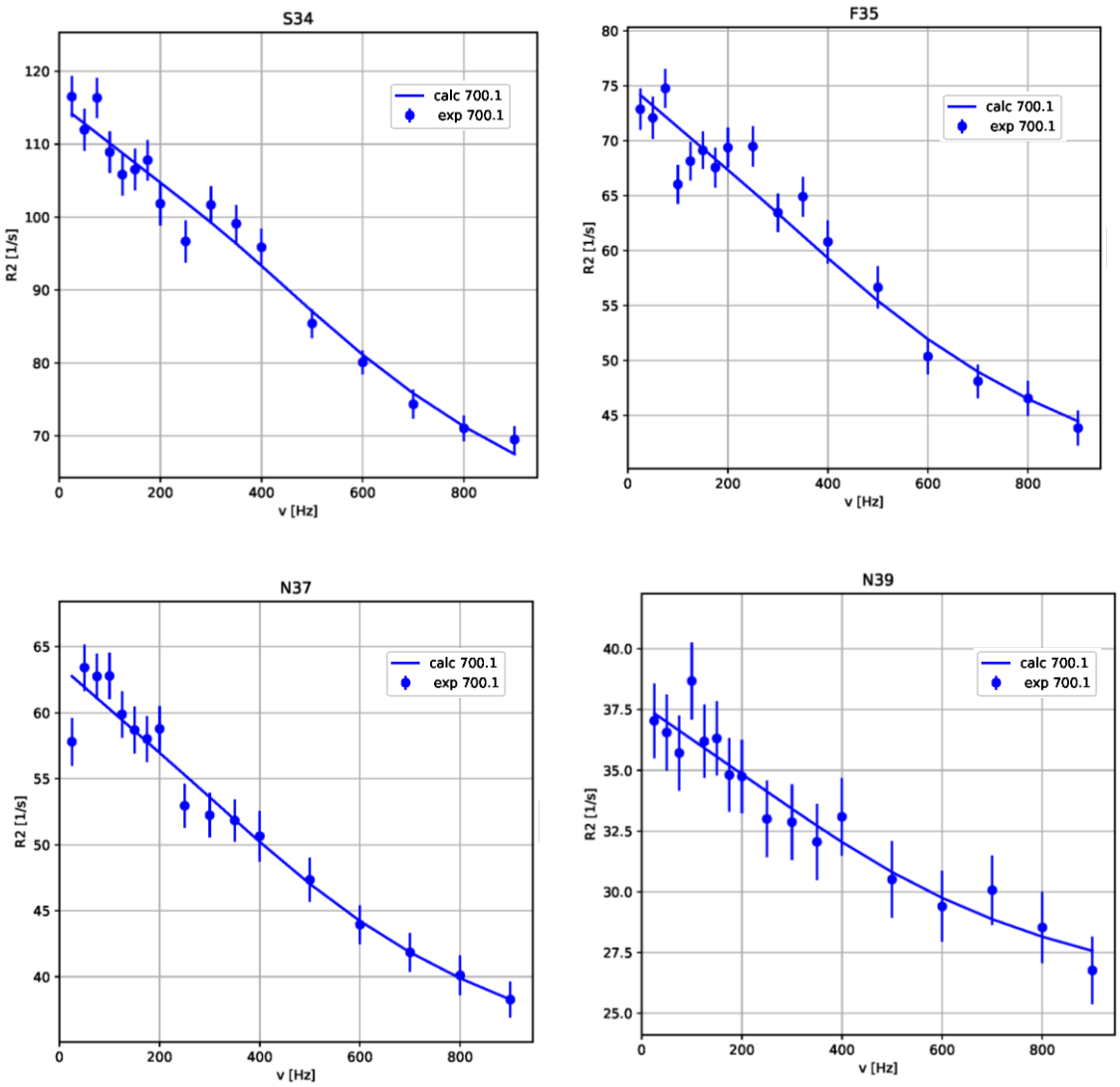
S34
F35
N37
N39
calc 700.1
exp 700.1
R2 [1/s]
v [Hz]

e

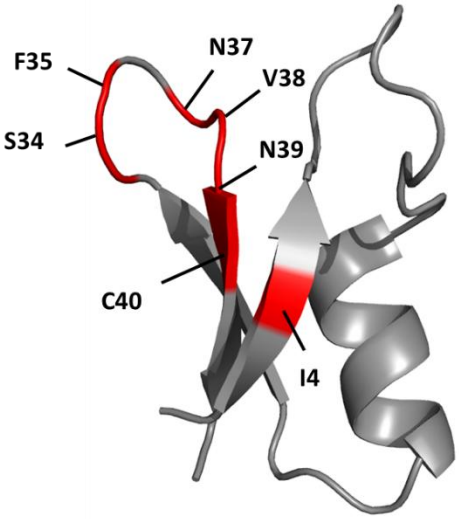
F35
N37
V38
S34
N39
C40
I4

Figure S4: ^{15}N-^{1}H backbone relaxation measurements for ETD151 free in solution. (a) R1, (b) R2, and (c) ^{1}H-^{15}N heteronuclear NOE plotted as a function of the residue name and number for ETD151. Values of R1 and R2 were obtained from the fit as a single exponential decay of the time dependence of the relaxation data measured. The error bars indicate the fitting error. (d) Relaxation dispersion curves fitted using the ShereKhan web application, for S34, F35, N37 and N39 of the ETD151 in the free state. Data were fitted to a global two-state exchange process based on the Carver–Richards model for intermediate-slow exchange. (e) Ribbon representation of ETD151 highlighting the seven residues (I4, S34, F35, N37, V38, N39 and C40) in conformational exchange in red.

Conclusion and Perspectives

ETD151 a-44 amino acids peptide carries three amino acid substitutions as compared with its wild-type counterpart, the insect defensin Heliomicin. ETD151 has been previously reported to have potent broad-spectrum antifungal activity against several unicellular as well as filamentous fungal pathogens. In particular, it has been shown to inhibit the growth of *Botrytis cinerea*, causal agent of an economically important gray mold disease in fruits and vegetables. The study of its mechanism of action (MOA) on *B. cinerea* revealed multifaceted mechanisms, including morphogenic changes, disrupts of 300 proteins belonging to 6 different pathways, and membrane permeabilization. Moreover, ETD151 has been shown to localize mostly in the cell wall/plasma membrane of *B. cinerea* hyphal cells although intracellular entry of this peptide could not be ruled out. Inspired by studies of MOA of plant defensins especially RsAFP2 defensin, it has been suggested that ETD151 peptide may interact with cell wall/plasma membrane component(s) as a first step of its antifungal mechanism. Glucosylceramide (GlcCer), sphingolipids present in fungal membranes and the membrane partner of RsAFP2 and Heliomicin, have been proposed as a putative membrane target for the ETD151 peptide. Prior to my thesis, GlcCer has been shown to be necessary for the antifungal activity of peptide, as demonstrated by the absence of activity on *Saccharomyces cerevisiae* yeast or on Δ*gcs* mutants (e.g., lacking GlcCer in their membranes) of *Candida albicans* and *Pichia pastoris*. However, its direct molecular target(s) in the fungal cells is (are) remains unknown/unconfirmed.

To continue the deciphering of the MOA of ETD151 peptide, this thesis work through multidisciplinary approaches has enabled us to identify GlcCer as the membrane target of ETD151 peptide and to get insights at molecular and atomic level about how this antifungal peptide interacts with this target.

As a first step, using high performance thin layer chromatography, GlcCer have been extracted from the mycelia of *B. cinerea* and two species of this sphingolipid have been identified by mass spectrometry with the structures d19:2/h16:1 and d19:2/h16:0. This work is the first in which the glycosphingolipids of *B. cinerea* have been structurally characterized, increasing our knowledge of the membrane composition of this pathogenic fungus. Although these identified GlcCer share the conserved sphingoid base (9-methyl-4,8 sphingadienine) present in fungi, they possess a C16 chain fatty acid as opposed to a C18 chain found in the majority of other fungal species. Performing further analyses on membrane lipid extracts of *B. cinerea* to extend the identification to other membrane lipids of *B. cinerea* would add considerable value to the data already obtained. In fact, the literature in this field is still very scarce.

Direct interaction of ETD151 with the isolated GlcCer has been demonstrated through microscale thermophoresis (MST) using the fluorescently monolabeled-ETD151 (Atto647-ETD151) and *B. cinerea* GlcCer-containing phosphatidylcholine (PC) liposomes. This analysis for the first time allowed the determination of strong binding affinity with the K_d value of 0.5 ± 0.3 μM. Several plant defensins have

been reported to target GlcCer, including RsAFP2, psd1, and Psd2, however, no K_d values are available for defensin-GlcCer binding. This result therefore can be a reference for further studies using MST assay to test defensin-liposome interaction. In addition, the direct binding of ETD151 with fungal GlcCer has been confirmed through liposome binding assays. Overall, these data suggest that the affinity of ETD151 for the cell wall/plasma membrane of *B. cinerea* is at least partly due to GlcCer binding. Evaluation of a Δ*gcs* mutant of *B. cinerea* would fully support this point.

To fight against phytopathogenic fungi which mainly target crops, antifungal defensins from plants and insects have been proposed as promising candidates as alternatives to chemical fungicides in the fields. The phytosanitary application of defensins have been reported by two approaches: the development of transgenic plants highly expressed defensins to reduce plant disease due to fungi [1, 2], or, the use directly of defensins as fungicides to kill or inhibit fungal growth by targeting specifically fungal component(s). GlcCer is considered as a potential target for developing antifungal with innovative MOAs. Indeed, numerous studies elucidating the role of GlcCer as growth and virulence determinant in fungi, in addition to the differences in GlcCer structures between fungi, plants and mammals. Understanding therefore how a defensin target GlcCer is crucial to enhance the value of its application. Unfortunately, little is known about this interaction between the two partners, which seems to differ from one defensin to another.

As a second step, studies of the interaction at the molecular/atomic level between ETD151 and GlcCer-containing liposomes have been conducted to highlight key elements about this interaction, such as the essential sites for the peptide. For this part of work, a commercial fungal GlcCer (d19:2/h16:0) with the same chemical structure as one of the identified GlcCer from *B. cinerea,* has been used. Because the C9-methyl in the spingoid base is a feature characteristic for fungal GlcCer, a GlcCer lacking this methyl has been used in parallel to investigate the role of this methyl in the molecular interaction. Collectively MST and isothermal titration calorimetry (ITC) shows that ETD151 preferentially binds to PC-liposomes with methylated rather than unmethylated GlcCer. The area of ETD151 that would monopolize this binding has been identified by solution Nuclear Magnetic Resonance (NMR), which includes the two adjacent hydrophobic loops. Based on our NMR relaxation data of ETD151 in free state, conformational and/or dynamic peptide changes are not excluded as a part of the binding mechanism. Indeed, defensins psd1 and Sd5 showed changes in their dynamics and structural conformational adaptation when recognizing GlcCer-containing membrane models [3, 4]. During the thesis, NMR relaxation studies of ^{15}N-ETD151 in the presence of GlcCer-containing liposomes were initiated but unfortunately failed. Further optimization of these experiments will be necessary to obtain valid results. Moreover, our NMR data did not rule out the modification of the oligomerization state of ETD151 (formation of dimer or oligomer) when interacting with GlcCer-containing membrane. The ability of lipid-binding defensins to oligomerize is being increasingly recognized as a critical feature underlying their antimicrobial activities. In plants, the activity of certain defensins depends on the

engagement of specific membrane components, which trigger the formation of defensin-phospholipid oligomers (example of NaD1 and NsD7 defensins) [5, 6]. Finally, solid-state NMR showed that ETD151 specifically inserted into and fluidifies phosphatidylcholine (PC) lipid vesicles containing methylated GlcCer. The major role revealed for C9-methyl in the ETD151-GlcCer interaction provides evidence for the selectivity of ETD151 towards methylated fungal GlcCer, which is important for the selectivity of the activity spectrum. Although all these data have been obtained on the ETD151-GlcCer binding process, the exact ETD151 binding sites and the part of GlcCer involved in the interaction are still not identified. Note that these precisions are not known for any GlcCer-targeting defensin in a membrane environment. Structure resolution of the ETD151-GlcCer complex by crystallography and/or cryoEM experiments is planned and could provide additional structural information.

Overall, this structural and biochemical characterization of ETD151-GlcCer can serve as a basis for testing ETD151 mutants or fragment-derived GlcCer peptides, for selecting molecules with the highest affinity in vitro, and for assessing their activity on fungal cells. Moreover, the fact that in the literature there are no affinity studies with K_d estimation, testing other GlcCer-defensins using MST and ITC assays provides structure-GlcCer binding data. This data will be used to create a library of mutant and/or reduced-size peptides (< 5 kDa) and verify the conservation of antifungal activity compared with the native ETD151 peptide. These candidates can be screened *in vitro, in planta* on various phytopathogenic fungi, including *B. cinerea*, and in mice infected with human pathogenic fungi.

Identifying a partner crucial to the molecule's/peptide's activity is an essential step in understanding its mode of action, and thus in defining the molecule's potency. In this thesis work, the efficacy of ETD151 has been proposed to correlate with the presence of GlcCer on microorganisms' membranes. Insect defensins from the Heliomicin family - including ETD151 - are generally stated to display antifungal activities and to be devoid of antibacterial activity. Most bacteria cells naturally lack glycosphingolipid in their membranes.

As a third step, we investigated whether the presence of GlcCer in microbial membranes can modulate the peptide effect. *Novosphingonium capsulatum* is among the rare bacteria that possess glycosphingolipids (GSL). ETD151 exhibits a weak bacteriostatic effect against *N. capsulatum* with slightly membrane permeabilization. The fluorescence-labeled ETD151 (Atto647-ETD151) was used to reveal the targeting location of bacteria. Using confocal microscopy, ETD151 has been shown to localize mostly in the cell wall/plasma membrane of *N. capsulatum*, where GSL are located. This indicates the dependence of this peptide for its antimicrobial activity on the presence of glycosphingolipid in the microbial cell wall/plasma membrane.

This link between the target-binding step and ETD151 activity could extend the potential of this peptide to other human pathologies. Indeed, dysregulated glucosylceramide metabolism has been reported as a hallmark of several diseases such as lysosomal storage disorders (LSDs), Gaucher disease, and certain

types of cancer (e.g. breast, colon, prostate, melanoma, leukemia). In cancer cells, elevated levels of GlcCer can affect tumor progression, metastasis and chemotherapeutic drug resistance. This accumulation of GlcCer in some cancer has been reported in multi-drug resistant (MDR) cancer cells [1, 2]. These diverse contributions of GlcCer in some cancers underscore its potential as a therapeutic target. Lately, the biological application of some GlcCer-associated plant defensins as potential anticancer agents are deliberated. It has been suggested that Psd1 could be a promising prototype for human lung anti-metastatic melanoma therapy [9]. Recently, MsDef1 has been demonstrated to sensitizer MDR cancer cells to Doxorubicin chemotherapy, enhancing chemotherapy response [10]. PvD1 modulates the membrane composition of breast cancer-derived exosomes (exosome-mediated anticancer action of PvD1) [11]. However, more research is needed to fully elucidate the mechanisms involved and to develop effective therapies targeting glucosylceramide metabolism in cancer. These data encourage to test the activity of ETD151 against some cancer cells with elevated GlcCer level.

As a take-home message, getting insights about the MOA of ETD151 and other GlcCer-targeting defensins as potential antimicrobial and anticancer agents may open a new prospect in medicine, human health, and agriculture. Furthermore, molecules directly targeting glucosylceramides have been reported to offer a low risk of resistance [12]. The potential of defensins like ETD151 needs to be more exploited to show off their strengths, starting with a better understanding of their molecular mechanisms of action.

References

[1] N. Banzet, M.-P. Latorse, P. Bulet, E. François, C. Derpierre, et M. Dubald, « Expression of insect cystein-rich antifungal peptides in transgenic tobacco enhances resistance to a fungal disease », *Plant Science*, vol. 162, nº 6, Art. nº 6, juin 2002, doi: 10.1016/S0168-9452(02)00053-5.

[2] A. Lacerda, É. A. R. Vasconcelos, P. B. Pelegrini, et M. F. Grossi-de-Sa, « Antifungal defensins and their role in plant defense », *Front. Microbiol.*, vol. 5, 2014, doi: 10.3389/fmicb.2014.00116.

[3] L. Neves de Medeiros *et al.*, « Backbone dynamics of the antifungal Psd1 pea defensin and its correlation with membrane interaction by NMR spectroscopy », *Biochimica et Biophysica Acta (BBA) - Biomembranes*, vol. 1798, nº 2, p. 105-113, févr. 2010, doi: 10.1016/j.bbamem.2009.07.013.

[4] V. S. de Paula, G. Razzera, E. Barreto-Bergter, F. C. L. Almeida, et A. P. Valente, « Portrayal of Complex Dynamic Properties of Sugarcane Defensin 5 by NMR: Multiple Motions Associated with Membrane Interaction », *Structure*, vol. 19, nº 1, p. 26-36, janv. 2011, doi: 10.1016/j.str.2010.11.011.

[5] M. Järvå *et al.*, « X-ray structure of a carpet-like antimicrobial defensin–phospholipid membrane disruption complex », *Nat Commun*, vol. 9, nº 1, Art. nº 1, mai 2018, doi: 10.1038/s41467-018-04434-y.

[6] M. J. A. Hein, M. Kvansakul, F. T. Lay, T. K. Phan, et M. D. Hulett, « Defensin-lipid interactions in membrane targeting: mechanisms of action and opportunities for the development of antimicrobial and anticancer therapeutics », *Biochem Soc Trans*, vol. 50, nº 1, p. 423-437, févr. 2022, doi: 10.1042/BST20200884.

[7] Y. Y. Liu, T. Y. Han, A. E. Giuliano, et M. C. Cabot, « Expression of glucosylceramide synthase, converting ceramide to glucosylceramide, confers adriamycin resistance in human breast cancer cells », *J Biol Chem*, vol. 274, nº 2, p. 1140-1146, janv. 1999, doi: 10.1074/jbc.274.2.1140.

[8] H. Huang *et al.*, « LC-MS based sphingolipidomic study on A549 human lung adenocarcinoma cell line and its taxol-resistant strain », *BMC Cancer*, vol. 18, nº 1, p. 799, août 2018, doi: 10.1186/s12885-018-4714-x.
[9] V. S. G. do Amaral *et al.*, « Pisum sativum Defensin 1 Eradicates Mouse Metastatic Lung Nodules from B16F10 Melanoma Cells », *Int J Mol Sci*, vol. 21, nº 8, p. 2662, avr. 2020, doi: 10.3390/ijms21082662.
[10] R. Pandurangi, A. Karwa, U. S. Sagaram, K. Henzler-Wildman, et D. Shah, « Medicago Sativa Defensin1 as a tumor sensitizer for improving chemotherapy: translation from anti-fungal agent to a potential anti-cancer agent », *Front Oncol*, vol. 13, p. 1141755, 2023, doi: 10.3389/fonc.2023.1141755.
[11] J. Skalska *et al.*, « Plant defensin PvD1 modulates the membrane composition of breast tumour-derived exosomes », *Nanoscale*, vol. 11, nº 48, p. 23366-23381, déc. 2019, doi: 10.1039/C9NR07843F.
[12] R. Rollin Pinheiro, « Sphingolipids as targets for treatment of fungal infections | Future Medicinal Chemistry ». Consulté le: 24 janvier 2022. [En ligne]. Disponible sur: https://www.future-science.com/doi/10.4155/fmc-2016-0053

Part II.

AvBD103b a promising antibacterial trans-defensin

Chapter 4: Introduction

Table of contents

I. Antibioresistance concern

1. Bacterial infections and antibiotics

Based on the characteristics of their cell wall, bacteria are classified as Gram-positive or Gram-negative. The two classes of bacteria differ in their susceptibilities to antibiotics. Clinically, Gram-negative bacteria differ from Gram-positive bacteria, by the tendency to produce an endotoxin causing tissue destruction. Bacterial infections can be transmitted to humans through contact (e.g. Streptococcus, Salmonella), air (e.g. Tuberculosis, legionella), water, food, or living vectors (e.g. Lyme disease, Shigella) [1]. Antibiotics are small molecules that can inhibit the growth of bacteria (bacteriostatic activity) or kill bacterial pathogens (bactericidal activity).

The first antibiotic, salvarsan, was deployed in 1910. In just over 100 years, antibiotics have radically changed modern medicine and extended the average lifespan by 23 years. The discovery of penicillin in 1928 marked the beginning of the golden age of natural antibiotic discovery, which reached its peak in the mid-1950s. Since then, there has been a discovery void and development of antibiotics and the evolution of drug resistance in many human pathogens have led to the current resistance crisis [2]. In 1943, Selman Waksman discovered streptomycin, the first effective treatment for tuberculosis, marking a decisive step forward in the fight against infectious diseases. Shortly afterwards, other major classes of antibiotics were discovered: tetracyclines (1945), chloramphenicol (1947), and erythromycin (1952). The discovery of vancomycin in 1953 led to the development of a powerful treatment for resistant Gram-positive infections, notably Staphylococcus aureus. The development of cephalosporins in 1964 offered a broad-spectrum alternative to penicillin. In the 1970s, carbapenems emerged as powerful antibiotics of last resort against multi-resistant bacteria. Although important discoveries have been made since then, such as linezolid in 2000, the pace of new antibiotic development has slowed considerably in recent decades, contributing to the current antibiotic resistance crisis as bacteria evolve to resist these once miraculous drugs (Figure 1).

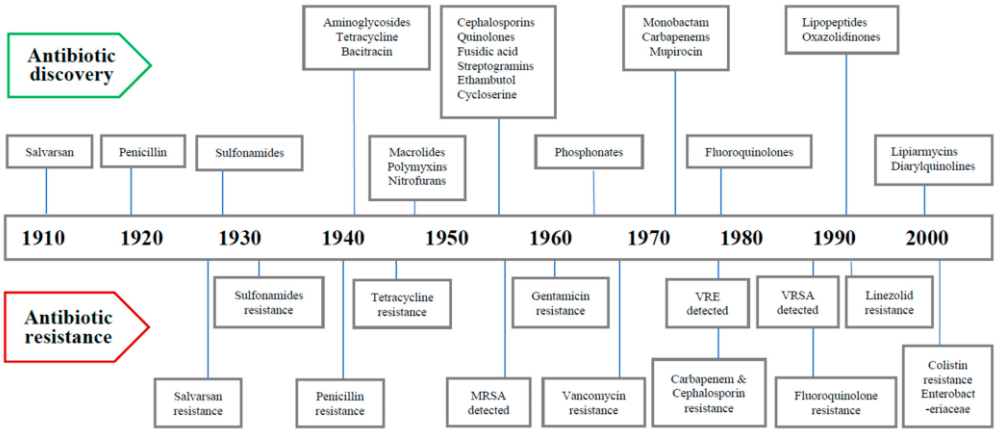

Figure 1: Timeline of discovery of major antibiotics and antibiotic resistance (adapted from ref [3])

2. Drug-resistance in bacteria and lack of new antibiotics

The worldwide increase in antibiotic resistance has become one of the most important global health challenges of the 21st century. Antibiotic resistance is a major threat, as it reduces the effectiveness of common antibiotics against widespread bacterial infections. The misuse and abusive use of antibiotics in medicine, agriculture, and animal husbandry has accelerated the development of resistance in many bacterial species. This phenomenon occurs when bacteria develop mechanisms to evade the effects of antibiotics, giving raise to multi-drug resistant (MDR) bacteria. As a result, infections caused by MDR bacteria are increasingly difficult to treat, leading to prolonged illness, higher medical costs, and higher mortality rates. Globally, infections caused by antibacterial-resistant (ABR) pathogens represent a significant burden of disease. In 2019, an estimated 1.27 million deaths has been attributed to antibiotic-resistant bacteria and 5 million associated deaths (WHO) [4]. Unfortunately, according to the WHO, this figure is set to rise considerably unless urgent action is taken. Moreover, in low- and middle-income countries, where healthcare infrastructure may be lacking, the burden of antibiotic resistance is especially high, exacerbating existing health inequalities.

Pathogens such as *Escherichia coli*, *Staphylococcus aureus* and *Mycobacterium tuberculosis* have developed multi-drug resistance, complicating treatment options. The median rates reported in 76 countries of 42% for third-generation cephalosporin-resistant *E. coli* and 35% for methicillin-resistant *S. aureus* are cause for great concern. As for urinary tract infections caused by *E. coli*, one in five cases showed reduced sensitivity to standard antibiotics such as ampicillin, cotrimoxazole and fluoroquinolones in 2020 [3]. *Klebsiella pneumoniae*, a common intestinal bacterium, also showed high levels of resistance to essential antibiotics. Rising levels of resistance can lead to increased use of drugs of last resort such as carbapenems, for which resistance is in turn observed in many regions (carbapenem-resistant bacteria are classified in the critical group in WHO list).

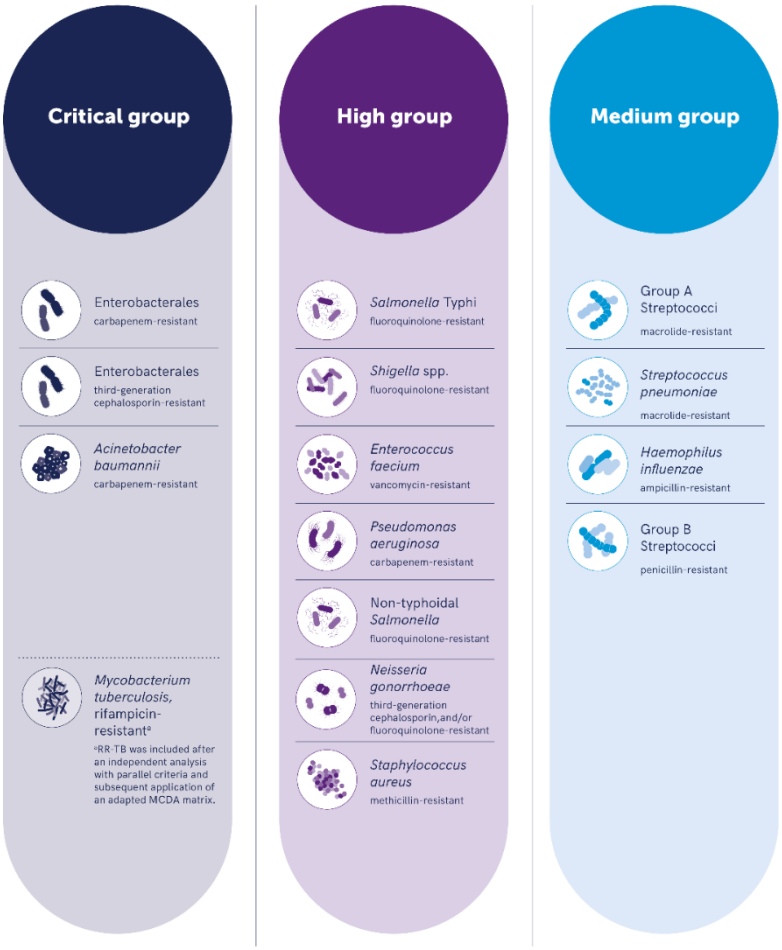

Figure 2: WHO Bacterial Priority Pathogens List, 2024 update (adapted from ref [5])

As the effectiveness of these last-resort drugs is compromised, the risk of untreatable infections increases. Projections by the Organization for Economic Cooperation and Development (OECD) indicate that resistance to last-resort antibiotics is set to double by 2035, compared with 2005 levels, underscoring the urgent need for rigorous antimicrobial stewardship practices and improved surveillance coverage worldwide. Also, emphasizing the need for the development of new antibiotics, alternative treatments, and stronger regulatory measures to reduce antibiotic misuse.

However, the pace of new drug discovery has lagged far behind the rapid emergence of resistance, raising fears that the world may soon face a post-antibiotic era where even common infections could once again become life-threatening. Combating antibiotic resistance requires a multi-faceted approach, including public awareness, research into new therapies, global surveillance, and strict policies to reduce antibiotic misuse in all sectors.

The ineffectiveness of current available antibiotics against MDR combined with the lack of new antibiotics for 50 years, make an alarming situation in both human and veterinary medicine. One of the solutions to tackle this emergence and the spread of antimicrobial resistance is the discovery of new

antibacterial drugs. Antimicrobial peptides (AMPs) are one of the promising avenues of research for alternatives to so-called conventional antibiotics, which lead to the rapid acquisition of resistance.

II. Alternatives to traditional antibiotics

Faced with the growing crisis of drug resistance and the fact that there are few antibiotics available to treat MDR bacteria, scientists are painstakingly exploring new alternatives to traditional antibiotics to treat bacterial infections. Traditional antibacterial agents are small organic molecules with a molecular weight of less than 1,000 Da that act directly to kill bacteria or inhibit their growth. They are referred as "Antibiotics". Non-traditional agents gather anything that is different from these direct-acting small organic compounds, such as bacteriophages, antibodies, peptides, antivirulence agents, biofilms disruptor, microbiome modifying agents, or immunomodulators [6].

According to the WHO, 97 antibacterial drugs are in clinical development, including 57 antibiotics (59%) and 40 non-traditional antibacterials (41%) [7]. Of these, 32 antibiotics and 30 non-traditional antibacterial agents target WHO priority bacterial pathogens (BPPs). Of the 32 traditional antibiotics under development against BPPs, 18 are expected to have some activity against at least one critical priority pathogen, and 12 meet at least one of the four WHO criteria for innovation, namely a new target (new molecular binding site), a new mode of action, a new class (scaffold) and no (known) cross-resistance to existing antibiotics.

1. Agents in clinical development

Thirty promising non-traditional antibacterial agents are under clinical development and are classified into six categories (Figure 3): (i) bacteriophages and phage-derived enzymes (44%), (ii) antibodies (23%), (iii) anti- virulence agents (10%), (iv) miscellaneous agents (13%), (v) immunomodulating agents (7%), and (vi) microbiome modulating agents (3%). Some characteristics of the two main categories of agents in clinical development are presented below.

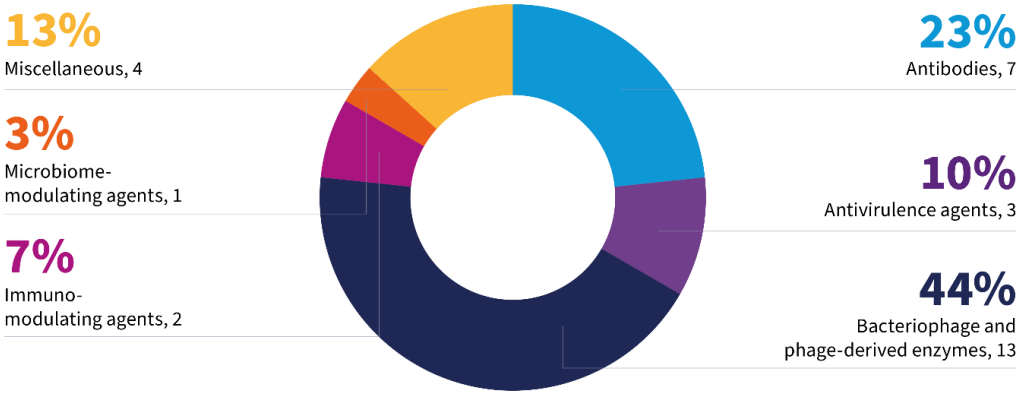

Note: Agents with activity against C. difficile, drug-resistant TB and H. pylori are not included in these figures.

Figure 3: Non-traditional antibacterial agents in the clinical pipeline (adapted from ref [7])

Bacteriophages and phage-derived enzymes

Promising alternatives include phages capable of directly lysing pathogenic bacterial populations (Figure 4) and/or phages designed as nanodelivery vehicles. Because of their particular properties, such as low intrinsic toxicity, lack of antibiotic resistance, and simple availability, phages are excellent substitutes for antibiotics. In addition, advances in genetic engineering make it possible to modify phages to increase their efficacy and stability, making phage therapy an area of growing interest. However, there are real obstacles to the practical implementation of phage therapy in the clinic, including a likely immunological response, effective formulations and a limited host range [8]. At least four bacteriophages for the inhalation treatment of chronic *P. aeruginosa* lung infection in cystic fibrosis patients are currently in phase 1 and 2 clinical trials, such as AP-PA02 (NCT04596319) and YPT-01 (NCT04684641).

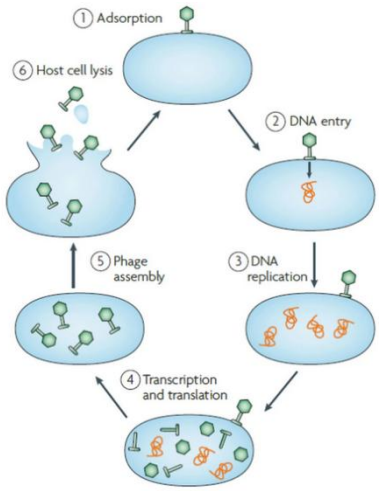

Figure 4: The phage replication cycle (adapted from ref [8]). Lytic phages' mode of action starts with attachment to the membrane (adsorption phase) of one specific bacterial species. The genetic material

of the phage is then injected into the bacterium, where it is reproduced by bacterial enzymes. The bacteria will also generate the lipids and proteins needed to create capsids. After the components have assembled to create virions, the bacterium will lyse and release a new phage population, which will initiate a new lytic development cycle.

Antibodies

Antibodies work by binding to and inactivating a pathogen, its virulence factors, or its toxin(s). Because of their relatively low risk and ease of technical feasibility, they are widely regarded as one of the alternative approaches most likely to have a major clinical impact. Tosatoxumab (registration code NCT03816956) and Suvratoxumab (NCT05331885), intravenous monoclonal antibodies (mAb) against *S. aureus*, are currently in phase 3 clinical trials.

Unfortunately, despite recently approved antibiotics and the diversity of clinical pipelines, this is still not enough to meet the challenge of the increasing emergence and spread of antimicrobial resistance. Consequently, the discovery of new therapies, including antimicrobial peptides (AMPs), is the focus of preclinical development.

2. Agents in preclinical development

A large number and wide variety of products (total number = 224) are in preclinical development. Although the majority are traditional agents, there are 93 non-traditional products representing 38.1% of the preclinical pipeline, the largest groups being direct-acting AMPs followed by bacteriophages (Figure 5). As promising alternatives, the number of AMPs compounds in preclinical trials has risen from 10% of total products in 2021 (30 AMPs out of 292 compounds) to 13.5% in 2023 (34 AMPs out of 244 compounds) [7], [9].

Product type	2023 Number	2023 %
Small molecule – direct acting	115	47.1
Small molecule – indirect acting[a]	23	9.4
Peptide – direct acting	33	13.5
Peptide – indirect acting[a]	1	0.4
Large molecule – direct acting[a]	17	7.0
Large molecule – indirect acting[a]	3	1.2
Bacteriophage / bacteriophage products[a]	29	11.9
Biologic (antibody or other biotherapeutic)[a]	7	2.9
Nucleic acid-based product[a]	1	0.4
Immunomodulators[a]	9	3.7
Microbiome-modifying agents[a]	3	1.2
Decolonization agents	3	1.2
Total	**244**	**100.0**

[a] Non-traditional agent.

Figure 5: Antibacterial agents under preclinical development, WHO 2023 (adapted from ref [7]).

III. Antimicrobial peptides (AMPs)

AMPs, also known as host defense peptides (HDPs), are naturally occurring peptides produced by many organisms, including mammals, amphibians, microorganisms and insects, as a primary defense mechanism against invading pathogens [10], [11]. They possess multifunctional properties, including antiviral, antifungal, antibacterial, anticancer and immunomodulatory activities [12]. In addition, several AMPs have been shown to inhibit or eradicate biofilms [13]. **AMPs can be classified according to their biosynthetic origin, ribosomal or non-ribosomal. The peptides in preclinical development reported by WHO in figure 5 are mainly non-ribosomal peptides (NRPs) and ribosomally synthesized and post-translationally modified peptides (RiPPs)** [15, 16] (figure 6).

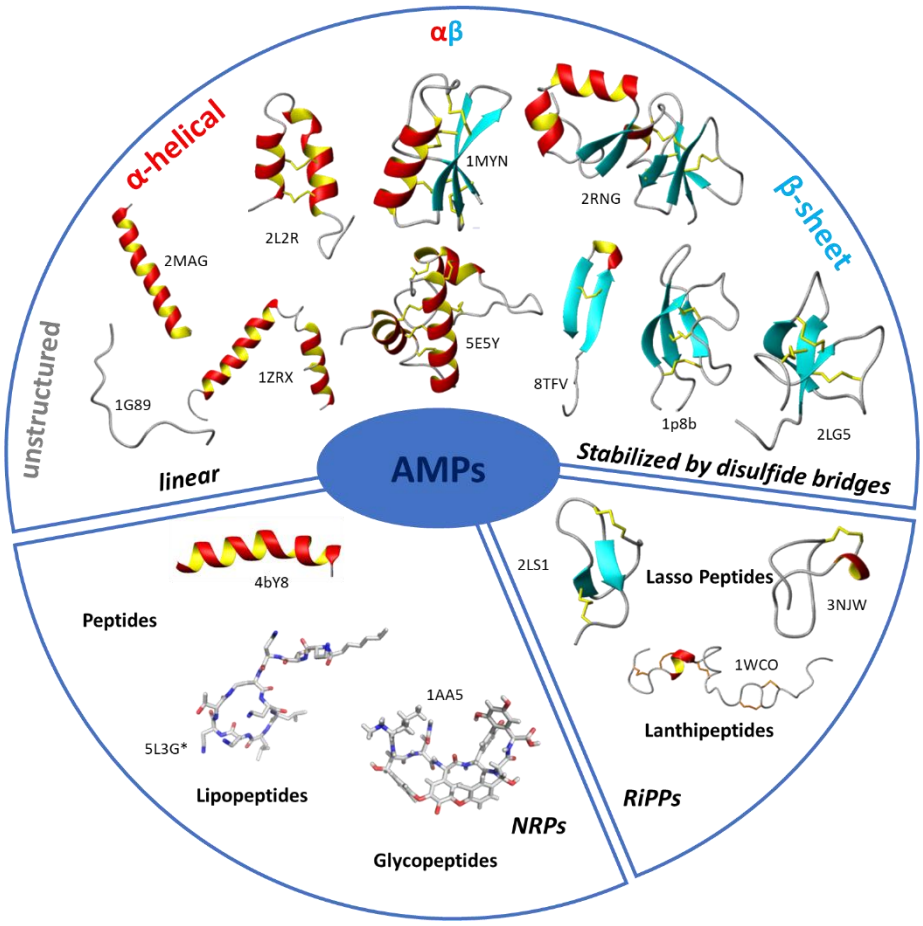

Figure 6: Origin of AMPs biosynthesis and structural diversity (adapted from MuFoPAM). NRPs stand for "non-ribosomal peptides" and RiPPs for "ribosomally synthesized and post-translationally modified peptides".

1. Non-ribosomal peptides (NRPs)

NRPs are usually produced by microorganisms like bacteria and fungi which possess large multifunctional enzymes, the so-called non-ribosomal peptide synthetases (NRPSs). NRPs distinguish

from ribosomally synthetized peptides by containing non-proteinogenic amino acids (e.g., D-isomers, carboxylic acids, N-methylated amino acids), incorporation of heterocyclic rings and fatty acids, and post NRPS-synthetic modifications like glycosylation. Many of NRPs have long been studied for their antibacterial activity and currently used as pharmaceuticals [15] (Figure 7). **Penicillin** belongs to this family was the first one approved by FDA in 1963. **Gramicidin** is the first antibiotic used to treat wound infections. It is a mixture of hydrophobic linear polypeptides composed of 15 amino acids (Gramicidin A, B and C) and naturally produced by Gram-positive *Brevibacillus brevis* commonly found in soil [16]. Gramicidin D was approved by the FDA in 1955 as a constituent in Neosporin® [17], a triple antibiotic ointment for treating bacterial conjunctivitis **Polymyxin E**, also known as colistin, is a cyclic lipopeptide composed of 10 amino acids, including 6 lysines, and a fatty acid (6-methyl octanoic acid). This antibacterial agent, with potent activity against several Gram- bacteria such as Pseudomonas aeruginosa, Klebsiella pneumoniae and Acinetobacter spp., was approved by the FDA in 1962. **Vancomycin** is a cyclic lipoglycopeptide approved by the FDA as an oral solution in 1983. Its derivatives, oritavancin, dalbavancin and telavancin are more bactericidal than their prototype, vancomycin, and are effective against vancomycin-resistant bacteria. Oritavancin and dalbavancin were approved by the FDA in 2014, and telavancin in 2009, for the treatment of complicated skin and skin structure infections due to Gram-positive pathogens. **Daptomycin** is a cyclic lipopeptide consisting of 13 residues produced naturally by *Steptomyces roseosporus* [18]. Daptomycin and its derivative Cubicin were approved in 2003 by the FDA to treat or prevent infectious diseases due to drug-resistant Gram-positive bacteria [19].

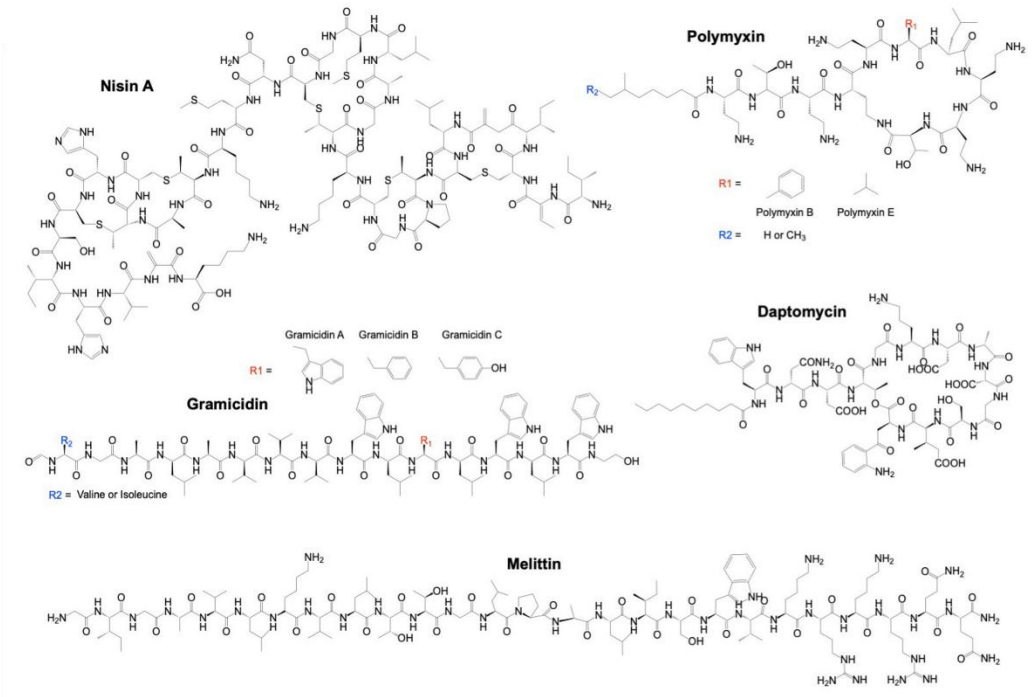

Figure 7: Chemical structures of AMPs have been approved for clinical use. They include α-helical, i.e., gramicidin and melittin, and cyclic AMPs, i.e., nisin A, polymyxin and daptomycin (adapted from ref [15])

2. Ribosomally synthetized antimicrobial peptides

They can be classified into two categories: **unmodified ribosomally synthesized peptides** and **ribosomally synthesized and post-translationally modified peptides (RiPPs)**.

a. RiPPs

For RiPPS, following ribosomal synthesis of the linear precursor peptide, the peptide's N-terminal leader region is recognized by modifying enzymes, while the peptide's C-terminal core region receives post-translational modifications (PTMs). These PTMs increase the structural diversity of RiPPs, which exploit only the 20 proteinogenic amino acids. Because of their antibacterial properties, many RiPPs are considered as potential alternatives to traditional antibiotics. Among these RiPPs, **Nisin** is a polycyclic peptide with 34 amino acids (Figure 7) produced by Gram-positive bacteria such as *Lactococcus* and *Streptococcus* species. Nisin has an activity against drug-resistant bacterial strains such as methicillin-resistant *S. aureus* (MRSA) and *Clostridium difficile* [3]. It has been used for several decades in the food industry in over 50 countries to combat food-borne pathogens [20]. Nisin is currently the only purified bacteriocin approved by the DFA in 1988 for use as a food preservative [21].

b. Unmodified ribosomally synthesized antimicrobial peptides

Unmodified ribosomally synthesized antimicrobial peptides are short peptides (< 50 amino acids), cationic (average net charge +3) and hydrophobic (content average 42%) [22].

Structural diversity

The term “unmodified ribosomally synthesized antimicrobial peptides” covers a wide diversity of primary, secondary and 3D structures. These AMPs can be classified as follows (i) Unstructured peptides with sequences rich in proline, arginine or histidine residues, (ii) linear α-helical peptides, which are generally amphipathic (e,g., cathelicidins), (iii) β-sheet peptides stabilized by disulfide bridges, which are usually cationic with hydrophobic patches dispersed on the surface (e.g.,protegrin) , and (iv) αβ peptides that contain both α-helical and β-sheet structures (e.g., insect defensins) (Figure 6). Note that this classification is far too be perfect. For example, linear α-helical peptides adopt their 3D structure in membrane-mimicking media only [23]. Otherwise, they are unstructured. On the contrary, so-called “unstructured peptides” can adopt a highly structured form when in contact with their biological partner (example the insect-derived proline-rich Oncocin onc112).

Development as antibacterial agents

Many peptides belonging to this group of AMPs are now under investigation for preclinical or clinical trials. For examples (i) **linear peptides** such as melittin, LL-37, analog of magainin, derivative of indolicidin. Melittin is the main component of *Apis mellifera* bee venom. It is composed of 26 amino

acids and adopts an α-helical conformation when interacting with cell membrane [24]. Melittin has antiviral and antibacterial activity against resistant bacteria [25], as well as anti-inflammatory activity [26]. The FDA approved melittin (Figure 7) to relieve pain and swelling associated with rheumatoid arthritis, tendonitis, bursitis and multiple sclerosis [27]. The human cathelicidin LL-37 exhibit broad spectrum of activity against various Gram-positive and Gram- bacteria including drug-resistant bacterial strains, alone and/or in combination [28]. In addition, this AMP has immunomodulatory properties by which it can reduce the inflammatory response [29]. Currently, LL-37 is under clinical trials phase 2 for topical use to treat leg ulcers [30]. Pexiganan is analog of magainin has failed in phase 3 clinical trials [31]. Omiganan a derivative of indolicin has completed the phase 2 in clinical trials for topical use as antisepsis and to prevent from catheter infection [32].

(ii) Some **β-sheet peptides** such as protegrin analogues; an analog named Murepavadin [33] is currently in clinical trials for the treatment of pneumonia, but another synthetic analog known as Iseganan [34] failed phase 3 clinical trials. (iii) **αβ peptides** are far less explored than the two other classes. A variant of plectasin is the first defensin under clinical development for topical treatment for fungal nail disease [15]. Plectasin is a defensin from *Pseudoplectania nigrella*, a saprophytic ascomycete, shows a potent activity in vitro and in mouse models against Gram +, especially *S. aureus* and *Staphylococcus epidermidis* [35].

3. Mechanisms of action of AMPs

AMPs can be classified into two main categories depending on their MOAs: membrane-active peptides (known also as lytic peptides) and non-membrane permeabilizing peptides (known also as non-lytic) AMPs [36]. The mode of action of membrane-active peptides is based on their immediate membranolytic effect. However, the mode of action of non-permeabilizing peptides relies on other mechanisms, in addition to or in place of their non-extensive ability to disrupt/permeabilize membranes.

In the membrane-active mechanism, AMPs disrupt bacterial cytoplasmic membranes, their primarily target, via non-specific interactions. Before that, AMPs have to pass through the peptidoglycan (PG) layer of Gram-positive bacteria and the outer membrane (OM) which is a complex structure containing lipopolysaccharide (LPS) of Gram- bacteria [37], [38] (Figure 8).

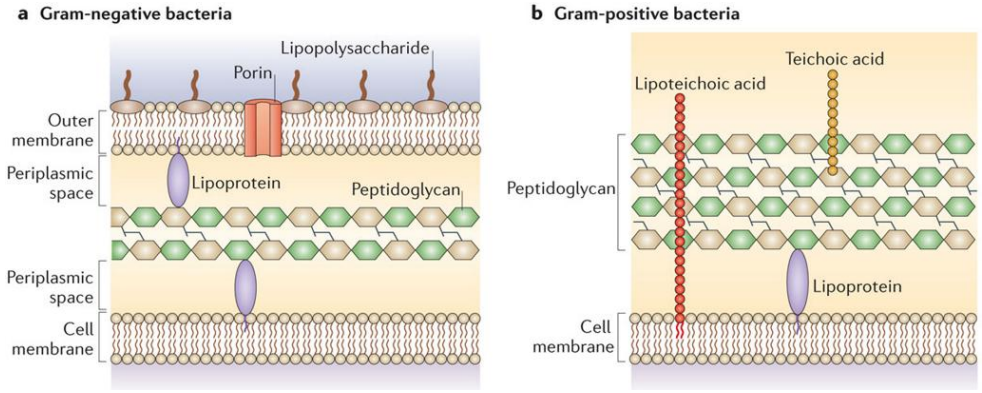

Figure 8: Cell envelope structure of (a) Gram-negative bacteria and (b) Gram-positive bacteria (adapted from ref [39]). Gram-negative bacteria are surrounded by a thin peptidoglycan (PG) cell wall, which itself is surrounded by an outer membrane containing lipopolysaccharide (LPS). Gram-positive bacteria lack an outer membrane but are surrounded by layers of PG many times thicker than is found in the Gram-negatives. Once past the cell wall, positively charged AMPs approach negatively charged phospholipids in the cytoplasmic membrane via electrostatic interaction. Subsequently, the insertion into the phospholipid bilayer, the hydrophobic regions of AMPs are close to the lipid hydrophobic core of the membrane, leading to the formation of pores or micelles. The result is leakage of intracellular contents and cell death. To date, different models of membrane rupture mechanisms have been described, namely the sinking raft, the barrel stave, and the toroidal model (Figure 9).

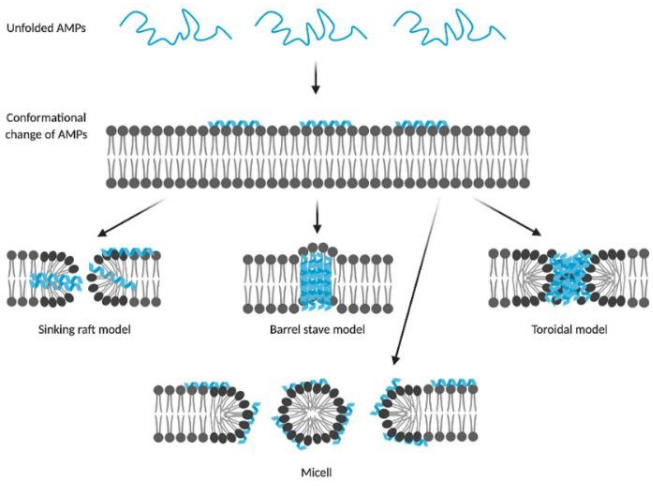

Figure 9: Membrane-active mechanism of AMPs (adapted from ref [15]).

Among FDA-approved AMPs there are membrane-active peptides. **Gramicidin** is a pore forming peptide which forms an ion channel in membranes as a transmembrane dimer, leading to membrane depolarization, osmotic swelling and cell lysis [40]. **Melittin** shows to create large toroidal pores in the plasma membrane of the targeted bacteria [40, 41]. **Colistin** forms pore-like aggregates in the bacterial cell membrane, disrupting membrane integrity, ultimately leading to cell death by lysis [40, 41].

The disruption of microbial membranes has been the most widely described activity for AMPs, probably because the lytic helical peptides have been the most extensively studied. Their rapid activity targeting bacterial membranes makes it energetically unfavorable for bacteria to develop resistance [10]. Unfortunately, these peptides are toxic to mammalian cells causing membrane lysis. Although this drawback has limited their development as potential therapeutic antibacterial agents, it has favored their development as anticancer agents (example of the lytic peptide melittin [45]).

In a non-membrane permeabilizing mechanism, AMPs can cross membranes, reach the cytoplasm and interact with intracellular target components and/or disrupt vital cellular processes. During crossed membranes, AMPs could perturbate the integrity of the cell wall, and/or permeabilize cytoplasmic membrane without causing extensive permeabilization. When reaching the cytoplasm, they can target DNA, RNA, or protein synthesis or inhibit cell division or enzymes [36] (Figure 10).

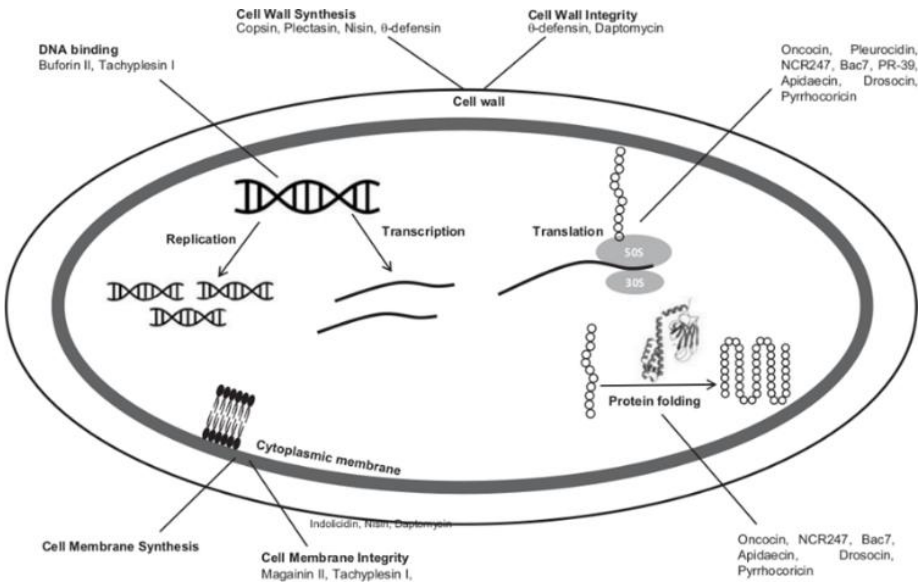

Figure 10: Schematic representation of proposed targets for membrane-active and non-membrane permeabilizing AMPs (adapted from ref [36]).

Nisin inhibits bacterial growth by forming pores in cytoplasmic membrane causing cell lysis and/or interfering cell wall biosynthesis through specific binding with lipid II, a precursor molecule that is essential for bacterial cell wall biosynthesis [23]. **Daptomycin,** which inhibits cell wall synthesis, causes membrane permeabilization and cell division impairment [46]. **Oncocin** inhibits the protein synthesis by binding to chaperone DnaK and inhibits bacterial protein translation at the 70 S ribosome [24, 25]. **Plectasin** defensin inhibits the cell wall synthesis by targeting specifically Lipid II [49]. **Teixobactin**, nonribosomal peptide, inhibits bacterial cell wall synthesis by targeting conserved non-proteinogenic

molecules (Lipid II and III) in the cytoplasmic membrane [50], [51], making the development of bacterial resistance against teixobactin is difficult.

Despite growing interest in AMPs as promising alternatives to antibiotics, since the approval of daptomycin in 2003, no new AMPs have been approved as antibacterials. In addition, peptides with more complex structures than linear peptides are largely unexplored, particularly those with disulfide bridges, including defensins. Current understanding of the modes of action of non-linear AMPs indicates that they act by a more complex mechanism than that of membrane activity. Further work is needed to discover their modes of action, which may be novel and/or multifaceted mechanisms less likely to induce resistance.

IV. Vertebrate defensins

Defensins are a family of vertebrate AMPs involved in host defense against microbial infections [52]. They are found predominantly in cells, particularly granules, and tissues. Vertebrate defensins are synthesized as prepropeptides, which are inactive precursors consisting of short signal peptides, propieces often but not always anionic, and mature peptides. The latter are cationic with β-sheet rich fold, and characterized by the presence of six strictly conserved cysteine residues [53]. The presence of disulfide bonds confers high stability to temperature, pH, and proteolysis [53]. Vertebrate defensins exhibit broad-spectrum antimicrobial activity against Gram-positive and Gram- bacteria, certain fungi and enveloped viruses, as well as immunomodulatory activities and LPS-neutralization [54]. **Vertebrate defensins** are classified intro three subclasses (**α, β, and θ)** depending on the connectivity of the three intramolecular disulfide bridges [52]. The **α**-defensins, which are mammalian specific, β-defensins, which are universal in vertebrates, and **θ**-defensins which have been only discovered in primates. The cysteine-bridging pattern for α-defensins is C1-C6, C2-C4, and C3-C5, whereas for β-defensins it is C1-C5, C2-C4, and C3-C6. θ-defensins form a macrocyclic structure by a head-to-tail ligation of two truncated α-defensins (figure 11).

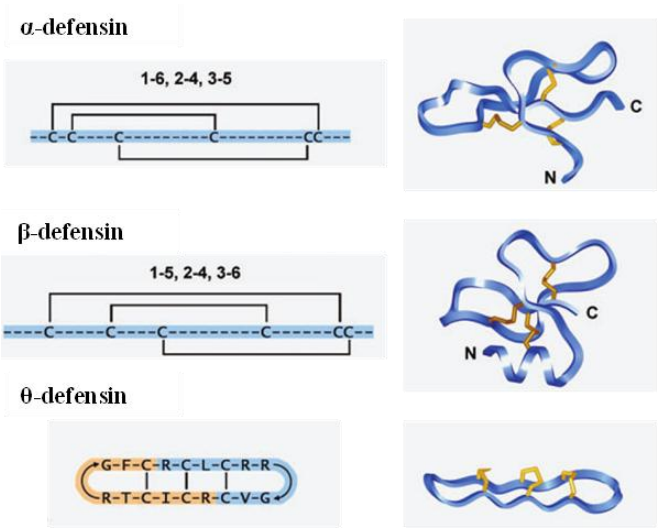

Figure 11: Three families of vertebrate defensins: α, β, and θ-defensins (adapted from ref [53]). Schemes of the three different disulfide bridges connectivity and the three-dimensional structures are of rabbit α-defensin RK-1 (top), human β-defensin-1 (middle) and θ-defensin RTD-1 (bottom).

β-defensins represent the largest family of vertebrate defensins, found in mammals (including Human, mouse, bovine, pig and rat), avian, fish... They are thought to be emerged from an ancestral big defensin gene similar to the one found in cephalochordates, mollusks and arthropods at least 520 million year [10, 11] (Figure 12). Although being not common, multipatterned β-defensins were initially identified in a few reptiles, including lizards, Gila monsters, and Komodo dragons, and suggested to originate from internal genetic duplications [13, 14, 15]. In addition to classical β-defensins, some proteins/peptides have been reported as β-defensin-like or β-defensin-related. They display a non-canonical cysteine spacing and/or do not display the canonical 3 stranded β-sheet that defines the β-defensin fold. For example, pelovaterin from Turtle [60], Crotamin from Snake [61], and DLP1, DLP2 and DLP4 from Platypus [62, 63].

Today, we recognize approximately 30 α-defensins isolated only from mammals including Human, Rhesus monkey, mouse, rabbit and guinea pig. As α-defensins family is not reported in evolutionarily ancient vertebrates such as fish and birds, this family is believed to arise from β-defensins by diversification and duplication of genes (Figure 12) , under positive selection [64]. The α-defensins have retained the antiparallel 3-stranded β-sheet of the β-defensins, but are stabilized by a different disulfide bridge network (C1-C6, C2-C4, and C3-C5) [65]. θ-defensins are believed to have evolved from α-defensins encoded by an α-defensin pseudogene [66].

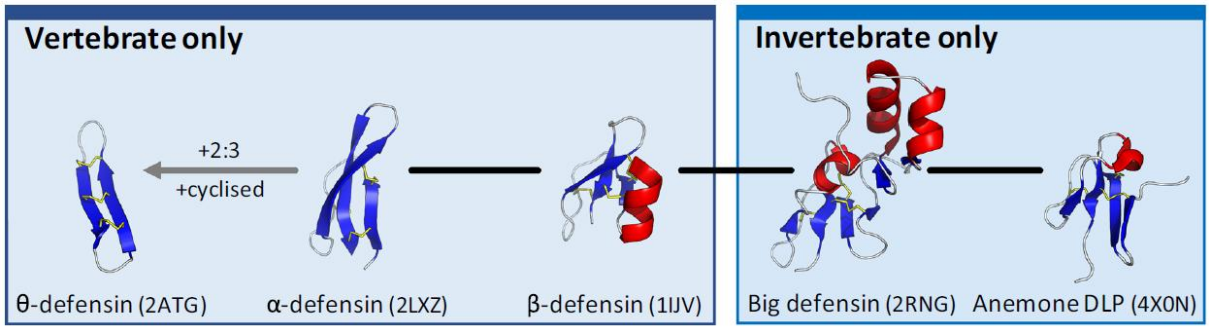

Figure 12: Evolution of the vertebrate defensins (adapted from ref [56]).

V. Avian β-defensins (AvBDs)

In birds, HDPs comprise two main families: cathelicidins and defensins. Avian β-defensins (AvBDs) are small cationic peptides that range from 36 to over 70 amino acids. Most of these AvBDs exhibit antimicrobial activity against various pathogens, including Gram-negative, Gram-positive bacteria, fungi, and viruses as well as immunomodulatory activity [67, 68, 69]. Structurally, AvBDs are defined by a conserved 3 stranded antiparallel β-sheet which is stabilized by 3 highly conserved disulfide bridges (C1-C5, C2-C4, C3-C6 cysteine pairing), typically to the β-defensin family [56]. Generally, an α-helix is also present at the N-terminal region.

In addition to the classic β-defensins, there is a specific group of avian β-defensin related family known as ovodefensins [70]. This group's name alludes to their preferred expression in the oviduct, where they are highly prevalent in the egg white [70]. Structurally, ovodefensins have six cysteines forming a disulfide bond identical to that of β-defensins, however they have a different spacing between the cysteines [71].

There is a lot of information scattered in the literature on AvBDs, but there is no synthetic review. We therefore propose here a report summarizing what is known about the antibacterial activity of AvBDs, the structural modulations around their global β-defensin fold and available information on their antibacterial MoAs. This chapter will form the basis of a review dedicated to avian defensins.

1. Discovery of AvBDs

AvBDs were originally named gallinacins/gallopavins/spheniscins/ostricacins, according to the name of the bird, and associated with uncoordinated numbers across species, prior to a nomenclature update in 2007 [72]. Initially in **1994,** four chicken β-defensins, known as "Gallinacins" (Gal-1, Gal-2, Gal-3, and Gal-1α), were isolated from leukocytes by Harwig and colleagues [73]. Meanwhile, E. W. Evans et al. identified two bactericidal peptides against *S. aureus* and *E. coli*, extracted from heterophilic granules, namely CHP1 and CHP2, known as "chicken heterophilic peptides" [74]. In **2001**, Zhoa and colleagues

reported that Gal-3 is widely expressed in non-myeloid cells, in contrast to Gal-1, 1α, Gal-2, whose expression is restricted to bone marrow cells. In addition, Gal-3 is particularly expressed in the tongue and trachea following infection with *Haemophilus paragallinarum*, the causative agent of infectious coryza, an economically important disease for the poultry industry [75]. Then in **2004**, Lynn and colleagues identified by bioinformatics algorithms 7 gallinacins (named from Gal-4 to Gal-10) [76], whereas, Xiao and coworkers reported a total of 13 different β-defensins (named from Gal-1 to Gal-13) that the chicken genome encodes by genome-wide screening [77]. Afterward, two novel chicken peptides have been identified in silico, named Gal-11 and Gal-12, in **2005** [78]. Finally, with the completion of chicken genome sequencing **in 2007**, a total of 14 genes located on the same chromosome 3 were identified to encode 14 chicken defensins known as "avian β-Defensins" (AvBDs) (AvBD1-14) [72], replacing the term "gallinacins".

As most chicken β-defensins were discovered simultaneously by two research groups, some confusion arose due to differing nomenclatures. For convenience, both the original avian β-defensin nomenclature and the updated standard nomenclature proposed by Lynn et al [72] are mentioned.

In addition to chicken (*Gallus gallus*), AvBDs have been isolated in various tissues of bird including the turkey [74], ostrich [79], and king penguin [80]. From **Turkey,** three β-defensins have been extracted known as THP for Turkey heterophil peptides. Four isolated β-defensins from **Ostrich** (initially named Ostricacins) have been reported. Two β-defensins (initially named Spheniscins) have been isolated from the stomach of the **king penguin** male, AvBD103a (known as Sphe-1) and AvBD103b (known as Sphe-2). These two defensins are highly expressed during the last part of egg incubation, contributing to preserve the food intact in the stomach of the male penguin. Besides these classical β-defensins, three ovodefensins have been identified named gallin 1-3 preferentially expressed in the oviduct with abundant presence in the chicken egg white [70].

2. Multiplicity of AVBD genes in each species

Besides the isolated AvBDs mentioned before, many additional AvBDs sequences have also been predicted in various bird species genome including the duck (*Anas platyrhynque*) [81], Chinese painted quail [82], goose (*Anser Cygnoides*) [83], king pigeon, and zebra finch [84]. Unlike most mammalian β-defensin genes, which consist mainly of two exons, chicken β-defensin genes consist of four exons. Except for AvBD12 and -14, the genes appear to have only two exons.

All the genes encoded for the 14 chicken AvBDs are located in a single cluster on chromosome 3. The availability of bird genome sequences has made it possible to compare the evolutionary history of the AvBDs gene cluster between species that shared a common ancestor around 100 million years ago (figure 13). The AvBDs gene cluster has the particularity of evolving, expanding the repertoire of

AvBDs with a wide variety of biological functions, including antimicrobial activities in the host defense system.

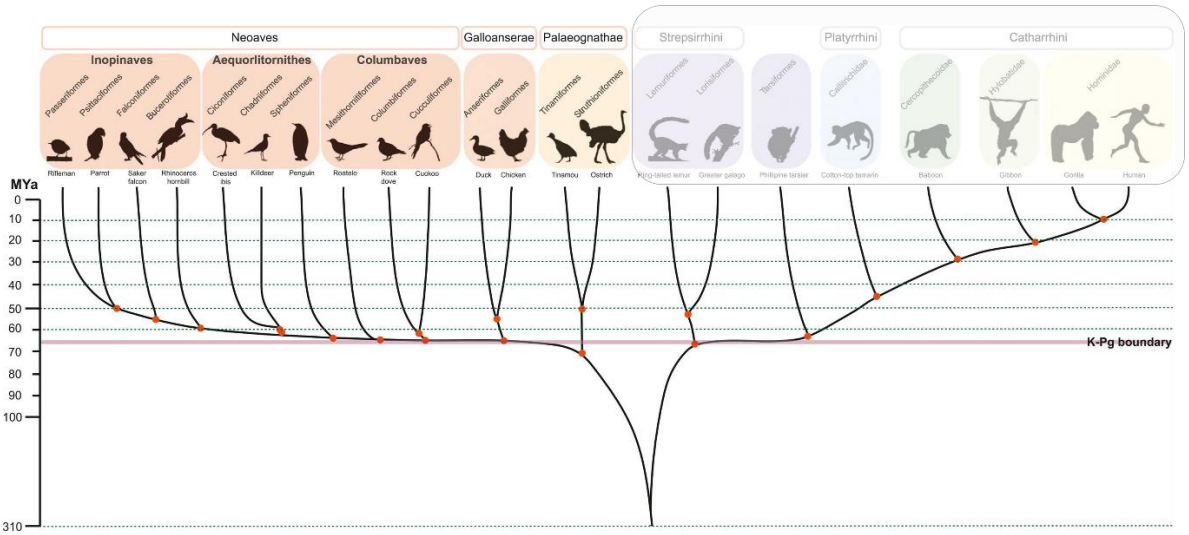

Figure 13: Evolutionary tree of avian and primate evolution (adapted from ref [85]).

Genomic comparison of the AvBDs gene cluster from Japanese quail, Coturnix japonica, with chicken, revealed a cluster of 14 AvBDs. However, the cluster lacks the AvBD3 and -7 loci, while genetic duplication of the orthologous AvBD6 locus gave rise to the CjAvBD101α, -101β and -101θ loci in the CjAvBD cluster after differentiation between Coturnix and Gallus [86]. Analysis of the mallard duck genome revealed the presence of 16 genes encoding β-defensins [87], which is slightly higher than the 14 genes found in chicken. In the zebra finch genome, 10 of the 22 total genes were identified as highly conserved compared with the chicken AvBDs gene cluster. However, the remaining 12 genes are thought to be the result of recent gene duplication events following the Galliformes-Passeriformes split [84].

Phylogenetic analysis of all available AvBDs revealed the existence of some species-specific AvBDs genes. While nine avian β-defensin genes are largely conserved, gene duplication and pseudogenization, e.g., AvBD1, AvBD3, AvBD7, and AvBD14, are possible explanations for the expansion in the defensin gene repertoire in duck and zebra finches. In zebra finches, the AvBD1 gene appears to have duplicated and diversified into three paralogous genes (AvBD123, 124, and 125), despite being preserved in chicken, turkey, goose, quail, and ostrich. The zebra finch genome now contains eight paralogs of the AvBD3 gene and lacks AvBD6 gene, which is present in the chicken, turkey, goose, and mallard duck genomes. Since no orthologs of the AvBD14 gene were discovered in other bird species, it appears to be unique to chickens.

A particular gene in birds is AvBD11, which encodes a unique double-β-defensin (AvBD11) and is present in the genome of every bird (over 300 genomes currently known) [88]. AvBD11 is most likely derived from the fusion of two ancestral genes encoding cell monodomain β-defensins from turtles or

crocodiles [89]. To date, no double-β-defensins have been reported in other vertebrates that birds (mammals, fish, or amphibians), apart from a few multiple β-defensins in reptiles.

Ovodefensins genes do not belong to the AvBD gene cluster, but it has been proposed that ovo- and avian defensins may have diverged from a common ancestor [37].

The co-evolution of defensins with the bacteria that surround the living organism is an intriguing way to gain inspiration for fighting bacterial infections. This evolutionary diversity of defensins in each species is an asset for understanding mechanisms as well as a natural asset for learning strategies to induce little or no bacterial resistance.

3. Biological activities of Avian β-defensins

The increased expression of β-defensins in several tissues in birds, particularly in immune tissues after bacterial infection, strongly suggests that these antimicrobial peptides may play a central role in the host defense of different bird species against infections. For example, Chicken AvBD3 (originally named Gal-3) was found widely expressed in non-myeloid cells, particularly in the tongue and trachea following *Haemophilus paragallinarum* infection [75]. In the Chinese goose (*Anser cygnoides*), four anser_AvBDs (2, 5, 9 and 10) were significantly upregulate in various immune tissues after *Salmonella enteritidis* infection [90]. AvBD7 from *Anas platyrhynchos* was significantly upregulated in the liver in response to duck hepatitis virus (DHV) infection [91]. Based on these observations, the in vitro antimicrobial activity of certain natural AvBDs directly extracted from avian tissues or produced chemically or biologically was evaluated.

a. Antibacterial activity

Some of AvBDs were successfully tested for their antibacterial activity in their native forms, e.g., directly extracted or chemically synthetized with correctly folded. These defensins include **chicken AvBDs AvBD1, -2, -6, -7, -9, and -12 , turkey AvBD1 and -2, ostrich AvBDs AvBD1, -2, -7, and -8, and penguin AvBD103b** [92] [79], [93] [80]. The activity of the mature **double β-defensin AvBD11** with 82 amino acids purified from chicken eggs also is reported [88]. Finally, the antibacterial activity of only one **ovodefensin,** chicken gallin, is investigated [71]. Table 1 summarizes the antibacterial activity of these AvBDs.

Chicken defensins

Most chicken β-defensins are active against a broad spectrum of Gram-positive and Gram-negative bacteria, and sometimes exhibit antifungal activity, usually in the lower micromolar range. However, their efficacy varies according to the pathogen. Chicken AvBD2 (called Gal-2) is slightly less effective against *E. coli* than chicken AvBD1 (originally called CHP1 [74] and Gal-1 [73]), while their activity against *L. monocytogenes* is almost identical [73]. The three chicken AvBD1 (+8), AvBD2 (+4) and AvBD7 (+6) show similar activity against Gram-positive bacterial strains (e.g., *S. aureus*, *B. subtilis*, *L.*

monocytogenes) [92], suggesting that there is no direct correlation between the protein's net charge and its activity against Gram-positive bacteria. AvBD2 is less effective against Gram-negative bacteria, particularly *Enterobacter cloacae*, than AvBD1 and AvBD7 [92]. This lower activity of AvBD2 is probably linked to its less charged N-terminal part than that of AvBD1 and AvBD7 [92]. Interestingly, *in vivo* antimicrobial efficacy was demonstrated for intraperitoneal administration of chicken AvBD7 in a lethal systemic salmonellosis model in mice, reducing the bacterial load in the liver and improving survival rates [94].The correctly folded chicken synthetic defensins AvBD6 and AvBD12 show higher activity against *E. coli* than against *S. Typhimurium* and *P. aeruginosa*, with much reduced activity against *S. aureus* (MIC = 256 µM) under low-salinity, low-nutrient conditions. While both defensins have a similar % hydrophobicity, AvBD6 is more positively charged than AvBD12 (+7 vs. +1 net charge). This difference in charge has an impact on antibacterial activity, revealing that AvBD6 is more potent than AvBD12 against all bacteria tested under similar conditions [95]. The synthetic folded form of chicken AvBD9 (called Gal-6) shows high activity against *C. perfringens* (MIC 1.8 µM), low activity against *S. pyogenes* and *E. coli*, and no activity against *P. aeruginosa*, *S. aureus* and *B. cereus* at the concentration tested [96].

Turkey defensins

Turkey AvBD1 (originally named THP1) has broad activity against Gram-negative bacteria, with the exception of *P. multocida*, and is most effective against *C. jejuni* and *S. typhimurim* (MIC 2 - 4 µg/ml) [74]. However, turkey AvBD2 (THP2) shows bactericidal activity against gram-positive *S. aureus* bacteria, but not against gram-negative *E. coli* [97].

Ostrich defensins

Ostrich defensins display similar effectiveness against bacterial growth as other chicken and turkey β-defensins with MIC values in the same range [76, 90]. The positively charged N-terminal was proposed to explain the strongest activity of ostrich AvBD2 (Osp-2) towards *E. coli* compared to AvBD1 (Osp-1), AvBD7 (Osp-3) and AvBD8 (Osp-4), which have fewer positive residues in this extremity (see sequence in Figure 14). Among the four ostrich defensins, AvBD8 exhibit the weakest activity, with MIC values 10 times higher than those obtained with AvBD1 [76, 90].

King penguin defensins

The synthetic folded version of King penguin β-defensin, AvBD103b (Sphe-2) displays a broad antimicrobial activity against a large panel of microorganisms with MIC values generally between 0.4 - 6 µM against a range of Gram-positive bacteria [80]. However, AvBD103b activity is less potent against Gram-negative bacteria (MIC values between 1.5 - 50 µM) with a very reduced efficacy against *K. pneumoniae* and no activity against *Enterobacter cloacae* and *A. faecalis* up to 100 µM [80].

AvBD103b shows mainly a bactericidal effect against Gram-positive and a bacteriostatic effect against Gram-negative bacteria [80].

Double avian-β-defensins

While all currently available bird genomes contain the gene for a double β-defensin, only one AvBD11 defensin (chicken *Gga*-AvBD11) has been purified to date, and biological data are therefore published. With high cationic net charge (+9), *Gga*-AvBD11 shows high activity (MIC values < 1 µM) against *L. monocytogenes*, *S. enteritidis*, *S. Typhimurium*, and *E. coli*. This antibacterial activity is similar to that of AvBD103b (with a net charge of +10), except against *S. aureus*, where *Gga*-AvBD11 was less effective [88]. Interestingly, both defensins are active against *S. enteritidis* LA5, a strain isolated in the field and responsible for contaminating chicken eggs [88].

Ovodefensins

Unlike classical β-defensins, ovodefensins generally do not have any discernible antibacterial activity, which is the case of proteins isolated from avian egg whites, e.g., duck BPS1 and BPS2 [98] and turkey meleagrin [99]. The only known ovodefensin having antibacterial activity is from chicken gallin, however it seems to have a limited spectrum range. When tested against a number of common Gram-negative and Gram-positive bacteria, chicken gallin only shown efficacy against *E. coli*; unlike *Salmonella*, *S. aureus* and *Listeria monocytogenes*, which were not sensitive to gallin [71]. Therefore, it is believed that ovodefensins have another biological role than antibacterial one.

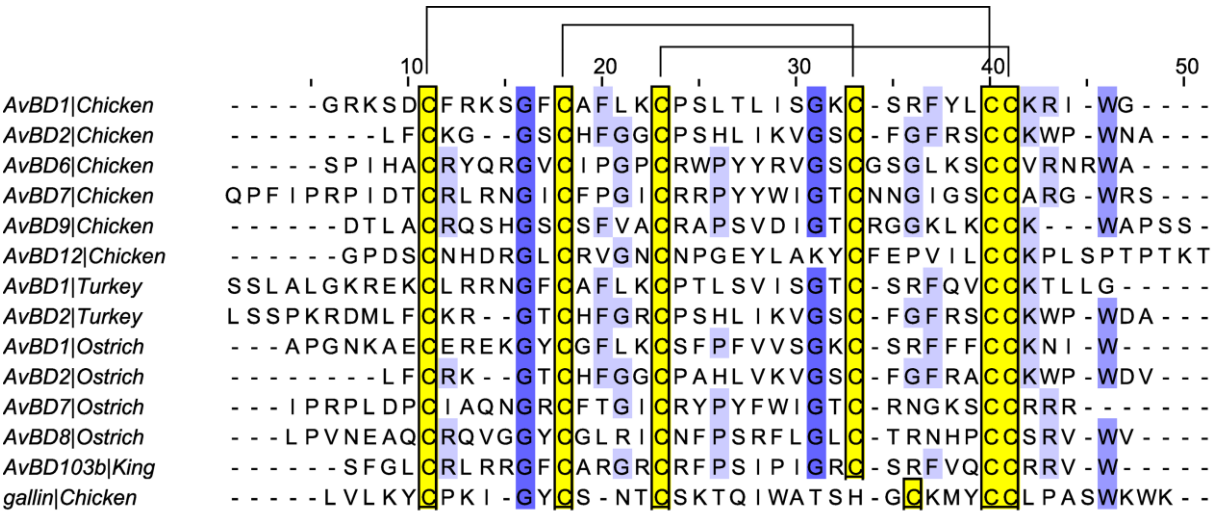

Figure 14: Sequence alignment of the avian β-defensins whose antibacterial activity has been reported (except the double β-defensin).

AvBDs in non-native form

It should be noted that the antibacterial activity of some chemically synthesized avian β-defensins in their linear form, e.g., without the formation of the disulfide bridges, has been reported in the literature.

Two reasons encourage the study of linear forms of avian defensins: i) several mammalian β-defensins have similar antimicrobial activities in their linear/reduced or folded/oxidized forms [100] [45, 46], and ii) If the 3D fold does not influence the activity, peptide synthesis of linear forms simplifies the production process and reduces cost (without oxidative folding).

The four chicken β-defensins AvBD1, AvBD2, AvBD6, and AvBD9 show *in vitro* bactericidal activity against five pathogenic bacteria of economic, public health, and poultry production importance: *E. coli*, *C. jejuni*, *S. enteritidis*, *S. Typhimurium*, and *C. perfringens*. AvBD1 displays the highest bactericidal effects against all bacteria (MIC range: 0.83–1.66 µM), while the other three defensins showed weaker inhibitory activities [103]. Interestingly, the *in ovo* administration of these defensins has been demonstrated to prevent early chick mortality due to bacterial infections [103]. A unique comparative study has evaluated the relative antibacterial activity of the 14 chicken β-defensins (AvBD1-14) linear forms on *E. coli* under the same experimental conditions. All peptides showed strong antibacterial activity at 5 µM against *E. coli*, except for AvBD5, AvBD8, AvBD10 and AvBD12. Among all linear chicken β-defensins, AvBD4 displayed the strongest antibacterial effect, killing 50% of *E. coli* at very low concentration (0.5 µM) [104]. The three predicted mature anser_AvBD1, AvBD3 and AvBD6 peptides, both in N-terminally acetylated synthetic linear forms showed antibacterial activity at 50 and 100 µg/mL against G+ bacteria, e.g., *S. aureus*, *B. subtilis*, *Lactobacillus*, but were only active against *P. aeruginosa* and *P. multocida* on G- bacteria [83]. Finally, note that the antibacterial activity of some predicted GST-tagged β-defensins from other bird species has also been reported, including those from quail [79, 103], and duck [106] [91].

Table 1: Antibacterial activity of the avian β-defensins (AvBDs) extracted from avian species or chemical synthetized with the correct folding. Note that this table is not exhaustive, and the minimal inhibitory concentration (MIC) values are obtained in different experimental conditions (growth media, pH, temperature, salt concentrations…).

Species	Defensins	Gram-positive bacteria (MIC)	Gram-negative bacteria (MIC)	Comments
Chicken	**AvBD1**	*Staphylococcus aureus* [74], *Listeria monocytogenes* [73] *Bacillus subtilis* (0.19 µM), *Bacillus cereus* (0.21 µM), *S. aureus* (0.08 µM), *Staphylococcus haemolyticus* (0.14 µM), *Staphylococcus saprophyticus* (0.16 µM), *L. monocytogenes* (0.26 µM) [92]	*Escherichia coli* (3.5 µM), *Salmonella enteriditis* (3.5 µM), *Salmonella typhimurium* (1.75 µM), *Campylobacter jejuni* (0.43 µM), *Bordetella avium* (3.5 µM), *Mycoplasma gallisepticum* (3.5 µM) [97] *S. enteritidis* (0.17 µM), *S. Typhimurium* (0.15 µM), *Enterobacter cloacae* (0.20 µM), *Klebsella pneumoniae* (0.10 µM), *E. coli* (0.27 µM), *Pseudomonas aeruginosa* (0.27 µM) [92]	-Bactericidal against *E. coli* and *S. aureus* [74] -Activity against *C. albicans* (1.75 µM), no ability to neutralize Infectious Bronchitis Virus (IBV) [97]
	AvBD2	*L. monocytogenes* [73], *S. aureus* (1 µM) [107] *B. subtilis* (0.28 µM), *B. cereus* (0.47 µM), *S. aureus* (0.42 µM), *S. haemolyticus* (0.25 µM), *S. saprophyticus* (0.22 µM), *L. monocytogenes* (0.22 µM) [92]	*E. coli* [73], *S. enteriditis* (1.66 µM), *S. typhimurium* (0.8 µM), *C. jejuni* (0.8 µM), *B. avium* (3.3 µM), *M. gallisepticum* (3.3 µM) [97] *E. coli* (3 ± 2 µM) [107] *S. Enteritidis* (0.80 µM), *S. Typhimurium* (2.39 µM), *E. cloacae* (> 64 µM), *K. pneumoniae* (0.71 µM), *E. coli* (0.72 µM), *P. aeruginosa* (1.86 µM) [92]	-Bactericidal against *E. coli* and *S. aureus*[74] -Ineffective against *C. albicans* at 83 µM [73] -Loss of the antibacterial activity in the presence of proteases [107]
	AvBD7	*S. aureus* (0.5 µM), *L. monocytogenes* (0.7 µM), *Streptococcus salivarius* (0.7 µM) [107] *B. subtilis* (0.21 µM), *B. cereus* (0.20 µM), *S. aureus* (0.11 µM), *S. haemolyticus* (0.21 µM), *S. saprophyticus* (0.16 µM), *L. monocytogenes* (0.31 µM) [92]	*E. coli* (1 µM), *S. Typhimurium* (2.6 µM), *Pseudomonas aeruginosa* (0.7 µM) [107] *S. Enteritidis* (0.16 µM), *S. Typhimurium* (0.21 µM), *E. cloacae* (0.32 µM), *K. pneumoniae* (0.32 µM), *E. coli* (0.28 µM), *P. aeruginosa* (0.33 µM) [92]	-Antibacterial activity is stable even in presence of proteases [107]
	AvBD6	*S. aureus* (54 µM) [95]	*E. coli* (27 µM) [95]	-

	AvBD9	*Clostridium perfringens* (1.8 µM), *Streptococcus pyogenes* (14.5 µM) [96] *Streptococcus bovis* (1.45 µM), *Staphylococcus epidermidis* (1.45 µM), *S. aureus* (1.45 µM) , *Enterococcus faecalis* (1.45 µM), *Micrococcus luteus* (1.45 µM) [108]	*C. jejuni* (14.5 µM), *E. coli* (14.5 µM) [96] *E. coli* (1.45 µM), *P. aeruginosa* (1.45 µM), *S. typhimurium* (1.45 µM), *K. pneumonia* (1.45 µM), *Shigella sonnei* (1.45 µM) [108]	-Antifungal activity against *C. albicans* (1.8 µM) and *S. cerevisiae* (1.8 µM) [96] -Antifungal activity against *C. albicans* (1.45 µM), *Aspergillus flavus* (0.72 µM), *Aspergillus* niger (0.72 µM) [108]
	AvBD-12	-	*E. coli* (52 µM) [95]	-
	AvBD-13	*L. monocytogenes*, *S. pyogenes* [78]	*E. coli*, *S. typhimurium* [78]	-Completely killing *L. monocytogenes* and *S. typhimurium* at 114 µM [78] -Bacteriostatic activity against *E. coli* and *S. pyogenes* at 114 µM [78]
	AvBD11 (Hen egg)	*S. aureus* (0.9 µM), *L. monocytogenes* (0.18 µM) [88]	*S. enteritidis* (0.35 µM), *S. Typhimurium* (0.32 µM), *E. coli* (0.05µM) [88], *S. enterica* (0.31 µM) [109]	-Antiparasitic activity against infectious sporozoites of *Eimeria tenella* [109]
Turkey	**AvBD1**	*S. aureus* [97]	*E. coli* (1.6 µM), *S. enteriditis* (1.6 µM), *S. typhimurium* (0.8 µM), *C. jejuni* (0.8 µM), *B. avium* (1.6 µM), *M. gallisepticum* (1.6 µM) [97]	-Bactericidal against *E. coli* and *S. aureus* [74] -Activity against *C. albicans* (1.6 µM) [97] -No ability to neutralize IBV [97]
	AvBD2	*S. aureus* [74]	-	-Bactericidal against only *S. aureus* [74] -No activity against *E. coli* [74]
Ostrich	**AvBD1**	*S. aureus* [79]	*E. coli* [79]	-No activity detected against *C. albicans* [79]
	AvBD2	*S. aureus* 1056 MRSA (0.26 µM) [93] *S. aureus, B. cereus, Streptococcus agalactiae* [110]	E. coli O157:H7 (0.2 µM) [93] *P. multocida, E. coli, Salmonella choleraesuis* [110]	-Activity against *C. albicans* (1.3 µM) [93]
	AvBD7	*S. aureus* 1056 MRSA [93] *S. aureus, B. cereus, S. agalactiae* [110]	*E. coli* O157:H7 [93] *P. multocida, E. coli, S. choleraesuis* [110]	-No activity detected against *C. albicans* [93]
	AvBD8	*S. aureus* 1056 MRSA [93]	*E. coli* O157:H7 [93]	- No activity detected against *C. albicans* [93]

King penguin	**AvBD103b**	*M. luteus* (1.5-3 µM), *B. subtilis* (0.8-1.5 µM), *B. cereus* (3-6 µM), *Bacillus megaterium* (0.4-0.8 µM), *S. aureus* (1.5-3.0 µM), *S. saprophyticus* (1.5-3.0 µM), *Staphylococcus haemolyticus* (1.5-3.0 µM), *Nocardia asteroides* (0.8-1.5 µM), *Aerococcus viridans* (0.4-0.8 µM), *L. monocytogenes* (6-12 µM) [80] *S. aureus* (0.16 µM), *L. monocytogenes* (0.14 µM) [88] *Listeria ivanovii* (3 µM), *Streptococcus suis* (1.5µM), *Enterococcus faecium* (0.75 µM), *Enterococcus faecalis* (0.75 µM) [111]	*E. coli* (1.5-3.0 µM), *S. typhimurium* (6-12 µM), *K. pneumoniae* (50-100 µM), *P. aeruginosa* (6-12 µM), *Vibrio metshnikovii* (25-50 µM), *Vibrio anguillarum* (25-50 µM) [80] *S. enteritidis* (0.31 µM), *S. Typhimurium* (0.2 µM), *E. coli* (0.09µM) [88] *S. enteritidis* (1.5 µM), *P. aeruginosa* (1.5 µM) [111]	-Bactericidal effect against all Gram-positive tested bacteria, except against *S. saprophyticus* [80] -Bacteriostatic activity against all Gram-negative tested bacteria, except against *E. coli* and *V. metshnikovii* [80] -No activity detected against *Enterobacter cloacae* and *A. faecalis* up to 100 µM [80] -Activity against yeast and filamentous fungi: *Candida glabrata* (>100 µM), *C. albicans* (50-100 µM), *Candida tropicalis* (1.5- 3 µM), *Neurospora crassa* (3-6 µM), and *Aspergillus fumigatus* (3-6 µM) [80]

b. Other activities than antibacterial

In addition to antibacterial activity, the antimicrobial activity of avian β-defensins extent to antifungal and antiviral effects. **Chicken AvBD1** is active against *C. albicans* at 8 µg/mL [73] contrary to AvBD2, which was ineffective against *C. albicans* at 400 mg/ml [73]. The synthetic folded form of **chicken AvBD9** (named Gal-6) shows an activity against *S. cerevisiae* and *C. albicans* [96]. Ostrich β-defensins are found devoid of activity against *C. albicans*, except for AvBD-2 (MIC 6.20 µg/mL) [93]. Penguin AvBD103b defensin exhibit an antifungal activity principally against *N. crassa* (3-6 µM) and *A. fumigatus* (3-6 µM). The linear form of N-terminal acetylated of chicken AvBD4 and AvBD10 exhibit an antifungal activity against *C. albicans* and *A. flavus* (MFC range: 25 – 100 µg/mL) [112]. Duck β-defensins (Apl_AvBDs), Apl_AvBD4, 7 and 12 in both GST-tagged recombinant and synthetic linear forms exhibited significant antiviral activity against duck hepatitis virus (DHV) [91].

Besides having direct microbicidal activities, AvBDs have increasingly been shown to play a pivotal role in regulating host immune responses to infections by actively involved in chemotaxis and activation of immune cells, similarly to mammalian defensins [113], [114]. Furthermore, several AvBDs directly bind and neutralize lipopolysaccharides (LPS), bacterial membrane component, suppressing therefore the LPS-induced proinflammatory cytokines production. Chicken AvBD6 and AvBD12 are effective LPS neutralizers and are broad-spectrum chemoattractant molecules for avian and mammalian immune cells. Both peptides are mildly chemotactic for chicken macrophages and strongly chemotactic for CHO-K1 cells expressing chicken chemokine receptor 2 (CCR2). Also, AvBD-12 at a relatively high concentration (64 µg/ml) induced chemotactic migration of murine immature dendritic cells (DCs) [95]. The immunomodulatory potential of duck AvBD2 was shown by chemotaxis of DT-40 chicken B-lymphocytes [106].

4. 3D Structures

To date, the tertiary structures of two chicken β-defensins (AvBD2, AvBD7), a penguin β-defensin (AvBD103b), a duck β-defensin (AvBD3), a chicken ovodefensin (gallin), and the unique double β-defensins chicken AvBD11, have been determined, all by nuclear magnetic resonance (NMR) in solutions (Table 2). Unlike mammalian defensins, which have been reported as dimers or multimers in several crystal structures [77, 78], all avian defensins have been reported as monomers in solution, although the authors could not completely rule out the formation of a perfect symmetric dimer [117]. However, it is not clear which form, monomeric or multimeric, is biologically relevant, or whether the same form is relevant for any defensin.

Table 2: Summary of the avian β-defensins and variants for which the tridimensional structure has been solved by solution NMR.

Bird species (common name)	**Defensin** (previous name)	**Length sequence**	**3D structure (PDB Code)**	**Main results**	**Date** (Ref.)
Aptenodytes patagonicus (King Penguin)	**AvBD103b** (Sphenicin-2)	38	**1UT3** 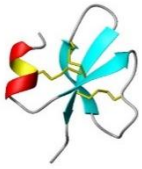	-N-terminus is mainly organized into an α-helical	**2004** [118]
Gallus Gallus (Chicken)	**AvBD2** (Gallinacin-2)	36	**2LG5** 	-N-terminal short sequence -Lacks the N-terminal α-helix	**2012** [119]
	AvBD2-K31A	36	**2LG6** 	-The mutation induces the appearance of an additional short anti-parallel β-strand	**2012** [119]
	AvBD7 (Gallinacin-7)	47	**5LCS** 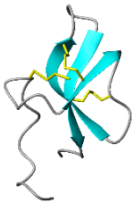	-A long N-terminal tail, without showing any propensity to form an N-terminal helix.	**2016** [107]
	Gga-AvBD11 (Gallinacin-11)	82	**6QEU** 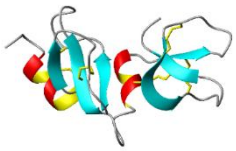	-Double size defensin -α-helix in the N-terminus -the two domains are packed together via a hydrophobic cluster.	**2020** [109]
	Gallin (Ovo-defensin)	41	**2MJK** 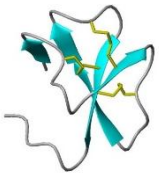	-the presence of an additional short two-stranded β-sheet -unusual long C-terminal part	**2014** [71]
Anas platyrhynchos (Mallard Duck)	**AvBD3**	37	**7LZL** 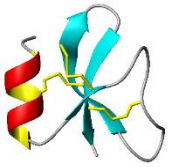	-N-terminus is organized into an α-helical	To be published

Typical β-defensins

The first structure (PDB code 1UT3) was performed on the king penguin AvBD103b defensin (initially named spheniscin-2), which revealed a three-dimensional structure most similar to the first mammalian β-defensin structures available at that time, e.g., human HBD1-3 defensins, murine mBD7-8 and bovine BNBD12 (PDB codes 1KJ6, 1E4T and 1BNB respectively). Indeed, AvBD103b possess the typical three-stranded antiparallel β-sheet of mammal defensin and its N-terminus is mainly organized (5/10 deposited structures) into an α-helical [117]. There is little doubt that the strong propensity to form a helix described at the time could, with today's computational means, be refined into a well-shaped helix, comparable for example to the recently determined Duck Mallard AvBD3 (PDB code 7lzl, unpublished). The second NMR structure of the avian β-defensin family, is AvBD2 from the chicken *Gallus gallus* [92]. AvBD2 structure (PDB code 2LG5) is restricted to the typical 3 stranded antiparallel β-sheet of β-defensins, but lacks the N-terminal α-helix [119]. In fact, it lacks the ability to form an N-terminal α-helix due to its shorter sequence (only two residues before the first cysteine in the sequence). Similar to chicken AvBD2, the additional N-terminal α-helix is absent in the bovine BNBD12 defensin (PDB code 1BNB) [120].

The third NMR structure of the avian β-defensin family, is AvBD7 from the chicken *Gallus gallus* [107]. The resolved structure (PDB code 5LCS) demonstrates a long N-terminal region (10 residues before the first Cys residues at position 11) of chicken AvBD7, which does not show any propensity to form an N-terminal helix [107].

Subfamily of ovodefensins

The 3D structure of gallin (PDB code 2MJK), which is the only ovodefensin structure to have been solved, contains the antiparallel three-stranded β-sheet typical of vertebrate β-defensins, and stabilized by 3 disulfide bridges with the following spacing cysteine pattern: C_1-X5-C_2-X3-C_3-X11-C_4-X3-C_5-C_6. Gallin, and presumably the other ovo-defensins, can therefore be unambiguously classified as a β-defensin [71]. However, the presence of an additional short two-stranded β-sheet reveals a new variation in the β-defensin fold, which is directly related to slight differences in cysteine spacing. In addition, the gallin sequence contains an unusual long C-terminal part (10 residues after the last cys residue), that does not form any secondary structure but is packed against the protein core (Table 2).

The double β-defensin AvBD11

The protein *Gga*-AvBD11 (corresponding to the 11th AvBD gene in the AvBD cluster of *Gallus gallus*) is a double size defensin (82 residues, 12 cysteine residues) found in the vitelline membrane of the hen egg. The determination of its 3D NMR (PDB code 6QEU) structure allows the definition of a new β-defensin subfamily, without equivalent in vertebrates other than birds, and named avian-double-β-defensin (Av-DBD) [109]. Indeed, the N-terminal domain adopts a typical β-defensin fold, with the 3

stranded antiparallel β-sheet and the α-helix. Although its inter-cysteine spacing is not canonical, the C-terminal domain also adopts a β-defensin fold, with a slightly distorted helix. Under the experimental conditions of the NMR solution, the two domains are packed together via a hydrophobic cluster [109]. However, there is no evidence that the compact form described is maintained *in vivo* and corresponds to the active form, or even that the double defensin is not cleaved into two monodomain defensin during chick development.

5. Structure-Activity Relationships

This paragraph brings together the scattered information on the structure-activity relationship, namely the impact of overall charge, the presence of disulfide bridges and N-terminal helix, the distribution of hydrophobic and basic surface residues, and the effect of a single mutation on the antibacterial activity of AvBDs.

Global charge

Even if the global fold is conserved within the β-defensin family, the extremely low sequence identity induces high variations in the distribution of the charged and hydrophobic residues at the surface, which may explain the differences in their antimicrobial spectra and potency.

Although cationicity is essential for AvBDs activity, it is not possible to establish a direct link between the overall charge of a defensin and its antibacterial activity. The activity of three chicken defensins, AvBD1, AvBD2 and AvBD7 with different charges, +8, +4 and +6, respectively, was evaluated on a panel of bacteria [92]. The three defensins exhibited comparable potencies against Gram-positive bacteria although the positive net charge of AvBD2 (+4) is one of the lowest among the AvBDs. Among the three defensins, AvBD2 has the lowest activity against Gram-negative bacteria. However, the fact that AvBD1 and AvBD7 show similar levels of activity against Gram-negative bacteria indicates that there is no direct correlation between overall charge and the activity on bacteria [92]. This study clearly shows that an AvBD is not necessarily more active simply because it is more cationic.

The high cationicity of AvBD103b, which sequence contains 10 Arg over 38 residues unbalanced by any Glu or Asp, is presumably the critical factor for its retained activity in high salt concentrations (which is related to its natural environment, the stomach of the penguin) [117], unlike the vast majority of β-defensins (e.g., chicken defensins, ostrich AvBD2 and AvBD7 [39, 40] [122], mammalian defensins [53]) which lose their antibacterial activities at physiological salt concentrations. Indeed, AvBD103b remains active *in vitro* against bacteria (*S. aureus* and *E. coli*) in high salt concentration, approximately 324 mOsm/L, an osmolarity equal to one found in penguin stomach content, and even up to an osmolarity approx. 1000 mOsm/L, close to one of the seawaters, against *S. aureus* [117]. Along with AvBD103b, the highly cationic human β-defensin HBD3 (+11) is the second known salt-insensitive β-defensin.

Reduced or oxidized states

Although the structural role of conserved disulfide bridges in defensins to ensure high stability and enzymatic resistance is undisputed, their role in antimicrobial activity is unclear, as some reduced defensins retain their activity. Unlike many mammalian β-defensins (bovine BNDB-2 and BNDB-12 or human hBD3) whose structural integrity showed a minimum impact on the antibacterial activity [100], [123], [124], [125], chicken AvBD2 requires the presence of the folded structure for maximum antimicrobial activity [126]. In fact, blocking cysteine pairing in synthetic version of chicken AvBD2 (AvBD2-Acm) show a drastic loss of activity against a range of bacterial strains, particularly Gram-positive bacteria, compared to its oxidatively folded counterpart (AvBD2). For example, AvBD2-Acm is 10 and 16 times less effective against *B. cereus* and *L. monocytogenes* than the folded form. The loss of AvBD2-Acm activity was less significant against Gram-negative bacteria, with no impact on activity against *E. coli* [126].

N-terminal helix

In contrast to what has been shown for certain mammalian defensins (HBD3 for example [127]), the N-terminal α-helix appears to be nonessential for the antibacterial activity of AvBDs. Indeed, chicken AvBD2, lacking the N-terminal helix, shows activity against bacterial strains as AvBD103b [126]. The truncated peptidoform of AvBD7 lacking the first three N-terminal residues maintains antibacterial activity, except against *S. aureus* [107]. It has been suggested that the α-helix in the N -terminus may be involved in the selectivity of AvBDs antimicrobial activity (antifungal activity, for example), since AvBD103b is known to be fungicidal [117] compared to the lack of potency of chicken AvBD2 against *Candida albicans* [126].

The long N-terminal region (10 residues before the first Cys residues at position 11) of chicken AvBD7 is stabilized by a β-turn formed by a salt bridge between residues D9 and R12, and it covers the C-terminal part, which is a key feature to confer AvBD7 an unusual resistance to proteolysis [107].

Surface Distribution of hydrophobic and charged residues at the surface

Similar to ovodefensins, Gallin exhibits atypical surface properties showing a non-random distribution of hydrophobic and basic residues [71]. The 3D fold variations and/or atypical surface hydrophobic properties of Gallin compared with other avian β-defensins could be related to its unexpected spectrum of activity (restricted activity against *E. coli*), and/or to other as yet unknown functions.

Impact of the single mutation K31A

A fine comparison of chicken AvBD2 and king penguin AvBD103b structures revealed a series of well (but not strictly) conserved residues that may be involved in the antimicrobial properties and/or bacterial strain specificity of avian defensins. The potential strategic role of K31 (AvBD2 numbering), located in the hydrophobic environment provided by accessible and well-conserved hydrophobic residues, was highlighted. The AvBD2-K31A (PDB code 2LG6) mutant was chemically synthesized and, as expected

exhibited a marked decrease in the antibacterial activity against both Gram-positive and Gram-negative bacteria [126]. Surprisingly, this mutation at position 31 induces substantial N-terminal structural modifications, with the appearance of an additional short anti-parallel β-strand (Table 2) [126]. The reduction of disulfide bonds rendered the lysine-alanine substituted AvBD2 nearly completely inactive in killing bacteria [126]. This study demonstrates that a single mutation can have a dramatic impact on structure and activity.

6. Antibacterial mechanisms of action (MOAs)

Despite their potential antibacterial activity *in vitro*, the mechanisms by which avian defensins inhibit growth or kill bacterial cells have yet to be fully elucidated. Like other cationic AMPs, defensins primarily target bacterial cell membranes via initial electrostatic interactions with negatively charged components of bacterial surfaces, such as lipoteichoic acids (LTAs) in Gram-positive bacteria, LPS in Gram-negative bacteria and also anionic phospholipids. Indeed, it is well known that the outer membrane of bacteria is stabilized by the presence of divalent cations such as Ca^{2+} and $Mg^{2+,}$ whose binding sites are attractive to defensin-type cationic peptides. Defensins compete for these binding sites and displace the divalent cations, thus disrupting membrane stability/organization. This interaction is diminished by the presence of salts or divalent cations, which simply inhibit the initial attraction between the cationic peptide and its anionic target [128]. As a result of this perturbation, the hydrophobic part of the peptide is inserted into the membrane. Local accumulation of the peptide can lead to complete membrane rupture, such as pore formation, and ultimately cell lysis and death [121]. Other peptides induce transient membrane permeabilization to facilitate their passage across the membrane into the cytoplasm, where they interact with intracellular component(s). These translocated peptides can interfere with vital biological processes such as interfering with cell wall synthesis by inhibiting peptidoglycan synthesis, interfering with cytoplasmic membrane septum formation, binding to DNA, RNA or inhibiting proteins/enzymes [39, 95].

For most of the avian β-defensins studied (from ostrich, chicken, and penguin), a multifaceted antibacterial mechanism combining membrane disruption and intracellular targeting has been reported, which is less likely to readily induce resistance in bacterial strains.

Ostrich AvBD1 (3-fold MIC) and **AvBD2** (5-fold MIC) defensins were shown to cause slow, partial depolarization of ***E. coli*** outer and cytoplasmic membranes by binding weakly to bacterial LPS [130]. This slight membrane disruption failed to cause bacterial death. It was therefore suggested that ostrich defensins could cross the bacterial membrane, reach the cytoplasm, and interact with intracellular molecules. Given that ostrich defensins were effective in altering the mobility of bacterial DNA in a gel electrophoresis assay, it was proposed that DNA could be the molecular target of defensin [130].
The **chicken defensins AvBD6** and **AvBD12** (1-fold MIC) have been shown to induce ultrastructural changes in ***S. Typhimurium***, resulting in a fuzzy membrane, cytoplasmic membrane shrinkage and loss

of cytoplasmic content by transmission electron microscopy (TEM). This suggests that both defensins disrupt the bacterial membrane in addition to interfering with other intracellular functions such as cell division, resulting in morphological changes. Potential interference with transcription and translation was also suggested after demonstrating the ability of both defensins to retard bacterial DNA migration in a gel retardation assay, with AvBD6 being significantly more effective than AvBD12 [95]. These chicken defensins also display significant LPS-neutralizing capabilities, which are essential for attenuating the inflammatory response during bacterial infections [95].

Chicken AvBD9 induced morphological changes in ***C. perfringens*** in a dose-dependent manner, as revealed by TEM observations, without inducing cell lysis as the primary killing mechanism [96]. Indeed, at low concentrations (< MIC), AvBD9 causes granulation of intracellular material and the formation of irregular septa in dividing cells, however, at high concentrations (> MIC), lysis of dividing cell septa, degradation of the cytoplasmic membrane and complete cell lysis were observed [95].

This dual mechanism of action has been also proposed for the salt-insensitive **king penguin AvBD103b** defensin on ***Salmonella enteritidis*** [111]. Indeed, Teng et al. suggested that AvBD103b disrupted the integrity of both membranes after binding electrostatically to the cell surface, then reached the cytoplasm and interfered with intracellular DNA by intercalating the base pair, ultimately causing cell death [111]. This non-membrane-disrupting mechanism for the antibacterial activity of AvBD103b was confirmed by Landon et al [131], demonstrating a delayed transient membrane permeabilization caused by the peptide (1-fold MIC) in real-time on ***E. coli***. Indeed, AvBD103b induces permeabilization of the outer and cytoplasmic membranes concomitantly after bacterial growth arrest. This permeabilization profile is different from that induced by the lytic peptides, LL37 and Cecropin A [99, 100]. The translocation of the highly cationic AvBD103b within the cell and binding to DNA and other anionic partners have also been suggested [131] (more details about this study in the chapter 5 of thesis).

In addition to multi-faceted antibacterial MOAs, some avian defensins act in favor of a non-specific mechanism, which is another favorable point for combating resistant bacteria through the development of mutations.

Because of steric incompatibility, it is widely known that the D-enantiomer of a native protein does not recognize the L-enantiomer's protein partners, and vice versa. The all-D enantiomer of chicken AvBD2 was synthetized and resulted in little difference in the activity against various bacterial strains, either Gram-positives or Gram-negatives, compared with the naturally all-L AvBD2 [126]. This indicates that chicken AvBD2 primarily disrupts the bacterial membrane through a nonchiral, nonspecific interaction, as is the case with magainin and cecropins. In addition to chicken AvBD2, the target of penguin defensin AvBD103b has been shown to be non-chiral. The D-enantiomer of this defensin not only exhibits similar activity against *E. coli*, but also the same cascade of events to attack *E. coli* as the native form (L-enantiomer) [131].

Despite their functional and structural similarities, the antibacterial mechanisms of avian defensins may be considerably different and are probably achieved by multiple actions. Unfortunately, the little we know about how avian defensins act on bacteria cell is deduced mainly from *in vitro* experiments with attached/fixed bacteria, at low salt concentrations and without a peptide concentration in the MIC range.

The experimental conditions and techniques used in the studies mentioned in this section are summarized in Table 3. To our knowledge, of all the previously cited references on the antibacterial mechanisms of avian defensins, only one study examined the MOA on living cells under physiological conditions and in real time, using an innovative single-cell fluorescence imaging technique [131] (more details about this technique in the next chapter of thesis).

Table 3: Summary of the main results obtained on the antibacterial mechanisms of action of avian β-defensins (obtained using different techniques and under various experimental conditions)

Mechanisms of action	Techniques and conditions	Main results
Chicken AvBD6 and AvBD12 [95] [122] Experiments were performed on wild type (oxidized) forms and reduced forms. Gram-negative bacteria: *Salmonella Typhimurium*		
Lipopolysaccharides (LPS)-neutralizing ability	**Limulus Amoebocyte Lysate (LAL) assay** *Medium: Endotoxin-free water* *Peptide concentration: ½ MIC, MIC, 2 × MIC* *S. Typhimurium LPS and Escherichia coli LPS (2 EU/ml)* *Incubation: 37 °C for 30 min*	-Both AvBD6 and AvBD12 neutralized LPS activity in a dose-dependent manner -The neutralizing capacity of AvBD6 was significantly stronger than AvBD12 -The presence of NaCl (from 17 to 137 mM) had no impact on AvBDs' ability to neutralize LPS
Ultrastructural changes	**Transmission electron microscopy (TEM)** *Medium: in the presence of 5 mM NaCl.* *10^8 CFU S. Typhimurium cells* *Peptide concentration: MIC* *Incubation: 37 °C for 30 min* *Cells were harvested by centrifugation, then fixed, dehydrated, and stained.*	-Treatment with oxidized resulted in fuzzy membrane, loss of cytoplasmic content, vacuole formation, membrane blebbing, and cytoplasmic membrane shrinking -Treatment with reduced AvBDs caused only fuzzy membrane and cytoplasmic leakage
	Scanning electron microscopy (SEM) *10^8 CFU S. Typhimurium cells* *Medium: 10 mM phosphate buffer saline (PBS)* *Peptide concentration: MIC* *Incubation: at 37 °C for 30 min.* *Bacterial pellets were fixed, washed, dehydrated then observed.*	-Treatment with defensins caused membrane damage and cell deformation
Binding to bacterial genomic DNA	**Gel retardation assay** *Peptide/DNA ratios: 0, 0.5, 1, 2, 4 and 8 (w/w).* *Incubation: RT for 10 min.*	-Both oxidized AvBDs were able to retard the *S. Typhimurium* genomic DNA migration (50 % at a mass ratio of 4:1 (peptide: DNA) and near completely at a ration 8:1) -AvBD6 was more effective than AvBD12 in retarding genomic DNA migration -Reduced AvBDs were less able than their respective Wild-type to retard *Salmonella* genomic DNA migration
Chicken AvBD9 [96] Gram-positive bacteria: *Clostridium perfringens*		
Ultrastructural changes	**Transmission electron microscopy (TEM)** *2 × 10^8 CFU/ml C. perfringens* *Medium: Tryptic Soy Broth (TSB) minimal medium* *sGal-6 concentration= 1.56 to 25 µg/ml*	Dose-dependent morphological effects: -At a concentration lower than MIC, treatment resulted on granulation of intracellular material and irregular septa in dividing cells

	Incubation: for 30 min at 37°C under anaerobic conditions.	-At a concentration higher than MIC, retracting cytoplasm and membrane leakage, whereas lysis at the septa of dividing cells became more prominent -At 3x MIC, the majority of cells developed a ghost-like appearance combined with detachment of the cytoplasmic membrane from its peptidoglycan layer and concomitant membrane fragmentation and resulted more often in complete lysis
Chicken AvBD9 [108] Gram- bacteria: *Shigella Sonnei* Gram-positive bacteria: *S. aureus*		
Effects on the bacterial morphology	**Transmission electron microscopy (TEM)** *Medium: PBS* *Peptide concentration: 2.5× and 5× MIC* *Incubation: 1h*	- Penetration to the bacterial cell membrane and successfully lead to the release of the cytoplasmic contents into the surrounding environment -Deterioration of the cell membrane ultrastructure, damage to the cell wall (i.e., holes and deep craters), loss of the cell wall, decrease in the cell volume, cell lysis and leakage of the cytoplasmic continents
Ostrich AvBD1 and AvBD2 [130] Gram-negative bacteria: *Escherichia coli*		
Binding affinity for LPS	**Fluorescence-based assay** *Peptide concentration = 1 µM (3-5 MIC)* *LPS (commercial lipid extract) at 3 µg/mL in the buffer* *Fluorescent dye: Dansyl polymyxin B (fluorescens when attached to LPS)* *Buffer: 5mM HEPES, pH 7.2*	-Both defensins were able to bind to LPS with low affinities
Outer membrane (OM) permeabilization assay	**Fluorescence-based assay** *-E. coli was grown in LB broth then resuspended in 5mM HEPES, 5mM glucose buffer, pH 7.4 to an $OD_{600\ nm}$ of 0.5.* *-Final concentration of peptide: 1 µM* *-Fluorescent dye: fluorophor 1-N-phenylnapthylamine (NPN) (normally impermeable to OM)* *-Positive control: polymyxin B*	-They were able to permeabilize partially the OM -AvBD1 caused permeabilization slightly higher than AvBD2
Cytoplasmic membrane (CM) depolarization assay	**Fluorescence-based assay** *-E. coli was grown in LB broth then resuspended in 5mM HEPES, 5mM glucose buffer, pH 7.4 to an $OD_{600\ nm}$ of 0.05.* *-Fluorescent dye: 3,3-dipropylthiacarbocyanine iodide [diSC3(5)] (membrane potential-sensitive dye)*	-Both defensins caused a slow and partial depolarization of the cytoplasmic membrane

	- Final concentration of peptide: 1 µM *-Positive control: gramicidin*	
Binding to bacterial genomic DNA	**DNA gel electrophoresis** *-Bacterial DNA used was λDNA/EcoRI (fragments).* *-Buffer: 100mM Tris, 200mM KCl, 10mM EDTA, 10mM DTT and 50% (v/v) glycerol* *-Positive control : Oabac5mini*	-At DNA: peptide 1:1 ratio, defensins were able to bind to a small fragment of the DNA, whereas at DNA: peptide 1:4 ratio, peptides interacted with all DNA fragments
King penguin AvBD103b [111] Gram-negative bacteria: *Salmonella enteritidis*		
Effect on the cell surface hydrophobicity	**Bacterial adherence to hydrocarbons (BATH) method** *Medium: Sterile normal saline + 0.1 KNO_3 (pH 6.2)* *Bacteria in stationary phase* *Peptide concentration: 1 ×, 2 ×, and 4× MIC* *Incubation: 37°C for 10 min.* *Lecture at Optical density at 600 nm*	-Increasing hydrophobicity of the cell surface by the peptide in a concentration dependent manner
OM permeability assay	**Uptake of N-phenyl-1-naphthylamine (NPN) dye** *Medium: 5 mM HEPES buffer (pH 7.2) containing 5 mM glucose* *Bacteria: 0.5 ($OD_{600\ nm}$)* *Concentration peptide: 2× or 4× MIC* *Lecture of fluorescence*	-AvBD103b was able to rapidly and highly permeabilize the outer membrane in a dose dependent manner, resulting in an increase of NPN uptake
Effect on CM permeabilization	**Potassium release assay by atomic absorption spectrometer** *Bacteria solution at 10^8 CFU/mL* *Concentration peptide: 2x and 4x MIC* *Incubation: 37°C from 0 to 120 min*	-AvBD103b treatment at 2x and 4x MIC caused an efflux of potassium ions from cells in a time-dependent manner suggesting an increase of the CM permeability
	Flow cytometric analysis using Propidium iodide (PI) dye *Medium: 10 mM PBS* *Bacteria: 10^8 CFU/mL* *Concentration labelled-peptide (FITC-AvBD103b): 1x and 5x MIC* *Incubation: 37°C for 5, 30 and 120 min then added 50 µg/mL PI*	-AvBD103b induced PI influx into the cells indicating the disruption of the cell membrane integrity

Effects on the bacterial morphology	**TEM Observation** *Medium: MH* *Bacteria: 10^8 CFU/mL* *Peptide concentration: 1x MIC* *Incubation: 37°C for 2h*	-Cells treated with peptide showed changes in the overall morphology: disappearance/ damage of membranes, leakage of intracellular contents, formation of ghost-like cells, and even complete cell lysis
Binding to bacterial genomic DNA	**DNA gel retardation** *Different peptide: DNA (w/w) ratios at: 0, 0.25, 0.5, 1.25, 2.5 and 5* *Incubation : 10 min at RT*	- AvBD103b could bind with *S. enteritidis* genomic DNA by inserting base pairs and changing the DNA conformation
	Circular dichroism spectroscopy analysis *Different peptide: DNA ratios at: 0, 0.5, 2.5 and 5 (w/w)* *Incubation : 10 min at RT*	
Cell cycle analysis	**Flow cytometric analysis** *Bacteria: 0.5 x 10^8 CFU/mL* *Medium: 10 mM PBS (pH 7.2)* *Peptide concentration: 1x MIC* *Incubation: 37°C for 5, 30 and 120 min then treatment with RNAse A and PI (50 µL, 0.5 mg/ml).*	-AvBD103b induced arrest of *S. enteritidis* cells in the I-phase, e.g., time from cell division to initiation of chromosome replication
King penguin AvBD103b [135] Experiments were performed using both isomers *L*- and *D*-AvBD103b Gram-negative bacteria: *E. coli*		
OM and CM permeabilization and bacterial growth effect in real time	**Single-cell imaging using fluorescence microscopy** **Real-time fluorescence microscopy on living bacteria under physiological salt condition** *Medium: EZ Rich Defined Medium (EZRDM), pH 7.2, ~280 mosm/L* *Bacteria: E. coli strain JCW10 expressing GFP in the periplasm at OD_{600nm} ~ 0.4* *Peptide (1/2 MIC, 1x MIC, and 2x MIC) injected under constant flow with the bacterial growth media in the presence of Sytox orange (DNA binding dye)* *Incubation: follow in real time for one-hour on living bacteria*	-AvBD103b attacked the bacteria in two phases: at the end of phase 1, it induced an osmotic effect and growth arrest, before causing abrupt transient permeabilization of MO and CM concomitantly at the start of phase 2. These observations point to a non-disruptive mechanism. -The two isomers L- and D-AvBD103b showed similar activity and a cascade of MOAs events indicating a lack of stereospecific interaction with the cellular target(s). -AvBD103b would enter the cell and interact non-specifically with a variety of polyanionic targets, leading indirectly to cell death.

VI. References

[1] S. Doron et S. L. Gorbach, « Bacterial Infections: Overview », *International Encyclopedia of Public Health*, p. 273-282, 2008, doi: 10.1016/B978-012373960-5.00596-7.

[2] M. Hutchings, A. Truman, et B. Wilkinson, « Antibiotics: past, present and future », *Current Opinion in Microbiology*, vol. 51, p. 72-80, oct. 2019, doi: 10.1016/j.mib.2019.10.008.

[3] M. A. Salam *et al.*, « Antimicrobial Resistance: A Growing Serious Threat for Global Public Health », *Healthcare*, vol. 11, nº 13, Art. nº 13, janv. 2023, doi: 10.3390/healthcare11131946.

[4] C. J. L. Murray *et al.*, « Global burden of bacterial antimicrobial resistance in 2019: a systematic analysis », *The Lancet*, vol. 399, nº 10325, p. 629-655, févr. 2022, doi: 10.1016/S0140-6736(21)02724-0.

[5] « WHO bacterial priority pathogens list, 2024: Bacterial pathogens of public health importance to guide research, development and strategies to prevent and control antimicrobial resistance ». Consulté le: 30 octobre 2024. [En ligne]. Disponible sur: https://www.who.int/publications/i/item/9789240093461

[6] V. Gigante *et al.*, « Multi-year analysis of the global preclinical antibacterial pipeline: trends and gaps », *Antimicrobial Agents and Chemotherapy*, vol. 68, nº 8, p. e00535-24, juill. 2024, doi: 10.1128/aac.00535-24.

[7] « 2023 Antibacterial agents in clinical and preclinical development: an overview and analysis ». Consulté le: 30 octobre 2024. [En ligne]. Disponible sur: https://www.who.int/publications/i/item/9789240094000

[8] C. Brives et J. Pourraz, « Phage therapy as a potential solution in the fight against AMR: obstacles and possible futures », *Palgrave Commun*, vol. 6, nº 1, p. 1-11, mai 2020, doi: 10.1057/s41599-020-0478-4.

[9] « 2021 antibacterial agents in clinical and preclinical development: an overview and analysis ». Consulté le: 30 octobre 2024. [En ligne]. Disponible sur: https://www.who.int/publications/i/item/9789240047655

[10] M. Zasloff, « Antimicrobial peptides of multicellular organisms », *Nature*, vol. 415, nº 6870, p. 389-395, janv. 2002, doi: 10.1038/415389a.

[11] G. Diamond, N. Beckloff, A. Weinberg, et K. O. Kisich, « The Roles of Antimicrobial Peptides in Innate Host Defense », *Current Pharmaceutical Design*, vol. 15, nº 21, p. 2377-2392, juill. 2009, doi: 10.2174/138161209788682325.

[12] T. Ganz, « The Role of Antimicrobial Peptides in Innate Immunity », *Integrative and Comparative Biology*, vol. 43, nº 2, p. 300-304, 2003.

[13] Y. Luo et Y. Song, « Mechanism of Antimicrobial Peptides: Antimicrobial, Anti-Inflammatory and Antibiofilm Activities », *International Journal of Molecular Sciences*, vol. 22, nº 21, p. 11401, oct. 2021, doi: 10.3390/ijms222111401.

[14] N. Mookherjee, « Antimicrobial host defence peptides: functions and clinical potential | Nature Reviews Drug Discovery ». Consulté le: 17 novembre 2021. [En ligne]. Disponible sur: https://www.nature.com/articles/s41573-019-0058-8

[15] G. S. Dijksteel, M. M. W. Ulrich, E. Middelkoop, et B. K. H. L. Boekema, « Review: Lessons Learned From Clinical Trials Using Antimicrobial Peptides (AMPs) », *Front. Microbiol.*, vol. 12, févr. 2021, doi: 10.3389/fmicb.2021.616979.

[16] T. Meikle, C. Conn, F. Separovic, et C. Drummond, « Exploring the structural relationship between encapsulated antimicrobial peptides and the bilayer membrane mimetic lipidic cubic phase: Studies with gramicidin A' », *RSC Adv.*, vol. 6, p. 68685-68694, juill. 2016, doi: 10.1039/C6RA13658C.

[17] J. W. Hallett, M. I. Wolkowicz, et I. H. Leopold, « Ophthalmic Use of Neosporin », *American Journal of Ophthalmology*, vol. 41, nº 5, p. 850-853, mai 1956, doi: 10.1016/0002-9394(56)91781-0.

[18] U. Hofer, « The central role of lipids in daptomycin action », *Nat Rev Microbiol*, vol. 14, n° 12, p. 729-729, déc. 2016, doi: 10.1038/nrmicro.2016.172.
[19] C. F. Carpenter et H. F. Chambers, « Daptomycin: Another Novel Agent for Treating Infections Due to Drug-Resistant Gram-Positive Pathogens », *Clinical Infectious Diseases*, vol. 38, n° 7, p. 994-1000, avr. 2004, doi: 10.1086/383472.
[20] J. Lubelski, R. Rink, R. Khusainov, G. N. Moll, et O. P. Kuipers, « Biosynthesis, immunity, regulation, mode of action and engineering of the model lantibiotic nisin », *Cell. Mol. Life Sci.*, vol. 65, n° 3, p. 455-476, févr. 2008, doi: 10.1007/s00018-007-7171-2.
[21] I. Jenson, L. Baird, et J. Delves-Broughton, « The Use of Nisin as a Preservative in Crumpets », *Journal of Food Protection*, vol. 57, n° 10, p. 874-877, oct. 1994, doi: 10.4315/0362-028X-57.10.874.
[22] G. Wang, X. Li, et Z. Wang, « APD3: the antimicrobial peptide database as a tool for research and education », *Nucleic Acids Research*, vol. 44, n° D1, p. D1087-D1093, janv. 2016, doi: 10.1093/nar/gkv1278.
[23] T.-H. Lee, K. N. Hall, et M.-I. Aguilar, « Antimicrobial Peptide Structure and Mechanism of Action: A Focus on the Role of Membrane Structure », *CTMC*, vol. 16, n° 1, p. 25-39, sept. 2015, doi: 10.2174/1568026615666150703121700.
[24] T. Terwilliger et D. Eisenberg, « The structure of melittin. », *The Journal of biological chemistry*, vol. 257, p. 6016-22, juill. 1982, doi: 10.1016/S0021-9258(20)65098-0.
[25] J. H. Choi *et al.*, « Melittin, a honeybee venom-derived antimicrobial peptide, may target methicillin-resistant Staphylococcus aureus », *Molecular Medicine Reports*, vol. 12, n° 5, p. 6483-6490, nov. 2015, doi: 10.3892/mmr.2015.4275.
[26] G. Lee et H. Bae, « Anti-Inflammatory Applications of Melittin, a Major Component of Bee Venom: Detailed Mechanism of Action and Adverse Effects », *Molecules*, vol. 21, n° 5, Art. n° 5, mai 2016, doi: 10.3390/molecules21050616.
[27] D. Son, J. Lee, Y. Lee, H. Song, C. Lee, et J. Hong, « Therapeutic application of anti-arthritis, pain-releasing, and anti-cancer effects of bee venom and its constituent compounds », *Pharmacology & Therapeutics*, vol. 115, n° 2, p. 246-270, août 2007, doi: 10.1016/j.pharmthera.2007.04.004.
[28] J. F. Shurko, R. S. Galega, C. Li, et G. C. Lee, « Evaluation of LL-37 antimicrobial peptide derivatives alone and in combination with vancomycin against S. aureus », *J Antibiot*, vol. 71, n° 11, p. 971-974, nov. 2018, doi: 10.1038/s41429-018-0090-7.
[29] A. Nijnik et R. E. Hancock, « The roles of cathelicidin LL-37 in immune defences and novel clinical applications »:, *Current Opinion in Hematology*, vol. 16, n° 1, p. 41-47, janv. 2009, doi: 10.1097/MOH.0b013e32831ac517.
[30] K. Brown *et al.*, « Host Defense Peptide LL-37 Selectively Reduces Proinflammatory Macrophage Responses », *Journal of immunology (Baltimore, Md. : 1950)*, vol. 186, p. 5497-505, mars 2011, doi: 10.4049/jimmunol.1002508.
[31] L. M. Gottler et A. Ramamoorthy, « Structure, membrane orientation, mechanism, and function of pexiganan — A highly potent antimicrobial peptide designed from magainin », *Biochimica et Biophysica Acta (BBA) - Biomembranes*, vol. 1788, n° 8, p. 1680-1686, août 2009, doi: 10.1016/j.bbamem.2008.10.009.
[32] E. Rubinchik, D. Dugourd, T. Algara, C. Pasetka, et H. D. Friedland, « Antimicrobial and antifungal activities of a novel cationic antimicrobial peptide, omiganan, in experimental skin colonisation models », *International Journal of Antimicrobial Agents*, vol. 34, n° 5, p. 457-461, nov. 2009, doi: 10.1016/j.ijantimicag.2009.05.003.
[33] N. Srinivas *et al.*, « Peptidomimetic Antibiotics Target Outer-Membrane Biogenesis in Pseudomonas aeruginosa », *Science*, vol. 327, n° 5968, p. 1010-1013, févr. 2010, doi: 10.1126/science.1182749.
[34] K. Garbacz, W. Kamysz, et L. Piechowicz, « Activity of antimicrobial peptides, alone or combined with conventional antibiotics, against Staphylococcus aureus isolated from the

airways of cystic fibrosis patients », *Virulence*, vol. 8, n° 1, p. 94-100, janv. 2017, doi: 10.1080/21505594.2016.1213475.

[35] P. Mygind *et al.*, « Plectasin is a peptide antibiotic with therapeutic potential from a saprophytic fungus », *Nature*, vol. 437, p. 975-80, nov. 2005, doi: 10.1038/nature04051.

[36] M. Scocchi, M. Mardirossian, G. Runti, et M. Benincasa, « Non-Membrane Permeabilizing Modes of Action of Antimicrobial Peptides on Bacteria », *Current Topics in Medicinal Chemistry*, vol. 16, n° 1, p. 76-88, janv. 2016.

[37] M.-H. Baek *et al.*, « Lipopolysaccharide-bound structure of the antimicrobial peptide cecropin P1 determined by nuclear magnetic resonance spectroscopy », *Journal of Peptide Science*, vol. 22, n° 4, p. 214-221, 2016, doi: 10.1002/psc.2865.

[38] N. Malanovic et K. Lohner, « Gram-positive bacterial cell envelopes: The impact on the activity of antimicrobial peptides », *Biochimica et Biophysica Acta (BBA) - Biomembranes*, vol. 1858, n° 5, p. 936-946, mai 2016, doi: 10.1016/j.bbamem.2015.11.004.

[39] L. Brown, J. M. Wolf, R. Prados-Rosales, et A. Casadevall, « Through the wall: extracellular vesicles in Gram-positive bacteria, mycobacteria and fungi », *Nat Rev Microbiol*, vol. 13, n° 10, p. 620-630, oct. 2015, doi: 10.1038/nrmicro3480.

[40] H. Huang, « Deformation free energy of bilayer membrane and its effect on gramicidin channel lifetime », *Biophysical Journal*, vol. 50, n° 6, p. 1061-1070, déc. 1986, doi: 10.1016/s0006-3495(86)83550-0.

[41] H. Raghuraman et A. Chattopadhyay, « Melittin: a Membrane-active Peptide with Diverse Functions », *Bioscience Reports*, vol. 27, n° 4-5, p. 189-223, août 2007, doi: 10.1007/s10540-006-9030-z.

[42] J. M. Leveritt, A. Pino-Angeles, et T. Lazaridis, « The Structure of a Melittin-Stabilized Pore », *Biophysical Journal*, vol. 108, n° 10, p. 2424-2426, mai 2015, doi: 10.1016/j.bpj.2015.04.006.

[43] T. Velkov, P. E. Thompson, R. L. Nation, et J. Li, « Structure−Activity Relationships of Polymyxin Antibiotics », *J. Med. Chem.*, vol. 53, n° 5, p. 1898-1916, mars 2010, doi: 10.1021/jm900999h.

[44] Y. F. Mohamed, H. M. Abou-Shleib, A. M. Khalil, N. M. El-Guink, et M. A. El-Nakeeb, « Membrane permeabilization of colistin toward pan-drug resistant Gram-negative isolates », *Brazilian Journal of Microbiology*, vol. 47, n° 2, p. 381-388, avr. 2016, doi: 10.1016/j.bjm.2016.01.007.

[45] G. Gajski et V. Garaj-Vrhovac, « Melittin: A lytic peptide with anticancer properties », *Environmental Toxicology and Pharmacology*, vol. 36, p. 697-705, juin 2013, doi: 10.1016/j.etap.2013.06.009.

[46] J. Pogliano, N. Pogliano, et J. Silverman, « Daptomycin-Mediated Reorganization of Membrane Architecture Causes Mislocalization of Essential Cell Division Proteins », *Journal of bacteriology*, vol. 194, p. 4494-504, août 2012, doi: 10.1128/JB.00011-12.

[47] D. Knappe, M. Zahn, U. Sauer, G. Schiffer, N. Sträter, et R. Hoffmann, « Rational Design of Oncocin Derivatives with Superior Protease Stabilities and Antibacterial Activities Based on the High-Resolution Structure of the Oncocin-DnaK Complex », *ChemBioChem*, vol. 12, n° 6, p. 874-876, 2011, doi: 10.1002/cbic.201000792.

[48] A. Krizsan, D. Volke, S. Weinert, N. Sträter, D. Knappe, et R. Hoffmann, « Insect-Derived Proline-Rich Antimicrobial Peptides Kill Bacteria by Inhibiting Bacterial Protein Translation at the 70 S Ribosome », *Angewandte Chemie International Edition*, vol. 53, n° 45, p. 12236-12239, 2014, doi: 10.1002/anie.201407145.

[49] T. Schneider *et al.*, « Plectasin, a Fungal Defensin, Targets the Bacterial Cell Wall Precursor Lipid II », *Science*, vol. 328, n° 5982, p. 1168-1172, mai 2010, doi: 10.1126/science.1185723.

[50] R. Shukla *et al.*, « Mode of action of teixobactins in cellular membranes », *Nat Commun*, vol. 11, n° 1, p. 2848, juin 2020, doi: 10.1038/s41467-020-16600-2.

[51] R. Shukla *et al.*, « Teixobactin kills bacteria by a two-pronged attack on the cell envelope », *Nature*, vol. 608, n° 7922, p. 390-396, août 2022, doi: 10.1038/s41586-022-05019-y.

[52] T. Ganz, « Defensins: antimicrobial peptides of innate immunity », *Nat Rev Immunol*, vol. 3, n° 9, p. 710-720, sept. 2003, doi: 10.1038/nri1180.

[53] M. E. Selsted et A. J. Ouellette, « Mammalian defensins in the antimicrobial immune response », *Nat Immunol*, vol. 6, nº 6, p. 551-557, juin 2005, doi: 10.1038/ni1206.
[54] F. Semple *et al.*, « Human β-defensin 3 has immunosuppressive activity in vitro and in vivo », *European Journal of Immunology*, vol. 40, nº 4, p. 1073-1078, 2010, doi: 10.1002/eji.200940041.
[55] S. Zhu et B. Gao, « Evolutionary origin of β-defensins », *Developmental & Comparative Immunology*, vol. 39, nº 1, p. 79-84, janv. 2013, doi: 10.1016/j.dci.2012.02.011.
[56] T. M. A. Shafee, F. T. Lay, T. K. Phan, M. A. Anderson, et M. D. Hulett, « Convergent evolution of defensin sequence, structure and function », *Cell. Mol. Life Sci.*, vol. 74, nº 4, p. 663-682, févr. 2017, doi: 10.1007/s00018-016-2344-5.
[57] B. G. Fry *et al.*, « Novel Venom Proteins Produced by Differential Domain-Expression Strategies in Beaded Lizards and Gila Monsters (genus Heloderma) », *Molecular Biology and Evolution*, vol. 27, nº 2, p. 395-407, févr. 2010, doi: 10.1093/molbev/msp251.
[58] L. Dalla Valle, F. Benato, S. Maistro, S. Quinzani, et L. Alibardi, « Bioinformatic and molecular characterization of beta-defensins-like peptides isolated from the green lizard Anolis carolinensis », *Dev Comp Immunol*, vol. 36, nº 1, p. 222-229, janv. 2012, doi: 10.1016/j.dci.2011.05.004.
[59] M. L. van Hoek *et al.*, « The Komodo dragon (Varanus komodoensis) genome and identification of innate immunity genes and clusters », *BMC Genomics*, vol. 20, nº 1, p. 684, août 2019, doi: 10.1186/s12864-019-6029-y.
[60] R. Lakshminarayanan *et al.*, « Structure, Self-Assembly, and Dual Role of a β-Defensin-like Peptide from the Chinese Soft-Shelled Turtle Eggshell Matrix », *J. Am. Chem. Soc.*, vol. 130, nº 14, p. 4660-4668, avr. 2008, doi: 10.1021/ja075659k.
[61] V. Fadel *et al.*, « Automated NMR structure determination and disulfide bond identification of the myotoxin crotamine from Crotalus durissus terrificus », *Toxicon*, vol. 46, nº 7, p. 759-767, déc. 2005, doi: 10.1016/j.toxicon.2005.07.018.
[62] A. M. Torres *et al.*, « Solution structure of a defensin-like peptide from platypus venom », *Biochemical Journal*, vol. 341, nº Pt 3, p. 785, août 1999.
[63] A. M. Torres, C. Tsampazi, D. P. Geraghty, P. S. Bansal, P. F. Alewood, et P. W. Kuchel, « D-Amino acid residue in a defensin-like peptide from platypus venom: effect on structure and chromatographic properties », *Biochemical Journal*, vol. 391, nº 2, p. 215-220, oct. 2005, doi: 10.1042/BJ20050900.
[64] C. a. M. Semple, K. Taylor, H. Eastwood, P. E. Barran, et J. R. Dorin, « Beta-defensin evolution: selection complexity and clues for residues of functional importance », *Biochem Soc Trans*, vol. 34, nº Pt 2, p. 257-262, avr. 2006, doi: 10.1042/BST20060257.
[65] A. Patil, A. L. Hughes, et G. Zhang, « Rapid evolution and diversification of mammalian α-defensins as revealed by comparative analysis of rodent and primate genes », *Physiological Genomics*, vol. 20, nº 1, p. 1-11, déc. 2004, doi: 10.1152/physiolgenomics.00150.2004.
[66] T. X. Nguyen, A. Cole, et R. Lehrer, « Evolution of primate theta-defensins: a serpentine path to a sweet tooth. », *Peptides*, 2003, Consulté le: 8 novembre 2024. [En ligne]. Disponible sur: https://www.semanticscholar.org/paper/Evolution-of-primate-theta-defensins%3A-a-serpentine-Nguyen-Cole/9610dfab6b23368301507ad7a9506d0ca7951066
[67] H. Sugiarto et P.-L. Yu, « Avian antimicrobial peptides: the defense role of β-defensins », *Biochemical and Biophysical Research Communications*, vol. 323, nº 3, p. 721-727, oct. 2004, doi: 10.1016/j.bbrc.2004.08.162.
[68] T. Cuperus, M. Coorens, A. van Dijk, et H. P. Haagsman, « Avian host defense peptides », *Dev Comp Immunol*, vol. 41, nº 3, p. 352-369, nov. 2013, doi: 10.1016/j.dci.2013.04.019.
[69] G. Zhang et L. T. Sunkara, « Avian Antimicrobial Host Defense Peptides: From Biology to Therapeutic Applications », *Pharmaceuticals*, vol. 7, nº 3, Art. nº 3, mars 2014, doi: 10.3390/ph7030220.

[70] D. Gong *et al.*, « Gallin; an antimicrobial peptide member of a new avian defensin family, the ovodefensins, has been subject to recent gene duplication », *BMC Immunology*, vol. 11, nº 1, p. 12, mars 2010, doi: 10.1186/1471-2172-11-12.
[71] V. Hervé *et al.*, « Three-dimensional NMR structure of Hen Egg Gallin (Chicken Ovodefensin) reveals a new variation of the β-defensin fold », *J Biol Chem*, vol. 289, nº 10, p. 7211-7220, mars 2014, doi: 10.1074/jbc.M113.507046.
[72] D. J. Lynn *et al.*, « Avian beta-defensin nomenclature: a community proposed update », *Immunol Lett*, vol. 110, nº 1, p. 86-89, mai 2007, doi: 10.1016/j.imlet.2007.03.007.
[73] S. S. Harwig *et al.*, « Gallinacins: cysteine-rich antimicrobial peptides of chicken leukocytes », *FEBS Lett*, vol. 342, nº 3, p. 281-285, avr. 1994, doi: 10.1016/0014-5793(94)80517-2.
[74] E. W. Evans, G. G. Beach, J. Wunderlich, et B. G. Harmon, « Isolation of antimicrobial peptides from avian heterophils », *J Leukoc Biol*, vol. 56, nº 5, p. 661-665, nov. 1994, doi: 10.1002/jlb.56.5.661.
[75] C. Zhao, T. Nguyen, L. Liu, R. E. Sacco, K. A. Brogden, et R. I. Lehrer, « Gallinacin-3, an inducible epithelial beta-defensin in the chicken », *Infect Immun*, vol. 69, nº 4, p. 2684-2691, avr. 2001, doi: 10.1128/IAI.69.4.2684-2691.2001.
[76] D. J. Lynn *et al.*, « Bioinformatic discovery and initial characterisation of nine novel antimicrobial peptide genes in the chicken », *Immunogenetics*, vol. 56, nº 3, p. 170-177, juin 2004, doi: 10.1007/s00251-004-0675-0.
[77] Y. Xiao *et al.*, « A genome-wide screen identifies a single β-defensin gene cluster in the chicken: implications for the origin and evolution of mammalian defensins », *BMC Genomics*, vol. 5, nº 1, Art. nº 1, août 2004, doi: 10.1186/1471-2164-5-56.
[78] R. Higgs *et al.*, « The synthetic form of a novel chicken beta-defensin identified in silico is predominantly active against intestinal pathogens », *Immunogenetics*, vol. 57, nº 1-2, p. 90-98, avr. 2005, doi: 10.1007/s00251-005-0777-3.
[79] P.-L. Yu, S. D. Choudhury, et K. Ahrens, « Purification and characterization of the antimicrobial peptide, ostricacin », *Biotechnology Letters*, vol. 23, nº 3, p. 207-210, févr. 2001, doi: 10.1023/A:1005623806445.
[80] C. Thouzeau *et al.*, « Spheniscins, avian beta-defensins in preserved stomach contents of the king penguin, Aptenodytes patagonicus », *J Biol Chem*, vol. 278, nº 51, p. 51053-51058, déc. 2003, doi: 10.1074/jbc.M306839200.
[81] D. Ma *et al.*, « Identification, expression and activity analyses of five novel duck beta-defensins », *PLoS One*, vol. 7, nº 10, p. e47743, 2012, doi: 10.1371/journal.pone.0047743.
[82] R. Wang *et al.*, « Identification and characterization of an avian β-defensin orthologue, avian β-defensin 9, from quails », *Appl Microbiol Biotechnol*, vol. 87, nº 4, p. 1395-1405, juill. 2010, doi: 10.1007/s00253-010-2591-6.
[83] D. Ma *et al.*, « Identification of three novel avian beta-defensins from goose and their significance in the pathogenesis of Salmonella », *Mol Immunol*, vol. 56, nº 4, p. 521-529, déc. 2013, doi: 10.1016/j.molimm.2013.05.227.
[84] O. Hellgren et R. Ekblom, « Evolution of a cluster of innate immune genes (beta-defensins) along the ancestral lines of chicken and zebra finch », *Immunome Res*, vol. 6, p. 3, avr. 2010, doi: 10.1186/1745-7580-6-3.
[85] A. van Dijk, R. Guabiraba, G. Bailleul, C. Schouler, H. P. Haagsman, et A.-C. Lalmanach, « Evolutionary diversification of defensins and cathelicidins in birds and primates », *Molecular Immunology*, vol. 157, p. 53-69, mai 2023, doi: 10.1016/j.molimm.2023.03.011.
[86] T. Ishige, H. Hara, T. Hirano, H. Mannen, T. Kono, et K. Hanzawa, « Basic characterization of avian β-defensin genes in the Japanese quail, Coturnix japonica », *Animal Science Journal*, vol. 87, nº 3, p. 311-320, 2016, doi: 10.1111/asj.12436.
[87] Y. Huang *et al.*, « The duck genome and transcriptome provide insight into an avian influenza virus reservoir species », *Nat Genet*, vol. 45, nº 7, p. 776-783, juill. 2013, doi: 10.1038/ng.2657.

[88] V. Hervé-Grépinet *et al.*, « Purification and Characterization of Avian β-Defensin 11, an Antimicrobial Peptide of the Hen Egg », *Antimicrobial Agents and Chemotherapy*, vol. 54, n° 10, p. 4401-4409, oct. 2010, doi: 10.1128/AAC.00204-10.

[89] N. Guyot, C. Landon, et P. Monget, « The Two Domains of the Avian Double-β-Defensin AvBD11 Have Different Ancestors, Common with Potential Monodomain Crocodile and Turtle Defensins », *Biology (Basel)*, vol. 11, n° 5, p. 690, avr. 2022, doi: 10.3390/biology11050690.

[90] D. Ma, C. Zhou, M. Zhang, Z. Han, Y. Shao, et S. Liu, « Functional analysis and induction of four novel goose (Anser cygnoides) avian β-defensins in response to salmonella enteritidis infection », *Comp Immunol Microbiol Infect Dis*, vol. 35, n° 2, p. 197-207, mars 2012, doi: 10.1016/j.cimid.2012.01.006.

[91] D. Ma *et al.*, « Three novel Anas platyrhynchos avian β-defensins, upregulated by duck hepatitis virus, with antibacterial and antiviral activities », *Mol Immunol*, vol. 49, n° 1-2, p. 84-96, oct. 2011, doi: 10.1016/j.molimm.2011.07.019.

[92] C. Derache *et al.*, « Primary Structure and Antibacterial Activity of Chicken Bone Marrow-Derived β-Defensins », *Antimicrobial Agents and Chemotherapy*, vol. 53, n° 11, p. 4647-4655, nov. 2009, doi: 10.1128/AAC.00301-09.

[93] H. Sugiarto et P.-L. Yu, « Identification of three novel ostricacins: an update on the phylogenetic perspective of beta-defensins », *Int J Antimicrob Agents*, vol. 27, n° 3, p. 229-235, mars 2006, doi: 10.1016/j.ijantimicag.2005.10.013.

[94] G. Bailleul *et al.*, « Systemic Administration of Avian Defensin 7: Distribution, Cellular Target, and Antibacterial Potential in Mice », *Front Microbiol*, vol. 10, p. 541, mars 2019, doi: 10.3389/fmicb.2019.00541.

[95] M. Yang, C. Zhang, X. Zhang, M. Z. Zhang, G. E. Rottinghaus, et S. Zhang, « Structure-function analysis of Avian β-defensin-6 and β-defensin-12: role of charge and disulfide bridges », *BMC Microbiology*, vol. 16, n° 1, p. 210, sept. 2016, doi: 10.1186/s12866-016-0828-y.

[96] A. van Dijk, E. J. A. Veldhuizen, S. I. C. Kalkhove, J. L. M. Tjeerdsma-van Bokhoven, R. A. Romijn, et H. P. Haagsman, « The beta-defensin gallinacin-6 is expressed in the chicken digestive tract and has antimicrobial activity against food-borne pathogens », *Antimicrob Agents Chemother*, vol. 51, n° 3, p. 912-922, mars 2007, doi: 10.1128/AAC.00568-06.

[97] E. W. Evans, F. G. Beach, K. M. Moore, M. W. Jackwood, J. R. Glisson, et B. G. Harmon, « Antimicrobial activity of chicken and turkey heterophil peptides CHP1, CHP2, THP1, and THP3 », *Veterinary Microbiology*, vol. 47, n° 3, p. 295-303, déc. 1995, doi: 10.1016/0378-1135(95)00126-3.

[98] S. NAKNUKOOL, S. HAYAKAWA, et M. OGAWA, « Multiple Biological Functions of Novel Basic Proteins Isolated from Duck Egg White: Duck Basic Protein Small 1 (dBPS1) and 2 (dBPS2) », *J. agric. food chem. (Print)*, vol. 59, n° 9, p. 5081-5086, 2011.

[99] S. Odani, T. Koide, T. Ono, Y. Takahashi, et J. Suzuki, « Covalent Structure of a Low-Molecular-Mass Protein, Meleagrin, Present in a Turkey (Meleagris gallopavo) Ovomucoid Preparation », *The Journal of Biochemistry*, vol. 105, n° 4, p. 660-663, 1989.

[100] Z. Wu *et al.*, « Engineering disulfide bridges to dissect antimicrobial and chemotactic activities of human β-defensin 3 », *Proceedings of the National Academy of Sciences*, vol. 100, n° 15, p. 8880-8885, juill. 2003, doi: 10.1073/pnas.1533186100.

[101] E. Klüver, S. Schulz-Maronde, S. Scheid, B. Meyer, W.-G. Forssmann, et K. Adermann, « Structure−Activity Relation of Human β-Defensin 3: Influence of Disulfide Bonds and Cysteine Substitution on Antimicrobial Activity and Cytotoxicity † », *Biochemistry*, vol. 44, p. 9804-16, août 2005, doi: 10.1021/bi050272k.

[102] C. Nehls *et al.*, « Influence of disulfide bonds in human beta defensin-3 on its strain specific activity against Gram-negative bacteria », *Biochimica et biophysica acta. Biomembranes*, vol. 1862, p. 183273, mars 2020, doi: 10.1016/j.bbamem.2020.183273.

[103] T. T. T. Nguyen, B. Allan, C. Wheler, W. Köster, V. Gerdts, et A. Dar, « Avian antimicrobial peptides: in vitro and in ovo characterization and protection from early chick mortality caused

by yolk sac infection », *Sci Rep*, vol. 11, n° 1, p. 2132, janv. 2021, doi: 10.1038/s41598-021-81734-2.

[104] M. O. Lee *et al.*, « Tissue expression and antibacterial activity of host defense peptides in chicken », *BMC Veterinary Research*, vol. 12, n° 1, p. 231, oct. 2016, doi: 10.1186/s12917-016-0866-6.

[105] D. Ma *et al.*, « Discovery and characterization of Coturnix chinensis avian β-defensin 10, with broad antibacterial activity », *Journal of Peptide Science*, vol. 18, n° 4, p. 224-232, 2012, doi: 10.1002/psc.1437.

[106] S. S. Soman, D. S. Arathy, et E. Sreekumar, « Discovery of Anas platyrhynchos avian beta-defensin 2 (Apl_AvBD2) with antibacterial and chemotactic functions », *Mol Immunol*, vol. 46, n° 10, p. 2029-2038, juin 2009, doi: 10.1016/j.molimm.2009.03.003.

[107] G. Bailleul *et al.*, « The Unusual Resistance of Avian Defensin AvBD7 to Proteolytic Enzymes Preserves Its Antibacterial Activity », *PLoS One*, vol. 11, n° 8, p. e0161573, 2016, doi: 10.1371/journal.pone.0161573.

[108] H. A. Yacoub *et al.*, « Biocidal activity of chicken defensin-9 against microbial pathogens », *Biochemistry and Cell Biology*, déc. 2015, doi: 10.1139/bcb-2015-0121.

[109] N. Guyot, « Structure, function, and evolution of Gga-AvBD11, the archetype of the structural avian-double-β-defensin family - PubMed ». Consulté le: 6 novembre 2022. [En ligne]. Disponible sur: https://pubmed-ncbi-nlm-nih-gov.insb.bib.cnrs.fr/31871151/

[110] S. Lu *et al.*, « Molecular cloning, characterization and tissue distribution of two ostrich β-defensins: AvBD2 and AvBD7 », *Gene*, vol. 552, n° 1, p. 1-7, nov. 2014, doi: 10.1016/j.gene.2014.08.019.

[111] D. Teng *et al.*, « A dual mechanism involved in membrane and nucleic acid disruption of AvBD103b, a new avian defensin from the king penguin, against Salmonella enteritidis CVCC3377 », *Appl Microbiol Biotechnol*, vol. 98, n° 19, p. 8313-8325, oct. 2014, doi: 10.1007/s00253-014-5898-x.

[112] H. A. Yacoub, A. M. Elazzazy, O. A. H. Abuzinadah, A. M. Al-Hejin, M. M. Mahmoud, et S. M. Harakeh, « Antimicrobial activities of chicken β-defensin (4 and 10) peptides against pathogenic bacteria and fungi », *Frontiers in Cellular and Infection Microbiology*, vol. 5, p. 36, 2015, doi: 10.3389/fcimb.2015.00036.

[113] D. Yang, A. Biragyn, L. Kwak, et J. Oppenheim, « Mammalian defensins in immunity: More than just microbicidal », *Trends in immunology*, vol. 23, p. 291-6, juill. 2002, doi: 10.1016/S1471-4906(02)02246-9.

[114] Y. Lai et R. L. Gallo, « AMPed Up immunity: how antimicrobial peptides have multiple roles in immune defense », *Trends in immunology*, vol. 30, n° 3, p. 131, févr. 2009, doi: 10.1016/j.it.2008.12.003.

[115] D. M. Hoover *et al.*, « The structure of human beta-defensin-2 shows evidence of higher order oligomerization », *J Biol Chem*, vol. 275, n° 42, p. 32911-32918, oct. 2000, doi: 10.1074/jbc.m006098200.

[116] D. J. Schibli *et al.*, « The Solution Structures of the Human β-Defensins Lead to a Better Understanding of the Potent Bactericidal Activity of HBD3 against Staphylococcus aureus », *Journal of Biological Chemistry*, vol. 277, n° 10, p. 8279-8289, mars 2002, doi: 10.1074/jbc.M108830200.

[117] C. Landon, C. Thouzeau, H. Labbé, P. Bulet, et F. Vovelle, « Solution structure of spheniscin, a beta-defensin from the penguin stomach », *J Biol Chem*, vol. 279, n° 29, p. 30433-30439, juill. 2004, doi: 10.1074/jbc.M401338200.

[118] C. Landon, C. Thouzeau, H. Labbé, P. Bulet, et F. Vovelle, « Solution structure of spheniscin, a beta-defensin from the penguin stomach », *J Biol Chem*, vol. 279, n° 29, p. 30433-30439, juill. 2004, doi: 10.1074/jbc.M401338200.

[119] C. Derache *et al.*, « Initial insights into structure-activity relationships of avian defensins », *J Biol Chem*, vol. 287, n° 10, p. 7746-7755, mars 2012, doi: 10.1074/jbc.M111.312108.

[120] G. R. Zimmermann, P. Legault, M. E. Selsted, et A. Pardi, « Solution Structure of Bovine Neutrophil .beta.-Defensin-12: The Peptide Fold of the .beta.-Defensins Is Identical to That of the Classical Defensins », *Biochemistry*, vol. 34, nº 41, p. 13663-13671, oct. 1995, doi: 10.1021/bi00041a048.
[121] A. van Dijk, E. J. A. Veldhuizen, et H. P. Haagsman, « Avian defensins », *Veterinary Immunology and Immunopathology*, vol. 124, nº 1, p. 1-18, juill. 2008, doi: 10.1016/j.vetimm.2007.12.006.
[122] M. Yang, C. Zhang, M. Z. Zhang, et S. Zhang, « Novel synthetic analogues of avian β-defensin-12: the role of charge, hydrophobicity, and disulfide bridges in biological functions », *BMC Microbiology*, vol. 17, nº 1, p. 43, févr. 2017, doi: 10.1186/s12866-017-0959-9.
[123] D. M. Hoover, Z. Wu, K. Tucker, W. Lu, et J. Lubkowski, « Antimicrobial Characterization of Human β-Defensin 3 Derivatives », *Antimicrob Agents Chemother*, vol. 47, nº 9, p. 2804-2809, sept. 2003, doi: 10.1128/AAC.47.9.2804-2809.2003.
[124] M. Mandal, M. V. Jagannadham, et R. Nagaraj, « Antibacterial activities and conformations of bovine β-defensin BNBD-12 and analogs:structural and disulfide bridge requirements for activity », *Peptides*, vol. 23, nº 3, p. 413-418, mars 2002, doi: 10.1016/S0196-9781(01)00628-3.
[125] V. Krishnakumari, S. Ambure, S. Singh, et R. Nagaraj, « Single Disulfide and Linear Analogues Corresponding to the Carboxy-Terminal Segment of Bovine β-Defensin-2: Effects of Introducing the β-Hairpin Nucleating Sequence d -Pro-Gly on Antibacterial Activity and Biophysical Properties † », *Biochemistry*, vol. 42, p. 9307-15, sept. 2003, doi: 10.1021/bi034403y.
[126] C. Derache *et al.*, « Initial Insights into Structure-Activity Relationships of Avian Defensins », *The Journal of biological chemistry*, vol. 287, p. 7746-55, déc. 2011, doi: 10.1074/jbc.M111.312108.
[127] M. Dathe et T. Wieprecht, « Structural features of helical antimicrobial peptides: their potential to modulate activity on model membranes and biological cells », *Biochim Biophys Acta*, vol. 1462, nº 1-2, p. 71-87, déc. 1999, doi: 10.1016/s0005-2736(99)00201-1.
[128] T. Ganz, « Defensins: antimicrobial peptides of innate immunity », *Nat Rev Immunol*, vol. 3, nº 9, p. 710-720, sept. 2003, doi: 10.1038/nri1180.
[129] K. A. Brogden, « Antimicrobial peptides: pore formers or metabolic inhibitors in bacteria? », *Nat Rev Microbiol*, vol. 3, nº 3, p. 238-250, mars 2005, doi: 10.1038/nrmicro1098.
[130] H. Sugiarto et P.-L. Yu, « Mechanisms of action of ostrich beta-defensins against Escherichia coli », *FEMS Microbiol Lett*, vol. 270, nº 2, p. 195-200, mai 2007, doi: 10.1111/j.1574-6968.2007.00642.x.
[131] C. Landon *et al.*, « Real-Time Fluorescence Microscopy on Living E. coli Sheds New Light on the Antibacterial Effects of the King Penguin β-Defensin AvBD103b », *International Journal of Molecular Sciences*, vol. 23, nº 4, Art. nº 4, janv. 2022, doi: 10.3390/ijms23042057.
[132] K. A. Sochacki, K. J. Barns, R. Bucki, et J. C. Weisshaar, « Real-time attack on single Escherichia coli cells by the human antimicrobial peptide LL-37 », *Proc Natl Acad Sci U S A*, vol. 108, nº 16, p. E77-81, avr. 2011, doi: 10.1073/pnas.1101130108.
[133] A. Agrawal et J. C. Weisshaar, « Effects of alterations of the E. coli lipopolysaccharide layer on membrane permeabilization events induced by Cecropin A », *Biochimica et Biophysica Acta (BBA) - Biomembranes*, vol. 1860, nº 7, p. 1470-1479, juill. 2018, doi: 10.1016/j.bbamem.2018.04.009.
[134] H. A. Yacoub, A. M. Elazzazy, O. A. H. Abuzinadah, A. M. Al-Hejin, M. M. Mahmoud, et S. M. Harakeh, « Antimicrobial activities of chicken β-defensin (4 and 10) peptides against pathogenic bacteria and fungi », *Front Cell Infect Microbiol*, vol. 5, p. 36, 2015, doi: 10.3389/fcimb.2015.00036.
[135] C. Landon *et al.*, « Real-Time Fluorescence Microscopy on Living E. coli Sheds New Light on the Antibacterial Effects of the King Penguin β-Defensin AvBD103b », *Int J Mol Sci*, vol. 23, nº 4, p. 2057, févr. 2022, doi: 10.3390/ijms23042057.

Chapter 5: Insights into AvBD103b's antibacterial mechanism

Table of contents

I. Introduction

1. The king penguin defensin AvBD103b

a. The discovery of AvBD103b

In the early 2000s and in the Possession Island, AvBD103b, initially named Spheniscin-2 (Sphe-2), was discovered in the stomach content of the male King penguin *Aptenodytes patagonicus*, and characterized by mass spectrometry (MS) analyses [1]. With other antimicrobial agents, AvBD103b preserves intact food in the penguin's stomach from attack by microorganisms for 2-3 weeks at body temperature. This enables the male to feed the newly born chick for ten days in case the return of the female is delayed [2].

b. Structural and functional peculiarities of AvBD103b

AvBD103b is a 38-amino acid defensin, possessing 10 Arginine residues and no anionic residue (Figure 1a), which makes it the most cationic (pI 12.95) of all avian defensins found to date. The solution NMR structure, the first one obtained for an avian defensin, reveals a three-dimensional structure similar to mammalian β-defensins with the presence of a three-stranded antiparallel β-sheet and a short α-helix in the N-terminus, stabilized by an array of three disulfide bridges, typical or vertebrate β-defensins [3] (Figure 1b). AvBD103b surface displays a hydrophobic patch, particularly preserved in avian defensins but not in mammalian β-defensins.

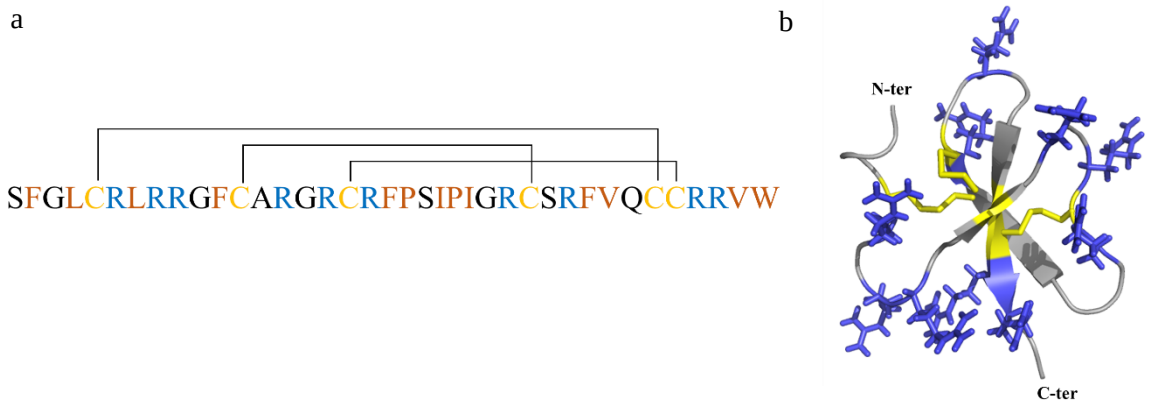

Figure 1: Structural features of AvBD103b defensin. (a) The primary sequence is composed of 38 residues with 10 Arg, highlighted in blue, and a high hydrophobic content, highlighted in orange. AvBDD103b has six cysteines shown in yellow in the sequence and is linked by three disulfide bridges as follows: C1-C5, C2-C4 and C3-C6. (b) 3D structure of AvBD103b (PDB:1ut3) resolved by solution NMR [3], showing a three-stranded antiparallel β-sheet and an α-helix structure at the N-terminus (N-ter).

AvBD103b is active against a large panel of microorganisms including Gram positive (Gram+) and Gram negative (Gram-) bacteria, and filamentous fungi [166, 172] (Table 1). This broad spectrum of

activity is thought to be largely due to its high cationicity [1], as AMPs activity depends on electrostatic interactions with negatively charged microbial membranes [5]. It has bactericidal activity against Gram+ bacteria, while it shows a bacteriostatic effect on the majority of Gram- bacteria [1]. The cytotoxicity of AvBD103b to mammalian cells assessed by its hemolytic activity in human red blood cells showed that even up to 48 µM peptide concentration, AvBD103b exhibited low hemolysis (~2.6%) [4]. Among all β-defensins, only two are reported to be salt-insensitive: AvBD103b and the human β-defensin HBD3 [1, 2]. AvBD103b retains its activity in physiological concentrations of salts (~308 mOsm/L and even higher) against *S. aureus* and *E. coli* [3]. Salt insensitivity is a considerable advantage in clinical therapeutics for combating pathogens capable of thriving under physiological conditions, but also in salt-rich body fluids, as in the case of cystic fibrosis patients. In these patients, the surface fluid of the respiratory tract has a high concentration of sodium chloride [8], and fighting infections developing in such environment requires antimicrobial compounds that are efficient in high concentration of salts [9].

Table 1: Antimicrobial activity of AvBD103b defensin. Data obtained from ref [1, 2, 3]

Pathogens	**MIC in µM**
Gram-positive bacteria	
M. luteus	1.5-3.0[1]
B. subtilis	0.8-1.5[1]
S. aureus	1.5-3.0[1]
S. saprophyticus	1.5-3.0[1]
S. haemolyticus	1.5-3.0[1]
L. monocytogenes	6-12[1]
Enterococcus faecalis	0.75[2]
Gram-negative bacteria	
***Escherichia coli* SBS 363**	0.8-1.5[1]
***Salmonella enteritidis* CVCC3377**	1.5[2]
***E. coli* 1106**	1.5-3.0[1]
Pseudomonas aeruginosa CVCC2087	1.5[2]
S. typhimurium	6-12[1]
K. pneumoniae	50-100[1]
***P. Aeruginosa* ATCC 82118**	6-12[1]
Fungi	
Neurospora crassa	3-6[1]
Aspergillus Fumigatus	3-6[1]

[1]The MIC value corresponded to the interval of concentration [a]-[b], where [a] is the highest concentration tested at which the bacteria are growing and [b] is the lowest concentration that cause 100% inhibitory growth [1].
[2]The MIC assay was conducted in Mueller-Hinton (MH) and determined as the lowest peptide concentration at which no bacterial growth was observed [4].

2. Mechanism of action of AvBD103b: state of the art

Our current understanding of how AMPs attack bacteria has been shaped by bulk assays, model membrane assays, and hypotheses based on studies of other AMPs, which may not reflect the real events and/or the complete picture of the MOA. Furthermore, only a few studies have examined the MOAs of avian β-defensins (see chapter 4), concluding that membrane interaction is unlikely to be the main cause of death. The majority of these data were obtained from experiments carried out at low salt concentrations, typically 5-10 nM total salts, which is far from physiological conditions. Finally, almost

all this knowledge about the modes of action of β-defensins is not collected on living bacteria, which is essential for dissecting the actual mechanism of how AMPs work in nature.

The effects of AvBD103b on *Salmonella enteritidis* have been investigated mostly under low salt concentrations and not on live bacteria [4]. This study supports the idea that AvBD103b acts by a complex antibacterial mechanism, involving other mechanisms than only causing membrane damage. Based on gel retardation assay, interference with intracellular DNA has also been suggested as a possible effect of AvBD103b [4]. Given the highly positive charge of AvBD103b (+10) and the absence of a control for comparison (with a similar net charge), binding to anionic DNA cannot be considered a specific interaction.

Recently, C. Landon and Coll. started to investigate the mechanism by which AvBD103b attacks living *Escherichia coli* bacteria in real time and at physiological concentration of salts. This study is based on the use of an innovative technique, single-cell fluorescence imaging, developed by J.C. Weisshaar. This approach had hitherto only been applied to study the antibacterial mechanism of membrane-active helical linear AMPs. Examples include the attack of labeled LL-37, a human antimicrobial peptide, and Cecropin A, an AMP isolated from the moth *Hyalophora cecropia*, on *E. coli* [10, 13]. Also, the membrane permeabilization effect of alamethicin, a fungal AMP produced by *Trichodermaon*, on *Bacillus subtilis* has been studied [12]. AvBD103b was the first β-defensin for which its MOA has been examined using this technique [13].

a. Single-cell fluorescence imaging to study AMPs' MOA

This technique has the enormous advantage of enabling the antibacterial mechanism of a MOA to be monitored in real time under physiological conditions (pH, temperature and salt concentrations) and on growing live bacteria. It is therefore a more effective method for exploring the "more real MOA" than other conventional techniques, under non-physiological conditions and/or on fixed or ingrowing bacteria.

Single-cell imaging is based on the use of time-resolved fluorescence microscopy to dissect the course of events during an AMP attack on a single cell of the Gram- bacterial specie, *E. coli* JCW10 a strain expressing green fluorescent protein (GFP) in the periplasm (see Figure 2). This technique enables simultaneous direct measurement of (i) cell growth judged by cell length measured from phase contrast images, (ii) outer membrane (OM) permeabilization, and (iii) cytoplasmic membrane permeabilization, on a single cell. The permeabilization of both membranes is judged by the fluorescence of the GFP and a DNA staining dye, Sytox orange. Directly monitoring the effects of an AMP on living cells by means

of the measurements mentioned should provide a better understanding of how AMPs attack bacterial cells, as close to reality as possible.

As reported in Chapter 4, AMPs can be classified, according to their MOAs, into membrane-active peptides and non-membrane-permeabilizing peptides. Although they all disrupt the cell envelope to a greater or lesser extent, the cascade of events in the MOA observed by single-cell fluorescence imaging will differ. Indeed, the speed, intensity and concomitance of disruption/permeabilization of the OM and/or CM are different between membrane-active and non-permeabilizing peptides.

This biophysical technique uses fluorophores, providing a less toxic approach to cell imaging than electron microscopy, which requires fixed cells. The use of fluorescence microscopy with a sensitive camera, powerful lasers for excitation, and fluorescent probes such as GFP and Sytox orange can be achieved with remarkable sensitivity. Moreover, fluorescence microscopy is coupled with the use of a microfluidic flow chamber, which allows constant renewal of the bacterial growth medium and the introduction of a constant flow of an AMP solution. This enables us to image growing cells with minimal disturbance other than the desired antimicrobial stress.

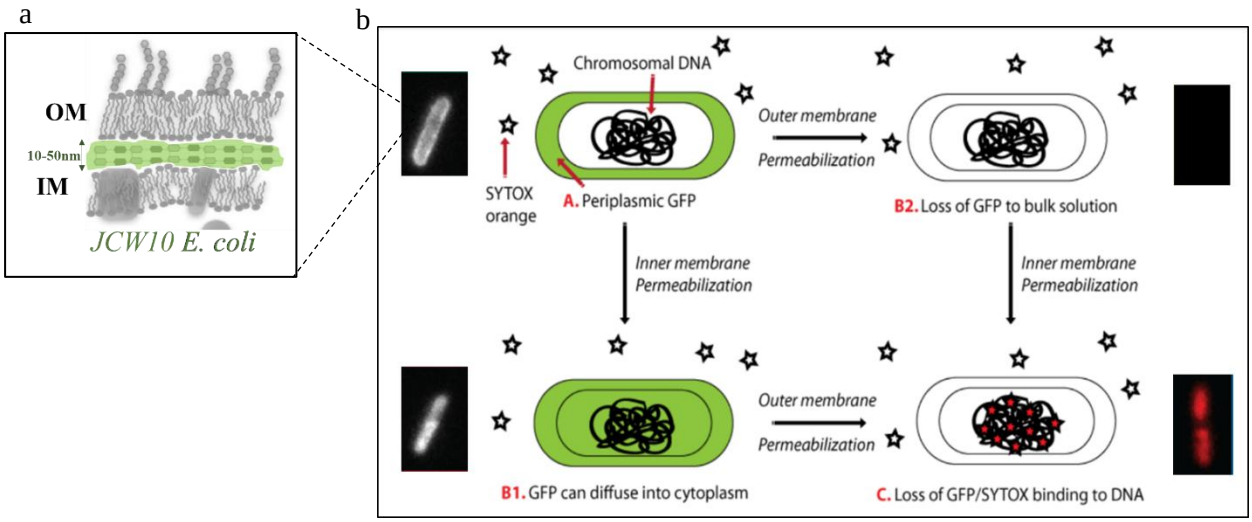

Figure 2: Schematic view of cell membrane permeabilization following AMP attack of bacteria using single-cell fluorescence microscopy. (a) *E. coli* JCW10 strain expressing GFP in the periplasm, the approximately 10-50 nm-thick space between the outer membrane (OM) and the cytoplasmic membrane (CM) of bacteria. (b) *E. coli* JCW10 with periplasmic GFP exposed to bacterial growth medium containing AMP and Sytox, a DNA-binding dye (A). There are two theoretical ways by which AMP could affects membrane permeabilization: either it first permeabilizes the OM, allowing the GFP to be lost into the bulk solution (B2), then it permeabilizes the CM, which can be seen by Sytox's strongly fluorescent binding to DNA (C); or AMP first breaks the CM, permitting periplasmic GFP to diffuse into the cytoplasm (B1), then it permeabilizes the OM, which allows Sytox entry, DNA binding, and fluorescence (C).

b. Mechanism of AvBD103b action using single-cell fluorescence imaging

To begin to understand the peptide's MOA, it is essential to study how the native version of the peptide, and not a labeled or modified version, deploys its antibacterial activity without risk interference with its mechanism. The effects of AvBD103b (1x MIC) on *E. coli* JCW10 were monitored in real time for one hour by widefield microscopy under physiological conditions (medium ~ 280 mOsmol/L, pH 7.4, 30°C). The use of widefield microscopy has the advantage of enabling the imaging and monitoring of peptide effects on a large number of bacterial cells at the same time. This study showed that AvBD103b inhibits *E. coli* growth in two phases (Figure 3) [13].

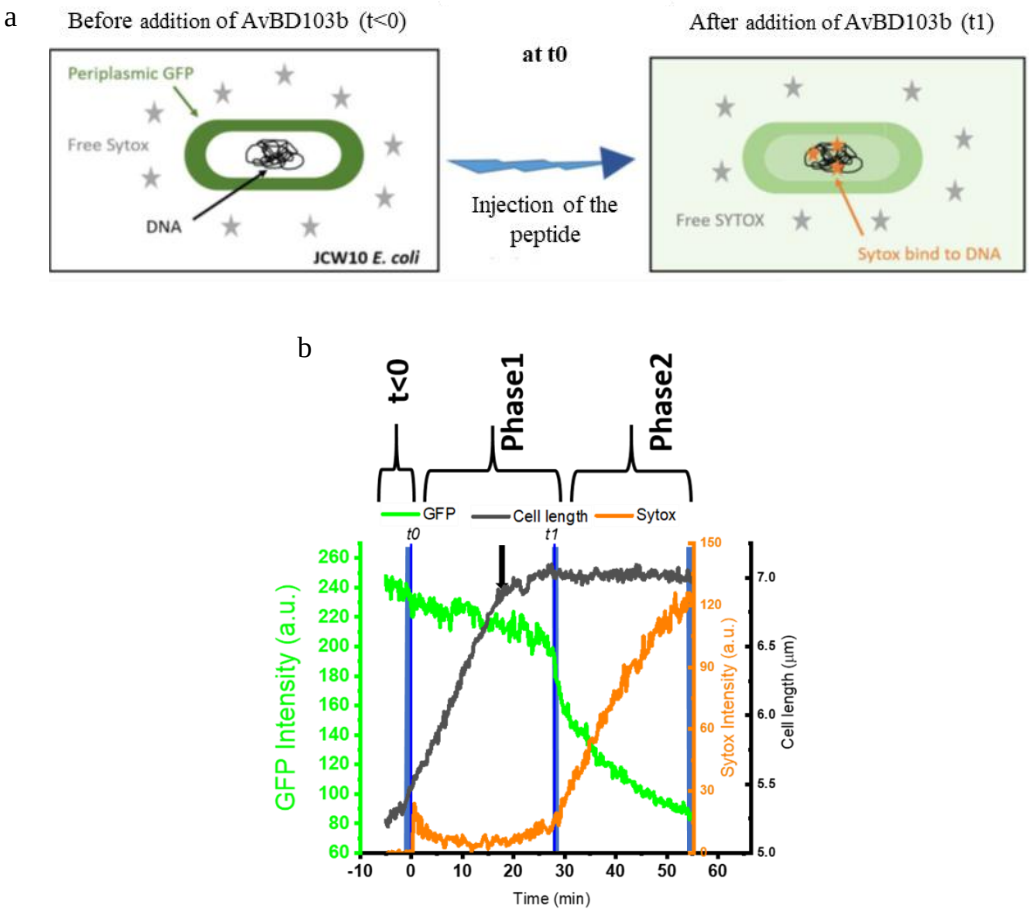

Figure 3: Effects of 1x MIC AvBD103b on a representative *E. coli* JCW10 strain expressing periplasmic GFP [13]**.** (a) Schematic view of *E. coli* JCW10 expressing periplasmic GFP at t<0 and at a time t1 after injected AvBD103b, a transient permeabilization of both the OM and CM membranes of the cell occurs. (b) Time dependence of total GFP intensity (in green, arbitrary units), of total Sytox intensity (in orange, arbitrary units), transition at time t1 (28 min for this example) is highlighted in blue. Cell length (in black, in µm) is calculated from phase contrast image. The black arrow indicates growth halting. The flow of peptide begins at t = 0. Abrupt transition at time t1 (28 min for this example) is highlighted in blue.

Growth halting

Phase 1 is characterized by a normal growth of the bacteria, as indicated by cell length measurements (Figure 3b, black arrow). The time when growth halts define the end of this phase 1. During phase 1, the total integrated GFP fluorescence intensity does not decrease, except by a weak photobleaching.

Slow and transient membrane permeabilization

During phase 2, a transient permeabilization of OM and IM occurs at a time t1, where two concomitant events occur (i) the abrupt loss of 15-20% of GFP fluorescence to bulk solution through the OM, and (ii) the appearance of a weak Sytox fluorescence signal, that is as a consequence of its DNA binding after crossing both OM and CM [13]. Note that for some bacteria, part of the GFP is able to reach the cytoplasm through the CM, suggesting that part of AvBD103b can enter the cell and interact with cytoplasmic partner(s).

AvBD103b causes a partial and transient concomitant permeabilization of the two *E. coli* membranes. These membranes permeabilization profiles are different from those observed for LL-37 cathelicidin for example, a typical lytic AMPs. Indeed, cathelicidin induces rapid release (within minutes of peptide injection) of periplasmic GFP completely into the cellular environment due to OM permeabilization, followed (not concomitantly) by a sharp increase in Sytox fluorescence due to CM permeabilization [10].

No stereospecific interaction

The mirror image of the natural *L*-AvBD103b, composed of *D*-amino-acids, showed the same activity (MIC assay) and the same cascade of events observed by single-cell fluorescence imaging in terms of membrane permeabilization and effects on cell growth. It would not be the case if AvBD103b acted through a strong, specific interaction with a given molecular partner [13]. The absence of any significant stereoselective interaction with a cellular partner at any stage of the process would prevent bacteria from developing a resistance mechanism, an undeniable advantage for the development of new antibiotics.

Overall, these preliminary data of AvBD103b' MOA study are in favor of a non-disruptive membrane mechanism involving possible disruption of simultaneous processes in a non-stereospecific way. The literature increasingly shows that many AMPs interact with many molecular targets, intracellular or membrane, rather than just one, and that they disrupt several cellular processes at once [14, 15]**. The possibility of a pathogen developing a mutation capable of resisting these AMPs is diminished by their multiple effects** [16, 17, 18]**.**

To date, based on the work of Landon and colleagues [13], several hypotheses are possible: (i) AvBD103b, or at least part of it, may be able to access the cell cytoplasm and interact non-specifically with a variety of polyanionic intracellular partners (i.e. DNA, RNA, proteins, etc.), like sand in a

gearbox. (ii) The peptide may remain on the cell surface and interact non-specifically with cell wall components such as the LPS layer or peptidoglycan. (iii) Nor can we rule out the possibility that part of AvBD103b remains on the surface and part reaches the cytoplasm. Further studies are needed to clarify these points concerning AvBD103b's MOA.

3. Aim of this work

My overall aim in this part of the thesis is to follow the real-time trajectory of a fluorescent version of AvBD103b on living bacteria using single-cell fluorescence imaging, the method described above. To achieve this, the following steps are required: **(i) transpose the refined method and adapt it to the standard widefield microscopy available in the CBM**. Control peptides, such as LL-37 and AvBD103b, are used for the implementation of this technique; (**ii) chemically label the defensin AvBD103b with a fluorescent dye and verify that the labeling has no impact on the activity or MOA of the native version of AvBD103b**; and **(iii)** perform preliminary experiments with fluorescently-tagged AvBD103b using single-cell fluorescence imaging **to define its precise localization(s) and spatial distribution throughout progression.** The goal is to hypothesize privileged partners that could engage with AvBD103b along the MOA process.

II. Results and discussion

1. Transposition of single-cell fluorescence imaging and control experiments

The aim of these fluorescence microscopy experiments is to monitor in real time the permeabilization effect of peptides on outer and cytoplasmic membranes vs. time on individual living bacterial cells under physiological conditions (salt concentration, pH and temperature). To achieve this, fluorescence images are interleaved with phase contrast images and are tracked over time. Fluorescence signals measurements from 2 channels provide a direct readout of membrane permeabilization events. A green channel monitors emission from GFP, which is expressed and transported to the 10–50 nm thick space between the OM and CM of bacteria. An Orange channel monitors emission from Sytox Orange, which is added to the growth bacterial media. For these experiments, the use of fluorescence microscopy is coupled to a home-built microfluidic chamber where bacteria are adhered to a previously deposited layer of poly-L-lysine. The flow of cell growth medium keeps the bacteria alive and growing in microfluidic chamber.

a. Considerations while transposing the fluorescence microscopy technique

Previous studies on the MOA of AMPs using single-cell fluorescence imaging have been carried out under optimized conditions, i.e., with a standard protocol for biological sample preparation and a microscope specifically optimized for this application (a non-standard microscope). This biophysical technique is particularly sensitive and directly dependent on experimental and/or instrumental parameters. Consequently, an important step in the transposition of this refined method was required to

adapt it to another cell growth medium and to a standard widefield microscope available in our laboratory.

Modification of the cell growth media

For these biophysical experiments, the growth medium must meet certain specifications to be suitable for not only fluorescence microscopy, but also GFP expression and induction in bacteria. Ideally, we would like a rich, chemically defined medium that has low background fluorescence, and provides doubling times similar to those of rich, undefined media (~20 min). All previous work by James C. Weisshaar's group have used EZ Rich Defined Medium (EZRDM) as a growth medium, formulated by Teknova and which works well for *E. coli*. Unfortunately, this medium, which is commercially available in the USA, is not resold in Europe. It is virtually impossible to have it delivered from the USA, and there is no guarantee that the temperature conditions during transport will be respected by the supplier. EZRDM medium contains vitamins, which are temperature-sensitive products (store at -20°C). To fix this issue, we tried a traditional growth media for bacteria i.e. LB media which gave fast doubling times (~25 min), however was not amenable to fluorescence microscopy. It contains contaminants that cause background fluorescence, and its chemical composition is not exactly defined. Besides, a good GFP expression in the bacterial periplasm could not be obtained, the expression of the GFP has been reported to depend of the growth media [19]. We finally settled on the chemically defined M9 minimal medium supplemented by 0.4% glucose (M9 supp. media) as carbon source. M9 supp. media has little background fluorescence, is suitable for GFP expression, but gave slower doubling times compared to EZRDM. The doubling time of *E. coli* length in M9 supp. media at 30 °C was ~80 min in bulk, compared to ~50 min in EZRDM media [181], which reduced experimental throughput.

Optimization of the parameters for time-lapse video acquisition

Imaging living cells with fluorescence microscopy has become an essential tool for researchers to understand biological processes at the cellular level. Among the fundamental considerations when designing and carrying out fluorescence microscopy experiments is the availability and suitability of equipment (hardware, e.g., excitation sources, detection systems..) for the intended applications [20].
The previous mechanistic study of AvBD103b was carried out using a non-standard microscope (figure 4a) specially adapted to this in vivo microscopic approach. At the CBM, where we performed all the fluorescence microscopy experiments in this part of the thesis, there is a standard widefield fluorescence microscope (Figure 4b) used for multiple biological applications.

a b

Figure 4: Fluorescence microscope used for single-cell imaging during AMP attack. (a) Widefield microscope previously used to study the MOA of AvBD103b (Madison university, WI, USA). (b) Widefield microscope used during the thesis experiments (CBM, Orléans).

The main material differences between the two microscopes are listed in Table 2.

Table 2: Major hardware differences between the microscope previously used to study the MOA of AvBD103b (Madison university, WI, USA) and the microscope used during the thesis experiments (CBM, Orléans)

Equipment	Previous work	Thesis work
Microscope	Nikon Eclipse Ti inverted microscope	Zeiss Axio Observer Z7 inverted
Camera	Electron Multiplying CCD Camera (EMCCD)	Complementary metal-oxide-semiconductor (CMOS)
Light source	Laser	Light Emitting Diode (LED)
Focus system	Perfect Focus System (PFS)	Auto focus (definite focus) module Zeiss
Light intensities	~5 W/cm2 and ~2.5 W/cm2 at 488 and 561 nm	Not determined/unknown
Heating system	Heater block	Incubation system
Filters	HQ510/20 and HQ600/50M for the green and orange channel	512/25 and 573/40 for the green and orange channel
Overall magnification	150x	100x

These differences have an impact on signal fluorescence detection, photobleaching, temperature regulation and hence bacterial growth, field of view size, resolution and focus maintenance. Consequently, the transposition of single-cell imaging by fluorescence microscopy must take this hardware difference into account, and optimizations for time-lapse video acquisition have therefore been carried out.

We first checked the localization of GFP and the absence of Sytox fluorescence before the onset of flow peptide (t < 0 min). The expressed GFP localization is characterized by a typical transverse "kamel" intensity profile from 488 nm channel along the white line (Figure 5). This indicates that the expression of the GFP is well induced and is mostly located in the periplasmic space as desired. An Orange channel monitors emission from Sytox Orange, which was added to the growth bacterial media at 20 nM as a final concentration. Prior to the onset of flow peptide (t < 0 min), no bacterial cells fluoresce at 548 nm due to Sytox dye binding to DNA, confirming the integrity of the bacterial membranes (Figure 5).

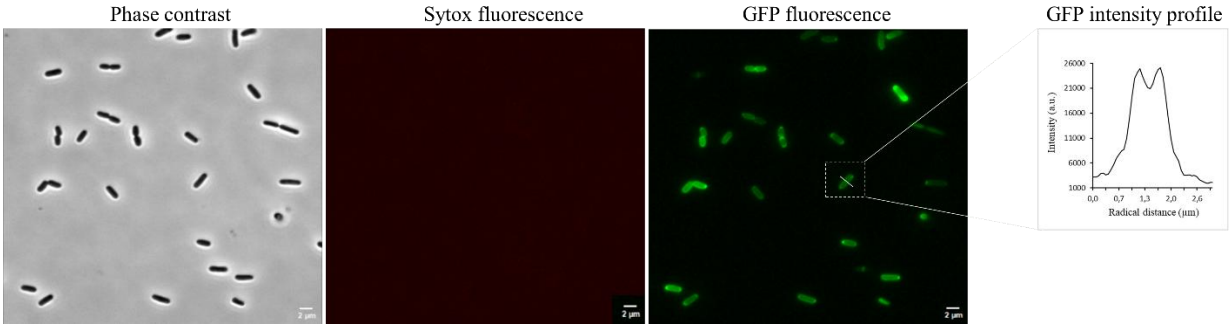

Figure 5: A snapshot of a typical field of cells monitored by time-lapse widefield microscopy at t < 0 before the set of peptide flow and typical double-peaked transverse intensity profile along the white line.

The second step was to optimize GFP excitation, to get a good initial fluorescence intensity, and to minimize photobleaching during the 60 min video monitoring (Table 3).

Table 3: Optimization of GFP excitation (exposure time and light intensity) to overcome the photobleaching problem over 60 minutes of video-microcopy with an image every 12 s.

Tested conditions	1	2	3	4	5
Light source intensity (%)	100	100	50	50	20
Exposure time (ms)	400	200	200	100	100

Finally, maintaining focus during 60 minutes of imaging under flow was also a challenge in these experiments. We unsuccessfully tried out the Z-stack, which allows us to take optical sections and create three-dimensional representations of a specimen, and finally we used the Auto focus module (also known as definite focus) from zeiss®.

b. Real-time effects of the control peptide LL-37 on bacterial membranes

To define the experimental parameters, we used the human cathelicidin LL-37 as a peptide control with a lytic mechanism. In two-color experiments (GFP Green and Sytox Orange), the effects of LL-37 on

membrane of single *E. coli* cells were monitored using time-lapse imaging over 48 min in our experimental set up conditions. A snapshot of a field of cells exposed to 16 µM (2x MIC) of LL-37 for t = 2.5 min and t = 47.5 min is shown in Figure 6. A typical effect on a single cell is demonstrated in Figure 7. Results indicate that LL-37 caused 50% loss of GFP, reflecting OM permeabilization, followed by an increase in Sytox fluorescence, reflecting both OM and CM permeabilization. Similar cascades of events have been reported previously for this peptide by J. C. Weisshaar and Colleagues [10]. However, in our conditions LL-37 permeabilization activity is relatively slow compared with the published experiments considered as reference. This is because the growth medium, e.g. Minimal M9 supp. 0.4% glucose, used in our experiments, is less rich than EZRDM medium, which slows bacterial growth and division and therefore slows peptide activity.

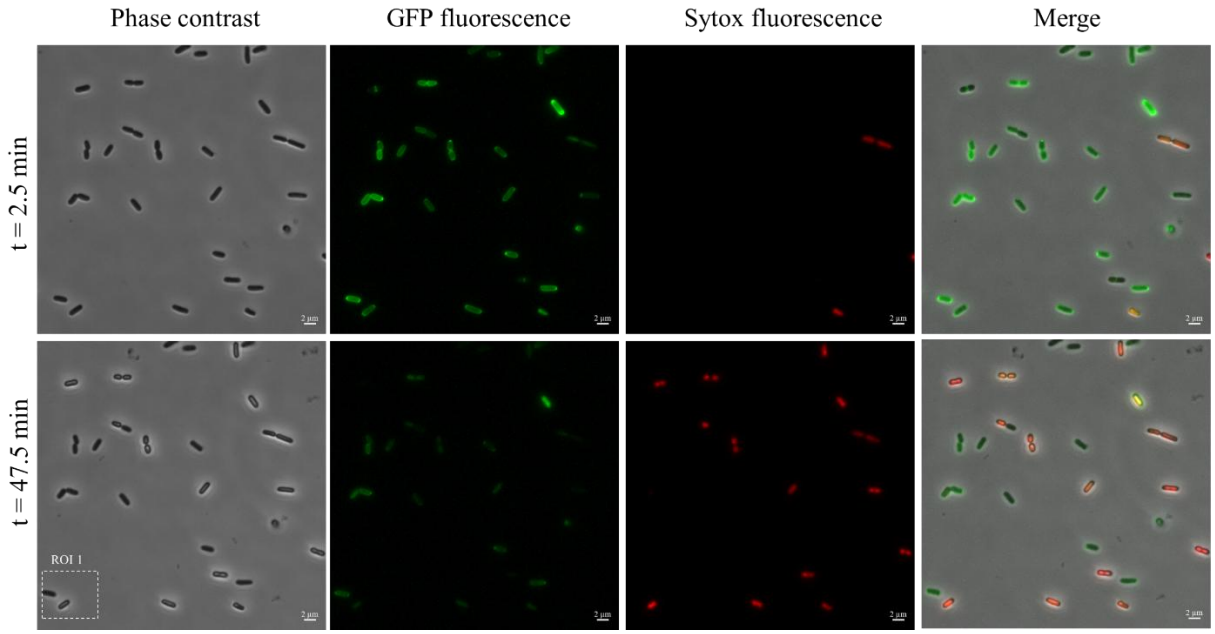

Figure 6: Microscopy field of cells exposed to a constant flow (0.2 mL/h) of 16 µM LL-37 under flow in the microfluidic chamber. Field of the view images are shown in phase contrast, GFP green fluorescence (488 nm) and Sytox Orange fluorescence (548 nm) at t = 2.5 min and t = 47.5 min**.**

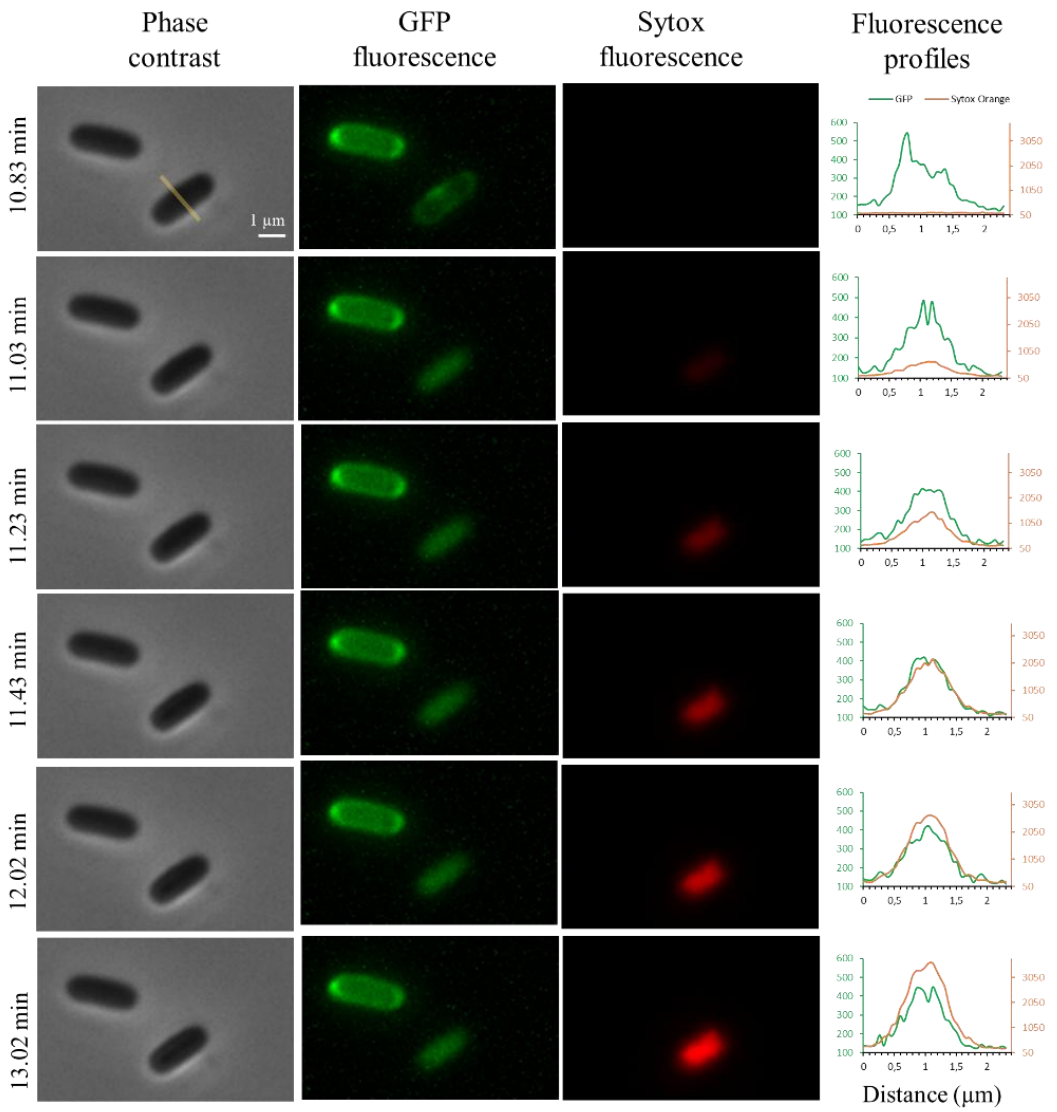

Figure 7: Imaging and analysis of one typical *E. coli* cell (ROI 1 in figure 6) during attack by LL-37. Sequence of events during attack by LL-37 at 16 µM of a single *E. coli* cell expressing periplasmic GFP. Medium also contains Sytox Orange at 20 nM. The snapshots are taken from a single movie at the times shown on the left. (Scale bar, 1 µm). For each event, images are shown in phase contrast, green fluorescence channel (488 nm, GFP) and then orange fluorescence channel (548 nm, Sytox Orange). Transverse intensity profiles of green and orange channels along the yellow line in the phase contrast snapshot are shown.

c. Preliminary experiments with *AvBD103b*

Preliminary experiments were carried out with the native version of AvBD103b. In two-color experiments (GFP Green and Sytox Orange), the effects of AvBD103b on membrane of single *E. coli* cells were monitored using time-lapse imaging over 70 min in our experimental set up conditions. A

snapshot of a field of cells exposed to 24 µM of the peptide for t = 0 and t = 70 min is shown in Figure 8. A typical effect on a single cell under our conditions is demonstrated in Figure 9. The results indicate that AvBD103b induced slow permeabilization (after ~37 min of treatment) of the OM and CM membranes, concomitantly. The increase in Sytox fluorescence was small compared with that observed with LL-37 treatment. Similar observations have been reported previously for this peptide by Landon and Colleagues [13].

Similar to LL-37, in our conditions the activity of AvBD103b is relatively slow compared with the published experiments considered as reference. This is because the growth medium, e.g. Minimal M9 supp. 0.4% glucose, used in our experiments, is less rich than EZRDM medium, which slows bacterial growth and division and therefore slows peptide activity.

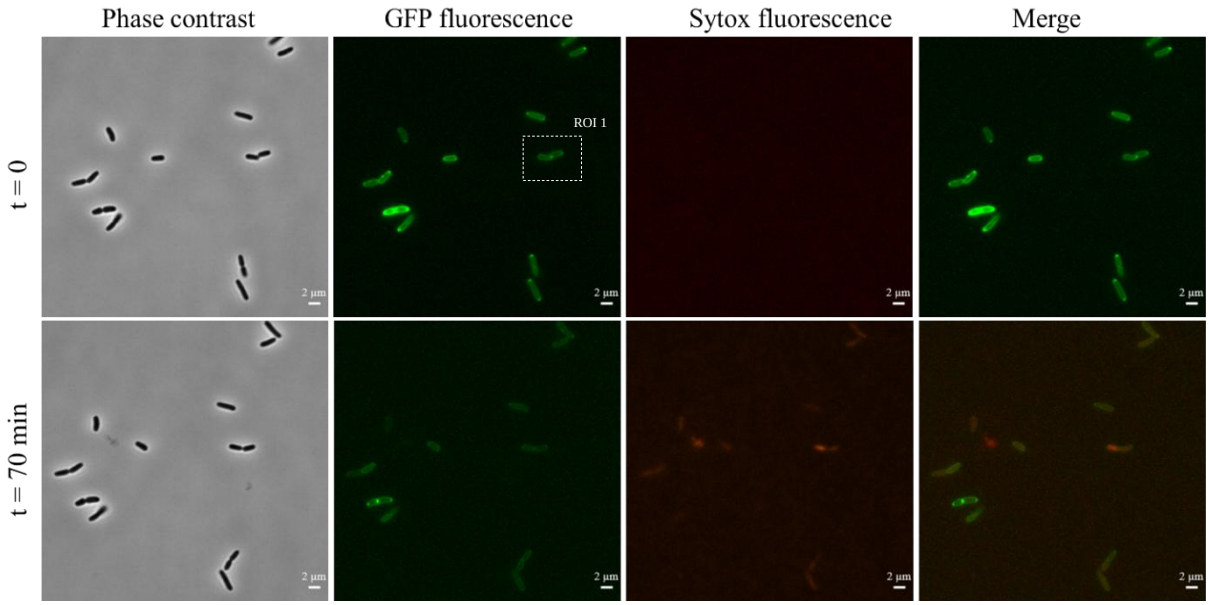

Figure 8: Microscopy field of cells exposed to a constant flow (0.2 mL/h) of 24 µM AvBD103b under flow in the microfluidic chamber. Field of the view images are shown in phase contrast, GFP green fluorescence (488 nm), Sytox Orange fluorescence (548 nm) and merge (GFP + Sytox) at t = 0 and t = 70 min.

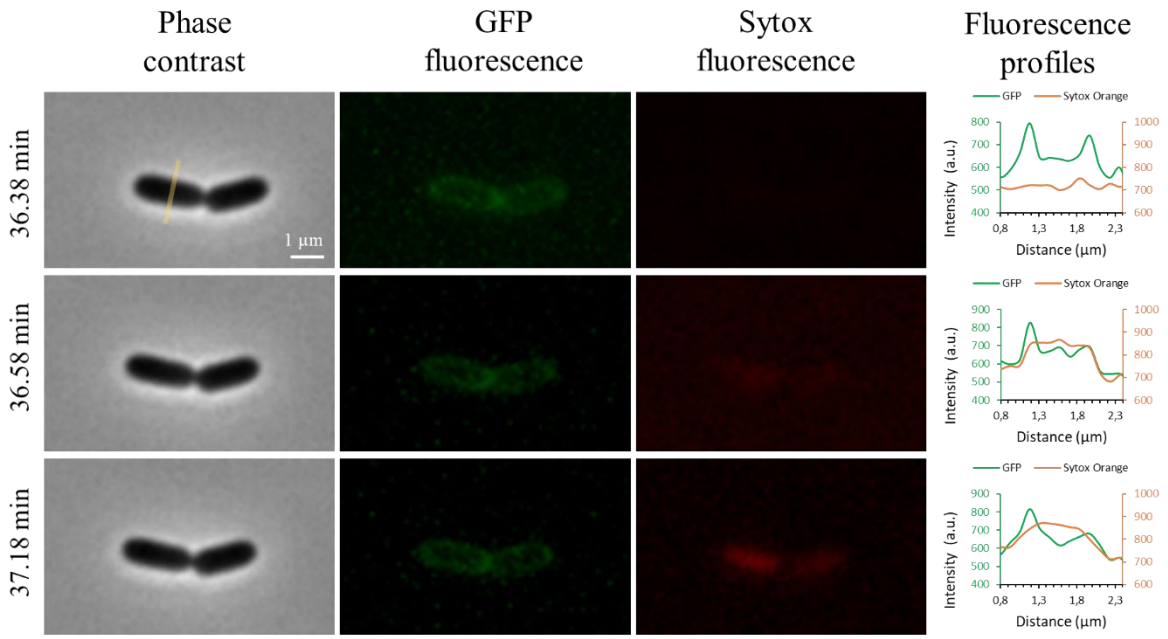

Figure 9: Imaging and analysis of one typical *E. coli* cell (ROI 1 in figure 8) during attack by AvBD103b. Sequence of events during attack by AvBD103b at 16 µM of a single *E. coli* cell expressing periplasmic GFP. Medium also contains Sytox Orange at 20 nM. The snapshots are taken from a single movie at the times shown on the left. (Scale bar, 1 µm). For each event, images are shown in phase contrast, green fluorescence channel (488 nm, GFP) and then orange fluorescence channel (548 nm, Sytox Orange). Transverse intensity profiles of green and orange channels along the yellow line in the phase contrast snapshot are shown.

2. AvBD103b chemically labeling and verification of the grafting dye effects

a. Fluorescently labeling and characterization of AvBD103b (Cy5-AvBD103b)

Selective chemical labeling of proteins is highly useful for probing protein localization and function in living biological systems [21]. However, it can be tough to selectively label a protein at a defined site without interfering with its activity and/or function, especially because proteins may have different active sites and/or functional groups. Furthermore, mild labeling conditions and the ability of reactions to take place in an aqueous solution are required to preserve the structural and functional stability of proteins. Consequently, it can be extremely challenging to label proteins in a chemoselective and site-specific way due to those restrictions [22].

Recent years have seen tremendous progress in chemical protein labeling, and many labeling strategies have been described. The strategies employed to achieve site-specific modification can be split into two major categories: direct modification of native proteins or protein modification via genetic manipulation.

Each labeling method has advantages and limitations, and the choice of a modification method should be based on the application of interest to not affect the conjugate application [22].

In our case, we should ensure that the grafting fluorescent dye in AvBD103b will not interfere with peptide activity and/or its antibacterial MOA and that the labeled version of AvBD103b reflects similar behavior as the native peptide. Therefore, a direct modification of endogenous AA was chosen as the strategy to label the native AvBD103b defensin. The N-terminus of a protein shows unique reactivity and can be site-specifically labeled or converted to a bioorthogonal handle [23]. One strategy for selective N-terminal protein labeling is to convert the N-terminal amino acid into a unique functional group, known as "N-terminal engineering," which can be further functionalized using a chemical ligation reaction (Figure 10) [183, 184].

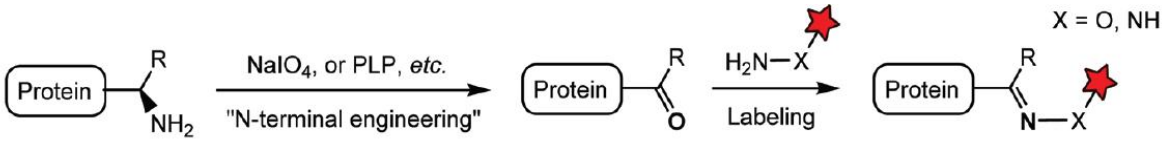

Figure 10: Strategy for chemoselective labeling of native proteins by N-terminal engineering [24].

As a first attempt, we have taken advantage of the presence of a Ser residue in the N-terminus, giving a 1,2-amino alcohol function, which can be easily converted to an aldehyde group by an oxidation reaction. The formed aldehyde can be conjugated to a reactive group present in a probe using a chemical ligation reaction. Additionally, except for Ser 1, AvBD103b sequence lacks Ser and/or Thr (Figure 1a), the two residues that can give a 1,2-amino alcohol function and thus can be converted to an aldehyde group and generate secondary reactions. Consequently, this labeling strategy enables selective labeling of the unique 1,2-amino alcohol function present in the N-terminal Ser residue and raises the possibility of greater reaction yield.

The chemical strategy designed for the covalent modification of AvBD103b consisted of two steps. The first one referred to the introduction of an aldehyde functional group through the oxidation with sodium m-periodate ($NaIO_4$) at neutral pH of the 1,2-amino alcohol function of the N-terminal Ser residue [25] of AvBD103b (Figure 11, Step I). In mild conditions, it is a very rapid oxidative reaction (~ 5 min) that takes place in an aqueous solution at neutral pH and requires the presence of a slight excess of $NaIO_4$. After a purification step to remove the excess of periodate, 880 µg (153 nmol) of the N-terminal aldehyde AvBD103b were recovered (see Appendix), associated with a yield of 88%.
The second step involved labeling the aldehyde derivative formed from AvBD103b using hydrazone ligation, in which the aldehyde group reacts with a reactive hydrazine group present in the probe (Figure 11, Step II). There are an increasing number of commercially available chemical probes that target aldehyde function. We choose to add Cyanine5 (Cy5) hydrazide, previously protected by Boc, to form

a hydrazone covalently bonded bioconjugate, Cy5-AvBD103b. After purification by High Performance Liquid Chromatography (HPLC), 500 µg (87 nmol) of N-terminal Cy5-AvBD103b with purity 98% (Figure 12) was recovered, associated with a yield of 50%.

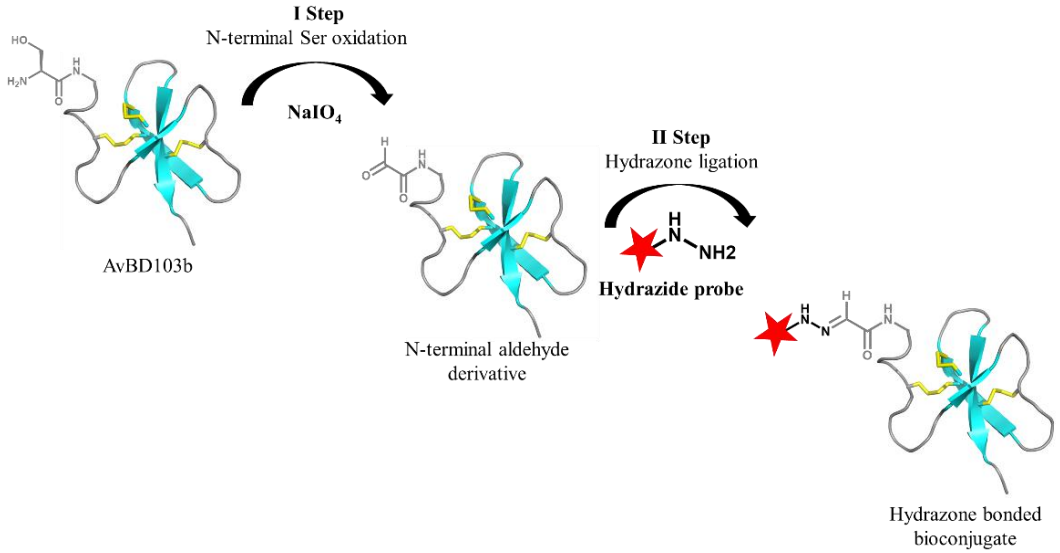

Figure 11: Chemical strategy designed for the labeling of AvBD103b. The bioconjugation strategy based on hydrazone chemical ligation reaction conjugating an N-terminal aldehyde derivative of the AvBD103b to a molecule probe harboring a hydrazide functional group, resulting in the covalently hydrazone-peptide conjugate.

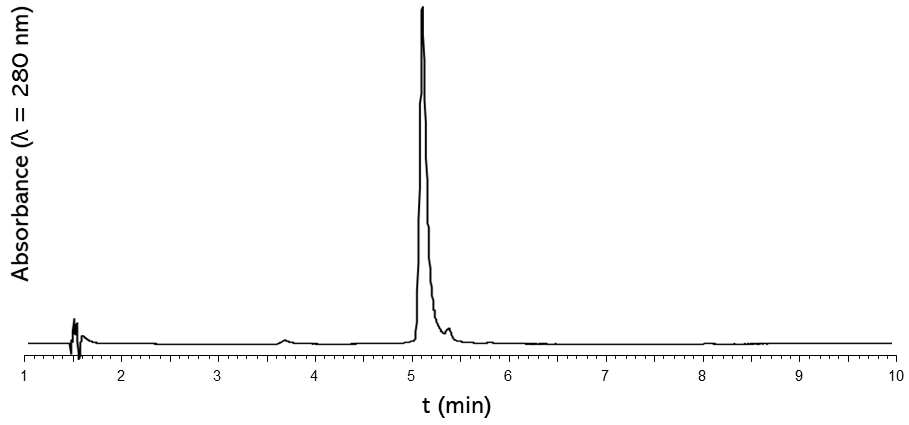

Figure 12: Chromatogram of the purified labeled peptide Cy5-AvBD103b used for MIC assay as well as for microscopy experiments. HPLC purification and analysis of the purified fraction (retention time = 5.1 min, purity 98% purity): gradient 25% - 45% solvent B (ACN + 0.1% TFA) for 10 minutes; UV-detection at 280 nm. Mass spectrometry (MS) analysis average masse deconvoluted corresponding to the major peak *m/z* 4948.

As a control, we synthesized a random peptide with Ser in the N-terminal (H-SERINENTER-NH_2) and labeled it with Cy5 dye (Cy5-SERINENTER) using the same strategy previously used for AvBD103b.

All results concerning the synthesis, labeling, and purification of this control peptide are described in the appendix.

The choice of Cy5 among all the commercially available fluorescent probes with a hydrazide reactive group was based on the physico-chemical and spectral properties of the dye. It has relatively small molecular weight (569.61 g/mol) and moderate solubility in water, compared to other fluorophores. It has high fluorescence quantum yield (0.2) and photostability and is widely used for imaging and flow cytometry analysis. Moreover, it is a far-red emitting fluorophore (λ excitation = 646 nm, λ emission = 662 nm), which is suitable to be used with GFP and Sytox Orange dyes in our microscopy imaging without spectra overlap (Figure 13).

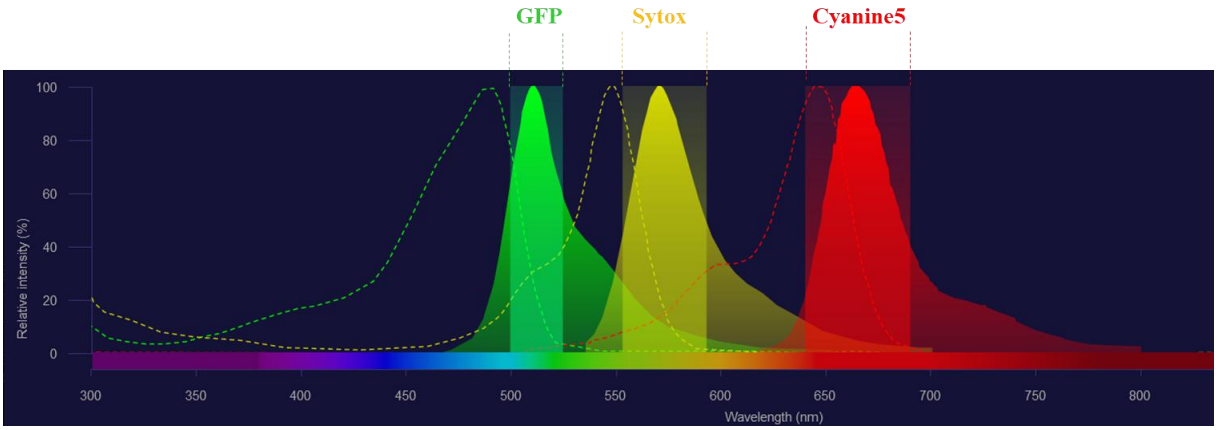

Emission Filters	Wavelength (nm)	Bandwidth
GFP	512	25
Sytox Orange	573	40
Cyanine5	665	50

Figure 13: Fluorescence Spectral viewer with the three fluorophores. (Top) Assessment of the spectral compatibility of the dyes used in our microscopy experiments using the "Fluorescence SpectraViewer" online tool developed by ThemoFisher®. The excitation (dashed line) and emission (solid line) spectra of each of the fluorophores GFP (green), Sytox Orange (yellow) and Cy5 (red) are shown. (Bottom) emission filters used for the detection of the emission fluorescence of each fluorophore.

Hydrazone ligation was chosen because of its various advantages, including high efficiency and selectivity, and the fact that it requires mild conditions and is carried out in an aqueous solution. In addition, hydrazones possess greater hydrolytic stability than other groups (e.g., imines) and are stable at physiological pH [26]. Furthermore, the strategy we have devised is biocompatible, cost-effective, and can be easily scaled up for larger-scale production.

As a general statement, fluorescent groups are often hydrophobic and large to a medium-sized biomolecule; therefore, affecting the activity of small proteins and/or peptides is possible. Unfortunately, many improperly reported results about mechanistic studies of fluorescently labeled AMPs could be suspected in the literature when no systematic control has been made. Before investigating the trajectory and spatial localization of Cy5-AvBD103b, we verified that the conjugation of AvBD103b by Cy5 did not impact the activity nor the MOA of the peptide native version.

b. Comparison between AvBD103b and Cy5-AvBD103b

Fluorophores are frequently covalently conjugated to proteins to improve their detection; however, the ensuing change in physico-chemical properties of the proteins may alter their biological properties. Cytotoxicity and large size are the main limitations of fluorescent probes, especially when grafted onto small proteins and/or peptides, the alteration of the molecule's structure and function is more likely than for large proteins [27].

Therefore, we investigated whether the conjugation of Cy5 fluorophore with AvBD103b defensin modified its activity against the *E. coli* JCW10 strain compared to the native peptide using MIC assay and flow cytometry experiment. We also tested whether the Cy5 fluorophore had an impact on the cellular localization of a labeled peptide using Cy5-SERINENTER as a control peptide on *E. coli* bacteria.

Antibacterial activity

Resazurin assay is a versatile colorimetric test that measures the metabolic activity of living cells by reduction of resazurin (purple-blue) to resorufin (pink). The resulted resorufin is fluorescent, thus its presence could be evaluated fluorometrically (λex520/λem590 nm), reflecting directly the metabolic activity of cells [189, 190]. Resazurin has already been used for determination of chemical cytotoxicity and MIC values of certain antibiotics [30].

Resazurin (alamarBlue®)-based 96-well plate microdilution method showed the same value of MIC (4 µM) for the native AvBD103b and Cy5-AvBD103b against *E. coli* JCW10 in the supplemented minimal M9 media (Table 4). Results showed a MIC = 8 µM for LL-37 peptide used as a positive control, in the same range (MIC = 4 µM) to that obtained in previous studies [190, 191], however in a different growth medium, EZRDM. Note that the negative control peptide, SERINENTER, does not show antibacterial activity against *E. coli* JCW10 (MIC > 64 µM).

Table 4: MIC values of AvBD103b (native peptide), Cy5-AvBD103b (the fluorescent version), LL-37 (peptide used as positive control), and SERINENTER (peptide used as negative control) against *E. coli* JCW10 strain in the indicated medium. MIC = minimum inhibitory concentration that inhibits the growth of ≥ 90% of cells. Data presented as means of experiments repeated three times.

		Bacterial strain: *E. coli* JCW10		
Culture media		**Minimal M9 supp. 0.4% glucose** 303 mOsmoL, pH 7.2		
Peptides	**AvBD103b**	**LL-37**	**Cy5-AvBD103b**	**SERINENTER**
MIC µM	**4 µM**	**8 µM**	**4 µM**	**>64 µM**

Membrane permeabilization

To assess whether the presence of the Cy5 dye could markedly modify AvBD103b's damage to the bacterial membrane, Propidium Iodide (PI) a DNA-binding stain was used. When the peptide disrupts cell membranes, the PI reaches the cytoplasm, binds to DNA and emits a fluorescent signal. Flow cytometry analysis indicated that treatment of *E. coli* cells with AvBD103b or Cy5-AvBD103b peptides enhanced in a very weak manner the uptake of PI, suggesting that the bacterial cell membrane was only slightly disrupted. Less than 10% and 5% cells stained with PI after exposure to AvBD103b and Cy5-AvBD103b, respectively, for 120 minutes at their MICs (Figure 14). This confirms that the membrane permeabilization is not the main effect of AvBD103b to inhibit bacterial growth, in accordance with the previous work [13], and that the presence of the Cy5 dye does not significantly impact membrane permeabilization.

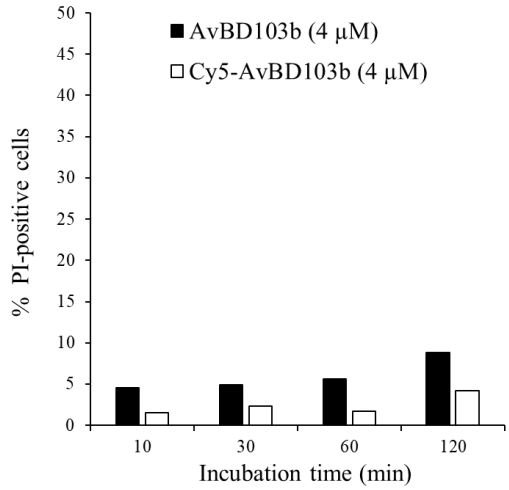

Figure 14: Membrane permeabilization of *E. coli* JCW10 produced by AvBD103b and its fluorescent labeled version, Cy5-AvBD103b at their MICs (4 µM) determined by flow cytometry with Propidium Iodide (membrane impermeable) stain.

Subcellular localization

Although we have previously verified that Cy5 labeling of AvBD103b defensin does not affect its activity against *E. coli* (MIC assay) or its membrane permeabilization activity (PI uptake assay), an impact in the cellular localization and/or molecular binding of AvBD103b by the fluorescent dye is possible and could not be excluded.

For most AMPs, electrostatic and hydrophobic interactions are involved in their binding to the microbial cell [33]. Therefore, the attachment of a hydrophobic and/or charged probe to AMPs, which are small peptides, could significantly affect the contribution of their interactions during the membrane association step as well as during a subsequent potential translocation event. For example, the fluorescent labeling of penetratin, a cell-penetrating peptide, has been shown to considerably change its mode of membrane interaction in vitro [34] and its cell-uptake, affecting its cellular distribution and cell viability [35].

To ensure that the dye conjugated to AvBD103b peptide has no significant influence on its MOA and localization, which we are seeking to study, we monitored in real time the membrane permeabilization and the cellular binding of the Cy5-SERINENTER model peptide on *E. coli* JCW10 using widefield fluorescence microscopy. A three-color experiment was performed for ~60 min in the flow chamber with 24 µM as a peptide final concentration and in the presence of Sytox Orange in the growth media. In addition to green and orange channels, a red channel monitors the emission of the fluorescently labeled version of Cy5-SERINENTER, enabling us to track its spatial localization over time. As seen in figure 15, even after 1 h of exposure, the GFP was still localized in the periplasmic space of bacteria cells, and no Sytox fluorescence in bacteria was detected, indicating the integrity of both membranes. Importantly, Cy5-SERINENTER fluorescence did not show a specific bacteria localization, demonstrating that the Cy5 dye (0.7 kDa) has no influence on the binding and cellular localization of the small, labeled peptide (1.2 kDa).

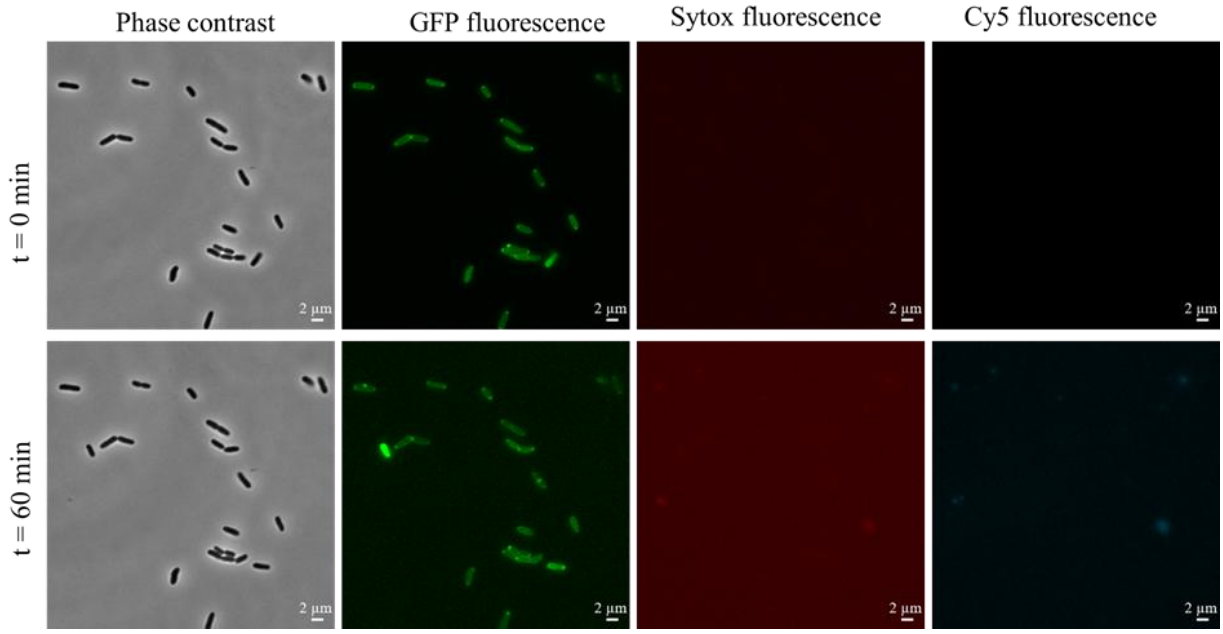

Figure 15: Widefield microscopy snapshots of the time lapse video of *E. coli* cells exposed to constant flow of 24 µM Cy5-SERINENTER at t = 0 (peptide injection time) and t = 60 min. Images in phase contrast, green fluorescence (488 nm, GFP showed in green), Orange fluorescence (548 nm, Sytox orange showed in red) and red fluorescence (650 nm, Cy5 showed in blue).

Overall, the antibacterial activity, membrane permeabilization, cellular localization, and binding of the AvBD103b defensin do not appear to be significantly affected by the conjugation with the fluorescent dye Cy5.

3. Preliminary fluorescence microscope experiments with Cy5-AvBD103b

a. Real-time effects of Cy5-AvBD103b on *E. coli*

We monitored the effects in real time of Cy5-AvBD103b on OM and CM permeabilization in live *E. coli* while following its cellular localization over a 75-min video with images interspersed with contrast phase, GFP, Sytox Orange, and Cy5-AvBD103b, every 20 s. All experiments using Cy5-AvBD103b were performed at 24 µM in the presence of 50 nM Sytox Orange and were repeated several times. The sequence of events is detailed below, with a typical example illustrated in Figure 16.

Before the onset of peptide flow (t = -0.6 min), GFP expression in the periplasmic space was characterized (Figure 16 A2), as shown by the axial intensity profile of the green channel (Figure 16 B). After ~ 12-20 min of peptide injection at a constant flow 0.2 mL/h, a slight loss of GFP fluorescence intensity is visible, with a modification of the GFP profile (Figure 16 B, profile intensity GFP), indicating a slight disruption of the OM membrane. Concomitantly, a very low fluorescence signal of Sytox appears (dashed circle Figure 16 A8, and profile intensity Sytox, figure 16 B), demonstrating a slight perturbation in the integrity of CM membrane, allowing its binding to DNA.

These profiles of membrane permeabilization, similar to those obtained with native AvBD103b [10], i.e. slow and weak disruption of OM and CM concomitantly confirm that the label (Cy5) does not disrupt the peptide's MOA.

The fluorescence signal of Cy5-AvBD103b appears at the same time (Figure 16 A7). Cy5-AvBD103b clearly has a preferential binding site at the septum (Figure 16 B, profile intensity of Cy5-AvBD103b), where the new cell wall is formed between two daughter cells as a result of cell division [36]. At this point, membranes are curved and nascent, relatively easier to be attacked than at the more mature cylindrical regions or membrane tips. Furthermore, the presence of cardiolipin (CL), a negatively charged phospholipid mostly located in curved membrane sites of bacteria [37], may help the highly positive AvBD103b to concentrate locally in the septal region.

This first direct localization of AvBD103b is in favor of a localization at the surface cell level of the peptide, without significant disruption of OM and/or CM membranes. In these experimental conditions, the ~5 kDa Cy5-AvBD103b had not crossed the membranes and reached the cytoplasm. After more than 1h of peptide exposure, Cy5-AvBD103b perturbates more importantly the integrity of membranes, generating a greater loss of GFP total fluorescence integration (Figure 16 B, profile intensity GFP) concomitant with an increase in Sytox fluorescence (Figure16 A12). However, the localization of the peptide, followed by Cy5 fluorescence, is not modified (Figure 16 A11).

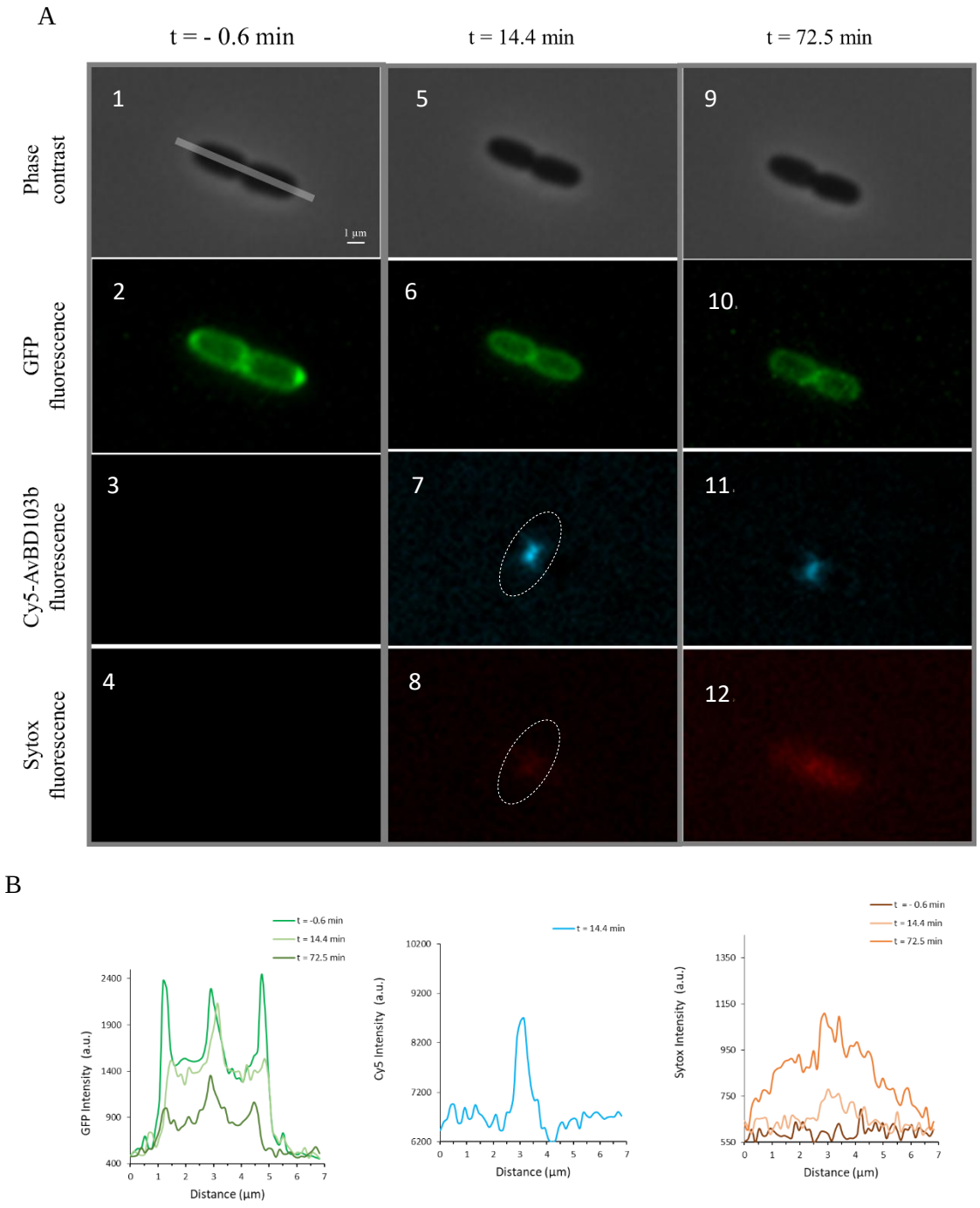

Figure 16: Real time localization of Cy5-AvBD103b on *E. coli* JCW10. (A) Widefield microscopy snapshots of the time lapse video of *E. coli* cells before (t = - 0.6 min) and during exposure to constant flow of 24 µM Cy5-AvBD103b (t = 14.4 min and t = 72.4 min). Images in phase contrast, green fluorescence (488 nm, GFP), Orange fluorescence (548 nm, Sytox orange) and red fluorescence (650 nm, Cy5) are shown. At t = 14.4 min, the weak fluorescence signal from Sytox and the fluorescence signal from Cy5-AvBD103b are highlighted in dashed circles. (B) Intensities profiles of GFP shown in green, Sytox orange shown in rouge and Cy5-AvBD103b shown in blue, at different times during the experiment.

Throughout time and after ~120 min of peptide injection, we observed a large number of bacteria. One of the recorded fields, representative to highlight the four-scenario observed, is shown in Figure 17.

(i) Some bacteria (represented by white rectangles) with GFP fluorescence localized in the periplasm, are weakly labeled with Cy5-AvBD103b, and not Sytox-labeled. This scenario suggests that if the local defensin concentration is insufficient, the membrane is not disrupted and there are no visible effects.

(ii) Some bacteria (highlighted by white arrows) with significant Cy5-AvBD103b labelling show a weak Sytox fluorescence, indicating a weak/transient disruption of membranes. Note that in this case, GFP fluorescence is periplasmic.

(iii) Some bacteria (represented by white triangles) labeled with Cy5-AvBD103b showed a high Sytox fluorescence intensity (indicating greater disruption of OM and CM) and a part of GFP entering in the cell cytoplasm. However, the precise localization of the peptide on the cell surface and/or inside the cell is not possible.

And finally (iv) in some cases (represented by white circles), the GFP signal fluorescence totally disappears, indication OM disruption, whereas the Sytox fluorescence indicates the CM disruption.

The Cy5-AvBD103b appears mainly concentrated in the middle and/or in the septum of cells. However, with widefield microscopy, it is not possible to localize precisely the peptide on the cell surface and/or inside the cell. In some cases, Cy5-AvBD103b may have finally entered the cell and reached the cytoplasm.

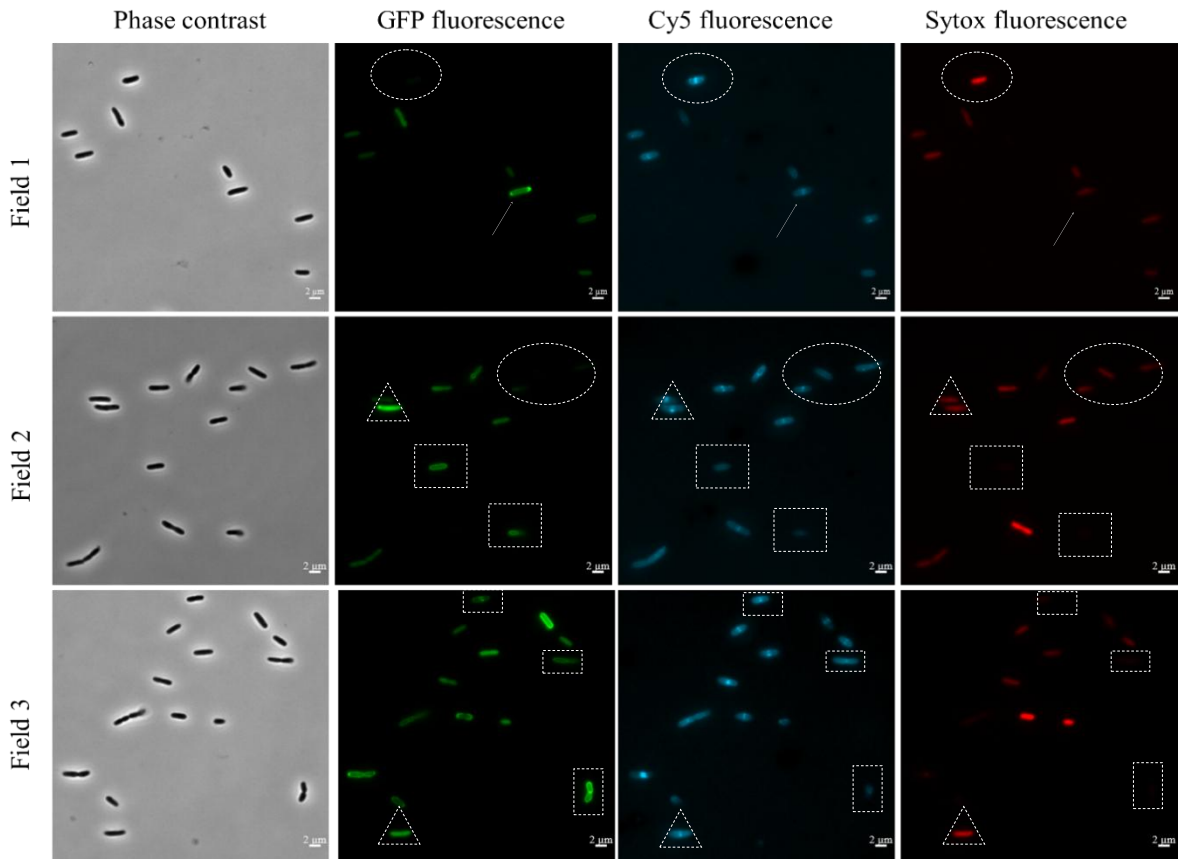

Figure 17: Snapshots of 3 different fields taken by widefield microscope of cells exposed for ~ 120 min to a constant flow (0.2 mL/h) of 24 µM Cy5-AvBD103b under flow in the microfluidic chamber. Field of the view images are shown in phase contrast, GFP green fluorescence (488 nm), Cy5-AvBD103b (650 nm) and Sytox Orange fluorescence (548 nm). White rectangles show bacteria with GFP fluorescence localized in the periplasm, weakly labeled with Cy5-AvBD103b, and not Sytox-labeled. White arrows indicate bacteria with significant Cy5-AvBD103b labelling, weak Sytox fluorescence, and GFP fluorescence is periplasmic. White triangles show bacteria labeled with Cy5-AvBD103b, with a high Sytox fluorescence intensity and a part of GFP entering in the cell cytoplasm. White circles show bacteria labelled Cy5-AvBD103b with Sytox fluorescence and GFP signal fluorescence totally disappears.

b. Subcellular localization of Cy5-AvBD103b by confocal microscopy

Our aim here is to visualize subcellular binding and localization with membrane permeabilization states using confocal microscopy, which offers much higher spatial resolution than widefield microscopy. To do so, we treated *E. coli* with 24 µM Cy5-AvBD103b and observed several fields after 120 min of treatment. The same experiment described for widefield microscopy was carried out (i.e., bacteria expressing periplasmic GFP were deposited on a layer of poly-L-lysine in the microfluidic chamber exposed to a constant flow (0.2 mL/h) of medium containing the peptide and 50 nM of Sytox Orange).

A large panel of bacteria (~73 cells) were observed in different fields, allowing us to approximate the percentage of cells labeled with Cy5-AvBD103b and the permeabilization status of both OM and CM membranes, indicated by GFP and Sytox fluorescence. As the bacterial culture was not synchronized, all phases of the cell cycles were present simultaneously. Cells that divide by showing a distinct septum are referred to as "septating cells," whereas those that do not are referred to as "nonseptating cells."

After 120 min exposure, 76% of cells (52/68 cells) were labeled with Cy5-AvBD103b (Table 5), which often accumulated at the septal point in septating cells and/or middle cell (midcell) in nonseptating cells (Figure 18).

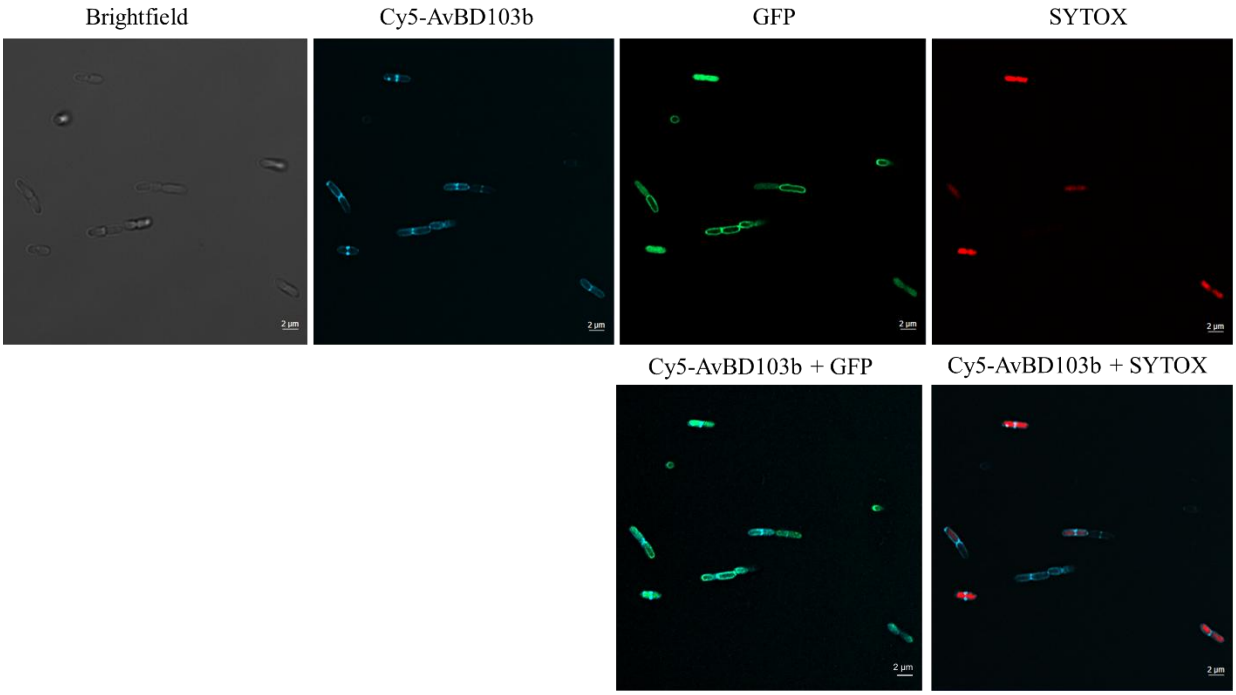

Figure 18: Confocal microscopy imaging on living *E. coli* JCW10 bacteria after one hour of the injection of 24 µM Cy5-AvBD103b at 0.2 mL/h with the presence of 50 nM Sytox Orange. Top: Example of a field of view containing 8 adherent bacteria shown in brightfield, Cy5-AvBD103b, GFP and Sytox fluorescence. Bottom: Superpositions of Cy5-AvBD103b fluorescence with that of GFP or Sytox.

For around 60% of Cy5-AvBD103b-positive cells (52/68 cells), GFP was localized in the periplasm and no Sytox fluorescence was observed (31/52 cells) (Table 5). The permeabilization of both OM and CM, judged by GFP enter in the cytoplasm and Sytox fluorescence signal, was observed in ~40% of Cy5-AvBD103b-positive cells (21/52 cells). Furthermore, among the total observed cells, Cy5-AvBD103b showed a preferential binding to septating cells rather than nonseptating cells. Indeed, ~90% of septating cells (33/36 cells) showed accumulation of Cy5-AvBD103b whereas only ~59% of nonseptating cells (19/32 cells) are labelled with the peptide.

Table 5: Proportion of cells with the different combinations of labeling, observed by confocal microscopy.

		Total cells observed = 68	
		Nonseptating cells	**Septating cells**
		32	36
Cy5-AvBD103b negative	Periplasmic GFP Sytox negative	13 (~ 36%)	3 (~ 8%)
Cy5-AvBD103b positive	Periplasmic GFP Sytox negative	9 (~ 25%)	22 (~ 60%)
	Cytoplasmic GFP Sytox positive	10 (~ 27%)	11 (~ 30%)

Figure 19 shows examples of Cy5-AvBD103b localization with the membrane permeabilization effect revealed by GFP and Sytox fluorescence on nonseptating cells (a and b) and septating cells (c). Independently whether bacteria cells are in division or not, the peptide shows a clearly preferential localization at the cell envelop cell with often highly intense fluorescence in the midcell and/or septal region. Although the peptide disrupts both membranes, its permeabilization of the CM appears to be greater than that of the OM, as evidenced by the entry of GFP into the cytoplasm (in the majority of cases) rather than its diffusion into the surrounding medium (rare observation). Unfortunately, we were unable in our experiments to estimate the fraction of the GFP diffusing in the media due to the OM permeabilization. The fluorescence of Sytox following DNA binding was our only indication of OM disruption.

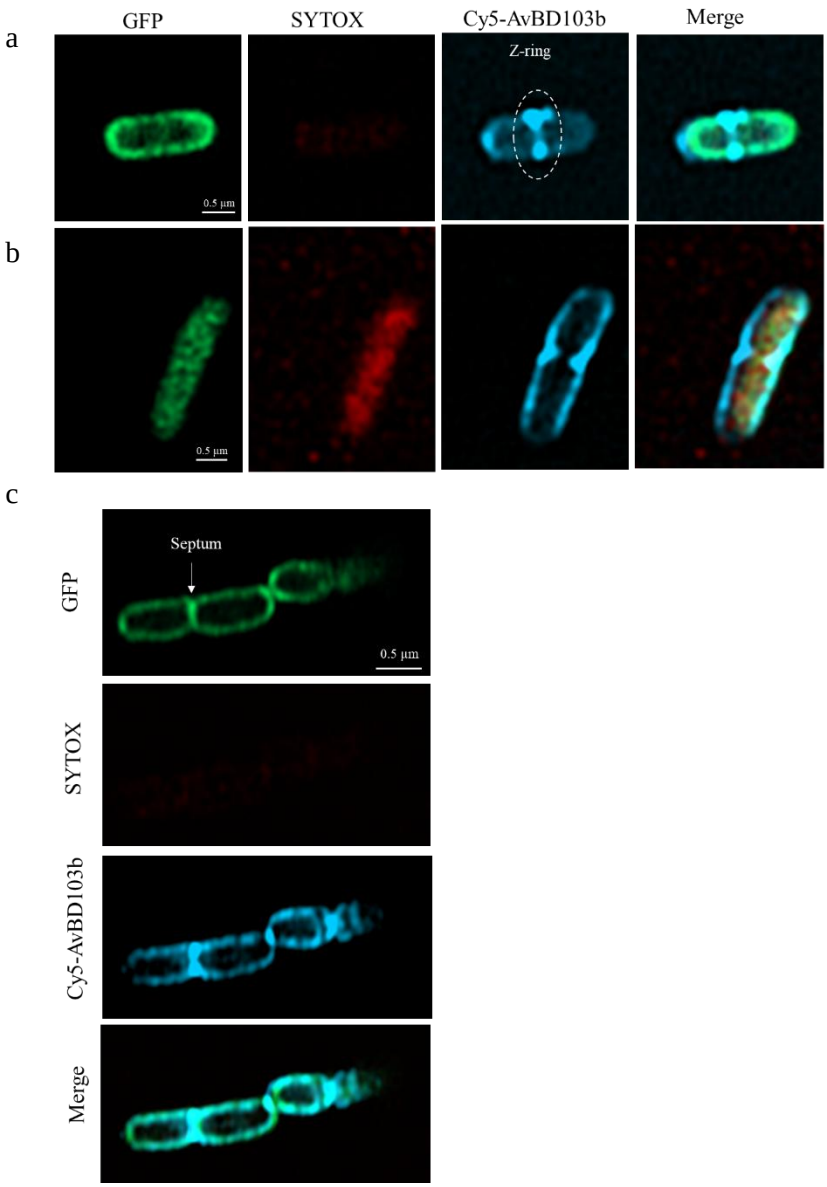

Figure 19: Confocal microscopy snapshots of the different possibilities of the localization of the peptide with membranes permeabilization effects. (a) Nonseptating cell with periplasmic GFP, very weak Sytox fluorescence and Cy5 fluorescence at the membranes, with high intensity at septal region. (b) Nonseptating cell with cytoplasmic GFP, Sytox binding to DNA and Cy5-AvBD103b binds to the membranes of bacteria. (c) Septating cell with periplasmic GFP, no Sytox fluorescence and Cy5 fluorescence at the membranes, with high intensity at septal region.

c. Preferred localization at the midcell and septal region

Cy5-AvBD103b shows a preferential subcellular localization in the middle of nonseptating *E. coli* cell and in the septum region in septating *E. coli* cells, where proteins involved in cell division are located

and biogenesis of CW components begins. This suggests that AvBD103b may (i) target bacterial cell division, and/or (ii) interfere with the synthesis of the CW, e.g., peptidoglycan layer, in the septum.

(i) Bacterial cell division

Cell division is an essential cellular process for cell reproduction and infection. To divide and proliferate, bacterial cells use membrane-associated proteins complexes that spatially and temporally organize the CW synthesis to split the mother cell into two daughter cells. Rod-shaped cells such as *E. coli* elongate their cell bodies by incorporating new peptidoglycan (PG) material at various points along the cylinder. This step is insured by the elongation machinery, known as elongasome [38]. Then, FtsZ protein, a homologue of eukaryotic tubulin, begins cell division process by forming the Z-ring in the middle of the cell, corresponds to the future cell division site. FtsZ ring recruits dozens of other proteins to the division site, assembling them together and constituting the "divisome" [36]. To create the transverse/septal wall between the dividing cells, the divisome promotes localized PG synthesis, known as septal PG (sPG). The daughter cells are initially linked by septal PG (sPG), which has to be metabolized in order to separate the newly formed cells [38] (Figure 20).

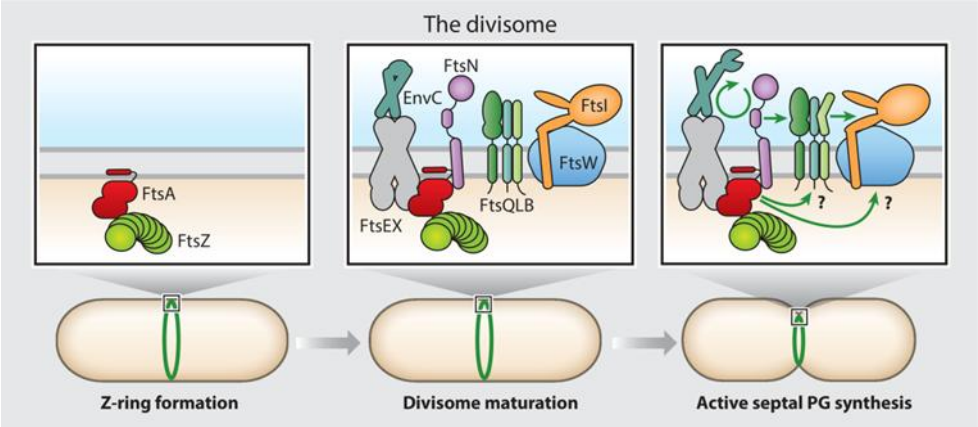

Figure 20: Steps of divisome assembly and activation in Gram-negative bacteria (adapted from ref [38]).

The strong affinity of Cy5-AvBD103b to the midcell where the divisome is located, suggests that AvBD103b could interfere with the cell division through possible mechanisms. AvBD103b could bind directly to one or multiple membrane-associated proteins at the Z-ring. Among these proteins, the tubulin-like protein FtsZ, involved in the crucial step of Z-ring formation at the beginning of the division process, is considered a promising target for development of new antibacterials [28, 29]. Different MoAs of FtsZ inhibitors including peptides, natural compounds and other synthetic small molecules, have been described [41]. For example, the antimitotic agent doxorubicin inhibits *E. coli* division by interacting with FtsZ [42]. Among AMPs, the amphibian Temporin with potent antibacterial activity was shown to

affect bacterial cell division by inhibiting FtsZ [43]. Finally, we cannot rule out the interference of AvBD103b with the cell division by another mechanism, independent of FtsZ protein.

(ii) PG biosynthesis

The cell wall of Gram-negative bacteria consists of a thin layer of peptidoglycan in the periplasmic space between the inner and outer lipid membranes [37]. The PG layer is an essential structural element, which defines bacterial cell shape and protecting them from osmotic lysis. PG cell wall consists of linear glycan chains cross-linked by short peptides. The glycan strands are made up of repeating disaccharide units of N-acetylglucosamine (GlcNAc) and N-acetylmuramic acid (MurNAc) residues. To each MurNAc sugar, a short peptide is attached and forms amide crosslinks between adjacent glycans, generating a covalent mesh surrounding the CM.

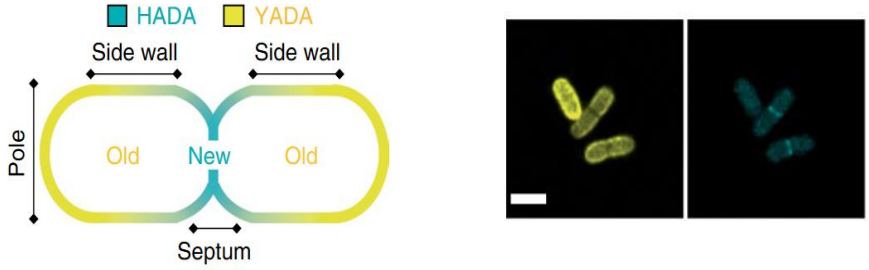

Figure 21: Labelling patterns of new cell wall material with HADA (blue), while old material is stained with YADA (yellow), on *E. coli* bacteria (adapted from ref [44]).

The Cy5-AvBD103b localization in the septum where components of the new CW are synthesized (Figure 21) suggests that AvBD103b could interfere with CW component biosynthesis. Given its high abundance in curved membranes, PG is a possible cellular partner. Like the LL-37 peptide [10], AvBD103b could bind directly to PG. A study of the *in vitro* interaction of AvBD103b with this component using membrane models could support this hypothesis. In addition, AvBD103b could bind to one of the PG precursors, such as the essential precursor lipid II, as has been demonstrated for certain defensins, oyster defensins [45], fungal defensin [46] or other antimicrobials [47]. Another possibility is that AvBD103b interferes with enzymes involved in PG biosynthesis, similar to the cyclic lipopeptide daptomycin, which disrupts the lipid II synthase MurG [48]. Finally, we cannot rule out the interference of AvBD103b with the cell envelope by another mechanism, independent of peptidoglycan.

III. Experimental part

1. Peptides

Unlabeled AvBD103b (Oxidized form, folded with 3 disulfide bridges) and LL-37 peptides were both purchased from Genepep SA (Montpellier, France) at >85% purity and used without further purification. The human cathelicidin LL-37 has the 37-residue sequence LLGDFFRKSKEKIGKEFKRIVQRIKDF-LRNLVPRTES.

2. AvBD103b defensin fluorescently labelling

The strategy used to label directly the N-terminal serine of AvBD103b by Cyanine5-hydrazide via periodate oxidation of a 2-amino alcohol is illustrated in Figure 22.

N-terminal serine oxidation to aldehyde

The oxidative cleavage of the N-terminal 1,2-amino alcohol function of AvBD103b was performed by treatment with excess NaIO4. 1 mg (174 nmol) of AvBD103b in 800 µL of 1x phosphate buffered saline (PBS) solution containing 0.01 M phosphate, 0.154 M NaCl, and a pH of 7.4 (peptide concentration of 1.5 mM) were treated with 1.3 eq of $NaIO_4$ (226 nmol) by adding to the peptide solution. The final resulted volume was 1.16 mL. The reaction mixture was incubated under stirring at room temperature for 5 min to ensure that the peptide was completely oxidized. One equivalent of Ser residue (175 nmol) was added to the mixture to remove $NaIO_4$ excess, followed by 5 min of incubation. Then, the aldehyde derivative AvBD103b was promptly purified by Sep-Pak® C18 6 cc Vrac Cartridge (WAT054955, Waters). Peak fractions of the aldehyde derivative AvBD103b were eluted with 0.1% TFA in H2O (solvent A) and 0.1% TFA in MeCN (solvent B) (50/50, v/v), pooled and verified by HPLC and MS analysis. All HPLC and MS equipment is detailed in the appendix. Quantities of lyophilized purified peptide was determined by UV spectrophotometry at $\lambda = 280$ nm (εTrp = 5500 and εSS bond = 125 $L.M^{-1}.cm^{-1}$) [49].

Labeling of aldehyde-AvBD103b by hydrazone ligation

Prior to the conjugation reaction, the reactive hydrazide was formed by removing the Boc protecting group with trifluoroacetic acid (TFA). 1.1 eq (191 nmol) of Cyanine-5-Boc hydrazide was dissolved in 200 µl of dichlomethane (DCM) and supplemented with TFA to give a final volume of 50/50 v/v. Organic solvents were completely evaporated using a rotary evaporator (DCM). Organic solvents were completely evaporated using a rotary evaporator (Rotavapor®) heated to 40°C. The resulting Cyanine5-hydrazide reagent was then dissolved in acetic acid (AcOH) and incubated with 1 mg (174 nmol) of the N-terminal aldehyde peptide AvBD103b in a 1x PBS solution containing 0.01 M phosphate, 0.154 M NaCl, and pH 7.4 (peptide concentration 2.5 mM). The final concentration of AcOH was 20% (v/v) in the mixture. Reaction kinetics were monitored by HPLC and mass spectrometry (MS) analysis over time. After 2 hours at 37°C, the reaction mixture was extensively diluted and a purification step carried

out. The purity and mass of the purified labeled fraction of AvBD103b were verified by HPLC and MS analysis. The final amount of lyophilized Cy5-AvBD103b was estimated by UV spectrophotometry at λ = 280 nm (εTrp = 5500, εSS bond = 125, εCy5 = 7500 L.M-1.cm-1) [182].

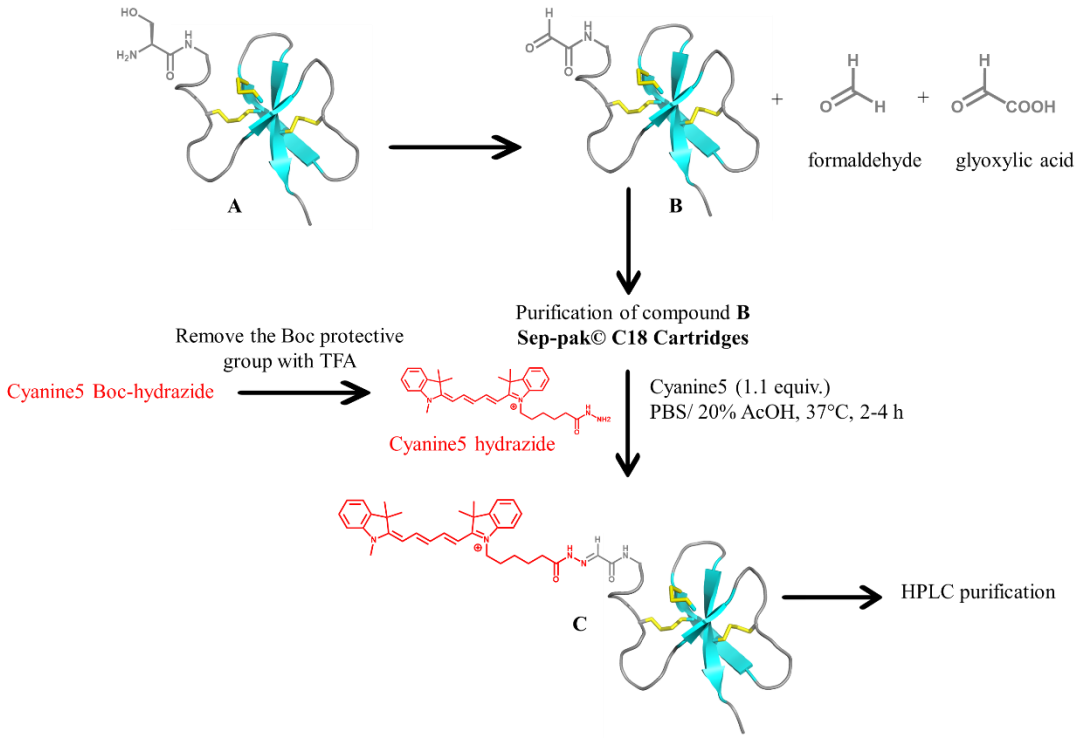

Figure 22: Strategy of the site-directed labeling of the N-terminal serine of AvBD103b by Cyanine5-hydrazide via periodate oxidation of a 2-amino alcohol. Step 1 consists of oxidation of 2-amino alcohol of the serine in N-terminal to aldehyde group. Step 2 consists of the conjugation reaction between aldehyde with hydrazide to form hydrazine bonds.

3. Peptide model synthesis and fluorescently labelling

The peptide model has the following sequence (Figure 23):

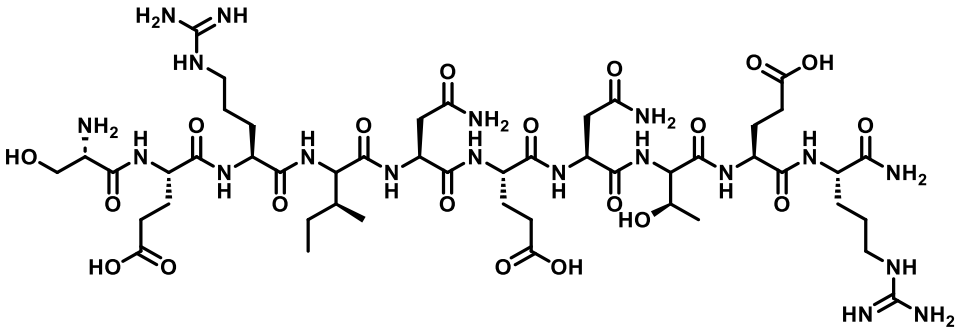

Figure 23: Sequence H-SERINENTER-NH_2

Peptide synthesis

Automated Fmoc-based solid phase peptide synthesis (SPPS) was carried out on a Prelude® synthesizer from Protein technologies to obtain the desired peptide model. The synthesis was performed at 0.050 mmol scale on Rink amide ChemMatrix® resin (0.45 mmol/g). The side-chain protecting groups used for Fmoc-L-amino acids were Ser(*t*Bu), Thr(*t*Bu), Glu(tBu), Arg(Pbf) and Asn (Trt). Protected amino acids (0.5 mmol, 10 equiv.) in DMF (1 mL) were coupled for 30 min using HATU (180mg, 0.475 mmol, 9.5 equiv.) in DMF (1 mL), DIEA (174 µL, 0.1 mmol, 20 equiv.) in NMP (1 mL) and additional NMP (1 mL). Capping of possible unreacted amine groups was achieved by treatment with acetic anhydride (286 µL, 3.02 mmol, 60 equiv.), DIEA (136 µL, 0.8 mmol, 15.5 equiv.) and HOBt (12 mg, 0.088 mmol, 1.8 equiv.) in NMP (5 mL) for 7 min after each coupling. Fmoc group was deprotected by three successive treatments with 20% v/v piperidine in NMP (4 mL) for 3 min.

Peptide cleavage from resin

The peptide was deprotected and cleaved from the resin through a treatment with TFA/H_2O/iPr_3SiH/Phenol 88:5:2:5 for 2 h into a polypropylene syringe fitted with a polypropylene frit from Torviq (Niles, USA). The peptide was then precipitated by dilution into an ice-cold diethyl ether/petroleum ether 1:1 mixture, recovered by centrifugation and washed twice with diethyl ether.

Analysis and Purification

The crude peptide was analyzed and purified by RP-HPLC (Reversed Phase High-Performance Liquid Chromatography) Chromolith High Resolution RP-18e (150 Å, 10 × 4.6 mm, 3 mL/min flow rate) column was used for analysis and purification of the peptide. As mobile phase, mixtures of 0.1% TFA in H_2O (A) and 0.1% TFA in MeCN (B) were used. HPLC analyses were carried out on a Chromaster system equipped with a 5160 pump, a 5430-diode array detector and a 5260-auto sampler. Semi-preparative purification was carried out on a Hitachi L-2130 pump, a Hitachi L-2455 diode array detector and a Hitachi L-2200 auto sampler.

The crude and purified peptide were characterized with high resolution ESI-MS analyses performed on a maXis ultra-high-resolution Q-TOF mass spectrometer (Bruker Daltonics, Bremen, Germany), using the positive mode. The multiply-charged envelope was deconvoluted using the Charge Deconvolution algorithm in Bruker Data Analysis 4.1 software to obtain the monoisotopic [M] value.

Peptide model labeling with Cy5

This peptide model was labelled following an identical protocol as for AvBD103b and illustrated in Figure 24. The purity and mass of the purified labeled fraction of the peptide were verified by LC-MS analysis.

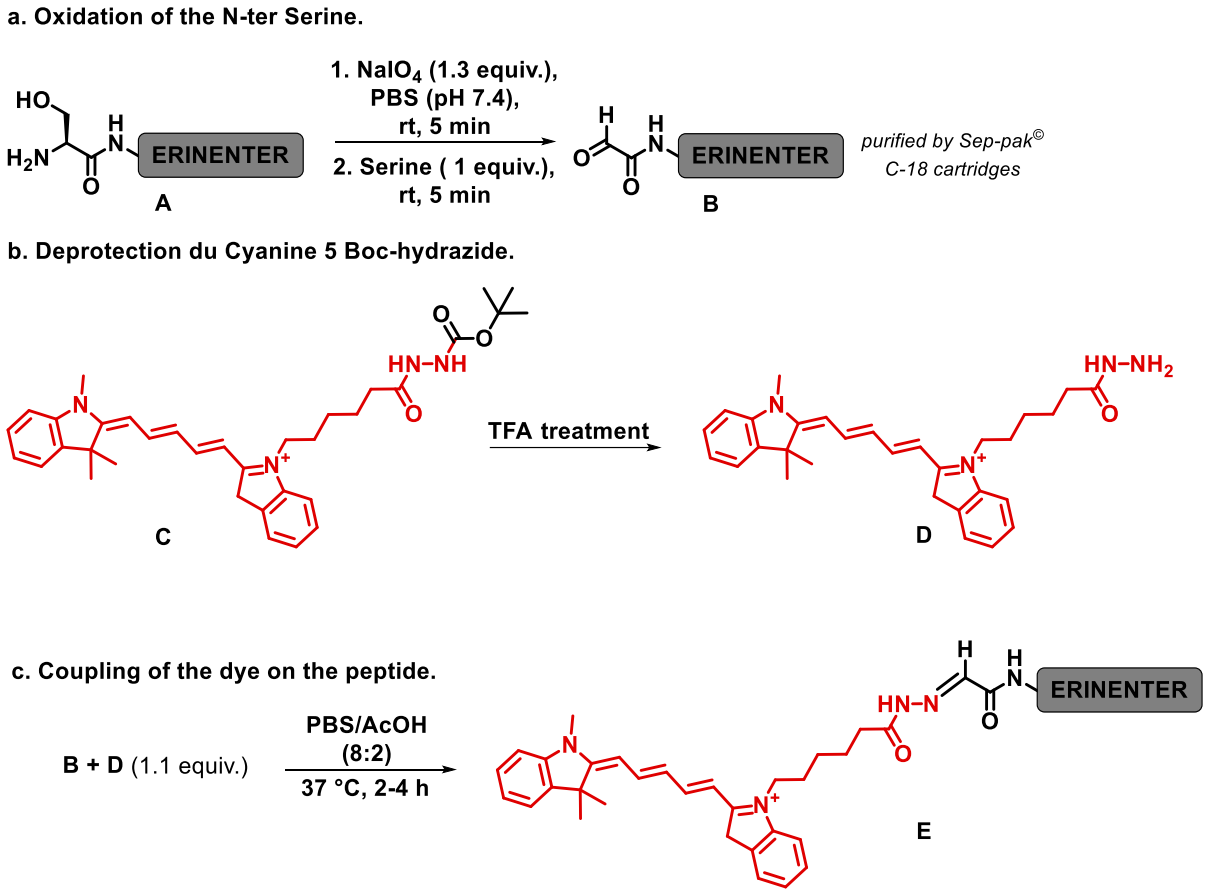

Figure 24: Site-directed labeling of the N-terminal serine of the peptide model H-SERINENTER-NH2 by Cyanine5-hydrazide via periodate oxidation of a 2-amino alcohol. *Step 1 consists of oxidation of 2-amino alcohol of the serine in N-terminal to aldehyde group. Step 2 consists of the conjugation reaction between aldehyde with hydrazide to form hydrazine bonds*.

4. Bacterial strain and growth conditions

The *E. coli* JCW10 strain, modified from *E. coli* K12 (MG1655) was kindly provided by Dr. James C. Weisshaar. JCW10 expresses the TorA-GFP fusion protein, composed of the twin-arginine signal peptide of TMAO reductase (TorA) and the 27 kDa green fluorescent protein (GFP), from the plasmid pJWA as previously described [19]. This plasmid has ampicillin resistance and a tetracycline-inducible promoter. On transport to the periplasm, the 10–50 nm thick space between OM and CM, the signal sequence is cleaved from GFP. The fluorescent signal of the mature, fully folded, periplasmic GFP can then be imaged. Bacterial cultures were grown overnight at 30 °C from a glycerol frozen stock solution in Luria-Bertani (LB) medium containing ampicillin (100 µg/mL) to stationary phase. All bacterial cultures were grown in low-fluorescence M9 minimal medium supplemented with 2 mM $MgSO_4$ and 4 mg/ml glucose as a carbon source. This medium is composed of a basic formulation of M9 minimal salts that can be supplemented with various amino acids and carbon sources. The exact recipe and concentrations of the various components of the M9 supp. medium used in this study are given in the

appendix. All bacterial cultures were grown at 30 °C under 180 rpm with 100 µg/mL ampicillin added to the medium.

5. Evaluation of the minimal inhibitory concentration

Bacterial subcultures were grown at 30 °C from the *E. coli* JCW10 overnight culture to exponential phase. Serial dilutions were performed for each peptide (Unlabeled AvBD103b and Cy5-AvBD103b) to estimate the MICs by the broth dilution method on a 96-well plate, each plate containing *E. coli* JCW10 (OD_{600} = 0.05) in the minimal M9 supplemented medium described below. After overnight at 30 °C under 180 rpm, resazurin, blue and low fluorescence dye was added to each well at 10% (v/v) as final concentration followed by 2h of incubation. Viable cells were detected via the formation of resorufin, pink and high fluorescence compound. The lowest concentration for which no viable cell is detectable at 600 nm is considered as the MIC. The antimicrobial peptide cathelicidin LL-37 (ref num, Genpep) was used as a positive control. This experiment was carried out in triplicate.

6. Evaluation of the membrane permeabilization

To verify, in our microscopy experiment conditions, that the dye conjugated to the peptide does not change the behavior/the toxicity of the native peptide on bacteria, we evaluated the membrane permeabilization of *E. coli* JCW10 by flow cytometry analysis. Bacteria at DO_{600nm}~ 0.4 were incubated with 4 µM of each peptide at room temperature (RT) over time in M9 supp. media. The cytotoxicity was evaluated by 30 µM propidium iodide (PI), red fluorescent when DNA-binding, at 10, 30, 60 and 120 min of incubation. Populations of 200,000 events were used. Measurements were carried out on independent triplicates. Results were analyzed and plotted using Prism software.

7. Preparation of PDMS microfluidic devices and flow chamber

Microfluidic patterned polydimethylsiloxane (PDMS) devices were prepared as previously described with Sylgard 184 silicone elastomer mixture. The final PDMS-based micro-fluidic chambers consist of a single rectilinear channel of uniform height of 150 µm, width of 6 mm and length of 11 mm. The chamber volume is 10 µL. To ensure optimal bacterial adhesion, the device is filled with 10 µL of an aqueous solution of 0.01% of poly-L-lysine (molecular weight > 150,000 Da) and kept overnight at 30 °C.

8. Fluorescence microscopy

Bacteria cells preparation

For imaging, subcultures were grown from the overnight culture at 30 °C, as previously mentioned (see paragraph 4.), until the exponential phase. A 3 ml subculture was prepared by 1:100 dilution from the overnight culture and then incubated until the culture's OD600 nm ~ 0.1-0.2 was reached. Periplasmic GFP expression was induced with 2.25 µL of 0.05 mg/mL tetracycline solution (37.5 µg/L final concentration) for 3 min following the previously described protocol [50]. To remove the inducer,

bacteria were harvested by centrifugation (13,000 rpm for 3 min), washed twice, and then resuspended in supplemented M9 minimal medium. Bacteria were ready for imaging after being re-incubated for 2 h at 30°C, which was necessary to achieve an OD600 nm ~ 0.3 with GPF mostly expressed in the periplasmic space. Directly, bacteria were gently injected into the flow chamber and held for several minutes to ensure adhesion to the poly-L-lysine layer. Once the bacteria were immobilized for observation, the flow chamber was purred with at least 1 ml to remove non-adhered cells. Effective expression and subcellular localization of GFP in the periplasm were verified using transverse intensity line scans. The culture was not synchronized so that all phases of the cell cycles were present simultaneously.

Widefield microscopy

All images were acquired on a carl Zeiss Axio Observer Z7 inverted video microscope with a 100× phase-contrast, 1.4 N.A., oil-immersion objective (Plan-Apochromat Ph3 M27, Zeiss). The microscope is equipped with a thermostatically controlled incubation chamber. All images were recorded by a back-illuminated CMOS camera with a pixel size of 6.5 µm (ORCA-Flash4.0, Zeiss). Colibri light-emitting diode (LED) light sources are directly coupled to the microscope (Colibri, Zeiss) for fluorescence imaging with a multiband filter for multichannel imaging. During the 60-minute video, the imaging sequence cycle was as follows: 488 nm excitation for GFP, 548 nm excitation for Sytox Orange, 650 nm excitation for Cy5-labeled peptide, and phase contrast illumination, repeated every 20 s. The exposure time was set at 100 ms for each channel, except for phase contrast, which was 20 ms. LED intensities were typically 20%, 50%, and 50% at 488 nm, 548 nm, and 650 nm, respectively. Emission filters (Chroma Technology) were 512/25 for GFP, 573/40 for Sytox Orange, and 665/50 for Cy5. Image size was 748 x 748 pixels (equivalent to 48.62 µm x 48.62 µm). ZEN 2.3 lite software was used to record and process the data.

Time-lapse microscopy experiment

Time-lapse imaging began when a field of view with an appropriate density of plated cells was found (typically 5-20 bacteria). Prior to peptide introduction, GFP expression and localization in the periplasmic space of *E. coli* JCW10 were checked, and the cells were then filmed for ~ 5 min to assess the effect of photobleaching (e.g., the permanent loss of fluorescence after extended exposure to light). This verification of the decrease in total GFP fluorescence due to photobleaching will allow us not to overestimate the effect of the peptide on MO permeabilization due to the loss of GFP fluorescence. The time t = 0 in the video corresponds to the injection of cell growth media (e.g., M9 media supplemented with 0.4% glucose) containing the peptide tested at a concentration of the order of the MIC with Sytox Orange (final concentration of 10 nM) using a syringe pump (Aladdin; World Precision Instruments, Berlin, Germany). This solution was prepared immediately prior to the experiment and mixed thoroughly. The flow rate was set at 0.2 ml/min for the first minute, then at 0.2 ml/h for the rest of the

experiment. During peptide injection, bacteria in the field of view were imaged with four channels (images interspersed with GFP, Sytox Orange, Cy5, and phase contrast) every 20 s, typically resulting in 180 images acquired to track MOA events in real time.

Experiments were carried out with 4 peptides: LL-37 was used as a lytic control peptide to ensure that the experimental set-up was working correctly; AvBD103b is the native version of the peptide of interest; a Cy5-peptide template was used to study whether the fluorescent dye has an impact on peptide localization; and finally, Cy5-AvBD103b is the fluorescent version of the working peptide. Control experiments were carried out without peptides under the same conditions to verify the absence of effects of all other components present in the medium, including the DNA dye, Sytox Orange.

Fluorescence confocal microscopy

Imaging was carried out using an inverted microscopy (Axio Observer.Z7, Zeiss) combined with a confocal laser scanning unit (LSM 980 AiryScan2, Zeiss). The latter was equipped with photomultiplier tubes, a transmitted light detector (ESID), three gallium phospho-arsenide detectors (GaAsP) and oil-immersion objective, Plan-Apochromat 100x/1.40. Images were captured and processed by Zen software (v2.3). Green (Ex/Em), Orange (excitation wavelength, 590 nm; emission wavelength, 618 nm) and far-red (excitation wavelength, 633 nm; emission wavelength, 668 nm) channels were used for GFP, Sytox and Cy5-AvBD103b fluorescence, respectively. Image analysis and intensity profiles were performed using ZEN 2.3 lite software.

Fluorescence profiles and microscopy data analysis

All images analysis and processing were performed using ImageJ.

IV. Annex

HPLC analysis

HPLC analyses were carried out on a Chromaster system equipped with a 5160 pump, a 5430-diode array detector and a 5260-auto sampler. Semi-preparative purifications were carried out on a LaChromElite system equipped with a Hitachi L-2130 pump, a Hitachi L-2455 diode array detector and a Hitachi L-2200 auto sampler. A Chromolith High Resolution RP-18e (150 Å, 10 × 4.6 mm, 3 mL/min flow rate) column was used for analysis and a Nucleosil C18 (300 Å, 5 µm, 250 × 10 mm, 3 mL/min flow rate) for purification. As mobile phase, mixtures of 0.1% TFA in H2O (A) and 0.1% TFA in MeCN (B) were used.

MS analysis

High resolution ESI-MS analyses were performed on a maXis ultra-high-resolution Quadrupole Time-of-Flight (Q-TOF) mass spectrometer (Bruker Daltonics, Bremen, Germany), using the positive mode. The multiply-charged envelope was deconvoluted using the Charge Deconvolution algorithm in Bruker Data Analysis 4.1 software to obtain the monoisotopic [M] value.

Labelling of AvBD103b by Cyanine5

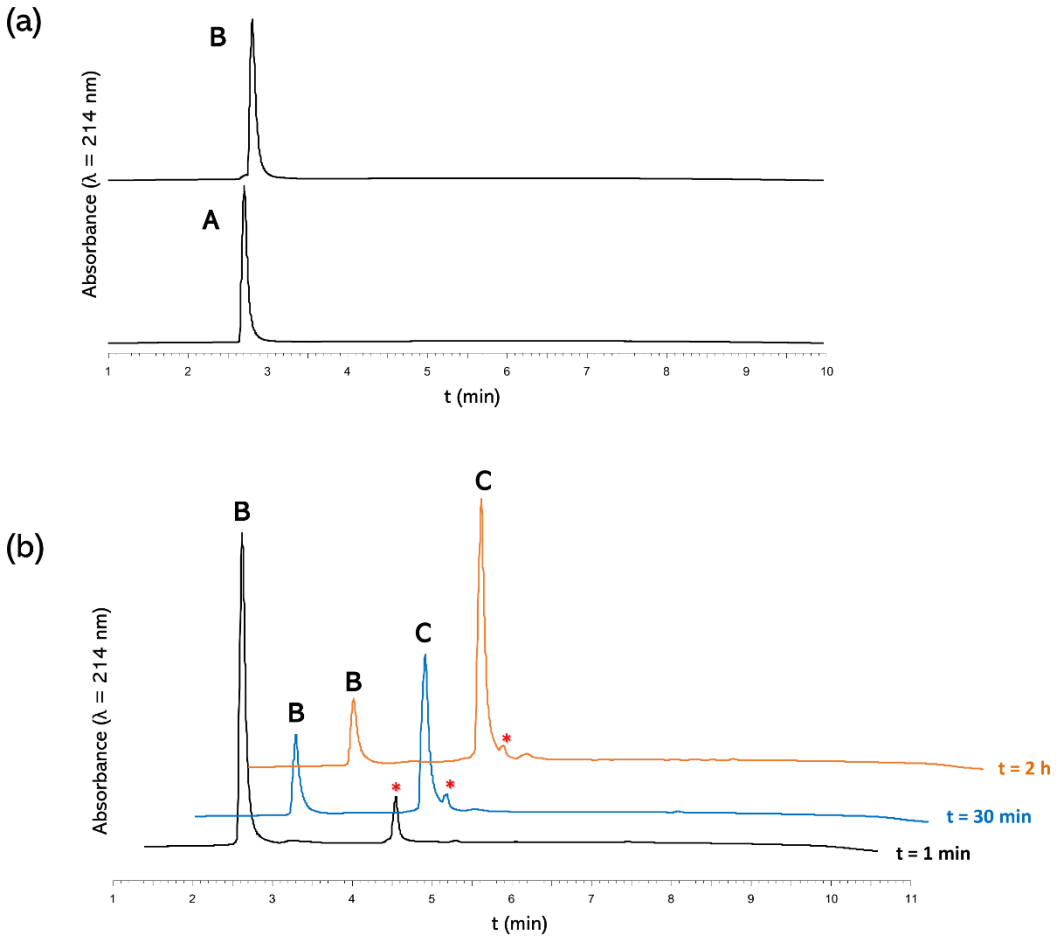

Peak	[M] (m/z) calculated	[M] (m/z) found	Attributed to
A	4500.36	4500.56	AvBD103b
B	4469	4469.81	Oxidized AvBD103b
D	4948	4947.94	Cy5-AvBD103b

Figure 1: HPLC traces of (a) oxidation of serine N-terminus of Sphe-2, (b) monitoring of the labelling reaction of oxidized Sphe-2 by Cyanine5.

SERINENTER peptide: purification and labelling

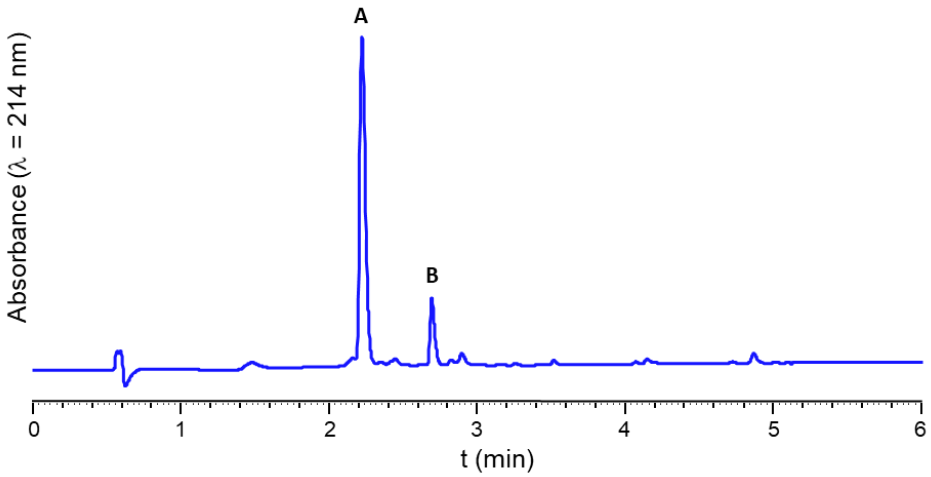

Peak	Retention time (min)	[M] (m/z) found	Attributed to
A	**2.24**	**1245.9**	**SERINENTER**
B	**2.69**	**1409.0**	**By-product:** linker attached to **SERINENTER** peptide

Figure 2: HPLC trace of crude SERINENTER peptide

ESI-MS (*m/z*): [M+H] calcd. for $C_{48}H_{84}N_{19}O_{20}^{+}$: 1246.6, found: 1245.9 (monoisotopic mass).

HPLC analysis: t_R = 2.24 min (Chromolith, gradient: 5-50% B/A over 5 min).

HPLC purification: [5 mg/mL], gradient: 5-50% B/A over 5 min, yield: 52%.

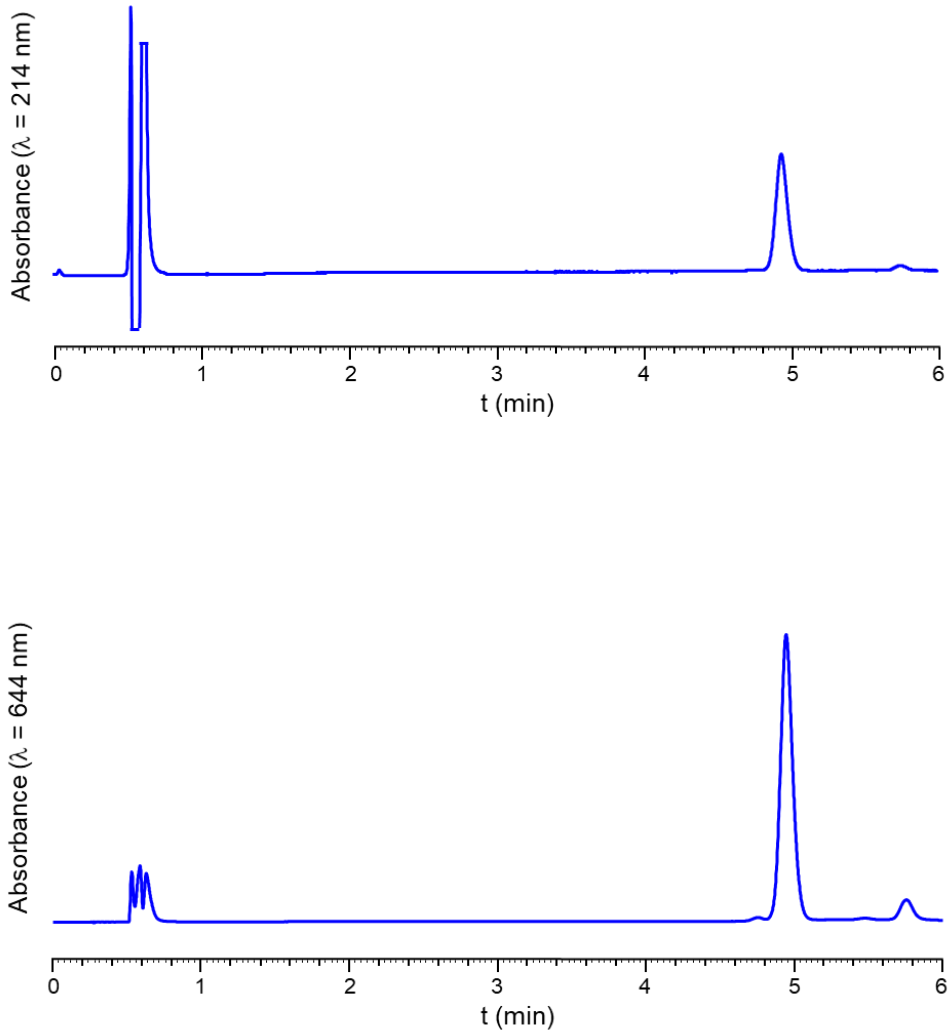

Figure 3: HPLC trace of purified labeled peptide Cy5-SERINENTER peptide at 214 nm and 644 nm.

ESI-MS (*m/z*): [M+H] calcd. for $C_{48}H_{84}N_{19}O_{20}^{+}$: 1683.0, found: 1685.5 (monoisotopic mass).

HPLC analysis: t_R = 4.80 min (Chromolith, gradient: 30-40% B/A over 5 min).

HPLC purification: [5 mg/mL], gradient: 5-50% B/A over 5 min, yield: 52%.

V. References

[1] C. Thouzeau *et al.*, « Spheniscins, Avian β-Defensins in Preserved Stomach Contents of the King Penguin, Aptenodytes patagonicus », *Journal of Biological Chemistry*, vol. 278, n° 51, p. 51053-51058, déc. 2003, doi: 10.1074/jbc.M306839200.

[2] M. Gauthier-Clerc, Y. Le Maho, Y. Clerquin, S. Drault, et Y. Handrich, « Penguin fathers preserve food for their chicks », *Nature*, vol. 408, n° 6815, p. 928-929, déc. 2000, doi: 10.1038/35050163.

[3] C. Landon, C. Thouzeau, H. Labbé, P. Bulet, et F. Vovelle, « Solution structure of spheniscin, a beta-defensin from the penguin stomach », *J Biol Chem*, vol. 279, n° 29, p. 30433-30439, juill. 2004, doi: 10.1074/jbc.M401338200.

[4] D. Teng *et al.*, « A dual mechanism involved in membrane and nucleic acid disruption of AvBD103b, a new avian defensin from the king penguin, against Salmonella enteritidis CVCC3377 », *Appl Microbiol Biotechnol*, vol. 98, n° 19, p. 8313-8325, oct. 2014, doi: 10.1007/s00253-014-5898-x.

[5] Q.-Y. Zhang *et al.*, « Antimicrobial peptides: mechanism of action, activity and clinical potential », *Military Medical Research*, vol. 8, n° 1, p. 48, sept. 2021, doi: 10.1186/s40779-021-00343-2.

[6] V. Sass *et al.*, « Human β-Defensin 3 Inhibits Cell Wall Biosynthesis in Staphylococci », *Infection and Immunity*, vol. 78, n° 6, p. 2793-2800, juin 2010, doi: 10.1128/iai.00688-09.

[7] B. Mathew et R. Nagaraj, « Variations in the interaction of human defensins with Escherichia coli: Possible implications in bacterial killing », *PLOS ONE*, vol. 12, n° 4, p. e0175858, avr. 2017, doi: 10.1371/journal.pone.0175858.

[8] S. Grandjean Lapierre *et al.*, « Cystic fibrosis respiratory tract salt concentration: An Exploratory Cohort Study », *Medicine*, vol. 96, n° 47, p. e8423, nov. 2017, doi: 10.1097/MD.0000000000008423.

[9] S. C. Langton Hewer et A. R. Smyth, « Antibiotic strategies for eradicating Pseudomonas aeruginosa in people with cystic fibrosis », in *Cochrane Database of Systematic Reviews*, The Cochrane Collaboration, Éd., Chichester, UK: John Wiley & Sons, Ltd, 2014, p. CD004197.pub4. doi: 10.1002/14651858.CD004197.pub4.

[10] K. A. Sochacki, K. J. Barns, R. Bucki, et J. C. Weisshaar, « Real-time attack on single Escherichia coli cells by the human antimicrobial peptide LL-37 », *Proceedings of the National Academy of Sciences*, vol. 108, n° 16, p. E77-E81, avr. 2011, doi: 10.1073/pnas.1101130108.

[11] N. Rangarajan, S. Bakshi, et J. Weisshaar, « Localized Permeabilization of E. Coli Membranes by the Antimicrobial Peptide Cecropin A », *Biochemistry*, vol. 52, août 2013, doi: 10.1021/bi400785j.

[12] K. J. Barns et J. C. Weisshaar, « Single-cell, time-resolved study of the effects of the antimicrobial peptide alamethicin on Bacillus subtilis », *Biochimica et Biophysica Acta (BBA) - Biomembranes*, vol. 1858, n° 4, p. 725-732, avr. 2016, doi: 10.1016/j.bbamem.2016.01.003.

[13] C. Landon *et al.*, « Real-Time Fluorescence Microscopy on Living E. coli Sheds New Light on the Antibacterial Effects of the King Penguin β-Defensin AvBD103b », *International Journal of Molecular Sciences*, vol. 23, n° 4, Art. n° 4, janv. 2022, doi: 10.3390/ijms23042057.

[14] J. Koehbach et D. Craik, « The Vast Structural Diversity of Antimicrobial Peptides », *Trends in Pharmacological Sciences*, vol. 40, p. 517-528, juill. 2019, doi: 10.1016/j.tips.2019.04.012.

[15] Z. Shang, S. Y. Chan, Q. Song, P. Li, et W. Huang, « The Strategies of Pathogen-Oriented Therapy on Circumventing Antimicrobial Resistance », *Research*, vol. 2020, sept. 2020, doi: 10.34133/2020/2016201.

[16] M. Mahlapuu, C. Björn, et J. Ekblom, « Antimicrobial peptides as therapeutic agents: opportunities and challenges », *Critical Reviews in Biotechnology*, vol. 40, p. 1-15, août 2020, doi: 10.1080/07388551.2020.1796576.

[17] A. Bin Hafeez, X. Jiang, P. Bergen, et Y. Zhu, « Antimicrobial Peptides: An Update on Classifications and Databases », *International Journal of Molecular Sciences*, vol. 22, p. 11691, oct. 2021, doi: 10.3390/ijms222111691.

[18] G. Upert, A. Luther, D. Obrecht, et P. Ermert, « Emerging peptide antibiotics with therapeutic potential », *Medicine in Drug Discovery*, vol. 9, p. 100078, mars 2021, doi: 10.1016/j.medidd.2020.100078.

[19] K. A. Sochacki, I. A. Shkel, M. T. Record, et J. C. Weisshaar, « Protein Diffusion in the Periplasm of E. coli under Osmotic Stress », *Biophysical Journal*, vol. 100, n° 1, p. 22, janv. 2011, doi: 10.1016/j.bpj.2010.11.044.

[20] S. M. Hickey *et al.*, « Fluorescence Microscopy—An Outline of Hardware, Biological Handling, and Fluorophore Considerations », *Cells*, vol. 11, n° 1, p. 35, déc. 2021, doi: 10.3390/cells11010035.

[21] C. D. Spicer et B. G. Davis, « Selective chemical protein modification », *Nat Commun*, vol. 5, n° 1, p. 4740, sept. 2014, doi: 10.1038/ncomms5740.

[22] E. A. Hoyt, P. M. S. D. Cal, B. L. Oliveira, et G. J. L. Bernardes, « Contemporary approaches to site-selective protein modification », *Nat Rev Chem*, vol. 3, n° 3, p. 147-171, mars 2019, doi: 10.1038/s41570-019-0079-1.

[23] L. De Rosa, R. Di Stasi, A. Romanelli, et L. D. D'Andrea, « Exploiting Protein N-Terminus for Site-Specific Bioconjugation », *Molecules*, vol. 26, n° 12, p. 3521, juin 2021, doi: 10.3390/molecules26123521.

[24] X. Chen et Y.-W. Wu, « Selective chemical labeling of proteins », *Org. Biomol. Chem.*, vol. 14, n° 24, p. 5417-5439, 2016, doi: 10.1039/C6OB00126B.

[25] K. F. Geoghegan et J. G. Stroh, « Site-directed conjugation of nonpeptide groups to peptides and proteins via periodate oxidation of a 2-amino alcohol. Application to modification at N-terminal serine », *Bioconjugate Chem.*, vol. 3, n° 2, p. 138-146, mars 1992, doi: 10.1021/bc00014a008.

[26] J. Kalia et R. T. Raines, « Hydrolytic Stability of Hydrazones and Oximes », *Angewandte Chemie International Edition*, vol. 47, n° 39, p. 7523-7526, 2008, doi: 10.1002/anie.200802651.

[27] A. Boaro, L. Castiñeiras, M. Torres, F. Bartoloni, et C. de la Fuente, « Light-Emitting Probes for Labeling Peptides », *Cell Reports Physical Science*, vol. 1, nov. 2020, doi: 10.1016/j.xcrp.2020.100257.

[28] E. Travnickova *et al.*, « Resazurin assay for assessment of antimicrobial properties of electrospun nanofiber filtration membranes », *AMB Express*, vol. 9, n° 1, p. 183, nov. 2019, doi: 10.1186/s13568-019-0909-z.

[29] M. Elshikh, S. Ahmed, S. Funston, R. Marchant, et I. Banat, « Resazurin-based 96-well plate microdilution method for the determination of minimum inhibitory concentration of biosurfactants », *Biotechnology Letters*, vol. 38, juin 2016, doi: 10.1007/s10529-016-2079-2.

[30] S. D. Sarker, L. Nahar, et Y. Kumarasamy, « Microtitre plate-based antibacterial assay incorporating resazurin as an indicator of cell growth, and its application in the in vitro antibacterial screening of phytochemicals », *Methods*, vol. 42, n° 4, p. 321-324, août 2007, doi: 10.1016/j.ymeth.2007.01.006.

[31] H. Choi, Z. Yang, et J. C. Weisshaar, « Oxidative stress induced in E. coli by the human antimicrobial peptide LL-37 », *PLOS Pathogens*, vol. 13, n° 6, p. e1006481, juin 2017, doi: 10.1371/journal.ppat.1006481.

[32] Y. Zhu, S. Mohapatra, et J. C. Weisshaar, « Rigidification of the Escherichia coli cytoplasm by the human antimicrobial peptide LL-37 revealed by superresolution fluorescence microscopy », *Proceedings of the National Academy of Sciences*, vol. 116, n° 3, p. 1017-1026, janv. 2019, doi: 10.1073/pnas.1814924116.

[33] A. Tossi, L. Sandri, et A. Giangaspero, « Amphipathic, α-helical antimicrobial peptides », *Peptide Science*, vol. 55, n° 1, p. 4-30, 2000, doi: 10.1002/1097-0282(2000)55:1<4::AID-BIP30>3.0.CO;2-M.

[34] S. F. Hedegaard *et al.*, « Fluorophore labeling of a cell-penetrating peptide significantly alters the mode and degree of biomembrane interaction », *Sci Rep*, vol. 8, n° 1, p. 6327, avr. 2018, doi: 10.1038/s41598-018-24154-z.
[35] D. Birch, M. Christensen, D. Staerk, H. Franzyk, et H. Nielsen, « Fluorophore labeling of a cell-penetrating peptide induces differential effects on its cellular distribution and affects cell viability », *Biochimica et Biophysica Acta (BBA) - Biomembranes*, vol. 1859, sept. 2017, doi: 10.1016/j.bbamem.2017.09.015.
[36] C. R. Mahone et E. D. Goley, « Bacterial cell division at a glance », *Journal of Cell Science*, vol. 133, n° 7, p. jcs237057, avr. 2020, doi: 10.1242/jcs.237057.
[37] E. Beltrán-Heredia, F.-C. Tsai, S. Salinas-Almaguer, F. J. Cao, P. Bassereau, et F. Monroy, « Membrane curvature induces cardiolipin sorting », *Commun Biol*, vol. 2, n° 1, p. 1-7, juin 2019, doi: 10.1038/s42003-019-0471-x.
[38] P. D. A. Rohs et T. G. Bernhardt, « Growth and Division of the Peptidoglycan Matrix », *Annual Review of Microbiology*, vol. 75, n° Volume 75, 2021, p. 315-336, oct. 2021, doi: 10.1146/annurev-micro-020518-120056.
[39] S. Tripathy et S. K. Sahu, « FtsZ inhibitors as a new genera of antibacterial agents », *Bioorganic Chemistry*, vol. 91, p. 103169, oct. 2019, doi: 10.1016/j.bioorg.2019.103169.
[40] P. Sass et H. Brötz-Oesterhelt, « Bacterial cell division as a target for new antibiotics », *Current Opinion in Microbiology*, vol. 16, n° 5, p. 522-530, oct. 2013, doi: 10.1016/j.mib.2013.07.006.
[41] H. Han *et al.*, « Recent progress of bacterial FtsZ inhibitors with a focus on peptides », *The FEBS Journal*, vol. 288, n° 4, p. 1091-1106, 2021, doi: 10.1111/febs.15489.
[42] P. Panda, A. C. Taviti, S. Satpati, M. M. Kar, A. Dixit, et T. K. Beuria, « Doxorubicin inhibits E. coli division by interacting at a novel site in FtsZ », *Biochemical Journal*, vol. 471, n° 3, p. 335-346, nov. 2015, doi: 10.1042/BJ20150467.
[43] A. di Somma, C. Canè, A. Moretta, et A. Duilio, « Interaction of Temporin-L Analogues with the E. coli FtsZ Protein », *Antibiotics*, vol. 10, p. 704, juin 2021, doi: 10.3390/antibiotics10060704.
[44] P. P. Navarro *et al.*, « Cell wall synthesis and remodelling dynamics determine division site architecture and cell shape in Escherichia coli », *Nat Microbiol*, vol. 7, n° 10, p. 1621-1634, oct. 2022, doi: 10.1038/s41564-022-01210-z.
[45] P. Schmitt *et al.*, « Insight into Invertebrate Defensin Mechanism of Action », *Journal of Biological Chemistry*, vol. 285, n° 38, p. 29208-29216, sept. 2010, doi: 10.1074/jbc.M110.143388.
[46] T. Schneider *et al.*, « Plectasin, a Fungal Defensin, Targets the Bacterial Cell Wall Precursor Lipid II », *Science*, vol. 328, n° 5982, p. 1168-1172, mai 2010, doi: 10.1126/science.1185723.
[47] J. Medeiros-Silva, S. Jekhmane, E. Breukink, et M. Weingarth, « Towards the Native Binding Modes of Antibiotics that Target Lipid II », *ChemBioChem*, vol. 20, n° 14, p. 1731-1738, 2019, doi: 10.1002/cbic.201800796.
[48] A. Müller *et al.*, « Daptomycin inhibits cell envelope synthesis by interfering with fluid membrane microdomains », *Proceedings of the National Academy of Sciences*, vol. 113, n° 45, p. E7077-E7086, nov. 2016, doi: 10.1073/pnas.1611173113.
[49] C. N. Pace, F. Vajdos, L. Fee, G. Grimsley, et T. Gray, « How to measure and predict the molar absorption coefficient of a protein », *Protein Science*, vol. 4, n° 11, p. 2411-2423, 1995, doi: 10.1002/pro.5560041120.
[50] Z. Yang, H. Choi, et J. C. Weisshaar, « Melittin-Induced Permeabilization, Re-sealing, and Re-permeabilization of E. coli Membranes », *Biophysical Journal*, vol. 114, n° 2, p. 368-379, janv. 2018, doi: 10.1016/j.bpj.2017.10.046.

Conclusion and Perspectives

The growing emergence of multidrug-resistant (MDR) bacteria, coupled with the lack of new antibiotics, is a threat to global health that requires an imminent solution. The discovery of new antibacterial drugs with new targets and/or innovative mechanisms of action is one of the recognized objectives in the fight against MDR bacteria. As alternatives to traditional antibiotics, the inspiration of antimicrobial peptides (AMPs) to develop a new class of antibacterials is a promising avenue of research.

AMPs are natural antibiotics produced by living organisms to defend themselves from an infection, a pathogen or an inflammatory process. Although they have been present in living organisms for hundreds of millions of years, most AMPs do not seem to induce bacterial resistance. Despite their potential antibacterial activity, only very few have been approved by the FDA. Many AMPs have failed in preclinical and clinical trials due to their toxicity to mammalian cells and lack of stability due to their degradation by proteases. However, these AMPs are mainly linear helical peptides that are widely studied, unlike complex disulfide-rich peptides (DRPs) such as defensins, which are less toxic and more resistant to proteolytic degradation. Defensins, like other DRPs, have been largely unexplored, partly due to the complexity of their production, which is no longer a problem today with advances in chemical peptide synthesis and/or peptide bioproduction.

Avian defensins (AvBDs) belong to the subfamily of β-defensins, which represents the largest family of vertebrate defensins. AvBDs have a potent activity against a large panel of Gram+ and Gram- pathogenic bacteria. The co-evolution of defensins with the bacteria that surround the living organism is an intriguing way to gain inspiration for fighting bacterial infections. This evolutionary diversity of defensins in each species is an asset for understanding mechanisms as well as a natural asset for learning strategies to induce little or no bacterial resistance. From the few data available on their modes of action, AvBDs do not appear to act via a lytic mechanism, but rather via a more complex one. Unfortunately, most of these studies are based on *in vitro* experiments under non-physiological conditions, which may therefore not reflect the actual MOAs.

Understanding how AMPs function in nature is the first essential step towards the rational engineering of highly effective compounds for clinical use, whether alone or in combination. Additional studies exploring AMPs bactericidal/bacteriostatic effects are necessary, particularly under conditions as close to reality as possible.

The king penguin defensin AvBD103b (known as Spheniscin-2) is an example of a highly interesting defensin as a promising therapeutic molecule, thanks to its physicochemical characteristics and atypical MOA. Indeed, this defensin is active against a wide panel of Gram+ and Gram- bacteria, with the advantage of being salt-insensitive, which is not the case of other β-defensins except the human HBD3. This particularity is highly valuable to fight against pathogens that thrive in salt-rich environments, for example in cystic fibrosis patients or during ocular infections. Moreover, the preliminary data of the

MOA of AvBD103b are in favor with a non-specific and multifaceted mechanism, which prevents bacteria from developing a resistance mechanism. This investigation of the antibacterial mechanism of AvBD103b using single-cell imaging fluorescence presents a unique real-time study conducted on living, growing bacteria under physiological conditions (salt concentrations) to understand the defensins' MOA. However, the MOA of AvBD103b remains not fully understood, particularly the peptide localization and trajectory during the attack of bacterial cells.

To continue deciphering the mechanism of action (MOA) of the peptide AvBD103b, this thesis work using the innovative single-cell fluorescence imaging technique has allowed us to provide new elements of MOA, particularly the direct spatial distribution of the peptide during its attack. This will pave the way for the investigation of putative molecular partners and/or cellular processes involved in the antibacterial mechanism of AvBD103b. This understanding is essential to explore the potential of AvBD103b as a candidate for the design of a new generation of antibacterial molecules.

As a first step, the single-cell fluorescence imaging technique develop in adaptative home-made fluorescence microscope (Weisshaar's group, Madison) has been implemented in a standard widefield microscope (CBM, Orléans). This technique presents numerous advantages; e.i., following in time-dependent manner the AMP effect on bacteria in growth and a reduced consumption of the AMP. Even more importantly, this technique can be used to study both membrane-active peptides and membrane-nonpermeabilizing peptides, as the cascade of events in the MOA differs. Studying the MOAs of several AMPs using this technique would add considerable value in the understanding of how these molecules "real" work. Although all the optimizations for the set-up of these experiments that have been carried out, several points remaining to be resolved for an optimal set-up, the change of growth media to optimize bacterial growth during the experiment is the most important one.

As a second step, the peptide has been fluorescently labelled by Cyanine5 dye (Cy5-AvBD103b) to allow monitoring precisely its spatial distribution during its bacterial attack. A direct selective strategy has been performed to label the N-terminal Ser. Despite two steps of the conjugation reaction, the global yield was good around 50%. We obtained 7.5 mg of Cy5-AvBD103b with high purity, which allows us to perform all our experiments easily (no restriction for the labeled peptide quantity). As the sub-localization of the peptide will be based on the signal fluorescence of the dye grafted on the peptide, MIC assay and cell localization have been carried out to verify that the dye does not interfere with the activity and the MOA of the native version of the peptide.

As a third step, the localization of Cy5-AvBD103b has been tricking in real time during bacteria attack, simultaneously with membrane permeabilization effect. Our preliminary results showed that AvBD103b localizes preferentially in the Z-ring, where cell division proteins are located, and in the septal region, where peptidoglycan synthesis is active. Throughout its attack, AvBD103b remains mainly on the cell

surface. However, part of the peptide may eventually reach cytoplasm and thus multiple potential intracellular molecular partners. The localization of AvBD103b indicates that cell division and/or CW biosynthesis, such as peptidoglycan (PG) synthesis, are putative partners of the peptide. The tubulin-like protein FtsZ involved in the Z-ring formation at the beginning of the division process may be one of the molecular partners(s) of AvBD103b. FtsZ is considered a promising target for the development of new antibacterials. Few peptides (e.i., Temporin, Octapeptides, NCR247) and molecules (e.i., Doxorubicin) have been reported as FtsZ inhibitors, inhibition of FtsZ assembly, inhibition of GTPase activity and the Z ring formation, degradation of FtsZ [1]. One way to support the hypothesis that FtsZ is a partner to AvBD103b, is to express GFP-tagged FtsZ in *E. coli* bacteria [2] and colocalize it with Cy5-AvBD103b. It's worth mentioning that the FtsZ protein is highly abundant, with around 5,000 to 20,000 monomers per *E. coli* cell during exponential growth [3]. The possibility that AvBD103b could interfere with the cell division by another mechanism, independent of FtsZ protein, cannot be ruled out. The interference with the biosynthesis of the CW is a putative target in the antibacterial AvBD103b's MOA, by directly targeting CW component(s), i.e., PG, or via indirect pathways. A study of the *in vitro* interaction of AvBD103b with PG lipid using membrane models could support the hypothesis that AvBD103b may interact with this cell envelop component. The interference with the CW biosynthesis has been reported to be part of the MOA of several AMPs via different ways. Lipid II is an important component in the synthesis of PG, which transports cell wall subunits across the cell membrane for polymerization and insertion into the existing cell wall [4]. Nisin [5], plectasin [6], and vancomycin [7] are representative AMPs, which target Lipid II to inhibit the PG synthesis. Teixobactin arrests CW synthesis by selectively inhibiting the transglycosylation of PG [8]. At this stage of the work, many questions remain unanswered, including the precise molecular partner(s) of AvBD103b.

Short-term perspectives

The understanding of the MOA AvBD103b by single-cell fluorescence microscopy will be pursued by a postdoctoral researcher as part of the project titled "ANTARBioTic" funded by the French National Research Agency (ANR). ANTARBioTic aims to explore the molecular diversity of King penguin defensins by combining original and multidisciplinary approaches (proteomics, spectroscopy, microscopy) and to tackle the challenge of deciphering the MOA of the most promising penguin defensins. This will have a significant impact, giving us a new and broader vision of the MOA of AMPs belonging to the defensin family.

Long-term perspectives

The transposition of the single-cell fluorescence imaging technique to a standard widefield fluorescence microscope makes this approach more accessible to researchers. One of the significant advantages of using the microfluidic flow chamber is the ability to work with small volumes and low concentrations (at the µL and µM scales, respectively), reducing the peptide consumption of the experiment, a common

obstacle in AMPs research. Therefore, this approach can be expanded to study the MOAs of other AMPs, including natural variants from different organisms, their mutants, or after chemical modifications. This allows us to identify key elements of peptide structure/characteristics concerning their antibacterial MOA. Study of the mechanism of synergistic effects of two antibiotics, e.g., an AMP and a conventional antibiotic, is also conceivable.

References

[1] H. Han *et al.*, « Recent progress of bacterial FtsZ inhibitors with a focus on peptides », *The FEBS Journal*, vol. 288, nº 4, p. 1091-1106, 2021, doi: 10.1111/febs.15489.

[2] X. Ma, D. W. Ehrhardt, et W. Margolin, « Colocalization of cell division proteins FtsZ and FtsA to cytoskeletal structures in living Escherichia coli cells by using green fluorescent protein », *Proceedings of the National Academy of Sciences*, vol. 93, nº 23, p. 12998-13003, nov. 1996, doi: 10.1073/pnas.93.23.12998.

[3] K. Dai et J. Lutkenhaus, « The proper ratio of FtsZ to FtsA is required for cell division to occur in Escherichia coli », *Journal of Bacteriology*, vol. 174, nº 19, p. 6145, oct. 1992, doi: 10.1128/jb.174.19.6145-6151.1992.

[4] C.-F. Le, C.-M. Fang, et S. D. Sekaran, « Intracellular Targeting Mechanisms by Antimicrobial Peptides », *Antimicrobial Agents and Chemotherapy*, vol. 61, nº 4, p. e02340, mars 2017, doi: 10.1128/AAC.02340-16.

[5] I. Panina, N. Krylov, D. Nolde, R. Efremov, et A. Chugunov, « Environmental and dynamic effects explain how nisin captures membrane-bound lipid II », *Scientific Reports*, vol. 10, p. 8821, juin 2020, doi: 10.1038/s41598-020-65522-y.

[6] T. Schneider *et al.*, « Plectasin, a Fungal Defensin, Targets the Bacterial Cell Wall Precursor Lipid II », *Science*, vol. 328, nº 5982, p. 1168-1172, mai 2010, doi: 10.1126/science.1185723.

[7] M. Hort *et al.*, « The Role of β-Glycosylated Wall Teichoic Acids in the Reduction of Vancomycin Susceptibility in Vancomycin-Intermediate Staphylococcus aureus », *Microbiology Spectrum*, vol. 9, nº 2, p. e00528, oct. 2021, doi: 10.1128/Spectrum.00528-21.

[8] P.-C. Wen, J. M. Vanegas, S. B. Rempe, et E. Tajkhorshid, « Probing key elements of teixobactin–lipid II interactions in membranes », *Chemical Science*, vol. 9, nº 34, p. 6997, juill. 2018, doi: 10.1039/c8sc02616e.

General Conclusion and Perspectives

Multidrug-resistant pathogens pose a significant threat to global health. AMPs, natural components of the immune system of living organisms, are promising alternatives for conventional antibiotics, especially when it comes to treating bacterial infections caused by pathogens that are multidrug-resistant. Understanding how these peptides work and their mechanisms of action is essential for developing effective therapeutic approaches to infectious disease treatment.

However, deciphering these mechanisms, particularly of non-membrane lytic AMPs, is complex and requires collaboration across various fields in the research area to achieve success. By leveraging the power of AMPs and adopting a multidisciplinary approach, innovative strategies can be developed to tackle resistant bacterial strains and improve overall health. Therefore, continued research in this field is essential, as it may lead to breakthroughs that could transform our approach to infectious diseases and safeguard public health for future generations.

However, further research is essential to optimize these AMPs for real-world applications. The main areas of interest are improving selectivity, ensuring safety and developing targeted delivery methods to fully exploit their therapeutic potential while protecting human cells.

Ons KHARRAT

Déchiffrer les mécanismes d'action de défensines prometteuses pour concevoir une nouvelle génération d'antimicrobiens

Avec l'augmentation spectaculaire de la résistance aux composés antimicrobiens et le nombre limité de nouveaux composés développés, il est urgent de mettre au point des alternatives thérapeutiques. Les peptides antimicrobiens (PAMs) sont des alternatives naturelles prometteuses, avec une grande diversité de mécanismes d'action (MOAs) optimisés depuis des millions d'années. Comprendre leurs MOAs à l'échelle moléculaire/atomique est essentiel pour concevoir des molécules efficaces dérivées des PAMs. L'objectif de ma thèse était de déchiffrer les MOAs de deux PAMs cationiques riches en ponts disulfure prometteurs : ETD151, un peptide antifongique de 44 résidus dérivé des défensines d'insectes (Partie I) et AvBD103b, un peptide antimicrobien de 38 résidus du manchot royal pour son activité antibactérienne (Partie II). La défensine ETD151 est très active contre les champignons pathogènes pour l'Homme et les plantes, et ne présente pas de toxicité. Son mécanisme multifacette nécessite la présence de glucosylcéramides (GlcCers), lipides de la membrane fongique déterminants pour la croissance cellulaire et la virulence du champignon, et donc considérés comme des cibles prometteuses. Cibler les GlcCers fongiques est peu susceptible d'induire rapidement une résistance. En utilisant des approches multidisciplinaires, nous avons prouvé l'interaction moléculaire directe entre ETD151 et le GlcCer fongique, et l'avons étudié à l'échelle atomique. La première étape a consisté à caractériser, par spectrométrie de masse, les deux principales formes de GlcCer du champignon *Botrytis cinerea*, révélant des structures de base sphingoïde méthylée d19:2/h16:0 et d19:2/h16:1. Nous avons ensuite révélé qu'ETD151 reconnaissait spécifiquement ces GlcCer de *B. cinerea* insérés dans des liposomes, avec un K_d estimé de l'ordre du micromolaire (µM) par thermophorèse à micro-échelle (MST). Par RMN, nous avons montré que les deux boucles hydrophobes adjacentes d'ETD151 jouaient un rôle majeur dans l'interaction, et aussi dans l'insertion spécifique et la fluidification des liposomes contenant du GlcCer fongique. Enfin, nous avons démontré que le méthyle C9 spécifique aux champignons (absent des GlcCer de mammifères et de plantes) jouait un rôle majeur dans l'interaction. Les éléments biochimiques et structuraux clés que nous avons révélés pour le mécanisme moléculaire par lequel ETD151 cible les GlcCer fongiques in vitro fournissent une base solide pour la conception d'antifongiques mimant les défensines et ciblant spécifiquement les GlcCers fongiques méthylés. La défensine aviaire AvBD103b appartient à une sous-famille différente de défensines. Elle est active contre un large spectre de bactéries Gram+ et Gram-, y compris en milieu salé, et ne présente pas de toxicité. L'hypothèse actuelle est que le MOA d'AvBD103b est non spécifique et multifacette, ce qui défavoriserait le développement de résistance. L'objectif ici est de marquer le peptide et de suivre précisément sa distribution spatiale au cours de son attaque. Pour ce faire, nous avons d'abord transposé une technique innovante d'imagerie par fluorescence sur cellule unique, permettant de disséquer le mécanisme antibactérien des PAMs en temps réel, sur des *Escherichia coli* vivantes et dans des conditions physiologiques. Nos résultats préliminaires ont montré qu'AvBD103b se localisait préférentiellement dans l'anneau Z où se trouvent les protéines de division cellulaire, et dans la région septale où la synthèse du peptidoglycane est active. Pendant son attaque, AvBD103b resterait principalement à la surface de la cellule. Cependant, une partie du peptide pourrait accéder au cytoplasme et atteindre ainsi de potentiels partenaires moléculaires intracellulaires. Ces nouveaux éléments du mécanisme sont essentiels pour concevoir une nouvelle génération de molécules antibactériennes, en particulier contre les pathogènes qui prospèrent dans des environnements riches en sel (patients atteints de mucoviscidose).

Mots clés : Résistance antimicrobienne, Défensine CSαβ antifongique, β-défensine antibactérienne, Glucosylcéramides, Interaction peptide-membrane, Microscopie de fluorescence

Deciphering the mechanisms of action of promising defensins to design a new generation of antimicrobials

With the dramatically increasing of antimicrobial resistance, coupled with the limited number of newly developed antimicrobials, therapeutic alternatives are urgently required. Antimicrobial peptides (AMPs) are promising natural alternatives with a wide diversity of mechanisms of action (MOAs) optimized over millions of years in nature. Understanding their MOAs at the molecular/atomic scale is essential for designing effective therapeutic molecules from AMPs. The aim of my thesis was to decipher the MOAs of two promising disulfide-rich cationic AMPs, namely ETD151, a 44-residue antifungal peptide optimized from insect defensins (Part I), and AvBD103b a 38-residue antimicrobial peptide from the king penguin for its antibacterial activity (Part II). The ETD151 defensin is highly active against human and plant pathogenic fungi without toxicity. Its multifaceted MOA requires the presence of glucosylceramides (GlcCers), fungal membrane lipids that are determinants of cell growth and virulence in fungi, and are therefore considered promising targets. Targeting fungal GlcCer is unlikely to quickly induce resistance. Using multidisciplinary approaches, we proved and studied at the atomic scale the direct molecular interaction between ETD151 and the fungal GlcCer. The first step was to characterize by mass spectrometry the two main forms of GlcCers from *Botrytis cinerea* fungus, revealing a methylated-sphingoid base structures, d19:2/h16:0 and d19:2/h16:1, respectively. Then, we revealed that ETD151 selectively recognizes these *B. cinerea* GlcCers containing in liposomes with a K_d estimated at ~ µM by microscale thermophoresis. By NMR, we identified that the two adjacent hydrophobic loops of ETD151 monopolize probably the binding, the specifically insertion into and fluidization of liposomes containing fungal GlcCer. Finally, we showed that the C9-methyl in the sphingoid base, a feature specific to fungi compared to mammals and plants, plays a major role in the ETD151-GlcCer interaction. The key biochemical and structural elements we have revealed for the molecular mechanism by which ETD151 targets fungal GlcCers in vitro, provide a solid structural basis for the design of defensin-mimetic antifungals specifically targeting methylated fungal GlcCer. The avian defensin AvBD103b belongs to a different subfamily of defensins. It is active against a wide panel of Gram+ and Gram- bacteria, with the advantage of being salt-insensitive, and without toxicity. The MOA of AvBD103b is supposed to be non-specific and multifaceted, preventing bacteria from developing a resistance mechanism. The aim here is to label the peptide, and monitor precisely its spatial distribution during its bacterial attack. To achieve this, we first implemented an innovative single-cell fluorescence imaging technique that allows to dissect the antibacterial mechanism of AMPs in real time, on living *Escherichia coli*, and in physiological conditions. Our preliminary results showed that AvBD103b localizes preferentially in the Z-ring, where cell division proteins are located, and in the septal region, where peptidoglycan synthesis is active. Throughout its attack, AvBD103b remains mainly on the cell surface. However, part of the peptide may eventually reach the cytoplasm and thus multiple potential intracellular molecular partners. The new MOA elements provided here are essential to design a new generation of antibacterial molecules, particularly against pathogens that thrive in salt-rich environments (cystic fibrosis patients).

Keywords: Antimicrobial resistance, CSαβ antifungal defensin, Antibacterial β-defensin, Glucosylceramides, Peptide-membrane interaction, Fluorescence microscopy

Centre de Biophysique Moléculaire
Rue Charles Sadron 45071 Orléans